UTS UNIVERSITY OF TECHNOLOGY SYDNEY

Behaviour of Bond Mechanism in Fibre Reinforced Polymer (FRP) Composites Externally Bonded to Timber

by Abbas Vahedian

Thesis submitted in fulfilment of the requirements for the degree of

Doctor of Philosophy

under the supervision of
Dr Rijun Shrestha
Prof. Keith Crews

University of Technology Sydney
Faculty of Engineering and Information Technology

April 2019

Dedication

In memory of my mother

and

To my beloved father, and

To my dearest wife.

Declaration

CERTIFICATE OF ORIGINAL AUTHORSHIP

I, Abbas Vahedian declare that this thesis, submitted in fulfilment of the requirements for the award of Doctor of Philosophy, in the School of Civil and Environmental Engineering, Faculty of Engineering and Information Technologies at the University of Technology Sydney.

This thesis is wholly my own work unless otherwise reference or acknowledged. In addition, I certify that all information sources and literature used are indicated in the thesis.

This document has not been submitted for qualifications at any other academic institution.

This research is supported by an Australian Government Research Training Program Scholarship.

Signature: Production Note: Signature removed prior to publication. Date: 10.04.2019

Acknowledgements

Acknowledgement and thanks are due first and foremost to my supervisors, Dr. Rijun Shrestha and Prof. Keith Crews, without whom this thesis would not have been possible. Your generous supervision, sound advice and guidance have been an endless source of inspiration and support. I am truly honoured to have been one of your PhD students.

I would also like to thank Dr. Saeed Mahini and Mr. Rex Glencross-Grant for their advice and assistance during early stage of my research study. My sincere and deep veneration goes to many people in the Faculty of Engineering and IT, especially Prof. Hadi Khabbaz, Dr. Emre Erkmen and Mrs. Van Le for their dedicated encouragement, attention and support throughout my PhD candidature. A particular gratefulness is given to Ms. Cynthia Zhang for her assistance in second stage of material tests. The assistance of laboratory staffs Mr. Mulugheta Hailu, Mr. Rami Haddad, Mr. David Dicker, Mr. Peter Brown and Mr. Laurence Stonard is highly appreciated. I would like to acknowledge and thank Sika Australia Pty. Ltd., who supplied the materials for this study. I would like to express my gratitude to Forest and Wood Products Australia Ltd (FWPA) for providing travel fund and supporting conference presentation. I am grateful to Dr. Hamidreza Farhoudi and Dr. Hojjat Badnava for their assistance in numerical analysis. I wish to express my regards to all of my friends especially Mr. Mehdi Aghayarzadeh for his assistance and encouragements.

Presentation of aspects of this research at several conferences gave me the exceptional opportunity to exchange ideas with and learn from the community of peers. I thank everyone I had the chance to meet and talk with. Thank you for viewing my presentations and for your thoughtful questions. I would like to acknowledge the support provided by Australian Government Research Training Program Scholarship.

I would like to express deepest and special thanks to my father, brother and sisters for their endless love, infinite support and encouragement to tackle this challenge. Without them, I could not have made it here. To my late mother, Zahra, who always believed in my ability to be successful and thank you for showing me that the key to life is enjoyment. You are gone but your belief in me has made this journey possible. I am grateful to my father-in-law and mother-in-law for their encouragement. Last but not least, I am greatly indebted to my beloved wife, Shamila. Thank you for your kindness, tremendous patience and for giving me the strength to endure this journey.

List of papers/publications

Refereed journal papers

1. Vahedian, A., Shrestha, R. & Crews, K. 2019, 'Experimental and analytical investigation on CFRP strengthened glulam laminated timber beams: Full-scale experiments', *Composites Part B: Engineering*, vol. 164, pp. 377-389.

2. Vahedian, A., Shrestha, R. & Crews, K. 2018, 'Analysis of externally bonded Carbon Fibre Reinforced Polymers sheet to timber interface', *Composite Structures*, vol. 191, pp. 239-250.

3. Vahedian, A., Shrestha, R. & Crews, K. 2018, 'Bond strength model for externally bonded FRP-to-timber interface', *Composite Structures*, vol. 200, pp. 328-339.

4. Vahedian, A., Shrestha, R. & Crews, K. 2018, 'Experimental investigation on the effect of bond thickness on the interface behaviour of fibre reinforced polymer sheet bonded to timber', *International Journal of Structural and Construction Engineering*, vol. 12, no. 12, pp. 1157-1163.

5. Vahedian, A., Shrestha, R. & Crews, K. 2017, 'Effective bond length and bond behaviour of FRP externally bonded to timber', *Construction and Building Materials*, vol. 151, pp. 742-754.

6. Vahedian, A., Shrestha, R. & Crews, K. 2017, 'Modelling of Factors Affecting Bond Strength of Fibre Reinforced Polymer Externally Bonded to Timber and Concrete', *International Journal of Structural and Construction Engineering*, vol. 11, no. 12, pp. 1567-1574.

Refereed conference papers

1. Vahedian, A., Shrestha, R. & Crews, K. 2018, 'Width effect of FRP externally bonded to timber', paper presented to the *Fibre-Reinforced Polymer (FRP) Composites in Civil Engineering (CICE 2018)*, Paris, France.

2. Vahedian, A., Shrestha, R. & Crews, K. 2018, 'Timber type effect on bond strength of FRP externally bonded timber', paper presented to the *The World Conference on Timber Engineering (WCTE 2018)*, Seoul, Korea.

3. Vahedian, A., Shrestha, R. & Crews, K. 2016, 'Modelling the bond slip behaviour of FRP externally bonded to timber', paper presented to the *The World Conference on Timber Engineering (WCTE 2016)*, Vienna, Austria.

List of abbreviations and acronyms

ACI	American Concrete Institute
AFRP	Aramid Fibre Reinforced Polymer
AS/NZS	Standards Australia
ASTM	American Society for Testing and Materials
BSI	British Standards Institution
BS	British Standards
CFRP	Carbon Fibre Reinforced Polymer
CoV	Coefficient of Variation
EB	Externally bonded
FEA	Finite Element Analysis
FRP	Fibre reinforced polymer
GFRP	Glass Fibre Reinforced Polymer
AFRP	Aramid Fibre Reinforced Polymer
Glulam	Glued-laminated timber
IAE	Integral Absolute Error
ISO	International Organization for Standardisation
LVDT	Linear variable differential transformer
LVL	Laminated veneer lumber
MOE	Modulus of Elasticity
NSM	Near-surface mounted
SR	Stepwise Regression
UTM	Universal testing machine
W	Increment of strain

List of notations

A_{eff}	Effective bonded area
A_f	FRP cross section area
A_t	Timber cross section area
b_t	Width of timber block
b_c	Concrete width
b_f	Width of FRP
d_t	Timber depth
E_{adh}	Adhesive elastic modulus
E_f	Elastic modulus of FRP plate
$E_f t_f$	Bond stiffness
E_L	Elastic modulus of timber parallel to grain
E_R	Elastic modulus of timber perpendicular to the grain
E_t	Elastic modulus of timber
E_T	Elastic modulus of timber tangential to the growth rings
f'_c	Concrete compressive strength
$f_{c,0}$	Compressive strength of timber parallel to grain
$f_{c,90}$	Compressive strength of timber perpendicular to grain
F_{c1t}	Plastic compressive loads in timber
F_{c2t}	Plastic compressive loads in timber
F_{ct}	Compression force in timber
f_t	Tensile strength of timber parallel to grain
F_{tf}	Tension force in FRP
F_{tt}	Tension force in timber
f_{ut}	Ultimate tensile strength of timber parallel to grain
G_a	Adhesive shear modulus
G_f	Interfacial fracture energy of FRP-to-timber interface
G_t	Timber shear moduli
L_e	Effective bond length of FRP-to-timber joint
L_f	Length of bonded FRP plate
L_t	Timber length
m	Slop of the plastic zone
M_u	Ultimate bending capacity of the composite beam
P_u	Maximum load before failure of joint and beam
$P_{u\ Anal.}$	Analytical maximum load of joint

$P_{u\ Num.}$	Numerical maximum load
$P_{u\ Exp.}$	Experimental maximum load of joint
s	Slip of FRP-timber interface
s_0	Slip of FRP plate at free unloaded end
s_1	Initial slip
s_i	Slip between adjacent strain gauges
s_{max}	Maximum slip for bond stress-slip model
s_x	Slip of FRP plate at location x
t_f	Thickness of FRP plate
t_{pl}	Measured thickness of the plate (or coupon specimen)
x_0	Variable location along FRP plate
y_c	Neutral axis
α	Effective bond length factor
β	Width ratio factor
Δl	Distance between adjacent strain gauges
Δ_{max}	Deflection of beam corresponding to ultimate load
ε	Strain of FRP plate
ε_{ct}	Maximum strains in compression
ε_{cu}	Ultimate strain in the plastic limit compression
ε_{cy}	Strain in the elastic limit compression
ε_{FRP}	Ultimate strain of FRP
$\varepsilon_{FRP,x}$	Strain of the FRP at point x
ε_t	Maximum strains in tension
ε_f	Strain at the loaded end
σ_{ct}	Maximum timber compression stress
σ_{FRP}	Axial stresses in FRP
σ_t	Maximum timber tensile stress
τ_1	Initial shear stress
τ_i	Average shear stress between two consecutive strain gauges
τ_u	Maximum bond stress for bond-slip model
τ_x	Shear stress of interface at location x
τ_v	Adhesive shear resistance
υ	Poisson ratio
γ_t	Timber type factor

Table of content

List of figures

List of tables

Abstract

Timber has been extensively used in construction for many centuries due to a number of advantageous properties such as aesthetics, strength-to-weight ratio, fire performance and acoustic properties. Besides, timber is only one of few renewable construction materials that can be used in large quantities. There has been an increase in the use of timber in modern structures in recent times with the advent of engineered wood products and growing interest in the use of environmentally sustainable materials in construction. Timber structures may need to be repaired and/or strengthened due to a number of reasons, such as, degradation as a result of biological and/or physical hazards, loss of strength or damage due to overloading or to meet increased load demands due to change in functionality or to comply with new code requirements. Therefore, either entire structures or key components may require strengthening, rehabilitation or replacement to maintain or upgrade their structural integrity.

Whilst demolition and replacement of degraded structures is a straightforward solution, it is often costly and time-consuming. Recent studies and applications have demonstrated that Fibre Reinforced Polymer composites (FRP) can effectively and economically be used for new structures, as well as in the strengthening and retrofitting of existing civil infrastructure. FRP is a material with high stiffness and strength to weight ratio, high Young's modulus and high fatigue performance. Moreover, additional advantageous properties of FRP such as being light in weight with superior corrosion resistance and flexibility in application make it a viable alternative to steel in reinforcing and/or repairing timber, especially in aggressive and extreme environments.

One of the most common problems associated with the use the externally bonded FRP sheets is the premature failure due to debonding which limits the full utilisation of the material strength of the FRP. Whilst the debonding mechanism in FRP bonded to concrete is well understood based on several previous studies, only limited attempts have been made to investigate the debonding behaviour of FRP bonded to timber. It is important to mention that there are some fundamental differences in the failure mechanism when FRP is bonded to timber compared to when it is bonded to concrete. Concrete is weak in tension; whilst

tensile strength of timber is much higher. Therefore, the models which work for FRP-to-concrete bond may not work for when FRP is bonded to timber. As such, a knowledge gap on potential parameters that influence bond behaviour of FRP-to-timber interface exists. Therefore, a sound understanding of the behaviour of FRP-to-timber interfaces needs to be developed and consequently, further understanding of the bond is essential.

The main goal of this research was to identify and investigate the potential parameters affecting the behaviour of the bond between timber and FRP. To achieve these outcomes, an extensive experimental program followed by analytical and numerical investigation was carried out. Through the experimental program, the influence of potential factors such as bond width, bond length, material properties and geometries on the bond strength was investigated. Investigation of the bond parameters showed that the bond strength significantly increases with increase in bond width and timber tensile strength. In addition, bond length has a major impact on the bond strength; however, bond strength cannot increase further once the bond length exceeds the effective bond length.

Whilst a number of analytical methods exist to predict the bond behaviour of FPR-to-concrete interface, analytical solutions to determine the interface behaviour of FRP-to-timber have not been fully investigated. Furthermore, existing analytical models for FRP-to-timber joints have been mostly derived based on the theoretical proposals where concrete had been used as a substrate and therefore, these models do not correlate particularly well with the experimental results. Novel theoretical models are proposed in this study to quantify the bond length, bond strength, the strain distribution profile, slip profile and shear stress relationships for FRP-timber joints. A good correlation could be obtained between the proposed models and experimental results.

Numerical simulation of FRP-to-timber joint is one of the most neglected fields of research. Numerical simulation has been undertaken to gain a better understanding about the interface behaviour of FRP-to-timber joints, and also to evaluate the feasibility of FRP application bonded to timber. It was found that by employment of proper constitutive behaviour for materials, the bond behaviour can be successfully predicted by FEA models.

The outcomes of FRP-to-timber joint tests and the models developed for the joints were then scaled up to FRP-strengthened timber beams. Finally, a design procedure for an FRP strengthened timber beam was developed to design and accurately predict the flexural capacity of strengthened timber beams.

The experimental, analytical and numerical works presented in this dissertation lead to a number of conclusions which are expected to make a significant contribution for understanding and modelling of FRP strengthened timber beams.

Chapter 1

INTRODUCTION

1.1. Introduction

This research aims to investigate the behaviour of the bond between timber and FRP and examine the potential factors affecting bond strength of FRP-to-timber joints. This chapter presents an introduction to FRP bonded to timber. Problem description aims and objectives of this study as well as thesis outline are described in this chapter.

1.2. Background and problem description

The requirement for lightweight, resistant, sustainable, and cost-effective structures has been increasingly demanded worldwide due to the reduction in raw material supplies and energy sources. The efficient and sustainable use of materials in building design and construction has received significant attention by civil engineers and environmentalists. Therefore, possessing all the foregoing characteristics, timber is being increasingly used as one of the main materials in civil infrastructure particularly in terms of aesthetics, fire protection, strength-to-weight ratio, acoustic properties, and seismic resistance. It is one of the oldest sustainable construction materials and still continues to be a popular choice in modern infrastructure (Sweeney 2012). However, without careful

detailing, timber degradation can occur as a result of physical hazards or biological decay of the elements and overloading that results in structural damage.

One of the main concerns of engineers is to evaluate the integrity of existing structures which were designed based on older codes, particularly those structures that were not designed for the earthquake actions. Structural degradation and deterioration from durability caused numerous bridges and roads to require repair throughout the world (Patnaik et al. 2008). During the 1950s and 1960s, a large number of bridges, highways and other infrastructure were built around the world and many of these are now in need of significant repairs and rehabilitation. In Australia alone, presently there are 12,000 timber bridges with spans over 7 m still in service most of which were built prior to 1940 (Kluft 2011). In addition, a vast number of damaged historical timber structures in the world are in urgent need of repair, strengthening, and rehabilitation using modern approaches due to either a change in their use or structural degradation. A large number of bridges of more than 30 years of age in Europe require strengthening to upgrade their structural capacity in order to tolerate increased loads caused by heavier vehicles and high volumes of traffic as well as requirements for more lanes (Motavalli and Czaderski 2007; Sweeney 2012). Many of these structures have reached the end of their planned service life. Moreover, change in functionality, infrastructure ageing, environmental action and increased service loads, have caused many structures to gradually deteriorate and led to significant reduction in load capacity and subsequent safety. Therefore, either entire structures or components require strengthening, rehabilitation or replacement (Banthia et al. 2002; Soleimani 2006). Whilst demolition and replacement of degraded structures with new structures is a straightforward solution; this can be costly and time consuming. Worldwide, the magnitude of the problem is estimated as costing $900 billion and this amount is increasing

constantly (Banthia et al. 2002). It is obviously clear that such a major challenge cannot be undertaken using old techniques. In this case, repairing and/or retrofitting of members based on modern standards is the only remaining alternative which is usually more feasible and cost effective than the replacement of deteriorated and damaged structures (Talukdar and Banthia 2010; Valipour and Crews 2011).

In the past, retrofitting and strengthening of deteriorated timber structures was primarily accomplished through the use of conventional methods such as cutting out damaged timber section and replacing with steel plates or connecting external steel plates to the surface of the structural members (Boyd 2000; Yang et al. 2013; Zhao and Zhang 2007). Bolted timber cover plates for strengthening of timber beams have been investigated to minimise the strength reducing effects of natural imperfections such as knots (Stanila et al. 2010). However, even though steel has a much higher Young's modulus and ultimate strength than wood, this may not be effective for strengthening as these plates are heavy, bulky and increase the dead load to the structure. Moreover, added steel plates are susceptible to corrosion and installation is usually difficult and requires heavy lifting equipment (Juvandes and Barbosa 2012; Valipour and Crews 2011). This repairing method also regularly needs long periods of service interruption as well as high maintenance cost and large amounts of labour (Banthia et al. 2002; Seica and Packer 2007). In addition, difficulties in handling and forming acceptable butt joints in the field make this method much less attractive (Boyd et al. 2008). Therefore, the use of steel plates and bolting is not desirable in many cases.

1.3. Strengthening timber structures using FRP composites

FRP composites can be either manufactured from fibre sheet and adhesive by hand known as wet lay-up plates or via pultruded plates. Initial use of FRP's focused on wet lay-up applications, as has been widely used in the

aerospace and marine industries. Wet lay-up is a flexible method, very cost competitive and easy to install. Wet lay-up process, with wide variety of components, can be used for structural elements having large and complex geometries. Application of pultruded profiles, on the other hand, has been considered as large-sized structural sections in bridge and building construction. This application can be categorised as an automated continuous moulding process in which the fibres are impregnated with resin by either drawing through a resin bath or injection of resin into the reinforcement. Different types of fibre can be used as reinforcement in pultrusion, such as roving, mats, fabrics, and braided preforms.

In recent years, FRP composites gained significant popularity for repairing and/or strengthening of existing structures because of their excellent structural characteristics. FRPs are light, highly resistant to corrosion, cost effective and have superior strength and stiffness properties (Hollaway 2010; Soleimani 2006; Triantafillou 1998). Currently, these composites have become a mainstream technology for strengthening of infrastructures such as steel, concrete and more recently, timber and masonry structures (Soleimani 2006). Results of previous studies on retrofitting timber structures using FRP composite have shown significant improvement in performance and load carrying capacity compared to an un-retrofitted structure. This improvement includes increasing loading carrying capacity both in tensile and compression zone, boosting stiffness of timber and also decreasing the compressive strain and tensile strain which lead to decrease the delamination (Lyons and Ahmed 2005).

To strengthen and retrofit timber elements, there are two main layouts of applications of FRP, namely externally bonding (EB) and near-surface mounting (NSM) as shown in Figure 1-1. As a composite strengthening material, externally bonded FRP has valuable advantages particularly where there are severe access restraints or high cost associated with

installation time (Hollaway and Teng 2008). To improve the flexural loading capacity and stiffness of timber beams, FRPs are usually bonded on the tensile section of elements. FRP strips/sheets which are externally bonded have been found to repair the biologically degraded or mechanically overloaded timber members. Near-surface mounted FRP bars, on the other hand, have been used to repair and retrofit historical timber structures (Kim and Harries 2010; Smith 2011; Valipour and Crews 2011). In the NSM strengthening method, a narrow groove is cut into the bottom face of member, and FRP composites plates or bars are inserted with a bonding agent. This is a relatively new strengthening technique which is an ideal choice for structures where the aesthetics of the original structure needs to be maintained. The NSM application increases the flexural rigidity, load carrying capacity and strength of the timber beams (Bisby and Fitzwilliam 2003; Valipour and Crews 2011). Alternatively, FRP sheets can be wrapped around the timber beams in which not only the flexural capacity of beam significantly increases but also this reinforcement may lead to increase the strength of the beam against splitting due to shear. Flexural and shear failures are the two main failure modes for normal unstrengthened timber beams.

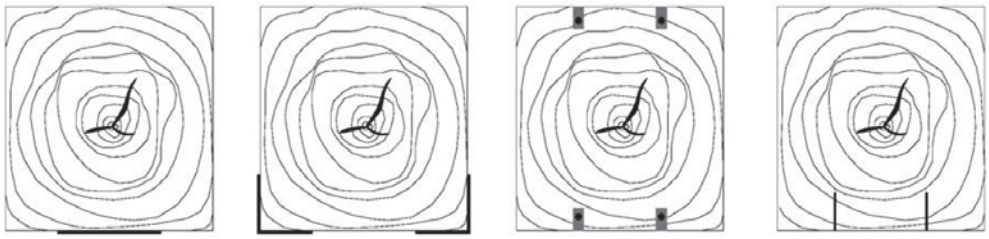

Figure 1-1 Outline of the timber section strengthened with FRP sheet or near-surface mounted bar.

1.3.1. Flexural strengthening

Research findings for FRP retrofitted beams show a significant increase in load capacity. However, if the reinforcement area ratio in the tension zone is adequate and large enough, the failure mode usually changes from a

brittle tensile to a more ductile compression (Pantelides et al. 2010; Valipour and Crews 2011). The part of timber yielding in compression spreads from the top of the beam to the bottom until the beam ultimately fails by tensile disconnection/rupture of the bottom wooden fibres. Therefore, more efficient use is made of the compressive strength of the timber. Simultaneously, as the FRP reinforcement prevents crack opening and restricts local rupture, the average ultimate tensile strain of the timber typically increases. This transition of failure mode causes not only an increase in strength but also enhanced ductility of the strengthened beam (Hollaway and Teng 2008). FRP also has other positive consequences when it is used to strengthen timber, because its presence reduces the effect of local "defects" (natural characteristics) that cause stress concentrations, such as deviations, knots, etc. As a result, the standard deviation of the beam lessens, which is highly desirable from a structural design perspective (Hollaway and Teng 2008; Valipour and Crews 2011).

1.3.2. Shear strengthening

Shear strengthening of timber beams must be considered if the beam is deficient in shear, or if its shear capacity is less than the flexural capacity after flexural strengthening. Timber has a low tensile strength perpendicular to the grain, and sometimes shear resistance parallel to the grain is also critical. This disadvantage may also be evidenced when the flexural capacity of a timber beam enhanced by external wrap; therefore, failure becomes shear-controlled. A wide variety of methods exist with the use of externally bonded FRP in shear strengthening. Popular techniques of bonding FRP shear reinforcement to a timber beam include side-bonding where the FRP is attached to the sides only, application of U-jacketing, where FRP U-jackets are bonded on both sides and the tension zone, and complete wrapping in which the FRP is wrapped around the entire cross-section. FRP also produces more consistent behaviour against splitting due

to shear resistance (Hollaway and Teng 2008). The scope of this dissertation is limited to flexurally FRP strengthened timber beams; however, further work still requires to be performed to consider shear strengthening of FRP externally bonded to timber beams.

The most common application of FRP composites which has been widely used in civil infrastructure, is the one where FRP is externally bonded to the substrate for flexural strengthening of structures. The application of externally bonded FRP was initially used for flexural strengthening of reinforced concrete; however, this application has been used to strengthen cast iron, modern steel, timber, and masonry in flexure and more recently received the greatest amount of research attention. Externally-bonded FRP composites can be used to address a variety of structural deficiencies. Nevertheless, to date, limited investigations of flexurally strengthened timber beams exist in the literature.

1.4. Bond behaviour of FRP externally bonded to timber

FRPs have a number of advantageous properties such as high elastic modulus, high fatigue performance, high stiffness and strength to weight ratios and superior resistance to corrosion (D'Ambrisi et al. 2014; Juvandes and Barbosa 2012; Valipour and Crews 2011; Xu et al. 2015). However, one of the most common problems associated with the use the externally bonded FRP sheets is the premature failure due to debonding which limits the full utilisation of the material strength of the FRP (Khelifa and Celzard 2014; Wu and Hemdan 2005). Debonding can be defined as the single most important failure mechanism of retrofitted beams (Coronado 2006) that occurs at much lower FRP strains than its ultimate strain (Mostofinejad and Shameli 2013). Debonding directly impacts the total integrity of the structure, with the subsequent outcome that the ultimate capacity and desirable ductility of the structure may not be achieved. Despite the large number of studies on externally bonded elements using FRP composites,

there is a significant knowledge gap on comprehensive understanding of potential parameters such as bond width, bond length, material properties and geometries that influence bond strength. Moreover, theories that have been developed to-date mostly cover FRP-to-concrete bond behaviour.

Mostofinejad and Shameli (2013) reported that several attempts have been made to improve the performance of FRP techniques to eliminate or postpone debonding failure of the FRP attached to concrete. Fracture mechanics - based models have been developed (both theoretically and experimentally) by many researchers to predict the initiation of debonding in retrofitted concrete elements and the peak load that the composite layers can resist before debonding (Achintha and Burgoyne 2011; Achintha and Burgoyne 2013; Täljsten 1996; Wu and Niu 2000). However, performance of FRP composite externally bonded to timber, considering debonding and failure modes, has not been fully investigated (Wan 2014) and to date, limited attempts have been made to investigate the bond behaviour of FRP to timber beams (CNR-DT 2007).

1.5. Scope and objectives

The lack of knowledge on the application of FRP to timber necessitates the need for a comprehensive program of study, and such knowledge gaps have motivated the research as is undertaken herein. The main goal of the present study is to contribute to the mitigation of the actual lack of knowledge and also to scrutinise the potential parameters affecting bond strength when FRP is bonded to timber. So far, majority of the research conducted on the application of FRP-to-timber have been confined to experimental investigations and the advancements in analytical and numerical modelling has been most limited. This research also focuses on development of functional and efficient analytical models to accurately predict the main characteristic of the interface including strain distribution profile, slip profile, shear stress and ultimate load. To achieve these

outcomes, supplementary experimental tests have been conducted in order to obtain the best alternative solution for externally bonded timber joints and timber beams using the FRP technique. For this purpose, the methodologies proposed for FRP-retrofitted concrete structures is adapted for timber substrates. To do this, the following objectives have been met in order of interrelation:

- Complete an in-depth review of previous relevant research conducted on using FRP as a technique for retrofitting timber structures including national and international standards;
- Develop a new test set-up to reliably measure the ultimate load, strain and slip of the interface with superior accuracy;
- Carry out laboratory experiments to investigate the behaviour of FRP-to-timber bonds;
- Investigate debonding failure of externally bonded FRP-to-timber joint;
- Investigate various parameters that effect on the interface response of the FRP-to-timber joints;
- Develop efficient and constitutive analytical interface models to predict the behaviour of the bond between FRP and timber;
- Establish and develop a suitable numerical model of bond strength model using a finite element analysis (FEA) software. The model should be generated in best-fit and design forms for possible incorporation into Standards and others design guidelines.

The most significant independent variables affecting bond strength and bond behaviour of FRP-to-timber joints are bond length, bond width, FRP thickness, timber modulus of elasticity and tensile strength, FRP-to-timber width ratio, bond stiffness and geometries of the interface. The above parameters have been investigated in this dissertation.

1.6. Thesis outline

This research is mainly divided into four components – (i) literature review to review the "state of art" and identify gaps in knowledge on behaviour of FRP-timber bond, (ii) experimental investigation to explore parameters affecting bond strength of FRP-to-timber joints, (iii) analytical model to predict the interfacial behaviour of FRP-to-timber joints and to establish predictive models for determination of effective bond length, strain distribution profile, slip profile, shear stress, and the bond strength of FRP-to-timber joints/beams, (iv) numerical model to simulate and predict all aspects observed during experiments.

The outcomes of these studies have been presented in this thesis in the form of eight chapters, organised as follows:

Chapter 1 – Presents an introduction to the research, the aims and objectives of the study, and also summarise the contribution of this work to knowledge.

Chapter 2 – Outlines a literature review on structural behaviour of timber, characteristics of FRP, and also provides information about different methods and techniques on retrofitting and strengthening of infrastructure. The possible failure modes of FRP-to-timber interface are mentioned in this chapter followed by the potential parameters that influence the interface behaviour. This chapter reviews development and use of FRP on timber joints/beams in order to investigate interfacial behaviour of externally bonded timber beams considering premature debonding failure.

Chapter 3 – Discusses the experimental details of externally bonded FRP-to-timber to failure subjected to monotonic tensile loading to investigate the behaviour of the bond between timber and FRP. Details of test setup, fabrication of test specimens, test procedures, equipment as well as

determination of materials properties have been described in this chapter. Through the experimental program, the influence of potential factors on the bond strength including bond width, bond length, material properties and geometries have been investigated.

Chapter 4 – Presents results of experimental investigation on externally bonded FRP-to-timber to failure for determining the effective bond length, bond strength, strain distribution profile, slip profile and shear stress along the interface. Through the experimental program, the sensitivity of the interface behaviour to potential factors such as bond width, bond length, FRP thickness, material properties and specimen geometry has been discussed in this chapter.

Chapter 5 – Describes the proposed analytical models for determining effective bond length, bond-slip relationship, strain and stress distribution profiles of FRP to timber substrates. The model established to predict the strength of the reinforced timber joints to examine the effect factors influence on the bond strength. In this chapter, numerical simulations through finite element analysis have been performed to consider and compare the interaction behaviour of FRP-to-timber bond against of experimental tests. Finite element analysis has been performed to validate the capability of the proposed analytical models and also to evaluate the feasibility of FRP application; failure load and failure mechanism of FRP-to-timber bonded interfaces.

Chapter 6 – Provides experimental details of flexurally reinforced FRP timber beams made of Glulam. Details of specimen's construction, test procedures, determination of materials properties as well as instrumentation have been described in this chapter. This chapter also represents results of unreinforced and strengthened timber beams. The load deflection of all beams, strain distribution profile, shear stress in the interface have been presented in this chapter. Following results of

experiments, an analytical model has been established to determine the ultimate flexural capacity of reinforced timber beam. The capability of the proposed model has been evaluated with the beam tests data.

Chapter 7 – Presents the design process for strengthened timber beam through a flowchart. To illustrate the design process, an example is also provided in this chapter.

Chapter 8 – Summarises the major outcomes of the research presented in this thesis and recapitulates the feasibility and applicability of fibre reinforce polymer methods on externally bonded timber joints and timber beams. This chapter also presents recommendations for future work.

Chapter 2

LITERATURE REVIEW

2.1. Introduction

Civil structures should be designed with the lowest cost and longest lifetime possible to function at theirs designated capacity without catastrophic service failure and major repairs. The efficient and sustainable use of materials in building design and construction has always been at the forefront for civil engineers and environmentalists. Timber exhibits these characteristics and is one of the best contenders and a more appropriate candidate than most other structural materials such as steel, concrete, and clay bricks. Timber is one of the oldest sustainable construction materials and still continues to be a popular choice in modern infrastructure (Raftery and Harte 2013; Thorhallsson et al. 2017). Timber is a natural, renewable, and energy efficient material, which can be recycled and reused at the end of its service life or converted into other re-manufactured products. Compared with other construction materials such as steel, concrete and clay bricks, timber is very light and offers a high strength-to-weight ratio. The construction time of timber structures is significantly less than other framing systems such as steel and concrete (Hollaway and Teng 2008; Rijal 2013). In addition to timber being one of only a few environmentally sustainable construction materials (Raftery and Harte 2013; Rescalvo et al. 2018), due to a number of advantageous properties such as aesthetics, strength-to-weight ratio, fire performance, acoustic properties, and seismic

resistance, there has been an increase in the use of timber in modern structures lately due to its low embodied energy and low environmental impacts.

On the other hand, although timber has been frequently used as a construction material, it certainly has limitations and its weaknesses must be accurately considered to have a precise analysis and design of timber structures (Juvandes and Barbosa 2012). High variability in the mechanical and physical properties of timber due to the influence of natural growth defects, such as knots and fibre misalignment can be defined as one the most difficulties in assessing existing timber elements. Timber structures may need to be repaired and/or strengthened due to a number of factors, such as, degradation of the timber due to biological and/or physical hazards, loss of strength or damage due to overloading or to meet increased load demands due to change in functionality or to meet new code requirements. Timber structures can be readily damaged by lack of inappropriate maintenance, surface degradation due to insect and fungal attack and environmental action. In addition, knots, defects, and pitch pockets significantly affect structural timber leading to gradually deteriorate and result in significant reduction in load capacity and subsequent safety (Juvandes and Barbosa 2012). Due to the reduction in strength, which may pose a serious threat to public safety, structures that have excessively deteriorated need to be repaired/ strengthened.

2.2. FRP materials

Recent studies and applications have demonstrated that Fibre Reinforced Polymer (FRP) composites have become a mainstream technology for repair and/or strengthening of infrastructures such as steel, concrete and more recently, timber and masonry structures (Kabir et al. 2016a; Manalo et al. 2010). FRP composites has emerged as an innovative and widespread

method for strengthening and retrofitting of infrastructure over the last three decades (Chen and Teng 2001; Juvandes and Barbosa 2012; Kabir et al. 2016b; Valipour and Crews 2011). FRPs are light, highly resistant to corrosion, cost effective and have superior strength and stiffness properties and its specific strengths remain high at elevated temperatures (Hollaway 2010; Soleimani 2006; Triantafillou 1998). FRP composite materials are able to carry high loads safely and increase the stability of structures. In some cases, they are the only reasonable and applicable materials that can be used for retrofitting, particularly in places where it is impossible to gain access for heavy machinery. These materials have a major role both in the field of strengthening and retrofitting of existing structures and in the new structural design (Juvandes and Barbosa 2012; Valluzzi et al. 2016). FRP may have additional advantages relating to aesthetic aspects and possibly to a better thermal compatibility which can be achieved by properly tailoring the composite material. FRP is a powerful and viable alternative to steel when considered as a retrofitting material for timber structures due to high compatibility of timber and FRP composites to their strains at failure. The high strain capacity of FRP reinforcement allows the compression fibres of the timber to reach their yield strains and the tension laminates to reach their ultimate tensile capacity. Constantly, in strengthening of timber structures where steel is the reinforcing material, the timber will not reach its full strain capacity prior to the yielding of the reinforcement (Gilfillan et al. 2003).

Whilst there are a number of fibre composite available, glass, carbon and aramid fibres are more commonly used in construction industry due to higher and more consistent properties of these fibres. The mechanical properties of these fibres are given in Table 2-1. Carbon FRP (CFRP) has sound fatigue strength; about three times that of steel along with a low axial coefficient of thermal expansion, favourable creep characteristics and resistance against abrasion (Gilfillan et al. 2003). Carbon fibres have the

most desirable properties and, based on the circumstances, are produced from one of three precursors: polyacylonitrile (PAN), rayon and mesophase/isotropic pitches (Banthia 2002; Burgoyne et al. 2007). Due to the variety of mechanical properties and modulus of elasticity of carbon fibre, several classes of carbon fibres are available. CFRPs are usually more expensive than glass fibres; however, they are extensively used in structural engineering applications to repair and strengthen infrastructure due to their outstanding properties. CFRPs have prominent characteristics such as high modulus of elasticity, low density, and resistance to thermal, chemical, and environmental effects. Carbon fibres can be used as the best strengthening materials for structures which are weight and/or deflection sensitive (Bisby and Fitzwilliam 2003).

Glass fibre is one of the most widely used materials in the field of structural retrofitting. It is an amorphous form of silica. Based on its mechanical properties, glass fibre is categorised in different classes (e.g. A-Glass, E-Glass, ECR-Glass, AR-Glass and the S-Glass). In terms of retrofitting to infrastructure, E-type glass fibres are mostly used due to their exceptional mechanical properties and relatively low cost. Although the tensile strength and modulus of elasticity of S-glass is higher than that of E-glass, the higher cost of S-glass fibres makes them less popular than E-glass.

Aramid (Kevlar™) is an organic fibre which is commonly used in composites. They have high strength, moderate modulus of elasticity, low density and are highly resistance to fire, heat and chemical components (André 2006; Bisby and Fitzwilliam 2003). All types of FRPs – carbon, glass and aramid – must be cured with the appropriate adhesives to carry out the tensile loads. The epoxy matrix not only plays an effective role in forcing the individual and flexible fibres to orientate in the same direction, but also transfer loads between the fibres and protect the fibres from environmental factor (Sweeney 2012). Figure 2-1 shows the typical stress-

strain diagrams for different uni-directional FRP composites under short-term uniform loading compared with steel (Du Béton 2001). It can be seen that CFRP has the higher tensile strength in comparison with GFRP, AFRP and even mild steel.

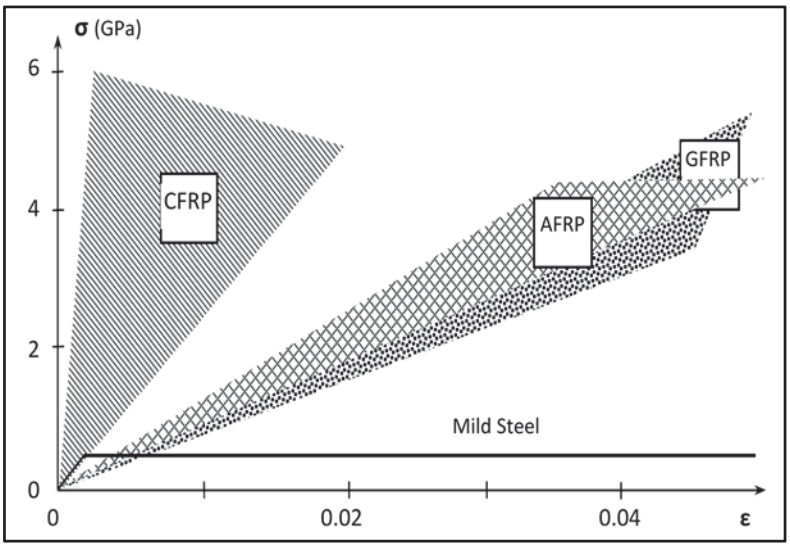

Figure 2-1 Uniaxial tension stress-strain diagrams for steel and unidirectional FRPs including carbon FRP, aramid FRP and glass FRP (Du Béton 2001).

Table 2-1 Properties of Composite and Comparison with Steel (Banthia 2002; Burgoyne et al. 2007)

Property	Steel	AFRP	CFRP	GFRP
Tensile strength [MPa]	300 -450	1720 - 2540	600 - 3690	480 - 1600
Modulus of Elasticity [GPa]	200	41 - 125	120 - 580	35 - 51
Rupture strain, %	7 - 13	1.9 - 4.4	0.5 - 1.7	1.2 - 3.1

2.3. Adhesive materials

In terms of strengthening and retrofitting of infrastructure, the selection of materials is a critical process. To achieve a satisfactory bonded joint, the effectiveness of the adhesive used, the quality and integrity of the composite adherent need to be considered (Hollaway and Teng 2008). Moreover, application conditions, surface preparation, cleanliness and temperature, significantly impact the strength of the bond.

2.3.1. Adhesives

The adhesives provide a shear load path between the composite material and the member surface. One of the most common types of structural adhesive is epoxy which is the result of mixing an epoxy resin (polymer) with a hardener. To achieve a successful application of an epoxy adhesive, adequate specifications require being taken into account. These provisions can be listed as adherent materials, surface treatment techniques, mixing/application temperatures and methods, curing temperatures, thermal expansion, creep properties, abrasion and chemical resistance (Deng et al. 2014; Du Béton 2001). In comparison with other polymers; such as adhesive agents, epoxy adhesives have remarkable advantages for civil engineering purpose including low shrinkage, low creep and high strength retention under sustained load, high cured cohesive strength, flexibility to accommodate irregular or thick bond lines and high surface activity and appropriate wetting properties for a variety of substrates (Du Béton 2001; Hollaway 2001; Zoghi 2013).

2.3.2. Matrices

In general, a polymer is referred to as resin system during processing and matrix after the polymer has cured. The main roles and structural requirements of a matrix are: to bind together the fibres, to protect the fibres against abrasion or environmental corrosion and to distribute the load and transfer stresses to the fibres (Burgoyne et al. 2007; Hollaway and Teng 2008; Zoghi 2013). Mechanical properties of the composite, including the transverse modulus and strength, shear properties and properties in compression highly depend on the type of matrix (Zoghi 2013). It is important to note that the physical and chemical characteristics of the matrix such as melting or curing temperature, viscosity and reactivity should be compatible with the fibres since these specifications play a vital role in controlling the overall stress-strain behaviour of the composite.

Therefore, appropriate selection of the matrix is of paramount importance and all physical and chemical characteristics of the matrix need to be taken into account when designing a composite system (Banthia 2002; Burgoyne et al. 2007; Du Béton 2001; Hollaway and Teng 2008).

As a structural composite material, the matrix can either be a thermoplastic type or a thermosetting type, with the second being the most common one (André 2006; Du Béton 2001; Zoghi 2013). However, the thermoplastic polymer is not intended for use as a matrix material for rehabilitation and retrofitting of civil infrastructure. Thermoplastics have high viscosity at the processing temperature, and as such, are difficult to process. In addition, their impregnation is impaired by high viscosity; therefore, special care must be taken to ensure that contact between the fibres and the polymeric resin is strong enough (Hollaway 2001; Zoghi 2013). Thermoplastics are also capable of being reshaped and repaired by application of heat and subjecting them to temperature cycles reaching values above their forming temperature. Polyether Ether Ketone (PEEK), Polyphenylene Sulphide (PPS) and Polysulfone (PSUL) are the most common thermoplastic resins for high performance applications (Burgoyne et al. 2007). Thermosetting resins are polymers which have strong bonds both with the molecules and in-between the molecules. When thermosetting resins have been cured, they retain their shape; however, at high temperatures they begin to thermally decompose. The most common thermosetting resins used in civil engineering applications are epoxy, polyesters and vinyl ester.

Epoxy resins generally have high specific strengths, temperature resistance, dimensional stability, durability and good resistance to solvents and alkalis, but, mostly have weak resistance to acids (Banthia 2002; Burgoyne et al. 2007; Hollaway 2001; Hollaway and Teng 2008). In addition, epoxy resins are highly resistant to corrosion and are less affected by water and heat

than other polymeric matrices. Epoxy resins can be formulated to have a wide range of stiffness and other mechanical properties as shown in Figure 2-2. The main disadvantages associated with epoxy resins are their relatively high cost and long curing period. The cost of epoxies varies depending on their performance, but generally polyesters and vinyl esters are cheaper than epoxy resins (Burgoyne et al. 2007; Deng et al. 2014; Zoghi 2013).

Polyester resins have been widely used in applications requiring corrosion resistance. Polyester resins have superior durability and are resistant to fibre erosion especially when styrene is supplemented with methyl methacrilate (MMA) (Burgoyne et al. 2007). Polyester resins, if properly formulated, can be one the best options to be used in outdoor applications since they act as a good UV protector. In addition, their formulations improve stiffness, glass transition temperature, and thermal stability (Burgoyne et al. 2007; Zoghi 2013). High volumetric shrinkage is identified as the main disadvantage of polyester resins. However, this volumetric shrinkage can be reduced by adding a thermoplastic component. Typical stress-strain curves for general purpose polyester matrices tested in tension and compression are shown in Figure 2-3 (Burgoyne et al. 2007).

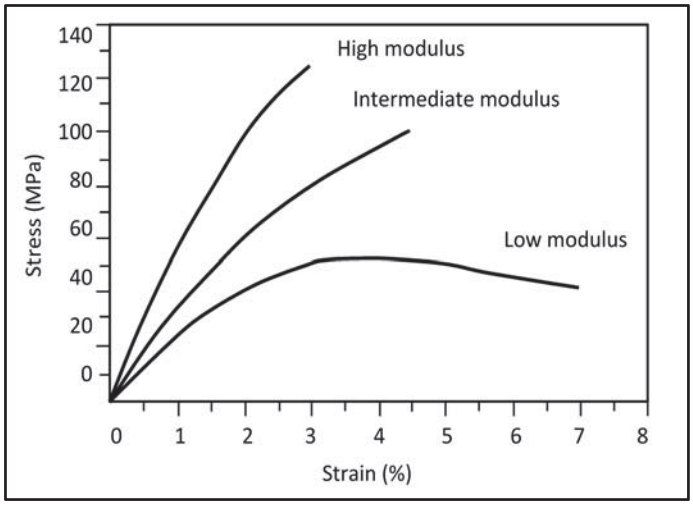

Figure 2-2 Stress-strain curves (tensile) of epoxy matrix resins of different modulus (Burgoyne et al. 2007)

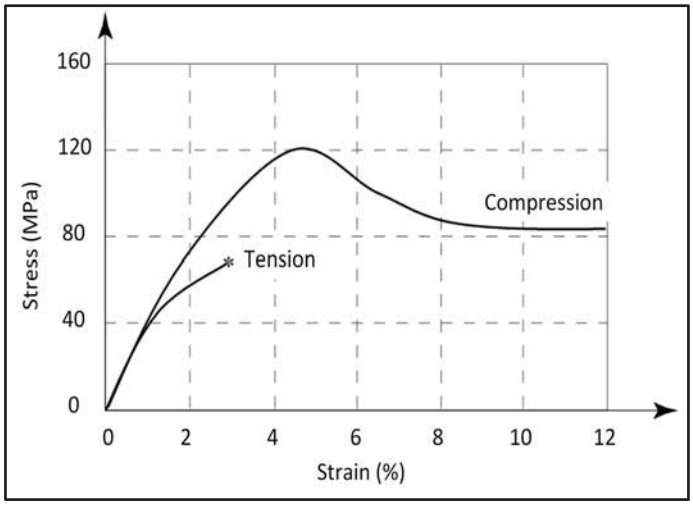

Figure 2-3 Stress-strain curves for general purpose polyester resin (Burgoyne et al. 2007).

Vinyl esters have higher fracture toughness and are more flexible than polyesters. They also have capable adhesion and very good wet-out when reinforced with glass fibres. In addition, vinyl esters exhibit some of the advantages of polyesters such as viscosity and fast curing as well as the advantages of epoxies such as chemical resistance and tensile strength (Zoghi 2013). Vinyl ester resins are appropriate to be used in applications requiring corrosion resistance. They are highly resistant to acids, alkalis, solvents and peroxides. However, in comparison with epoxy resins they have only moderate adhesive strength.

2.4. Previous studies of timber strengthening

Timber is one of the oldest structural material and still continues to be a popular choice in modern infrastructure. Timber can carry both tensile and compressive loads; and consequently it has been used extensively for millennia as the main component of civil infrastructure such as houses, bridges, railway sleeper, etc. (Lyons and Ahmed 2005; Smith 2011). In the last century, a large number of timber structures were built in all around the world. In Australia alone, there are 12,000 timber bridges still in service most of which were built prior to 1940 (Kluft 2011). Many of these

structures have reached the end of their planned service life. Therefore, either entire structures or components require strengthening, rehabilitation or replacement (Rescalvo et al. 2018; Valluzzi et al. 2016). In such structures, the deficient members and joints require strengthening to achieve acceptable levels of safety, and to avoid brittle failure during large load events. Furthermore, deteriorated timber elements need to be repaired in order to upgrade their structural capacity to tolerate increased loads caused by heavier vehicles and high volumes of traffic as well as requirements for more lanes, (Gandomi et al. 2013). A vast number of damaged historical timber structures in the world are in urgent need of repair, strengthening, and rehabilitation using modern approaches due to either a change in their use or structural degradation. Besides, prior to the introduction of new design codes and standards, most of the structures were designed based on vertical/gravity loads only. Thus, those structures might not satisfy the specific requirements of new codes and need to be replaced or retrofitted to upgrade their structural integrity in order to withstand standard loads (Raftery and Rodd 2015; Thorhallsson et al. 2017).

In order to strengthen and retrofit timber structures, attempts have been taken both for new and existing structures. Strengthening of timber structures can be performed to decrease the size of timber element and allow the utilisation of weaker species of timber providing a more efficient use of the timber resources. The strengthening techniques can also be used to enhance the performance of timber structure and increase the load-carrying capacity of existing timber elements to support higher loads than the original design of the structure leading to reduce the cost and material of a replacement structure.

2.4.1. Non-FRP materials

Throughout decades, various techniques have been employed to retrofit timber structures using different material. Some of the early investigations of strengthening of timber structures were accomplished through the use of metals for reinforcement.

Mark (1961) bonded aluminium plates to the bottom and top side of timber beams; in which the main failure modes were reported as the separation and buckling of the aluminium plates. The aluminium plates were bonded between laminations of glulam beams both horizontally and vertically in the study conducted by Sliker (1962). The failure mode was reported by buckling of the plates under concentrated loads, as well as delamination of the plates over time with dimensional changes in the timber. Bohannan (1962) bonded stranded steel cable and Peterson (1965) used steel plates bonded on the tensile soffit of timber beams to increase the flexural loading capacity and stiffness. An increased in bending strength of pre-stressed beams was observed in both studies; however, the stiffness enhancement was only obtained in the study conducted by Peterson (1965). Bulleit et al. (1989) strengthened glulam beams using both square and round cross-section steel bars. The rods were embedded in the tensile area of the beams and this area was covered with a layer of timber to reduce the possibility of splitting timber around the steel bars. Failures; however, occurred adjacent to the embedded bar by splitting wooden fibres inside the timber. Nevertheless, the stiffness and bending strength of the steel-reinforced glulam increased by 24-32% and 30%, respectively.

Del Senno et al. (2004) conducted experiments to investigate the behaviour of steel to timber joints as shown in Figure 2-4. It was concluded that the viscosity of the adhesive, rather than its mechanical properties, has more impact on the mechanical properties of the joint. It was also reported that the joint ultimate load and stiffness enhanced when the

thickness of adhesive increased from 1 mm to 2 mm. Issa and Kmeid (2005) conducted a series of tests on flexurally reinforced glulam beams with 1.5 mm thick steel plate subjected to four-point bending test as shown in Figure 2-5. The reinforced beams exhibited 36% and 67% increases in strength and stiffness, respectively, when compared with unreinforced beams. However, it was reported that the installation of streel plates was rather difficult and required at least two persons to be involved in the task to accomplish the strengthening. In addition, the steel plate needed to be pressed in a presser after laminating to the timber beams, and therefore required more special equipment.

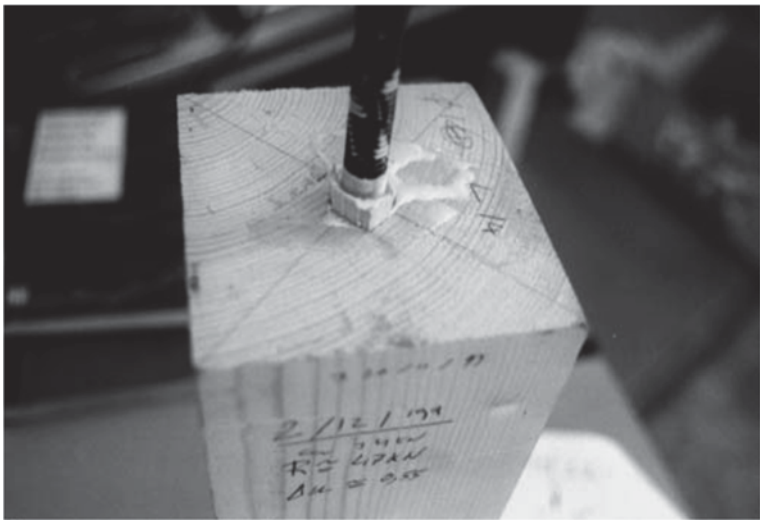

Figure 2-4 Strengthening of timber connections and joints using steel rods (Del Senno et al. 2004)

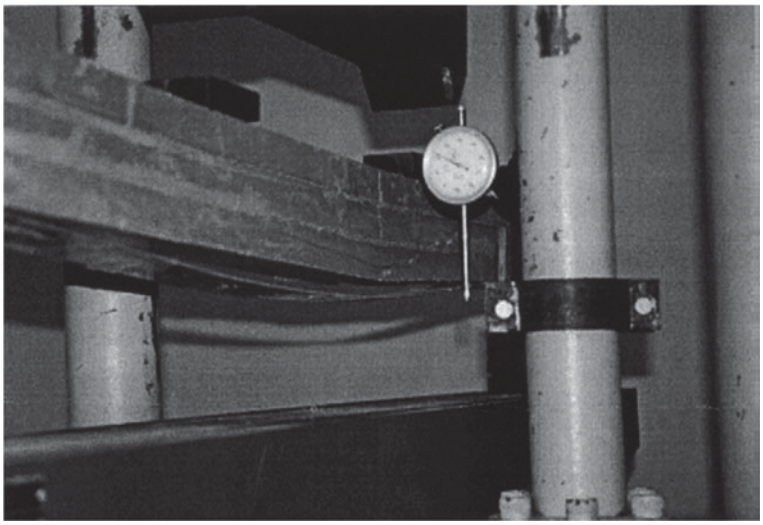

Figure 2-5 Glulam beam strengthened with steel plate (Issa and Kmeid 2005)

De Luca and Marano (2012) tested twelve unreinforced and reinforced glulam beams in which nine specimens were reinforced as shown in Figure 2-6. The reinforcement was accomplished through the insertion of steel bars to the top and bottom side of glulam beams by an adhesive, whereas in six reinforced beams the bottom bars were pre-tensioned by a force of 18 kN. It was reported that the pre-tensioned samples exhibited higher strength and stiffness with more ductile manner when compared with simply reinforced beams and unreinforced beams.

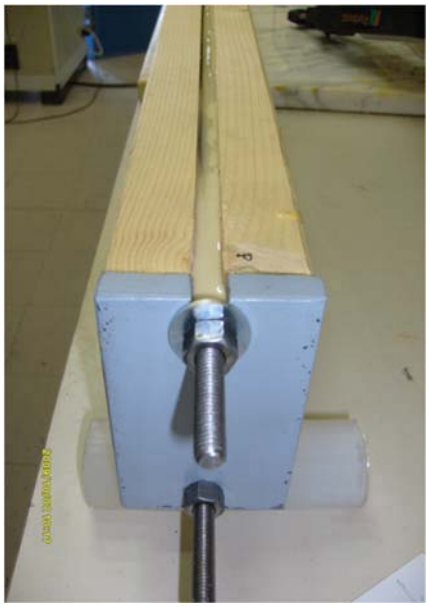

Figure 2-6 Reinforced glulam beams (De Luca and Marano 2012)

An attempt was made by Akbiyik et al. (2007) in which beam was repaired with hex bolts at every 610 mm as shown in Figure 2-7. The hex bolts were placed from bottom to the top of the stringers in predrilled holes at the centre of beam. The test results of the repaired beam showed 88% recovery of the original ultimate load as well as increase in residual capacity and ductility. Bolted timber splice plates used as a strengthening approach for axially loaded timber elements or flexural members as shown in Figure 2-8 (Stanila et al. 2010). This technique would be effective in minimising the effects of natural imperfections such as knots. Nevertheless, no tests were reported in such study, and hence its contribution to the literature is limited.

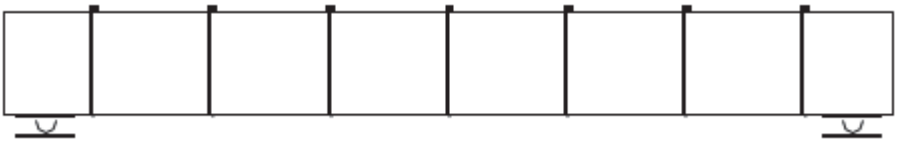

Figure 2-7 Repair method applied to timber stringer; long hex bolts (Akbiyik et al. 2007)

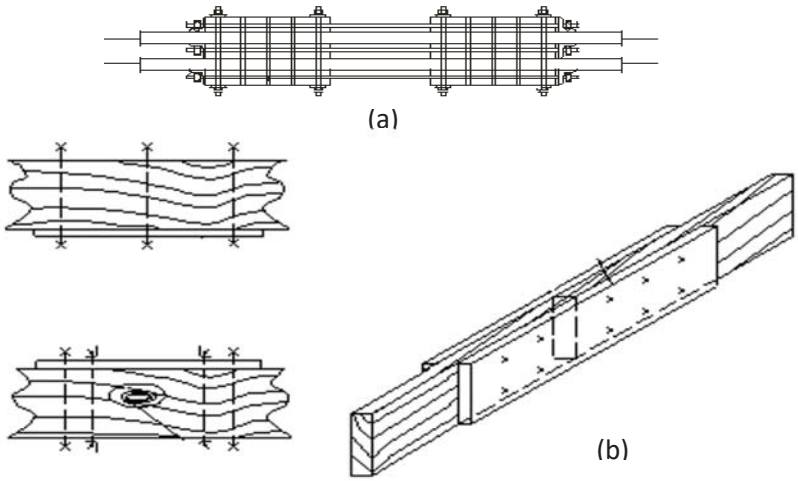

Figure 2-8 Timber lumber strengthened with wood plates; (a)tension-strengthening, (b) ending-strengthening (Stanila et al. 2010)

De Lima et al. (2018) have more recently carried out a study in strengthening of timber beams with steel plates, steel rebars, and steel cables. Strengthening with pre-stressed steel plate consists of a steel plate fixed to the bottom of the timber beam by commercial screws and the pre-stress applied using the camber technique. Strengthening with pre-stressed steel rebars consists on the installation of a steel rebar underneath of the beam and then connected to the timber beam through steel plates and screws. The pre-stress was then applied by tightening the steel nuts at each end of the rebar against the steel element. Timber beams strengthened with pre-stressed steel cables which were anchored to their ends on eyebolts and the eyebolts were pinned through a nut anchored to a U-channel profile, as shown in Figure 2-9. Strengthening systems showed at least 25% increase in the stiffness whilst the improvement of load carrying capacity was reported between 57% to 286% depending on the strengthening technique. Results of such investigations showed that the steel plate, screws and rebars remained undamaged while the maximum

tensile strength of timber was achieved in the first two test methods. In contrast, failure occurred in the anchorage of the steel cable in a more brittle manner leading to release steel cable after rupture which resulted in failure in timber beam.

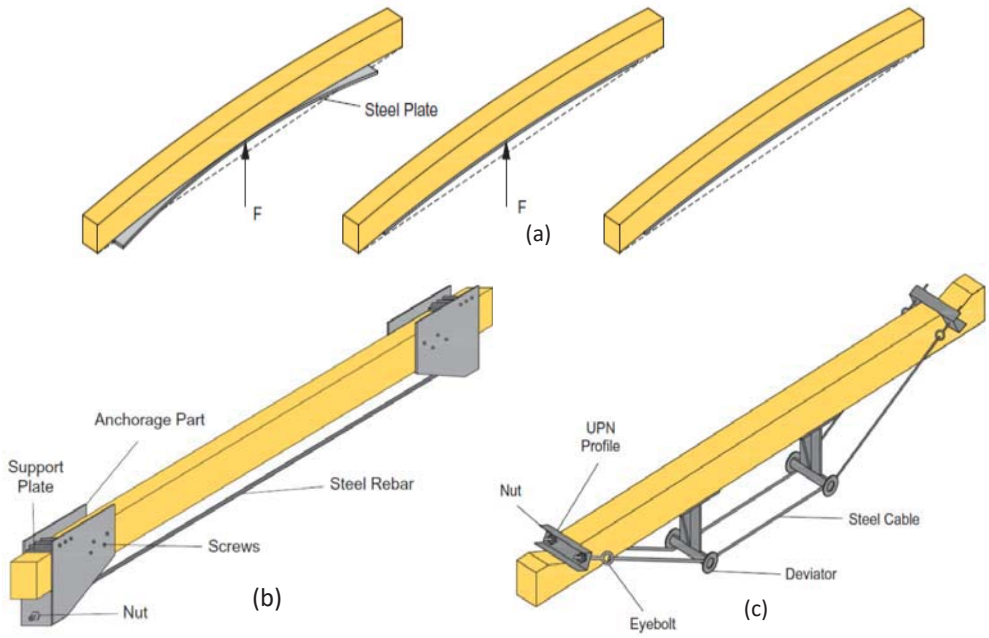

Figure 2-9 Strengthening procedure using; (a) pre-stressed steel plate, (b) pre-stressed steel rebar and (c) pre-stressed steel cables (De Lima et al. 2018)

In most of above studies, the load carrying capacity and stiffness of reinforced timber structures with metals have been increased; however, failure occurred in the timber beams in a brittle manner. Strengthening of timber structures with metals may not be effective as the added steel are heavy, bulky leading to increase the dead load of the structure. Even though steel has a much higher Young's modulus and ultimate strength than timber, the added steel plates and bars aspire to further corrosion damage; their installation is rather difficult and requires heavy lifting equipment. This repairing method appears time-consuming, requires complicated steps and regularly needs long periods of service interruption as well as high maintenance cost (Sieca et al., 2007). Bolted connections usually result in much higher stress concentrations where cracks occur. Bolted connections have some disadvantages including increase in

construction time and rise of the structure weight and cost (Jiang et al., 2012). Besides, bolted connections may not be feasible for all type of repair and strengthening. Therefore, an alternative method is essentially needed to avoid these difficulties.

2.4.2. FRP materials

Disadvantages associated with traditional rehabilitation methods, have resulted researchers to develop new techniques using new materials such as advanced fibre reinforced polymers (FRPs) (Talukdar and Banthia 2010). It is worth mentioning that all the proposals involving the use of metal for strengthening and retrofitting of timber structures can be adapted to advanced composite materials, substituting the metal plate with FRP (Yang et al. 2013). The FRP composites work in a similar manner to metal; however, the strength to weight ratio is much higher for FRP composites. Therefore, the same or even improved repair/strengthening effect can be achieved with FRP as for metal plates, but without added self-weight load.

Strengthening of structures using these composites materials has been enhanced by the continuous progress obtained in FRP materials due to wider availability in different materials and shapes leading to reductions in the cost of strengthening. These methods show promise and can provide a higher level of assurance of the integrity of a structure whilst minimising physical disturbance of the structure. These composite materials contribute tensile forces to the internal moment resistance leading to an increased load carrying capacity of the beam. To improve the flexural loading capacity and stiffness of timber beams, FRPs are usually bonded on the tensile face of timber elements. FRP plates have been mostly used to repair the biologically degraded or mechanically overloaded structural elements. The FRP sheets can be either made from fibre sheet and bonded to the substrate using epoxy and adhesive by hand (i.e. wet lay-up plates) or via pultrusion (i.e. pultruded plates). Near-surface mounted (NSM) FRP

bars have also been used to repair and retrofit historical structures (Kim and Harries 2010; Smith 2011; Valipour and Crews 2011). In the NSM strengthening method a narrow groove is cut into the bottom face of member, and FRP composites plates or bars are inserted with a bonding agent. This technique is an ideal choice for structures where the aesthetics of the original structure needs to be maintained (Bisby and Fitzwilliam 2003; Valipour and Crews 2011).

It is worth emphasising that the main focus of studies conducted to date is mostly for reinforced concrete and pre-stressed concrete applications; conversely, there are limited research studies to examine the use of FRP materials for the strengthening of timber beams considering the effect of above parameters. The body of knowledge on FRP-to-timber bonded interfaces and bonded systems is even more narrow and providing feasible guidelines or recommendations for such composite structures would be of crucial importance and hence limited field application uptake. Nevertheless, available studies in the literature are useful for understanding the performance of externally reinforced timber beams.

The application of FRP martials for repair and/or strengthening of timber structure was originated in the 1980s by Gustafsson (1987) and Meier (1987), and the research interest and development in the use of FRP for reinforcement of timber structures enhanced by Triantafillou and Plevris (1991),Triantafillou (1998), Kropf and Meierhofer (2000) and Gentile (2000). The following sections present an overview of research performed during the last two decades on repair and/or strengthening of timber structures with FRP.

2.4.2.1 FRP strengthened sheet

Borri et al. (2005) conducted a series of tests on flexurally strengthened old timber beams with CFRP sheets, pre-stressed sheets and CFRP bars. It was

found that the flexural capacity of the specimens reinforced with pre-stressed sheets was similar to that obtained for beams reinforced without the pre-stressing operations. The maximum flexural capacity of the strengthened beams enhanced by up to 60.3% compared to reference beams, whilst the stiffness of reinforced beams increased by up to 30% when compared to that of samples before reinforcement. Timber failure occurred immediately followed by CFRP fracture in the tension zone of beams reinforced with CFRP sheet, leading to collapse of the beams whilst no debonding occurred in pre-stressed beams.

The bond strength of FRP-strengthened timber joints was considered by Crews and Smith (2006) to determine the strength of the adhesive-to-timber interface as shown in Figure 2-10. It was reported that timber failure has been the main failure mode that occurred in their tests, indicating that the bond behaviour may be controlled by the properties of timber rather than that of the adhesive. The flexural performance of timber beams strengthened with CFRP and GFRP sheets were investigated by Yang et al. (2008). It was reported that the load carrying capacity of strengthened beams was up to 17.7% higher than that of un-strengthened beams.

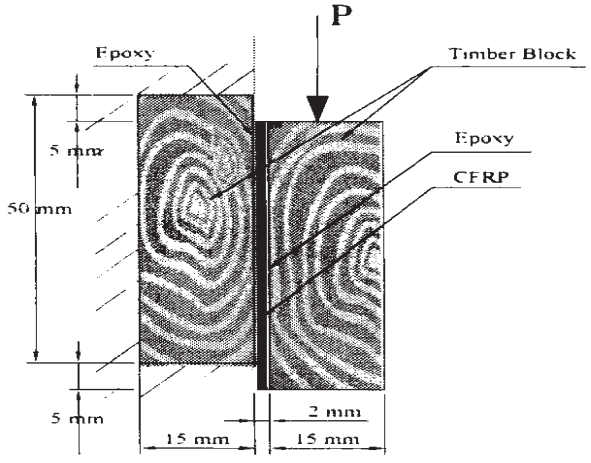

Figure 2-10 Side elevation of a typical test specimen (Crews and Smith 2006)

Yang et al. (2008) strengthened two types of timber beams with 1, 2 and 3 layers of CFRP. The reinforced beams were then subjected to four-point

bending test to investigate the flexural performance and load-displacement relationships of the strengthened timber beams. It was reported that timber flexural failure mostly occurred in the specimens strengthened with 2 and 3 layers of CFRP, whilst the failure mode in specimens strengthened with 1 ply of FRP was observed as a flexural failure with CFRP debond, and flexural failure with CFRP rupture as shown in Figure 2-11. The increased percentages of flexural strength ranged from 39% to 61%, depending timber type and number of CFRP used.

Hybrid fibre reinforced polymer (HFRP) has been used in the study conducted by Yang et al. (2013). This strengthening system consists of two or more types of reinforcing fibres (e.g. carbon fibre and/or glass fibre) within a single matrix. The fibres with higher strength provide the stiffness and load carrying qualities mainly, whereas the fibres with lower strength make the composite more damage tolerant and keep the composite element more cost effective. Three different fibres were used for strengthening of timber beams and then reinforced beams were tested as simply supported beams under four-point loading, over an effective span of 1800 mm. Strengthening of the beams resulted in an increased load carrying capacity between 7% to 58%. The maximum displacement of the hybrid strengthened beams was 106% higher than that of the specimens strengthened with CFRP only. No debonding failure of the FRP was reported.

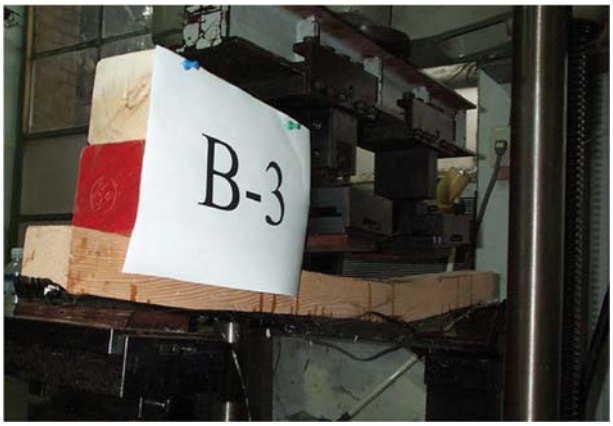

Figure 2-11 Failure mode of the retrofitted timber beams with 1 layer of CFRP sheet (Yang et al. 2008)

Wan et al. (2013) performed a series of tests on unreinforced and CFRP reinforced glulam timber beams and proposed a debonding strain model for externally strengthened timber beams. In this investigation, it was observed that all the reinforced timber beams achieved higher strength when compared with unstrengthened timber beam and the load carrying capacity of CFRP timber beams was enhanced by up to 60%. Timber cracking, shear failure and FRP debonding on adhesive-timber interface were reported as the main failure mode as shown in Figure 2-12. Wan (2014) has conducted a more extensive study on FRP-to-timber interface in which results of 86 single shear tests are reported. The main focus in that study was on bond length and types of adhesives, and limited variations in parameters such as bond width, FRP-to-timber width ratio, bond stiffness, FRP thickness, compressive strength of timber. It was concluded that the adhesives had not noticeably influenced the ductility of the bonded joints. This finding is in agreement with observations made by Crews and Smith (2006).

Figure 2-12 failure modes, failed beam and debonded FRP (Wan 2014)

Biscaia et al. (2016b) conducted a series of tests on flexurally strengthened old suspended timber floors with CFRP to investigate the effectiveness of externally bonding FRP to their soffits. It was reported the load carrying capacity of reinforced specimens was approximately 81.7% more than the reference/unstrengthened specimen. It was also reported that the stiffness

of reinforced specimens increased significantly; however, stiffness of reinforced samples or un-strengthened specimens were not clearly reported in the study. The specimens failed mainly due to the shear and knot-induced cracks when the timber was in its elastic state.

Different reinforcement layouts have been investigated in the study performed by Rescalvo et al. (2017). The experiment consists on old timber beams (200–300 years old/in service) reinforced with one layer of carbon fibre composite to examine the maximum bending capacity of such beams. Two different FRP-to-timber width ratios (60% and 100%) were investigated in which the width of timber beams was 75 mm, while 45 mm and 75 mm CFRP were bonded to the timber. Results of the study showed that specimens reinforced with wider CFRP (75 mm) exhibited higher bending strength with mean bending strength of 43.87 MPa; while the mean value for those specimens strengthened with 45 mm CFRP was reported as 30.28 MPa. This finding signifies that the bond width has a major impact on the bond strength.

2.4.2.2 Near-surface mounted FRP technique

Near-surface mounted (NSM) is relatively a new strengthening technique which is an ideal choice for structures where the aesthetics of the original structure needs to be maintained. Whilst this technique is outside the scope of this thesis; a short background of such technique is provided herein. This technique was investigated experimentally by Gentile et al. (2002) as shown in Figure 2-13. It was found that the flexurally strengthened timber beams failed at higher level of applied loads (between 18% to 46%) compared to unstrengthened beams. The rupture of FRP rods was not observed and the strengthened timber beams mainly failed by timber compression failure resulting in a more ductile behaviour. Such behaviour is desirable from a structural design point of view. The

unstrengthened beams, on the other hand, failed due to brittle tensile rupture, as expected.

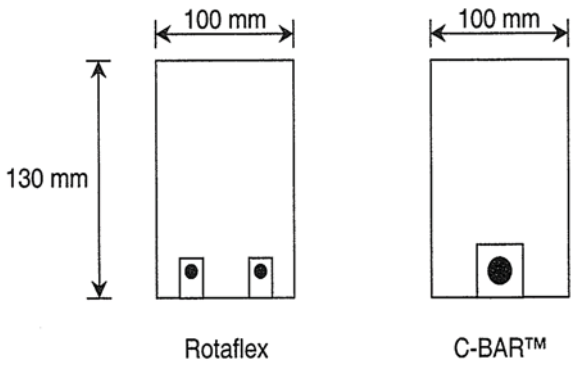

Figure 2-13 Cross-section of bond specimens (Gentile et al. 2002)

Micelli et al. (2005) performed an experimental program in which one and two NSM CFRP rods with a diameter of 12.5 mm were used for strengthening of glulam beams. The failure mode was reported as the ultimate strain of the timber in tension in both reinforced and control beams. Rupture of FRP rods or delamination of the reinforcement rods in the CFRP-epoxy region was observed and the maximum strain in the CFRP rods reached in the tests was 0.43%, which was much lower than the rupture strain (1.38%). The increment in bending strength and stiffness were found to be up to 82% and 19%, respectively, as a result of the FRP strengthening.

The performance of reinforced low-grade glued laminated timber in flexure with GFRP rods was investigate by Raftery and Whelan (2014). The beams subjected to four-point bending test arrangement with a span of 3420 mm. Reinforcement percentages studied ranged between 0 (control beam); 1.05% and 2.8%. Unreinforced beam failed through tensile failure with the failure cracks initiating from defects or irregularities in the timber as expected since low-grade of the timber was examined with significant defects in the bottom tension lamination. However, no compression failure was reported in the compression zone of any of the beams. The reinforced timber beams, on the other hand, failed as a result of excessive tensile

stresses in the bottom laminate of timber as a result of knots as shown in Figure 2-14. The stiffness and ultimate bending strength of reinforced beams increased in comparison to unreinforced control specimens.

The NSM technique has been also investigated numerically and analytically when FRPs have been used for strengthening of timber structures. Some of the most recent investigations are listed here (Khelifa and Celzard 2014; Raftery and Harte 2013; Wan 2014; Xu et al. 2017). This technique has been widely investigated experimentally, analytically and numerically when FRP composite materials were bonded to concrete beams, with some of the more recent studies listed as (Ghaib et al.; Jawdhari and Harik 2018; Rezazadeh and Carvelli 2018); and more recently in glass beams (Bedon and Louter 2017, 2018). However, such investigations are not explained herein as they are outside of the scope of the present study.

Figure 2-14 Tensile fracture by defect in bottom lamination (Raftery and Whelan 2014).

2.5. Failure mode and characterisation of FRP bonded to timber

Investigating and predicting the bond behaviour is extremely important for the efficient application of FRP bonding technology. In the retrofitted timber beam, the stress transfers from timber to the FRP composite through the bonded interface generating tensile stresses in FRP. Failure in an FRP reinforced timber beam can occur due to flexural failure of the

critical section, due to crushing of the timber in the regions subjected to compressive stresses (Figure 2-15), or by debonding of the FRP plate from the timber beam (Figure 2-16). Debonding is one of the most common problems associated with the use the externally bonded FRP sheets that limits the full utilisation of the material strength of the FRP (Khelifa and Celzard 2014; Wu and Hemdan 2005). Debonding has been identified as the single most important failure mechanism of retrofitted beams (Coronado 2006; Kabir et al. 2016b) that occurs at much lower FRP strains than its ultimate strain.

Debonding failures generally occur in the timber fibres, since the adhesive itself rarely fails due to its high characteristic strength (Chen and Teng 2001). FRP rupture is unlikely to occur unless more strengthening system such as mechanical anchorages are applied at both ends of FRP; whereas failure of timber may occur when extra amounts of FRP composite are used and the shear strength of the timber is not exceeded (Biscaia et al. 2016b). The initiation of debonding may take place in the high moment region or at the end of the FRP plate. The former is base of a flexural shear crack or a purely flexural crack. In this case, the flexure crack–induced interfacial debonding may lead large local stress concentration at such region, and when these stresses reach critical values, debonding starts to propagate towards one end of FRP plate as shown in Figure 2-16 (d). The later may occur due to short bonding anchorage which results in high interfacial shear and normal stresses at or near a plate end, that exceed the strength of the weakest element, generally the timber, as shown in Figure 2-16 (a and c). In this case, the debonding propagates towards the midspan of the beam (Biscaia et al. 2016b; Hollaway and Teng 2008). The premature rupture of a timber beam may be due to presence of knots as shown in Figure 2-16 (f).

Debonding directly impacts the total integrity of structure, with the subsequent outcome that the ultimate capacity and desirable ductility of the structure may not be achieved. Despite studies conducted in strengthening of timber beams using composite materials, knowledge of the interface behaviour between a timber beam and FRP is scarce and a comprehensive understating of the bond is essential. In the analysis and design of an FRP strengthened member, all the above failure modes must be appropriately considered in order to ensure satisfactory behaviour and load resistance.

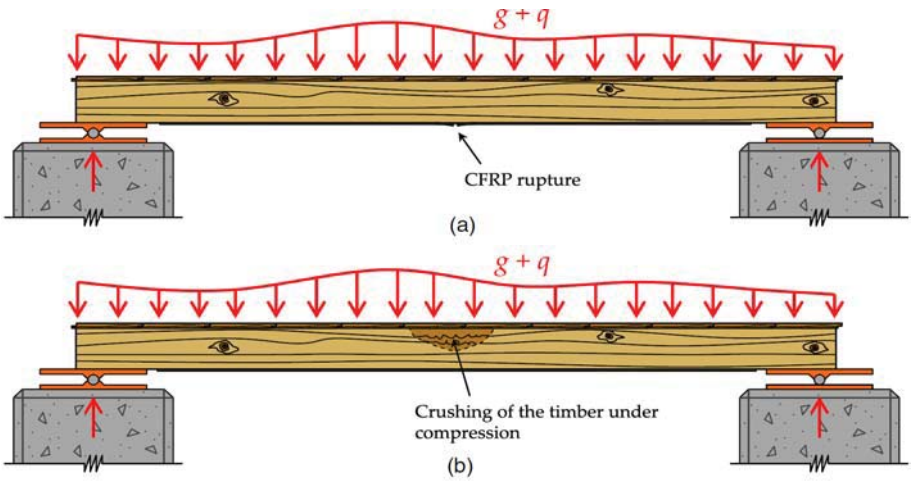

Figure 2-15 Failure modes in timber beams strengthened with FRP composites, (a) FRP rupture; (b) crushing of compressive timber (Biscaia et al. 2016b)

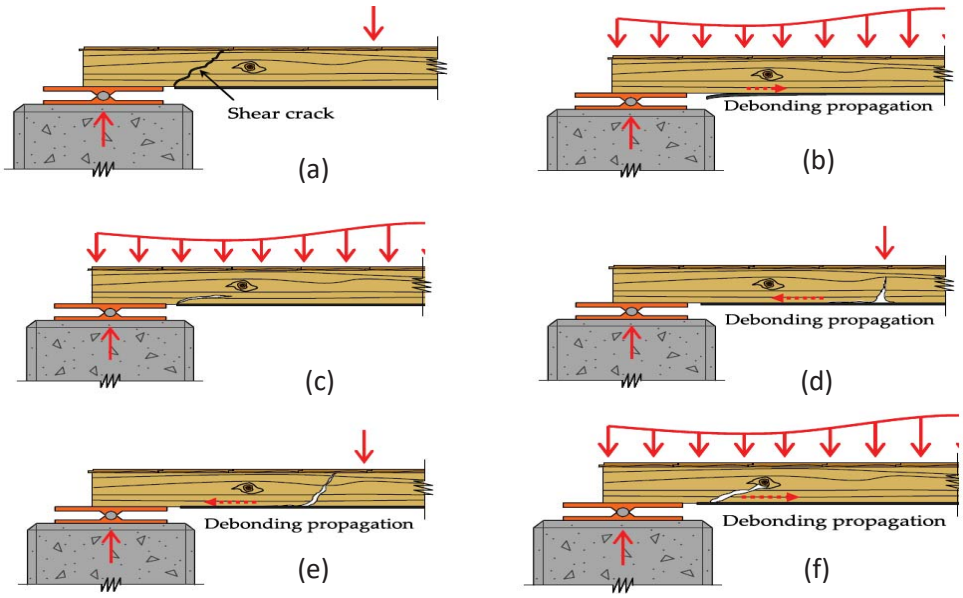

Figure 2-16 Debonding failure modes of an FRP reinforced timber beam; shear failure (a), debonding of the FRP composite at the end of the FRP free end (b),

shear crack due to an insufficient bonding anchorage length (c), flexure crack induced interfacial debonding (d), shear-flexure crack–induced interfacial debonding (e), and failure due to the existing knots of the timber (f) (Biscaia et al. 2016b)

2.6. Factors affecting bond strength

The interaction between timber and FRP is relatively complex and is influenced by several variables. The bond strength is typically defined as the peak load divided by the effective bonded area *($A_{eff} = b_f \times L_{eff}$);* where ($b_f$) is the width of FRP and L_{eff} is effective bond length. A number of studies have been carried out considering the behaviour of bond (Coronado 2006; Gómez and Svecova 2008; Hollaway and Teng 2008; Xu et al. 2015) and their results have shown that the bond strength is highly dependent on the timber mechanical properties, geometry of the bond, and boundary conditions. The bond strength also varies with the FRP stiffness, FRP width and thickness, bond length, FRP to timber width ratio, and also specimen alignment (Chen and Teng 2001; Rescalvo et al. 2017; Wan 2014).

Environmental conditions, moisture content, surface treatment, poor adhesive mix and inadequate curing period or incorrect curing temperature significantly impact on the bond strength (Hollaway and Teng 2008; Xu et al. 2015). Valluzzi et al. (2016) conducted a series of experimental tests to investigate the influence of moisture content on the bond strength of strengthened timber elements. In such investigations timber moisture content has been reported as the main reason of debonding in all specimens. Moreover, in studies conducted by Lyons and Ahmed (2005) and Raftery et al. (2009) it was observed that the bond strength in a dry environment achieved better results when compared with a specimen in the wet/soaked environment. Nevertheless, these factors are outside the scope this dissertation and the influence of differing moisture contents, durability and their impacts on the bond strength have not been considered in the test reports.

2.6.1. Timber mechanical properties

Existing experimental investigations have suggested that the main failure mode associated to the FRP bonded interface is timber failure under shear. Crews and Smith (2006) reported that timber failure has been the main failure mode that occurred in their tests, indicating that the bond behaviour may be controlled by the properties of timber rather than that of the adhesive. Yao et al. (2005) also stated that substrate failure most often take place in pull-out tests under shear, occurring generally at a few millimetres from the adhesive layer. In the study conducted by Wan (2014), two different types of timber were utilised, namely softwood (Pine) and hardwood (Camphor) timber to fabricate the joint specimens. Results of that study showed that specimens made from hardwood, has higher strength as opposed to samples made from softwood as shown in Figure 2-17. Similar observations were also reported in the studies performed by Custódio et al. (2009) and Franke et al. (2015). Therefore, it can be concluded that timber mechanical properties and its impact on the bond strength must be considered to evaluate the capability of the interface for both ultimate and serviceability limit state designs.

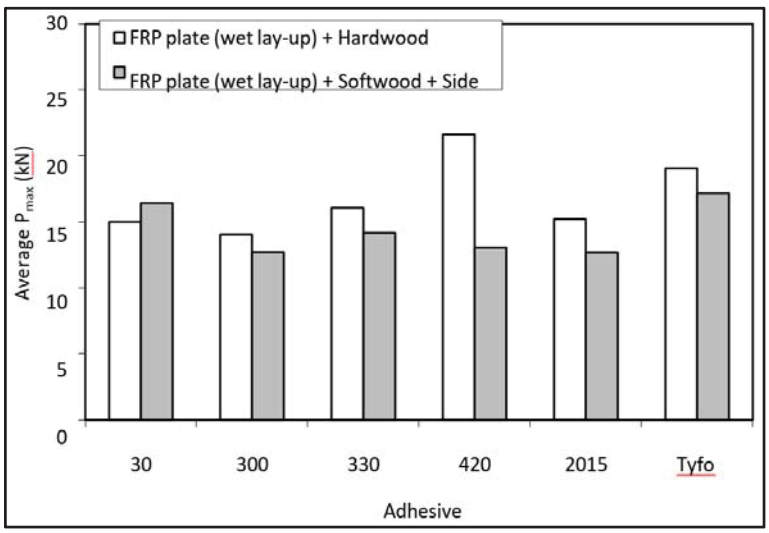

Figure 2-17 Joint strengths of externally bonded timber species series tests (Wan 2014).

2.6.2. Bond length

Another important parameter that influences predominantly on the bond strength is the bond length. However, effective bond length (EBL, also referred to as transfer length or critical anchor length in some literature) must always be taken into consideration. That is because, many experimental studies (Bizindavyi and Neale 1999; Coronado 2006; Franco and Royer Carfagni 2014; Yao et al. 2005) and fracture mechanics analyses (Yuan and Wu 1999; Yuan et al. 2001) have confirmed that there is no benefit in extending the bond length beyond that where there is no increase in the bond strength. Many researchers have experimentally defined effective bond length as the bond length over which the result of the shear contact stress is either at 97% or 99% (Chen et al. 2012; Kabir et al. 2016b; Lu et al. 2005a) of the ultimate strength of the bond. On the other hand, to accurately obtain an effective bond length, resistance strain gauges can be bonded to the surface of CFRP strip along the bond length and then, the effective bond length can be defined as the distance between the points that the strain decays from the maximum to the zero value (Franco and Royer Carfagni 2014; Mazzotti et al. 2009; Shen et al. 2015). In the study performed by Khalid et al. (2018), it was reported that there was a significant increase in bond shear stress (from 1.74 to 2.54 MPa) when the bonded length increased from 30 mm to 40 mm. However, the increase of shear stress was insignificant with further increment in bonded length. De Jesus et al. (2012) also reported that when the bond length was not long enough the improvement of strengthened beams was negligible as shown in Figure 2-18. It can be seen that specimens with longer bond length not only failed at higher level of loads, but also failed in a more ductile manner when compared with samples reinforced with shorter bond length. Therefore, the bond length has a major impact on the bond strength; however, bond strength cannot increase further once the bond length exceeds the effective bond length. Nonetheless, a longer bond

length improves the ductility of the flexurally reinforced beam (Hollaway and Teng 2008). Thus, determination of the effective bond length is of fundamental importance in the characterisation of the interface between FRP and timber.

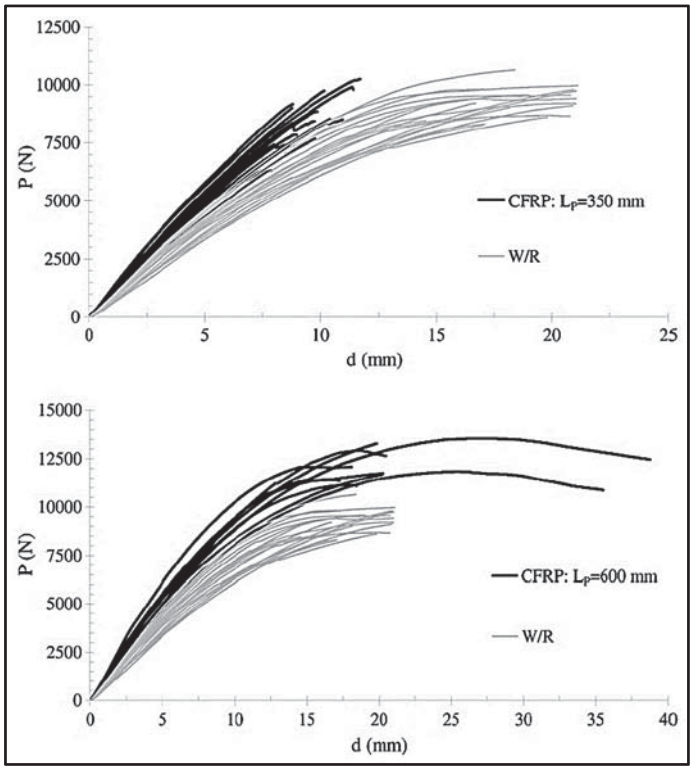

Figure 2-18 Two reinforced test series (De Jesus et al. 2012).

2.6.3. FRP thickness

FRP thickness is one of the parameters that impact on the bond strength and its effect on the bond strength needs to be investigated. Theoretically, if the reinforcement ratio in the tension zone is adequate and large enough, the failure mode in FRP strengthened timber changes from a brittle tensile to a more ductile compression, since the neutral axis position moves towards the tensile face leading to lower stress and strain in the tension area and, conversely higher strain in the compressive area (Borri et al. 2005). The part of timber yielding in compression spreads from the top of the beam to the bottom until the beam ultimately fails by tensile disconnection/rupture of the bottom wooden fibres. Therefore, more

efficient use is made of the compressive strength of the timber. This transition in failure mode leads to substantial enhancement in capacity and ductility of the strengthened beam. Simultaneously, as the FRP reinforcement prevents crack opening and restricts local rupture, the average ultimate tensile strength of the timber typically increases. Increasing in FRP reinforcing stiffness ($E_f.t_f$) will also lead to increase in effective bond length of FRP bonded member. The results of experimental investigations conducted by Bizindavyi and Neale (1999) agree that the effective bond length increases for samples with more layers of FRP; however, the joint tends to be more brittle while the load carrying capacity increases. To address this concern, Chen and Teng (2001) recommended that using FRP plates with higher modulus of elasticity and smaller thickness achieves high stress in externally bonded joints. Nakaba et al. (2001) and De Lorenzis et al. (2001) also reported that the effective bond length and load carrying capacity of FRP bonded member increase as the FRP stiffness increases. In general, it is recommended that using higher FRP stiffness (Chen and Teng 2001; Nakaba et al. 2001; Yoshizawa et al. 2000) and softer adhesives (Chen and Teng 2001; Dai et al. 2002) can increase the average bond strength.

2.6.4. FRP width

The influence of FRP width on the ultimate load has been reported in several research but the reported results were often inconsistent (Carloni et al. 2005; Kamel et al. 2004; Ueda et al. 1999). Whilst results of some studies showed that the bond width had negligible effect on the bond strength (Bizindavyi and Neale 1999; Rescalvo et al. 2018), other research studies have emphasised that the bond width has a major impact on the bond strength (Chen and Teng 2001; Rescalvo et al. 2017; Xu et al. 2015). For instance, two different bond widths (25 mm and 38 mm) were investigated experimentally to examine the influence of FRP width on the

bond strength in the studies performed by Subramaniam et al. (2007). Results of such investigations showed that the maximum load was higher for the wider FRP sheet as shown in Figure 2-19. More recently, a three-dimensional (3D) finite element model (FEM) was developed and assessed by Lin et al. (2017); in which it was reported that specimens reinforced with wider FRP width exhibited higher load. From these studies it can be concluded that, with the increase of FRP plate width, the interfacial bond strength increases, and ductility of the bonded interface reduces leading to the decrease of the interfacial slip during the softening-debonded stage. Furthermore, it is noted that when FRP-to-timber width ratio is low, the force transfers from the FRP to timber leads to a non-uniform stress distribution across the width of timber, leading to failure at lower load level. When FRP width is lower than that of timber width, the stress transfer occurs over a partial active area leading to local shear stress concentrations which may results in failure at lower level. Conversely, the area of the bond can be enhanced by extending bond width which allows the load to be distributed over a larger area, and consequently relieves the stress concentration in the FRP leading delay in the debonding failure (Xu et al. 2015). Therefore, understanding of the width effect on the ultimate load is essential for determining the optimal width of the FRP sheet in flexural strengthening applications.

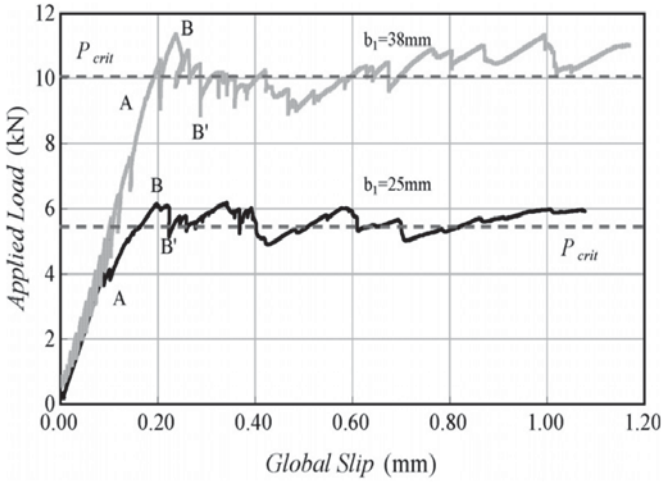

Figure 2-19 Load vs. global slip response for two different FRP widths, (Subramaniam et al. 2007).

2.6.5. Adhesive mechanical properties

Adhesive stiffness and strength also have an impact on the bond strength. Vallée et al. (2010) reported that stiffness of adhesive (E_A) as well as the level of plasticity significantly impact the stress–strain state inside bonded joints. The effectiveness of adhesive bonding technique depends on the joint design, type of adhesive, properties of timber, the type of FRP used, environmental conditions, surface preparation and in-service conditions. Wan (2014) conducted a more extensive study on FRP-to-timber interface and concluded that the properties of the adhesives may not have a substantial impact on the bond strength, which contradicts the findings of Vallée et al. (2010). Wu and Hemdan (2005) reported that when the interfacial stiffness of the adhesive increases, the effective bonding length decreases. However, for values of interfacial stiffness higher than 160 MPa/mm, interfacial stiffness has no substantial impact on the effective bonding length. Therefore, using an adhesive with low interfacial stiffness increases the effective bonding length and consequently relieves the stress concentration in the FRP that will cause delay in the debonding failure (Niu and Wu 2006; Wu and Hemdan 2005). It is important to note that different types of adhesive materials have not been investigated in this research study.

2.6.6. Surface preparation

Surface preparation is one of the most important phases in adhesive bonding and laminating; however, it is often not given the attention that it requires. A major barrier in achieving high strength bonds is a lack of understanding about appropriate surface preparation techniques, and the effect on adhesives and resins. The main purposes of surface preparation are to remove all contaminants and weak surface layers that can interfere with adhesion, and to develop a surface roughness with the intention of promoting and maximising the adhesion capacity of the bond (Hollaway

and Teng 2008; Mostofinejad and Shameli 2013). Surface treatment particularly has a much greater influence on long-term bond durability rather than short-term bond strength; therefore, a high standard of surface preparation is essential for promoting long-term bond integrity and durability (Wegman and Van Twisk 2012). Surface preparation techniques can be considered under four categories (Hollaway and Teng 2008):

- solvent degreasing;
- mechanical techniques;
- chemical techniques;
- physical techniques.

Contaminants and grease can be removed through solvent degreasing. However, toxicity, flammability and cost of the solvent are some of the issues that need to be taken into consideration for this method. Acetone, as a volatile solvent, is one the most popular solvent materials. Mechanical treatments are often undertaken to roughen the surface; however, their effects on adhesion are complex. Mechanical treatments remove weak surface layers and expose a clean and new surface. Control of the method and assessment of the surface are two major aspects of the mechanical method. Chemical methods, on the other hand, typically cause more complex changes to surfaces than do mechanical methods. Chemical treatments not only clean and remove weak layers, but also often roughen a surface microscopically (Hollaway and Teng 2008). One of the main disadvantages normally associated with chemical treatment is the toxicity of the materials and the need for proper waste disposal (Davis 1997). Physical techniques include methods that promote a strong oxidising reaction with the surfaces of materials. Although they are highly effective on inert plastics, like polypropylene, physical techniques also work well on thermoset–matrix composites (Hollaway and Teng 2008).

2.6.6.1 Surface preparation of timber

The surface layers of timber become oxidised and degrade over time. A well prepared timber surface not only provides a good substrate for adhesive bonding (Gómez and Svecova 2008), but also opens up the porous cellular structure of timber enabling penetration of the resin into the microstructure of the material. Thus surface preparation significantly promotes adhesion to cellulose and lignin components (Broughton and Hutchinson 2001). Therefore, it is essential to remove any weak layers and materials and then bond the surfaces relatively quickly, since freshly cut surfaces are ideal for optimum adhesion and bonding. The general surface treatments of timber elements are listed below (Hollaway and Teng 2008):

- cutting with a plane, saw, auger, chisel or similar sharp tools;
- removal of dust;
- localised drying, if necessary;
- application of an adhesive-compatible primer, if necessary.

The surfaces of the timber that have been sanded or sawn require careful cleaning prior to bonding to remove any loose dust. Acetone and compressed air are two effective ways that can be used to clean timber surfaces (Wan et al. 2013). A detailed consideration of this topic is given by Davis (1997).

2.6.6.2 Surface preparation of FRP materials

The surface of a composite material may be contaminated with mould release agents, lubricants or fingerprints as a result of the production process. In addition, the matrix resin may include waxes, flow agents and 'internal' mould release agents. Therefore, surface treatment of the composite materials is essential to exorcise and remove all contaminants from polluted areas. Surface preparation causes an increase in the surface area for bonding, promotes micro-mechanical interlocking and/or

chemically modifies a surface (Hollaway and Teng 2008). It is important to note that special care must be taken to ensure neither to break reinforcing fibres, nor to affect the bulk properties of the composite. ASTM-D2093-03 (2003) and BSI (1995) present detailed requirements for the surface preparation of composite materials using solvent degreasing, mechanical abrasion and the peel-ply technique. The basic sequence of steps in the process of surface preparation of composite materials the using above standards should be either:

- to use a suitable solvent, such as acetone or methyl ethyl ketone (MEK), to remove grease and dust, or
- to remove release agents and resin-rich surface layers by abrasion. This treatment can be accomplished by careful grinding, sanding or cryo-blasting with solid carbon dioxide pellets (ASTM D2093-03 2003).

More discussion on the surface preparations of adhesively bonded composite is given by US Department of Transportation (2004).

2.7. Bond test methods

The interfacial behaviour of the bond can be addressed by the bond-slip characteristics. In the FRP-strengthened materials, various bond testing methods have been carried out experimentally for determining bond-slip relationship, failure load and failure mode, interface stress, and effective bond length; including single shear tests (Biscaia et al. 2015; Coronado 2006; Dai et al. 2005; Juvandes and Barbosa 2012; Mazzotti et al. 2008; Wan 2014), double shear tests (Hiroyuki and Wu 1997; Maeda et al. 1997; Nakaba et al. 2001; Neubauer and Rostasy 1997), and modified beam tests shown in Figure 3-9 (Chen and Teng 2001; Wan 2014).

The test setup for single and double shear pull tests can be configured using two different approaches; near-end supported, and far-end

supported. The near-end support introduces compressive stress to the bonded surface, whilst far-end support introduces tensile stress to the bonded surface (Chen and Teng 2001; Wan 2014). In the single lap shear test, FRP plates are attached to one side of the substrate and placed on the test rig. Load can then be gradually applied either to the plate end or substrate end, depending on the test setup as shown in Figure 2-20. In this method, the FRP and substrate are subjected to uniformly distributed axial stresses (Cornetti and Carpinteri 2011), while the interface is predominantly subjected to the shear deformation. On the other hand, in the double shear lap test, FRP plates are symmetrically attached on both sides of the substrate. In this method, the loading system is identical to the single shear lap test; however, special consideration must be taken into account to minimise the possibility of the eccentricity of the acting forces in order to avoid error in the results (Nakaba et al. 2001). The bond strength of double-shear test is the lowest load applied to the both sides of the specimen. Results of previous studies conducted illustrated that double-shear test set up provides lower debonding values when compared with single-shear test setup (Brosens 2001). One reason may be attributed to the unavoidable asymmetry of the applied load when debonding occurs on one side of the sample test.

In order to predict the behaviour of FRP retrofitted beams, results of the pull-out tests may not represent the actual debonding phenomenon; that is because the loading type, boundary conditions, and deflections are different in FRP retrofitted beams from those of the FRP-to-timber joint under shear force in pull-out tests (Mohammadi 2014). The interfacial stress transfer in FRP strengthened beams produces high accuracy using bending tests rather than shear tests, since the interface is under both shear and flexural stresses simultaneously; however, such tests require a complex test setup and higher investment (Serbescu et al. 2013). In the beam tests, specimens may consist of two substrate blocks joined by a

steel plate on the bottom side or a substrate beam with a notch in the middle. In this method, the shear bond strength can be defined as an average stress along the bond length. A higher value of the bond strength has been generally obtained from beam tests when compared with single and double shear test set. The reason for this may be attributed to the compressive stress orthogonal to the FRP plate being introduced by the deformation of the beam.

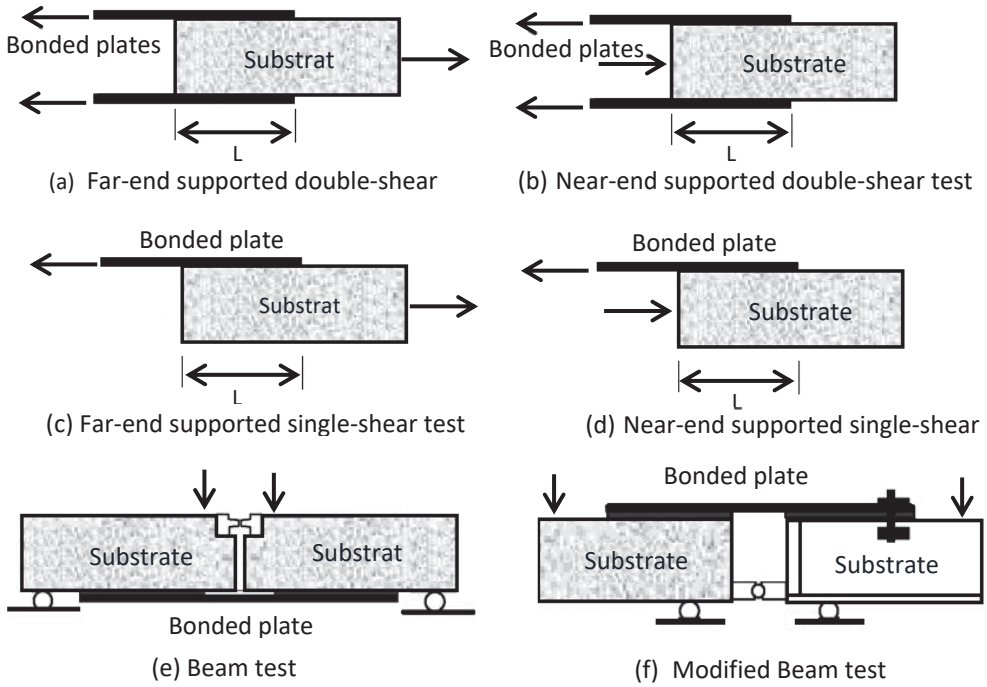

Figure 2-20 Bond tests classification (Chen and Teng 2001).

2.8. Existing interface modelling methods

Whilst a number of studies have been carried out experimentally (Cao et al. 2007; Mazzotti et al. 2008; Nakaba et al. 2001) and theoretically (Dai et al. 2006; Ferracuti et al. 2007) to address the behaviour of FRP bonded to concrete substrate there are limited studies on FRP-to-timber bond. The proposed models in the literature, in particular for FRP to concrete interface, can be divided into two main categories including 1) empirical models based directly on the regression of test data, 2) fracture mechanics

models based on the behaviour of bond stress-slip (Chen and Teng 2001; Wan 2014).

2.8.1. Empirical-based models

Empirical-based models are mainly dependent on the results of experimental tests where the bond relationships are predominantly determined from a regression analysis of the interface parameters. The formulation of these models is quite simple and straightforward, although their outcomes show high variability from one experiment to another. This appears to be due to the fact that the bond parameters are derived for specific experimental conditions including composition of the materials (substrate, FRP and adhesive properties), test setup, local stress concentrations and equipment. These conditions are not equivalent for all experiments and the assumptions and data used to derive the model requires verification. Due to these variations, a number of interface laws based on the test shape and bond parameters have been proposed for bonding FRP to concrete. Hiroyuki and Wu (1997) and Tanaka (1996) conducted a series of experimental tests based on which they derived Eqs. (2.1) and (2.2), respectively:

$\tau_u = 5.88 L_f^{-0.669}$ (MPa), where L is in centimetre (2-1)

$\tau_u = 6.13 - \ln L$ (MPa), where L is in millimetres (2-2)

A model developed by Maeda et al. (1997) in which the average bond shear stress at failure (τ_u) and effective bond length (L_e) can be calculated using Eqs. (2.3) and (2.4), respectively.

$\tau_u = 110.2 \times 10^{-6} E_f . t_f$ (MPa) (2-3)

$L_e = e^{6.13 - 0.580 \ln E_f t_f}$ (mm) (2-4)

where t_f (mm) is the FRP thickness and E_f is elastic modulus of the bonded plate. Note that E_f is in Mega Pascals and Giga Pascals in equations (2-3) and (2-4), respectively. It was shown that the effective bond length (L_e) was exponentially related to the FRP stiffness, and the ultimate bond strength can be determined by multiplying the effective bond area by bond shear stress (τ_u) (Chen and Teng 2001). This model is clearly unreliable if $L<L_e$.

Chen and Teng (2001) proposed a semi-empirical design model based on the combination of a fracture mechanics model (with rational simplifications) and regression models. This model was calibrated with a series of single shear and / or double shear pull out tests and is applicable to both externally bonded steel plate and FRP-to-concrete bonded joints. In Chen and Teng's (2001) model, the width ratio of the bonded plate to the substrate was one of the main parameters which had a major impact on the bond strength. Chen and Teng (2001) concluded that if concrete width (b_c) is greater than that of the bonded plate (b_p), stress distributes non-uniformly across the width of the concrete and consequently, may result in a higher shear stress in the adhesive at failure. By taking into account the above considerations, Chen and Teng (2001) developed a model where the ultimate strength of joint, stress in the bonded plate at failure and the effective bond length can be calculated as given in Eqs. (2-5), (2-6) and (2-7), respectively.

$$P_u = \alpha\beta_p\beta_L L_e b_p \sqrt{f'_c} \tag{2-5}$$

$$\sigma_f = \alpha\beta_f\beta_L \sqrt{\frac{E_f\sqrt{f'_c}}{t_f}} \tag{2-6}$$

$$L_e = \sqrt{\frac{E_f t_f}{\sqrt{f'_c}}} \tag{2-7}$$

$$\beta_L = 1 \quad \text{if} \quad L \geq L_e \tag{2-8}$$

$$\beta_L = \sin\frac{\pi L}{2L_e} \quad \text{if} \quad L < L_e$$

$$\beta_p = \sqrt{\frac{2 - b_f / b_c}{1 + b_f / b_c}} \tag{2-9}$$

Mega-Pascals, Newtons and millimetres are the units for the above equations, where P_u and σ_f are the ultimate strength and stress in the bonded plate at failure; L and L_e are the bond length and the effective bond length, respectively. t_f, E_f and b_f are thickness, elastic modulus and width of the bonded plate, respectively. b_c is concrete width and f'_c is the cylinder concrete compressive strength. β_L and βp are dimensionless parameters that are influenced by the bond length and bonded plate-to-concrete width ratio, respectively. A best fit value of α=0.427 was achieved by Chen and Teng (2001).

Wan (2014) has conducted a more extensive study on FRP-to-timber interface in which results of 86 single shear tests are reported and correspondingly developed a bond strength model and bond stress-slip model for FRP-to-timber bond using a *J*-integral approach as follow:

$$P_u = 0.012\,\gamma_t \gamma_e b_f L_e^{0.28} \sqrt{E_f t_f} \tag{2-10}$$

$$\tau_{(x)} = \frac{dJ}{dx} = A^2 B C_N e^{-Bs}(1 - e^{-Bs}) \tag{2-11}$$

In Eq. (2-10), γ_t and γ_e were referred to timber sides and adhesive type, respectively. b_f, L_e and $E_f t_f$ were referred to bond with, effective bond length and stiffness of FRP, respectively. In Eq. (2-11), A and B are experimental parameters that have been given based on Dai et al. (2005), s was corresponding slip at specific location and C_n was referred to elastic stiffness. The bond stress model proposed by Wan (2014), Eq. (2-11), has been derived based on the theoretical proposals of Qiao and Chen (2009)

and Dai et al. (2005) where concrete had been used as a substrate. In addition, the mechanical properties of timber was not considered in Eq. (2-10) because Wan (2014) believed that softwood, hardwood and glulam used in that study were not significantly different from one another. As such, the importance of timber properties that have a major factor influencing the failure of the interface reported by others (Crews and Smith 2006; Kim and Harries 2010) has been ignored in such model. Furthermore, in the same study (Wan 2014), the expression of the effective bond length was calculated using the model derived by Chen and Teng (2001). It is worth emphasising that Chen and Teng's model was derived based on results of FRP-to-concrete interface. It is notable that there are some fundamental differences between the failure mechanism in timber and concrete when bonded with FRP. Concrete is weak in tension; whilst tensile strength of timber is much higher. Debonding initiates when the tensile stress at the interface exceeds the bond strength. Therefore, the models which work for FRP-to-concrete bond may not work for FRP-to-timber bond due to these differences. As a result, the bond strength model proposed by Wan (2014) did not fit very well into the experimental results (Figure 2-21, with The coefficient of variation R^2=0.59). It is important to note that the main focus in study performed by Wan (2014) was on bond length and types of adhesive; whereas it was concluded that the adhesives used did not noticeably influence the bond strength. In that study, there were limited variations in parameters such as bond width, FRP-to-timber width ratio, tensile strength of timber, etc and their importance on the bond strength as explained earlier were not investigated.

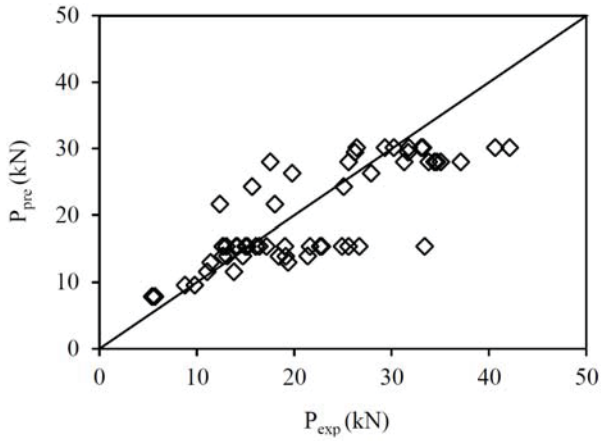

Figure 2-21 Performance of proposed FRP-to-timber bond strength model (Wan 2014)

More recently, Biscaia et al. (2015) performed experimental investigations on bonding between CFRP laminates and three different substrates: timber, concrete, and steel throughout pultrusion system. The geometry of timber was measured as 95 mm × 60 mm × 280 mm (width × high × length), whereas the CFRP composite used had a section of 10 mm × 1.4 mm. The bond length, one the other hands, had a range between 65 mm and 280 mm. Limited numbers of specimens were tested in such study. It was found that, CFRP-to-timber interface reached the highest strength compared to specimens where the substrates were concrete and steel. It was also reported that, CFRP-to-timber interfaces required a longer bond length to reach maximum strength in comparison with samples made from concrete and steel e.g. the longest effective bond length was reported for specimens made from timber. The initiation of crack due to lower tensile strength in concrete was reported as the main reason for such observation. Following the results obtained in the work developed by Biscaia et al. (2015), Biscaia et al. (2016a) developed analytical models for determining effective bond length and bond strength of CFRP-to-timber interface as follow:

$$L_e^{\max} = s_1 \sqrt{\frac{2E_f.t_f}{\tau_1.s_1}} \qquad (2\text{-}12)$$

$$P_u = b_f \cdot \sqrt{2G_f . E_f . t_f} \quad (2\text{-}13)$$

Where, s_1 and τ_1 are initial slip and shear stress while the entire bonded length is in an Elastic state and G_f is the Mode II fracture energy released during the debonding process. Although, these studies cover different debonding behaviour of FRP-to-timber interfaces analytically, similar to the study performed by (Wan 2014), the importance of other parameters such as bond width, FRP thickness, timber mechanical properties etc. were ignored. Consequently, for safe and economic design of FRP repair/strengthening of timber structures, further understanding of the bond is essential and thus, a new bond strength model for FRP-to-timber bonded interface is highly required to predict the ultimate load of the bond with better accuracy.

2.8.2. Fracture mechanics-based models

Fracture mechanics-based models are extremely practical in their application to adhesive joints; this is because the basic principle of these theories is that the strength of most real solids is governed by the presence of flaws. Adhesive joints subjected to physical loading generally fail by the initiation and propagation of flaws which lead to the failure of the structure. Figure 2-22 shows some existing bond-slip models in the literature. As can be seen, some models represent only the descending branch while the others consist of ascending and descending branches. In addition, the distribution of the shear stresses along the bonded length is expressed by linear or nonlinear curves.

One of the main specifications of fracture mechanics models is that the fracture energy, G_f, for a given joint, is geometry-independent. Another main specification of these models is that as long as the failure mode is noted the theory of brittle fracture is applicable equally to interfacial failures as it is to cohesive failures (Custódio et al. 2009). Mier (2012)

identified three common separate fracture modes-of-loading in classical fracture mechanics as depicted in Figure 2-23: the opening mode or mode I (a), in-plane shear or mode II (b), and out-of-plane shear or mode III (c). Mode I is the lowest energy fracture mode for isotropic materials, that has been usually used to assess adhesive toughness, adhesion and durability, and surface preparation techniques for investigating fracture energy, G_{If}, and fracture toughness, K_{If}. Crack propagation predominantly occurs under Mode I. Mode II, however, leads to the sliding of the crack surfaces. In the third mode loads applied to the crack in a way to tear the two crack surfaces apart. In adhesive joints most interest focuses on first two modes, and the other mode appears less frequently but is nevertheless of great importance (Custódio et al. 2009; Mier 2012).

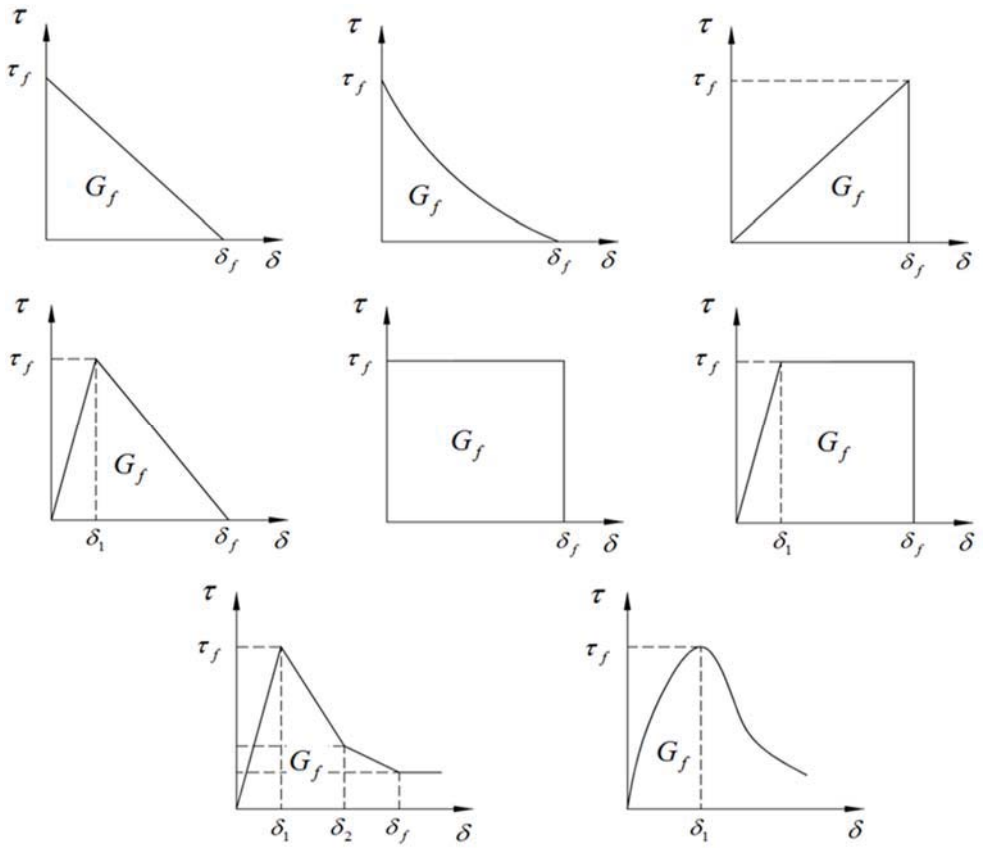

Figure 2-22 Shear-Slip Models for Plate to Concrete Bonded Joints (Yuan and Wu 1999)

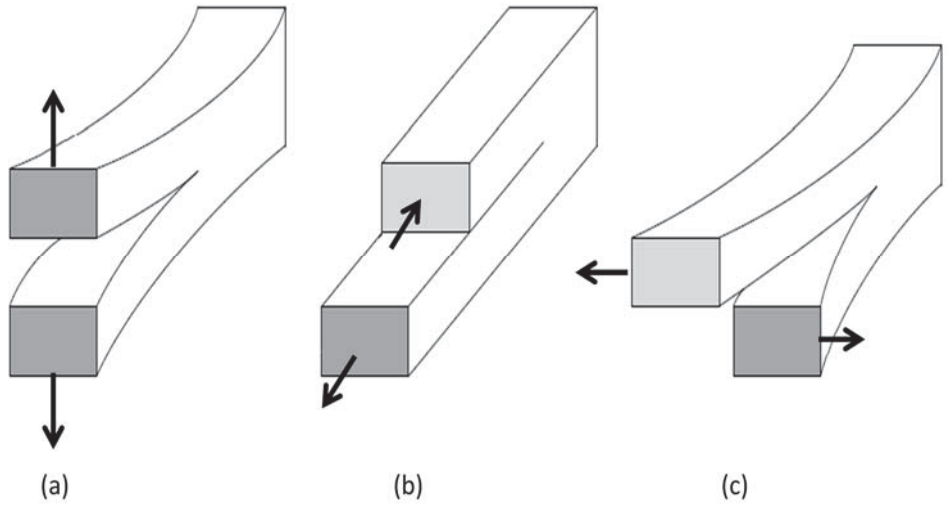

Figure 2-23 Three fracture modes: (a) opening mode I, (b) in-plane shear mode II, and (c) out-of-plane shear mode III (Mier 2012).

Custódio et al. (2009) reported that the brittle fracture energy of the bondline, G_f, considering linear elastic fracture mechanics (LEFM), can be determined for a given adhesive layer thickness t_a:

$$G_f = \frac{\tau_v^{\,2} t_a}{2G_a} \tag{2-14}$$

where τ_v and G_a are adhesive shear resistance and adhesive shear modulus, respectively. This method was initially developed for timber pull-out behaviour by Gustafsson (1987) that is currently the ideal method for determining the pull-out load of rods bonded into timber (Custódio et al. 2009). Holzenkämpfer (1994) considered the bond strength between concrete and steel plate using nonlinear fracture mechanics (NLFM). Niedermeier (1996) and Blaschko et al. (1996) modified the proposed model to calculate the bond strength by using

$$P_u = 0.78 b_f \sqrt{2G_f E_f t_f} \qquad \text{if} \qquad L \geq L_e \tag{2-15}$$

$$P_u = 0.78 b_f \sqrt{2G_f E_f t_f}\,\frac{L}{L_e}\left(2 - \frac{L}{L_e}\right) \qquad \text{if} \qquad L < L_e$$

where the fracture energy (G_f) and the effective bond length (L_e) can be derived by

$$G_f = c_f k_f^{\,2} f_{ctm} \quad \text{(N.mm/mm}^2\text{)} \tag{2-16}$$

$$L_e = \sqrt{\frac{E_f t_f}{4 f_{ctm}}} \quad \text{(mm)} \tag{2-17}$$

In the above equations, c_f is constant that can be determined in a linear regression analysis based on the results of double shear or similar tests; f_{ctm} (MPa) is the average surface tensile strength of concrete. The value of f_{ctm} can be determined using the results of pull-off test according to DIN1048 (Deutsches Institut für Normung 1991); and k_p is geometrical factor which is related to the width of the concrete (b_c) and also width of the bonded plate (b_p)

$$k_f = \sqrt{1.125 \frac{2 - b_f / b_f}{1 + b_f / 400}} \tag{2-18}$$

Neubauer and Rostasy (1997) investigated the behaviour of carbon fibre reinforced polymer to concrete bonded joints using a number of double shear tests. They concluded that the fracture energy can be calculated using

$$G_f = c_f f_{ctm} \tag{2-19}$$

in which f_{ctm} is the tensile strength of concrete. They also reported an average value of 0.204 mm for c_f (Chen and Teng 2001). Neubauer and Rostasy (1997) modified the model which was developed by Holzenkämpfer (1994) to calculate the bond strength by using

$$P_u = 0.64 k_f b_f \sqrt{E_f t_f f_{ctm}} \quad \text{if} \quad L \geq L_e \tag{2-20}$$

$$P_u = 0.64 k_f b_f \sqrt{E_f t_f f_{ctm}} \frac{L}{L_e}\left(2 - \frac{L}{L_e}\right) \quad \text{if} \quad L < L_e$$

$$L_e = \sqrt{\frac{E_f t_f}{2 f_{ctm}}} \tag{2-21}$$

The fracture mechanics based models for FRP-to-concrete interface have been extensively considered (Liu and Wu 2012; Seracino et al. 2007; Täljsten 1994; Woo and Lee 2010; Wu and Niu 2000; Yuan and Wu 1999; Yuan et al. 2001) and a series of formulae have been derived based on linear and non-linear shear stress-slip relationship. Table 2-2 and Table 2-3 provide references for existing bond-slip models which have been developed based on empirical and fracture mechanics-based theories.

Table 2-2 Existing empirical based models proposed in literature

Model	Shear Stress Profile		τ_{max}	s_0	P_u	L_e
	Ascending Branch $s \le s_0$	Descending Branch $s > s_0$				
Nakaba et al. (2001)	$\tau_{max} \frac{s}{s_0} \frac{3}{2+(s/s_0)^3}$		$3.5 f'_c{}^{0.19}$	0.065	--	--
De Lorenzis et al. (2001)	$k.\frac{F}{\alpha b_f E_f t_f \sinh \alpha L_f} \times \cosh \alpha x$		$0.0184\sqrt{(t_f E_f)}$	--	--	--
Seracino (2001)	--		--	--	$1.71\times10^8 \frac{f'_c A_f t_a}{E_c^{1.5}}.(\frac{E_f}{E_a})^{0.1}$	--
Monti et al. (2003)	$\tau_{max} \frac{s}{s_0}$	$\tau_{max} \frac{s_f - s}{s_f - s_0}$	$1.8 \beta_w ft$	$2.5\tau_{max}(\frac{t_a}{E_a}+\frac{50}{E_c})$	--	--
Savoia et al. (2003)	$\tau_{max}.\frac{s}{s_0}\left[\frac{2.86}{1.86+(s/s_0)^{2.86}}\right]$		$3.5 f'_c{}^{0.19}$	0.051	--	--
Guo et al. (2005)	$\tau_{max}.\frac{s_x}{s_0}\left[\frac{2.018}{1.018+(s_x/s_0)^{2.86}}\right]$		$0.7512 \quad f'_c{}^{0.5}$	0.046	--	--

Model		Shear Stress Profile		τ_{max}	s_0	P_u	L_e
		Ascending Branch $s \le s_0$	Descending Branch $s > s_0$				
Foster and Khomwan (2005)		$\tau_{int,\,x} = 12\,(\lambda - 2\lambda^2 + \lambda^3).\frac{\varepsilon_0 t_f E_f}{L_e}$ $s_x = (1-k).(2-2\lambda^2+0.6\lambda^2).(L_e\varepsilon_0\lambda^3)$		$\frac{16}{9}.\frac{\varepsilon_0 t_f E_f}{L_e}$	$\frac{7}{135}(1-k).(L_e\varepsilon_0)$	--	Ueda and Dai (2004)
Seracino et al. (2007)		--	$\tau_{max}\frac{s_{max}-s_x}{s_{max}}$	$(0.802+.078\varphi_f)f'_c{}^{0.6}$	$s_{max}=\frac{0.976\varphi_f{}^{0.526}}{0.802+0.078\varphi_f}$	$0.85\varphi_f{}^{0.25}f'_c{}^{0.33}\sqrt{A_f E_f L_{per}}$	
Zhou et al. (2010)	Infinite joint	$\tau_{int,s} = \frac{E_f t_f}{1+\rho}.\frac{\alpha}{\beta^2}.(1-e^{-\frac{s}{\alpha}})$		$\frac{E_f t_f}{4(1+\rho)}.\frac{\alpha}{\beta^2}$	--	$\frac{\alpha}{\beta}.E_f A_f$	$2\beta.(\frac{1+\delta}{1-\delta})$
	Finite joint	$\tau_{int,s} = \frac{E_f t_f}{1+\rho}.\frac{\alpha}{\beta^2}.\frac{x+\beta}{L_f}.\frac{e^{-\frac{x-x_0}{\beta}}}{(\frac{x}{L_f}+e^{-\frac{x-x_0}{\beta}})^2}$		$\frac{E_f t_f}{4(1+\rho)}.\frac{\alpha}{\beta^2}.(1+\frac{\beta}{x})$	--	$\frac{E_f A_f}{1+\rho}.\frac{\alpha}{\beta}.\frac{1}{1+e^{-\frac{L_f-x_0}{\beta}}}$	--
Liu and Wu (2012)		(Zhou et al. 2010) $s_x = \alpha.\ln\left(\frac{A^2-1}{2AB-2}\right)$		--	--	$E_f A_f \frac{\alpha}{\beta}\sqrt{(1-e^{-\frac{s_l}{\alpha}})^2-(1-e^{-\frac{s_f}{\alpha}})^2}$	244 mm

Table 2-3 Existing fracture-based models for adhesively bonded joints

Model	Shear Stress Profile		τ_{max} and s_0	G_f	P_u	L_e
	Ascending Branch $s \le s_0$	Descending Branch $s > s_0$				
Täljsten (1996)	$\frac{P_{max}}{\tau_{int,x} b_f (L_f - a)}$	--	--	--	$b_f \cdot \sqrt{\frac{2E_f t_f G_f}{1+\alpha}}$ $\alpha = \frac{E_f t_f}{E_c t_c}$	--
Neubauer and Rostasy (1997)	--		--	$0.204 f'_c$	$0.64 k_p b_f \sqrt{E_f t_f f'_c}$	$\sqrt{\frac{E_f t_f}{2 f'_c}}$
De Lorenzis et al. (2001)	--	--	$0.0184\sqrt{E_f t_f}$	--	--	$\frac{\sqrt{2E_f t_f G_f}}{\tau_{max}}$
Chen and Teng (2001)	--	--	--	--	$0.427 \beta_p \beta_L b_f L_e \sqrt{f'_c}$	$\sqrt{\frac{E_f t_f}{\sqrt{f'_c}}}$
Dai et al. (2005) and Ueda and Dai (2005)	$\varepsilon_s = A.(1 - \exp(B_s)$ $\tau_{int,s} = A^2 B.E_f t_f .e^{-Bs}.(1 - e^{-Bs})$		$\tau_{max} = 0.5BG_f$ $s_{max} = \frac{0.693}{B}$	$0.5A^2 E_f t_f$ $0.446 \frac{f_c^{0.236} (E_f t_f)^{0.023}}{(\frac{G_a}{t_a})^{0.352}}$	$(b_f + \Delta_{bf}) \cdot \sqrt{2E_f t_f G_f}$ $\Delta_{bf} = 3.7mm$	$\frac{1}{B}\sqrt{\frac{2E_f t_f}{G_f}}.\ln(\frac{1+\alpha}{1-\alpha})$ $0.74\sqrt{\frac{E_f t_f}{f'^{0.236}_c}}$

Model	Shear Stress Profile		τ_{max} and s_0	G_f	P_u	L_e
	Ascending Branch $s \le s_0$	Descending Branch $s > s_0$				
Lu et al. (2005a)	$\tau_{max}\sqrt{\frac{s}{s_0}}$	$\tau_{max} e^{-\alpha(\frac{s}{s_0}-1)}$	$s_0 = 0.0195\beta_w f_t$	$0.308\beta_w^2\sqrt{f_t}$	$\beta_l b_f \cdot \sqrt{2E_f t_f G_f}$	$\alpha + \frac{1}{\lambda_1}\ln\frac{\lambda_1 + \lambda_2 \tan(\lambda_2\alpha)}{\lambda_1 - \lambda_2 \tan(\lambda_2\alpha)}$
Ferracuti et al. (2007)	$\tau_{max} \cdot \frac{s_p}{s}\left[\frac{n}{(n-1)+(s_p/s)^n}\right]$		--	$\pi\left[\frac{1}{n-1}\right]^{\left(1-\frac{2}{n}\right)} \cdot \frac{1}{\sin\left(\frac{2\pi}{n}\right)}$	$b_f \cdot \sqrt{2E_f t_f G_f}$	--
Liu and Wu (2012)	--	--	--	$0.5 E_f t_f (\frac{\alpha}{\beta})^2$	--	--
Wan (2014)	$\tau_x = A^2 B C_N e^{-Bs}(1 - e^{-Bs})$		--	--	$0.012\gamma_l\gamma_e b_f L_f^{0.28}\sqrt{E_f t_f}$	$\sqrt{\frac{E_f t_f}{\sqrt{f'_c}}}$
Biscaia et al. (2016a)	--		--	--	$b_f \cdot \sqrt{2G_f E_f t_f}$	$s_1\sqrt{\frac{2E_f t_f}{\tau_1 . s_1}}$

2.9. Summary

This chapter has provided a literature review on structural behaviour of timber, characteristics of FRPs as well as a brief history of different methods and techniques on retrofitting and strengthening of timber structure. In terms of repairing and retrofitting civil structures, previous studies have reported that FRP composites materials have sound advantages compared to the traditional strengthen methods such as cutting out and replacing plates or connecting external steel plates to the surface of the structural members. A number of researches have been performed to date on FRP-to-concrete bond; conversely, very limited attempts have been conducted to investigate the FRP-to-timber bond. Nevertheless, the research findings of such studies have been reviewed with the intention of characterising and identifying of potential failure modes and bond behaviour of FRP-to-concrete and timber bonded interface. However, due to the limited success and applicability of these studies, further research in this area is highly desirable from a structural design perspective, to develop models that can properly predict debonding failure loads as well as associated failure criteria for FRP strengthened members.

The failure mode of externally bonded joints may occur in different ways, such as substrate failure, FRP delamination, FRP/adhesive separation, FRP rupture, cohesion failure, adhesive failure, and substrate-to-adhesive interfacial failure; although they may be mixed in an actual failure. However, the most common failure mode in the externally bonded elements is FRP debonding which directly impacts on total integrity of the structure causing devastating damages to the whole structure. Consequently, in order to investigate the debonding mechanism, numerous bond testing methods have been carried out experimentally; including

single shear tests, double shear tests, and modified beam tests. Considering these testing approaches, different factors have been reported in the literature to investigate their impact on the interfacial behaviour of the joints. The main parameters are but not limited to timber mechanical properties and geometries, adhesive stiffness and strength, interfacial fracture energy, FRP bonded length, FRP stiffness, FRP bonded width and FRP-to-timber width ratio.

Comprehensive test methods and guidelines are available, e.g. ACI (2005) and Canadian Standards Association (2002), covering above parameters and their impact on the FRP reinforced concrete structures; however, there is a significant knowledge gap to gain a comprehensive understanding of parameters that influence the bond strength of FRP bonded to timber. It is worth emphasising that, the research on the bond behaviour of FRP-to-timber is still in its infancy. While an understanding of the influence of bonded length on the ultimate load with the length of the FRP is emerging, less attention has been paid to the scaling in the ultimate load with the width of the FRP. Further investigations need to be carried out to determine the influence of the above-mentioned parameters on the bond behaviour FRP bonded to timber elements.

The knowledge gap observed in the literature, describing the above parameters has motivated the work reported in this dissertation. The main intention of this research study is therefore to investigate the bond strength and bond behaviour between timber and FRP and also to identify and assess the potential factors affecting FRP-to-timber interface. Therefore, to strengthen the bond, make it more resistant and also to consider compatibility of FRP and timber, an experimental investigation has to be undertaken, focusing on the bonding mechanisms between timber beam and fibre reinforced polymers. Moreover, a new bond strength model of the bond between FRP and timber is essential to be able

to accurately predict the ultimate load capacity of timber members repaired/strengthened with FRP.

Chapter 3

EXPERIMENTAL DETAILS: FRP-TO-TIMBER INTERFACE

3.1. Introduction

This chapter presents the experimental details of externally bonded CFRP-to-timber joints under monotonic tensile loading and discussion on the observed behaviour of the bond between timber and FRP. Test setup, test specimens and their fabrication, test procedures, test equipment and materials properties are described in this chapter.

3.2. Externally bonded FRP-to-timber interface

The experimental program consisted of 136 specimens with a modified single-shear CFRP-to-timber bonded interface. The parameters of the test specimens were determined by preliminary analysis on experimental results obtained from the literature, through a stepwise regression (SR) analysis, the results of which have been published (Vahedian et al. 2017b). Stepwise regression is a robust approach for selecting the best subset of independent variables that provides efficient prediction of the dependent variable. Stepwise regression analysis significantly reduces computing complexity compared to that required for all possible regressions (Campbell 2006). The stepwise regression analysis was carried out based on 446 experimental results of FRP-to-concrete bonded interface, covering a wide range for each parameter as reported in the literature (Chen and

Teng 2001; Dai et al. 2006; Ren 2003; Ueda et al. 1999; Wu et al. 2001; Yao et al. 2005; Zhou 2009) and an average of 198 experimental results of FRP-to-timber bonded interfaces as reported by Wan (2014). The stepwise analysis process has been performed using different possible combinations of independent variables including linear, polynomial, exponential model, reciprocal model and nonlinear multiple regression. Models considered for the stepwise regression process are given in Table 3-1. This analysis revealed that FRP width, FRP-to-substrate width ratio, FRP stiffness and bond length are the key parameters which affect the bond strength. Accordingly, decisions were made as to the factors that were to be considered for further detailed investigation.

Table 3-1 models considered in SR process

Model	Equation
Multiple regression model (linear regression)	$Y = b_0 + b_1x_1 + b_2x_2 + ... + b_mx_m$
Polynomial Regression	$Y = b_0 + b_1x + b_2x^2 + b_3x^3 + ... + b_mX^m$
Nonlinear multiple regression models	$Y = b_0 + b_1x_1b_2x_2b_3x_3b_mX_m$
Exponential model	$Ln\ Y = b_0 + b_1x_1 + b_2x_2 + b_3x_3$
Reciprocal model	$Y = 1 / (b_0 + b_1x_1 + b_2x_2 + ... + b_mx_m)$

3.3. Details of tested parameters

Two different types of timber, namely Laminated Veneer Lumber (LVL) made out of softwood (manufactured Radiata Pine, New Zealand) and hardwood sawn timber were utilised. Whilst the species of the hardwood samples were not identified, based on the tested density, tensile and compressive properties, the species would fall into SD4 strength group as per AS1720.1 (2010). The timber samples used were selected to be as free as possible from knots, naturally occurring “defects” and pitch, although this could not always be the case. The main intention of fabricating joints with different types of timber was to evaluate the effect of timber mechanical properties such as tensile strength and modulus of elasticity on the bond strength. The compatibility and failure mode of the interface can also be investigated through these test series.

Bond length is one the key parameters that impacts on the bond strength. The investigation presented in this section was undertaken in order to determine the effective bond length and correspondingly to address critical variables that impact on effective bond length different bond lengths. Five different bond lengths namely, 50 mm, 100 mm, 150 mm, 200 mm and 250 mm were examined for specimens made from LVL; whilst the hardwood samples contained bond lengths of 50 mm, 100 mm, 150 mm and 200 mm. Results of such an investigation can be used to determine the influence of bond length on the bond strength, and correspondingly to determine and propose a new effective bond length model for the externally bonded FRP-to-timber interface. The effect of timber mechanical properties on the effective bond length can also be addressed through these series of tests.

The bond strength is highly dependent to the geometry of the bond and also varies with the FRP width and FRP-to-timber width ratio. To examine the influence of bond width on the bond strength, three different bond widths namely, 35 mm, 45 mm, and 55 mm, were investigated in the joints made from LVL. Only one bond width, 45 mm, was tested for the hardwood samples. In this set, interface stress and strain distribution, as well as interface bond-slip, can be scrutinised. Through these tests, the influence of bond width on the effective bond length can also be considered.

The effect of bond stiffness on the bond strength has been investigated herein, where one or two plies of unidirectional wet-lay up of CFRP with a nominal thickness of 0.117mm (provided by manufacturer; MBRACE^{TM}) were externally bonded to the timber with an epoxy. The failure mode of the specimens was studied by a comparative analysis of all series, to investigate the behaviour of the interface and to determine how the ductility of the interface may change through adding extra FRP layers. The performance of adhesive stiffness on the bond strength has not been

reported in this dissertation (outside of the scope) and only one type of structural adhesive (Sikadur®-330) has been used for bonding FRP sheets to timber.

The joints were divided into 28 different series to evaluate the influence of various parameters on the bond strength. For each series, five specimens were fabricated as duplicates, except the samples with 250 mm bond length, where three specimens were made. The arrangements of the various series, the number of samples and test variables of each series are listed Table 3-2.

Table 3-2 Detail of the tested specimens

Timber type	Identification of specimen	FRP thickness (mm)	Bond length (mm)	Bond width (mm)	Number of specimens
Laminated Veneer Lumber	LVL[a]50[b]-35[c]-01[d]		50	35	5
	LVL 100-35-01		100	35	5
	LVL 150-35-01		150	35	5
	LVL 200-35-01	1 x 0.117	200	35	5
	LVL 50-35-02		50	35	5
	LVL 100-35-02		100	35	5
	LVL 150-35-02		150	35	5
	LVL 200-35-02	2 x 0.117	200	35	5
	LVL 50-45-01		50	45	5
	LVL 100-45-01		100	45	5
	LVL 150-45-01		150	45	5
	LVL 200-45-01	1 x 0.117	200	45	5
	LVL 150-45-02	2 x 0.117	150	45	5
Hardwood	H 50-45-01		50	45	5
	H 100-45-01		100	45	5
	H 150-45-01		150	45	5
	H 200-45-01	1 x 0.117	200	45	5
	H 50-45-02		50	45	5
	H 100-45-02		100	45	5
	H 150-45-02		150	45	5
	H 200-45-02	2 x 0.117	200	45	5
Laminated Veneer Lumber	LVL 50-55-01		50	55	5
	LVL 100-55-01		100	55	5
	LVL 150-55-01		150	55	5
	LVL 200-55-01		200	55	5
	LVL 250-55-01	1 x 0.117	250	55	3
	LVL 150-55-02	2 x 0.117	150	55	5
	LVL 250-55-02	2 x 0.117	250	55	3

a: Timber type, b: Bond length, c: Bond width and d: CFRP layers

3.4. Material properties

3.4.1. Timber mechanical properties

A total of 28 timber samples (14 LVL and 14 hardwood) divided into two groups were fabricated with different cross sections and tested in accordance with BS_EN_408 (2010) to establish the mechanical properties of the timber. These samples were cut from the same timber members which were used to make the FRP-timber bond test specimens. In compression, BS_EN_408 (2010) specifies that the test piece shall be of full cross section, and shall have a length of six times the smaller cross-sectional. The compression sample test specimens of the LVL had average cross-sectional dimensions of 64 mm by 29 mm and a length of 180 mm. The average dimensions of the hardwood samples were 34 mm by 33 mm and a length of 198 mm. The thickness of commercially available hardwood used in this study is less than that normally used for LVL. Thus, the main reason for the difference is due to ready availability of these materials. The end surfaces have been prepared to ensure that the end surfaces are plane and parallel to one another and perpendicular to the longitudinal axis of the sample. In tension, on the other hand, BS_EN_408 (2010) specifies that the test piece shall be of full structural cross section, and of sufficient length to provide a test length clear of the testing machine grips of at least nine times the larger cross-sectional dimension. The tension samples of LVL and hardwood possessed the mean cross-sectional dimensions of 65 mm x 38 mm and 42 mm x 42 mm with the lengths of 960 mm and 1000 mm, respectively. Setup details for the compression and tension tests for the LVL and hardwood samples are shown in Figure 3-2.

Eight preliminary tests (2 for tensile strength and 2 for compressive strength per each type of timber) were performed to find out the correct load rate for determination of compressive and tensile strength parallel to

the grain and modulus of elasticity. In the compression tests, two conditions were followed according to BS_EN_408 (2010); (a) the load rate for determination of modulus of elasticity is limited to not greater than 0.00005L mm/s where L refers to length of sample, (b) for determination of compression strength the maximum load should be reached within (300±120) s. To determine modulus of elasticity in tension, the rate of strain should be not greater than 0.00005L mm/s per second. Simultaneously, for determination of tensile strength the maximum load should be reached within (300±120) s. The constant uniaxial loads parallel to grain were applied until failure occurred in the specimens with the rates of 0.5 mm/min and 8 mm/min in compression and tension, respectively. The maximum load was achieved in the time recommended by BS_EN_408 (2010) as shown in Figure 3-1 which is within (300±120) s.

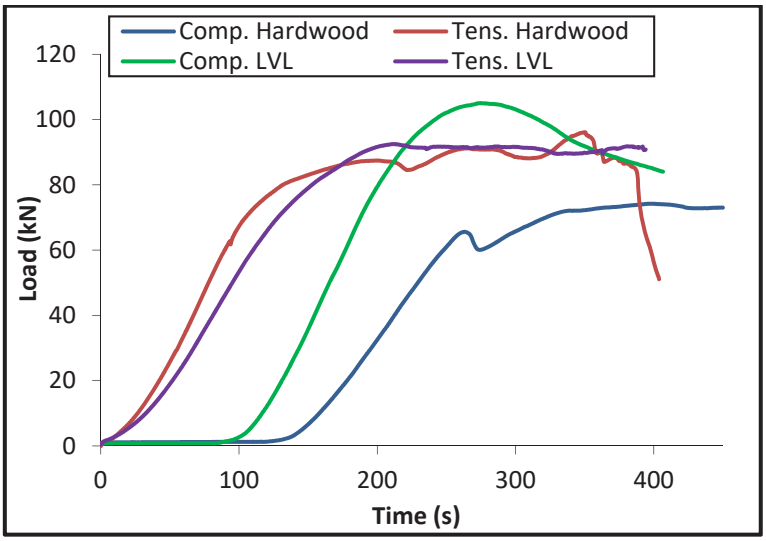

Figure 3-1 preliminary test results for determination of proper load rate in tension and compression

The compressive and tensile strength were calculated as the peak load divided by the measured minimum cross-sectional dimensions of the specimens. The mean values of test results are tabulated in Table 3-3 to Table 3-6, whilst all test results are presented in Appendix A. It can be noted that the compression and tensile strengths for the hardwood specimens were similar, with an average tensile to compression strength

ratio of 1.04. This ratio for LVL specimens was 0.79 the tensile strength for the LVL was much lower than its compressive strength.

Modulus of elasticity was determined from Eq. (3-1) using three strain gauges bonded parallel and perpendicular to three sides of the test samples.

$$MOE = \frac{L_1(F_2 - F_1)}{A(W_2 - W_1)} \tag{3-1}$$

Where F_2 - F_1 is an increment of load on the linear portion of the load deformation curve, in Newtons; W_2 - W_1 is the increment of strain corresponding to F_2 - F_1. A is cross-sectional area, in square millimetres and L_1 is gauge length for the determination of modulus of elasticity, in millimetres. The average modulus of elasticity in compression and tension for the hardwood were determined to be 19.70 GPa and 19.75 GPa, respectively. In the LVL samples, the mean values of modulus of elasticity in compression and tension were determined to be 17.68 GPa and 16.18 GPa respectively, as listed in Table 3-3 to Table 3-6. The elastic modulus of hardwood are approximately 1.2 times higher than that of LVL. Such a difference leads to higher stiffness in the bond, which is explained in the following chapter.

Poisson's ratio of the tested samples was derived from strain gauges located perpendicular and parallel to the grain in compressive and tensile tests over the linear portion of the strain against load plots. As listed in Table 3-3, the average Poisson's ratios of hardwood in radial and tangential direction to the grain were similar with a value of 0.36. However, the average Poisson's ratio of LVL parallel to the glueline was obtained as 0.6 which is double the average Poisson's ratio perpendicular to the glueline, as tabulated in Table 3-5. Poisson's ratios vary within and between species and are affected by moisture content and specific gravity. The large difference of Poisson's ratio in the LVL sample can be as a result of the

glueline. It is important to note that some of strain gauges during sample tests detached from surface of timber, and the data was not completely collected for such strain gauges. Thus, the associated Poisson's ratios are not reported in Table 3-3 and Table 3-5.

Figure 3-2 Timber specimen test in progress; (a) compressive test of LVL, (b) tensile test of LVL, (c) compressive test of Hardwood, (d) tensile test of Hardwood

Table 3-3 Hardwood compression test results (mean values)

Samples	P_u (kN)	Compressive Strength (MPa)	MOE (GPa)	Poisson Ratio	
				Parallel to the grain	Perpendicular to the grain
Average	76.82	64.93	19.70	0.37	0.36
CoV (%)	6.46	4.45	24.13	27.04	24.66

Table 3-4 Hardwood tensile test results (mean values)

	P_u (kN)	Tensile Strength (MPa)	MOE (GPa)
Average	96.80	67.53	19.75
CoV (%)	9.26	8.71	8.58

Table 3-5 LVL compression test results (mean values)

	P_u (kN)	Compressive Strength (MPa)	MOE (GPa)	Poisson Ratio	
				Parallel to the grain	Perpendicular to the grain
Average	100.58	56.26	17.68	0.60	0.30
CoV (%)	3.19	1.79	16.96	31.85	27.04

Table 3-6 LVL tensile test results (mean values)

	P_u (kN)	Tensile Strength (MPa)	MOE (GPa)
Average	107.83	44.31	16.18
CoV (%)	18.81	15.61	5.06

CoV: co-efficient of variation.

Both the LVL and hardwood used in this study, had been stored in the laboratory for a few years. Timber as a hygroscopic material attempts to balance its moisture content with its surrounding environment. As mentioned in Chapter 2, the influence of moisture content and environmental conditions on the bond strength are outside the scope this dissertation; nevertheless, the moisture content of LVL and hardwood were evaluated to ensure that this value for the specimens used herein lays between 9% and 14% with the average 11% following the recommendation of AS2796.1 (1999) and AS4785.1 (2002). In cases where the moisture content was above 14%, such specimens should not be used for the fabrication of joints. The moisture content of LVL and hardwood were evaluated according to the AS/NZS2098.1 (2006) and AS/NZS1080.1 (2012) using results of 50 samples that were cut on the same day when the joint tests were conducted. The average value of moisture content was 10.2% with a coefficient of variation 1.7% for the LVL samples, and 12.1% with a coefficient of variation 2.4% for the hardwood samples. The average density of 643 kg/m^3 (coefficient of variation 1.39%) and 804 kg/m^3

(coefficient of variation 0.52%) were measured for LVL and hardwood samples, respectively, as per ASTM-D2395 (2014).

3.4.2. FRP mechanical properties

The tensile tests of coupon samples were conducted for determining tensile strength and elastic moduli of CFRP. Surface treatment of the FRP materials has been performed following the recommendation of ASTM-D2093-03 (2003) to remove all contaminants such as mould release agents, lubricants, or fingerprints from surface of FRPs as a result of the production process. The unidirectional wet-lay up of CFRP (MBRACE^{TM}) with the nominal thickness of 0.117 mm were utilised. To fabricate the coupon samples, two plies of the fibres with the dimension of 300mm x 400mm were placed in a release film and bonded with an epoxy based from Sika (Sikadur® 330). ASTM-D2093-03 (2003) strongly recommends to use tabs when testing unidirectional materials in order to provide proper thickness of the end tapping. Thus, to make tabs for the coupon tests, three layers of CFRP were applied in both sides of the sample with the dimension of 80 mm x 400 mm, and then a release film is placed over the sample. An aluminium roller was used to remove trapped air, impregnate the fibres, and brush out the excessive epoxy from the specimen. The samples were then placed in the laboratory to be cured for at least 10 days. The specimen was then cut into the desired dimensions according to ASTM-D3039/D3039M (2014). The complete list of requirements for specimen shape, dimensions, and tolerances based on ASTM-D3039/D3039M (2014) and also the values adopted in this study are reported in Table 3-7. Prior to tension testing, the area of the specimen was measured at three places in the gauge section (as shown in Figure 3-3) using a micrometre with a flat anvil interface, and the minimum value of these three measurements was used in all calculations. To avoid failure at the tab ends due to excessive interlaminar stresses, the coupon inserted so that the grp jaws extend

approximately 10 to 15 mm past the beginning of the tapered portion of the tab.

Six CFRP coupons were prepared and tested (as shown in Figure 3-4) with average dimensions of 0.234 mm x 15.0 mm x 250 mm and standard head displacement rate of 2 mm/min following the ASTM-D3039/D3039M (2014). One strain gauge was bonded longitudinally in the middle of the coupon and the tensile strength and modulus of elasticity of the FRP can be determined from the stress verses strain curves as shown in Figure 3-5. From the tensile tests on CFRP, the values of mean tensile strength and modulus of elasticity were determined to be 2497 MPa with a coefficient of variation 6.5%, and 229 GPa with a coefficient of variation 10.22%, respectively. The Coupon test results are presented in Appendix A. The mean ultimate strain was also calculated as 0.013 with a coefficient of variation 16%. These values fall around the minimum values specified by the manufacturer (MBrace®Fibre 2011).

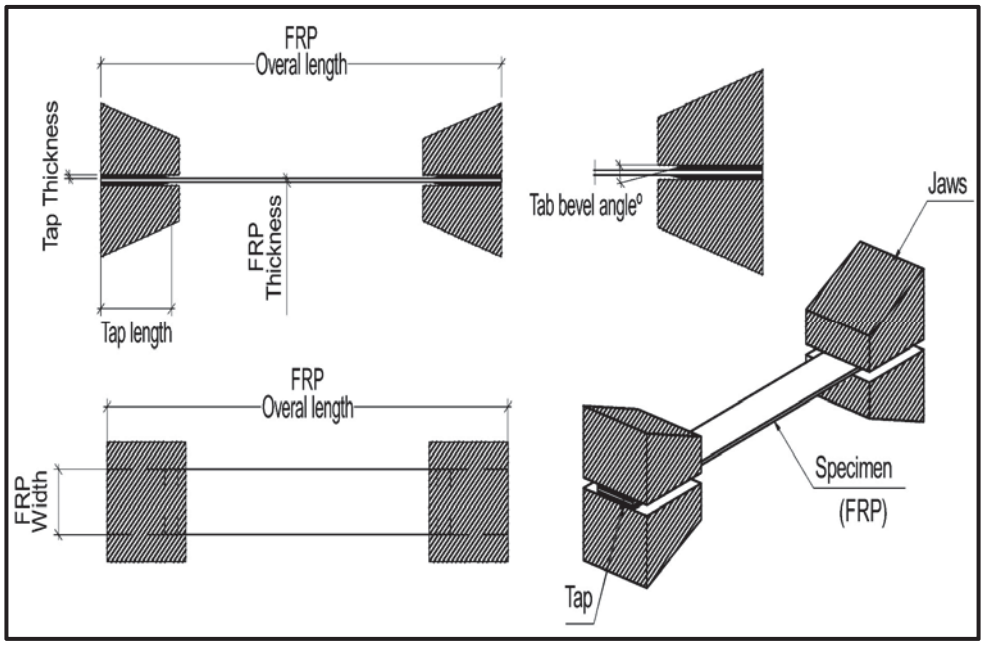

Figure 3-3 FRP coupon samples, a schematic view

Table 3-7 Tensile specimen geometry recommendations in standards and the values adopted in this study

	Overall length (mm)	Width (mm)	Thickness (mm)	Tap length (mm)	Tap thickness (mm)	Tab bevel angle°
ASTM D3039/D3039M	250	15 (±1%)	1.0 (±4%)	56	1.5 (±1%)	7-10
Current study	250	15	0.234	56	varied	7-10

Figure 3-4 FRP coupon test specimens

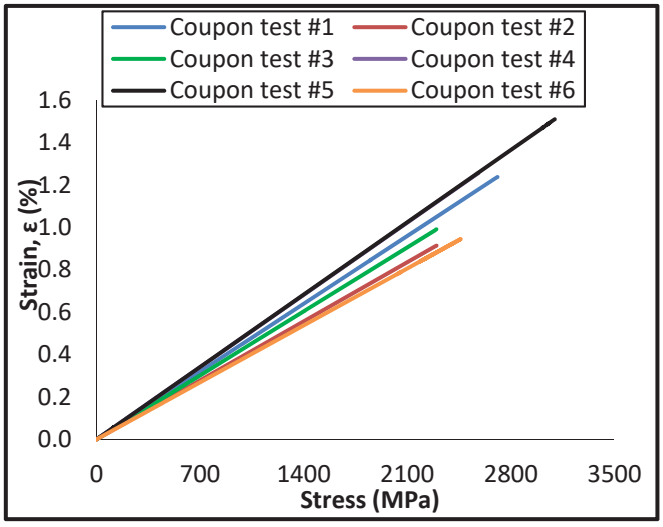

Figure 3-5 FRP coupon test results

The epoxy adhesive was not tested; however, based on manufacture's product data sheet (Sikadur®-330 2015), the values of elastic modulus and tensile strength of Sikadur®-330 were utilised to be 4.5GPa and 30MPa, respectively, and these values has been used in the analytical phase of this study. The average values of the sample tests are tabulated in Table 3-8.

Table 3-8 Material properties of timber, FRP and adhesive

Material	Tension (CoV%)		Compression (CoV%)		Poisson ratio % (CoV%)
	Tensile Strength MPa	Modulus of Elasticity, GPa	Compressive Strength MPa	Modulus of Elasticity, GPa	
Hardwood	67.53 (8.71)	19.75 (8.58)	64.93 (4.45)	19.70 (24.13)	0.36 (24.66)
LVL	44.31 (15.61)	16.18 (5.06)	56.26 (1.79)	17.68 (16.96)	0.30 (27.04)
FRP	2497 (6.45)	228.89 (10.2)	--	--	--
Sikadur®-330	30	4.5	--	--	--

CoV: co-efficient of variation.

3.5. Details of externally bonded test specimens

Two types of specimens were used depending on the type of timber used; the LVL samples consisted of 320 and 370 mm long with a 110 mm x 63 mm cross section, and the overall dimension of hardwood samples were 320 mm long x 110 mm wide x 35 mm deep. This was limited/governed by the size of timber commercially available used in this study. Figure 3-6 illustrates different stages of the timber cutting.

In order to promote and maximise the adhesion capacity of the bond, the surface of timber blocks sanded with 300 and 400 grit sandpaper as shown in Figure 3-7 before application of the FRP. Surface preparation was performed to remove all contaminants and weak surface layers that can potentially interfere with adhesion, and to develop a surface roughness. The timber surface was then cleaned with air spray and wiped with acetone. The surface of each of the CFRP sheets was prepared as per ASTM-D2093-03 (2003) to remove all impurities and potential contaminants such as mould release or fingerprints as a result of the production process. The bonded area was surrounded by masking tape to define the extent of the bonded CFRP as depicted in Figure 3-8.

Figure 3-6 Cutting of the timber specimens.

Figure 3-7 Surface preparation of timber block

Figure 3-8 Manufacturing of timber joints

Carbon fibres were cut in three different widths namely 35 mm, 45 mm, and 55 mm. The full length of FRPs vary due to different bond lengths ranging between 50 mm to 250 mm; however, to properly fit and grip the specimens into the universal testing machine, at least 300 mm extra length was allocated for each FRP sheet. In all specimens, a 20 mm unbonded zone was provided to prevent boundary conditions effects and also to minimise failure in the timber prism at the loaded end. Following the instructions of the manufacturer, a two-part epoxy based impregnating resin (Sikadur®-330) was mixed manually and applied to the bonded area of timber prism. The fibre composite was then placed in such area and an aluminium roller was used to remove trapped air, impregnate the fibres, and brush out the excessive epoxy from the specimen. A similar procedure was followed for the

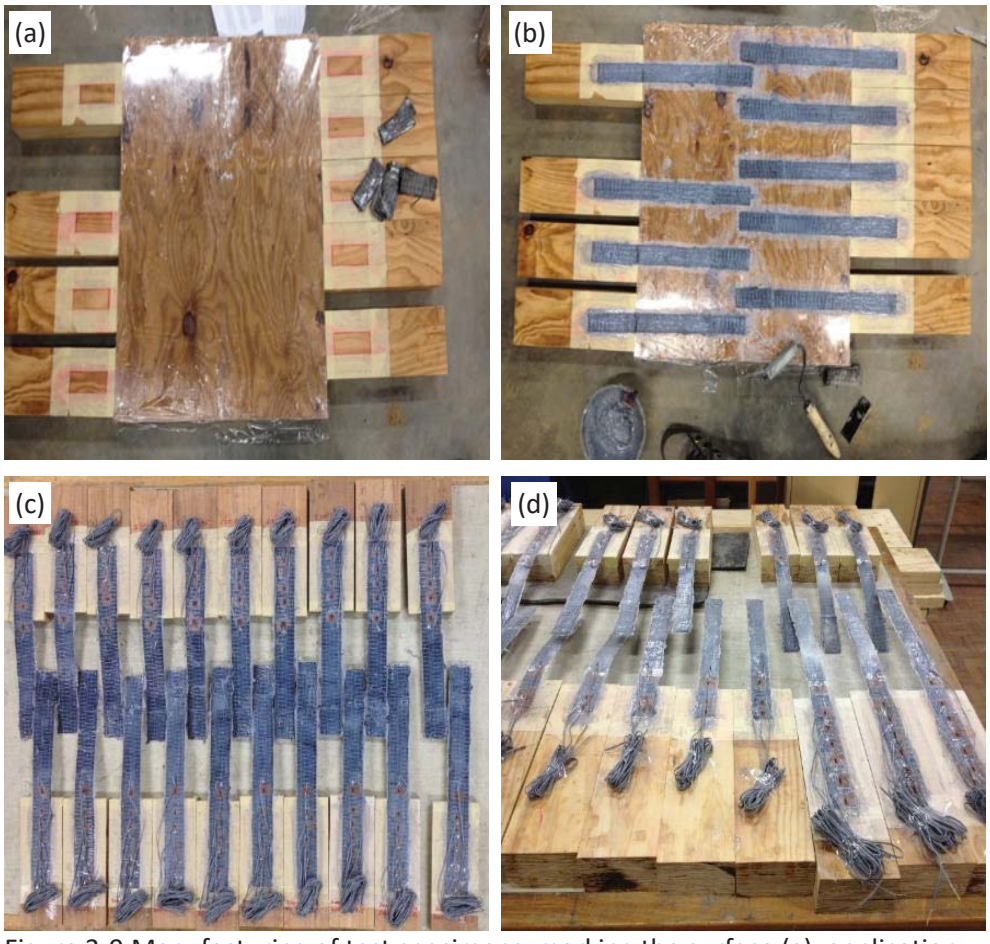

Figure 3-9 Manufacturing of test specimens, marking the surface (a), application of FRP and curing FRP (b), fabricated FRP-to-timber joints (c and d)

alternate layers of the fibres. Two additional 100 mm long layers of FRP were applied on each face of the free end of the FRP to form a tab and also to provide proper thickness of end tapping. The purpose of the tab is to prevent slippage between the grip face and the FRP that may lead gripping damage to the FRP. Figure 3-9 illustrates the procedure for fabrication of FRP-to-timber joints. Figure 3-10 schematically shows details of FRP-to-timber joints.

All specimens were fabricated and stored in the laboratory for at least 10 days for epoxy curing in the laboratory environment. The temperature and humidity of laboratory were monitored during fabrication and testing of specimens which ranged between 20°C to 22°C and 60% to 70%, respectively.

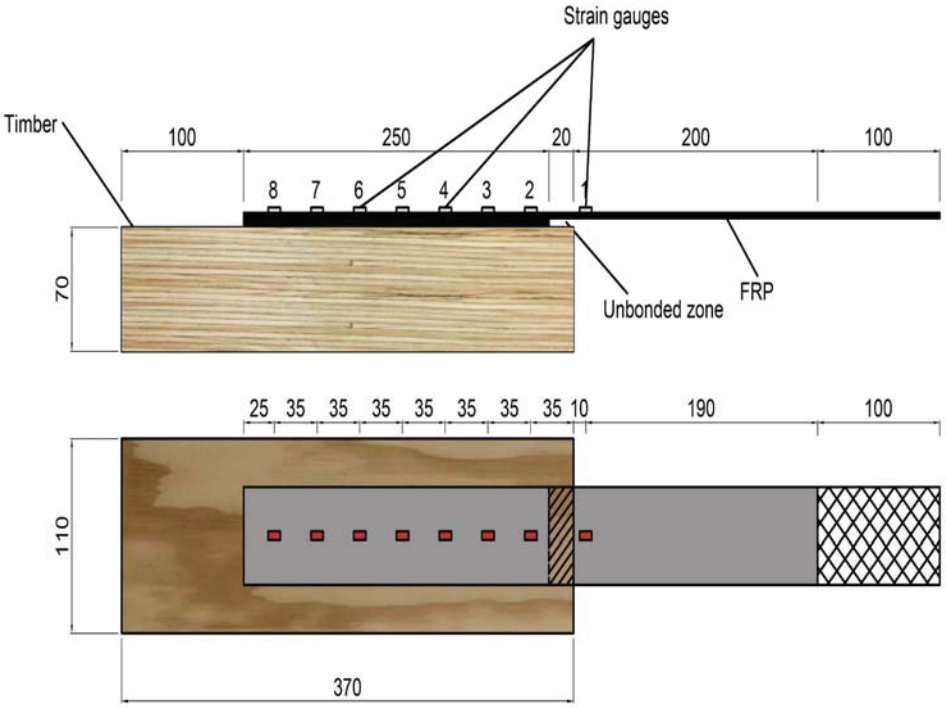

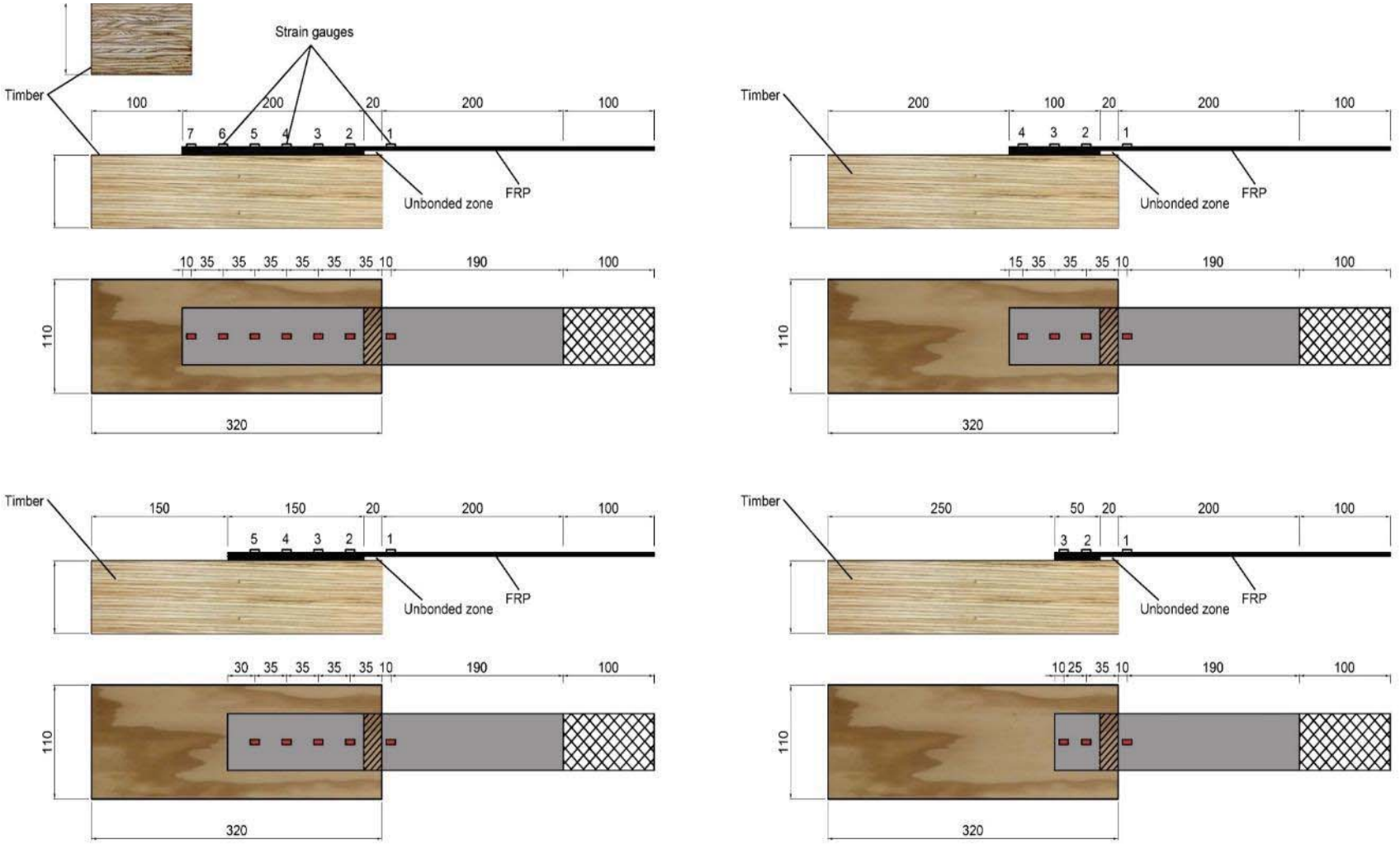

Figure 3-10 Application of the strain gauges on the bonded joint

3.6. Details of test setup

Debonding initiates when the tensile stress at the interface exceeds the bond strength. In other words, debonding is accompanied by slip between timber and FRP. Fracture mechanism of the FRP-to-timber interface revealed that, the slip value is quite small (Wan 2014) and any error in the test set-up can lead to scattered results. One reason for scattered results observed in the literature may be attributed to the test setup due to unexpected out of plane movements, since the interface is under both shear and flexural stresses simultaneously. For instance, in previous a test setup (Wan 2014), two or more LVDTs were used for measuring the bond slip between timber and FRP; however, the slip was finally derived using the strain gauge profiles, since it was believed that the data collected from LVDTs were not reliable due to timber out-of-plane movement. Furthermore, the timber block may not be cut perfectly rectangular, so that these blocks cannot be tightly fitted and held in the frame. Consequently, any out of plane movement of timber block can be expected to influence the test results.

Different test setups have been carried out to date in order to investigate the interfacial characteristics of adhesively bonded joints such as; single shear test, double shear test, and beam test as explained in Chapter 2. Accordingly, the bond-slip responses proposed by other researchers vary between a number of experimental studies. Disadvantages associated with the double shear test setup and beam tests have caused researchers to widely use the single shear test set up as the most reliable configurations for investigation of FRP bonded to timber. Nevertheless, there is not still a comprehensive formula to precisely predict the bond behaviour of FRP-to-timber interface. Consequently, in order to monitor bond behaviour and bond-slip relationships accurately and also to address and minimise the above-mentioned issues, a modified single shear test setup has been

adopted herein as shown in Figure 3-11. In the proposed modified test setup, the timber block was restrained in a steel rig and load was applied to the free end of the FRP. The slip between timber and CFRP was measured by one LVDT which was mounted on the surface of timber block as shown in Figure 3-11. One of the key advantages of the present test setup when compared with previous ones, is that when the timber block experiences any unexpected out of plane movements, both the timber and LVDT simultaneously have the same displacement. Moreover, at least one LVDT is omitted from the test; compared with previous test setup in the literature, and the slip of the interface can be measured with higher precision using only one LVDT placed at the loaded end. Therefore, the proposed test setup can minimise the effects of out of plane movements in shear tests.

Strain gauges were attached to the CFRP surface to investigate the interfacial stresses and also to measure the strain variation along the bond length. Strain gauges of 5 mm gauge length with 120.3 ± 0.5 Ω resistance were bonded to the CFRP surface for each sample. One strain gauge was placed at the unbonded zone of the CFRP surface, and other strain gauges were distributed on the centre-line of FRP along the bond length as shown in Figure 3-10 and summarised in Table 3-9. Due to the different bond lengths, the number of strain gauges installed varied between three and eight. The strain gauges were bonded to the FRP with an identical spacing of 35 mm in all sample tests except samples with 50 mm bond length, where the strain gauges were attached to FRP with 25mm spacing.

The pull-out tests were performed using a Class A universal testing machine which had a capacity of 500kN. However, the machine was operated only at a maximum load range of 30 kN based on predicted load capacity of sample tests and results of preliminary test samples which were in the range of 17 - 20 kN. During pull-out tests, an initial 2 kN load was

applied and reloaded for all specimens and then the load was applied at the rate of 0.3 mm/min as per ISO6238 (2001) and ASTM-D905-03 (2003). This increment in displacement allows the user to capture data over a small period of time, improving the accuracy of the results. A data logger was specifically prepared to collect data from the actuator, LVDT, and strain gauges.

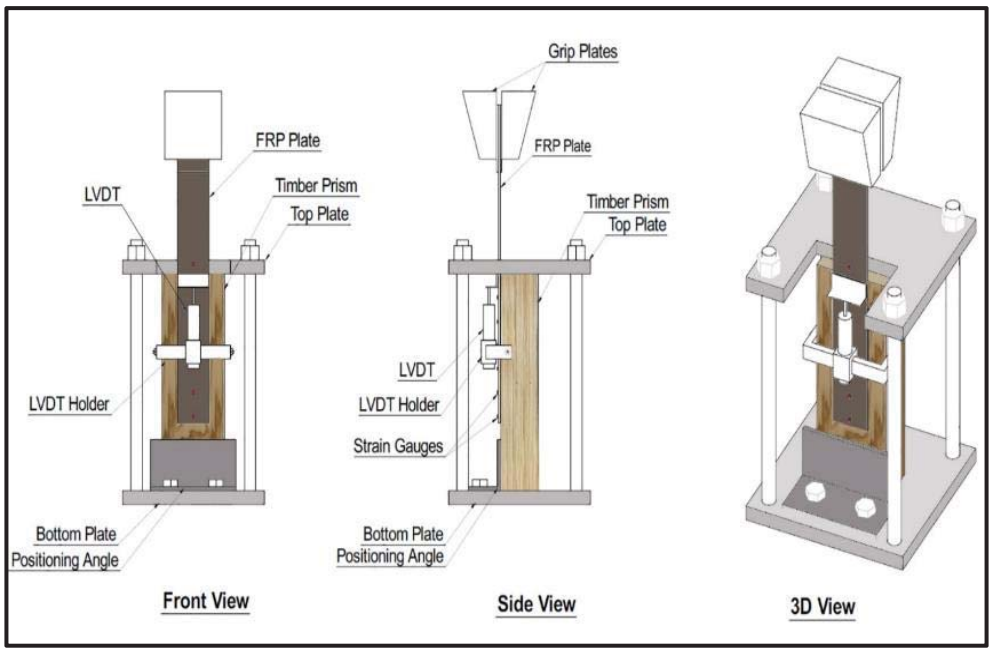

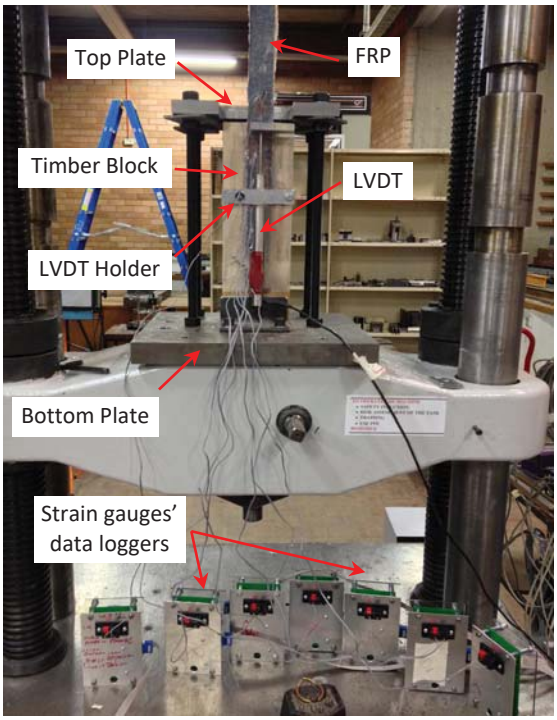

Figure 3-11 Modified test setup

Table 3-9 Position of the strain gauges along the bonded length

Bond length	Distance of the strain gauges from the loaded end (mm)						
	Strain gauge No. 2	Strain gauge No. 3	Strain gauge No. 4	Strain gauge No. 5	Strain gauge No. 6	Strain gauge No. 7	Strain gauge No. 8
50	15	40					
100	15	50	85				
150	15	50	85	120			
200	15	50	85	120	155	190	
250	15	50	85	120	155	190	225

3.7. Summary

This chapter presents the experimental work on externally bonded CFRP-to-timber joints subjected to monotonic tensile loading. A modified single shear test setup was successfully developed to minimise any unexpected out of plane movements of sample tests. This test set up is applicable for investigating not only FRP-to-timber joints, but also other combinations of materials. In addition, this setup offers the possibility of obtaining the bond-slip using only one LVDT and the slip of interface can be measured with higher precision than other methods. Details of the test setup, fabrication of test specimens, test procedures and equipment have been described in this chapter.

In the first stage of each experiment, properties of timber and FRP used in the fabrication of CFRP-timber joint samples were experimentally identified based on tensile and compressive tests on clear timber samples and tensile tests on FRP coupons. The moisture content and density of the timber materials used in the joint tests have been also measured.

The entire experimental program was divided in four phases focusing on the potential parameters affecting on the bond strength. The parameters that are investigated herein are the timber mechanical properties, bond length, FRP thickness, and bond width including the CFRP-to-timber width ratio. Results of the experimental investigation are presented and described in detail in the following chapter.

Chapter 4

EXPERIMENTAL RESULTS: FRP-TO-TIMBER INTERFACE

4.1. Introduction

This chapter presents the results and relevant discussion of the experimental program investigating externally bonded CFRP-to-timber joints, presented in Chapter 3. A parametric study of the bond behaviour is also presented in this chapter. The test data, which includes data from strain gauges attached to the surface of FRP, LVDT readings for measuring slip and the bond strength, quantifies the interfacial behaviour between timber and FRP. The parameters that are investigated herein are:

- Timber mechanical properties
- Bond width
- FRP layers
- Bond length

In summary, timber failure under shear, which occurred generally a few millimetres away from the adhesive layer, was observed as the main failure mode of interface. Failure of interface occurred at 28% to 100% of the ultimate tensile capacity of FRP sheets depending on bond geometries with an average value of 64% and coefficient of variation (CoV) of 27% as shown in Figure 4-1. Complete FRP rupture was recorded in only one sample, which occurred when 95% or more of the FRP ultimate tensile strength was

reached. Due to overall similarity of bond behaviour among tested samples, representative results are presented in this chapter and complete details of test results for each specimen can be found in Appendices B-I.

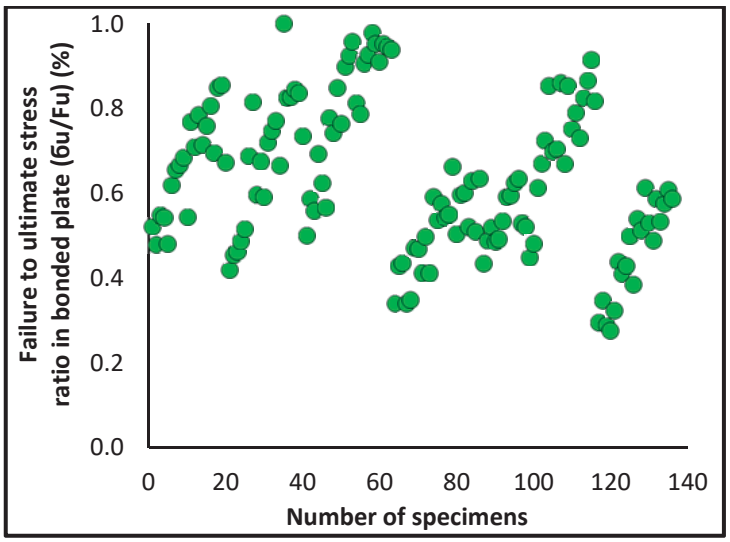

Figure 4-1 Peak FRP stress at bond failure

4.2. Effect of timber mechanical properties

Joint samples were fabricated from two different timbers namely Laminated Veneer Lumber (LVL) made out of softwood and kiln dried hardwood sawn timber. The effect of timber mechanical properties on the interface behaviour and bond strength are presented in this section. Results from 65 samples (Table 4-1) with identical bond width (45 mm) and variable bond length and FRP layers have been compared.

4.2.1. Behaviour and failure modes

Failures of samples are categorised into different modes; timber splitting (TS), FRP delamination (FD), FRP rupture (FR), adhesive failure (AD), and failure at timber-adhesive interface (FT). Timber splitting (TS) is referred to as failure in which at least a few millimetres thick timber was attached to the FRP after the joint samples failed. FRP Delamination (FD) named light-fibre-tear failure (LFT) according to ASTM-D5573-99 (2012),

Table 4-1 Results of timber species series tests

Identification	Timber				FRP			b_f / b_t	Pu (kN)							Failure modes
	L_t (mm)	b_t (mm)	d_t (mm)	type	t_f (mm)	L_f (mm)	B_f (mm)		Individual					Average	CoV (%)	
50-45-01-1~5	320	110	65	LVL	0.117	50	45	0.41	5.52	5.99	6.09	6.42	6.81	6.17	7.83	TS-FT
100-45-01-1~5	320	110	65	LVL	0.117	100	45	0.41	9.07	10.74	7.87	8.89	7.80	8.88	13.41	TS-FT
150-45-01-1~5	320	110	65	LVL	0.117	150	45	0.41	9.48	9.83	10.15	8.77	13.18	10.28	16.51	TS-AD-FT-FD
200-45-01-1~5	320	110	65	LVL	0.117	200	45	0.41	10.88	10.90	11.13	11.02	9.69	10.72	5.49	TS-AD-FT-FD
150-45-02-1~5	320	110	65	LVL	0.234	150	45	0.41	16.61	13.44	16.75	11.46	12.89	14.23	16.51	TS-FT
50-45-01-1~5	320	110	35	Hardwood	0.117	50	45	0.41	6.97	6.87	5.92	6.34	8.09	6.84	11.95	TS-FT
100-45-01-1~5	320	110	35	Hardwood	0.117	100	45	0.41	8.83	9.55	11.24	9.20	9.27	9.62	9.81	TS-FT-FD
150-45-01-1~5	320	110	35	Hardwood	0.117	150	45	0.41	11.32	8.82	11.24	9.91	10.41	10.34	10.01	TS-FD-FT
200-45-01-1~5	320	110	35	Hardwood	0.117	200	45	0.41	9.63	10.87	11.39	12.03	10.76	10.94	8.13	TS-FT
50-45-02-1~5	320	110	35	Hardwood	0.234	50	45	0.41	7.81	9.16	7.66	7.28	8.56	8.09	9.35	TS-FT
100-45-02-1~5	320	110	35	Hardwood	0.234	100	45	0.41	11.56	10.81	11.28	13.18	10.15	11.39	9.92	TS-FT
150-45-02-1~5	320	110	35	Hardwood	0.234	150	45	0.41	14.22	13.53	16.13	13.97	12.89	14.15	8.60	TS-AD-FT
200-45-02-1~5	320	110	35	Hardwood	0.234	200	45	0.41	15.49	14.04	15.20	16.05	15.50	15.26	4.89	TS-FT-FD

Note: TS = Timber splitting; AD = Adhesive failure; FD= FRP Delamination; FR= FRP Rupture; FT = Failure at timber-adhesive interface (very thin layer of timber attached)

refers to the failure within the FRP adherent near the surface in which a thin layer of the FRP resin matrix is transferred from the adherent and remained on the adhesive. FRP rupture (FR) is referred to failure of FRP in unbonded area in which only FRP failed due to high level of applied load whilst no failure occurred in the interface or timber. Adhesive failure (AD), Figure 4-2 (a and b), is referred to the failure that purely occurred in adhesive in which partial or entire adhesive split. Timber-adhesive interface failure (FT), Figure 4-2 (a), is referred to as failure in which a very small amount of timber fibre is peeled off. Whilst no FRP rupture (FR), Figure 4-2 (c), was reported in the current section, timber splitting (TS), Figure 4-2 (b and d), was the main failure in the experiments that was observed in all tested joints. This failure mode was even more evident in case of LVL due to its lower tensile strength. For hardwood timber joints, due to the higher tensile strength of hardwood timber compared to LVL, only a very thin layer of timber was observed to be attached to the FRP after failure. Although adhesive failure (AD) was recorded among the failure modes in some samples, this failure mode was not common and rarely occurred. It should be noted that the percentage of the attached adhesive to timber or FRP was less than 10 percent of the bond area where adhesive failure was seen.

One of the most common problems associated with the use the externally bonded FRP sheets is debonding which limits the full utilisation of the material strength of the FRP (Khelifa and Celzard 2014; Wu and Hemdan 2005). Debonding failures generally occur in the timber fibres, since the adhesive itself rarely fails due to its high characteristic strength (Chen and Teng 2001). Therefore, except the FRP rupture, all of the above failure modes can be related to the debonding of interface. Debonding initiation was generally unstable and propagated rapidly in the samples made from hardwood; however, samples made from LVL failed gradually. Photographs

of all tested samples showing the failure mode of the externally bonded FRP is given in Appendices J and K.

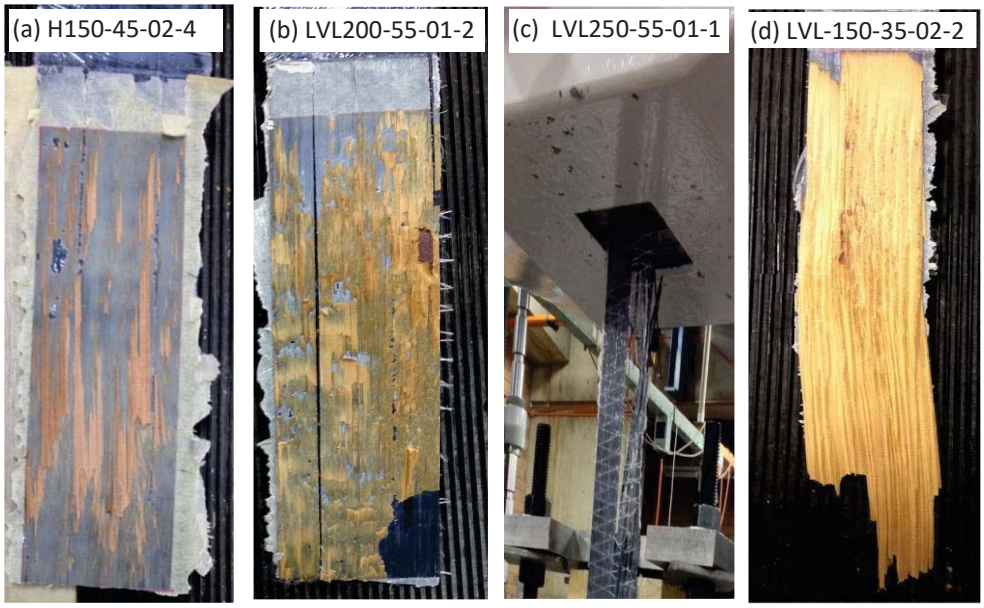

Figure 4-2 Failure modes; TS: timber splitting (b,d); AD: adhesive delamination (a,b); FD: FRP delamination (b); FR: FRP rupture (c); FT: failure at timber-adhesive interface (a)

4.2.2. Load-slip response, strain and stress distributions

Figure 4-3 shows bond slip behaviour of selected samples made from LVL and hardwood with identical bond geometry. Since the slip is measured by a modified test set-up at the loaded end side, the slip here refers to the global relative displacement between FRP and timber. During the first stage of loading, increase in the load is accompanied with a slight increase in the slip and the load-slip curves is linear. With a continuous increase in the applied load, the response becomes non-linear up to ultimate load and then the slip becomes plateau near a constant load. This trend denotes that the debonding has been occurred in the interface. Therefore, the ultimate load that can be carried by the interface is attained and simultaneously, the effective bond zone shifts away from the loaded end to the free end of the FRP. Therefore, the ultimate load (*Pu*) remains almost constant. As can be seen in Figure 4-3, the bond slip in specimen fabricated from LVL is higher than that of samples made from hardwood for identical

loads. Such observations can be attributed to the difference in stiffness of the timber. The elastic modulus of hardwood was approximately 1.22 times higher than that of LVL (as explained in Chapter 3), which results in a higher stiffness in the bond. A larger slip is evident from the relatively constant load level (refer to Appendices D and E) in the samples made from LVL. On the other hands, in samples made from hardwood, when the ultimate load is being reached there is not a distinct load-slip plateau. The joints then failed suddenly in a brittle manner. The ductile and brittle behaviour can be defined as; if the joint has no strength after failure, the failure mode is brittle; however, if the joint after failure experiences a load capacity approximately equal to the load at failure, the failure mode is ductile (Kirkegaard et al. 2011). One reason for brittle failure mode can be higher tensile strength of hardwood. The other reason can be related to the inability of the epoxy to penetrate properly into the timber fibre due to higher density of hardwood (Wan 2014); density of hardwood used herein was 1.25 higher than LVL (refer to Chapter 3).

Figure 4-4 shows the strain distribution profiles along bonded length at various load level for the two samples considered in Figure 4-3. There is a bilinear tendency in the strain distribution with a transition point occurring at the limit of the initial transfer area. The bilinear trend in strain distribution is different from the theoretical relationship between the FRP sheet strain and the distance from the loaded end (Shen et al. 2015) since it is expected to have a linear descending trend towards free end for completely homogeneous material. This phenomenon may be due to material heterogeneity or stress concentration in the FRP plate and timber at a meso-scale. The other reason for such observation can be due to propagation of the debonding between FRP and timber and possible bending of the plate (Dai et al. 2006; Xu et al. 2015).

In the majority of samples, the maximum strain in the samples made from LVL was higher than the maximum strain in the joints made from Hardwood; even though joints with LVL failed at lower load. This observation can be related to the elastic modulus and stiffness of timber. Due to lower stiffness and modulus of elasticity of LVL more ductile tendency with higher strain can be expected in the interface resulting in a higher shear stress in the bond at failure. This finding is consistence with the results reported in studies conducted by Talukdar (2008) and Wan (2014) in which FRP sheets was bonded to hardwood and softwood. It is also notable to mention that such observation in strain distribution has been achieved when FRP was bonded to concrete (Dai et al. 2005; Lu et al. 2005a; Shen et al. 2015; Yao et al. 2005; Zhou et al. 2010) in which the maximum strain was reported in joint made with concrete with lower modulus of elasticity and stiffness. The other potential reason for this observation can be related to the impregnation of the epoxy into the timber. Hardwoods are more difficult to bond than softwoods because of their higher densities (Hollaway and Teng 2008) leading to a more brittle failure mode with little timber attached to the debonded FRP.

Results of samples with bond length 150 mm showed that the strain gauges near the far end of bond experience quite minimal strain values in LVL samples; whilst high strain was recorded for samples made from hardwood at similar point. This phenomenon signifies that the effective bond length (effective bond length has been explained in Section 4.5) in joints made from hardwood is longer than joints made from LVL due to higher tensile strength of hardwood, and as such the ultimate load that can be carried by the interface is attained in the LVL series. In contrast, the hardwood series can still carry out higher load level; however, due to insufficient bond length the strain at the free end experiences high value and then joints failed before the peak load attained.

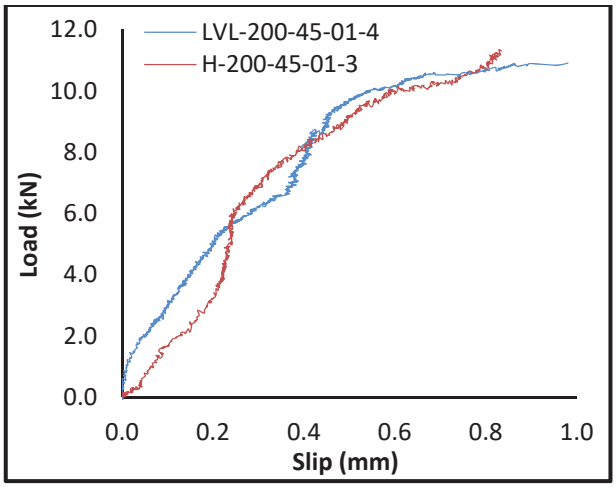

Figure 4-3 Load-slip response related to timber type series

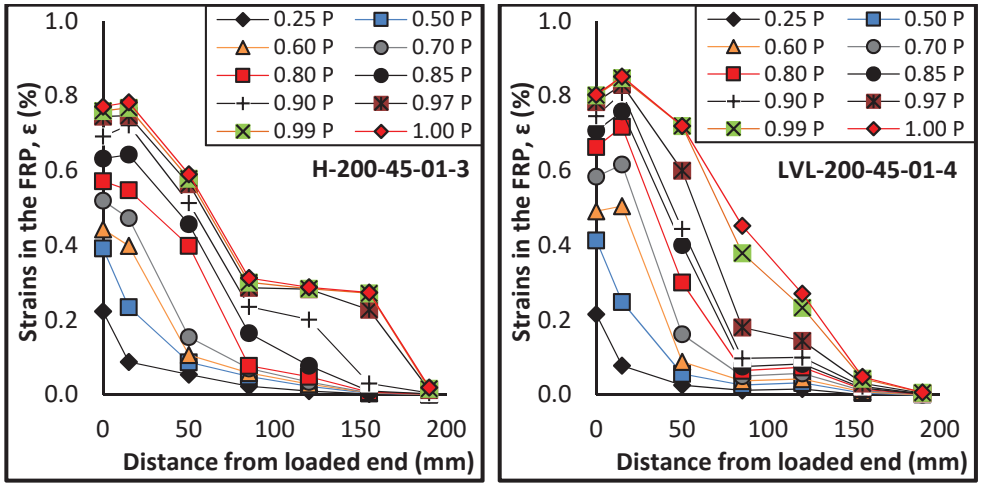

Figure 4-4 Relationship between FRP strain and distance from the loaded end related to timber type series

The average shear stress between two consecutive gauge positions and thus the shear stress distribution can be determined as follows (Bizindavyi and Neale 1999):

$$\tau_{i-j} = \frac{t_f \times E_f \times (\varepsilon_i - \varepsilon_j)}{\Delta l_{i-j}} \qquad (4\text{-}1)$$

In Eq. (4-1), ε_i and ε_j are two strain gauges at positions *i* and *j*, and Δl_{i-j} is the distance between these two gauges. E_f and t_f are elastic modulus and thickness of the laminate, respectively. Proceeding in this way for all gauge positions, the selected results of the distribution of bond stress along the

interface shown in Figure 4-5 and 4-6. As can be seen from Figure 4-5, when the load is first applied, the bond stresses are higher at the loaded end of the FRP and decrease along the bonded length to zero. However, with the increase in applied load, the peak bond stress is observed to move along the length of the plate signifying debonding propagation along interface.

Figure 4-6 illustrates the evaluation of shear stress in different parts of the bond as a function of the relative load for two samples when 1 ply of FRP with 200 mm bond length and 45 mm bond width was bonded to LVL and hardwood. The interfacial bond stress in the region near the bearing end reaches a peak (*Pu*) and then begins to decrease abruptly, while simultaneously the shear stress in the adjacent region is beginning to increase. The decrease of the shear stress signifies failure in one region, while ascending shear stress in the adjacent region indicates that the load is being transferred there and accordingly the effective bond zone is being shifted inward along the bond length and away from the loaded end of the FRP. This phenomenon was consistently observed such that the region of high stress transferred from one area to the adjacent area until total bond failure occurred.

Whilst higher ultimate load capacity was achieved for samples made from hardwood, Figures 4-5 and 4-6 show that shear stress in the samples made from LVL was higher than that of samples made from Hardwood. Moreover, when the ultimate load was achieved, shear stress near the far end of bond experiences relatively high values in the samples made from hardwood; in contrast, such values are nearly zero in LVL series as shown in Figure 4-5. This observation can be attributed to the stiffness of the bond and dissimilar interfacial material properties, since the joint made from LVL has lower modulus of elasticity which results lower stiffness of the interface. Therefore, in the LVL series, higher strain can be expected in the

interface resulting in a higher shear stress in the interface. Thus, higher shear stress can be achieved for samples made from LVL.

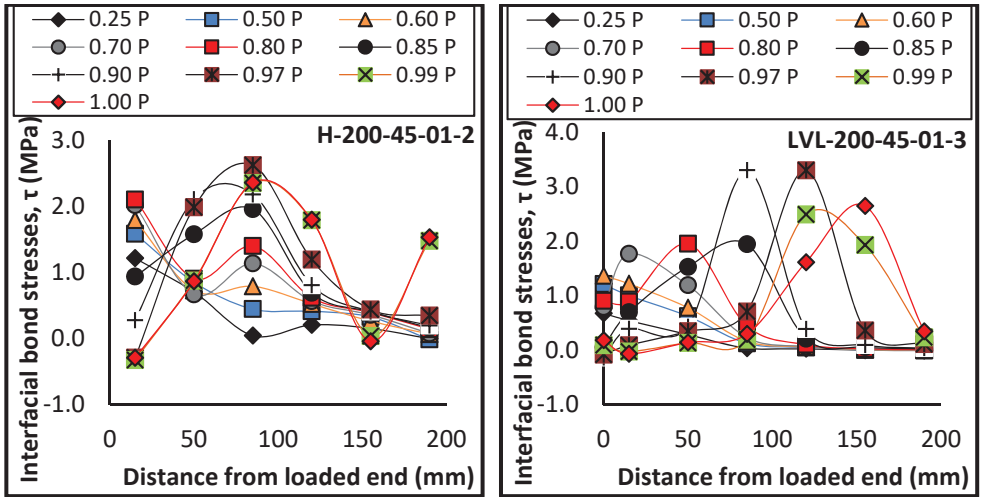

Figure 4-5 Relationship between bond stress and distance from the loaded end related to LVL and Hardwood used

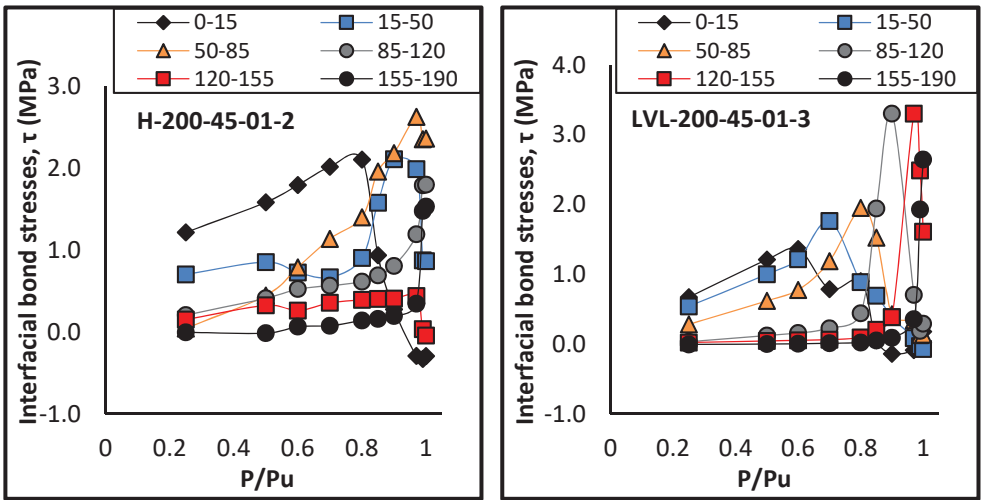

Figure 4-6 Shear stress as function of relative load level related to LVL and Hardwood used

4.2.3. Bond strength relationship

The tensile and compressive strength of the hardwood timber used in the present study were similar; while LVL samples are stronger in compression. The average ratio of tensile to compression strength of hardwood and LVL was 1.04 (67.53 MPa / 64.93 MPa) and 0.79 (44.31 MPa / 56.26 MPa), respectively. Results of tested samples showed that higher ultimate loads were recorded for samples made from hardwood compared to samples

made from LVL, as shown in Figure 4-7. It is noted that all bond characteristics in samples shown in Figure 4-7 are identical, except the timber type. As can be seen, in all bond lengths, the ultimate load of samples made from hardwood exhibited approximately 6.5% to 8.5% higher load compared with the same samples made from LVL.

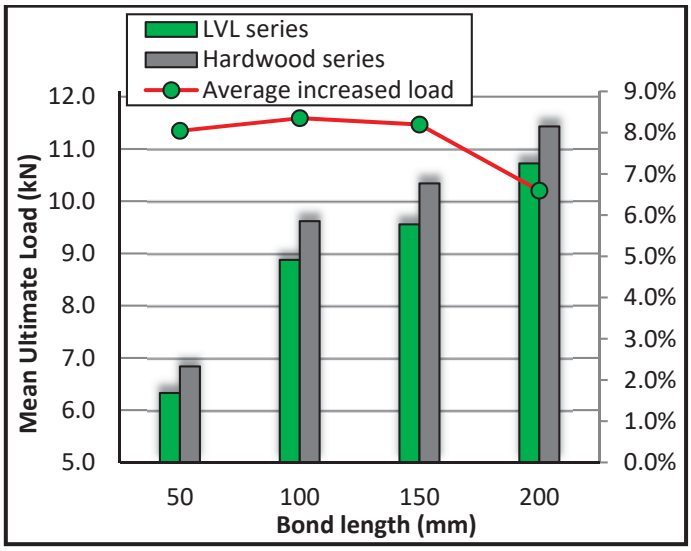

Figure 4-7 Relationship between ultimate applied load and timber type

4.2.4. Concluding remarks

Timber density impacts the test results; timbers with higher density, e.g. hardwood, have higher joint strength as opposed to timbers with lower density such as LVL used. This is due to higher bond strength arising from higher density and elastic modulus of timber. It was observed that with increase of timber tensile strength, modulus of elasticity and stiffness, the interfacial pull-out force increases whilst the interfacial slip decreases during the softening-debonded stage. Furthermore, samples made from hardwood failed suddenly in a brittle manner; whilst joints made from LVL exhibited more ductile behaviour. The ductile behaviour of the joints was more distinguished where the bond length was relatively long. In addition, it was observed that shear stress in the samples fabricated from LVL was higher than that of samples made from hardwood due to lower elastic

modulus that results lower stiffness of the interface, and consequently leading to higher strain and stress in the interface.

4.3. Effect of bond width

In this section, results of LVL series, in which three different bond width (35 mm, 45 mm, and 55 mm) were tested, are used to discuss the effect of bond width and FRP-to-timber width ratio on the bond strength, bond stress and the local slip of externally bonded FRP-to-timber interface. The FRP-to-timber width ratio for these three bond widths were 32%, 41% and 50%, respectively. Results of 73 joints (Table 4-2) are compared and selected data and graphs shown in this section. Graphs for all samples are given in Appendices B – I.

4.3.1. Behaviour and failure modes

Timber splitting (TS) and failure at timber-adhesive interface (FT) were observed predominately in the majority of experiments categorised in this section. In some samples, one layer of LVL (around 3 mm) was attached to the FRP when failure occurred. FRP delamination (FD) as well as adhesive failure (AD) were observed in a few samples in which very small amount of adhesive was attached to timber or FRP. When the bond width increased from 35 mm to 45 mm, no significant changes in failure mode was observed. However, in the samples where the bond width was 55 mm (FRP-to-timber width ratio was 50%) and bond length was 250 mm, FRP rupture occurred. The FRP rupture in progress is shown in Figure 4-8. As can be seen, such failure initially occurred approximately between bonded end of the joint and the grip starting from one side of FRP and then propagated towards the other side of the bond.

Table 4-2 Results of bond width series tests

Identification	Timber				FRP			b_f / b_t	Pu (kN)							Failure modes
									Individual					Average	CoV	
	L_t (mm)	b_t (mm)	d_t (mm)	type	t_f (mm)	L_f (mm)	B_f (mm)								(%)	
50-35-01-1~5	320	110	65	LVL	0.117	50	35	0.32	5.33	4.92	5.62	5.57	4.93	5.27	6.41	TS-FT
100-35-01-1~5	320	110	65	LVL	0.117	100	35	0.32	6.35	6.71	6.83	7.02	5.57	6.50	8.80	TS-FT-FD-AD
150-35-01-1~5	320	110	65	LVL	0.117	150	35	0.32	7.86	7.27	8.03	7.32	7.78	7.66	4.44	TS-AD-FT-FR
200-35-01-1~5	320	110	65	LVL	0.117	200	35	0.32	8.25	7.12	8.70	8.75	6.90	7.94	11.08	TS-FT-FR-FD
50-45-01-1~5	320	110	65	LVL	0.117	50	45	0.41	5.52	5.99	6.09	6.42	6.81	6.17	7.83	TS-FT
100-45-01-1~5	320	110	65	LVL	0.117	100	45	0.41	9.07	10.74	7.87	8.89	7.80	8.88	13.41	TS-FT
150-45-01-1~5	320	110	65	LVL	0.117	150	45	0.41	9.48	9.83	10.15	8.77	13.18	10.28	16.51	TS-AD-FT-FD
200-45-01-1~5	320	110	65	LVL	0.117	200	45	0.41	10.88	10.90	11.13	11.02	9.69	10.72	5.49	TS-AD-FT-FD
50-55-01-1~5	320	110	65	LVL	0.117	50	55	0.50	8.05	9.47	9.00	11.14	10.07	9.55	12.13	TS-FT-FD-AD
100-55-01-1~5	320	110	65	LVL	0.117	100	55	0.50	9.12	12.50	11.94	13.67	12.31	11.91	14.18	TS-FT-FD-FR-AD
150-55-01-1~5	320	110	65	LVL	0.117	150	55	0.50	14.48	14.90	15.42	13.08	12.66	14.11	8.40	TS-AD-FD-FT
200-55-01-1~5	320	110	65	LVL	0.117	200	55	0.50	14.60	14.91	15.74	15.32	14.67	15.05	3.18	TS-FT-FD-FR-AD
250-55-01-1-3	370	110	65	LVL	0.117	250	55	0.50	15.32	15.22	15.11	--	--	15.21	0.70	TS-AD-FT-FR
150-35-02-1~5	320	110	65	LVL	0.234	150	35	0.32	12.15	10.99	11.80	11.14	11.29	11.47	4.22	TS-FT
150-45-02-1~5	320	110	65	LVL	0.234	150	45	0.41	16.61	13.44	16.75	11.46	12.89	14.23	16.51	TS-FT
150-55-02-1~5	320	110	65	LVL	0.234	150	55	0.50	16.72	15.65	15.85	17.22	19.04	16.90	8.04	TS-AD-FT-FD

Note: TS= Timber splitting; AD= Adhesive failure; FD= FRP Delamination; FR= FRP Rupture; FT = Failure at timber-adhesive interface (very thin layer of timber attached

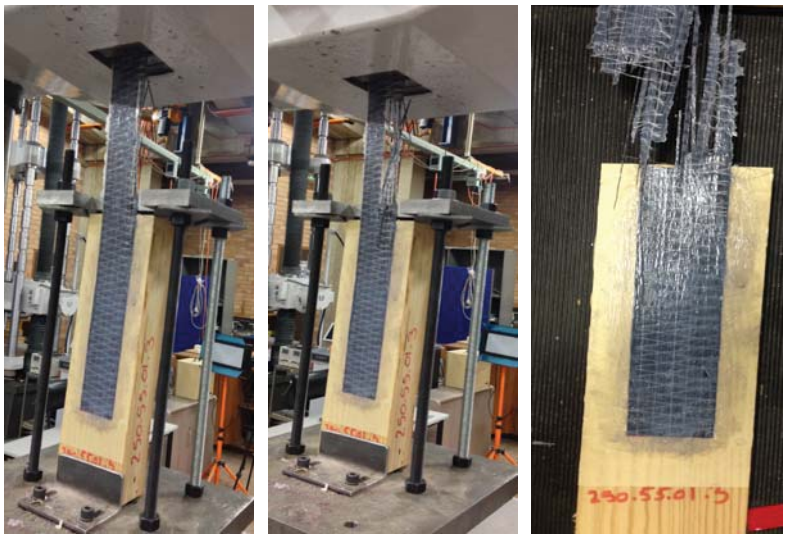
Figure 4-8 FRP rupture in progress

As listed in Table 4-2, only three samples were tested where the bond width and bond length were 55 mm and 250 mm. In these samples, the strain gauges were only attached to one of the samples. Therefore, no strain was recorded in the samples shown in Figure 4-8. It is important to note that, complete or partial FRP ruptures occurred in samples with 55 mm bond width in which 95% or more of the FRP ultimate tensile strength was reached. The minimum and mean tensile strength of FRP were determined to be 2349 MPa and 2497 MPa, respectively (Chapter 3, Section 3.4.2). The recorded tensile stress was around 2200 MPa in the samples where their bond width was 55 mm with the bond length equal or longer than 150 mm. Such tensile stress is relatively close to the ultimate stress of FRP; therefore, complete or partial FRP rupture can be expected in such samples.

4.3.2. Load-slip response, strain and stress distributions

The slip between timber prism and the FRP was measured with a LVDT mounted on the surface of timber block. Figure 4-9 shows typical load versus slip curves along bonded length for FRP with 35 mm, 45 mm and 55 mm width. The bond lengths of the selected samples shown in Figure 4-9 are 150 mm and 200 mm. Complete results are shown in Appendices D and

E. In the majority of tests, it was observed that samples with wider FRP sheet exhibited higher slope in the initial elastic deformation. The slip increased linearly when the applied load was relatively low. Such observation indicates that there is no interfacial softening or debonding along the interface. However, when the failure occurs at the FRP-to-timber interface, there is a rapid increase in slip with increasing applied load and then slip tends to plateau until failure. At the same load level, the slip is lower for samples with higher FRP-to-timber width ratio and the ultimate interfacial slip at the bonded joint decreased when wider FRP is bonded to the timber. As can be seen from Figure 4-9, when the samples with 35 mm bond width reached their ultimate load and slip, samples with 55 mm bond width are still in the elastic state and slip is increasing linearly. Figure 4-10 shows interfacial bond stress versus slip curves along bonded length for FRP-to-timber width ratio 32%, 41% and 50% and various bond lengths. Figure 4-10 (b) for instance shows that, when the bond stress was around 1.5 MPa, the average slips of 0.88 mm, 0.76 mm and 0.64 mm were recorded for samples where the FRP widths are 35 mm, 45 mm and 55 mm, respectively. Similar trend observed in the other tested series is shown in Figure 4-10 (a and c). This phenomenon can be attributed to distribution of load over a larger area of the bond. When FRP-to-timber width ratio is large enough, a larger area of the bond is active, and the stress distributes more uniformly across the width of timber leading to fail the interface at higher load level.

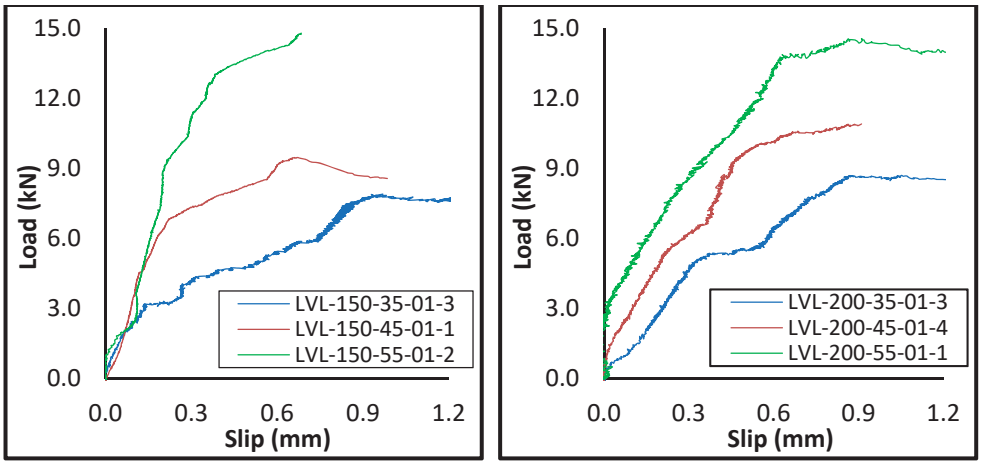

Figure 4-9 Load-slip response related to FRP width series

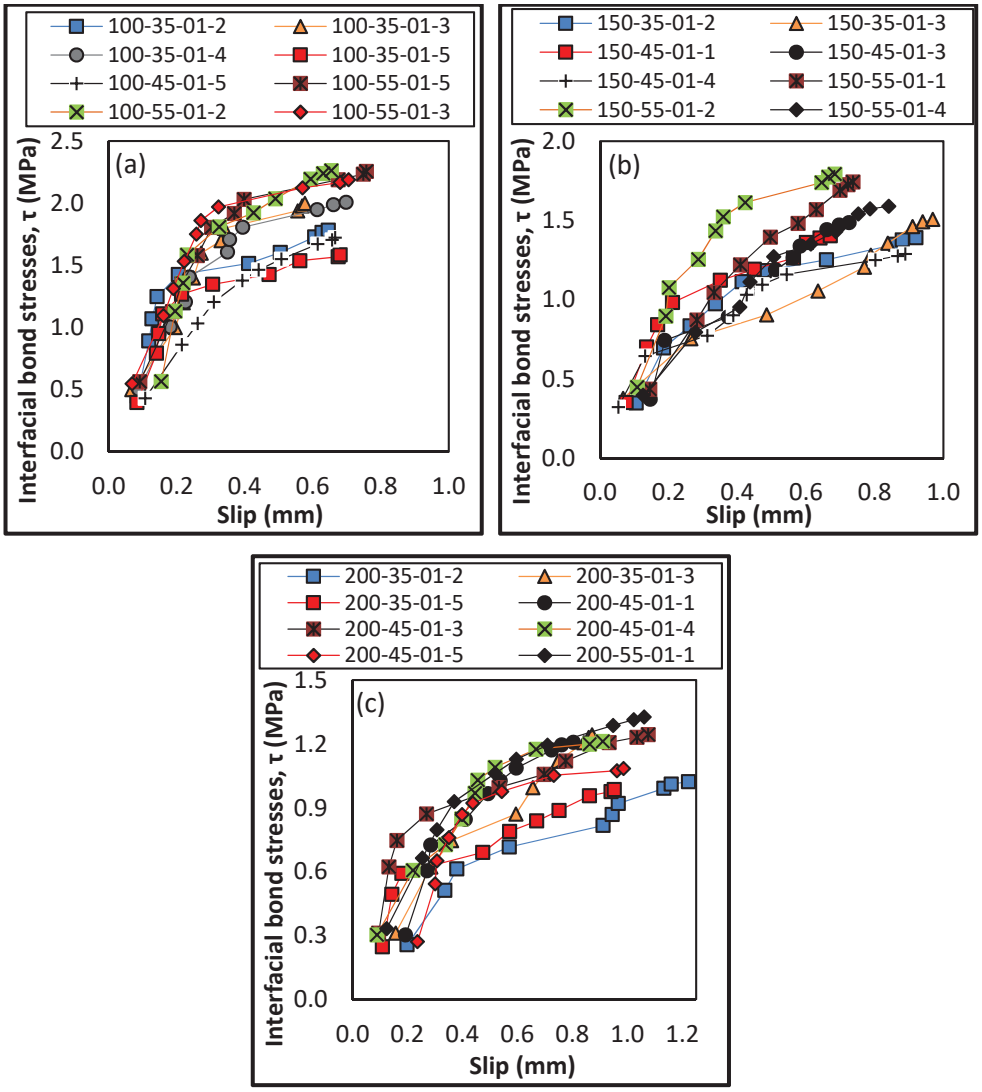

Figure 4-10 Relationship between shear stress and local slip related to bond width series

The strain distribution profile along the bonded length for selected samples are shown in Figure 4-11. Almost all of test results showed that the strains at failure for different bond widths with identical bond length, were approximately similar. However, it is important to emphasise that samples with wider bond width failed at higher load level. Table 4-2 for instance shows that, when the bond length was 200 mm, the ultimate loads with the average values of 7.94 kN, 10.92 kN, and 15.05 kN were achieved for samples with the bond widths of 35 mm, 45 mm and 55 mm, respectively. This finding represents that the strain of interface decreases with the increase of FRP plate width which leads to decreased shear stress between FRP and timber and consequently increase the bond strength.

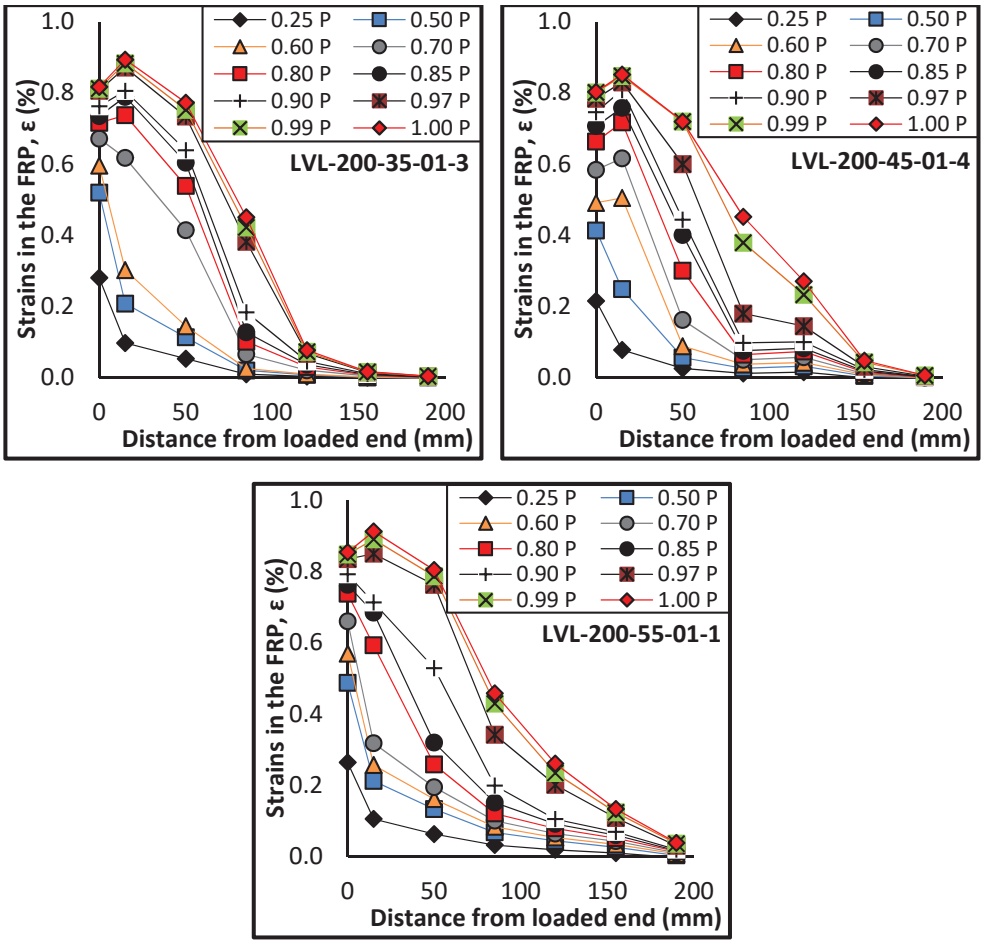

Figure 4-11 Relationship between FRP strain and distance from the loaded end related to bond width series

Figures 4-12 and 4-13 show shear stress along the FRP-timber interface at various load level for different bond width for selected samples. Complete diagrams for strain and stress distribution profiles can be found in Appendices B - I. In the majority of samples, it was observed that the maximum shear stress decreases with the increase in FRP-to-timber width ratio as can be seen in Figures 4-12 and 4-13 where timber type and all bond characteristics for the shown samples were identical except bond width. When FRP-to-timber width ratio is low, the force transfers from the FRP to timber leads to a non-uniform stress distribution across the width of timber leading to failure of the interface at lower load level. Furthermore, a smaller FRP width compared to the timber width may result in a higher stress in the bond at failure; directing stress from bonded area to the timber outside of the bonded zone. The distribution of the maximum shear stress and strain in the timber beneath the FRP plate along the transverse direction can be expected to be more uniform with the increase of FRP plate width.

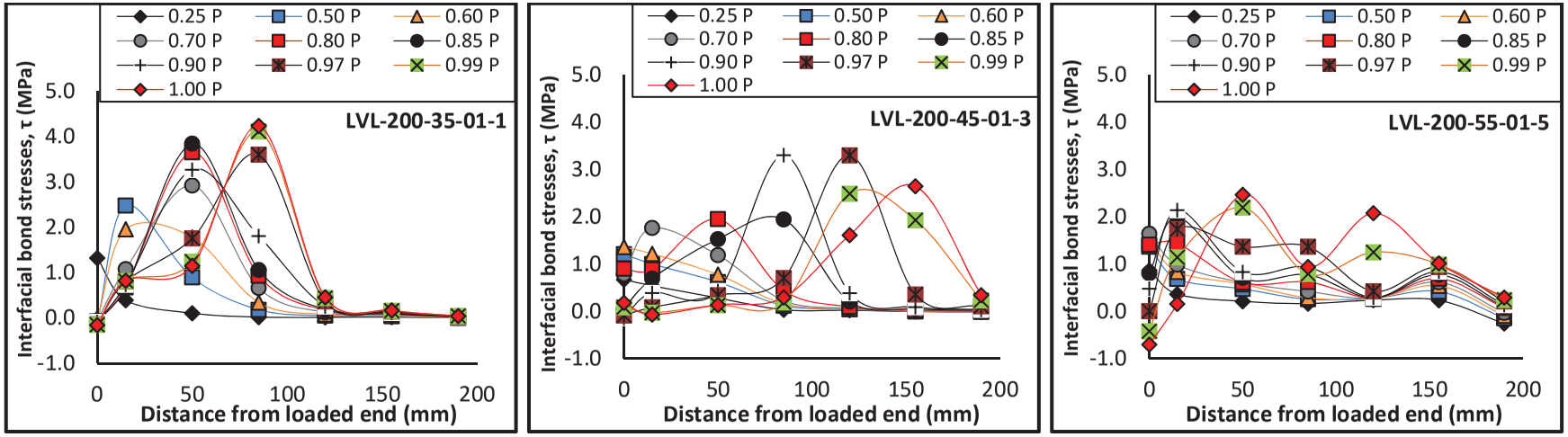

Figure 4-12 Relationship between bond stress and FRP-to-timber width ratio

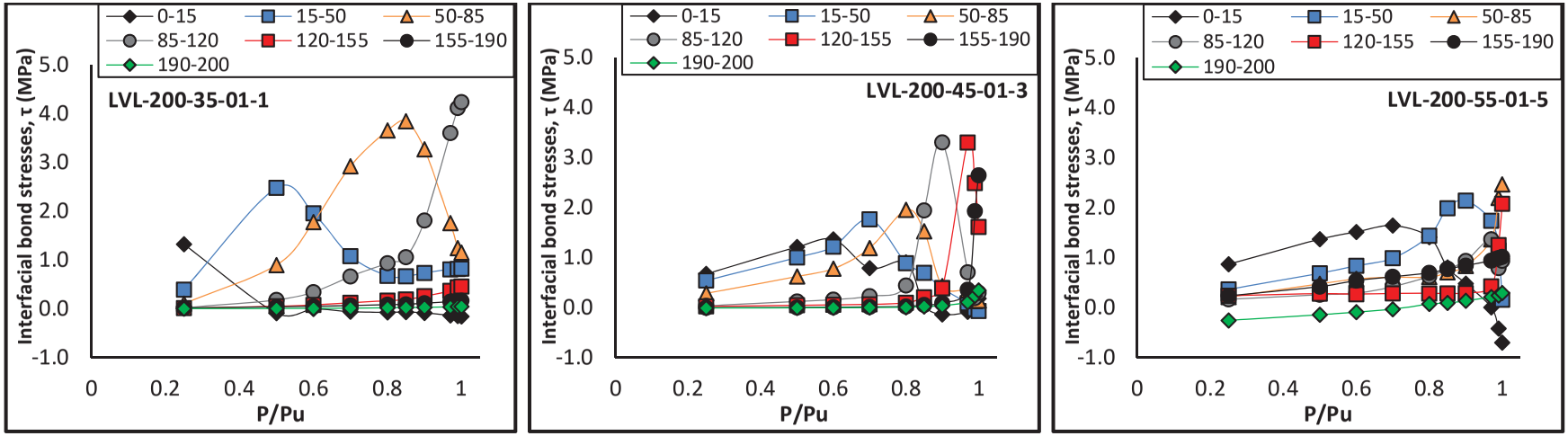

Figure 4-13 Shear stress as function of relative load level related to FRP width series

4.3.3. Bond strength relationship

The relationship between bond strength and bond width is discussed in this section. It is notable to mention that samples with different bond widths (35 mm, 45 mm, and 55 mm) when the other parameters (e.g. bond length, FRP layers and timber type) were identical have been investigated and compared together. Results of the tests showed that the interfacial pull-out force and accordingly bond strength increases with the increase of the FRP plate width. Figure 4-14 shows the average load of five samples in each series under various bond widths and bond lengths. As can be seen in Figure 4-14, for various bond lengths (50 mm, 100 mm, 150 mm and 200 mm), the greater the width of FRP plate, the higher interfacial bond strength of FRP-to-timber. However, this difference is more noticeable for samples with higher FRP-to-timber with ratio (50%). It can be seen that the ultimate load increased by around two times when the bond width increased from 35mm to 55mm for all bond lengths. This is because when FRP width is lower than timber prism, the FRP-timber interface is subjected to higher stress concentration, especially at the edges of FRP. Thus, increasing bond width not only increases the area of the bond interface but also allows the load to be distributed over a larger area resulting in reduced stress concentration. The bond strength of samples shown in Figure 4-14 illustrated that when the bond width is constant and the bond length increase from 150 mm to 200 mm, the bond strength remains almost unchanged. This condition signifies the concept of effective bond length that there is no benefit in extending the bond length beyond that where there is no increase in the bond strength. Therefore, although increasing bond length increases the area of bond interface, bond strength cannot increase further once the bond length exceeds the effective bond length. The effective bond length will be explained in detail in section 4.5.

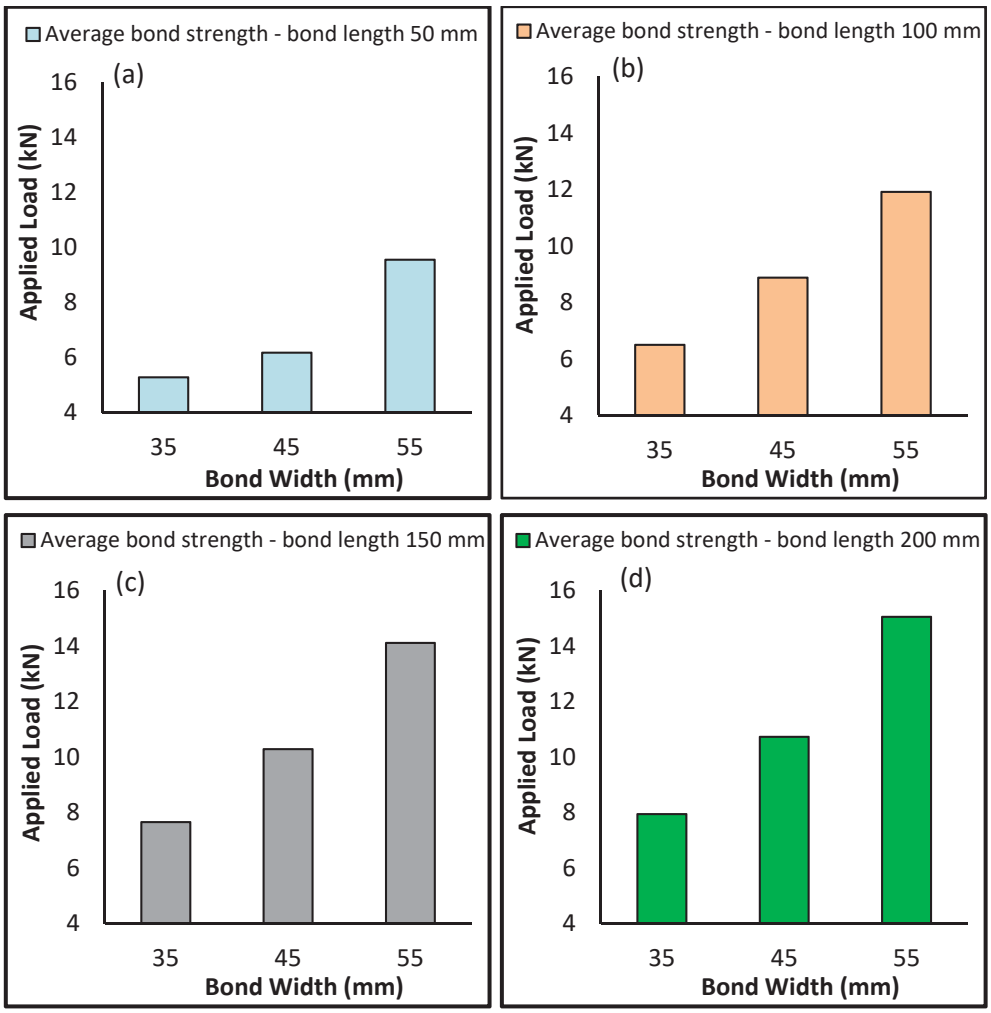

Figure 4-14, Recorded average bond strength for 35 mm, 45 mm and 55 mm bond widths for bond length (a) 50 mm, (b) 100 mm, (c) 150 mm and (d) 200 mm.

4.3.4. Concluding remarks

Results of experimental tests showed that the bond width significantly affects the bond strength such that with the increase of the FRP plate width, the bond strength increases, and interface reaches higher level of load. The bond strength doubled when the FRP width increased from 35 mm to 55 mm. Conversely, at the same level of applied load, experimental results illustrated that the local slip decreased during the softening-debonded stage when wider FRP bonded to timber. That is because the interface has a higher effective bonded area that leads to more uniform stress distribution across the width of the FRP. In addition, the maximum

bond stress decreased with the increase of FRP-to-timber width ratio due to more uniform stress distribution in the interface and reduction of stress concentration.

4.4. Effect of number of FRP layers

In this section, the effect of FRP layers on the interface behaviour is discussed based on samples with one and two plies of FRP. Nominal thickness of the single ply FRP was 0.117 mm. The bond width in the samples made from hardwood was 45 mm, whilst this parameter in the majority of samples made from LVL was 35 mm. Hundred six samples (Table 4-3) are compared herein and selected data and graphs are shown in this section.

4.4.1. Behaviour and failure modes

Almost all of samples made either from hardwood or LVL exhibited timber splitting (TS), and failure at timber-adhesive interface (TF). The joints made from LVL either with one or two layers of FRP failed in more ductile behaviour, especially for higher FRP-to-timber width ratio. However, unstable and brittle failure was observed for joints with hardwood. The brittle failure of joints was more common when two layers of FRP were bonded to the hardwood. This observation was mainly due to higher tensile strength and stiffness of hardwood. FRP delamination (FD) and adhesive failure (AD) were rarely observed in the sample made from hardwood; however, LVL series exhibited mixture of different failure modes and partial FRP rupture (FR) were only observed in the LVL series. When FRP delamination was observed, a very small amount of fibre was peeled off from the laminate. The number of FRP layers did not have a significant impact on the failure mode; however, brittle failure was mostly observed for samples with two layers of FRP. The last column of Table 4-3 summarises failure modes of samples investigated in this series.

Table 4-3 Results of FRP layers series tests

Identification	Timber				FRP			b_f / b_t	Pu (kN)							Failure modes
									Individual					Average	CoV	
	L_t (mm)	b_t (mm)	d_t (mm)	type	t_f (mm)	L_f (mm)	B_f (mm)								(%)	
50-35-01-1~5	320	110	65	LVL	0.117	50	35	0.32	5.33	4.92	5.62	5.57	4.93	5.27	6.41	TS-FT
100-35-01-1~5	320	110	65	LVL	0.117	100	35	0.32	6.35	6.71	6.83	7.02	5.57	6.50	8.80	TS-FT-FD-AD
150-35-01-1~5	320	110	65	LVL	0.117	150	35	0.32	7.86	7.27	8.03	7.32	7.78	7.66	4.44	TS-AD-FT-FR
200-35-01-1~5	320	110	65	LVL	0.117	200	35	0.32	8.25	7.12	8.70	8.75	6.90	7.94	11.08	TS-AD-FT-FR
50-35-02-1~5	320	110	65	LVL	0.234	50	35	0.32	7.00	8.81	8.95	7.00	7.17	7.78	12.88	TS-FT-AD
100-35-02-1~5	320	110	65	LVL	0.234	100	35	0.32	9.66	9.61	8.45	10.20	8.44	9.27	8.52	TS-FT-AD
150-35-02-1~5	320	110	65	LVL	0.234	150	35	0.32	12.15	10.99	11.80	11.14	11.29	11.47	4.22	TS-FT
200-35-02-1~5	320	110	65	LVL	0.234	200	35	0.32	13.57	10.34	12.21	12.32	10.66	11.82	11.19	TS-AD-FT-AD
150-45-01-1~5	320	110	65	LVL	0.117	150	45	0.41	9.48	9.83	10.15	8.77	13.18	10.28	16.51	TS-FT-FD-AD
150-45-02-1~5	320	110	65	LVL	0.234	150	45	0.41	16.61	13.44	16.75	11.46	12.89	14.23	16.51	TS-FT
150-55-01-1~5	320	110	65	LVL	0.117	150	55	0.50	14.48	14.90	15.42	13.08	12.66	14.11	8.40	TS-AD-FT-FR
150-55-02-1~5	320	110	65	LVL	0.234	150	55	0.50	16.72	15.65	15.85	17.22	19.04	16.90	8.04	TS-FT-FD-AD
250-55-01-1~3	370	110	65	LVL	0.117	250	55	0.50	15.32	15.22	15.11			15.21	0.70	TS-AD-FT-FR
250-55-02-1~3	370	110	65	LVL	0.234	250	55	0.50	19.16	20.10	20.40			19.88	3.27	TS-FT-FD
50-45-01-1~5	320	110	35	Hardwood	0.117	50	45	0.41	6.97	6.87	5.92	6.34	8.09	6.84	11.95	TS-FT
100-45-01-1~5	320	110	35	Hardwood	0.117	100	45	0.41	8.83	9.55	11.24	9.20	9.27	9.62	9.81	TS-FT-FD
150-45-01-1~5	320	110	35	Hardwood	0.117	150	45	0.41	11.32	8.82	11.24	9.91	10.41	10.34	10.01	TS-FT-FD
200-45-01-1~5	320	110	35	Hardwood	0.117	200	45	0.41	9.63	10.87	11.39	12.03	10.76	10.94	8.13	TS-FT
50-45-02-1~5	320	110	35	Hardwood	0.234	50	45	0.41	7.81	9.16	7.66	7.28	8.56	8.09	9.35	TS-FT
100-45-02-1~5	320	110	35	Hardwood	0.234	100	45	0.41	11.56	10.81	11.28	13.18	10.15	11.39	9.92	TS-FT
150-45-02-1~5	320	110	35	Hardwood	0.234	150	45	0.41	14.22	13.53	16.13	13.97	12.89	14.15	8.60	TS-AD-FT
200-45-02-1~5	320	110	35	Hardwood	0.234	200	45	0.41	15.49	14.04	15.20	16.05	15.50	15.26	4.89	TS-FT-FD

Note: TS= Timber splitting; AD= Adhesive failure; FD= FRP Delamination; FR= FRP Rupture; FT = Failure at timber-adhesive interface (very thin layer of timber attached)

4.4.2. Load-slip response, strain and stress distributions

Two different bond thicknesses were tested using one and two layers of FRP. Figure 4-15 shows the load versus slip at the loaded end for selected samples. In almost all of samples, it was observed that the load-slip plot had a similar pattern when one and two layers of FRP were bonded either to LVL or hardwood and the load-slip relationship was reasonably linear prior to the initiation of failure/debonding and exhibited a nonlinear behaviour afterwards. However, the ratio of ultimate load for identical samples with two and one layer of FRP was approximately 1.5. In addition, with the increase of FRP layers, the global slip corresponding to the ultimate load decreased. Such finding distinctly indicates that with more number of FRP plies, the load carrying capacity increases but the interface fails in more brittle manner. Thus, it can be concluded that when strength criteria are essential to be met for strengthening of timber structures, increase in the FRP layers may lead to higher load carrying capacity; however, such increase proportional to the increase in FRP layers.

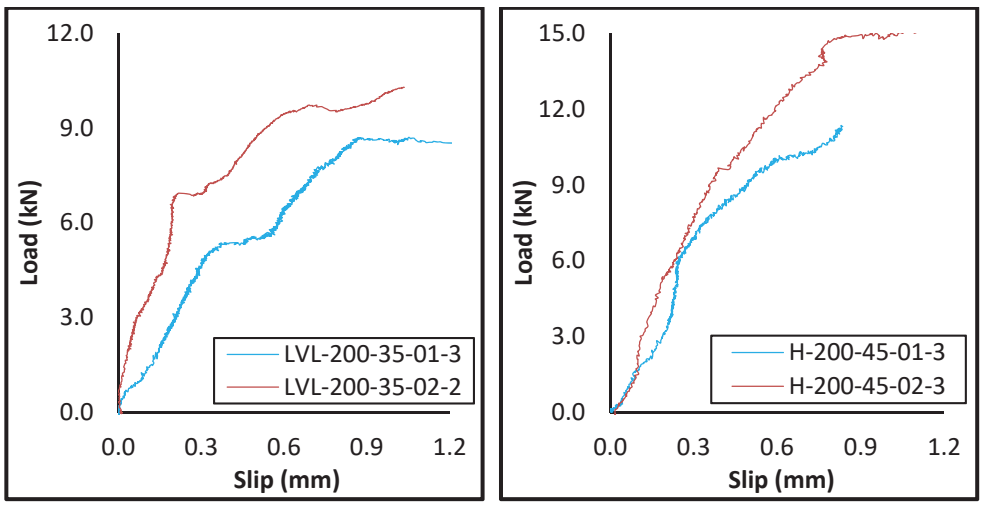

Figure 4-15 Load-slip response related to FRP layers series

For further investigation, the strain distribution profile and shear stress along interface are studied when one and two layers of FRP were bonded to the timber (Figure 4-16). The maximum strain occurred at the loaded end, indicating that most of the applied load is carried by the FRP near the

loaded end and when the bond length was long enough, strain gauges close to the free end exhibited a small amount of strain even at the final stages of loading. Maximum strain in samples with one and two plies of FRP was quite similar, although the applied load in thicker interfaces was around 50% higher than thinner interfaces. The main reason for this behaviour of interface can be explained based on strain distribution profile (Figure 4-16), which shows that the effective bonded length for samples with thicker FRP is longer i.e. the load is transferred over a larger shear area.

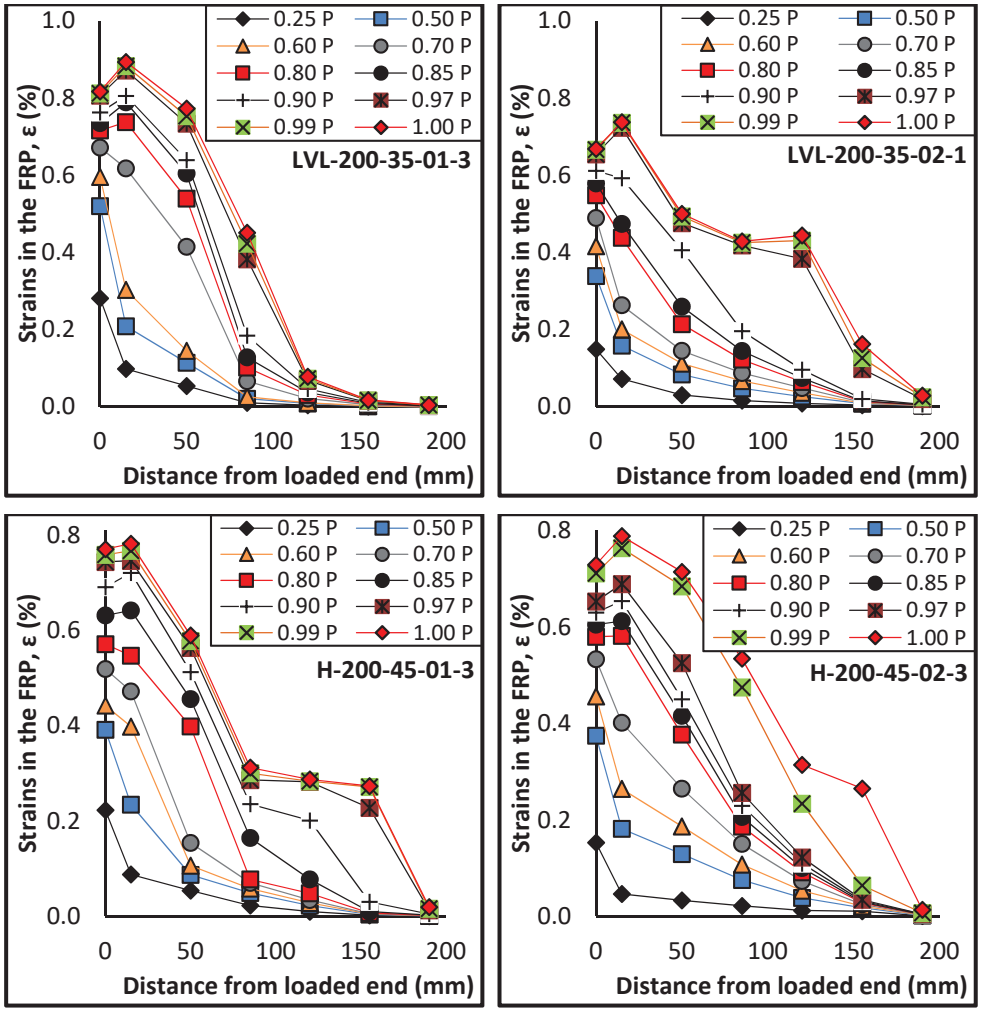

Figure 4-16 Relationship between FRP strain and distance from the loaded end related to FRP layers series

Figure 4-17 shows the interfacial bond stress between two consecutive gauges calculated using Eq. (4-1). Whilst the samples with two layers of FRP

failed at much higher load compared to samples with one layer of FRP, distribution of the interfacial bond stress over a larger area because of longer effective bond length means that the stress is only marginally higher for samples with two layers FRP. Additionally, while the stiffness ($E_f.t_f$) of the interface doubled for the thicker application, it can be expected that a larger and deeper surface of the bond gets involved in the interfacial stress transfer, and thus the stress distributes more uniformly along the interface. Therefore, the interface fails at a higher load level. Similar observation has been found in the studies conducted by Chen and Teng (2001) and Hollaway and Teng (2008) on FRP to concrete bond.

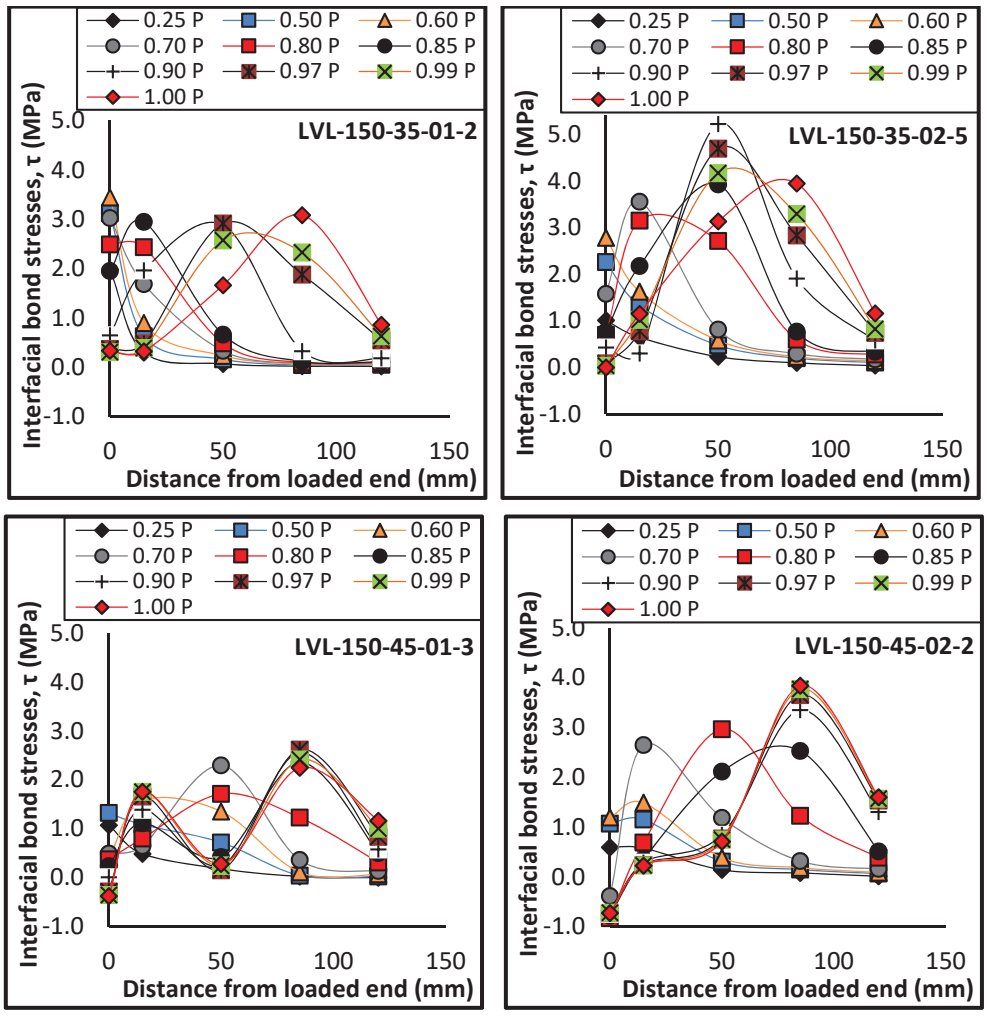

Figure 4-17 Relationship between bond stress and distance from the loaded end related to FRP layers series

4.4.3. Bond strength relationship

The relationship between bond strength, ultimate interfacial pull-out force and number of FRP layers obtained from the experiments is shown in Figures 4-18 and 4-19. The bond strength of interface improved by adding layers of FRP. It can be seen that, samples with two layers of FRP exhibited 43 % to 50 % higher load than samples where only one ply of FRP was bonded to the LVL. The ultimate load increased by 18% when number of FRP layers was doubled for the joints made from hardwood with relatively shorter bond length. On the other hand, the ultimate pull-out force increased between 40 % to 42 % when two layers of FRP with bond length equal or longer than effective bond length were bonded to the surface of hardwood. The main reason for dissimilar enhancement of bond strength when more layers of FRP was attached to hardwood can be expressed as: due to more density of hardwood and accordingly differences in the fibre/cellular structure between hardwood and softwood, when the bond length is not long enough, the applied load is not able to be efficiently distributed along the interface. Therefore, failure occurs at a lower load level. However, LVL showed more efficient compatibility with the adhesive and FRP in which constant increase was observed in the bond strength when FRP layers increased. It is important to state that the concept of optimum FRP layers need to be considered in studying the interfacial behaviour of FRP-to-timber joints. That is because, when the number of FRP layers increase, more adhesive needs to be used accordingly. Therefore, the risk of flaws in the adhesive is higher which may lead stress concentrations in the interface. In addition, adhesives are designed to cure in thin layer, and application of thick layers can change physical properties of the epoxy when epoxy cured. From the chemical point of view, the more adhesive used the more polymerisation shrinkage and thus, internal stress. It is important to mentioned that in the present study thickness of adhesive was not used neither in analysis of experimental results nor analytical

model. In the present study thickness of bond refers to number of FRP layers bonded to the timber.

Figure 4-19 illustrates the relationship between FRP layers and bond strength obtained from experimental tests, where the bond length was constant, 150 mm, and bond width varied. When of the number of FRP layers was changed from one to two, the strength enhancement was found to increase but the enhancement also depended upon factors such as FRP-to-timber width ratio. For example, the bond strength increased by 50% between one and two layers of FRP for samples with 35 mm bond width. but such enhancement was approximately 40% and 20%, for the samples with 45 mm and 55 mm bond width, respectively. The main reason can be defined as when FRP width is relatively narrower than width of timber, increase on FRP layers leads to further increase in the effective bond length which results enhancement of effective bonded area. When one layer of FRP with 35 mm bond width was bonded to LVL, the average effective bond length was measured as 126 mm. However, the average effective bond length increased to 137 mm when two layers of FRP were bonded to the surface of LVL. Therefore, more efficient use of interface can be expected to be achieved leading to further improvement of bond strength. However, when the bond length was 150 mm and FRP 55 mm were bonded to the LVL, increasing thickness of FRP mostly improved the stiffness of interface and had an insignificant impact on the effective bonded zone, since the effective bond length was already reached even when one layer of FRP was used. Therefore, the bond strength increased by 20%.

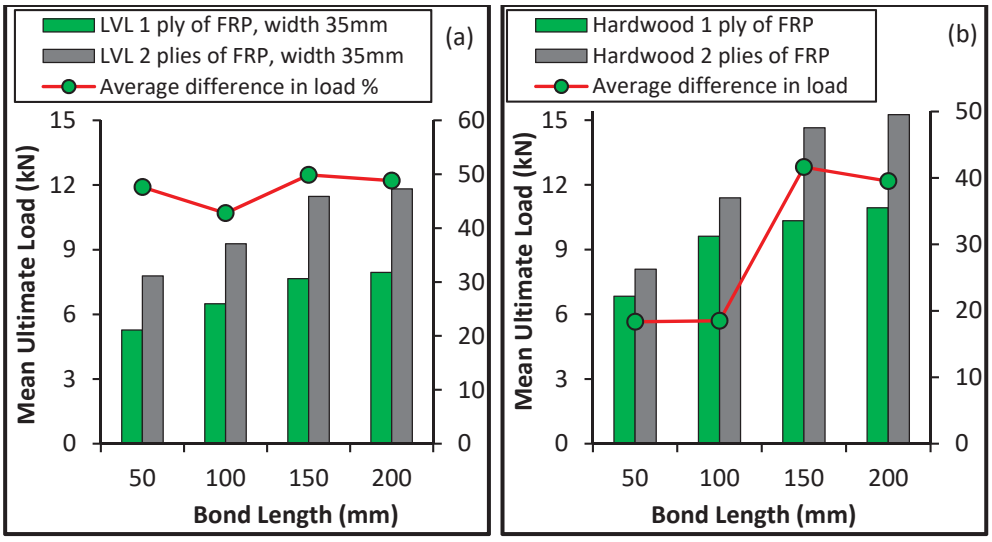

Figure 4-18 Relationship between bond strength and FRP layers; (a) LVL samples (b) hardwood samples

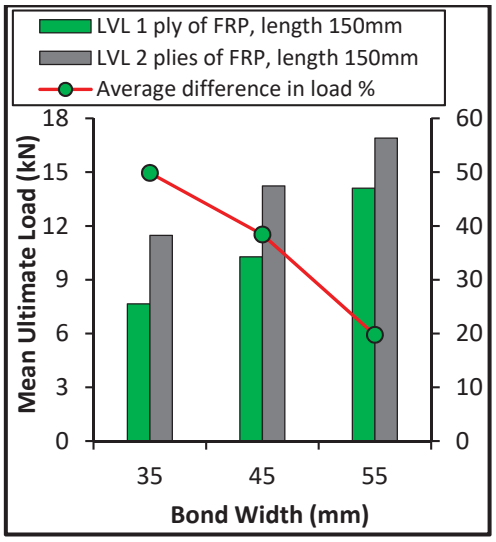

Figure 4-19 Relationship between bond strength and FRP layers for different bond widths

4.4.4. Concluding remarks

Experimental results showed when the bond length is equal or longer than the effective bond length, by adding extra layer of FRP, the effective bond length increases which results enhancement of effective bonded area. Thus, the interfacial bond stress distributes more uniformly over a larger and deeper surface of the bond. The maximum shear stress also increases by increase in FRP layers; however, such increase may not be proportional with the increase in the number of FRP layers. Furthermore, by using more

FRP layers the stiffness of bond increases which leads to decrease the slip of interface. Therefore, further increase in the FRP layers leads to obtain higher bond strength. Consequently, more efficient use of the interface can be obtained by adding extra layers of FRP. However, when strength criteria govern the design for the strengthening of timber structures, increase in FRP layers lead to higher load carrying capacity. Higher thickness leads to more brittle failure due to stress concentration at the corners of the join, such that, thinner interface may be more appropriate when a ductile behaviour is expected from the FRP-strengthened system.

4.5. Effect of bond length

This section represents the effect of bond length and accordingly effective bond length on the interface. Many experimental studies (Bizindavyi and Neale 1999; Coronado 2006; Franco and Royer Carfagni 2014; Yao et al. 2005) and fracture mechanics analyses (Yuan and Wu 1999; Yuan et al. 2001) have confirmed that there is no benefit in extending the bond length beyond that where there is no increase in the bond strength. Such bond length so-called as effective bond length. To accurately obtain an effective bond length, resistance strain gauges were bonded to the surface of FRP along the bond length and then, the effective bond length was defined as the distance between the points that the strain decays from the maximum to the zero value. One strain gauge was placed at the unbonded zone of the FRP, and other strain gauges were distributed on the centre-line of FRP along the bond length. The number of strain gauges varied between three to eight depending bond length.

This section covers results of all samples (Table 4-4). Samples with both timber types, LVL and hardwood, and one and two layers of FRP are discussed in this section. In the LVL series, four different bond lengths namely 50 mm, 100 mm, 150 mm and 200 mm with bond width of 35 mm,

45 mm and 55 mm were utilised. An additional bond length (250 mm) was also used for samples with bond width of 55 mm. The hardwood samples contained bond lengths of 50 mm, 100 mm, 150 mm and 200 mm with a constant bond width (45 mm).

Table 4-4 Results of bond length series tests

Identification	Timber				FRP			b_f / b_t	Pu (kN)							Failure modes
	L_t (mm)	b_t (mm)	d_t (mm)	type	t_f (mm)	L_f (mm)	B_f (mm)		Individual					Average	CoV (%)	
50-35-01-1~5	320	110	65	LVL	0.117	50	35	0.32	5.33	4.92	5.62	5.57	4.93	5.27	6.41	TS-FT
100-35-01-1~5	320	110	65	LVL	0.117	100	35	0.32	6.35	6.71	6.83	7.02	5.57	6.50	8.80	TS-FT-FD-AD
150-35-01-1~5	320	110	65	LVL	0.117	150	35	0.32	7.86	7.27	8.03	7.32	7.78	7.66	4.44	TS-FT-FR-AD
200-35-01-1~5	320	110	65	LVL	0.117	200	35	0.32	8.25	7.12	8.70	8.75	6.90	7.94	11.08	TS-FT-FD-FR
50-45-01-1~5	320	110	65	LVL	0.117	50	45	0.41	5.52	5.99	6.09	6.42	6.81	6.17	7.83	TS-FT
100-45-01-1~5	320	110	65	LVL	0.117	100	45	0.41	9.07	10.74	7.87	8.89	7.80	8.88	13.41	TS-FT
150-45-01-1~5	320	110	65	LVL	0.117	150	45	0.41	9.48	9.83	10.15	8.77	13.18	10.28	16.51	TS-FT-FD-AD
200-45-01-1~5	320	110	65	LVL	0.117	200	45	0.41	10.88	10.90	11.13	11.02	9.69	10.72	5.49	TS-FT-FD
50-55-01-1~5	320	110	65	LVL	0.117	50	55	0.50	8.05	9.47	9.00	11.14	10.07	9.55	12.13	TS-AD-FT
100-55-01-1~5	320	110	65	LVL	0.117	100	55	0.50	9.12	12.50	11.94	13.67	12.31	11.91	14.18	TS-FT-FD-AD-FR
150-55-01-1~5	320	110	65	LVL	0.117	150	55	0.50	14.48	14.90	15.42	13.08	12.66	14.11	8.40	TS-FT-FD-AD-FR
200-55-01-1~5	320	110	65	LVL	0.117	200	55	0.50	14.60	14.91	15.74	15.32	14.67	15.05	3.18	TS-FT-FD-AD
250-55-01-1~3	370	110	65	LVL	0.117	250	55	0.50	15.32	15.22	15.11			15.21	0.70	TS-FT-FR-AD
50-35-02-1~5	320	110	65	LVL	0.234	50	35	0.32	7.00	8.81	8.95	7.00	7.17	7.78	12.88	TS-AD-FT
100-35-02-1~5	320	110	65	LVL	0.234	100	35	0.32	9.66	9.61	8.45	10.20	8.44	9.27	8.52	TS-AD-FT
150-35-02-1~5	320	110	65	LVL	0.234	150	35	0.32	12.15	10.99	11.80	11.14	11.29	11.47	4.22	TS-FT
200-35-02-1~5	320	110	65	LVL	0.234	200	35	0.32	13.57	10.34	12.21	12.32	10.66	11.82	11.19	TS-AD-FT
150-45-02-1~5	320	110	65	LVL	0.234	150	45	0.41	16.61	13.44	16.75	11.46	12.89	14.23	16.51	TS-FT
150-55-02-1~5	320	110	65	LVL	0.234	150	55	0.50	16.72	15.65	15.85	17.22	19.04	16.90	8.04	TS-AD-FT
250-55-02-1~3	370	110	65	LVL	0.234	250	55	0.50	19.16	20.10	20.40			19.88	3.27	TS-FT-FD
50-45-01-1~5	320	110	35	Hardwood	0.117	50	45	0.41	6.97	6.87	5.92	6.34	8.09	6.84	11.95	TS-FT
100-45-01-1~5	320	110	35	Hardwood	0.117	100	45	0.41	8.83	9.55	11.24	9.20	9.27	9.62	9.81	TS-FT-FD
150-45-01-1~5	320	110	35	Hardwood	0.117	150	45	0.41	11.32	8.82	11.24	9.91	10.41	10.34	10.01	TS-FT-FD
200-45-01-1~5	320	110	35	Hardwood	0.117	200	45	0.41	9.63	10.87	11.39	12.03	10.76	10.94	8.13	TS-FT
50-45-02-1~5	320	110	35	Hardwood	0.234	50	45	0.41	7.81	9.16	7.66	7.28	8.56	8.09	9.35	TS-FT
100-45-02-1~5	320	110	35	Hardwood	0.234	100	45	0.41	11.56	10.81	11.28	13.18	10.15	11.39	9.92	TS-FT
150-45-02-1~5	320	110	35	Hardwood	0.234	150	45	0.41	14.22	13.53	16.13	13.97	12.89	14.15	8.60	TS-AD-FT
200-45-02-1~5	320	110	35	Hardwood	0.234	200	45	0.41	15.49	14.04	15.20	16.05	15.50	15.26	4.89	TS-FT-FD

Note: TS= Timber splitting; AD= Adhesive failure; FD= FRP Delamination; FR= FRP Rupture; FT = Failure at timber-adhesive interface

4.5.1. Behaviour and failure modes

Whilst timber splitting (TS) and timber-adhesive interface failure (FT) were observed in samples made from hardwood, FRP and adhesive failure (FT) rarely occurred and no full FRP rupture (FR) was recorded. However, brittle failure occurred in majority of samples which was more prominent when two layers of FRP were bonded to the timber.

In the LVL series, a mix of all failure modes were recorded as listed in the last column of Table 4-4. As explained in section 4.2.1. , very small amount of adhesive was attached to LVL or FRP where adhesive failure occurred. Timber splitting (TS) and timber-adhesive interface (FT) failure were recorded in almost all of samples made from LVL. Adhesive failure (AD) was mostly observed when the bond length was around or longer than effective bond length. A couple of partial FRP rupture occurred during joint tests as listed in Table 4-4; however, complete FRP rupture was only recorded when 1 ply of FRP with 250 mm bond length and 55 mm bond width was bonded to LVL.

4.5.2. Load-slip response, strain and stress distributions

Figure 4-20 shows representative load-slip curves of samples with bond length of 150 mm and 200 mm for two types of timber. Load-slip curves for all tested samples are given in Appendices D and E. The load-slip responses illustrated in Figure 4-20 represent different trends in the interface behaviour. The initial part of the response is predominantly linear. However, after initiation of debonding, the slope of the curve becomes lower (closer to the horizontal). The presence of the plateau in the response indicates that the effective bond length of the interface has been reached and the ultimate strength of interface has been achieved. In each series, when the bond length was very short the increase in the load is accompanied with a slight increase in the slip. Further increase in the load

leads to complete failure of the interface. Thus, the load-slip curves show almost linear behaviour. Further increase in the bond length enhanced the bond strength; however, as the bond length was still relatively short compared to the effective bond length, the stress may not be transferred from FRP to the substrate. In this situation, the failure occurs before the maximum load is being reached, and accordingly the ultimate strength of interface cannot be expected to be attained. Accordingly, debonding initiates and rapidly propagates towards free end and the slip experiences a bilinear tendency. On the other hand, when the bond length was equal to or longer than the effective bond length; the interface exhibited peak load, and accordingly, the slip between timber and FRP was increased. In samples with relatively longer bond length, the load-slip relationship was reasonably linear prior to the initiation of debonding and an almost flat shape was ultimately formed afterwards. The constant portion of load-slip was mostly observed when LVL was the substrate of the joint, in contrast, the constant load-slip was rarely recorded for the joints made from hardwood. This finding is due to shorter effective bond length in LVL series. Therefore, after initiation of debonding the remaining portion of the bond length allows for further transfer of load along interface. Accordingly, whilst the applied load is almost constant, further increase in slip can be expected being occurred. In contrast, due to longer effective bond length in hardwood series, whilst the applied load is increasing which leads to further increase in the slip, the applied load is not able to be efficiently distributed along the interface resulting a rapid failure in the interface.

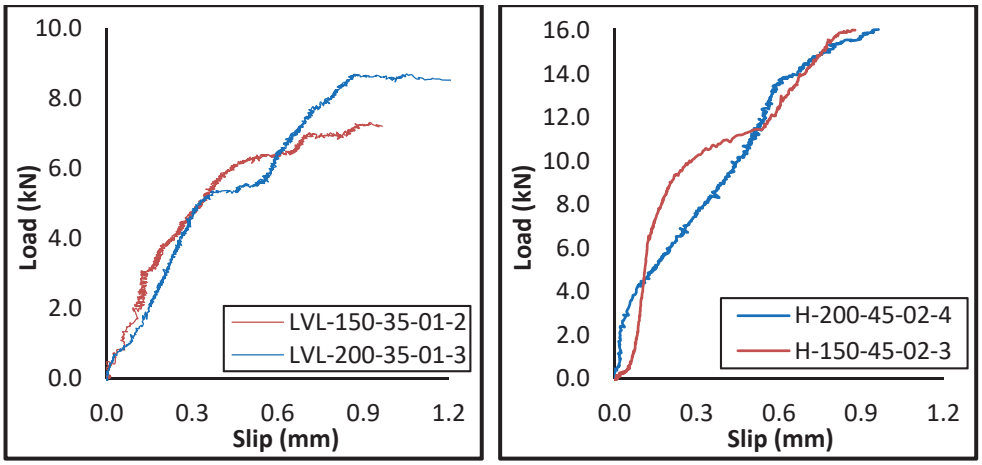

Figure 4-20 Load-slip response related to bond length series

Figure 4-21 shows the strain distribution profiles along bonded length at various load levels for 1-ply and 2 plies FRP-to-timber joints. Strain on point zero refers to the strain in the unbonded area. When the bond length is relatively short (e.g. 50 mm and 100 mm), the strain decreases linearly from the loaded end of the joint to the unloaded end. Further increase in the load leads to complete failure of interface at much lower FRP strains than its ultimate strain. On the other hand, when the bond length is sufficiently long (Figure 4-21 b, d, e and f), three distinct profile stages can be identified from these strain distribution diagrams, based on the level of applied loads. At low load levels, the strain distribution exhibited a linear descending shape towards the end of the bond. This linear downward pattern represents that the entire length of the interface is in an elastic stress state and only part of the interface is stressed.

The second trend shows that the strain increased gradually between strain gauges 2 and 4 until crack initiated in the interface. In the majority of samples, it was observed that the maximum load associated with this strain distribution occurred approximately at 60% to 65% of the ultimate applied load, depending on bond geometries. This observation is more evident when the bond length was equal or longer than effective bond length as shown in Figure 4-21 (b, d and f). The distance from loaded end to the

point where the strain profile reaches zero defines the so-called initial transfer length. Once a crack is formed, the effective bond zone propagates from the loaded end toward the unloaded end and a further increase in strain distribution was observed until the applied loading P reached ultimate load P_u.

In the third trend, as shown in Figure 4-21, there is a bilinear tendency in the strain distribution with a transition point occurring at the limit of the initial transfer area. In the majority of samples tested herein, this transition point generally coincided with approximately 75% of the ultimate load, and in some other samples around 80% of the ultimate load was recorded. The bilinear trend in strain distribution is different from the theoretical relationship between the FRP sheet strain and the distance from the loaded end since it is expected to be uniform for completely homogeneous material. This phenomenon may be due to material heterogeneity or stress concentration in the FRP plate and timber at a meso-scale.

Effective bond length is the length over which strain decreases from the maximum value to a zero value, as measured from the strain profile in the FRP by strain gauges. Experimental test results revealed that, interface stiffness, timber tensile strength, and FRP width directly impact on the effective bond length in which the effective bond length increased when these critical parameters are increased. Effective bond lengths extracted from strain distribution profiles are listed in Table 4-5.

As expressed earlier, interfacial bond stress can be determined using Eq. (4-1). At small loads, there is no interfacial softening or debonding along the FRP-to-timber interface, thus the entire length of the interface is in an elastic stress state. The peak value of shear stress at the elastic stage takes place at the FRP loaded end and then decrease along the bonded length tending to zero. Further increase in the applied load leads to debonding at the vicinity of the loaded end. Therefore, the bonded length is divided into

two distinct regions. One continues in an elastic state and another is a softening state, where the bond stress decreases. The maximum bond strength and accordingly maximum shear stress is attained in this stage. Nevertheless, if the bond length is not long enough, the interface may fail rapidly in which the stress at the free end remains at high value. In contrast, when the bond length is equal or longer than the effective bond length, the initiated debonding propagates along the interface by a slight increase or a constant bond stress distribution within the interface. As debonding propagates, the peak shear stress moves towards the unloaded end of the bonded FRP. Figure 4-22 illustrates an example of such observation. Although bond strength cannot increase further once the bond length exceeds the effective bond length, a longer bond length can improve the ductility of the interface. As shown in Figure 4-22, the bond stress at the vicinity of free end is close to zero when the bonded length exceeds effective bond length.

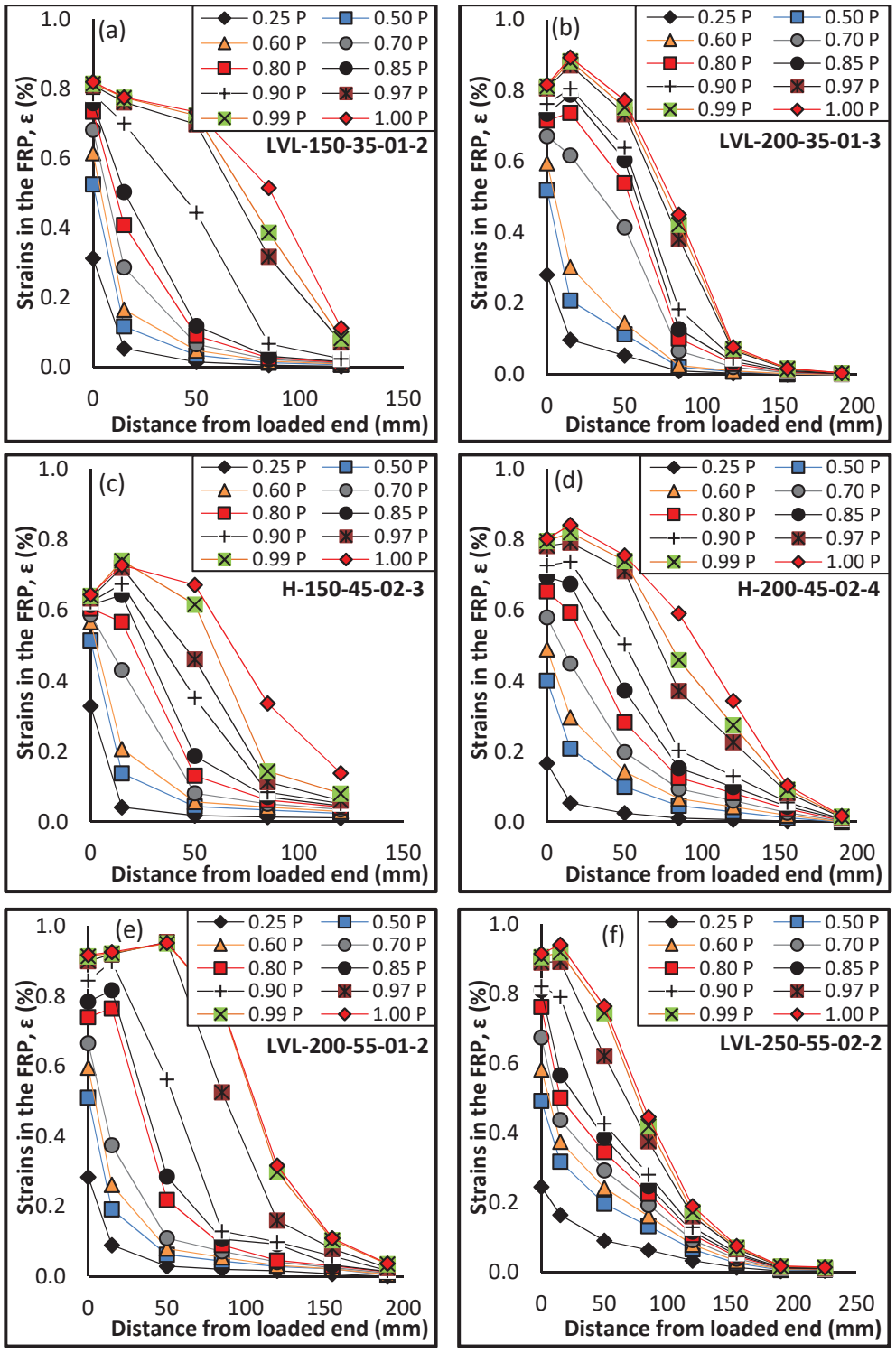

Figure 4-21 Relationship between FRP strain and distance from the loaded end related to bond length series

Table 4-5 Measured effective bond length

Identification	Effective bond length (mm)	Identification	Effective bond length (mm)	Identification	Effective bond length (mm)	Identification	Effective bond length (mm)
LVL 50-35-01-1~5	>50	LVL 150-45-01-4	132	LVL 200-35-01-5	136	H 100-45-02-1~5	>100
LVL 50-35-02-1~5	>50	LVL 150-45-01-5	136	LVL 200-35-02-1	165	H 150-45-01-1	154
LVL 50-45-01-1~5	>50	LVL 150-45-02-1	151	LVL 200-35-02-2	200	H 150-45-01-2	161
LVL 50-55-01-1~5	>50	LVL 150-45-02-2	149	LVL 200-35-02-3	179	H 150-45-01-3	158
LVL 100-35-01-1~5	>100	LVL 150-45-02-3	151	LVL 200-35-02-4	149	H 150-45-01-4	157
LVL 100-35-02-1~5	>100	LVL 150-45-02-4	158	LVL 200-35-02-5	189	H 150-45-01-5	149
LVL 100-45-01-1~5	>100	LVL 150-45-02-5	150	LVL 200-45-01-1	156	H 150-45-02-1	152
LVL 100-55-01-1~5	>100	LVL 150-55-01-1	169	LVL 200-45-01-2	158	H 150-45-02-2	184
LVL 150-35-01-1	123	LVL 150-55-01-2	175	LVL 200-45-01-3	182	H 150-45-02-3	161
LVL 150-35-01-2	129	LVL 150-55-01-3	178	LVL 200-45-01-4	155	H 150-45-02-4	182
LVL 150-35-01-3	129	LVL 150-55-01-4	160	LVL 200-45-01-5	147	H 150-45-02-5	--
LVL 150-35-01-4	126	LVL 150-55-01-5	153	LVL 200-55-01-1	180	H 200-45-01-1	163
LVL 150-35-01-5	125	LVL 150-55-02-1	180	LVL 200-55-01-2	165	H 200-45-01-2	185
LVL 150-35-02-1	142	LVL 150-55-02-2	178	LVL 200-55-01-3	161	H 200-45-01-3	187
LVL 150-35-02-2	140	LVL 150-55-02-3	181	LVL 200-55-01-4	--	H 200-45-01-4	191
LVL 150-35-02-3	145	LVL 150-55-02-4	180	LVL 200-55-01-5	180	H 200-45-01-5	176
LVL 150-35-02-4	130	LVL 150-55-02-5	191	LVL 250-55-01-2	190	H 200-45-02-1	189
LVL 150-35-02-5	128	LVL 200-35-01-1	144	LVL 250-55-02-2	194	H 200-45-02-2	186
LVL 150-45-01-1	139	LVL 200-35-01-2	158	H 50-45-01-1~5	>50	H 200-45-02-3	170
LVL 150-45-01-2	136	LVL 200-35-01-3	137	H 50-45-02-1~5	>50	H 200-45-02-4	185
LVL 150-45-01-3	146	LVL 200-35-01-4	136	H 100-45-01-1~5	>100	H 200-45-02-5	189

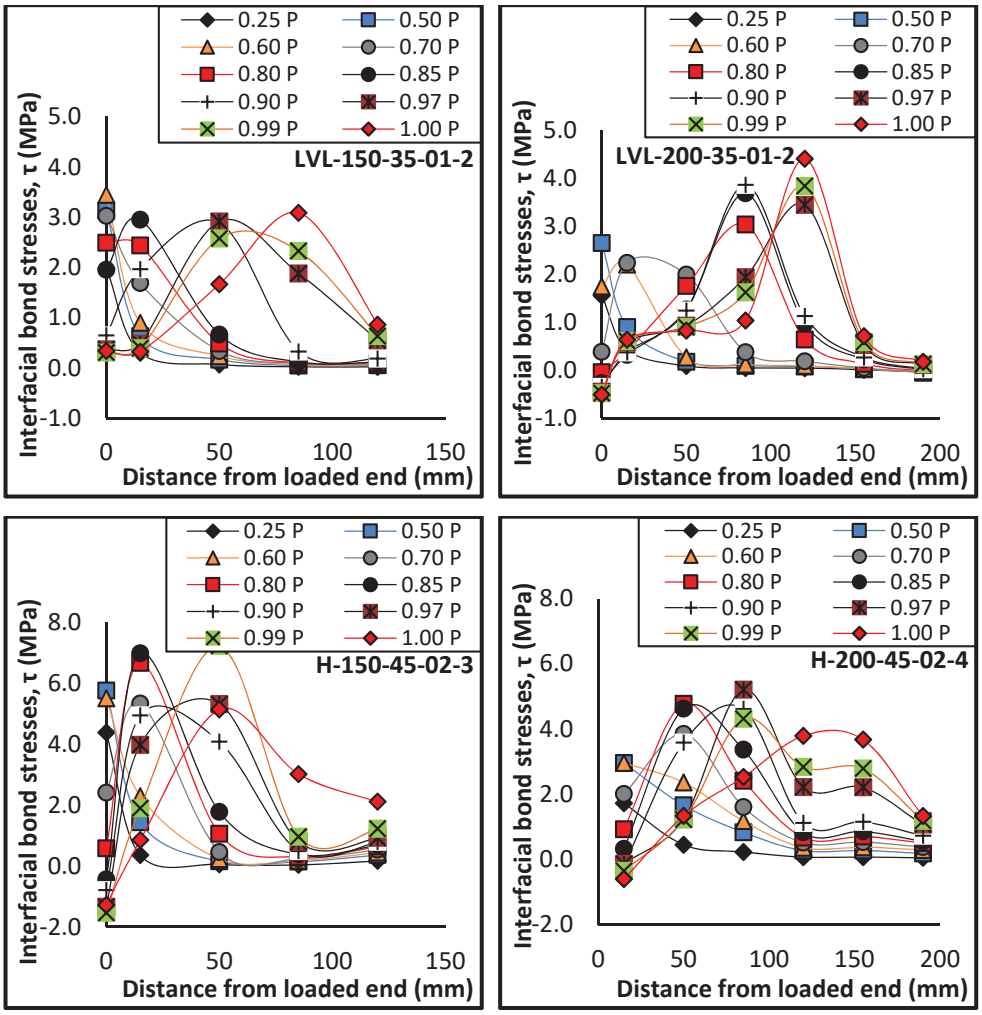

Figure 4-22 Relationship between bond stress and distance from the loaded end related to bond length series

4.5.3. Bond strength relationship

Although increasing bond length increases the area of bond interface, there is no benefit in extending the bond length beyond the effective bond length where there is no increase in the bond strength. However, when the bond length is longer than the effective bond length, the remaining portion of the bond length allows for further transfer of loads that exceeded the ultimate load leading to more ductile tendency in failure mode. As shown in Figure 4-23, the bond strength increases with increase in the bond length but once the effective bond length is reached, there is no further increment in the bond strength. Such observation was made in all series of

samples tested; however, the effective bond length varied with the type of timber and bond width and FRP layers as explained in previous sections.

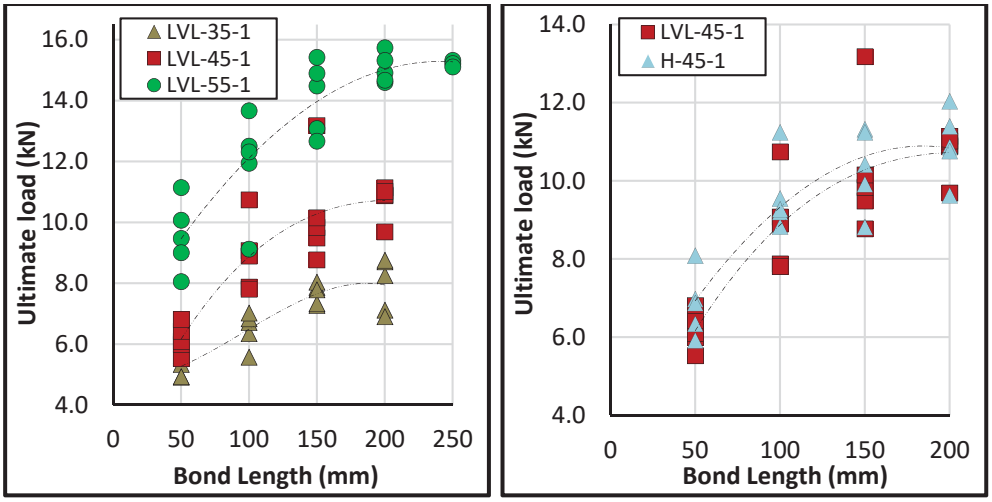

Figure 4-23 The effect of bond length on the bond strength

4.5.4. Concluding remarks

The concept of the effective bond length has been verified from the tests conducted in this study. It was observed that the bond strength increased with increase in the bond length; however, such enhancement was negligible in the samples with the bond length longer than effective bond length. It was found that number of FRP layers, timber mechanical properties, and FRP-to-timber width ratio impact on the effective bond length in which the effective bond length increases when these critical parameters are increased. Samples with longer bond length exhibited more ductile behaviour at ultimate load and failed gradually whilst brittle failure occurred in the samples with shorter bond length. Minimal interface shear stress was observed close to the free end of samples with sufficient bond length. In contrast, high interface shear stress was observed at the free end of samples where their bond length was insufficient.

4.6. Summary

Modified single lap shear tests of FRP-to-timber joints and their results have been presented in this chapter. The influence of parameters affecting bond strength and the interfacial behaviour of the adhesively bonded joints are discussed based on these results. Investigated parameters were (i) timber species, (ii) bond width, (iii) FRP layers, and (iv) bond length. The main findings from the experimental test results are summarised as:

- The main failure mode for both LVL and hardwood samples was predominately timber failure at the interface between adhesive and FRP plate. Samples made from LVL exhibited more ductile failure, conversely, hardwood samples failed in a brittle manner.
- The slip between timber and FRP was measured during the tests with a LVDT which was mounted on the surface of timber block. At an identical load level, the bond slip in specimen made from LVL was found to be higher than that of sample made from hardwood. Lower slip was exhibited to the wider bonded interface at failure. In samples with bond length equal to or longer than effective bond length, the value of ultimate slip at failure was approximately equal. At an identical load level, lower slip was obtained when more layers of FRP were bonded to the timber.
- The strain variation and shear stress of the interface derived from strain gauges which were attached to the FRP surface. The maximum strain in specimen made from LVL was higher than the maximum strain in the joints made from Hardwood. Although samples with wider bond width failed at higher load level, almost similar strain was found at failure for different bond widths. Similarly, whilst the applied load in thicker interfaces was around 50% higher than thinner interfaces, maximum strain in samples with one and two plies of FRP was approximately similar.

- It was found that, maximum shear stress decreases with the increase of FRP-to-timber width ratio due to a non-uniform stress distribution across the width of timber. Moreover, in the samples where the bond length was short, the joints failed rapidly with a high value of shear stress at the free end. Conversely, such value was near to zero at failure for the samples with longer bond length. Also, thicker interface exhibited higher ultimate shear stress during applied load. In addition, shear stress in the samples fabricated from LVL was higher than that of samples made from hardwood.
- Various effective bond length has been identified for each series of tested samples depending on timber type, bond width and interface stiffness. In samples made with LVL, the effective bond length was relatively shorter the effective bond length achieved in samples made with hardwood. In addition, samples with more layers of FRP and higher FRP-to-timber width ratio exhibited longer effective bond length.
- Results of experimental tests showed that bond width, tensile strength and modulus of elasticity of timber impact the bond strength in which the interfacial bond strength improves when these parameters increased leading to interface reaches higher level of load. It was also observed that the bond strength increases by increasing bond length; however, such enhancement was negligible in the samples with the bond length longer than effective bond length. It was also found that higher layers of FRP increase the effective bond length which results enhancement in the ultimate load carrying capacity.

Chapter 5

FRP-TO-TIMBER JOINTS: ANALYTICAL AND FINITE ELEMENT MODELS FOR INTERFACIAL BOND

5.1. Introduction

A number of methods including indirect analytical methods and/or finite element analysis have been established and developed to reduce the inconsistency of effective bond length, bond-slip relationship, shear stress and bond strength obtained from the experimental results when FPR was bonded to concrete. However, analytical solutions to determine the interface behaviour of FRP to timber have not been fully investigated. Furthermore, existing analytical models for FRP-to-timber joints have been mostly derived based on the theoretical proposals of Qiao and Chen (2009) and Dai et al. (2005) where concrete had been used as a substrate. There are some fundamental differences between the failure mechanism in timber and concrete when bonded with FRP and the models which work for FRP-to-concrete bond may not work for FRP-to-timber bond. Therefore, existing FRP-to-timber interface models do not correlate particularly well with the experimental results or such models are not empirically verified.

To overcome these issues, functional and efficient analytical models have been established and presented in this chapter to accurately predict the behaviour of FRP-to-timber joints. Novel theoretical models have been developed through Stepwise Regression (SR) analysis leading to establishing new predictive models for determination of the effective bond

length and bond strength for FRP-to-timber joints. The non-linear and continuously differentiable strain function have been solved based on boundary conditions, and accordingly interfacial models have been proposed. The proposed models can be used to determine strain distribution profile, slip profile and shear stress for FRP externally bonded to timber at different loading stages. All the proposed models in this chapter have been verified and calibrated with experimental test results presented in previous chapter. A comparative analysis of the results of the experimental pull-out tests results and those predicted from the analytical model indicates a satisfactory correlation is achieved between measured and predicted parameters.

5.2. Limitation of existing interface modelling methods

A summary of exiting interface models has been explained in Chapter 2. Two of the most recent proposed models (Biscaia et al. 2016a; Biscaia et al. 2015; Wan 2014) for FRP externally bonded to timber have been fully described in Chapter 2. Although, these studies presented analytical methods for modelling different debonding behaviour of FRP-to-timber interfaces, the importance of parameters such as bond width, FRP thickness, timber mechanical properties etc. were ignored. As a result, the proposed models did not align with the experimental results presented previously in this thesis.

5.3. Stepwise regression analysis; a brief explanation

When dealing with a large group of potential independent variables, stepwise regression (SR) can be employed to determine the most significant variables in predicting the dependent variable (Cevik et al. 2010). Stepwise regression is a robust approach for selecting the best subset of independent variables that provides efficient prediction of the dependent variable. In addition, such analysis significantly reduces

computing complexity that is required for all possible regressions (Campbell 2006). The determination of the best subset models can be obtained either by trying out one independent variable into the regression model that produces the highest value of "R-Squared" if statistical significance of model is kept (Forward selection), or by including all potential independent variables in the regression model and removing those that are least significant (Backward selection). Stepwise regression is a combination of these two methods, selecting variable(s) that has the highest effect on the residual sum of squares; and conversely, removing the variable(s) that has the least significant on the residual sum of squares. In stepwise regression analysis, after each step in which a variable is added or removed, all candidate variables in the model are checked to ensure whether or not their significance has been reduced below the specified tolerance level. If a non-significant variable is then found, it will be removed from the model. It should be noted that stepwise regression analysis consecutively adds or deletes variables while there is no further contribution of independent variables to remain or enter to the model, then variable selection process will be terminated (Cevik et al. 2010; Hintze 1998).

One way to test the model proposed by SR is not to rely on the significance or R-squared or model's P-value (an indicator that describes whether or not a variable has statistically significant predictive capability in the presence of the other variable), but instead, assess the model against an "independent" data set that was not used to create the model (Mark and Goldberg 1988). Thus, a model can be built based on a sample of the dataset available (e.g., 70%) and then, assess the accuracy of the model using the remaining 30% dataset (Myers and Forgy 1963). The stepwise regression analysis has been performed using Statistical Analysis Software (SAS®). SAS® permits choosing the stepwise variable selection option by providing the opportunity to specify the method as "Forward" or

"Backward". Fully stepwise analysis has been selected (both Forward and Backward methods) allowing the software to perform a straight multiple regression using all the variables. At the next step, a significance level of a variable must be specified before it can be entered into the model (F-to-enter) prior to analysis, and then to remain in the model after each step of analysis (F-to-remove). Therefore, the options SLENTRY=0.05 and SLSTAY=0.1 have been set as the level of significance for a variable to enter and remain in the model, respectively. Dependent and independent variables have been defined to the model and program, then preceded analysis automatically. It is important to note that when the procedure terminates, all variables added and deleted must be checked, since it is possible that the addition or removal of a few more variables might not lead to improvement to the model. Furthermore, the value of the adjusted "R-squared" of the model must always be checked, because the adjusted "R-squared" should increase consistently as the stepwise process works; however, it may sometimes decrease. Hence, variables that tend to reduce the value of "adjusted R-squared" must be manually removed from the model.

5.4. Effective bond length

To achieve a satisfactory bonded joint and also for assessment and analysis of the characterisation and performance of the interface between timber and FRP, the effectiveness of bond length needs to be accurately considered. That is because, there is no benefit in extending the bond length beyond the effective bond length and the bond strength does not increase once the effective bond length achieved. Stepwise regression analysis has been performed to analysis experimental results in order to develop and establish an analytical model for determining effective bond length when FRP was bonded to timber. A database including 100 experimental results of the FRP-to-timber joint has been used to create the

model (predict) and remaining 36 sets of data have been used to test the measurement accuracy of SR model. Prior to the modelling phase, the correlation of each variable including FRP thickness, bond length, mechanical properties of material used, bond width etc. on output (dependent variable) which is the effective bond length has been determined. The most common measure of correlation in statistics is the Pearson Correlation, which is a measure of the strength of the linear relationship between two sets of data. The symbol for Pearson's correlation is "*r*" with the range from -1 to 1. An *r* of adjacent to 1 and -1 indicates a perfect positive and negative linear relationship between variables, respectively; while a *r* of 0 indicates no linear relationship between variables (Reddy, 2014). Pearson correlation coefficient can be calculated by Eq. (5-1).

$$r = \frac{\sum xy - n\overline{x}\,\overline{y}}{\left(\sqrt{\sum x^2 - n\overline{x^2}}\right)\left(\sqrt{\sum y^2 - n\overline{y^2}}\right)} \tag{5-1}$$

where *x* and *y* are independent and dependent variables, respectively. $\ddot{x}$ and $\bar{y}$ are mean of x and y values, and *n* is the number of samples. Results of the analysis show that FRP width (b_f), FRP to timber width ratio (b_f/b_t) FRP stiffness ($E_f t_f$) as a function of FRP thickness (t_f) and elastic modulus (E_f) , and ultimate tensile strength of timber block (f_{ut}) are the most significant independent variables affecting the effective bond length, as shown in Table 5-1.

Table 5-1 Pearson's correlation of independent variables on effective bond length

	timber tensile strength	FRP thickness	FRP width	FRP stiffness	FRP to timber width ratio
effective bond length	0.30	0.29	0.57	0.29	0.57

Regression analysis has been performed in order to consider the effect of all factors on the effective bond length. Uniform shear stress distribution

along the FRP laminates was assumed, and the effective bond length can be determined as follow:

$$L_e = \alpha \times \beta \times \ln(E_f t_f) \times (f_{ut})^{0.25} \quad \text{if} \quad L_e < L \tag{5-2}$$

$$L_e = L \quad \text{if} \quad L \le L_e$$

$$\beta = \frac{1.25 + \frac{b_f}{b_t}}{2 \times (2.5 - \frac{b_f}{b_t})} \tag{5-3}$$

Megapascal, Newton, and millimetres are units for the above equations. The effect of FRP to timber width ratio (*β*) (Eq. 5-3) was determined based on linear regression analysis using the test data of all specimens where b_f and b_t are widths of FRP laminates and timber block, respectively. From the test results, the constant α was determined with the value of 4.5π. Table 5-2 shows the comparison of measured effective bond length using strain profile with the predicted effective bond length using Eqs. (5-2) and (5-3).

It is also essential to note that apart from regression analysis, the performance of the fitted model and also the reliability of the derived model was assessed based on the Integral Absolute Error (IAE, %). In Eq. (5-4), O_i and P_i are the observed and predicted values, respectively. The value of zero rarely occurs for IAE; however, having a regression model with a low value of the IAE demonstrates that the derived model is reliable. For an acceptable regression equation, a range of 0 to 10% is suggested in the literature (Arıoglu et al. 2006; Girgin et al. 2007). The Integral Absolute Error of 7.34% was obtained using Eq. (5-4) for the proposed model against experimental results which is in agreement with recommendations made in the literature (Arıoglu et al. 2006; Girgin et al. 2007).

$$IAE = \sum \frac{\sqrt{(O_i - P_i)^2}}{\sum O_i} \times 100 \tag{5-4}$$

Table 5-2, Theoretical (Equation 5-2) and measured effective bond length

Identification of specimen	Effective bond length (mm)		Identification of specimen	Effective bond length (mm)		Identification of specimen	Effective bond length (mm)		Identification of specimen	Effective bond length (mm)	
	Measured	Predicted		Measured	Predicted		Measured	Predicted		Measured	Predicted
LVL 50-35-01-1~5	>50	134	LVL 150-45-01-4	132	148	LVL 200-35-01-5	136	134	H 100-45-02-1~5	>100	175
LVL 50-35-02-1~5	>50	143	LVL 150-45-01-5	136	148	LVL 200-35-02-1	165	143	H 150-45-01-1	154	164
LVL 50-45-01-1~5	>50	148	LVL 150-45-02-1	151	158	LVL 200-35-02-2	200	143	H 150-45-01-2	161	164
LVL 50-55-01-1~5	>50	163	LVL 150-45-02-2	149	158	LVL 200-35-02-3	179	143	H 150-45-01-3	158	164
LVL 100-35-01-1~5	>100	134	LVL 150-45-02-3	151	158	LVL 200-35-02-4	149	143	H 150-45-01-4	157	164
LVL 100-35-02-1~5	>100	143	LVL 150-45-02-4	158	158	LVL 200-35-02-5	189	143	H 150-45-01-5	149	164
LVL 100-45-01-1~5	>100	148	LVL 150-45-02-5	150	158	LVL 200-45-01-1	156	148	H 150-45-02-1	152	175
LVL 100-55-01-1~5	>100	163	LVL 150-55-01-1	169	163	LVL 200-45-01-2	158	148	H 150-45-02-2	184	175
LVL 150-35-01-1	123	134	LVL 150-55-01-2	175	163	LVL 200-45-01-3	182	148	H 150-45-02-3	161	175
LVL 150-35-01-2	129	134	LVL 150-55-01-3	178	163	LVL 200-45-01-4	155	148	H 150-45-02-4	182	175
LVL 150-35-01-3	129	134	LVL 150-55-01-4	160	163	LVL 200-45-01-5	147	148	H 150-45-02-5	--	175
LVL 150-35-01-4	126	134	LVL 150-55-01-5	153	163	LVL 200-55-01-1	180	163	H 200-45-01-1	163	164
LVL 150-35-01-5	125	134	LVL 150-55-02-1	180	174	LVL 200-55-01-2	165	163	H 200-45-01-2	185	164
LVL 150-35-02-1	142	143	LVL 150-55-02-2	178	174	LVL 200-55-01-3	161	163	H 200-45-01-3	187	164
LVL 150-35-02-2	140	143	LVL 150-55-02-3	181	174	LVL 200-55-01-4	--	163	H 200-45-01-4	191	164
LVL 150-35-02-3	145	143	LVL 150-55-02-4	180	174	LVL 200-55-01-5	180	163	H 200-45-01-5	176	164
LVL 150-35-02-4	130	143	LVL 150-55-02-5	191	174	LVL 250-55-01-2	190	163	H 200-45-02-1	189	175
LVL 150-35-02-5	128	143	LVL 200-35-01-1	144	134	LVL 250-55-02-2	194	163	H 200-45-02-2	186	175
LVL 150-45-01-1	139	148	LVL 200-35-01-2	158	134	H 50-45-01-1~5	>50	164	H 200-45-02-3	170	175
LVL 150-45-01-2	136	148	LVL 200-35-01-3	137	134	H 50-45-02-1~5	>50	175	H 200-45-02-4	185	175
LVL 150-45-01-3	146	148	LVL 200-35-01-4	136	134	H 100-45-01-1~5	>100	164	H 200-45-02-5	189	175

5.5. Development of the new interfacial bond models

5.5.1. Governing equations

A simple mechanical model can be established for the FRP-to-timber joint to define governing equations describing strain, shear stress and slip of the interface. In this model effect of environmental exposure, local defects in timber such as deviations, knots etc. and poor adhesive mix, inadequate curing period or incorrect curing temperature have not been considered. Uniform bond between timber and FRP has been considered which is consistent with previous studies (Kim and Harries 2010; Valipour and Crews 2011). Accordingly, it can be assumed that the two adherents (timber and FRP) are mainly subjected to axial deformation while the adhesive layer is subjected to shear deformation (Yuan et al. 2004). Therefore, both the timber and FRP are assumed to be subjected to uniformly distributed axial stress and the effect of bending in the joint are ignored. Adhesive layer is correspondingly assumed to be under shear stress which is constant across the adhesive thickness. These assumptions along with equilibrium considerations shown in Figure 5-1 lead to the following equations:

$$\frac{d\sigma_f(x)}{dx} - \frac{\tau_{(x)}}{t_f} = 0 \tag{5-5}$$

$$\frac{d\sigma_t(x)}{dx} + \frac{b_f \tau_{(x)}}{b_t t_t} = 0 \tag{5-6}$$

$$\sigma_f(x) b_f t_f + \sigma_f(x) b_t t_t = 0 \tag{5-7}$$

where t_t and t_f are thickness of timber and FRP, respectively and b_t, and b_f are width of timber and FRP, respectively. σ_f and σ_t are axial stresses in FRP and timber prism and τ is shear stress in the adhesive layer. The stress-strain relationship can be defined as per Hooke's law:

$$\sigma_f(x) = E_f \frac{du_f(x)}{dx} \tag{5-8}$$

$$\sigma_t(x) = E_t \frac{du_t(x)}{dx} \tag{5-9}$$

where E_f and E_t are FRP and timber modulus of elasticity, respectively; du_f/dx and du_t/dx also represent strains in FRP and timber, respectively. The interfacial slip(s) which is the relative displacement between timber and FRP along the bond length can be determined:

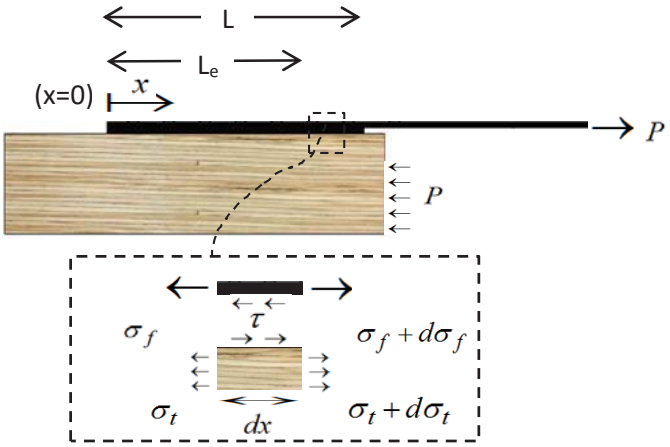

Figure 5-1 Equilibrium of bonded joint and free body diagram of an infinitesimal segment *dx*

$$s(x) = u_f(x) - u_t(x) \tag{5-10}$$

where u_f and u_t are the displacements in the FRP sheet and timber prism. Differentiating Eq. (5-10) leads Eq. (5-11) and substituting Eqs. (5-8) and (5-9) into Eq. (5-11) gives Eq. (5-12):

$$\frac{ds(x)}{dx} = \frac{du_f(x)}{dx} - \frac{du_t(x)}{dx} \tag{5-11}$$

$$\frac{ds(x)}{dx} = \frac{\sigma_f(x)}{E_f} - \frac{\sigma_t(x)}{E_t} \tag{5-12}$$

Differentiating Eq. (5-12) yields to

$$\frac{d^2 s(x)}{dx^2} = \frac{1}{E_f}\frac{d\sigma_f(x)}{dx} - \frac{1}{E_t}\frac{d\sigma_t(x)}{dx} \quad (5\text{-}13)$$

Following second order differential equation is obtained by substituting Eqs. (5-5) and (5-6) into Eq. (5-13):

$$\frac{d^2 s(x)}{dx^2} = \frac{1}{E_f}\frac{\tau(x)}{t_f} + \frac{1}{E_t}\frac{\tau(x).b_f}{b_t t_t} \quad (5\text{-}14)$$

$$\frac{d^2 s(x)}{dx^2} = \tau(x).(\frac{1}{E_f t_f} + \frac{b_f}{E_t b_t t_t}) \quad (5\text{-}15)$$

Eq. (5-15) is the governing differential equation for the FRP-to-timber joints shown in Figure 5-1. The following sections represent the step-by-step procedures for predicting of strain and stress distribution profile as well as local slip profile for CFRP-to-timber interfaces.

5.5.2. Strain profile

Results of experimental tests revealed that the polynomial expression fits the experimental results with a high correlation. Figure 5-2 shows the strain distribution and the fitted 3rd order polynomial function (Eq. 5-16) along the bonded length corresponding to 60%, 80% and the ultimate load level. It was observed that the values of Coefficient of Determination (R^2) between the experimental data and the polynomial function lie between 0.8877 and 0.9999.

$$\varepsilon_f(x) = \frac{ds(x)}{dx} = Ax^3 + Bx^2 + Cx + D \quad (5\text{-}16)$$

where *s(x)* is the slip between timber and FRP, x is the interval of gauges along the bond length (Figure 5-1) in which x = 0 refers to the free end and x = L corresponds to the FRP loaded end. The constant parameters A, B, C, and D can be defined depending on the boundary conditions. Based on

strain values at location x=0 (refer to Figure 5-1) and x=L_e, the boundary conditions for the FRP-to-timber bond interface can be expressed as:

$$\varepsilon_f = 0 \qquad when \qquad x = 0$$
$$\frac{d\varepsilon_f(x)}{dx} = 0 \tag{5-17}$$

$$\varepsilon_f = \varepsilon_1 \qquad when \qquad x = L_e$$
$$\frac{d\varepsilon_f(x)}{dx} = 0 \tag{5-18}$$

Where L_e and ε_f are effective bond length and strain at the loaded end, respectively. While the bonded length is in the elastic state, the strain (ε_1) in the FRP sheet can be obtained from Hooke's law as:

$$\varepsilon_1 = \frac{P}{E_f A_f} = \frac{P}{E_f t_f b_f} \tag{5-19}$$

where P, and A_f are applied load and FRP cross section, respectively. With the boundary conditions introduced in Eqs. (5-17) and (5-18) and solving Eq. (5-16), following expressions are obtained:

$$C = D = 0 \tag{5-20}$$

$$AL_e^3 + BL_e^2 = \varepsilon_1 \tag{5-21}$$

$$3AL_e^2 + 2BL_e = 0 \tag{5-22}$$

The solution of Eqs. (17 and 18) leads to:

$$A = -\frac{2\varepsilon_1}{L_e^3} \tag{5-23}$$

$$B = \frac{3\varepsilon_1}{L_e^2} \tag{5-24}$$

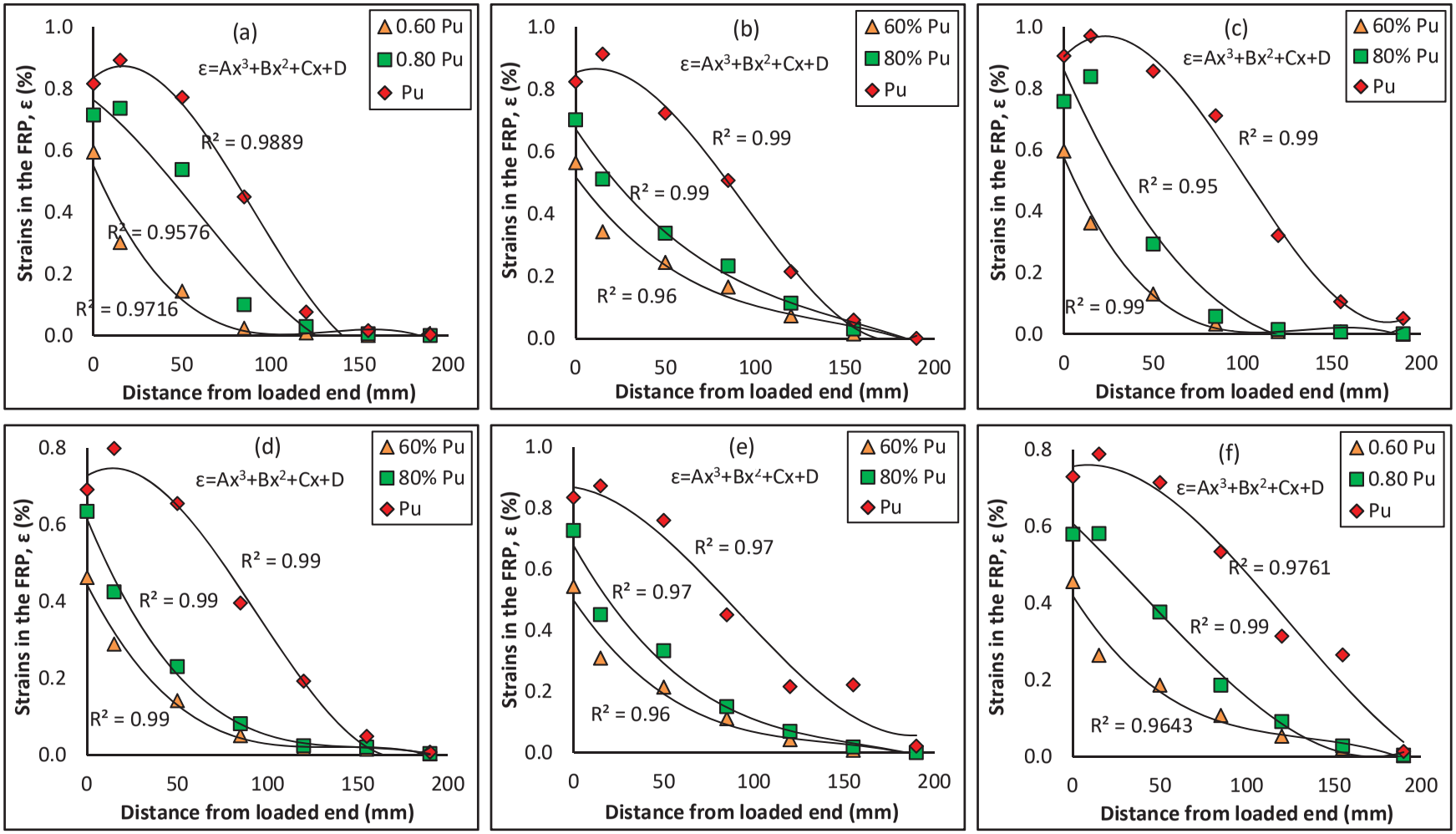

Figure 5-2, Strain distribution and interpolation curves of samples; (a) LVL 200-34-01-3, (b) LVL 200-45-01-2, (c) LVL 200-55-01-3, (d) H200-45-01-5 and (e) H200-45-01-2 and (f) H200-45-02-3

and then Eq. (5-16) can be expressed as

$$\varepsilon_f = -\frac{2\varepsilon_1}{L_e^{\,3}}x^3 + \frac{3\varepsilon_1}{L_e^{\,2}}x^2 \tag{5-25}$$

by substituting Eq. (5-19) into Eq. (5-25):

$$\varepsilon_f = -\frac{\frac{2P}{E_f t_f b_f}}{L_e^{\,3}}x^3 + \frac{\frac{3P}{E_f t_f b_f}}{L_e^{\,2}}x^2 \tag{5-26}$$

and then Eq. (5-26) can be simplified to

$$\varepsilon_f(x) = \frac{P}{E_f t_f b_f L_e^{\,2}}(3 - \frac{2}{L_e}x)x^2$$

(5-27)

Thus, the strain distribution in the FRP composite can be determined as:

$$\varepsilon_f = \frac{ds(x)}{dx} = -\frac{2\varepsilon_1}{L_e^{\,3}}x^3 + \frac{3\varepsilon_1}{L_e^{\,2}}x^2 \quad (a) \qquad for \quad 0 < x \le L_e$$

$$\varepsilon_f = \varepsilon_1 = \frac{P}{E_f A_f} = \frac{P}{E_f t_f b_f} \qquad (b) \qquad for \quad L_e < x \le L \tag{5-28}$$

In the initial stage of loading, only part of the interface near the loaded end of FRP plate is stressed whilst the stresses elsewhere are very small, indicating that the entire of bonded length is in an elastic stress state. Therefore, the strain can be determined from part (b) of Eq. (5-28) based on Hooke's law. As the tensile load on FRP plate increases, interfacial softening or debonding along the interface may occur and the region of high strain gradient appears to gradually shift inward along the length of the FRP plate. In this stage, the strain can be determined from part (a) of Eq. (5-28). The strain distribution of interface derived by Eq. (5-28) is compared with the experimental results, and the applicability of the proposed equation is presented in section 5.5.4.

5.5.3. Bond stress – slip relationships

The shear stress of the FRP-to-timber joint can be determined from strain distribution along the bond length and FRP stiffness based on Eqs. (5-5 to 5-8). Therefore, the interfacial bond stress can be obtained as

$$\tau_{(x)} = \frac{t_f . d\sigma_f(x)}{dx} = E_f t_f \frac{d\varepsilon_f(x)}{dx} \tag{5-29}$$

By derivation of Eq. (5-28) and substituting Eq. (5-19) into Eq. (5-30) the shear stress along the bonded length can be expressed as

$$\tau_{(x)} = E_f t_f (\frac{6\varepsilon_1 x}{L_e^{\,2}} - \frac{6\varepsilon_1 x^2}{L_e^{\,3}}) \tag{5-30}$$

$$\tau_{(x)} = \frac{6P}{b_f L_e^{\,2}} (1 - \frac{x}{L_e}).x \tag{5-31}$$

By derivation of Eq. (5-31) equal to zero and substituting result into Eq. (5-31) the maximum shear stress along the bonded length can be expressed as:

$$\tau_{(\max)} = \frac{3P_u}{2b_f . L_e} \tag{5-32}$$

The axial stress in the FRP sheet can also be derived from the following integration equation:

$$\sigma_f(x) = \int \frac{\tau_{(x)}}{t_f} dx = \frac{1}{t_f} \int \tau_{(x)} \tag{5-33}$$

By substituting Eq. (5-31) into Eq. (5-33) the axial stress in the FRP can be simplified as:

$$\sigma_f(x) = \frac{6 \times P}{t_f b_f L_e^{\,2}} (\frac{1}{2} - \frac{x}{3L_e}) x^2 \tag{5-34}$$

As mentioned in Eq. (5-6), the relative displacement between timber and FRP can be determined from the integration of strain profile along the bonded length:

$$s(x) = \int \varepsilon_f dx - \int \varepsilon_t dx \tag{5-35}$$

Therefore, the relative displacement between two adherents can be determined from following expressions:

$$u_f(x) = \int \varepsilon_f dx = \int (-\frac{2\varepsilon_1}{L_e^{\,3}} x^3 + \frac{3\varepsilon_1}{L_e^{\,2}} x^2) dx \tag{5-36}$$

$$u_f(x) = -\frac{\varepsilon_1 x^4}{2L_e^{\,3}} + \frac{\varepsilon_1 x^3}{L_e^{\,2}} \tag{5-37}$$

$$u_t(x) = \int \varepsilon_t dx = \frac{b_f}{A_t E_t} \iint \sigma(x)\ dx^2 \tag{5-38}$$

$$u_t(x) = \frac{b_f}{A_t E_t} \iint E_f t_f .(\frac{6\varepsilon_1 x}{L_e^{\,2}} - \frac{6\varepsilon_1 x^2}{L_e^{\,3}})dx^2 \tag{5-39}$$

$$u_t(x) = \frac{\varepsilon_1 E_f A_f}{A_t E_t L_e^{\,2}} x^3 .(1 - \frac{x}{2L_e}) \tag{5-40}$$

Therefore, Eq. (5-41) is the governing equation for the slip between timber and FRP considering Eqs. (5-32 to 5-36):

$$s(x) = -\frac{\varepsilon_1 x^4}{2L_e^{\,3}} + \frac{\varepsilon_1 x^3}{L_e^{\,2}} - \frac{\varepsilon_1 E_f A_f x^3}{A_t E_t L_e^{\,2}} + \frac{\varepsilon_1 E_f A_f x^4}{2 A_t E_t L_e^{\,3}} \tag{5-41}$$

Experimental results of the FRP-to-timber joints indicated that the displacement of the timber is negligibly small relative to the displacement of FRP sheet, since the axial stiffness of timber (the cross-sectional area of timber multiple by modulus of elasticity e.g. Eq. (5-41) is large.

Consequently, the slip in the timber can be neglected and equations (5-41) can be simplified as:

$$s = -\frac{\varepsilon_1 x^4}{2L_e^{\,3}} + \frac{\varepsilon_1 x^3}{L_e^{\,2}} \qquad for \qquad 0 < x \le L_e$$

$$s = \varepsilon_1 x - \frac{\varepsilon_1 L_e}{2} \qquad for \qquad L_e < x \le L \tag{5-42}$$

5.5.4. Validation of the generated analytical models against experimental results

The load-slip curve, strain distribution profile and shear stress obtained from the bond test specimens were compared with the results from the analytical model at different load levels to evaluate the accuracy of the analytical model. The strain distribution profiles along the bond length at various applied load (60%, 80% and the ultimate load) derived from proposed analytical model, Eq. (5-28), and experimental test results for selected number of tested specimens with different bond length and timber type are shown in Figure 5-3. It is important to note that the effective bond length of FRP-to-timber joints needs to be determined to calculate strain using Eq. (5-28). Therefore, the effective bond length proposed in Eq. (5-2) has been adopted. The trend in the predicted strain profiles is similar to the strain distribution profiles derived from experimental tests. Nevertheless, since the strain monitored at specific points over a very short length (depending on the gauge length of the strain gauge), it cannot be expected that experimental and analytical results fit perfectly, due to the inherent variability of localised timber properties. It is important to note that bond width and thickness of FRP have also been considered in Eq. (5-28); therefore, the proposed model is capable of appropriately predicting the strain profile for FRP-to-timber joint with different bond characteristics. Although all results of the

experimental pull-out tests result and those predicted from the analytical model are not shown in Figure 5-3, it was observed that the proposed model for determination of strain profile slightly overestimates the strain distribution profile when the applied load is around 80% of the ultimate load, while it underestimates it at the ultimate load. Such observations could be due to local stresses and any out of plane movements at the loaded end. Furthermore, when debonding occurs, the stress shifts over a partial active area leading to local shear stress concentrations.

Comparisons between the load-slip profile from experimental tests and the proposed analytical model are shown in Figure 5-4. At small loads, the slip increases linearly indicating that there is no interfacial softening or debonding along the interface. However, when the micro cracks occur at the FRP-to-timber interface, there is a rapid increase in slip without noticeable change in load. This trend is seen in both the experimental and analytical results. Whilst the slip curves derived from proposed analytical model for specimens shown in Figure 5-4 are slightly lower than that of slip curve obtained from experimental tests at lower load level, the predicted slip is quite similar to the experimental results at ultimate load level for majority of specimens. When the bond length is not long enough, slip at the free end occurs although strain in the FRP remains minimal at that location and indicates a smooth and gradual change. However, as the applied load on FRP plate increases, crack along the interface may form, and simultaneously the effective bond zone is being shifted towards the free end of the bond resulting in a rapid increase in the slip. Similar observations are seen in Figure 5-3 (specimen H150-45-01-1), where the bond length was not sufficiently long. The bond length of this specimen was 150 mm, while the measured and predicted effective bond length for this sample are 164 mm and 174 mm, respectively. Therefore, premature debonding can be expected to occur at lower FRP strains than the ultimate

strain, reducing the full utilisation of the bond. This finding is in agreement with the observations made by Dai et al (Dai et al. 2006).

The slip obtained from the theoretical prediction did not completely fit the experimental results; however, their similarities are evident. The possible reason for this difference may be attributed to unexpected out of plane movements since when eccentric effects occur, the interface is subjected to both shear and flexural stresses simultaneously. As noted previously, the timber block may not be cut perfectly rectangular, so that these blocks cannot be tightly fitted and held in the frame. In addition, FRP sheets may not be bonded exactly in the centre of timber block; therefore, the eccentricity of FRP and timber can impact on the strain distribution profile, slip profile and shear stress.

The evaluation of shear stress in different parts of the bond, as a function of the relative load corresponding to experimental results and analytical model, are shown in Figure 5-5. The average experimental shear stress between two consecutive gauge positions and thus the shear stress distribution can be determined as follows (Bizindavyi and Neale 1999):

$$\tau_{i-j} = \frac{t_f \times E_f \times (\varepsilon_i - \varepsilon_j)}{\Delta l_{i-j}} \tag{5-43}$$

In Eq. (5-43), ε_i and ε_j are two strain gauges at positions *i* and *j*, and Δl_{i-j} is the distance between these two gauges. As can be seen in Figure 5-5, the maximum shear stress of experimental tests is slightly higher than the predicted one. However, this difference is more noticeable for samples with lower FRP-to-timber with ratio. Although in the current study strain gauges were not bonded in the transverse direction, it has been proven that when FRP to timber width ratio is low, the force transfers from the FRP to timber leads to a non-uniform stress distribution across the width of timber resulting in a higher shear stress in the bond at failure (Hollaway

and Teng 2008). Therefore, with increase of FRP plate width, the interfacial bond strength increases, leading to a decrease of the interfacial slip during the softening-debonded stage. This trend has been also observed in experimental tests results where Figure 5-6 shows that the maximum shear stress decreased with the increase of FRP-to-timber width ratio. It is important to note that all bond characteristic and timber type in samples shown Figure 5-6 are identical, except the bond width.

Whilst, an analytical model is devolved in Chapter 6 for determining the ultimate bending capacity of the reinforced composite timber, the analytical models developed herein can be used to calculate the strain and shear stress at which debonding failure of the FRP may occur in strengthened timber beams.

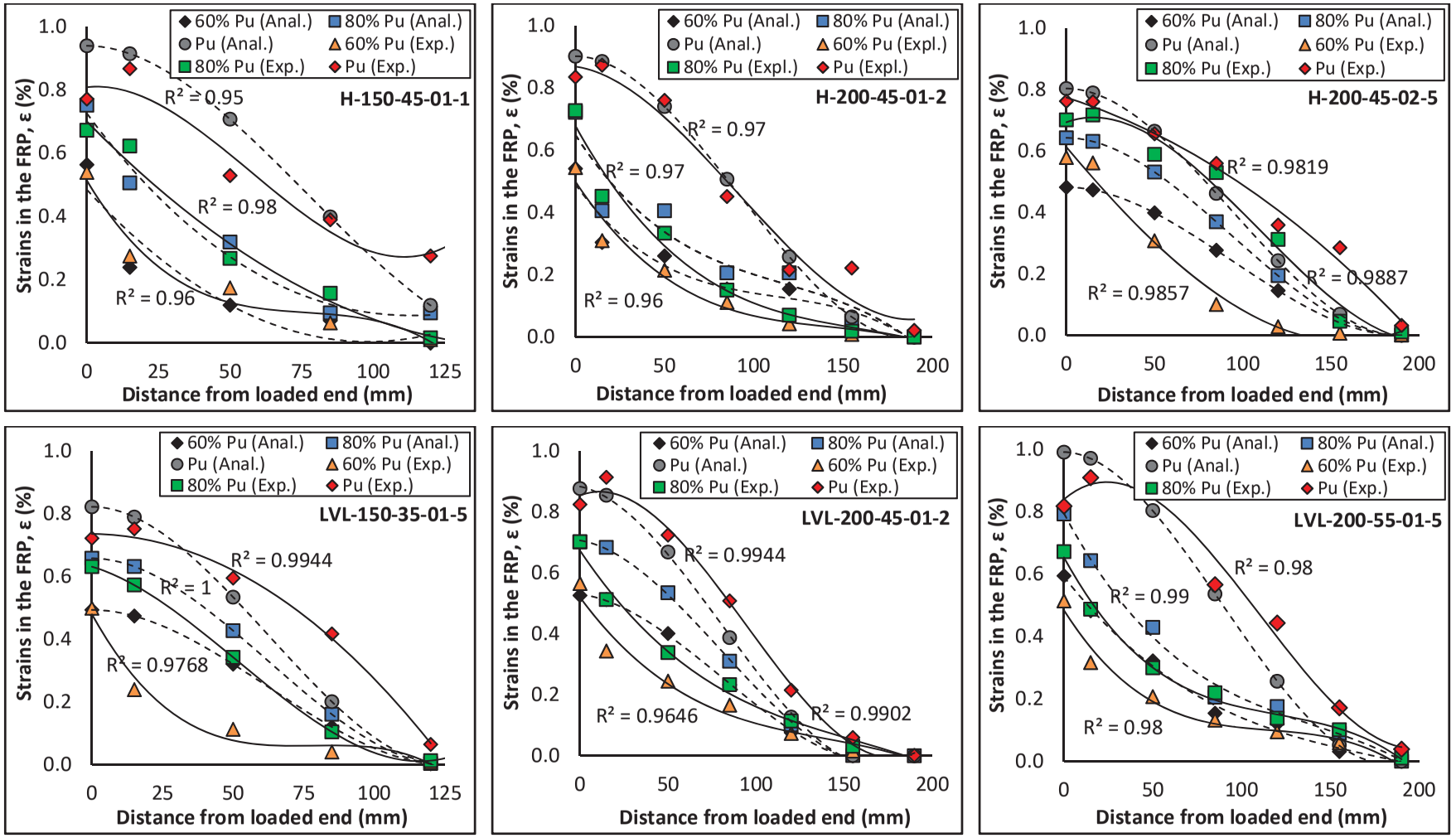

Figure 5-3, Strain distribution corresponding to 60%, 80% and the ultimate applied load

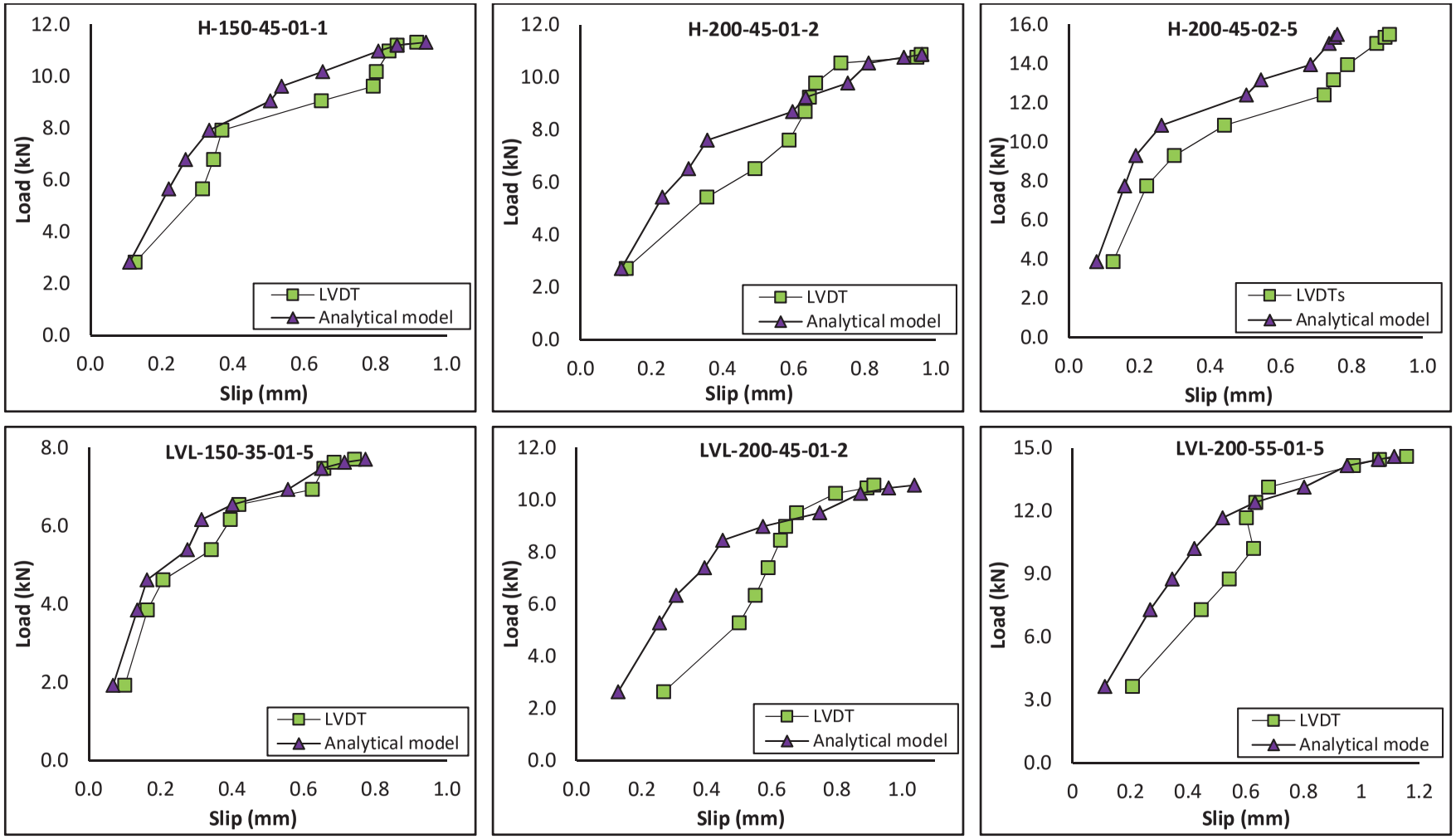

Figure 5-4, Slip profile corresponding to 60%, 80% and the ultimate applied load

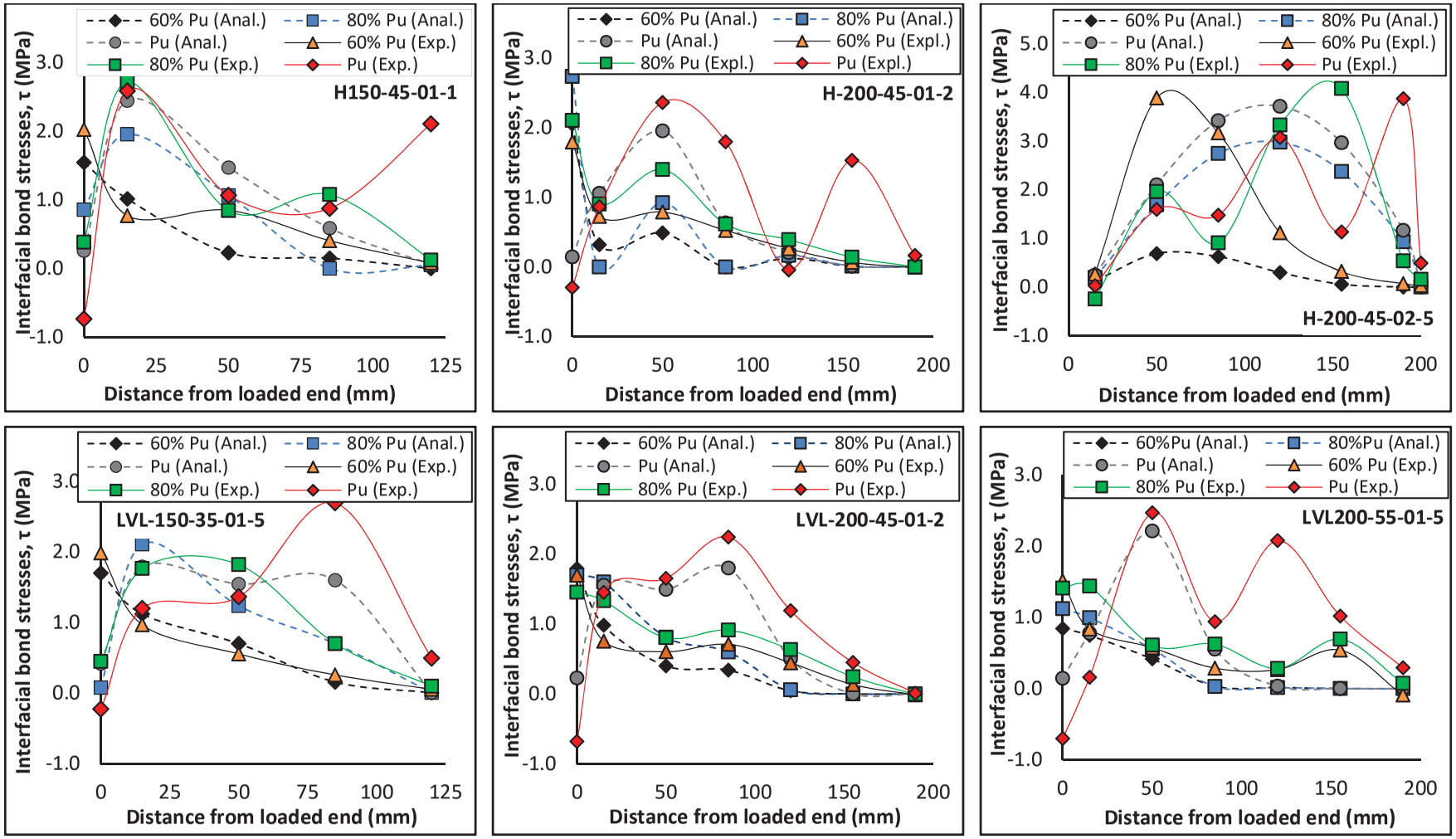

Figure 5-5, Shear stress corresponding to 60%, 80% and the ultimate applied load

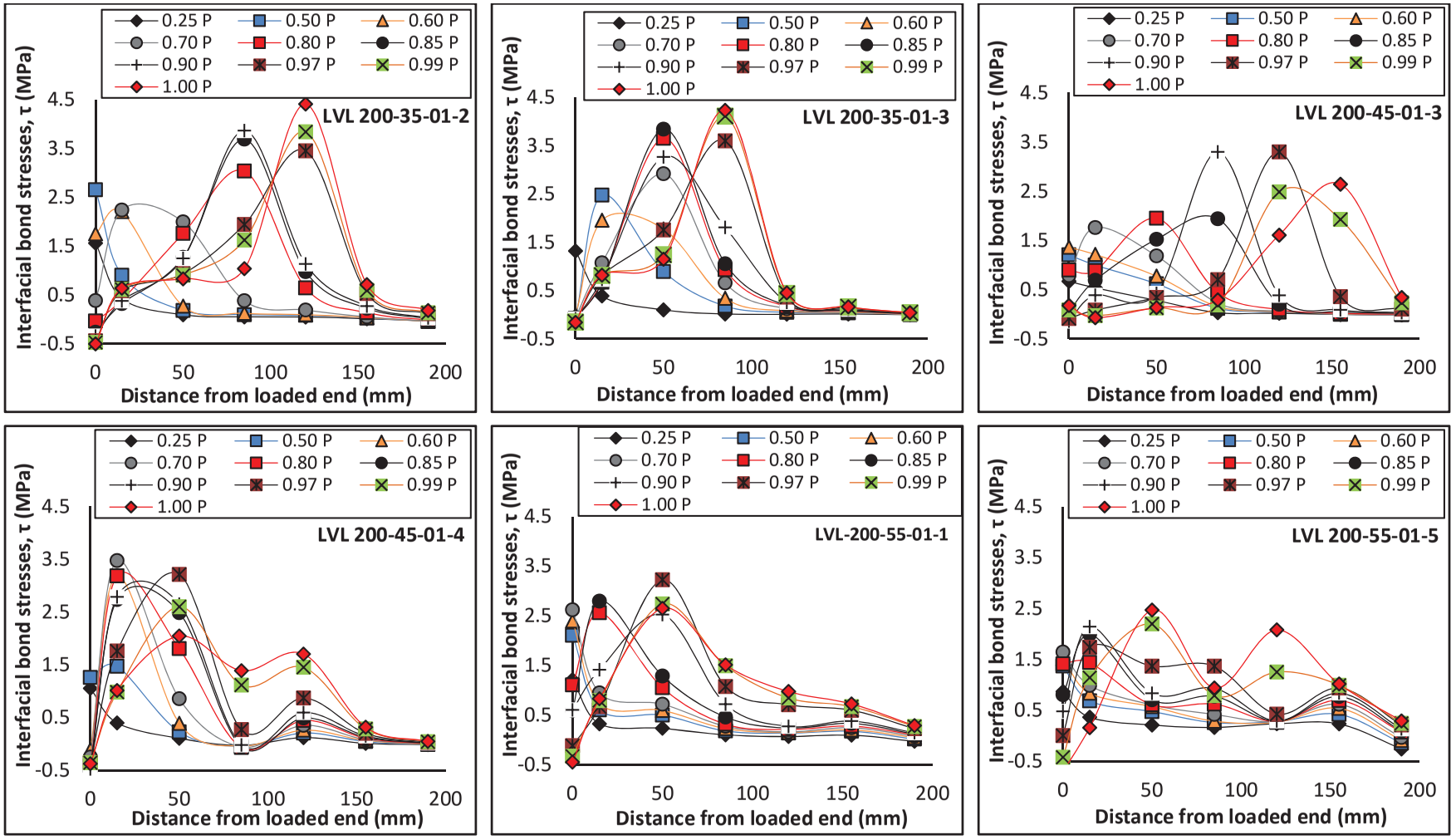

Figure 5-6, Relationship between bond stress and FRP-to-timber width ratio; (a) 32%, (b) 41% and (c) 50%

5.6. Proposed bond strength model

The bond strength model is developed for FRP-to-timber interface based on the approaches of stepwise regression analysis. The regression analysis stages have been already explained in section 5.3. and 5.4. Prior to the analysis, the Pearson Correlation of each variable on output (the ultimate bond strength) was determined using Eq. (5-1). As a result of such analyses, FRP length (L_f), FRP width (b_f), FRP to timber width ratio (b_f/b_t), FRP stiffness ($E_f t_f$) as a function of FRP thickness (t_f) and elastic modulus (E_f) , and ultimate tensile strength of timber block (f_{ut}) were determined and used as the most significant independent variables affecting the bond strength, as shown in Table 5-3.

Table 5-3 Pearson's correlation of independent variables on bond strength

	bond length	timber tensile strength	FRP thickness	FRP width	FRP stiffness	FRP to timber width ratio
Bond strength	0.65	0.22	0.39	0.59	0.39	0.59

Results of the Pearson Correlation showed that the bond strength is mainly influenced by the FRP width, FRP-to-timber width ratio and FRP length within the regression line. Longer bond length and width means larger FRP to timber interface areas, which leads to increased bond strength. However, bond strength cannot increase further once the bond length exceeds the effective bond length. Conversely, increasing bond width allows the load to be distributed over a larger area, reducing stress concentration and resulting in higher bond strength. FRP stiffness and timber tensile strength were identified as factors affecting bond strength.

The joint tests presented in Chapter 4 were used to calibrate the model proposed for FRP-to-timber joints. The test data covered a wide range for each parameter e.g. two types of timber (LVL and Hardwood), two bond thickness (1 and 2 plies of FRP), three bond width (35 mm, 45 mm and 55

mm) and five bond length (50 mm, 100 mm, 150 mm, 200 mm and 250 mm) providing a reliable benchmark for theoretical models. A full stepwise analysis has been selected (both Forward and Backward methods) allowing the software to perform a straight multiple regression using all the variables. The stepwise selection process has been performed using different possible combinations of independent variables including linear, polynomial, exponential model, reciprocal model and nonlinear multiple regression. Accordingly, stepwise regression analysis was performed using two-third of specimens and the remaining one-third results were used to test the proposed model. It is important to note that, uniform stress between timber and FRP was considered.

There are several reasons for this assumption including; (i) difficulty in capturing non-linear local interface through observation of local strain information of FRP in pull out tests, (ii) the debonding of interface may be affected by timber characteristics such as knots, grains and defects, (iii) difficulty in evaluating timber surface preparation conditions since the surface preparation of timber may not be uniform in entire of interface, and (iv) the debonding usually occurs rapidly, hence the data logger may not record sufficient data points. By taking into account the above considerations, a simple analytical formula has been derived covering those critical variables that influence on the bond strength and the ultimate interfacial pull-out force can be expressed as follows:

$$P_u = \gamma_t \cdot \sqrt{L_e \cdot f_{ut} . E_f t_f . \left(\frac{b_f}{b_t} \right)^3} \qquad (5\text{-}44)$$

The units for the above equation are: Megapascals, Newtons, and millimetres, where, b_f, E_f and t_f are the FRP width, elastic modulus and thickness of FRP sheet, respectively. f_{ut} and b_t refer to the ultimate tensile strength and width of the timber prism, respectively. L_e is the effective

bond length derived from Eq. (5-2). The latter parameter γ_t is related to the timber types, in which γ_t is equal to 0.1 and 0.08 for LVL and hardwood, respectively. To evaluate the capability of the proposed model, experimental results and those predicated from proposed bond strength model, Eq. (5-44), are compared as shown in Figure 5-7. The coefficient of determination (R^2=0.89) of the stepwise regression analysis signifies that the proposed model is able to reliably predict the ultimate load applied to the interface through experimental tests and is a more accurate predictor than the existing model proposed by (Wan 2014).

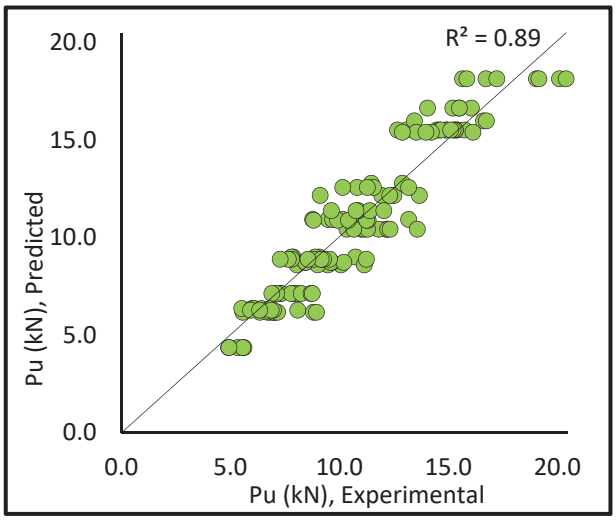

Figure 5-7 Comparison of predicted bond strength against experimental results

Reliability of the derived model was also assessed based on the Integral Absolute Error (IAE, %) to evaluate the performance of the fitted model. The Integral Absolute Error of 0.9% was obtained using Eq. (5-4) for the proposed model against experimental results which is quite low and is in agreement with recommendations made in the literature (Arıoglu et al. 2006; Girgin et al. 2007), emphasising the reliability of proposed model. Table 5-4 provides the configuration and bond strength obtained from experimental tests and the current proposed bond strength model for the entire set of specimens. The ratio of the predicted bond strength to the bond strength obtained from experimental results tests has an average value of 1.00 with the coefficient of variation of 8.5%.

Table 5-4, Theoretical (Equation 5-5) and experimental ultimate bond strength

Identification of specimen	Bond Strength (kN)		Ratio $P_{u,Exp.}/P_{u,Anal}$	Identification of specimen	Bond Strength (kN)		Ratio $P_{u,Exp.}/P_{u,Anal}$	Identification of specimen	Bond Strength (kN)		Ratio $P_{u,Exp.}/P_{u,Anal}$	Identification of specimen	Bond Strength (kN)		Ratio $P_{u,Exp.}/P_{u,Anal}$
	$P_{u,Exp}$	$P_{u,Anal}$			$P_{u,Exp}$	$P_{u,Anal}$			$P_{u,Exp}$	$P_{u,Anal}$			$P_{u,Exp}$	$P_{u,Anal}$	
LVL 50-35-01-1	5.33	4.37	1.22	LVL 150-45-01-5	13.18	10.95	1.20	LVL 100-35-02-1	9.66	8.74	1.10	H 100-45-01-2	9.55	8.90	1.07
LVL 50-35-01-2	4.92	4.37	1.12	LVL 200-45-01-1	10.88	10.95	0.99	LVL 100-35-02-2	9.61	8.74	1.10	H 100-45-01-3	11.24	8.90	1.26
LVL 50-35-01-3	5.62	4.37	1.29	LVL 200-45-01-2	10.90	10.95	1.00	LVL 100-35-02-3	8.45	8.74	0.97	H 100-45-01-4	9.20	8.90	1.03
LVL 50-35-01-4	5.57	4.37	1.27	LVL 200-45-01-3	11.13	10.95	1.02	LVL 100-35-02-4	10.20	8.74	1.17	H 100-45-01-5	9.27	8.90	1.04
LVL 50-35-01-5	4.93	4.37	1.13	LVL 200-45-01-4	11.02	10.95	1.01	LVL 100-35-02-5	8.44	8.74	0.97	H 150-45-01-1	11.32	10.90	1.04
LVL 100-35-01-1	6.35	6.18	1.03	LVL 200-45-01-5	9.69	10.95	0.88	LVL 150-35-02-1	12.15	10.45	1.16	H 150-45-01-2	8.82	10.90	0.81
LVL 100-35-01-2	6.71	6.18	1.09	LVL 50-55-01-1	8.05	8.61	0.93	LVL 150-35-02-2	10.99	10.45	1.05	H 150-45-01-3	11.24	10.90	1.03
LVL 100-35-01-3	6.83	6.18	1.10	LVL 50-55-01-2	9.47	8.61	1.10	LVL 150-35-02-3	11.80	10.45	1.13	H 150-45-01-4	9.91	10.90	0.91
LVL 100-35-01-4	7.02	6.18	1.14	LVL 50-55-01-3	9.00	8.61	1.05	LVL 150-35-02-4	11.14	10.45	1.07	H 150-45-01-5	10.41	10.90	0.96
LVL 100-35-01-5	5.57	6.18	0.90	LVL 50-55-01-4	11.14	8.61	1.29	LVL 150-35-02-5	11.29	10.45	1.08	H 200-45-01-1	9.63	11.40	0.84
LVL 150-35-01-1	7.86	7.15	1.10	LVL 50-55-01-5	10.07	8.61	1.17	LVL 200-35-02-1	13.57	10.45	1.30	H 200-45-01-2	10.87	11.40	0.95
LVL 150-35-01-2	7.27	7.15	1.02	LVL 100-55-01-1	9.12	12.18	0.75	LVL 200-35-02-2	10.34	10.45	0.99	H 200-45-01-3	11.39	11.40	1.00
LVL 150-35-01-3	8.03	7.15	1.12	LVL 100-55-01-2	12.50	12.18	1.03	LVL 200-35-02-3	12.21	10.45	1.17	H 200-45-01-4	12.03	11.40	1.06
LVL 150-35-01-4	7.32	7.15	1.02	LVL 100-55-01-3	11.94	12.18	0.98	LVL 200-35-02-4	12.32	10.45	1.18	H 200-45-01-5	10.76	11.40	0.94
LVL 150-35-01-5	7.78	7.15	1.09	LVL 100-55-01-4	13.67	12.18	1.12	LVL 200-35-02-5	10.66	10.45	1.02	H 50-45-02-1	7.81	8.90	0.88
LVL 200-35-01-1	8.25	7.15	1.15	LVL 100-55-01-5	12.31	12.18	1.01	LVL 150-45-02-1	16.61	16.00	1.04	H 50-45-02-2	9.16	8.90	1.03
LVL 200-35-01-2	7.12	7.15	1.00	LVL 150-55-01-1	14.48	15.53	0.93	LVL 150-45-02-2	13.44	16.00	0.84	H 50-45-02-3	7.66	8.90	0.86
LVL 200-35-01-3	8.70	7.15	1.22	LVL 150-55-01-2	14.90	15.53	0.96	LVL 150-45-02-3	16.75	16.00	1.05	H 50-45-02-4	7.28	8.90	0.82
LVL 200-35-01-4	8.75	7.15	1.22	LVL 150-55-01-3	15.42	15.53	0.99	LVL 150-45-02-4	11.46	12.80	0.90	H 50-45-02-5	8.56	8.90	0.96
LVL 200-35-01-5	6.90	7.15	0.97	LVL 150-55-01-4	13.08	15.53	0.84	LVL 150-45-02-5	12.89	12.80	1.01	H 100-45-02-1	11.56	12.59	0.92
LVL 50-45-01-1	5.52	6.37	0.87	LVL 150-55-01-5	12.66	15.53	0.82	LVL 150-55-02-1	16.72	18.16	0.92	H 100-45-02-2	10.81	12.59	0.86
LVL 50-45-01-2	5.99	6.37	0.94	LVL 200-55-01-1	14.60	15.53	0.94	LVL 150-55-02-2	15.65	18.16	0.86	H 100-45-02-3	11.28	12.59	0.90

LVL 50-45-01-3	6.09	6.37	0.96	LVL 200-55-01-2	14.91	15.53	0.96	LVL 150-55-02-3	15.85	18.16	0.87	H 100-45-02-4	13.18	12.59	1.05
LVL 50-45-01-4	6.42	6.37	1.01	LVL 200-55-01-3	15.74	15.53	1.01	LVL 150-55-02-4	17.22	18.16	0.95	H 100-45-02-5	10.15	12.59	0.81
LVL 50-45-01-5	6.81	6.37	1.07	LVL 200-55-01-4	15.32	15.53	0.99	LVL 150-55-02-5	19.04	18.16	1.05	H 150-45-02-1	14.22	15.42	0.92
LVL 100-45-01-1	9.07	9.01	1.01	LVL 200-55-01-5	14.67	15.53	0.94	LVL 250-55-02-1	19.16	18.16	1.05	H 150-45-02-2	13.53	15.42	0.88
LVL 100-45-01-2	10.74	9.01	1.19	LVL 250-55-01-1	15.32	15.53	0.99	LVL 250-55-02-2	20.10	18.16	1.11	H 150-45-02-3	16.13	15.42	1.05
LVL 100-45-01-3	7.87	9.01	0.87	LVL 250-55-01-2	15.22	15.53	0.98	LVL 250-55-02-3	20.40	18.16	1.12	H 150-45-02-4	13.97	15.42	0.91
LVL 100-45-01-4	8.89	9.01	0.99	LVL 250-55-01-3	15.11	15.53	0.97	H 50-45-01-1	6.97	6.29	1.11	H 150-45-02-5	12.89	15.42	0.84
LVL 100-45-01-5	7.80	9.01	0.87	LVL 50-35-02-1	7.00	6.18	1.13	H 50-45-01-2	6.87	6.29	1.09	H 200-45-02-1	15.49	16.66	0.93
LVL 150-45-01-1	9.48	10.95	0.87	LVL 50-35-02-2	8.81	6.18	1.42	H 50-45-01-3	5.92	6.29	0.94	H 200-45-02-2	14.04	16.66	0.84
LVL 150-45-01-2	9.83	10.95	0.90	LVL 50-35-02-3	8.95	6.18	1.45	H 50-45-01-4	6.34	6.29	1.01	H 200-45-02-3	15.20	16.66	0.91
LVL 150-45-01-3	10.15	10.95	0.93	LVL 50-35-02-4	7.00	6.18	1.13	H 50-45-01-5	8.09	6.29	1.28	H 200-45-02-4	16.05	16.66	0.96
LVL 150-45-01-4	8.77	10.95	0.80	LVL 50-35-02-5	7.17	6.18	1.16	H 100-45-01-1	8.83	8.90	0.99	H 200-45-02-5	15.50	16.66	0.93

5.7. Nonlinear finite element model of FRP-to-timber joints

Numerical simulations through finite element analysis (FEA) have been performed to consider and compare the interaction behaviour of FRP-to-timber bond against of experimental tests. Since failure of the interface generally occurs very quickly, qualifying the interface behaviour is rather difficult. Therefore, finite element analysis may assist to gain a better understanding about the interface behaviour.

The mechanical properties of timber and FRP used in the simulation models are adopted from tensile and compression tests results presented in Chapter 3. Results of experimental tests presented in Chapter 4 indicated that timber failure was the most frequent failure mode on externally bonded FRP-to-timber interfaces. Therefore, in the present work, a timber damage plasticity model was selected as the most appropriate model for simulating the inelastic behaviour of timber in tension including damage parameters and tensile cracking in timber. Failure modes which occurred rarely in the FRP sheets and adhesive materials are not considered herein. The bond behaviour of FRP-to-timber joints is predicted numerically through a nonlinear 3D FEA using the Abaqus finite element simulation software (ABAQUS-Inc 2013). Accordingly, in the FEA, uniaxial tensile behaviour of timber is identified by plasticity deformations. Thus, the simulation considers the different material constitutive laws for mechanical orthotropic timber and isotropic FRP behaviours.

5.7.1. Material behaviour laws

5.7.1.1 Timber behaviour without damage

Materials can be defined as ideally elastic materials if the produced deformations by loads are completely recoverable when loads are removed. Timber cannot be categorised as an ideally elastic material since

deformation from loading is not immediately recovered when the load is removed. However, after a period of time residual deformations are gradually recoverable. Timber is commonly described as an orthotropic material with unique and independent mechanical properties. Its mechanical properties can be defined using a Cartesian coordinate system: along timber grain (longitudinal), perpendicular to the grain in the radial direction (radial) and perpendicular to the grain but tangential to the growth rings (tangential) as shown in Figure 5-8 (Bergman et al. 2010).

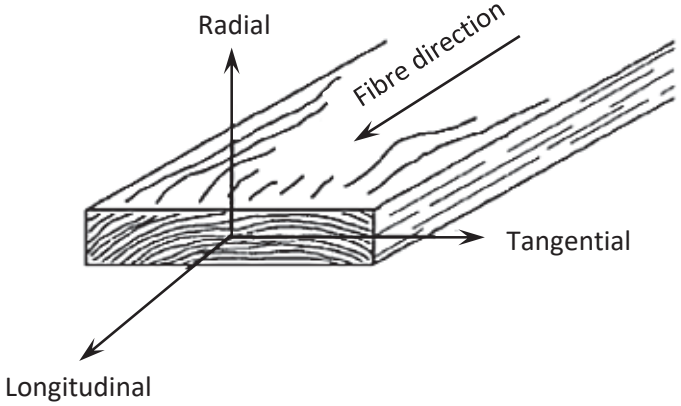

Figure 5-8 The principal axes useful for modelling wood as an orthotropic material (Bergman et al. 2010)

The relationship between modulus of elasticity parallel to grain, E_L, and the other moduli (E_R, E_T) can be determined from below relationships (Bodig and Jayne 1982).

$$E_L : E_R : E_T \sim 20 : 1.6 : 1 \tag{5-45}$$

Accordingly, a sensitivity analysis has been undertaken on the values of these modulus of elasticity. Results of such analysis revealed that variability in the mentioned modulus of elasticity has negligible influence on the FEA model predictions. The relations of timber shear moduli can be defined as follow (Bodig and Jayne 1982):

$$\begin{aligned} &G_{LR} : G_{LT} : G_{RT} \sim 10 : 9.4 : 1 \\ &E_L = G_{LR} \sim 14 : 1 \end{aligned} \tag{5-46}$$

However, similar behaviour in the radial and transverse directions is assumed in for FE as suggested by other researchers (Carlberg and Toyib 2012; Hellgren and Lundberg 2011) which translates into:

$$E_R = E_T; \quad G_{RT} = G_{TR}; \quad G_{LR} = G_{LT}; \quad \upsilon_{RT} = \upsilon_{TR}; \quad \upsilon_{LR} = \upsilon_{LT} \tag{5-47}$$

As mentioned earlier, since timber failure was the most frequent failure mode in the laboratory, the damaged finite elasto-plastic behaviour of timber and the expressions for FEA presented in previous studies (Khelifa and Celzard 2014; Khelifa and Khennane 2013; Khennane et al. 2014) is adopted herein. The plasticity model of timber is taken into account based on Hill's yield criterion with isotropic hardening. The Hill's stress function (Hill 1948) can be written as:

$$f(\sigma) = \sqrt{H(\sigma_x - \sigma_y)^2 + G(\sigma_x - \sigma_z)^2 + F(\sigma_y - \sigma_z)^2 + 2N\tau_{xy}^{\ 2} + 2M\tau_{xz}^{\ 2} + 2L\tau_{yz}^{\ 2}} - R - \sigma_{yield} \tag{5-48}$$

Where *F, G, H, L, M, N* are constants characteristic of the current state of anisotropy, σ_{yield} and *R* are the limit yield stress and the isotropic hardening stress, respectively. The constitutive equations are given as follows:

(a) State relations

$$\underline{\sigma} = \underline{\underline{\Lambda}} : \underline{\varepsilon^e} \tag{5-49}$$

$$R = Q \times r \tag{5-50}$$

Where $\underline{\sigma}$ and $\underline{\underline{\Lambda}}$ are the Cauchy stress tensor and the fourth order symmetric elastic properties tensor, respectively. The $\underline{\varepsilon^e}$ represents the tensor of elastic strain. *r* and *Q* are the isotropic hardening and the isotropic hardening modulus, respectively. The fourth order symmetric elastic properties tensor, $\underline{\underline{\Lambda}}$, can be given as (Bodig and Jayne 1982):

$$\underline{\underline{\Lambda}}^{-1}=\begin{bmatrix} \frac{1}{E_L} & -\frac{\nu_{RL}}{E_R} & -\frac{\nu_{TL}}{E_T} & 0 & 0 & 0 \\ -\frac{\nu_{LR}}{E_L} & \frac{1}{E_R} & -\frac{\nu_{TR}}{E_T} & 0 & 0 & 0 \\ -\frac{\nu_{LT}}{E_L} & -\frac{\nu_{RT}}{E_R} & \frac{1}{E_T} & 0 & 0 & 0 \\ 0 & 0 & 0 & \frac{1}{G_{LR}} & 0 & 0 \\ 0 & 0 & 0 & 0 & \frac{1}{G_{RT}} & 0 \\ 0 & 0 & 0 & 0 & 0 & \frac{1}{G_{LT}} \end{bmatrix} \quad (5\text{-}51)$$

(b) Complementary equations

$$\dot{\underline{\varepsilon}}^{p}=\dot{\lambda}\underline{n} \quad (5\text{-}52)$$

$$\dot{r}=-\dot{\lambda}(1-b\,r) \quad (5\text{-}53)$$

Where $\dot{\varepsilon}^{p}$, $\dot{\lambda}$ and $\underline{n}$ are plastic strains rate tensor, plastic multiplier and the normal to the Hill's stress function (Eq. (5-48)), respectively. $\dot{r}$ and b are the isotropic hardening strain rate and non-linear isotropic hardening parameter, respectively.

5.7.1.2 Timber behaviour with damage

There are varieties of constitutive law (e.g. nonlinear elasticity, plasticity and continuum damage etc.) with a diverse range of accuracy and generality to model behaviour of timber. In the present study, timber damage plasticity model was employed as the most proper model for the inelastic behaviour of timber in tension. Such model undertakes tensile cracking in timber as the main failure mechanism which is highly relevant to the failure mode optioned during experiments. Hence, the internal state variables used herein include: $\underline{\sigma}$ and $\underline{\varepsilon^{e}}$ for the plastic flow, r and R for the isotropic hardening and, D and Y for the isotropic ductile damage. Therefore, the constitutive equations can be given as follows:

(a) State relations

$\underline{\sigma} = (1-D)\underline{\underline{\Lambda}} : \underline{\varepsilon^e}$ Cauchy stress tensor (5-54)

$R = (1-D)Q \times r$ Isotropic hardening stress (5-55)

$Y = 0.5\underline{\varepsilon^e} : \underline{\underline{\Lambda}} : \underline{\varepsilon^e}$ Isotropic damage driving force (5-56)

(b) Complementary equations

$$\dot{\underline{\varepsilon}}^{p} = \dot{\lambda}\frac{\underline{\underline{H}} : \underline{\sigma}}{\sqrt{1-D}\,\|\sigma\|} = \frac{\dot{\lambda}}{\sqrt{1-D}}\underline{n} \tag{5-57}$$

$$\dot{r} = -\dot{\lambda}\left[\frac{1}{\sqrt{1-D}} - br\right] \tag{5-58}$$

$$\dot{D} = \dot{\lambda}\left(\frac{Y}{S}\right)^{s} \tag{5-59}$$

$$\|\underline{\sigma}\| = \sqrt{\underline{\sigma} : \underline{\underline{H}} : \underline{\sigma}} \tag{5-60}$$

Where $\dot{D}$ and S are the isotropic ductile damage parameter and ductility of the material; respectively. The exponent s is used to accelerate or delay the occurrence of damage. $\underline{\underline{H}}$ is the classical Hill anisotropic tensor defining the initial plastic anisotropy, which is given as follows (Khelifa et al. 2015):

$$\underline{\underline{H}} = \begin{bmatrix} G+H & -H & -G & 0 & 0 & 0 \\ -H & F+H & -F & 0 & 0 & 0 \\ -G & -F & F+G & 0 & 0 & 0 \\ 0 & 0 & 0 & 2N & 0 & 0 \\ 0 & 0 & 0 & 0 & 2M & 0 \\ 0 & 0 & 0 & 0 & 0 & 2L \end{bmatrix} \tag{5-61}$$

The expression for plastic flow f, Hill yield criterion, (Hill 1948) associated to isotropic hardening and the isotropic ductile damage can be stated as follows:

$$f = \frac{\|\sigma\| - R}{\sqrt{1-D}} - \sigma_{yield} \leq 0 \tag{5-62}$$

5.7.1.3 CFRP behaviour

The FRP material is idealised as linear elastic and isotropic up to its ultimate strength. Since the FRP does not experience noticeable plastic deformations, linear elastic isotropic behaviour with no damage and plastic strain is adopted. From the tensile tests on CFRP, presented in Chapter 3, the values of mean tensile strength and modulus of elasticity were determined to be 2497 MPa, and 229 GPa. The Poisson's ratio with the value of 0.3 and the ultimate strain of 0.013 were adopted for the isotropic model.

5.7.1.4 Cohesive model

Two different approaches, either cohesive element or surface-based cohesive behaviour; specifying the cohesive behaviour between the surfaces, can be used for modelling the adhesive interaction in Abaqus software (ABAQUS-Inc 2013). The functionality of these two methods are very similar; however, there is no need to create additional elements when surface-based cohesive behaviour is implemented. In addition, Lu et al. (2005a) and Lu et al. (2005b) stated the effect of the adhesive layer stiffness is negligible when the shear stiffness of adhesive is greater than 2.5 GPa/mm. Thus, the nodes of FRP element can be connected directly to timber element. In the present work, the thickness of the adhesive used was negligibly small. Therefore, it is more appropriate to simulate timber and FRP by specifying surface-based cohesive behaviour, as is often assumed in previous studies (Lu et al. 2005b; Tao and Chen 2014; Xu et al. 2015) which leads to significantly reduce computational cost. Accordingly, surface-based cohesive behaviour was employed for such simulation and the desirable and intended failure mode, which is failure with a thin layer of timber skin being pull-off from the timber block, was considered.

5.8. Numerical modelling and setup

Finite element analysis has been undertaken to further understand and explain the interfacial stress transfer mechanism, validate the capability of the proposed analytical models and also to evaluate the feasibility of FRP application bonded to timber. Since the bond strength is more relevant to effective bond length, only samples with bond length of 150 mm and 200 mm are considered here. However, key parameters including bond width, FRP thickness and stiffness, bond length and timber mechanical properties have been considered to numerically capture their effect on bond behaviour and interface. In total, thirteen different samples have been simulated considering the above-mentioned parameters. Figure 5-9 illustrates loading and boundary conditions in which a displacement-controlled mode of loading was applied to the FE model.

The mechanical properties of FRP and timber were adopted based on experiments, where Eqs. (5-45) and (5-46) were used for the calculation of timber properties in radial and tangential directions. The mechanical properties of timber and FRP are listed in Table 5-5. The FRP sheet and timber were modelled using solid elements. The plain timber block with the nominal dimensions of 320 mm (length), 110 mm (width) and 63 mm (depth) was modelled and meshed with the 8-node solid elements type C3D8R (80136 cubic elements) reduced integration (three degrees of freedom per node) in the ABAQUS/Explicit library. The FRPs were modelled by a 4-node shell element with reduced integration (six degrees of freedom per node) due to relatively thin layer of FRP. The FRP sheet with 150 mm and 200 mm in length, 0.117 and 0.234 mm in thickness with three different widths of 35 mm, 45 mm and 55 mm were bonded in the middle upper surface of plain timber (hardwood and LVL).

The size of cubic element for the FRP was selected to be 2 mm x 2 mm x 0.117 mm; however, the number of cubic elements in the meshed FRP

varies depending bond length and width. The FRP elements were directly attached to the surface of timber using surface-based cohesive behaviour. In the numerical computation, modified Mohr–Coulomb strength criterion reported by others (Longcope and Forrestal 1983; Pearce et al. 2000) was adopted in which a stressed element can be damaged in shear or in tension.

The loading was applied as an imposed displacement at the rate of 0.3 mm/min along the longitudinal direction which is equivalent to the displacement control applied during laboratory tests. At each step, some elements may reach the strength criterion and then being damaged and weakened according to the rules specified by the strength criterion. The stress and deformation distribution throughout the specimen are then adjusted instantaneously to reach a new equilibrium state.

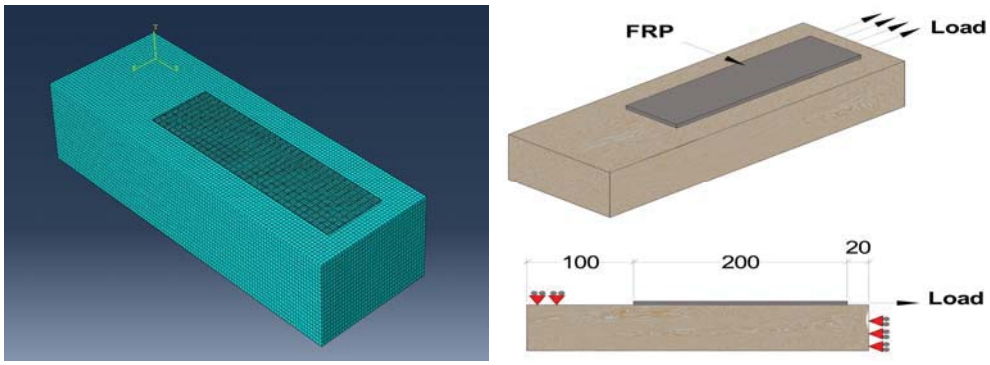

Figure 5-9 Geometrical configuration and boundary conditions of the numerical model.

Table 5-5 Material properties of timber and FRP

LVL	Elasticity	E_L = 16.8 GPa E_R = 0.84 GPa E_T = 0.84 GPa	$\upsilon_{LR} = \upsilon_{LT}$ = 0.3 υ_{RT} = 0.4 υ_{TR} = 0.4	G_{LR} = 1.2 GPa G_{LT} = 1.2 GPa G_{RT} = 0.12 GPa
	Plasticity	σ_{yield} = 44.3 MPa	Q = 17 MPa; b =1.7	F = G = H = 0.5; L = M = N = 1.5
	Damage	S = 3-5.5 MPa	s =2	
Hardwood	Elasticity	E_L = 19.8 GPa E_R = 0.99 GPa E_T = 0.99 GPa	$\upsilon_{LR} = \upsilon_{LT}$ = 0.36 υ_{RT} = 0.37 υ_{TR} = 0.37	G_{LR} = 1.4 GPa G_{LT} = 1.4 GPa G_{RT} = 0.14 GPa
	Plasticity	σ_{yield} = 67.5 MPa	Q = 17 MPa; b =1.7	F = G = H = 0.5; L = M = N = 1.5
	Damage	S = 4-5 MPa	s =2	
FRP	Elasticity	E = 229 GPa	G = 88 GPa	υ = 0.3

5.9. Numerical modelling results and discussion

5.9.1. Bond strength

In the numerical investigation the key factors affecting bond strength of FRP-to-timber bonded interfaces have been investigated e.g. bond width, bond length, FRP thickness and substrate material. Similar to the experimental tests, results of these simulations illustrated that the above-mentioned parameters have a significant impact on the bond strength; with the increase of these parameters, the interfacial bond strength increases. The numerical prediction of ultimate load carrying capacity of the FRP-to-timber joints compared against the experimental results as listed in Table 5-6. From the data presented, it can be seen that the discrepancy between predicated ultimate loads against test results varies between approximately ±13%; signifying that the numerical model is capable of appropriately predicting bond strength of FRP externally bonded to timber.

Table 5-6 Ultimate bond strength experimental versus numerical results

Specimen	$P_{u\ Exp.}$ (kN)	$P_{u\ Num.}$ (kN)	$\frac{P_{u\ Exp.}}{P_{u\ Num..}}$	Specimen	$P_{u\ Exp.}$ (kN)	$P_{u\ Num.}$ (kN)	$\frac{P_{u\ Exp.}}{P_{u\ Num.}}$
150-35-01	7.66	8.84	0.87	150-45-02	14.23	14.37	0.99
200-35-01	7.94	8.88	0.89	150-55-02	16.90	15.23	1.11
150-45-01	10.28	11.37	0.90	150-45-01	10.34	10.66	0.97
200-45-01	10.72	11.51	0.93	200-45-01	10.94	12.13	0.90
150-55-01	14.11	12.28	1.15	150-45-02	14.65	14.94	0.98
200-55-01	15.05	13.08	1.15	200-45-02	15.26	15.84	0.96
150-35-02	11.47	12.43	0.92				

5.9.2. Failure process of FRP-to-timber

Numerical simulation of FRP bonded to timber showed the damage of interface and the transfer of shear stress under various bond length, widths and thickness have a similar pattern. Typical evolution of shear stress in the timber prism and timber failure of FRP-to-timber joint with two layers of FRP, bond width 35 mm and bond length 150 mm (150-35-02) are shown in Figure 5-10. Whilst steps 1, 5, 10, 15, 30 and 42 are shown in Figure 5-10, it

was observed that in the initial stage of loading, significant stresses concentrated at the loaded end of the interface in which the stress distribution is basically uniform as shown in step 1 of Figure 5-10 (a).

With the increase of applied load on the FRP, the shear stress in the region near the loaded end reaches a peak and then begins to decrease abruptly, while simultaneously the shear stress in the adjacent region is beginning to increase. The decrease of the shear stress signifies failure in one region, while ascending of shear stress in the adjacent region illustrates that the load is being transferred there and accordingly the effective bond zone is being shifted inward along the bond length, as shown in step 10 to step 42 of Figure 5-10 (a).

Whilst some elements of timber may damage and fail in tension at the initial stage of loading, as shown in step 1 of Figure 5-10 (b), it can be seen that stress is approximately zero at the free end. With the increase of applied load, damage in the timber elements concentrates near the loaded end as shown in step 10 to step 42 of Figure 5-10 (b) as indicated by red zones which imply failure of timber. This phenomenon was constantly observed in all simulated models such that the region of high stress transferred from one area to the adjacent area until the total failure of the bond occurred. Whilst final experimental and numerical failure of interface for the specimen associated to Figure 5-10 are shown in Figure 5-11 (the red elements represent numerical failure of timber), all failure of the interface have been shown in Appendix J and Appendix K. It can be seen that interface failure of numerical simulations is in good agreement with the observed results in laboratory indicating that the numerical simulation is capable to identify and characterise the different stages of microstructural damage of interface.

(a)

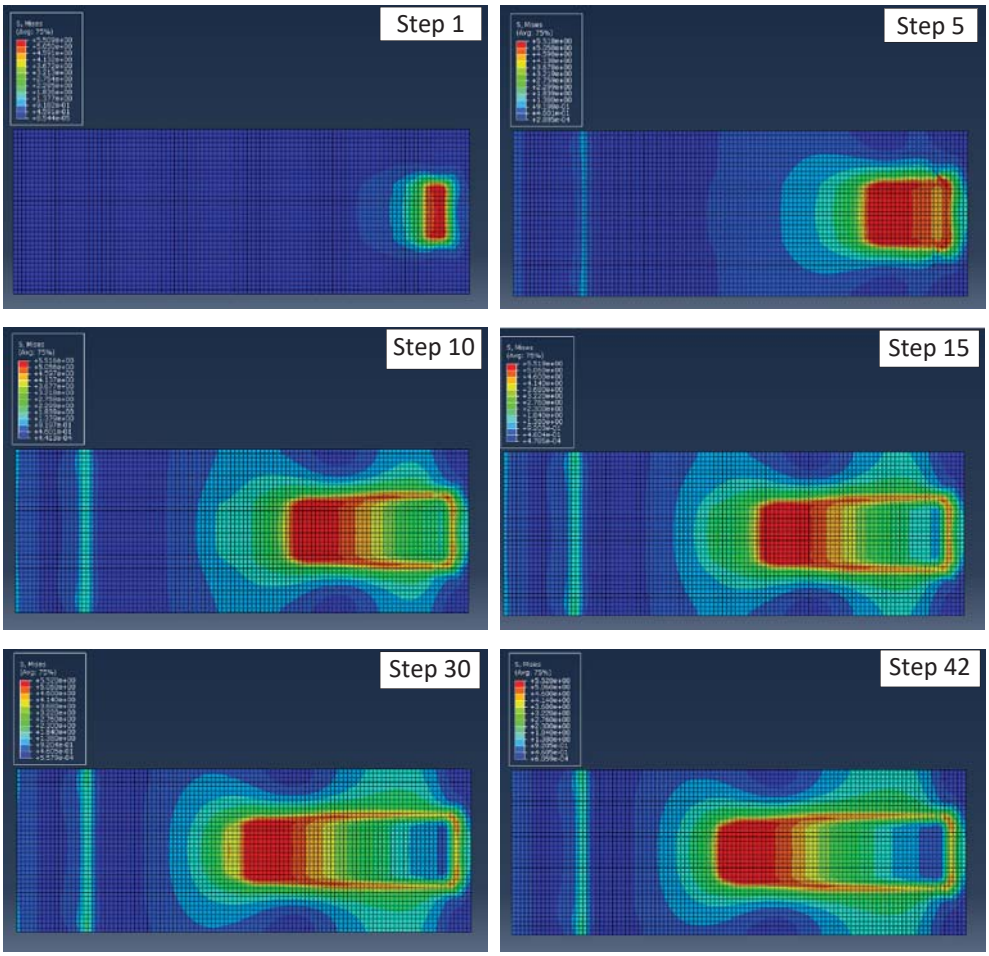
Step 1
Step 5
Step 10
Step 15
Step 30
Step 42

(b)

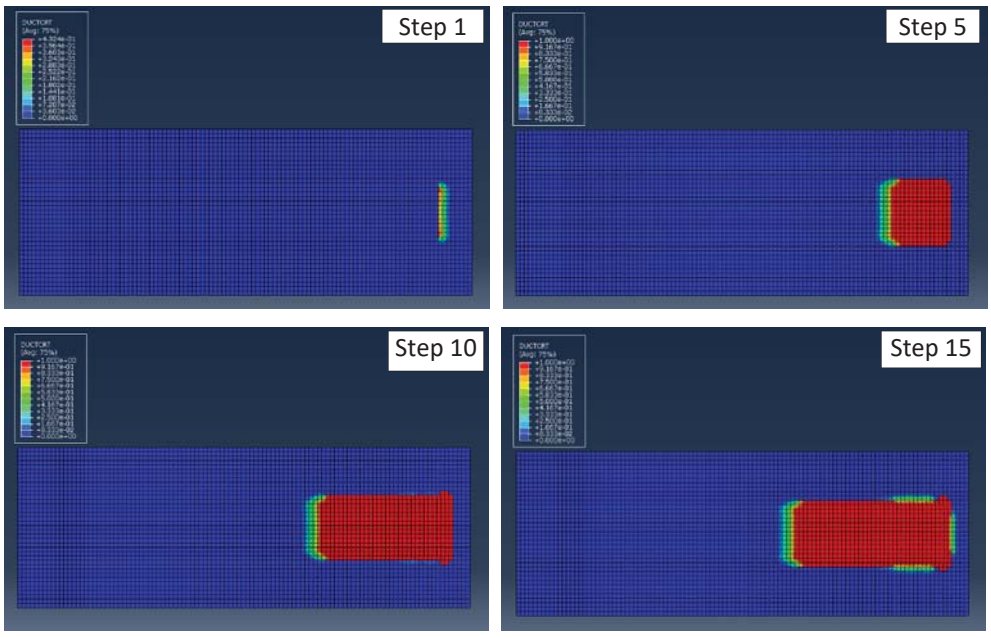
Step 1
Step 5
Step 10
Step 15

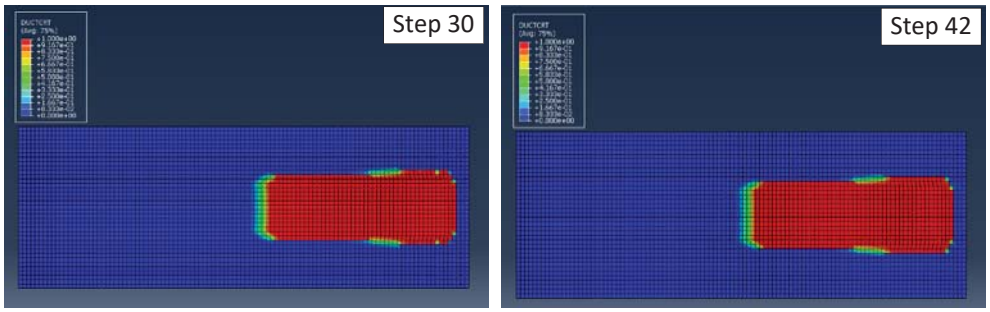

Figure 5-10 Numerically simulated (a) shear stress fields evolution, (b) interface failure for model 150-35-02

Figure 5-11 Comparison between failure of experimental and numerical result for sample 150-35-02

5.9.3. Strain distribution profile

Figure 5-12 shows the strain distribution profiles along bonded length at various load level obtained from numerical model for selected specimens. Results for all simulated models are given in Appendix P and Appendix R. Similar to the experimental results, the strain distribution exhibited a linear descending shape towards the end of the bond as the load was initially applied. This downward pattern indicates that the stress transfer length has been constant. The second trend shows that the strain increased gradually until timber failure initiated in the interface. Once failure of the timber occurred, the effective bond zone propagated from the loaded end toward the unloaded end and a further increase in strain distribution was observed until the applied loading P reached ultimate load P_u.

As mentioned in Chapter 4, the distance from the loaded end of the joint to the point where the strain profiles reach zero strain defines the effective bond length. Thus, when the bond length is long enough, the strain gauges near the far end of bond experience quite minimal strain. However,

interface stiffness, timber tensile strength, and FRP-to-timber width ratio directly impact on the effective bond length in which the effective bond length increases when these critical parameters are increased. The effective bond lengths obtained from numerical simulation were quite similar to those obtained from laboratory tests in which the shorter effective bond length (around 125 mm) was associated to the specimen modelled with one layer of FPR and bond width of 35 bonded to LVL. However, longer effective bond length (around 185 mm) was obtained in the model in which bond width was 45 mm and two layers of FRP were bonded to hardwood. The average values of the shortest and longest effective bond length obtained from laboratory tests for similar specimens were 132 mm and 184 mm, respectively.

Results of the numerical models showed that the maximum strain in the specimens made from LVL was higher than the maximum strain in the joints made from Hardwood; even though joint with LVL substrate failed at lower load. As explained in Chapter 4, this observation can be related to the elastic modulus of substrate and stiffness of interface; in which due to lower stiffness and modulus of elasticity of LVL, higher strain can be expected to occur in the interface.

It was also observed that at the same level of applied load, samples with higher FRP-to-timber bond ratio experienced lower strain when their results compared with those specimens with lower FRP-to-timber with ratio. Furthermore, comparison of simulated models with identical bond geometries except bond thickness revealed that, the maximum strain in samples with one and two plies of FRP was approximately similar, although the applied load in thicker interfaces was higher than thinner interfaces.

The main reason for this behaviour of interface can be explained based on strain distribution, in which apparently the effective bonded zone for samples with thicker bond is higher, hence the strain distributed between

adherents (FRP and timber) and adhesive over the longer interface toward the free end of the FRP. All above findings from numerical models are quite similar to those obtained from experimental tests presented in chapter 4 signifying that the numerical models are highly capable to predict the strain distribution profile along the interface for when the bond geometries vary.

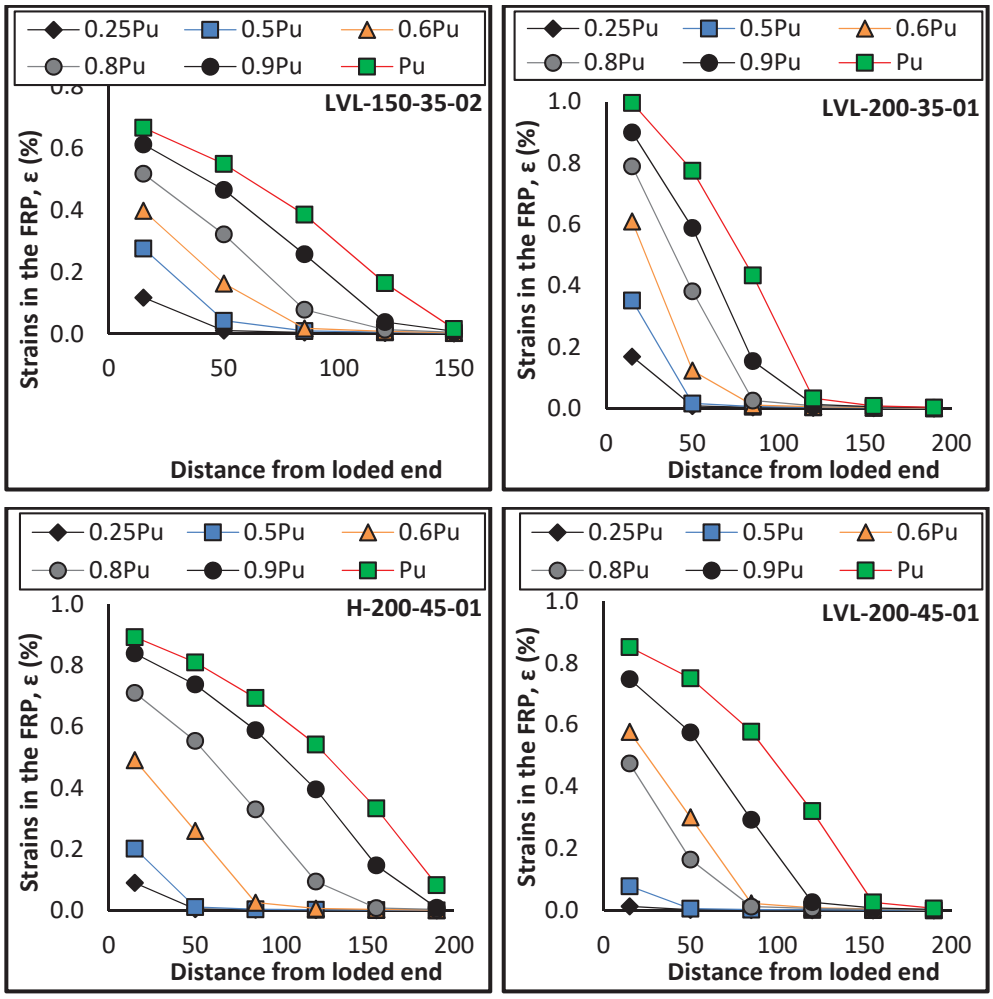

Figure 5-12 Strain distribution profile of simulated specimens

5.9.4. Bond stress

Figures 5-13 and 5-14 show shear stress along interface at various load level for selected models (same models as used in Figure 5-12). Full results for all simulated models can be found in Appendix O and Appendix Q. The interface shear stress in the LVL series was found to be higher than that for the hardwood series for similar models. A similar trend was observed in the

experimental tests. When the bond length was equal or longer than the effective bond length, shear stress near the far end of bond experiences relatively high values in the hardwood series at the ultimate load; in contrast, such values are near to zero in the LVL series as shown in Figure 5-13. This observation can be attributed to the stiffness of the bond, since LVL has lower modulus of elasticity which results lower stiffness of the interface. In addition, due to the lower stiffness and modulus of elasticity of LVL, higher strains can be expected to occur in the interface, resulting a higher shear stress in the interface. Therefore, similar to the laboratory test results, numerical results showed that a higher shear stress can be achieved for specimens made from LVL.

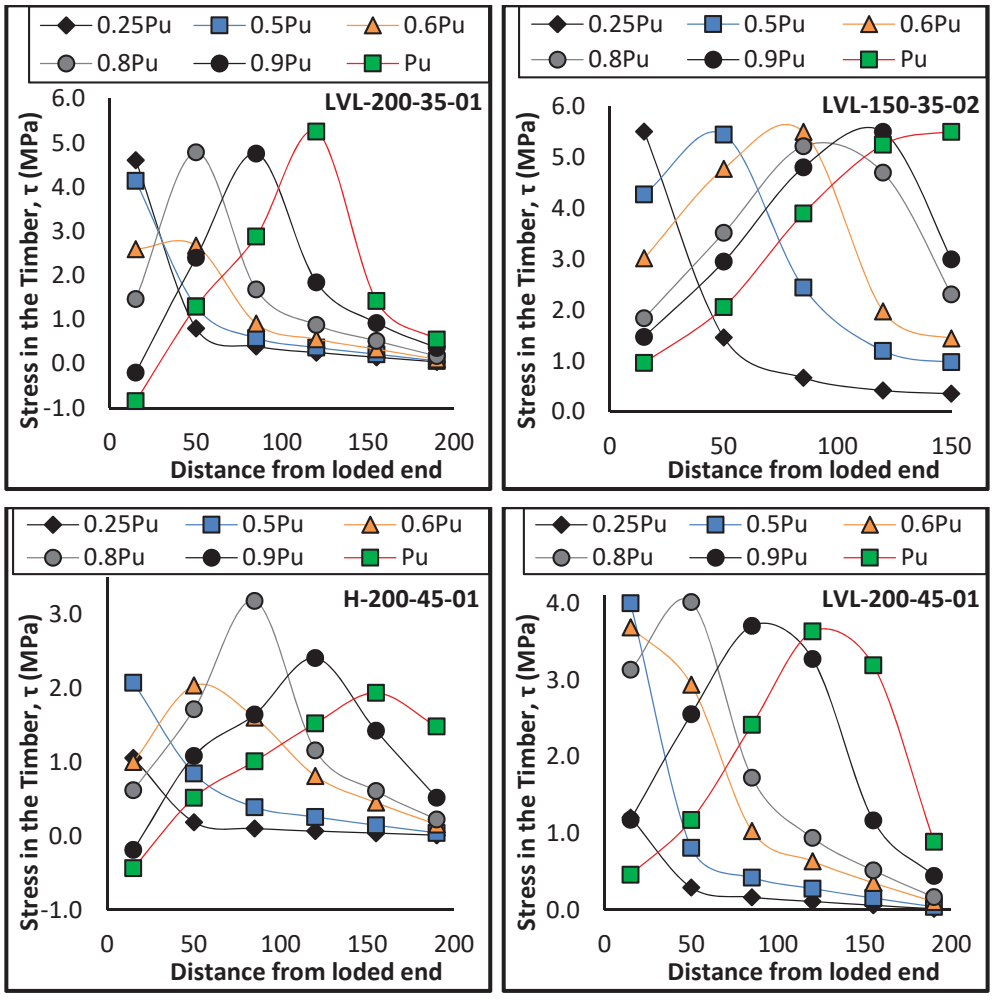

Figure 5-13 Relationship between bond stress and distance from the loaded end for selected samples

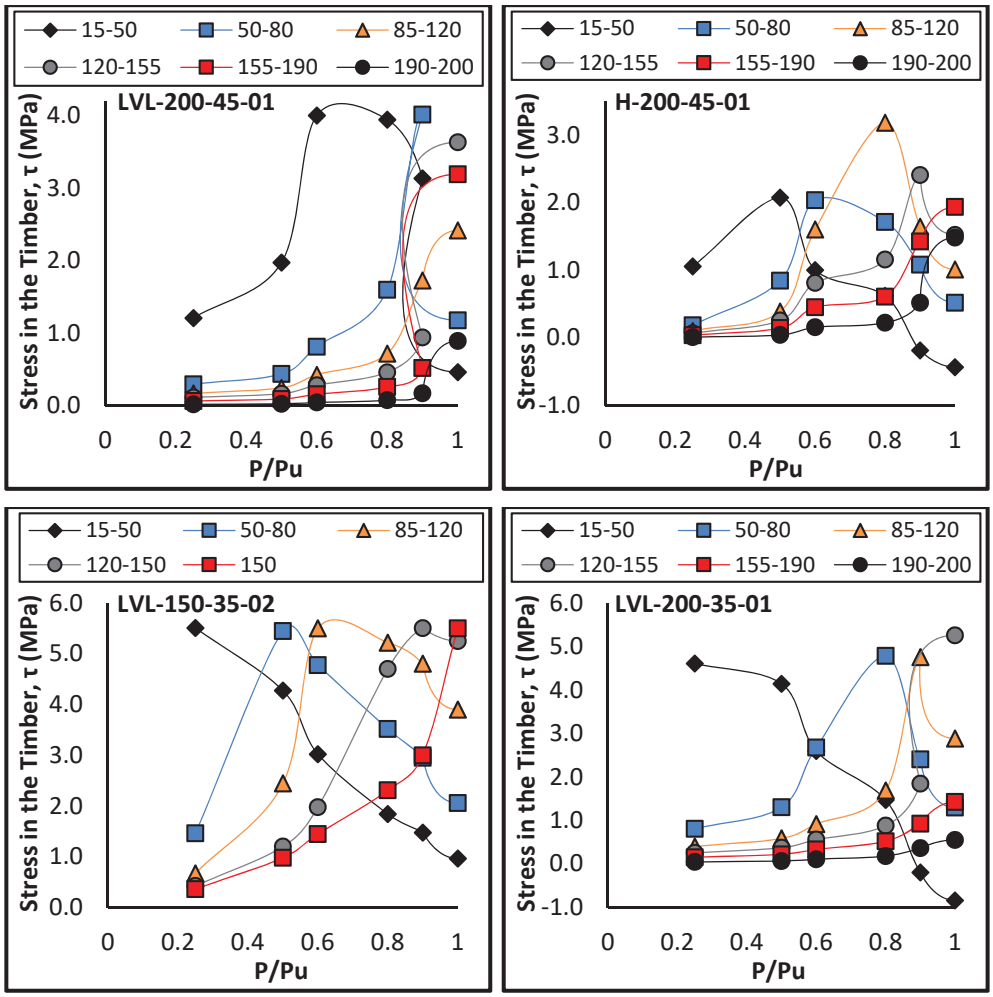

Figure 5-14 Shear stress as function of relative load level for selected specimens

Similar to the observation of the experimental results, the numerical models illustrated that the maximum shear stress decreases with the increase of FRP-to-timber width ratio. For instance, approximately 6 MPa is the maximum shear stress achieved for model LVL-200-35-01 (32% FRP-to-timber width ratio). However, the value for model LVL-200-45-01 (41% FRP-to-timber width ratio) is around 4 MPa as shown in Figure 5-13. When FRP-to-timber width ratio is low, the force transfers from the FRP to timber leads to a non-uniform stress distribution across the width of timber leading to interface failure at lower load level. Furthermore, a smaller FRP width compared to the timber width may result in a higher shear stress in the bonded zone. The distribution of the shear stress and strain in the timber beneath the FRP plate along the transverse direction will become

more uniform with the increase of FRP plate width. Numerical results also illustrated that shear stress increases when the thickness of the FRP increases. While the stiffness of the bond doubled for the thicker application, it can be expected that a larger and deeper surface of the bond get involved in the interfacial stress transferring, and thus the stress distributes more uniformly along the interface. This finding is in close agreement with the experimental test results.

5.10. Summary

In this chapter results of the experimental tests have been investigated and analysed. Accordingly, analytical models have been developed to predict the interfacial behaviour of FRP-to-timber joints. Effective bond length, FRP width and thickness, timber type and bond stiffness are the key parameters considered in the proposed models. The proposed models can be used to determine the strain distribution profile, slip profile and shear stress for FRP externally bonded to timber at different loading stages. A reliable correlation is obtained between the model prediction of strain distribution profile, slip profile and interfacial shear stress and experimental results.

Furthermore, a novel empirical model has been derived for determining of the effective bond length. The proposed model is a function of bond stiffness, timber geometries, and timber tensile strength. The effective bond length model is obtained by using strain profile and predicted shear stress along the interface. Reliable correlation is obtained for the proposed effective bond length model against the experimental results. In addition, a novel and simple predictive bond strength model with a higher accuracy for FRP-to-timber joints has been developed, considering all relevant parameters affecting the interface. The proposed model is a function of bond stiffness, timber tensile strength, FRP to timber width ratio and bond length. A comparative analysis of the results of the experimental pull-out

tests results and those predicted from the analytical model demonstrated the capability of the model in prediction of the ultimate load.

Behaviour of the FRP-timber joints was also modelled through finite element analysis (FEA) using Abaqus software. Comparing results of FEA and those obtained from laboratory tests indicated that by employment of proper constitutive behaviour for materials, the bond behaviour can be successfully predicted by FEA models. Such comparison reveals that the numerical simulation is capable of appropriately predicting the shear stress, strain distribution of interface and bond strength of FRP externally bonded to timber, with acceptable reliability and accuracy.

Chapter 6

FRP-STRENGTHENED TIMBER BEAMS: EXPERIMENTAL AND ANALYTICAL INVESTIGATION

6.1. Introduction

This chapter presents results of experimental tests on strengthened glulam laminated timber beams investigating potential parameters affecting flexural strength and ultimate load carrying capacity of timber beams strengthened with carbon FRP sheets. Eight full-scale timber beams with and without CFRP reinforcement were tested where the bonded length, width, and thickness of the CFRP was varied for the strengthened beams. Test setup, test specimens and their fabrication, test procedures, test equipment and materials properties are described in this chapter. An analytical model has been established to determine the ultimate flexural capacity of strengthened timber beam.

6.2. Failure modes for timber beam in bending

The behaviour of timber in bending highly depends on the relative values of compression and tension strengths. Buchanan (1990) stated that four separate modes of failure can take place for timber in bending.

Mode One

For materials with a lower failure stress in tension than the proportional limit stress in compression, bending failures occur in the tension zone, without any compression yielding. As can be seen in Figure 6-1, the moment-curvature relationship is linear to failure. It is notable that this behaviour is characteristic of weak pieces of commercial timber.

Mode Two

For timber materials that have an intermediate ratio of tension to compression strength, tension zone is still subjected to the maximum moment and a brittle tension failure occurs; however, some compression yielding has occurred. In this case, the compression yielding leads to the neutral axis shifts toward the tension face. Tension stress is still increasing until failure occurs as a rupture in the tension zone. The moment-curvature relationship starts curving when compression stresses exceed the proportional limit. The stronger pieces of commercial timbers have this specification. In this type of material, bending strength depends on both tension and compression strengths.

Mode Three

For materials with a high ratio of tension to compression, the ultimate bending strength is governed by compression behaviour alone. When compression yielding occurs, the moment reaches its maximum amount beyond which moment begins to decrease. However, tension stress is still increasing until rupture occurs in the tension zone at a moment below peak moment. This mode is shown graphically in Figure 6-1. Depending on the ratio of tension to compression strength, small clear specimens of timber generally fail in modes two or three.

Mode Four

For materials that are significantly stronger in tension than in compression, maximum moment is again associated with compression yielding; however, tension failure will not occur.

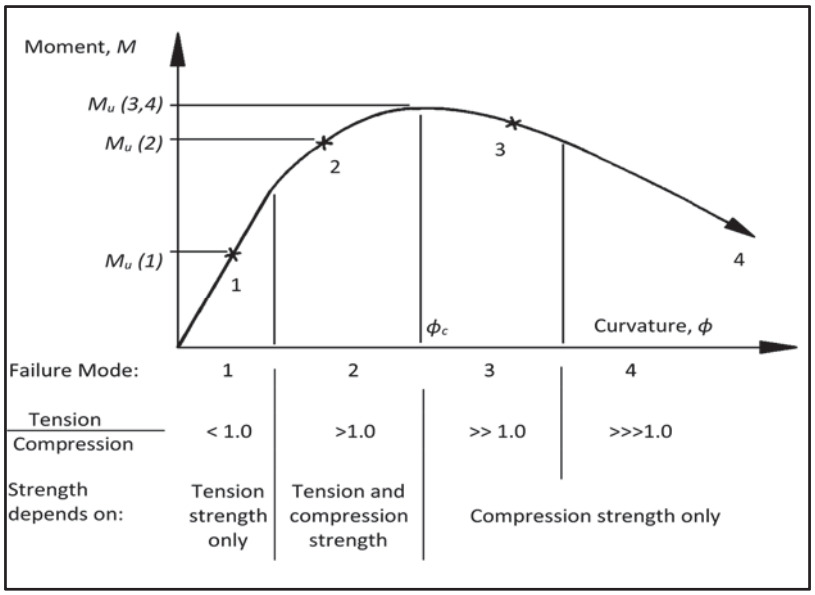

Figure 6-1 Moment curvature relationship for various failure modes (Buchanan 1990)

6.3. FRP-to-timber beams

The bond quality between timber and FRP was reported as the main concern of the retrofitted timber beams (Raftery and Rodd 2015; Valipour and Crews 2011). One of the most important failure mechanism of retrofitted timber beams is the premature failure due to debonding (Coronado 2006) which typically take place at much lower FRP strains than its ultimate strain (Biscaia et al. 2016b). Debonding directly affects the total integrity of the structure that limits the full utilisation of the material strength of the FRP (Wu and Hemdan 2005), with the subsequent outcome that the ultimate capacity and desirable ductility of the structure may not be achieved. The body of knowledge with the use of FRP strengthened glued laminated timber beams, glulam, is even more narrow and providing feasible guidelines or recommendations for such composite beams would

be of crucial importance. Glulam, as an engineered wood product, has been used in the building and construction industry for well over a century (Thorhallsson et al. 2017). Figure 6-2 illustrates the strength of standard timber products and glulam, in which the glulam products have higher strength, higher characteristic strength f_k, and lower variance when compared with standard timber products. One reason can be associated to the distribution of natural defects in the glulam timber, as they are distributed more evenly throughout the sections resulting an increased strength of the glulam element (Porteous and Kermani 2013; Thelandersson and Larsen 2003).

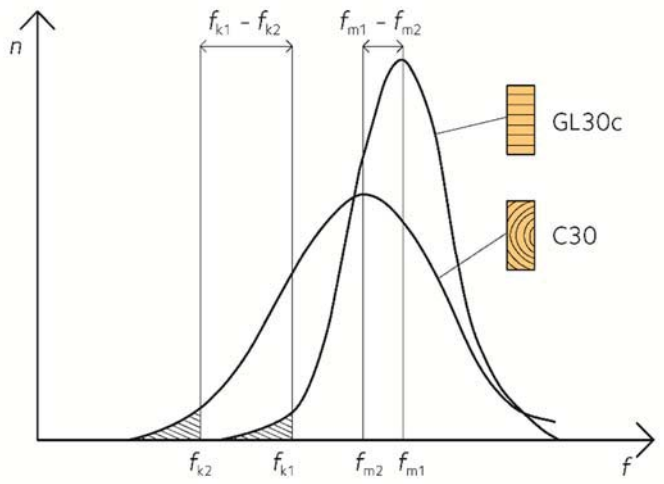

Figure 6-2 Strength properties of standard building timber and glulam. The *f* axis denotes the strength and the *n* axis is number of samples tested (Carling 1995).

The span of a timber beam is not necessarily limited by the strength of the material, but rather it is also important to consider the serviceability limit state designs and capability of the completed structural element. Although glulam timber beams have widespread use and are accepted internationally, they still have some important limitations. The design of a glulam beam is more often limited by the deflection of the beam rather than that of the strength. One way to deal with is to increase the height of the cross section of the beam; however, this approach is not always desirable and economical due to various reasons. To overcome this

weakness, FRP martials can be used as a strengthening material for glulam to obtain more strength (Thorhallsson et al. 2017).

As explained in section6.2., the most frequent failure mechanism of the retrofitted timber beams is associated with the tension failure, with or without partial plasticisation of the compressed zone, depending on the quality of the timber. In the strengthened timber beam, if the ratio of reinforcement in the tension area is adequately large, compression yielding propagates from compressive zone towards the tension area, and accordingly the neutral axis position moves downward, allowing greater strain in the compression region. Then, the strengthened beam ultimately may fail by tensile rupture of the bottom wooden fibres; or the failure mode may change from brittle tensile failure to a more ductile compression failure. Therefore, more efficient use is made of the compressive strength of the timber (Borri et al. 2005). This transition in failure mode (from mode one to mode two or three) leads substantial enhance in capacity and ductility of the strengthened beam.

6.3.1. Specimen design

Prior to manufacturing and testing specimens, the beams have been designed to ensure that either the FRP will debond or tensile failure occurs prior to timber compressive failure. The retrofitted timber beams were initially designed using section analysis proposed by Hollaway and Teng (Hollaway and Teng 2008). A linear variation of strain throughout the depth of the section has been assumed. A linear elasticity in tension and a bilinear relationship in compression area of timber have been also assumed, whilst the CFRP has been assumed to be linear-elastic as shown in Figure 6-3. Furthermore, assuming that CFRPs and timber are perfectly bonded the analysis requires satisfaction of equilibrium as per:

$$f_{ct} + f_{tt} + f_{tfrp} = 0 \qquad (6\text{-}1)$$

where f_{ct} and f_{tt} are the timber compressive force and timber tension force, respectively, and f_{tf} is the FRP tension force. Considering the above assumptions, failure of a reinforced timber beam is associated with one of the following states: both timber and FRP are linear-elastic; timber is linearly-elastic and FRP has ruptured; timber has yielded and FRP is linearly-elastic; and timber has yielded and FRP has ruptured.

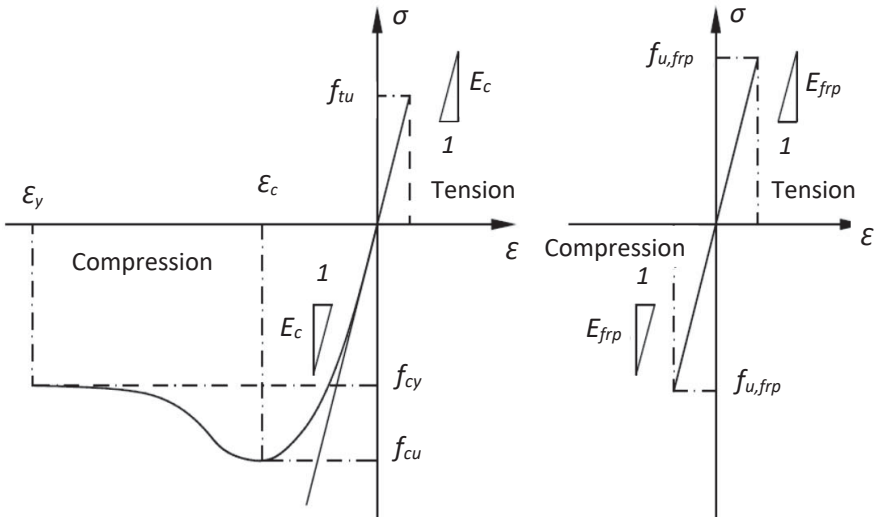

Figure 6-3 Schematic outline of the adopted stress–strain relationship for (a) timber, (b) FRP sheet

The theory and the procedure to solve Eq. (6-1) has been explained in (Bisby 2006; Hollaway and Teng 2008). The strain at which debonding failure of the FRP may occur in the strengthened beams have been modelled based on results of FRP-timber joints discussed in Chapters 3 and 4 in order to relate the joint tests results to the design of strengthened timber beams. Solution of Eq. (6-1) provided a FRP width 36.4 mm for the beams; however, CFRPs widths of 30 mm and 45 mm have been chosen which are approximately consistent with the plate width used in the joints. The FRP-to-timber width ratio of retrofitted timber beams were 66.67% and 100%. In addition, these two widths provide the opportunity to consider the effect of FRP width and FRP-to-timber width ratio in a retrofitted timber beam.

6.4. Experiments and details of test specimens

Eight timber beams, including plain timbers and reinforced specimens, have been fabricated (as listed in Table 6-1) and tested under monotonic load in four-point bending according to the AS/NZS-4063.1:2010 (2010) and BS_EN_408 (2010) Standards. The timber was GL10 grade glulam. All beams were 45 mm wide, 90 mm deep with the total length of 1800 mm and were tested with a clear span of 1620 mm. The timber beams were made of four layers of Pine in which the thickness of each layer was 22.5 mm.

Whilst the design bending strength and modulus of elasticity of the GL10 glulam beam was known to be 22 MPa and 10 GPa (Buchanan 2007) , tensile and compression tests were performed following the recommendation of (BS_EN_408 2010) to find out the actual mechanical properties of the specimens as discussed in Section 6.5, and these values have been used in the analytical phase of this study.

Six different FRP strengthening configurations were investigated by varying (i) number of layers of FRP sheet – two and four layers of FRP sheet were tested, (ii) length of the FRP – 1000 and 1300 mm lengths were used and (iii) FRP widths – 30 mm and 45 mm. Detail of the tested beams are summarised in Table 6-1. In all cases, the CFRP sheets were attached to the tensile face (soffit) of the timber beams using a wet lay-up process. Nominal thickness of the FRP sheet was 0.167 mm and epoxy used for bonding the FRP was Sikadur®-330. The fibre direction of FRP was aligned with the length of the beams. Prior to bonding CFRPs, the timber surface was wiped clean with acetone, and surface of FRP sheets was cleaned and prepared as per ASTM-D2093-03 (2003) and BSI (1995). The epoxy-based adhesive was then applied to the surface of timber beams and CFRP sheets, and an aluminium roller was used to remove trapped air, impregnate the fibres, and brush out the excessive epoxy from the

specimen. The epoxy adhesive was not tested; however, the values of elastic modulus and tensile strength of Sikadur®-330 were 4.5 GPa and 30 MPa, respectively as per manufacture's product data sheet (Sikadur®-330 2015).

Table 6-1 Detail of the tested timber beams

Identification of Specimen	Timber Beam			FRP			FRP-to-Timber Width Ratio (%)
	Length (mm)	Width (mm)	Height (mm)	Thickness (mm)	Length (mm)	Width (mm)	
B1	3000	45	90	N/A	N/A	N/A	N/A
B2	3000	45	90	N/A	N/A	N/A	N/A
B3	3000	45	90	2 x 0.167	1000	30	67
B4	3000	45	90	4 x 0.167	1000	30	67
B5	3000	45	90	4 x 0.167	1300	30	67
B6	3000	45	90	2 x 0.167	1000	45	100
B7	3000	45	90	2 x 0.167	1300	45	100
B8	3000	45	90	4 x 0.167	1300	45	100

Beam B1 - B2

The first two beams, without any reinforcement, have been fabricated and used as the control beams for determination of bending strength, load carrying capacity, timber elastic modulus in bending and also to determine the response of an unstrengthened timber beam.

Beam B3 - B4

In this series, two and four piles of CFRP with the width of 30 mm were centrally bonded to the bottom surface of the timber beam. The length of FRP for both beams was 1000 mm; however, two and four layers of FRP bonded to beams B3 and B4, respectively. The CFRP sheets were terminated 310 mm from each support in both beams B3 and B4. As the width of FRP is lower than that of timber beam, two unreinforced zones with a width of 7.5 mm were placed in both sides of the FRP along the length of timber beam. The intentions of testing these beams were to

evaluate the effect of FRP-to-timber width ratio and FRP layers and stiffness when CFRPs were attached to timber beam.

Beam B5

All bond characteristic and timber beam geometries in this sample were identical to beam B4, except the bond length. Four layers of CFRP were bonded to the timber beam. The length of the FRPs was 1300 mm and the FRP-to-timber width ratio was 66.67%. The FRP sheets were terminated 160 mm from each support. The main goal of testing this sample was to consider the effect of FRP layers/thickness and bond length on the bond strength and bond stiffness. In addition, when results of this beam are compared with beam B4, it is possible to determine how the ductility of the reinforced timber beam may change by adding extra length of FRP to the tensile zone of the timber beam.

Beam B6 - B7

The effect of bond width and FRP-to-timber width ratio have been investigated in these series. Two layers of CFRP with the width of 45 mm were attached to the tensile zone of these beams. The bond lengths; however, were selected to be 1000 mm and 1300 mm and the CFRP sheets were terminated 310 mm and 160 mm from each support for beam B6 and B7, respectively. The main aim of testing these beams was to consider the influence of bond width on the strength of a retrofitted timber beam. Moreover, the effect of bond width on the effective bond length can be assessed when results of these beams compared with beams B3 and B4. Furthermore, the deflection of these samples can be checked with the unreinforced timber beams (beams B1 and B2) as well as reinforced beams B3 and B4 to investigate the serviceability of a strengthened timber beam and also to consider which beam behaves in a more ductile manner and fails gradually.

Beam B8

This beam was strengthened with four layers of CFRP with the bond length and bond width of 1300 mm and 45 mm, respectively. Four layers of CFRP were bonded to the beam. The main objective of testing this sample was to consider the effect of FRP layers/thickness on the bond strength and bond stiffness while the FRP-to-timber width ratio was 100%. Moreover, when results of this beam are compared with those of beam B7, is possible to determine how the ductility of the reinforced timber beam may change by adding extra FRP to the tensile zone of the timber beam. Besides, it can be concluded whether extra FRP can impact on total deflection of a reinforced beam considering the serviceability of a strengthened timber beam.

6.5. Material properties

6.5.1. Timber mechanical properties

The standards and methodology used herein to obtain mechanical properties of glulam timber is exactly the same as those discussed in Chapter 3. However, the number of samples, timber cross-section and height of specimens were different. In addition to those, compressive strength perpendicular to the grain of glulam timber has been performed to ensure that such strength of glulam is adequate and unreinforced beams will not fail in compression area. The specimens used for material tests on timber were cut from the same timber used to make the beam tests. In total, ten specimens divided into two groups have been loaded parallel and perpendicular to grain for determination of tensile and compressive strength of timber specimens. The tests include four samples in tension and three samples in compression parallel to the grain; and three samples in compression perpendicular to the grain.

Tensile and compressive strength of the timber was determined based on tests of small samples according to BS_EN_408 (2010). In the compression tests parallel to grain, the specimens had the average cross-sectional dimensions of 45 mm by 90 mm and a height of 270 mm. Timber end surfaces have been accurately prepared to make them flat and parallel to one another and perpendicular to the axis of the piece. The samples used in tension had the mean cross-sectional dimensions of 45 mm x 90 mm with the length of 900 mm following the requirement of BS_EN_408 (2010). Based on the BS_EN_408 (2010) Standard, the ultimate loads either in tension or compression must be reached within (300±120)s. Accordingly, the load rates for the tests were determined from results of preliminary tests (two specimens for tensile strength and one sample for compressive strength) and were 0.5 mm/min and 8 mm/min in compression and tension, respectively (refer to Figure 6-4). Tensile and compression strength parallel to grain were determined as the peak load divided by the cross-sectional area of the specimens. Modulus of elasticity was determined from Eq. (6-2) based on the stress-strain relationship for the test samples.

$$MOE = \frac{L_1(F_2 - F_1)}{A(W_2 - W_1)} \tag{6-2}$$

Where F_2 - F_1 is an increment of load on the straight-line portion of the load deformation curve, in Newtons; W_2 - W_1 is the increment of strain corresponding to F_2 - F_1. The compressive strength perpendicular to the grain can be determined from Eq. (6-3), where *b* and *l* are width and length of specimen, respectively. The compression tests perpendicular to grain possessed the average dimensions of 45 mm width by 90 mm height and 70 mm long according to BS_EN_408 (2010). A strain gauge with gauge length of 60 mm located centrally in the test samples height. The samples were mounted vertically between the test machine platens and an initial

load applied. To prevent rotation or angular movement, the loading-heads were locked during the test. Consistent load concentrically applied perpendicular to grain with the rate of 0.7 mm/min; obtained from preliminary tests. The method for determining $F_{c,90,max}$ is given in Section 19.3 of BS_EN_408 (2010). The mean values of test results are tabulated in Table 6-2. All sample tests results are listed in Appendix L.

$$f_{c,90} = \frac{F_{c,90,\max}}{bl} \tag{6-3}$$

Table 6-2 Mean values of Glulam material properties

Test setup	Tension		Compression		Poisson ratio % (CoV%)
	Tensile Strength MPa (CoV%)	Modulus of Elasticity, GPa (CoV%)	Compressive Strength MPa (CoV%)	Modulus of Elasticity, GPa (CoV%)	
Parallel to the grain	26.22 (12.69)	16.38 (15.91)	40.78 (1.52)	13.56 (15.43)	0.3 --
Perpendicular To the grain	-- --	-- --	1.89 (9.91)	0.45 (2.23)	-- --

CoV: co-efficient of variation.

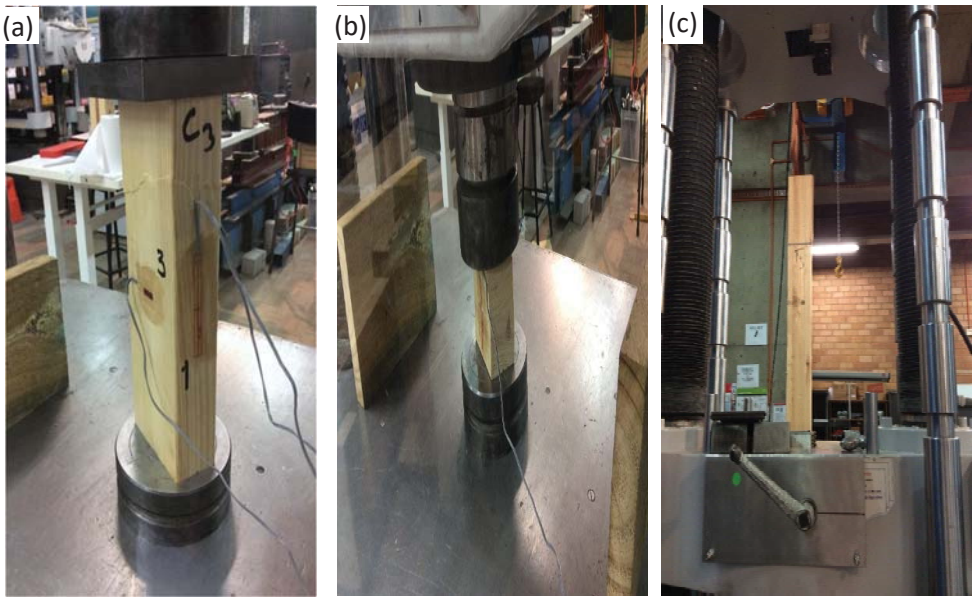

Figure 6-4 Timber specimens test in progress; (a) compressive test parallel to the grain, (b) compressive test perpendicular to the grain, and (c) tensile test parallel to the grain.

6.5.2. FRP tensile tests

The tensile tests of coupon specimens were conducted to obtain tensile strength and modulus of elasticity of CFRP. Prior to fabrication of the samples, surface of the FRP materials was wiped clean to remove all contaminants from surface of FRP according to ASTM-D2093-03 (2003) and BSI (1995). The fabrication process of coupon samples the methodology used was exactly similar to those discussed in section 3.4.2.

Five CFRP coupons were prepared and tested with average dimensions of 0.334 mm x 15.0 mm x 250 mm and standard head displacement rate of 2 mm/min following the ASTM-D3039/D3039M (2014) Standard as shown in Figure 6-5. One strain gauge was bonded longitudinally in the middle of the coupon (gauge section) and the tensile strength and modulus of modulus of elasticity of the FRP can be determined from the stress verses strain curves. From tensile tests of coupon samples, the average values of 2649 MPa and 245 GPa have been obtained for FRP tensile strength and elastic moduli, respectively. The tensile strength and modules of elasticity specified by the manufacturer are 2600 MPa and 210 GPa, respectively that are close to the tested specimens. The mean ultimate strain was also obtained 0.011 with a co-efficient of variation of 18.09%.

Figure 6-5 FRP coupon test specimens.

6.6. Detail of test setup and procedure

Figure 6-6 shows the schematic diagram of the four-point bending test setup where the end supports were designed to simulate a pin and a roller configuration. The photograph of the tests in progress are shown Figure 6-7. Each beam had an overall length of 20 times the depth of the section and the length of the test span was 18 times the depth of the section. Bearing plates were placed at the loading points and supports to prevent crushing indentation. Load was applied symmetrically at the third points of the test span using a universal testing machine (UTM) which had a capacity of 500 kN. Maximum load range of 30 kN was applied based on predicted load capacity of sample tests as well as results of preliminary test samples which were in the range of 10-12 kN. Load was applied at the constant rate of 0.15 mm/s (9 mm/min) until failure occurred; where the maximum load was reached within 300 ±120 s. AS/NZS-4063.1:2010 (2010) and BS_EN_408 (2010) were followed for the test setup and procedure.

A Laser Displacement Sensor (LDS) was mounted underneath the beams at the mid-span to determine mid-span deflection of the tested beams. For FRP strengthened beams, strain gauges were attached to the CFRP surface to measure the strain variation along the CFRP length. A mix of strain gauges with 60 mm and 10 mm gauge lengths and 120.3 ± 0.5 Ω resistance were bonded to the surface of CFRP. In total, eight strain gauges were used in specimens with 1000 mm bond length; while for samples with 1300 mm bond length, nine strain gauges were bonded to the centreline of the CFRP sheets along the bonded length (Figure 6-6). Since the bond length among the tested beams varies, the last strain gauge was placed near the end of the bond to measure strain at this point.

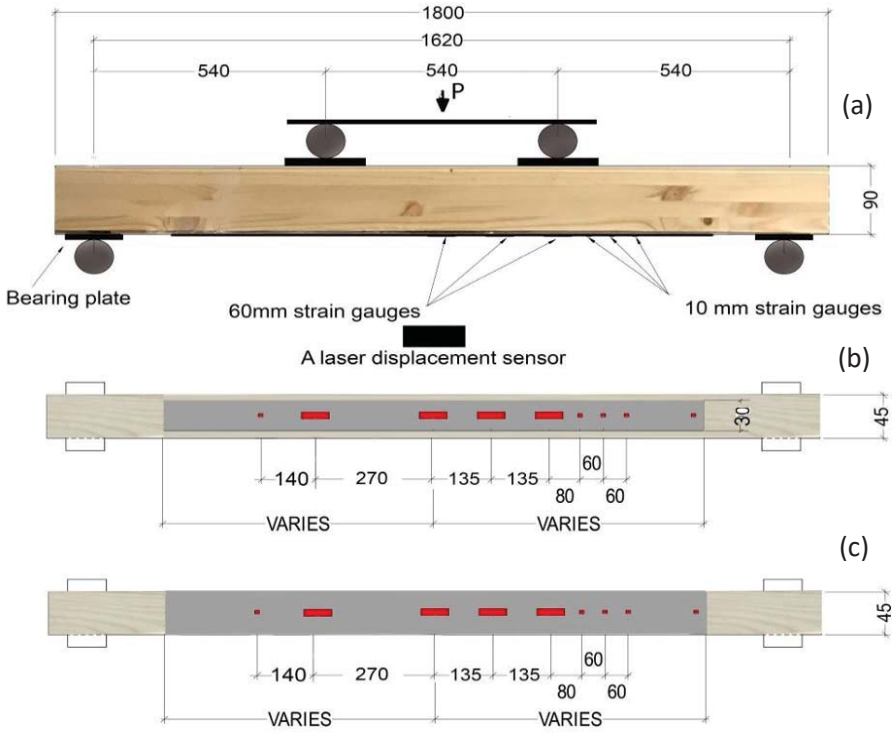

Figure 6-6 Detail of test set-up; (a) a schematic view, (b) 30 mm bond width, (c) 45 mm bond width

Figure 6-7 Fabricated FRP-to-timber beams

6.7. Analysis and discussion of the experimental results

6.7.1. Failure modes of the samples

The behaviour of timber in bending highly depends on the relative values of compressive and tensile strengths. The ratio of tensile to compressive strength of timber materials used herein is 64 %. Thus, due to lower tensile strength of unstrengthened timber beams, a brittle tension failure occurred in both unstrengthened beams as shown in Figure 6-8 (a) without any sign of compressive failure. However, experimental tests of strengthened beams showed that failure may occur with partial plasticisation of the compressed zone because of natural defect like knot followed by failure at tension zone as shown in Figure 6-8 (b). However, when the bonded length of the FRP was shorter than the effective bond length, the failure was due to plate end debonding in which crack initiated at the end of the FRP reinforcement followed by its propagation through interface leading strengthened timber beams ultimately fail in tension as shown in Figure 6-8 (c). The main reason for this observation can be attributed to the initiation of crack due to stress concentration at the end of the CFRP. On the other hand, in specimens where the bond length was 1300 mm, beams failed in a more ductile manner and the observed failure mode was associated with splitting of timber beams due to combination of timber shear and FRP debonding between the load and support points, as illustrated in Figure 6-8 (d). No FRP delamination or rupture was observed during the tests and the maximum strain measured in the FRP was around 75% of the minimum ultimate strains of FRPs achieved from coupon tests. FRP debonding was observed at the end of the FRP reinforcement especially for samples with shorter bond length.

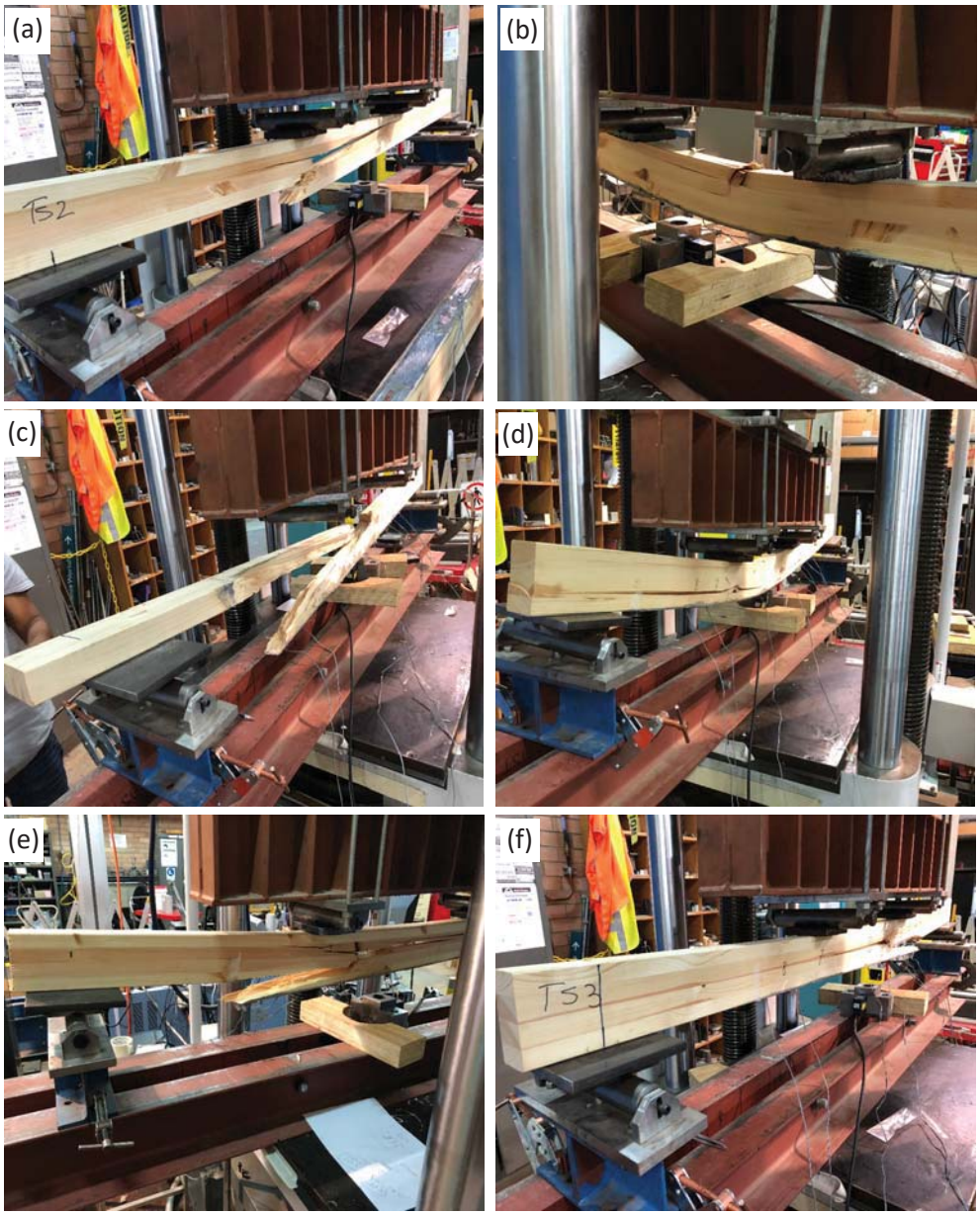

Figure 6-8 Failure mode of timber beams; (a) B2, (b) B4, (c) B6 and (d) B7, (e and f) B3

6.7.2. Load-deflections results

The load-displacement plot for beams B1 to B8 at the mid-span are shown in Figure 6-9. The ultimate load and the corresponding mid-span deflection at ultimate load of the beams are listed in Table 6-6. The load-displacement response of the control beams was almost linear up to failure and the failure was sudden and brittle. It is obvious that the addition of FRP strengthening leads to increased stiffness of the strengthened beams. As a

result, the strengthened beams exhibited higher initial stiffness as can be seen from the slopes of the load-displacement responses. For all strengthened beams, except for beams B3 and B4, the load displacement plot was observed to be linear until failure in the FRP strengthening initiated. This observation indicates that there is not interfacial softening or debonding along the FRP-to-timber beam. Therefore, the entire length of the interface is in an elastic stress state. In this stage of loading, the interfacial shear stress distribution is smaller than the local bond strength.

However, once the maximum shear stress reached, softening commences at the interface and further increase in the applied load leads to the initiation of failure in the interface propagating along the interface. At this stage, the slope of the load-displacement curve gradually flattened with increasing load until the strengthened beams FRP fully failed. At this point, the ultimate load that can be carried by the interface is attained and simultaneously, the effective bond zone shifts toward end of beam. Therefore, the ultimate load (P_u) remains almost constant. This observation is in agreement with the previous study conducted by (Wan 2014).

In Beams B3 and B4, on the other hand, when the ultimate load was reached, the strengthened beam failed suddenly at the end of the FRP. The stress concentration at the end of the FRP plate due to inadequate bond length, and consequent release of high energy at this point, appears to be the main reason for the sudden failure in this beam. Figure 6-9 and Table 6-3 illustrate that there is a significant increase in both strength and stiffness when FRPs are bonded to timber. As can be seen, the mid-span deflections of the control beams at failure were approximately 29 mm and 26 mm for beams B1 and B2, respectively; whereas, the mid-span displacement of the FRP strengthened beams at same level of applied load were around 19 mm to 13 mm for beams B3 and B8, respectively. Analysis of the results presented in this table shows that the stiffness values of

strengthened beams increased by around 31% for 1000 mm reinforcement; whilst; longer reinforcements (1300 mm) provided around 45% increase in stiffness when compared with control beams. In addition, results of beams B8 and B5 demonstrate that the stiffness increased by 43% and 64%, respectively when the bond width increased.

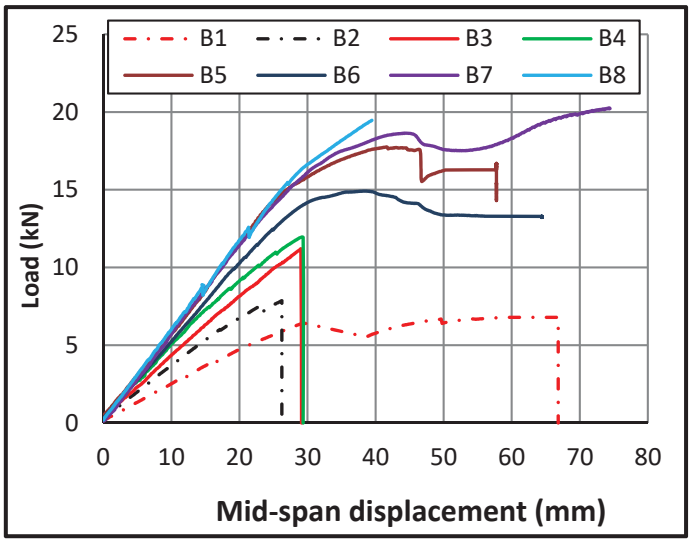

Figure 6-9 Load–displacement curves (mid-span measures).

6.7.3. Effect of FRP layers/thickness

The ultimate load in beams B3 and B4 increased by 43% and 52%, respectively, compared to unstrengthened beams (B1 and B2). Whilst the width and length of FRP for these two beams were identical; two and four layers of FRP were bonded to beams B3 and B4, respectively. Increasing the bond thickness by two times increased the load carrying capacity but the increment was not proportional to the increased thickness of the FRP. The main reason for this observation can be attributed to distribution of the applied load and consequently shear stress, over a larger area of the FRP. Accordingly, when thickness of the FRP plate increases, at the same level of applied load, the strain of plate becomes smaller and the effective bond length increases. Thus, shear stress distributes over more area of the interface and therefore shear stress decreases in the interface. This phenomenon results in enhancement of the load carrying capacity of a

beam (Wan 2014). Nevertheless, with a thicker bond, the risk of flaws occurring in the adhesive is higher, which may lead to stress concentrations in the interface. In addition, adhesives are designed to cure in thin layers and application of thick layers can change physical properties of the epoxy when the epoxy cures. Nevertheless, the increase of FRP layers enhances the stiffness of a strengthened beam, leading to reduced deflection of strengthened beams at similar loads. For instance, approximately 29 mm displacement was recorded for beam B3 at failure; whilst, at the same level of applied load approximately 24 mm mid-span displacement was recorded for beams B4, which is approximately an 18% reduction in mid-span displacement at the same level of load.

6.7.4. Effect of FRP width

Bending strength was significantly enhanced when the width of the interface increased. To investigate the effect of bond width on the load carrying capacity of the beam, results of beams B3 and B4 (bond width 35 mm) can be compared with beam B6 where the bond width was 45 mm. As can be seen in Table 6-3 and Figure 6-9, the ultimate load of beam B6 increased by around 90% which is more than double of the increased load achieved in beam B3. Beam B6 is even stronger than beam B4 in which 4 layers of FRP were used. A similar trend was observed when beam B8 is compared to beam B5, where the two beams were identical except for the width of FRP. This finding indicates that with an increase of the FRP width, the bond strength also increases. When the FRP-to-timber width ratio is low, the force transfers from the FRP to timber, leading to a non-uniform stress distribution across the width of timber and consequently shear stress increases at the interface leading to interfacial failure at lower load level. This finding is in agreement with the previous studies when the FRP was bonded to concrete (Chen and Pan 2006; Xu et al. 2015; Ye and Yao

2008). In addition, a smaller FRP width compared to the timber width may result in a higher shear stress at the FRP-timber interface.

6.7.5. Effect of bonded length

Results of beams B4, B5, B6 and B7 highlight that the bond length significantly impacts on the bending strength and load carrying capacity of strengthened beam. The bond length in beams B5 and B7 were 300 mm longer than beams B4 and B6. As shown in Figure 6-9, beams B7 and B5 failed at higher level of loads (18.29 kN and 17.25 kN) when compared with beams B6 and B4 (14.92 kN and 11.91 kN), respectively.

It was observed that the ultimate loads were higher for the series with longer FRP reinforcement and the mid-span deflection decreased when bond length increased. The typical failure mode in the test series with the smaller reinforcement length, was characterised by cracks initiating at the end of the reinforcement due to stress concentrations followed by brittle failure of beams. However, when the bond length is sufficiently long, the stress is distributed over a large area, leading to reduced shear stress in the bond and consequently resulting in increased strength. This finding agrees to the observation reported in (De Jesus et al. 2012) which signifies that the stiffness of beams strengthened with longer FRP was higher than that of those beams strengthened with shorter FRP.

However, it is important to note that the effective bond length must always be taken into consideration, since many studies (Franco and Royer Carfagni 2014; Vahedian et al. 2017a; Yuan et al. 2004) have confirmed that the bond strength cannot increase further once the bond length exceeds the effective bond length. That is because, when the effective bond length is attained, the effective bond zone shifts towards the free end of the bond. Therefore, the ultimate load (P_u) remains almost constant.

Table 6-3 Experimental results from the beams tested

Member	FRP Layers No.	FRP Width (mm)	FRP length (mm)	Peak load (kN)	Maximum bending moment (kN.m)	Maximum bending stress (MPa)	Maximum mid-span displacement (mm)	Stiffness (EI) * 10^9 N.mm^2	Modulus of elasticity (MOE) (MPa)	Increase in peak load (%)	Increase in stiffness (%)
B1	--	--	--	6.81	1.84	30.28	29.15	17.63	6450	N/A	N/A
B2	--	--	---	7.86	2.12	34.93	26.22	22.62	8273	N/A	N/A
B3	2	30	1000	11.19	3.02	43.63	29.01	29.62	9779	0.42	0.31
B4	4	30	1000	11.91	3.22	41.38	28.76	31.34	9477	0.52	0.39
B5	4	30	1300	17.75	4.79	61.66	41.59	32.43	9804	1.26	0.43
B6	2	45	1000	14.92	4.03	54.61	38.20	29.73	9383	0.90	0.31
B7	2	45	1300	18.29	4.94	66.96	46.87	32.80	10352	1.33	0.45
B8	4	45	1300	19.48	5.26	60.70	39.44	37.13	10414	1.48	0.64

6.7.6. Strain distributions along the FRP length

The maximum strain observed in the FRP bonded to the timber beams was 0.6% and was at the mid-span of beams B5 as shown in Figure 6-10. The level of FRP strain observed in the four-point bending tests was much lower than the strain in FRP at ultimate limit state recorded during the FRP coupon tests. This observation indicates that the bending strength of reinforced timber beam is not limited by the tensile strength of fibre composites; but timber mechanical properties, bond geometries and the interfacial strength are the main parameters that impact on the flexural strength of the strengthened timber beam.

Figure 6-10 shows strain distribution profiles along bonded length at various load levels for tested beams where the bond widths were 30 mm and 45 mm, the bond lengths were 1000 mm and 1300 mm, and two and four layers of FRP were bonded to timber beams. The obtained strain distributions are essentially similar to the bending moment diagram of the four-point bending test, with a bilinear tendency that is constant between applied loads, and a linear portion between loads and supports. The dissimilar strain distribution diagrams (refer to Figure 6-10) on either side of the mid-span are different from the theoretical relationship between the FRP sheet strain and the distance from the mid-span, which was expected to be identical for a completely homogeneous material. This phenomenon may be due to material heterogeneity or stress concentration in the FRP plate and timber at a meso-scale.

It is worth emphasising that beam B5 failed at lower load level compared to beam B8, however, it was observed that the maximum strain in beam B5 at failure was even higher than that of beam B8. A similar trend is observed when beams B3 and B6 are compared to each other. The only difference between beams B5 and B8 and beams B3 and B6 is the FRP width. This

observation can be related to the stiffness and modulus of elasticity of the composite beams; where due to lower stiffness of composite beams B5 and B3, more mid-span deflection with higher strain can be expected resulting in a higher shear stress in the bond compared to beams B8 and B6.

In addition, since the width of FRP is lower than that of timber width, the stress shifts over a partial active area leading to local shear stress concentrations which may results in a higher strain at failure. Furthermore, the strain distribution profile of beams B7 and B8 shows that higher stiffness of bond reduces the strain at failure; although the ultimate load of both beams was relatively similar. It is important to note that, all bond characteristic and timber cross-section of beams B7 and B8 were identical except FRP layers where beams B7 and B8 were strengthened with two and four layers of FRP, respectively.

Theoretically, if the reinforcement ratio in the tension zone is adequate and sufficiently large, the failure mode changes from a brittle tensile to a more ductile compression mode, since the neutral axis position moves towards the tension face, leading to lower stress and strain in the tension area and, conversely higher strain in the compressive zone. The part of timber crushing in compression spreads from the top of the beam to the bottom until the beam ultimately fails by tensile rupture of the bottom wooden fibres. Therefore, more efficient use is made of the compressive strength of the timber. This transition in failure mode leads to substantial enhancement in capacity and ductility of the strengthened beam. Simultaneously, as the FRP reinforcement prevents crack opening and restricts local rupture, the average ultimate tensile strength of the timber typically increases.

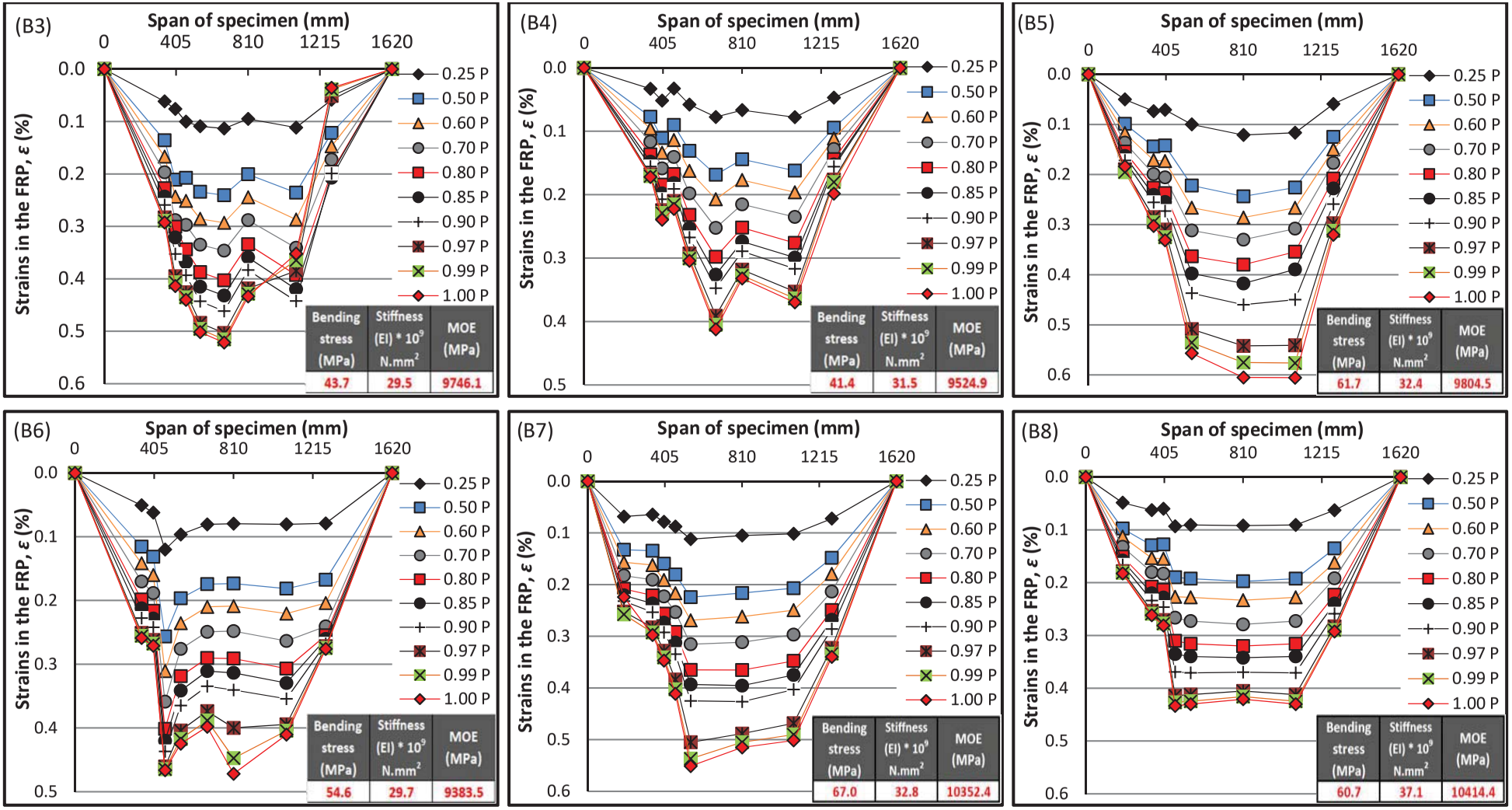

Figure 6-10 Strains in the CFRP sheets

6.7.7. Bond stress distributions in the FRP sheets

The average interfacial bond stress or shear stress distribution within the strengthened beam can be determined from two consecutive strain gauge positions as follows (Dai et al. 2005):

$$\tau_{i-j} = t_f . E_f . \frac{(\varepsilon_i - \varepsilon_j)}{\Delta l_{i-j}} \quad (6\text{-}4)$$

In Eq. (6-4), ε_i and ε_j are two strain gauges at positions *i* and *j*, and Δl_{i-j} is the distance between these two gauges. Figure 6-11 illustrates interfacial bond stress as function of relative load and bond length for beams B4 to B7. It is important to note that, the graphs on Figure 6-11 show interfacial stresses for limited load (i.e. not up to failure) for B5 and B7. As can be seen in the charts, beam B4 experienced higher level of stress at failure; whilst, at the same level of applied load, lower interfacial bond stress has been obtained in specimen B5. A similar trend is observed, when Beam B6 is compared with beam B7. Bond length is the only difference between beams B4 and B5 and between beams B6 and B7.

When the bond length was shorter than the effective bond length, cracks may have formed in the bond at lower strain leading to debonding in the interface. Nevertheless, as the applied load on FRP plate increases, cracking along the interface propagates and simultaneously the region of high stress transferred from one area to the adjacent area until the total debonding of the bond occurs. Therefore, at the same time, only a limited area of the bond is activated, and the applied load is carried by this area. When such an active area reaches the end of bonded interface, the bond shear stress increases, since the FRP reinforcement no longer contributes to the flexural stiffness of the section and any increase in applied load must be carried by the timber beam. As a result, since the ultimate bending strength of timber beam is significantly lower than that of strengthened

beam, failure occurs abruptly. Therefore, it can be concluded that bond length has a major contribution to shear stress distribution in the interface, that directly impacts on the bending strength as well as the failure mode of strengthened timber beams.

Theoretically, in the four-point bending test, the axial bond stress at both sides of the mid-span is expected to be identical for completely a homogeneous material; however, there is a noticeable spatial variation in the interfacial bond stress derived from the strain data as shown in Figure 6-11. These fluctuations in the bond stress can be related to the eccentricity of the attached strain gauges, local variation in the properties as the gauges only measuring strain over a very short length e.g. 5-10 mm, and material heterogeneity in the FRP and timber. Figure 6-11 also shows that shear stress between applied loads are relatively low; whereas the interfacial bond stress between loading points and supports are more pronounced. This trend can be attributed to the fact that in the four-point bending test, the bending moment between mechanical loading is constant and accordingly, the strains are constant likewise (Figure 6-10). Consequently, using Eq. (6-4), a constant strain distribution leads to zero interfacial bond stress.

Figure 6-12 shows the relationship between interfacial bond stress and bond width at various load levels expressing that the shear stress decreases with the increase of FRP-to-timber width ratio. Higher bond stress has been achieved in specimens B3 and B5 when compared with beams B6 and B8, respectively. FRP-to-timber width ratio for specimens B3 and B5 was 67%, whilst, this ratio for beams B6 and B8 was 100%. Although, in the current study strain gauges were not bonded in the transverse direction, it has been proven that when the FRP to timber width ratio is low, the force transfers from the FRP to timber leads to a non-uniform stress distribution across the width of timber resulting in a higher

shear stress in the bond at failure (Hollaway and Teng 2008). Therefore, with increase of FRP width, the interfacial bond strength increases, leading to a decrease of slip during the softening-debonded stage.

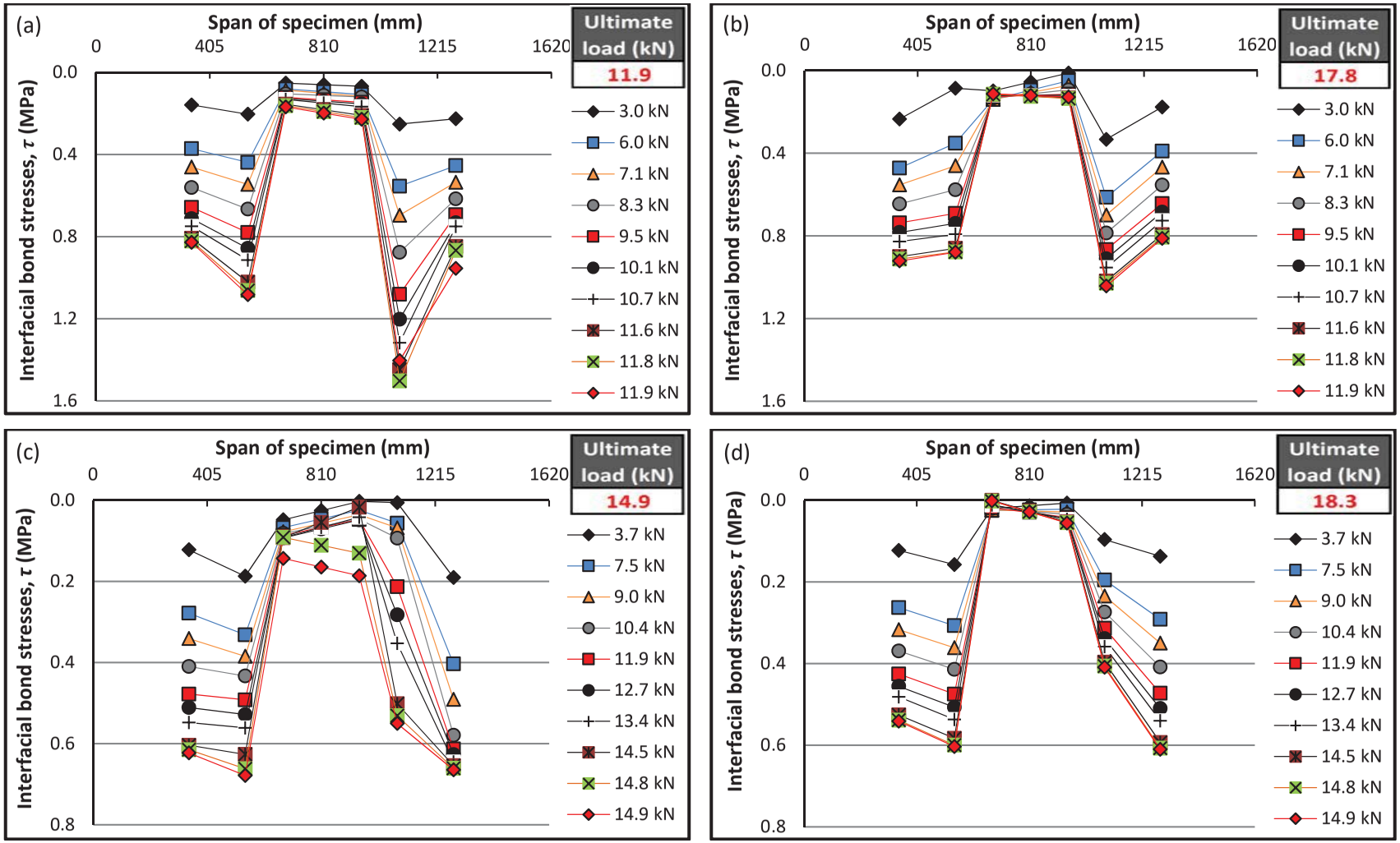

Figure 6-11 Shear stress as function of relative load level (limited load level i.e. not up to failure for B5 and B7) and bond length in the interface for selected specimens, (a) B4, (b) B5, (c) B6 and (d) B7

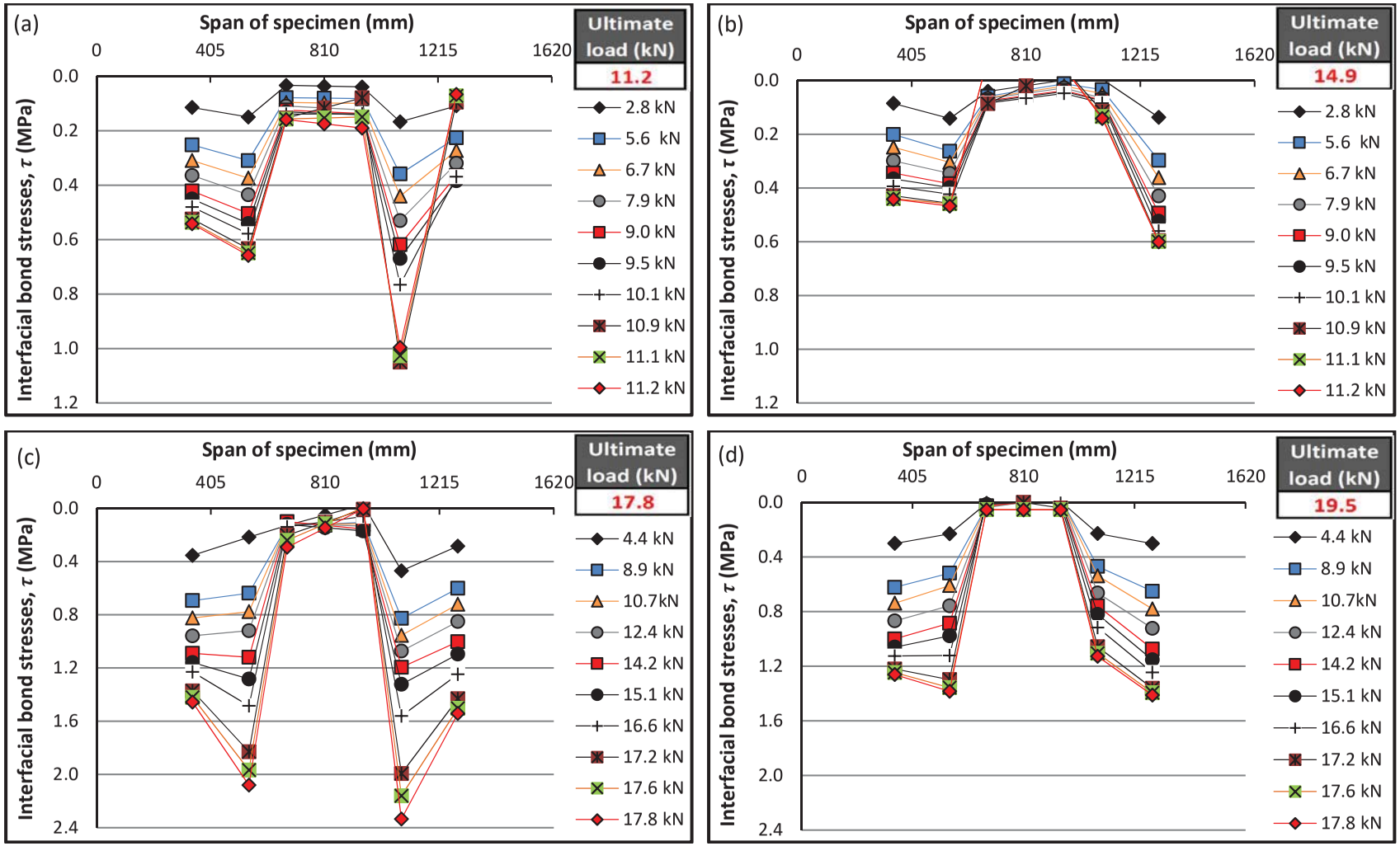

Figure 6-12 Shear stress as function of relative load level (limited load level i.e. not up to failure for B6 and B8) and bond width for selected specimens, (a) B3, (b) B6, (c) B5 and (d) B8

6.8. Prediction of ultimate moment capacity of CFRP- strengthened timber beam

With reference to the prediction model proposed by Borri et al. (2005) and the following assumptions, an analytical model based on a cross-section analysis (as shown in Figure 6-13) was developed to predict the flexure capacity of a timber beam strengthened with CFRP.

1. Timber beams are orthotropic materials with two orthogonal planes of symmetry;
2. The Bazan–Buchanan law (Bazan 1980) for the stress–strain relationships of timber was assumed in which timber is linearly elastic until failure in tension and bilinear in compression;
3. A full composite action between timber and FRP is assumed; debonding or slipping does not occur between FRP and timber;
4. As no rupture of FRP occurred during experiments, the failure of beams is defined by limiting strain in the timber, in either tension or compression.

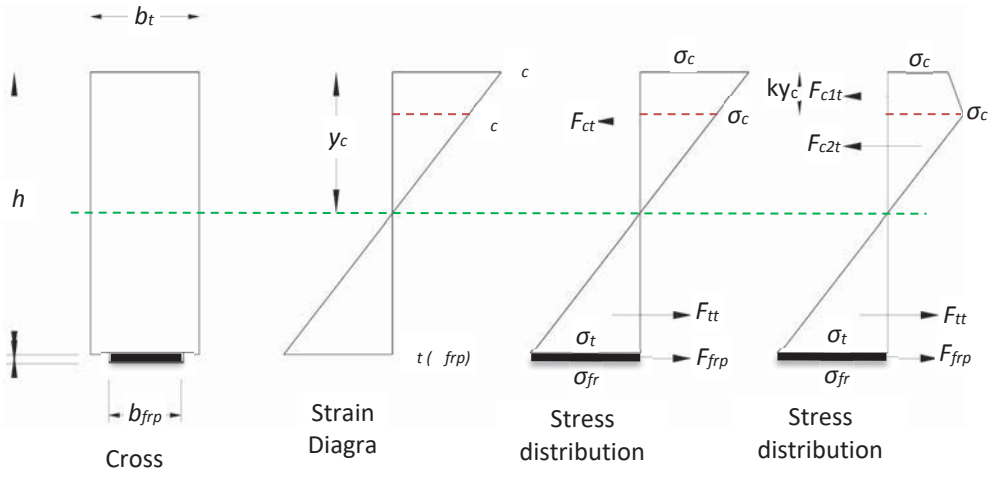

Figure 6-13 Elastic and ultimate limit scheme of a timber section

Where σ_t is maximum timber tensile stress, σ_{ct} is the maximum timber compression stress, $_t$ and $_{ct}$ are maximum strains in tension and

compression, respectively. ε_{cy} is the elastic limit compression strain and σ_{cy} is the elastic timber compression stress. F_{tt} and F_{ct} are tensile and compressive force in the timber, respectively. The tensile force in the FRP (F_{FRP}) can be calculated based on the strain (ε_{FRP}); in which a strain greater than 0.011 (the average ultimate strain achieved from coupon tests) would result in failure of the FRP. The stress distribution along the cross section is linear when maximum strains in tension is lower than strain in the elastic limit compression, $\varepsilon_{ct} < \varepsilon_{cy}$; however, plastic deformation occurs on the compression area when $\varepsilon_{cy} < \varepsilon_{ct} < \varepsilon_{cu}$. As such, two separate cases are considered depending on the strain in the cross section:

Case 1 if $\varepsilon_{ct} \leq \varepsilon_{cy}$

$$F_{ct} = F_{tt} + F_{frp} \tag{6-5}$$

$$F_{ct} = \frac{1}{2}\sigma_{ct} b_t y_c \tag{6-6}$$

$$F_{tt} = \frac{1}{2}\sigma_{tt} b_t (h - y_c) \tag{6-7}$$

$$F_{frp} = \sigma_{frp} b_{frp} t_{frp} \tag{6-8}$$

$$\varepsilon_{ct} = \frac{y_c \varepsilon_t}{h - y_c} \tag{6-9}$$

From the Bazan–Buchanan law (Bazan 1980) when $\varepsilon_{ct} < \varepsilon_{cy}$

$$\sigma_{ct} = E_t \varepsilon_{ct} \tag{6-10}$$

$$\sigma_{tt} = E_t \varepsilon_t \tag{6-11}$$

$$\sigma_{frp} = E_{frp} \varepsilon_{frp} \tag{6-12}$$

The neutral axis location can be determined by substituing Eqs. (6-6 - 6-12) to Eq. (6-5) as expressed

$$\frac{1}{2}E_t\varepsilon_{ct}y_cb_t-\frac{1}{2}E_t\varepsilon_{tt}(h-y_c)b_t-E_{frp}\varepsilon_{frp}(h-y_c+\frac{t_{frp}}{2})b_{frp}=0 \quad (6\text{-}13)$$

Once the location of the neutral axis determined from Eq. (6-13), the ultimate bending capacity of the composite beam can be obtained from moment equilibrium, i.e. by taking the moment about the neutral axis which can be expressed as follow:

$$M_u=\frac{2}{3}F_{ct}y_c+\frac{2}{3}F_{tt}(h-y_c)+F_{frp}(h-y_c+\frac{1}{2}t_{frp}) \quad (6\text{-}14)$$

for control beams $F_{FRP}=0$

Case 2 if $\varepsilon_{cy}<\varepsilon_{ct}<\varepsilon_{cu}$

Compression area of timber beam in this stage may be partially or fully plastic. Thus, the load in the compression zone will be divided into two parts. From the condition of equilibrium (Figure 6-13) it follows that

$$F_{c1t}+F_{c2t}=F_{tt}+F_{frp} \quad (6\text{-}15)$$

$$F_{c1t}=\frac{\sigma_{ct}+\sigma_{cy}}{2}b_tky_c \quad (6\text{-}16)$$

$$F_{c2t}=\frac{1}{2}\sigma_{cy}b_t(1-k)y_c \quad (6\text{-}17)$$

$$\frac{\varepsilon_{ct}}{y_c}=\frac{\varepsilon_t}{h-y_c}=\frac{\varepsilon_{cy}}{y_c(1-k)}=\frac{\varepsilon_{frp}}{h+d-y_c} \quad (6\text{-}18)$$

K is a constant value, F_{c1t} and F_{c2t} are the plastic compressive loads in timber. From the Bazan–Buchanan law

$$\sigma_{ct}=\sigma_{cy}-m.(\varepsilon_{ct}-\varepsilon_{cy}) \quad (6\text{-}19)$$

m represents the slop of the plastic zone in the model proposed by Bazan-Buchannan

$$m=\frac{\sigma_{cy}-\sigma_{ctu}}{\varepsilon_{ctu}-\varepsilon_{cy}} \tag{6-20}$$

$$M_u=\sigma_{cy}b_t(\frac{ky_c^{\ 2}}{2}-\frac{k^2y_c^{\ 2}}{3})+\sigma_{ct}b_t(\frac{ky_c^{\ 2}}{2}-\frac{k^2y_c^{\ 2}}{6})+(\sigma_{ct}+\sigma_{cy})b_tk(1-k)\frac{y_c^{\ 2}}{3} + \frac{1}{3}\sigma_{tt}b_t(h-y_c)^2+\sigma_{frp}b_{frp}t_{frp}(h-y_c+\frac{t_{frp}}{2}) \tag{6-21}$$

The values associated to the above parameters are obtained during tensile and compression tests of timber and FRP as explained in Section 6.5. as well as tested strengthened beams explained in Section 6.7. Using those values, the location of y_c determined and accordingly the ultimate bending capacity and ultimate load of each beam have been calculated using Eq. (6-14) and Eq. (6-21) and results as tabulated in Table 6-4. The analytical prediction of ultimate bending moment and load carrying capacity for all specimens are also compared against the experimental results. From Table 6-4, it can be seen that the discrepancy between predicated ultimate bending moment and actual failure loads against test results, varies between -9 % to +12 %. It is believed that this might be due to uncertainty associated with material heterogeneity and model simplifications.

Table 6-4 Experimental versus analytical results

Member	$y_{c\ Exp.}$ (mm)	$y_{c\ anal.}$ (mm)	$\frac{y_{c\ Exp.}}{y_{c\ anal.}}$	$M_{u\ Exp.}$ $(kN.m)$	$M_{u\ anal.}$ $(kN.m)$	$\frac{M_{u\ Exp.}}{M_{u\ anal.}}$	$P_{u\ Exp.}$ (kN)	$P_{u\ anal.}$ (kN)	$\frac{P_{u\ Exp.}}{P_{u\ anal.}}$
B1	45.00	45.00	1.00	1.84	1.67	1.10	6.82	6.20	1.10
B2	45.00	45.00	1.00	2.12	1.91	1.11	7.86	7.07	1.11
B3	46.28	48.33	0.96	3.03	3.09	0.98	11.22	11.45	0.98
B4	47.46	51.67	0.92	3.22	3.17	1.01	11.91	11.74	1.01
B5	47.46	52.51	0.90	4.79	5.18	0.93	17.75	19.18	0.93
B6	47.04	50.00	0.94	4.03	4.43	0.91	14.92	16.42	0.91
B7	47.04	50.63	0.93	4.94	5.35	0.92	18.29	19.83	0.92
B8	48.86	53.99	0.91	5.26	4.68	1.12	19.48	17.35	1.12

6.9. Summary

This chapter has provided details of test setup, fabrication of test specimens, test procedures and equipment used for testing CFRP strengthened timber beams. Key results and parameters affecting bond strength and behaviour of the interface in FRP-to-timber joints used for FRP strengthened beams have been presented and discussed. These parameters include bond length and effective bond length, bond width and FRP-to-timber width ratio, and thickness of the FRP. Prior to the fabrication of the test samples, properties of the timber and FRP used in the fabrication of CFRP-timber beams were experimentally quantified, based on tensile and compressive tests on clear timber samples and tensile tests on FRP coupons.

This experimental program has been performed to investigate the feasibility of strengthening glulam beams by carbon fibre reinforced polymer composites and to examine the effect of bond geometries on the ultimate flexural capacity, stiffness, deflection, and failure mode of FRP strengthened beam. To achieve these outcomes, eight full-scale timber beams with and without FRP reinforcement were tested. The test results indicate that reduction of stress concentrations can enhance the mechanical performance of the strengthened beams. The ultimate load carrying capacity and flexural strength of reinforced beams improved significantly when bond length and bond width increased.

Results of the experiments also showed that increasing the FRP layers predominantly improves stiffness and ductility of the strengthened timber beams, which has a significant enhancement in stiffness and the serviceability limit state. Finally, an analytical model has been developed to determine the ultimate flexural capacity of strengthened timber beam. Satisfactory correlation was achieved between measured and predicted flexural capacity, signifying the validity of the new models.

Chapter 7

DESIGN PROCESS FOR A FRP STRENGTHENED TIMBER BEAM

7.1. Introduction

This chapter presents a design procedure and design example for the strengthened FRP composite timber beam based on the models presented in chapter 5 and 6. The scope of design procedure discussed in this chapter is limited to ultimate limit state design for strength under short term loads only.

7.2. Proposed design procedure

The most frequent failure mechanism of the retrofitted timber beams is associated with the tension failure, with or without partial plasticisation of the compressed zone, depending on the quality of the timber. The model proposed in Chapter 6 for the calculation of ultimate flexural capacity of strengthened timber beam is based on a limiting strain for the FRP plate and strain in the tension or compression zone of timber. The following assumptions have been made to predict the flexure capacity of composite beam:

- Timber beams are orthotropic materials with two orthogonal planes of symmetry;
- A full composite action between timber and FRP is assumed;

- A linear variation of strain throughout the depth of the section has been assumed;
- A linear elasticity in tension and a bilinear relationship in compression area of timber have been assumed, whilst the FRP has been assumed to be linear-elastic;
- Beam is under Uniformly Distributed Load (UDL);
- The failure of the beams is defined by limiting strain in timber either in tension or compression.

The flexural capacity is then calculated based on the assumption of plane sections remaining plane and such calculations involve two steps, (i) determination of failure mode, and (ii) calculation of flexural capacity. The aim of the first step is to determine whether failure will occur on the compressive or tensile side. The failure of the compressive side can only be caused by timber crushing, while failure on the tensile side can be triggered by either timber fibre rupture or failure of the FRP strengthening. Since FRP rupture occurs rarely, the failure of beams is defined by limiting strain in the timber, in either tension or compression. The strain at which debonding failure of the FRP may occur in the strengthened beams can be determined based on the models proposed in Chapter 5 (Eq. 5-27). Accordingly, to predict the failure mode, the balanced cross-section area of the strengthened timber beam is calculated (refer to Eq. 6.5 in Section 6.8). Therefore, depending on the timber type and ratio of strengthening, the FRP strengthened timber beam should fail on tensile or compressive sides. However, FRP strengthening failure can be further separated into FRP debonding failure and FRP rupture. The second step is to calculate the flexural capacity of the timber beam with the assumption that plane section remains plane after bending. The design process for an FRP strengthened timber beam is illustrated in the following flowcharts (Figure 7-1). This flowchart illustrates the key design steps in the design processes

which are developed, based on the research outcomes of this thesis as discussed below.

A. Mechanical properties of FRP and timber

The structural engineer should rely on the mechanical properties either supplied by the manufacturer, based on the grade of the material or directly determined by laboratory testing. In case of material properties obtained from laboratory tests, the related design values can be determined following the recommendation of AS/NZS-4063.2 (2010) or ISO-12122-1 (2014).

B. Target timber cross section, length and FRP geometries

The cross-section area of timber, FRP width, FRP length and number of FRP layers need to be set. A preliminary static design is required to ensure the cross-section turns over-reinforced (e.g. using a terminology familiar for RC). That is because, if the reinforcement area ratio in the tension zone of timber beam is adequate and large enough, the failure mode usually changes from a brittle tensile to a more ductile compression–flexural failure.

C. Calculation of FRP sheet length

The effective bond length and accordingly entire FRP length can be calculated using data discussed in parts A and B. The expression for the calculation of effective bond length is based on results of FRP-to-timber connection presented in Section 5.4 in Chapter 5. It should be noted that if the calculated bond length is longer than the bond length set in part B, some adjustment may be needed (e.g. increase bond length, change number of FRP layers, and/or FRP geometries) until the calculated bond length becomes equal to or longer than the bond length set in part B. To eliminate the initiation of debonding due to stress concentration at the end

of the FRP, it is recommended that the actual bond length in the strengthened beam should be always longer than the calculated bond length.

It is important to emphasise that bond width is the most significant variable influencing the bond strength. In addition, increasing or decreasing FRP layers will change the stiffness and accordingly deflection of a reinforced timber beam. Thus, appropriate adjustment of the bond width and number of FRP layers needs to be performed in cases the calculated bond length was longer than the bond length determined in part B.

D. Calculate ultimate bond strength

The bond strength can be determined from the model developed in this study (Eq. 5.44) which was discussed in Section 5.6. The material properties discussed in the previous sections will be used in the model. Following determination of the bond strength, the strain at which debonding failure of the FRP may occur in the strengthened beams can be determined based on the models proposed in Section 5.5.2 (Eq. 5.27). The shear stress along the interface at various load level can also be calculated based on the model proposed in Section 5.5.3 (Eq. 5.31).

E. ***Prediction of ultimate moment capacity of strengthened timber beam***

The stress distribution along the cross section is linear when the maximum strain in tension is lower than the strain at the elastic limit in compression, ($\varepsilon_{ct}<\varepsilon_{cy}$); however, plastic deformation occurs on the compression area when $\varepsilon_{cy} < \varepsilon_{ct} < \varepsilon_{cu}$. The neutral axis can be calculated from either Eq. 6.13 or Eq. 6.18 depending on the validity of either $\varepsilon_{ct} < \varepsilon_{cy}$ or $\varepsilon_{cy} < \varepsilon_{ct} < \varepsilon_{cu}$ conditions. Once the neutral axis position is determined, it is possible to proceed to the calculation of the ultimate bending moment of the section from either Eq. 6.14 or Eq. 6.21. To illustrate the design process, an example is included in Section 7.3.

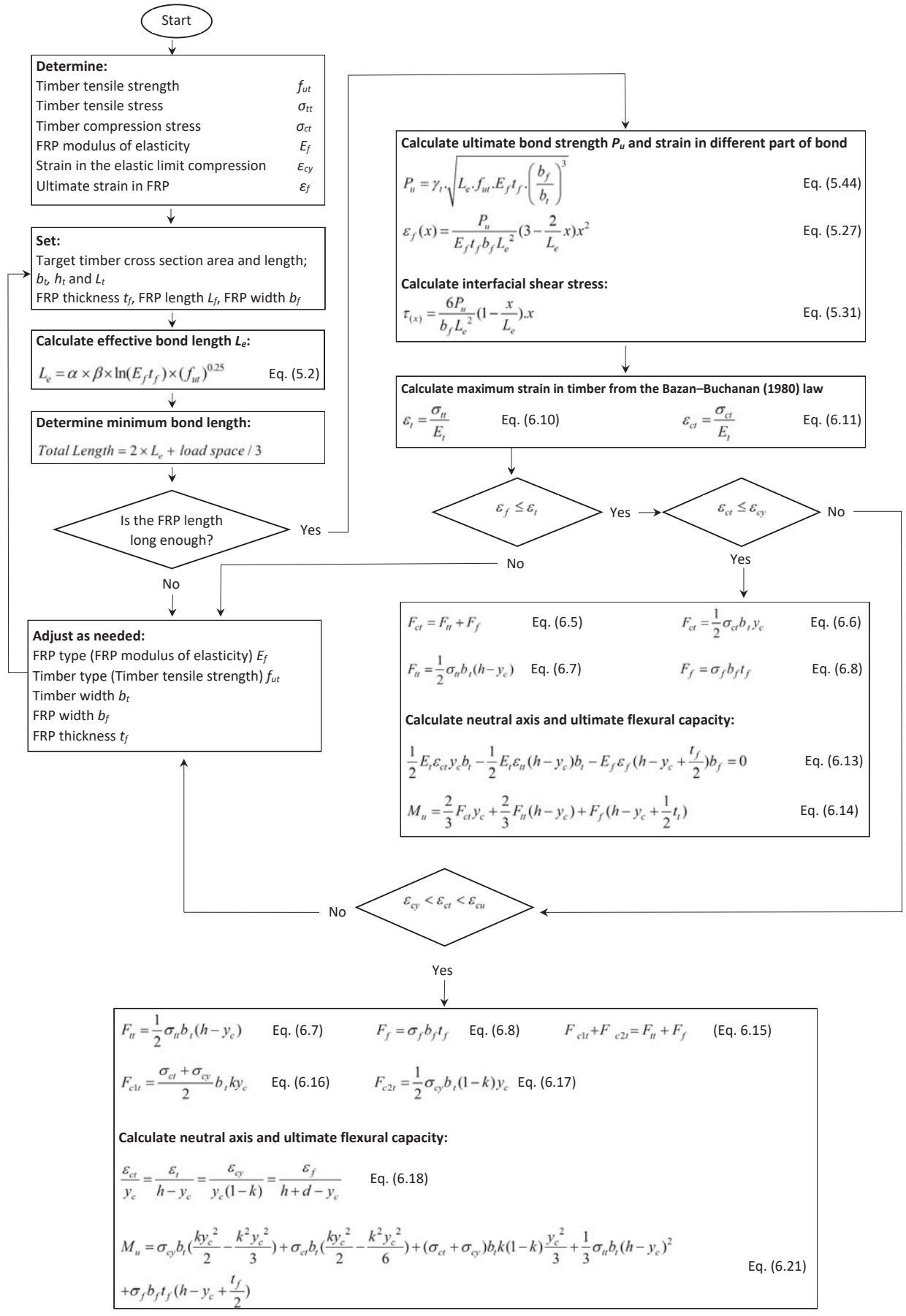

Figure 7-1 Proposed algorithm for the design process of FRP strengthened timber beam

7.3. Design example

To illustrate the design process, an example is provided in this Section. The example outlines the design of a strengthened timber beam with four layers of FRP, 45 mm bond width and total FRP length of 1300 mm as shown in Figure 7-2. Sample geometries and mechanical properties of materials used in this example are listed in Table 7-1.

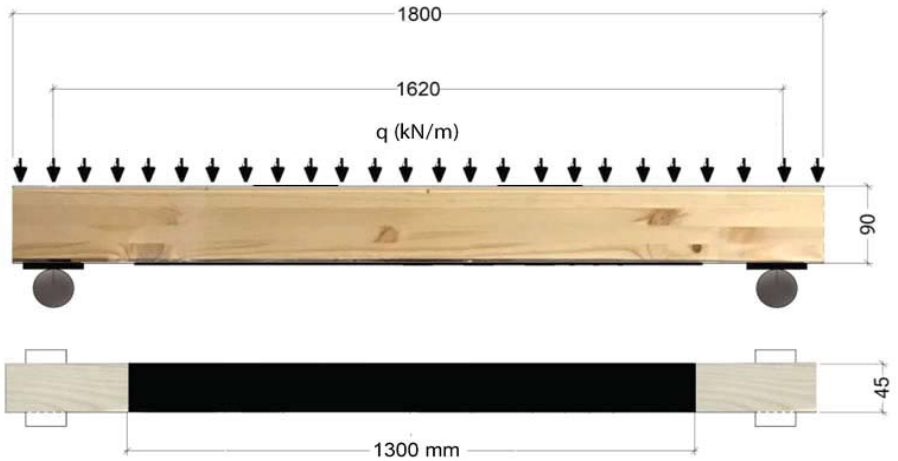

Figure 7-2 a schematic view of the strengthened beam

Table 7-1 Geometry and mechanical properties of timber and FRP used in the worked example

Material	Geometry (mm)	Tension			Compression	
		Strength (MPa)	MOE (GPa)	$\varepsilon_{ct}{}^{a}$	Strength (MPa)	$\varepsilon_{cy}{}^{b}$
Timber	45 x 90 x 1620	8	10	0.004	18	0.0042
FRP	B_f = 45 t_f = 0.664 L_f = 1300	2600	210	0.011	--	--

a: strains in tension zone of timber, b: strain in compression zone of timber

The timber would assume to be GL10 grade glulam which its mechanical properties obtained from manufacturer's datasheet (StoraEnso 2013). The mechanical properties of FRP obtained from manufacturer's datasheet (GESS-Pty-Ltd. 2015) as listed in Table 7-1. Following the assumed sample geometries and material properties, the effective bond length has been calculated based on the model proposed in Chapter 5 (Eq. 5.2) and was found to be approximately 290 mm. Accordingly, the minimum bond

length can be calculated to be at least 1120 mm; i.e. two times of the effective bond length plus one-third of shear span. Therefore, the assigned bond length of 1300 mm will be sufficient. Table 7-2 summarises the results obtained from the design calculation determined from the proposed frame work (Figure 7-1) and the steps provided above. The strain and accordingly shear stress at different part of the bond at various load level have been determined using Eq. 5.27 and 5.23. It can be seen that the condition of $\varepsilon_{ct} \leq \varepsilon_{cy}$ is valid for this example. This condition represents that the stress distribution along the cross section is linear; and the tension zone will be subjected to the maximum stress leading to a tension failure. The neutral axis and the ultimate bending moment have been calculated using Eqs. 6.13 and 6.14. The ultimate moment capacity of strengthened timber beam has been found to be 4.7 kNm. The elastic calculation of a "plain" timber beam without reinforcement, using mechanical properties listed in Table 7-1, indicates that the maximum bending moment would be around 2.43 kNm. The results indicate that FRP strengthening almost doubles the bending moment capacity of the beam. The maximum load that can be applied on the strength timber beam explained in the example work shall not be higher than 14.3 kN/m (Eq. 7-1).

$$M_u = \frac{q.L^2}{2} \tag{7-1}$$

Table 7-2 Design results for the worked example

τ_{max} (MPa)	σ_{tt} (MPa)	σ_{ct} (MPa)	*Yc* (mm)	M_u(kN.m)	*q* (kN/m)
1.5	73	60	54	4.70	14.3

7.4. Summary

A flowchart for the design process of FRP strengthened timber beam has been developed in this chapter. A worked example has also been presented to demonstrate the application of the design process to

calculate ultimate bending moment and load carrying capacity of a strengthened timber beam.

Chapter 8

CONCLUSIONS AND RECOMMENDATIONS

Advanced fibre reinforced polymers have been used for several decades for retrofitting and upgrade of infrastructure. These methods show promise and can provide a higher level of assurance of the integrity of a structure whilst minimising physical disturbance to the structure. The interfacial bond behaviour between FRP and concrete for FRP strengthened concrete structure has been thoroughly well investigated to the present time through decades of research. However, to-date, only a limited number of studies have investigated the performance of FRP composite bonded externally to timber. In these studies, the bond quality between timber and FRP has been identified and reported as the main concern of the retrofitted timber beams. The principal objective of this thesis has been to investigate the behaviour of the bond between timber and FRP and examine the factors affecting bond strength of the FRP-to-timber interface. Through a comprehensive experimental, analytical and numerical research program, the key objectives of this dissertation, as explained in Chapter 1, have been successfully achieved. The following sections present a summary of the significant contributions of this study, key findings / outcomes and recommendations for future studies.

8.1. Key Contributions

An extensive literature review followed by a sensitivity analysis using the data collected from the literature (Chen and Teng 2001; Crews and Smith

2006; Dai et al. 2006; Ren 2003; Ueda et al. 1999; Wan 2014; Wu et al. 2001; Yao et al. 2005; Zhou 2009) was performed. The results of this analysis were then used to identify the critical variables in a new bond-slip model to predict the ultimate capacity of the bond. The outcomes of FRP-to-timber joint tests and the models developed for the joints were then applied to FRP-strengthened timber beams. Eight full-scale timber beams with and without FRP reinforcement were then tested under monotonic loading in four-point bending. Finally, a design procedure for an FRP strengthened timber beam was developed to design and accurately predict the flexural capacity of strengthened timber beams.

The experimental, analytical and numerical works presented in this dissertation lead to a number of conclusions which are expected to make a significant contribution for understanding and modelling of FRP strengthened timber beams. The main contributions of the present research study on FRP externally bonded to timber are summarised as below:

- A modified single shear test setup was adopted to accurately monitor the behaviour of FRP-timber interface. Such a test set up allows the measurement of slip between timber and FRP using only one LVDT which provides more accurate and reliable results. The experimental errors and scattered results reported in the previous test methods, with two or more LVDTs, were minimised and eliminated when one LVDT was used. The significance of this test setup, when compared with previous test setups, is more obvious when the interface is subjected to unexpected out of plane movements. In the modified test setup, both timber and LVDT simultaneously have the same displacement; therefore, the slip of interface can be measured with higher precision using only one LVDT placed at the loaded end.

- The extensive experimental test conducted in the current study provides a better understanding of interface mechanisms between timber and FRP. The key parameters including bond width, bond length, timber mechanical properties and number of FRP layers that have a major impact in the behaviour of the interface, failure mode and failure load, have been investigated.
- This study has developed efficient and functional analytical interface models to accurately predict the ultimate behaviour of FRP-to-timber joints forming a composite beam. The proposed models can be used for determination of the interface characteristics including effective bond length, strain distribution profile, slip profile, shear stress and the bond strength along the interface at different loading stages. The strain profile, shear stress profile and bond-slip were expressed by the nonlinear continuously differentiable functions. The proposed analytical models are capable of appropriately predicting interface behaviour. The proposed models are a function of the FRP modulus of elasticity, FRP layers/thickness, timber mechanical properties, FRP to timber width ratio and bond length. The models presented were verified by comparing results of the proposed analytical model with the existing models from the literature. A substantial improvement in prediction of bond behaviour was achieved signifying that the proposed models from this study can be used advantageously in comparison to other existing models.
- Although timber mechanical properties and bond width are among the key parameters affecting bond strength, these factors were ignored in the previous predictive models. Furthermore, in the existing models (Bizindavyi and Neale 1999; Wan 2014), the expression of the effective bond length for FRP-to-timber joints was derived based on the model proposed for FRP-to-concrete interface. However, analytical models developed in the present study can be used for determining the

effective bond length, bond strength, strain and stress specifically for externally bonded FRP-to-timber joints. The predictive models developed in this research study cover key variables that impact on the bond strength and bond behaviour of FRP-to-timber interface.

- A Numerical investigation has also been undertaken to further understand and explain the interfacial stress transfer mechanism, validate the capability of the proposed analytical models and also to evaluate the feasibility of FRP bonded to timber. Therefore, finite element analysis may assist to gain a better understanding about the interface behaviour. Results of the numerical simulation revealed that the bond behaviour can be successfully predicted by employment of proper constitutive behaviour for materials.
- The analytical strain-stress and bond strength models derived for FRP-to-timber joints can be used for determining the maximum stress and strain in FRP strengthened or repaired timber beams. In addition, the expression of effective bond length developed through FRP-to-timber joints tests can be used for determining the overall required bond length of FRP for strengthening of timber beam. Building on the variables identified in FRP-to-timber joints, e.g. stress and strain in the interface, minimum required bond length etc., an analytical model to determine the ultimate flexural capacity of strengthened FRP-timber beams has been established. A substantial improvement for predicting flexural strength and load carrying capacity of strengthened timber beams was achieved signifying that the proposed model can be used advantageously in comparison to other existing models.
- Comprehensive test methods and guidelines are available, e.g. ACI (2005) and Canadian Standards Association (2002), for FRP bonded to concrete structures. However, determination of bond behaviour and bond strength has not been incorporated in current timber standards due to the limited research and knowledge base currently available for

strengthening of timber structures with FRP. Therefore, to fill this knowledge gap, a simple design approach has been developed that can be used as a guide for design of FRP strengthened timber beam. The proposed design procedure provides a step-by-step process for ultimate limit strength design of FRP strengthened timber beam under short-term loads.

8.2. Key findings

Results of experimental tests along with statistical analysis illustrated that bond length, bond width and width ratio, number of FRP layers, and timber mechanical properties were the most significant parameters affecting the bond strength and bond behaviour of interface. The main findings of the present research study on FRP externally bonded to timber are:

- In the present study various bond lengths were tested and it was observed that bond strength cannot increase further once the bond length exceeds the effective bond length. However, a longer bond length can improve the ductility of the interface. It was also found that number of FRP layers, timber mechanical properties, and FRP-to-timber width ratio impact on the effective bond length in which the effective bond length increases when these critical parameters are increased. However, the effective bond length was not proportional to either the amount of reinforcement nor timber tensile strength.
- Results of experimental tests revealed that the bond width significantly impacts on the bond strength; with the increase of the FRP plate width, the interfacial bond strength increases, and interface reaches higher levels of load. Furthermore, with the increase of bond width, the strain of interface and shear stress between FRP and timber decreases. The main reason for such observation can be attributed to the larger involved effective bonded area of the interface which results stress distributes more uniformly across the width of timber leading to delay in

interfacial softening or debonding along the interface. As a result, the distribution of the maximum shear stress and strain in the timber beneath the FRP plate along the transverse direction will become more uniform with the increase of FRP plate width.

- Results also showed that the maximum strain in samples with one and two plies of FRP was approximately similar, although the applied load in thicker interfaces was around 50% higher than thinner interfaces. The main reason for this behaviour of interface can be attributed to the effective bonded zone which found to be higher when two layers of FRP were bonded to timber. Hence the strain distributed between adherents (FRP and timber) and the adhesive over the longer interface toward the free end of the FRP. In addition, while the stiffness of the interface doubled for the thicker application, it can be expected that a deeper and larger surface of the timber under the FRP get involved in the interfacial stress transferring, and thus the stress distributes more uniformly along the interface. Therefore, failure occurred at higher load level.
- Experimental results demonstrated that with the increase of timber tensile strength and modulus of elasticity, the bond strength increases. Whilst a higher ultimate load was achieved for samples made from hardwood, higher maximum strain was observed in samples made from LVL. This observation appears to be related to the tensile strength of substrate; the lower tensile strength of the LVL resulted in higher ductility, with higher strain to be expected to occur in the interface, resulting a higher shear stress in the bond at failure.

8.3. Recommendations for future studies

Whilst the objectives of the present study have been achieved, there are a number of areas for further research to advance the understanding of the failure phenomenon and behaviour of the FRP-to-timber interface. To

facilitate future research directions, the following recommendations are offered:

- The scope of the present study was limited to short-term experimental tests on the FRP-timber interface. However, the effect of parameters such as environmental conditions, moisture content, timber surface treatment, curing time of the adhesive, high temperatures and fire, creep, fatigue etc. on the behaviour of FRP-to-timber interface needs to be investigated with respect to both short term and particularly time dependent, long term performance and duration of load effects on both stiffness and strength.
- The derived models are considered to be generally applicable to externally bonded FRP-to-timber joints. Additional research will be needed to address long-term performance and reliability.
- The FRP can be subjected to mechanical and physical deterioration with time, load, and exposure to various harmful environments and potentially may be damaged if used inappropriately in aggressive environments. Therefore, it is important to ensure that sufficient consideration is given to structural performance, qualification, and application of FRP materials in structural applications. Accordingly, further research may be needed to consider the effect of aggressive environments, alkalinity and corrosion, and chemical material on the application of FRP. All the above factors need to be addressed to ensure optimum durability of the composite system.
- The large consistent set of experimental data obtained from FRP-to-timber joints and beams along with supplementary consideration of other parameters e.g. moisture content, epoxy curing time, surface treatment etc. on the interface behaviour can be used for further investigation and modelling in future studies for use in repair and strengthening of timber structures.

- A wider range of epoxies can be considered especially when the substrate is relatively dense and/or hardwood. Results of such investigation then can be compared with the experiments conducted in the present study in order to investigate whether or not epoxy mechanical properties can change the interface behaviour significantly.
- Anchorage devices, which can be used to further delay the debonding of the interface between timber and FRP, can be investigated both experimentally and theoretically.
- For further contribution of the interfacial stresses into the timber substrate the effect of different surface preparation techniques can be investigated.
- The proposed analytical and numerical models are versatile and could be applied to various FRP-to-timber joints and beams. In the future, the predictions will be further compared with additional experiments under different loading tests, timber moisture content, temperature and boundary conditions.
- Whilst FRP thickness/layer has a major impact on the bond behaviour, further research can be performed for finding the optimum number of FRP layers.

References:

ABAQUS-Inc 2013, *ABAQUS Analysis User's Guide Ver. 6.13*, vol. II, © Dassault Systèmes, Providence, Rhode Island, USA.

Achintha, M. & Burgoyne, C. 2011, 'Fracture mechanics of plate debonding: Validation against experiment', *Construction and Building Materials*, vol. 25, no. 6, pp. 2961-2971.

Achintha, M. & Burgoyne, C. 2013, 'Fracture energy of the concrete–FRP interface in strengthened beams', *Engineering Fracture Mechanics*, vol. 110, pp. 38-51.

ACI 2005, *ACI Committee 440.2R-08, Guide for the design and construction of externally bonded FRP system for strengthening concrete structures.*, American Concrete Institute, MCP 2005. ACI. Michigan (USA).

Akbiyik, A., Lamanna, A.J. & Hale, W.M. 2007, 'Feasibility investigation of the shear repair of timber stringers with horizontal splits', *Construction and building materials*, vol. 21, no. 5, pp. 991-1000.

André, A. 2006, *Fibres for strengthening of timber structures*, Luleå tekniska universitet/Civil and Environmental Engineering/Structural Engineering.

Arıoglu, N., Girgin, Z.C. & Arıoglu, E. 2006, 'Evaluation of ratio between splitting tensile strength and compressive strength for concretes up to 120 MPa and its application in strength criterion', *ACI Materials Journal*, vol. 103, no. 1, pp. 18-24.

AS1720.1 2010, *Australian Standard: Timber Structures Part 1: Design methods*.

AS2796.1 1999, *Timber - Hardwood - Sawn and milled products Product specification*, Standards Australia, Australia.

AS4785.1 2002, *Timber - Softwood - Sawn and milled products Product specification*, Standards Australia, Australia.

AS/NZS1080.1 2012, *Timber—Methods of test Moisture content*, Standards Australia, Australia.

AS/NZS2098.1 2006, *Methods of test for veneer and plywood - Moisture content of veneer and plywood*, Standards Australia, Australia.

AS/NZS-4063.1:2010 2010, *Characterization of structural timber Part 1: Test methods*, Joint Technical Committee TM-001, Timber Structures, Australia.

AS/NZS-4063.2 2010, *Characterization of structural timber - Determination of characteristic values*, Australia.

ASTM-D905-03 2003, *Standard test method for strength properties of adhesive bonds in shear by compression loading*, West Conshohocken, PA, USA,.

ASTM-D2093-03 2003, *Standard Practice for Preparation of Surfaces of Plastics Prior to Adhesive Bonding.*, West Conshohocken, PA, USA.

ASTM-D2395 2014, *Standard test methods for density and specific gravity (relative density) of wood and wood-based materials*, West Conshohocken, PA, USA,.

ASTM-D3039/D3039M 2014, *Standard test method for tensile properties of polymer matrix composite materials*, West Conshohocken, PA, USA,.

ASTM D2093-03 2003, *Standard Practice for Preparation of Surfaces of Plastics Prior to Adhesive Bonding.*, West Conshohocken, PA., USA,.

Banthia, N. 2002, 'Fiber Reinforced Polymers in Concrete Construction and Advanced Repair Technologies', *Department of Civil Engineering University of British Columbia*, p. 37.

Banthia, N., Nandakumar, N. & Boyd, A. 2002, 'Sprayed fiber-reinforced polymers: From laboratory to a real bridge', *Concrete international*, vol. 24, no. 11.

Bazan, I.M.M. 1980, 'Ultimate bending strength of timber beams', Technical University of Nova Scotia.

Bedon, C. & Louter, C. 2017, 'Numerical analysis of glass-FRP post-tensioned beams–review and assessment', *Composite Structures*, vol. 177, pp. 129-140.

Bedon, C. & Louter, C. 2018, 'Numerical investigation on structural glass beams with GFRP-embedded rods, including effects of pre-stress', *Composite Structures*, vol. 184, pp. 650-661.

Bergman, R., Cai, Z., Carll, C., Clausen, C., Dietenberger, M., Falk, R., Frihart, C., Glass, S., Hunt, C. & Ibach, R. 2010, *Wood handbook: wood as an engineering material*.

Bisby, L.A. 2006, *ISIS Canada educational module no. 1: Mechanics Examples Incorporating FRP Materials*, Canada.

Bisby, L.A. & Fitzwilliam, J. 2003, 'ISIS Educational Module 2: FRP Composites for Construction'.

Biscaia, H., Cruz, D. & Chastre, C. 2016a, 'Analysis of the debonding process of CFRP-to-timber interfaces', *Construction and Building Materials*, vol. 113, pp. 96-112.

Biscaia, H.C., Chastre, C., Borba, I.S., Silva, C. & Cruz, D. 2015, 'Experimental evaluation of bonding between CFRP laminates and different structural materials', *Journal of Composites for Construction*, vol. 20, no. 3, p. 04015070.

Biscaia, H.C., Chastre, C., Cruz, D. & Franco, N. 2016b, 'Flexural Strengthening of Old Timber Floors with Laminated Carbon Fiber–Reinforced Polymers', *Journal of Composites for Construction*, vol. 21, no. 1, p. 04016073.

Bizindavyi, L. & Neale, K. 1999, 'Transfer lengths and bond strengths for composites bonded to concrete', *Journal of composites for construction*, vol. 3, no. 4, pp. 153-160.

Blaschko, M., Niedermeier, R. & Zilch, K. 1996, 'Bond failure modes of flexural members strengthened with FRP', *Fiber Compos. in Infrastruct, 2nd International Conference on Composites in Infrastructure*, eds H. H. Saadatmanesh & M.R. Ehsani, vol. 1, pp. 315-327.

Bodig, J. & Jayne, B. 1982, *Mechanics of Wood and Wood Composites*, New York: Van Nostrand Reinhold Company.

Bohannan, B. 1962, 'Prestressed wood members', *Forest Products Journal*, vol. 12, no. 12, pp. 596–602.

Borri, A., Corradi, M. & Grazini, A. 2005, 'A method for flexural reinforcement of old wood beams with CFRP materials', *Composites Part B: Engineering*, vol. 36, no. 2, pp. 143-153.

Boyd, A.J. 2000, 'Rehabilitation of reinforced concrete beams with sprayed glass fiber reinforced polymers', University of British Columbia, Vancouver, Canada.

Boyd, A.J., Liang, N., Green, P.S. & Lammert, K. 2008, 'Sprayed FRP repair of simulated impact in prestressed concrete girders', *Construction and Building Materials*, vol. 22, no. 3, pp. 411-416.

Brosens, K. 2001, 'Anchorage of externally bonded steel plates and CFRP laminates for the strengthening of concrete elements'.

Broughton, J. & Hutchinson, A. 2001, 'Adhesive systems for structural connections in timber', *International journal of adhesion and adhesives*, vol. 21, no. 3, pp. 177-186.

BS_EN_408 2010, *Timber structures - structural timber and glued laminated timber - determination of some physical and mechanical properties*, British Standards Institution, London, UK,.

BSI 1995, *Structural Adhesives – Guidelines for the Surface Preparation of Plastics*, British Standards Institution, London, UK,.

Buchanan, A. (ed.) 2007, *New Zealand Timber Design Guide*, Timber Industry Federation.

Buchanan, A.H. 1990, 'Bending strength of lumber', *Journal of structural engineering*, vol. 116, no. 5, pp. 1213-1229.

Bulleit, W.M., Sandberg, L.B. & Woods, G.J. 1989, 'Steel-reinforced glued laminated timber', *Journal of Structural Engineering*, vol. 115, no. 2, pp. 433-444.

Burgoyne, C., Taranu, N., Pilakoutas, K., Serbescu, A., Tamuzs, V. & Weber, A. 2007, 'FRP reinforcement in RC structures', *FIB Technical Rep., Sprint Digital Druck, Stuttgart, Germany*.

Campbell, M.J. 2006, *Statistics at square two: understanding modern statistical applications in medicine*, BMJ Books/Blackwell.

Canadian Standards Association 2002, *Design and construction of building components with fibre-reinforced polymers*, Canadian Standards Association.

Cao, S., Chen, J., Pan, J. & Sun, N. 2007, 'ESPI measurement of bond-slip relationships of FRP-concrete interface', *Journal of Composites for Construction*, vol. 11, no. 2, pp. 149-160.

Carlberg, J. & Toyib, B. 2012, 'Finite element modelling of interlaminar slip in stress-laminated timber decks, friction interaction modelling using Abaqus', Chalmers University of Technology, Gothenburg, Sweden.

Carling, O. 1995, *Limtra: arkitektmanual*, Svenskt limtra AB, Stockholm.

Carloni, C., Ali-Ahmad, M. & Subramaniam, K. 2005, 'Scaling effect in FRP/concrete interface debonding', *Proceedings of the 7th International Conference on Mesomechanics*, pp. 1-4.

Cevik, A., Göğüş, M.T., Güzelbey, İ.H. & Filiz, H. 2010, 'Soft computing based formulation for strength enhancement of CFRP confined concrete cylinders', *Advances in Engineering Software*, vol. 41, no. 4, pp. 527-536.

Chen, G., Teng, J. & Chen, J. 2012, 'Process of debonding in RC beams shear-strengthened with FRP U-strips or side strips', *International journal of solids and structures*, vol. 49, no. 10, pp. 1266-1282.

Chen, J. & Pan, W. 2006, 'Three dimensional stress distribution in FRP-to-concrete bond test specimens', *Construction and Building Materials*, vol. 20, no. 1, pp. 46-58.

Chen, J. & Teng, J. 2001, 'Anchorage strength models for FRP and steel plates bonded to concrete', *Journal of Structural Engineering*, vol. 127, no. 7, pp. 784-791.

CNR-DT 2007, *Guidelines for the design and construction of externally bonded FRP systems for strengthening existing structures–timber structures*, National Research Council, , Rome, Italy.

Cornetti, P. & Carpinteri, A. 2011, 'Modelling the FRP-concrete delamination by means of an exponential softening law', *Engineering Structures*, vol. 33, no. 6, pp. 1988-2001.

Coronado, C. 2006, 'Characterization, modeling and size effect of concrete-epoxy interfaces', The Pennsylvania State University.

Crews, K. & Smith, S.T. 2006, 'Tests on FRP-strengthened timber joints', *Proceedings, 3rd International Conference on FRP Composites in Civil Engineering, CICE 2006*, pp. 677-680.

Custódio, J., Broughton, J. & Cruz, H. 2009, 'A review of factors influencing the durability of structural bonded timber joints', *International journal of adhesion and adhesives*, vol. 29, no. 2, pp. 173-185.

D'Ambrisi, A., Focacci, F. & Luciano, R. 2014, 'Experimental investigation on flexural behavior of timber beams repaired with CFRP plates', *Composite Structures*, vol. 108, pp. 720-728.

Dai, J., Sato, Y. & Ueda, T. 2002, 'Improving the load transfer and effective bond length for FRP composites bonded to concrete', *Proceedings of the Japan Concrete Institute*, vol. 24, no. 1, pp. 1423-1428.

Dai, J., Ueda, T. & Sato, Y. 2005, 'Development of the nonlinear bond stress–slip model of fiber reinforced plastics sheet–concrete interfaces with a simple method', *Journal of Composites for Construction*, vol. 9, no. 1, pp. 52-62.

Dai, J., Ueda, T. & Sato, Y. 2006, 'Unified analytical approaches for determining shear bond characteristics of FRP-concrete interfaces through pullout tests', *Journal of Advanced Concrete Technology*, vol. 4, no. 1, pp. 133-145.

Davis, G. 1997, 'The performance of adhesive systems for structural timbers', *International journal of adhesion and adhesives*, vol. 17, no. 3, pp. 247-255.

De Jesus, A.M.P., Pinto, J.M.T. & Morais, J.J.L. 2012, 'Analysis of solid wood beams strengthened with CFRP laminates of distinct lengths', *Construction and Building Materials*, vol. 35, pp. 817-828.

De Lima, L.C., Costa, A.A. & Rodrigues, C.F. 2018, 'On the use of prestress for structural strengthening of timber beams: assessment with numerical support and experimental validation', *International Journal of Architectural Heritage*, pp. 1-16.

De Lorenzis, L., Miller, B. & Nanni, A. 2001, 'Bond of fiber-reinforced polymer laminates to concrete', *ACI Materials Journal*, vol. 98, no. 3, pp. 256-264.

De Luca, V. & Marano, C. 2012, 'Prestressed glulam timbers reinforced with steel bars', *Construction and building materials*, vol. 30, pp. 206-217.

Del Senno, M., Piazza, M. & Tomasi, R. 2004, 'Axial glued-in steel timber joints—experimental and numerical analysis', *Holz als Roh-und Werkstoff*, vol. 62, no. 2, pp. 137-146.

Deng, S., Djukic, L., Paton, R. & Ye, L. 2014, 'Thermoplastic-epoxy interactions and their potential applications in joining composite structures–A review', *Composites Part A: Applied Science and Manufacturing*.

Deutsches Institut für Normung, e.V. 1991, *DIN1048, Augsgabe 6.91,*, Beuth Verlag, Berlin (in German).

Du Béton, F.I. 2001, 'Externally bonded FRP reinforcement for RC structures', *Bulletin*, vol. 14, p. 138.

Ferracuti, B., Savoia, M. & Mazzotti, C. 2007, 'Interface law for FRP–concrete delamination', *Composite structures*, vol. 80, no. 4, pp. 523-531.

Foster, S. & Khomwan, N. 2005, 'Determination of bond stress versus slip for externally bonded FRP from standardized bond strength tests', *Proceedings of the International Symposium on Bond Behaviour of FRP in Structures (BBFS 2005)*.

Franco, A. & Royer Carfagni, G. 2014, 'Effective bond length of FRP stiffeners', *International Journal of Non-Linear Mechanics*, vol. 60, pp. 46-57.

Franke, S., Franke, B. & Harte, A.M. 2015, 'Failure modes and reinforcement techniques for timber beams–State of the art', *Construction and Building Materials*, vol. 97, pp. 2-13.

Gandomi, A.H., Yang, X.-S., Talatahari, S. & Alavi, A.H. 2013, *Metaheuristic applications in structures and infrastructures*, Newnes.

Gentile, C., Svecova, D. & Rizkalla, S.H. 2002, 'Timber beams strengthened with GFRP bars: development and applications', *Journal of Composites for Construction*, vol. 6, no. 1, pp. 11-20.

Gentile, C.J. 2000, 'Flexural strengthening of timber bridge beams using FRP', University of Manitoba, Winnipeg, Manitoba, Canada.

GESS-Pty-Ltd. 2015, 'Fiber reinforced polymer epoxy adhesive + fabric (FRP)', Global Engineering Systems and Solutions Pty Ltd., Form No.: RND004-005-REV00, Product Data Sheet.

Ghaib, M., Shateri, M., Thomson, D. & Svecova, D., 'Study of FRP bars under tension using acoustic emission detection technique', *Journal of Civil Structural Health Monitoring*, pp. 1-16.

Gilfillan, J., Gilbert, S. & Patrick, G. 2003, 'The use of FRP composites in enhancing the structural behavior of timber beams', *Journal of reinforced plastics and composites*, vol. 22, no. 15, pp. 1373-1388.

Girgin, Z.C., Arioglu, N. & Arioglu, E. 2007, 'Evaluation of strength criteria for very-high-strength concretes under triaxial compression', *ACI structural journal*, vol. 104, no. 3, p. 278.

Gómez, S. & Svecova, D. 2008, 'Behavior of split timber stringers reinforced with external GFRP sheets', *Journal of Composites for Construction*, vol. 12, no. 2, pp. 202-211.

Guo, Z., Cao, S., Sun, W. & Lin, X. 2005, 'Experimental study on bond stress-slip behaviour between FRP sheets and concrete', *FRP in construction, proceedings of the international symposium on bond behaviour of FRP in structures*, pp. 77-84.

Gustafsson, P. 1987, 'Analysis of generalized Volkersen-joints in terms of non-linear fracture mechanics', Paris, pp. 139-150.

Hellgren, J. & Lundberg, L. 2011, 'Finite element modelling of local interlaminar slip in stress-laminated-timber bridges', Chalmers University of Technology, Gothenburg, Sweden.

Hill, R. 1948, 'A theory of the yielding and plastic flow of anisotropic metals', *Proc. R. Soc. Lond. A*, vol. 193, no. 1033, pp. 281-297.

Hintze, J. 1998, 'NCSS statistical software', *NCSS, Kaysville, UT*.

Hiroyuki, Y. & Wu, Z. 1997, 'Analysis of debonding fracture properties of CFS strengthened member subject to tension', paper presented to the *Non-Metallic (FRP) Reinforcement for Concrete Structures, Proceedings of the Third Symposium*, Sapporo, Japan.

Hollaway, L.C. 2001, *Advanced polymer composites and polymers in the civil infrastructure*, Elsevier.

Hollaway, L.C. 2010, 'A review of the present and future utilisation of FRP composites in the civil infrastructure with reference to their important in-service properties', *Construction and Building Materials*, vol. 24, no. 12, pp. 2419-2445.

Hollaway, L.C. & Teng, J.-G. 2008, *Strengthening and rehabilitation of civil infrastructures using fibre-reinforced polymer (FRP) composites*, Elsevier Reference Monographs, North America by CRC Press.

Holzenkämpfer, P. 1994, 'Ingenieurmodelle des Verbunds geklebter Bewehrung für Betonbauteile ', Technische Universität Braunschweig, Braunschweig, Germany.

ISO6238 2001, *Adhesives -- Wood-to-wood adhesive bonds -- Determination of shear strength by compressive loading*.

ISO-12122-1 2014, *Timber structures — Determination of characteristic values — Part 1: Basic requirements*.

Issa, C.A. & Kmeid, Z. 2005, 'Advanced wood engineering: glulam beams', *Construction and Building Materials*, vol. 19, no. 2, pp. 99-106.

Jawdhari, A. & Harik, I. 2018, 'Finite element analysis of RC beams strengthened in flexure with CFRP rod panels', *Construction and Building Materials*, vol. 163, pp. 751-766.

Juvandes, L. & Barbosa, R. 2012, 'Bond Analysis of Timber Structures Strengthened with FRP Systems', *Strain*, vol. 48, no. 2, pp. 124-135.

Kabir, M.I., Samali, B. & Shrestha, R. 2016a, 'Fracture properties of CFRP–concrete bond subjected to three environmental conditions', *Journal of Composites for Construction*, vol. 20, no. 4, p. 04016010.

Kabir, M.I., Shrestha, R. & Samali, B. 2016b, 'Effects of applied environmental conditions on the pull-out strengths of CFRP-concrete bond', *Construction and Building Materials*, vol. 114, pp. 817-830.

Kamel, A.S., Elwi, A. & Cheng, R. 2004, 'Experimental investigation on FRP sheets bonded to concrete', *Emirates Journal for Engineering Research*, vol. 9, no. 2, pp. 71-76.

Khalid, H.R., Ha, S., Park, S., Wang, Z. & Lee, H. 2018, 'Bond characteristics of SFRP composites containing FRP core/anchors coated on geopolymer mortar', *Composite Structures*, vol. 189, pp. 435-442.

Khelifa, M., Auchet, S., Méausoone, P.-J. & Celzard, A. 2015, 'Finite element analysis of flexural strengthening of timber beams with carbon fibre-reinforced polymers', *Engineering Structures*, vol. 101, pp. 364-375.

Khelifa, M. & Celzard, A. 2014, 'Numerical analysis of flexural strengthening of timber beams reinforced with CFRP strips', *Composite Structures*, vol. 111, pp. 393-400.

Khelifa, M. & Khennane, A. 2013, 'Numerical analysis of the cutting forces in timber', *Journal of Engineering Mechanics*, vol. 140, no. 3, pp. 523-530.
Khennane, A., Khelifa, M., Bleron, L. & Viguier, J. 2014, 'Numerical modelling of ductile damage evolution in tensile and bending tests of timber structures', *Mechanics of Materials*, vol. 68, pp. 228-236.
Kim, Y.J. & Harries, K.A. 2010, 'Modeling of timber beams strengthened with various CFRP composites', *Engineering Structures*, vol. 32, no. 10, pp. 3225-3234.
Kirkegaard, P.H., Sørensen, J.D., Čizmar, D. & Rajčić, V. 2011, 'System reliability of timber structures with ductile behaviour', *Engineering structures*, vol. 33, no. 11, pp. 3093-3098.
Kluft, C. 2011, 'The UNSW Canberra at ADFA Journal of Undergraduate Engineering Research, Vol 4, No 1'.
Kropf, F.W. & Meierhofer, U. 2000, 'Strengthening, retrofitting and upgrading of timber structures with high-strength fibres', *Structural engineering international*, vol. 10, no. 3, pp. 178-181.
Lin, J.-P., Wu, Y.-F. & Smith, S.T. 2017, 'Width factor for externally bonded FRP-to-concrete joints', *Construction and Building Materials*, vol. 155, pp. 818-829.
Liu, K. & Wu, Y.-F. 2012, 'Analytical identification of bond–slip relationship of EB-FRP joints', *Composites Part B: Engineering*, vol. 43, no. 4, pp. 1955-1963.
Longcope, D. & Forrestal, M. 1983, 'Penetration of targets described by a Mohr-Coulomb failure criterion with a tension cutoff', *Journal of Applied Mechanics*, vol. 50, no. 2, pp. 327-333.
Lu, X., Teng, J., Ye, L. & Jiang, J. 2005a, 'Bond–slip models for FRP sheets/plates bonded to concrete', *Engineering structures*, vol. 27, no. 6, pp. 920-937.
Lu, X., Ye, L., Teng, J. & Jiang, J. 2005b, 'Meso-scale finite element model for FRP sheets/plates bonded to concrete', *Engineering structures*, vol. 27, no. 4, pp. 564-575.
Lyons, J.S. & Ahmed, M.R. 2005, 'Factors affecting the bond between polymer composites and wood', *Journal of Reinforced Plastics and composites*, vol. 24, no. 4, pp. 405-412.
Maeda, T., Asano, Y., Sato, Y., Ueda, T. & Kakuta, Y. 1997, 'A study on bond mechanism of carbon fiber sheet', *Non-Metallic (FRP) Reinforcement for Concrete Structures, Proceedings of the Third Symposium*, vol. 1, Sapporo, Japan, pp. 279-286.
Manalo, A., Aravinthan, T., Karunasena, W. & Islam, M. 2010, 'Flexural behaviour of structural fibre composite sandwich beams in flatwise and edgewise positions', *Composite Structures*, vol. 92, no. 4, pp. 984-995.
Mark, J. & Goldberg, M.A. 1988, 'Multiple regression analysis and mass assessment: A review of the issues', *Appraisal Journal*, vol. 56, no. 1.
Mark, R. 1961, 'Wood-aluminum beams within and beyond the elastic range', *Forest Products Journal*, vol. 11, no. 10, pp. 477-484.
Mazzotti, C., Savoia, M. & Ferracuti, B. 2008, 'An experimental study on delamination of FRP plates bonded to concrete', *Construction and Building Materials*, vol. 22, no. 7, pp. 1409-1421.
Mazzotti, C., Savoia, M. & Ferracuti, B. 2009, 'A new single-shear set-up for stable debonding of FRP–concrete joints', *Construction and Building Materials*, vol. 23, no. 4, pp. 1529-1537.

MBrace®Fibre 2011, *Unidirectional Carbon Fibre sheeting Glass and Aramid sheeting used with resin lay up method*, Product Data Sheet.

Meier, U. 1987, 'Bridge repair with high performance composite materials', *Material und Technik*, vol. 4, pp. 125-128.

Micelli, F., Scialpi, V. & La Tegola, A. 2005, 'Flexural reinforcement of glulam timber beams and joints with carbon fiber-reinforced polymer rods', *Journal of Composites for Construction*, vol. 9, no. 4, pp. 337-347.

Mier, J.G.V. 2012, *Concrete fracture: a multiscale approach*, CRC press.

Mohammadi, T. 2014, 'Failure mechanisms and key parameters of FRP debonding from cracked concrete beams', Marquette University, Milwaukee, Wisconsin.

Monti, G., Renzelli, M. & Luciani, P. 2003, 'FRP adhesion in uncracked and cracked concrete zones', *Proceedings of the Sixth International Symposium on FRP Reinforcement for Concrete Structures (FRPRCS-6)*, vol. 1, World Scientific, pp. 183-192.

Mostofinejad, D. & Shameli, S.M. 2013, 'Externally bonded reinforcement in grooves (EBRIG) technique to postpone debonding of FRP sheets in strengthened concrete beams', *Construction and Building Materials*, vol. 38, no. Complete, pp. 751-758.

Motavalli, M. & Czaderski, C. 2007, 'FRP composites for retrofitting of existing civil structures in Europe: state-of-the-art review', *Proceedings of the American Composites Manufacturers Association 2007*.

Myers, J.H. & Forgy, E.W. 1963, 'The development of numerical credit evaluation systems', *Journal of the American Statistical Association*, vol. 58, no. 303, pp. 799-806.

Nakaba, K., Kanakubo, T., Furuta, T. & Yoshizawa, H. 2001, 'Bond behavior between fiber-reinforced polymer laminates and concrete', *ACI Structural Journal*, vol. 98, no. 3.

Neubauer, U. & Rostasy, F. 1997, 'Design aspects of concrete structures strengthened with externally bonded CFRP-plates', *Proceedings of the 7th international conference on structural faults and repair, 8 july 1997. Volume 2: concrete and composites*.

Niedermeier, R. 1996, *Stellungnahme zur richtlinie für das verkleben von betonbauteilen durch ankleben von stahllaschen–entwurf märz 1996*, Technische Universität München, Munich, Germany (in German).

Niu, H. & Wu, Z. 2006, 'Effects of FRP-concrete interface bond properties on the performance of RC beams strengthened in flexure with externally bonded FRP sheets', *Journal of materials in civil engineering*, vol. 18, no. 5, pp. 723-731.

Pantelides, C., Romero, P. & Reaveley, L. 2010, 'Rehabilitation of splice connections of wood trusses with FRP composites', *Construction and Building Materials*, vol. 24, no. 1, pp. 37-45.

Patnaik, A., Bauer, C. & Srivatsan, T. 2008, 'The extrinsic influence of carbon fibre reinforced plastic laminates to strengthen steel structures', *Sadhana*, vol. 33, no. 3, pp. 261-272.

Pearce, C., Thavalingam, A., Liao, Z. & Bićanić, N. 2000, 'Computational aspects of the discontinuous deformation analysis framework for modelling concrete fracture', *Engineering Fracture Mechanics*, vol. 65, no. 2-3, pp. 283-298.

Peterson, J. 1965, 'Wood beams prestressed with bonded tension elements', *Journal of the Structural Division*, vol. 91, no. 1, pp. 103-120.

Porteous, J. & Kermani, A. 2013, *Structural timber design to Eurocode 5*, John Wiley & Sons.

Qiao, P. & Chen, F. 2009, 'Interface crack between two interface deformable piezoelectric layers', *International Journal of Fracture*, vol. 156, no. 2, pp. 185-201.

Raftery, G.M. & Harte, A.M. 2013, 'Nonlinear numerical modelling of FRP reinforced glued laminated timber', *Composites Part B: Engineering*, vol. 52, pp. 40-50.

Raftery, G.M., Harte, A.M. & Rodd, P.D. 2009, 'Bonding of FRP materials to wood using thin epoxy gluelines', *International Journal of Adhesion and Adhesives*, vol. 29, no. 5, pp. 580-588.

Raftery, G.M. & Rodd, P.D. 2015, 'FRP reinforcement of low-grade glulam timber bonded with wood adhesive', *Construction and Building Materials*, vol. 91, pp. 116-125.

Raftery, G.M. & Whelan, C. 2014, 'Low-grade glued laminated timber beams reinforced using improved arrangements of bonded-in GFRP rods', *Construction and building materials*, vol. 52, pp. 209-220.

Ren, H. 2003, 'Study on basic theories and long time behavior of concrete structures strengthened by fiber reinforced polymers', Dalian University of Technology, Dalian, China.

Rescalvo, F.J., Valverde-Palacios, I., Suarez, E. & Gallego, A. 2017, 'Experimental Comparison of Different Carbon Fiber Composites in Reinforcement Layouts for Wooden Beams of Historical Buildings', *Materials*, vol. 10, no. 10, p. 1113.

Rescalvo, F.J., Valverde-Palacios, I., Suarez, E. & Gallego, A. 2018, 'Experimental and analytical analysis for bending load capacity of old timber beams with defects when reinforced with carbon fiber strips', *Composite Structures*, vol. 186, pp. 29-38.

Rezazadeh, M. & Carvelli, V. 2018, 'A damage model for high-cycle fatigue behavior of bond between FRP bar and concrete', *International Journal of Fatigue*, vol. 111, pp. 101-111.

Rijal, R. 2013, 'Dynamic Performance of Timber and Timber-Concrete Composite Flooring Systems', University of Technology, Sydney, Sydney, Australia.

Savoia, M., Ferracuti, B. & Mazzotti, C. 2003, 'Non linear bond-slip law for FRP-concrete interface', *Proc. of 6th international symposium on FRP reinforcement for concrete structures. Singapore: World Scientific Publications*, World Scientific, pp. 163-172.

Seica, M.V. & Packer, J.A. 2007, 'FRP materials for the rehabilitation of tubular steel structures, for underwater applications', *Composite Structures*, vol. 80, no. 3, pp. 440-450.

Seracino, R. 2001, 'Axial intermediate crack debonding of plates glued to concrete surfaces', *FRP Composites in Civil Engineering. Proceedings of the International Conference on FRP composites in Civil Engineering*.

Seracino, R., Raizal Saifulnaz, M. & Oehlers, D. 2007, 'Generic debonding resistance of EB and NSM plate-to-concrete joints', *Journal of Composites for Construction*, vol. 11, no. 1, pp. 62-70.

Serbescu, A., Guadagnini, M. & Pilakoutas, K. 2013, 'Standardised double-shear test for determining bond of FRP to concrete and corresponding model development', *Composites Part B: Engineering*, vol. 55, pp. 277-297.

Shen, D., Shi, H., Ji, Y. & Yin, F. 2015, 'Strain rate effect on effective bond length of basalt FRP sheet bonded to concrete', *Construction and Building Materials*, vol. 82, pp. 206-218.

Sikadur®-330 2015, *2-part epoxy impregnation resin, Product Data Sheet*.

Sliker, A. 1962, 'Reinforced wood laminated beams', *Forest Products Journal*, vol. 12, no. 1, pp. 91-96.

Smith, S.T. 2011, 'Strengthening of concrete, metallic and timber construction materials with FRP composites', *Advances in FRP Composites in Civil Engineering*, Springer, pp. 13-19.

Soleimani, S.M. 2006, 'Sprayed glass fiber reinforced polymers in shear strengthening and enhancement of impact resistance of reinforced concrete beams', The University of British Columbia, Vancouver, Canada.

Stanila, O., Isopescu, D. & Hohan, R. 2010, 'Timber Elements: Traditional and Modern Strengthening Techniques', *Buletinul Institutului Politehnic din lasi. Sectia Constructii, Arhitectura*, vol. 56, no. 3, p. 75.

StoraEnso 2013, 'Glue Laminated Structural Timber', Stora Enso, Division Wood Products, Sales Australia.

Subramaniam, K.V., Carloni, C. & Nobile, L. 2007, 'Width effect in the interface fracture during shear debonding of FRP sheets from concrete', *Engineering Fracture Mechanics*, vol. 74, no. 4, pp. 578-594.

Sweeney, R. 2012, 'The UNSW Canberra at ADFA Journal of Undergraduate Engineering Research, Vol 5, No 1 '.

Täljsten, B. 1994, 'Strengthening of existing concrete structures with externally bonded steel or fibre reinforced plastics', University of Technology., Luleå, Sweden.

Täljsten, B. 1996, 'Strengthening of concrete prisms using the plate-bonding technique', *International journal of Fracture*, vol. 82, no. 3, pp. 253-266.

Talukdar, S. 2008, 'Strengthening of timber beams using externally-bonded sprayed fibre reinforced polymers', The University of British Columbia, Vancouver, Canada.

Talukdar, S. & Banthia, N. 2010, 'Performance of Sprayed Fiber Reinforced Polymer Strengthened Timber Beams', *Advances in Materials Science and Engineering*.

Tanaka, T. 1996, 'Shear resisting mechanism of reinforced concrete beams with CFS as shear reinforcement', Hokkaido University, Japan.

Tao, Y. & Chen, J.-F. 2014, 'Concrete damage plasticity model for modeling FRP-to-concrete bond behavior', *Journal of composites for construction*, vol. 19, no. 1, p. 04014026.

Thelandersson, S. & Larsen, H.J. 2003, *Timber engineering*, John Wiley & Sons.

Thorhallsson, E.R., Hinriksson, G.I. & Snæbjörnsson, J.T. 2017, 'Strength and stiffness of glulam beams reinforced with glass and basalt fibres', *Composites Part B: Engineering*, vol. 115, pp. 300-307.

Triantafillou, T.C. 1998, 'Composites: a new possibility for the shear strengthening of concrete, masonry and wood', *Composites Science and Technology*, vol. 58, no. 8, pp. 1285-1295.

Triantafillou, T.C. & Plevris, N. 1991, 'Post-strengthening of R/C beams with epoxy-bonded fiber composite materials', *Advanced Composites Materials in Civil Engineering Structures*, ASCE, pp. 245-256.

Ueda, T. & Dai, J. 2004, 'New shear bond model for FRP–concrete interface–from modeling to application', *FRP Composites in Civil Engineering-CICE 2004: Proceedings of the 2nd International Conference on FRP Composites in Civil Engineering-CICE 2004, 8-10 December 2004, Adelaide, Australia*, Taylor & Francis, p. 69.

Ueda, T. & Dai, J. 2005, 'Interface bond between FRP sheets and concrete substrates: properties, numerical modeling and roles in member behaviour', *Progress in Structural Engineering and Materials*, vol. 7, no. 1, pp. 27-43.

Ueda, T., Sato, Y. & Asano, Y. 1999, 'Experimental study on bond strength of continuous carbon fiber sheet', *ACI Special Publication*, vol. 188.

US Department of Transportation, F.A.A. 2004, *Effects of surface preparation on the long-term durability of adhesively bonded composite joints, final report*.

Vahedian, A., Shrestha, R. & Crews, K. 2017a, 'Effective bond length and bond behaviour of FRP externally bonded to timber', *Construction and Building Materials*, vol. 151, pp. 742-754.

Vahedian, A., Shrestha, R. & Crews, K. 2017b, 'Modelling of Factors Affecting Bond Strength of Fibre Reinforced Polymer Externally Bonded to Timber and Concrete', *International Journal of Structural and Construction Engineering*, vol. 11, no. 12, pp. 1567-1574.

Valipour, H.R. & Crews, K. 2011, 'Efficient finite element modelling of timber beams strengthened with bonded fibre reinforced polymers', *Construction and Building Materials*, vol. 25, no. 8, pp. 3291-3300.

Vallée, T., Tannert, T., Murcia-Delso, J. & Quinn, D.J. 2010, 'Influence of stress-reduction methods on the strength of adhesively bonded joints composed of orthotropic brittle adherends', *International Journal of Adhesion and Adhesives*, vol. 30, no. 7, pp. 583-594.

Valluzzi, M.R., Nardon, F., Garbin, E. & Panizza, M. 2016, 'Multi-scale characterization of moisture and thermal cycle effects on composite-to-timber strengthening', *Construction and Building Materials*, vol. 102, pp. 1070-1083.

Wan, J. 2014, 'An investigation of FRP-to-timber bonded interfaces', The University of Hong Kong Pokfulam, Hong Kong.

Wan, J., Smith, S.T., Qiao, P. & Chen, F. 2013, 'Experimental Investigation on FRP-to-Timber Bonded Interfaces', *Journal of Composites for Construction*.

Wegman, R.F. & Van Twisk, J. 2012, *Surface preparation techniques for adhesive bonding*, William Andrew.

Woo, S.-K. & Lee, Y. 2010, 'Experimental study on interfacial behavior of CFRP-bonded concrete', *KSCE Journal of Civil Engineering*, vol. 14, no. 3, pp. 385-393.

Wu, Z. & Hemdan, S. 2005, 'Debonding in FRP Strengthened Flexural Members with Different Shear-Span Ratios', *Proceeding of the 7th International Symposium on Fiber Reinforced Composite Reinforcement for Concrete Structures*, vol. 1, Michigan, USA, pp. 411-426.

Wu, Z. & Niu, H. 2000, 'Shear transfer along FRP-concrete interface in flexural members', *J. Mater., Conc. Struct., Pavements, JSCE*, vol. 49, no. 662, pp. 231-245.

Wu, Z., Yuan, H., Yoshizawa, H. & Kanakubo, T. 2001, 'Experimental/analytical study on interfacial fracture energy and fracture propagation along FRP-concrete interface', *ACI Special Publications*, vol. 201, pp. 133-152.

Xu, Q., Chen, L., Harries, K.A., Zhang, F., Wang, Z. & Chen, X. 2017, 'Experimental study and numerical simulation of long-term behavior of timber beams strengthened with near surface mounted CFRP bars', *Materials and Structures*, vol. 50, no. 1, p. 45.

Xu, T., He, Z., Tang, C., Zhu, W. & Ranjith, P. 2015, 'Finite element analysis of width effect in interface debonding of FRP plate bonded to concrete', *Finite Elements in Analysis and Design*, vol. 93, pp. 30-41.

Yang, H., Liu, W., Shao, J. & Zhou, Z. 2008, 'Study on flexural behavior of timber beams strengthened with FRP', *Journal of Building Materials*, vol. 11, no. 5, pp. 591-597.

Yang, Y.-l., Liu, J.-w. & Xiong, G.-j. 2013, 'Flexural behavior of wood beams strengthened with HFRP', *Construction and Building Materials*, vol. 43, pp. 118-124.

Yao, J., Teng, J. & Chen, J. 2005, 'Experimental study on FRP-to-concrete bonded joints', *Composites Part B: Engineering*, vol. 36, no. 2, pp. 99-113.

Ye, F. & Yao, J. 2008, 'A 3D Finite Element Study on The Effect of FRP Plate Width on Interfacial Stress between FRP and Concrete [J]', *Bulletin of Science and Technology*, vol. 24, no. 6, pp. 853-859.

Yoshizawa, H., Wu, Z., Yuan, H. & Kanakubo, T. 2000, 'Study on FRP-concrete interface bond performance', *PROCEEDINGS-JAPAN SOCIETY OF CIVIL ENGINEERS*, DOTOKU GAKKAI, pp. 105-120.

Yuan, H., Teng, J., Seracino, R., Wu, Z. & Yao, J. 2004, 'Full-range behavior of FRP-to-concrete bonded joints', *Engineering Structures*, vol. 26, no. 5, pp. 553-565.

Yuan, H. & Wu, Z.S. 1999, 'Interfacial fracture theory in structures strengthened with composite of continuous fiber', *Proceedings of symposium of China and Japan: Science and technology of 21st century*, pp. 142-155.

Yuan, H., Wu, Z.S. & Yoshizawa, H. 2001, 'Theoretical solutions on interfacial stress transfer of externally bonded steel/composite laminates', *J. Struct. Mech. and Earthquake Engrg.,*, no. 675, pp. 27-39.

Zhao, X.-L. & Zhang, L. 2007, 'State-of-the-art review on FRP strengthened steel structures', *Engineering Structures*, vol. 29, no. 8, pp. 1808-1823.

Zhou, Y.-W., Wu, Y.-F. & Yun, Y. 2010, 'Analytical modeling of the bond–slip relationship at FRP-concrete interfaces for adhesively-bonded joints', *Composites Part B: Engineering*, vol. 41, no. 6, pp. 423-433.

Zhou, Y. 2009, 'Analytical and experimental study on the strength and ductility of FRP-reinforced high strength concrete beam', Dalian University of Technology, Dalian, China.

Zoghi, M. 2013, *The International Handbook of FRP Composites in Civil Engineering*, CRC Press.

Appendix A.

Material properties – FRP to timber joints

Table A-1 Hardwood compression test results

Samples	P_u (kN)	Compressive Strength (MPa)	MOE (GPa)	Poisson Ratio	
				Parallel to the grain	Perpendicular to the grain
C1	74.20	62.83	20.55	0.03	0.41
C2	83.49	67.32	19.87	0.53	0.37
C3	79.83	64.19	14.37	0.18	0.49
C4	76.21	62.27	23.71	0.53	0.43
C5	81.70	66.76	14.21	0.27	0.36
C6	71.11	61.27	15.29	0.39	--
C7	67.18	61.09	28.18	0.41	0.28
C8	77.07	67.71	19.70	0.54	--
C9	77.30	68.40	16.39	0.23	--
C10	80.11	67.44	24.77	0.58	0.22
Average	76.82	64.93	19.70	0.37	0.36
CoV (%)	6.46	4.45	24.13	27.04	24.66

Table A-2 Hardwood tensile test results

Samples	P_u (kN)	Tensile Strength (MPa)	MOE (GPa)
T1	80.34	57.01	20.58
T2	96.08	66.77	21.51
T3	100.10	69.75	21.03
T4	93.89	64.93	18.01
T5	100.52	70.50	20.18
T6	108.08	74.58	18.60
T7	97.13	67.81	20.15
T8	111.19	77.25	22.28
T9	90.28	63.79	17.66
T10	90.41	62.87	17.53
Average	96.80	67.53	19.75
CoV (%)	9.26	8.71	8.58

Table A-3 LVL compression test results

Samples	P_u (kN)	Compressive Strength (MPa)	MOE (GPa)	Poisson Ratio	
				Parallel to the grain	Perpendicular to the grain
C1	99.65	56.24	17.95	0.67	0.25
C2	97.36	55.64	18.79	--	0.39
C3	97.71	54.72	19.11	0.73	0.20
C4	99.21	57.29	13.74	0.29	--
C5	95.28	57.98	15.64	0.58	0.28
C6	101.84	55.22	--	--	--
C7	102.78	55.78	13.65	0.40	0.37
C8	103.21	56.02	20.44	0.90	--
C9	105.03	56.53	22.65	0.68	--
C10	103.73	57.21	17.11	0.57	--
Average	100.58	56.26	17.68	0.60	0.30
CoV (%)	3.19	1.79	16.96	31.85	27.04

Table A-4 LVL tensile test results

Samples	P_u (kN)	Tensile Strength (MPa)	MOE (GPa)
T1	92.48	41.05	16.83
T2	81.46	35.77	16.73
T3	116.61	48.38	16.71
T4	86.07	35.34	15.19
T5	89.74	37.48	15.67
T6	108.27	44.21	16.58
T7	115.17	45.90	17.32
T8	131.18	53.25	16.50
T9	143.26	55.07	15.27
T10	114.08	46.62	15.00
Average	107.83	44.31	16.18
CoV (%)	18.81	15.61	5.06

Table A-5 FRP tensile test results

Samples	Tensile Strength (MPa)	MOE (GPa)	Ultimate Strain
1	2369	219	0.013
2	2449	251	0.010
3	2418	232	0.013
4	2675	205	0.013
5	2724	205	0.016
6	2349	261	0.012
Average	2497	229	0.013
CoV (%)	6.5	10.22	15.99

Appendix B.

Strain in the FRP – Hardwood Series

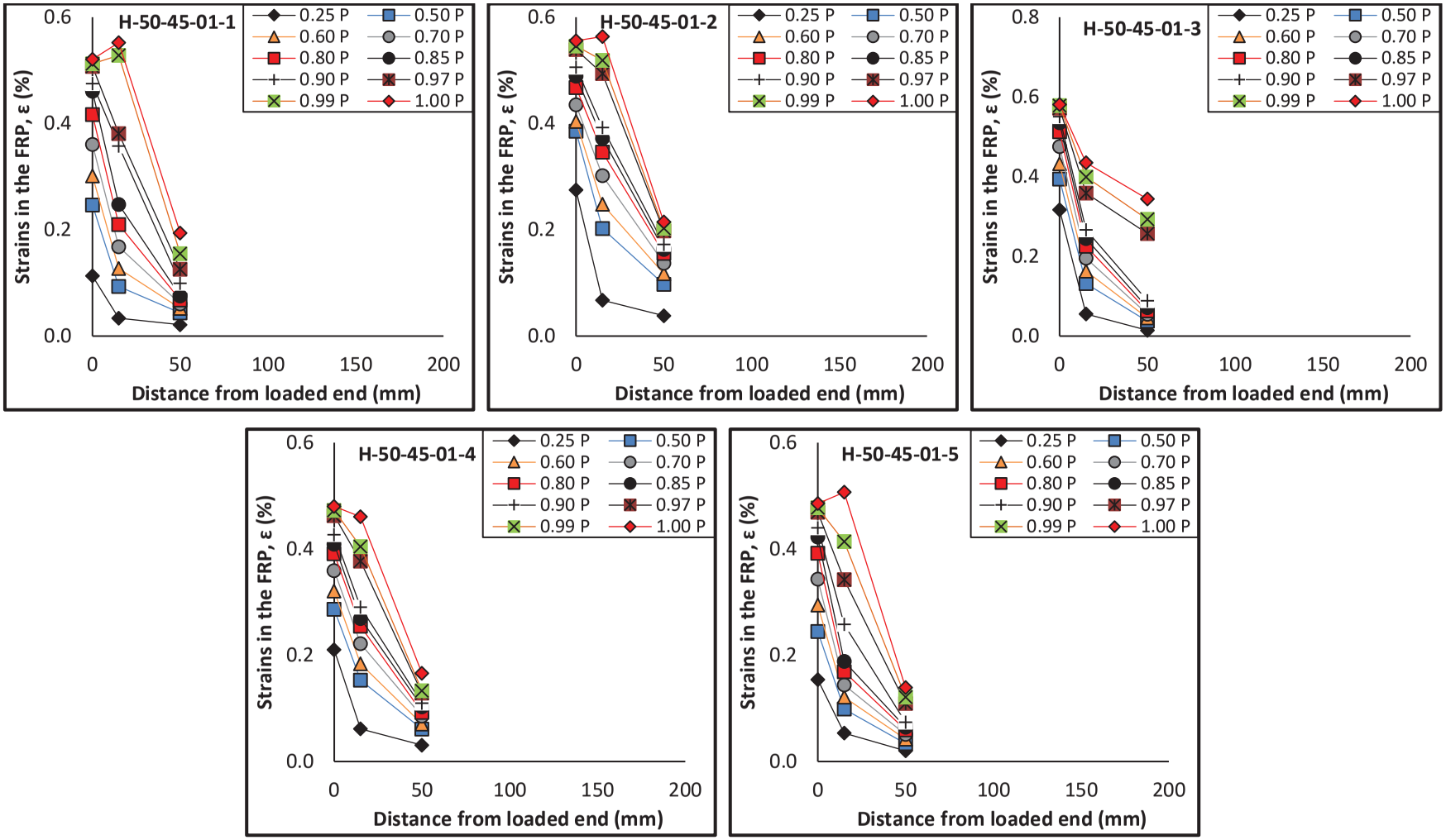
H-50-45-01-1
H-50-45-01-2
H-50-45-01-3
H-50-45-01-4
H-50-45-01-5
0.25 P
0.50 P
0.60 P
0.70 P
0.80 P
0.85 P
0.90 P
0.97 P
0.99 P
1.00 P
Strains in the FRP, ε (%)
Distance from loaded end (mm)

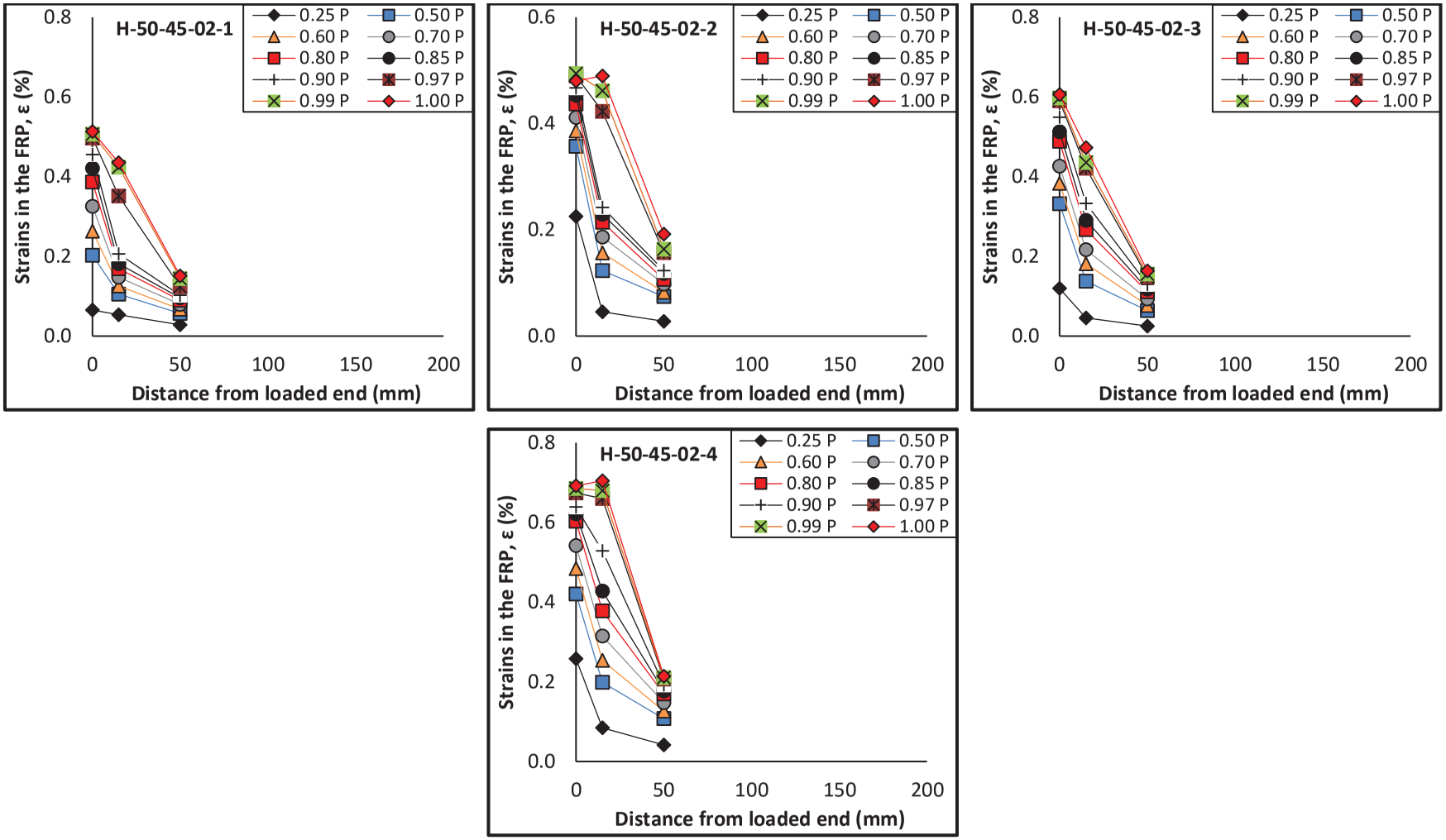
H-50-45-02-1
H-50-45-02-2
H-50-45-02-3
H-50-45-02-4
0.25 P
0.50 P
0.60 P
0.70 P
0.80 P
0.85 P
0.90 P
0.97 P
0.99 P
1.00 P
Strains in the FRP, ε (%)
Distance from loaded end (mm)
0.0
0.2
0.4
0.6
0.8
0
50
100
150
200

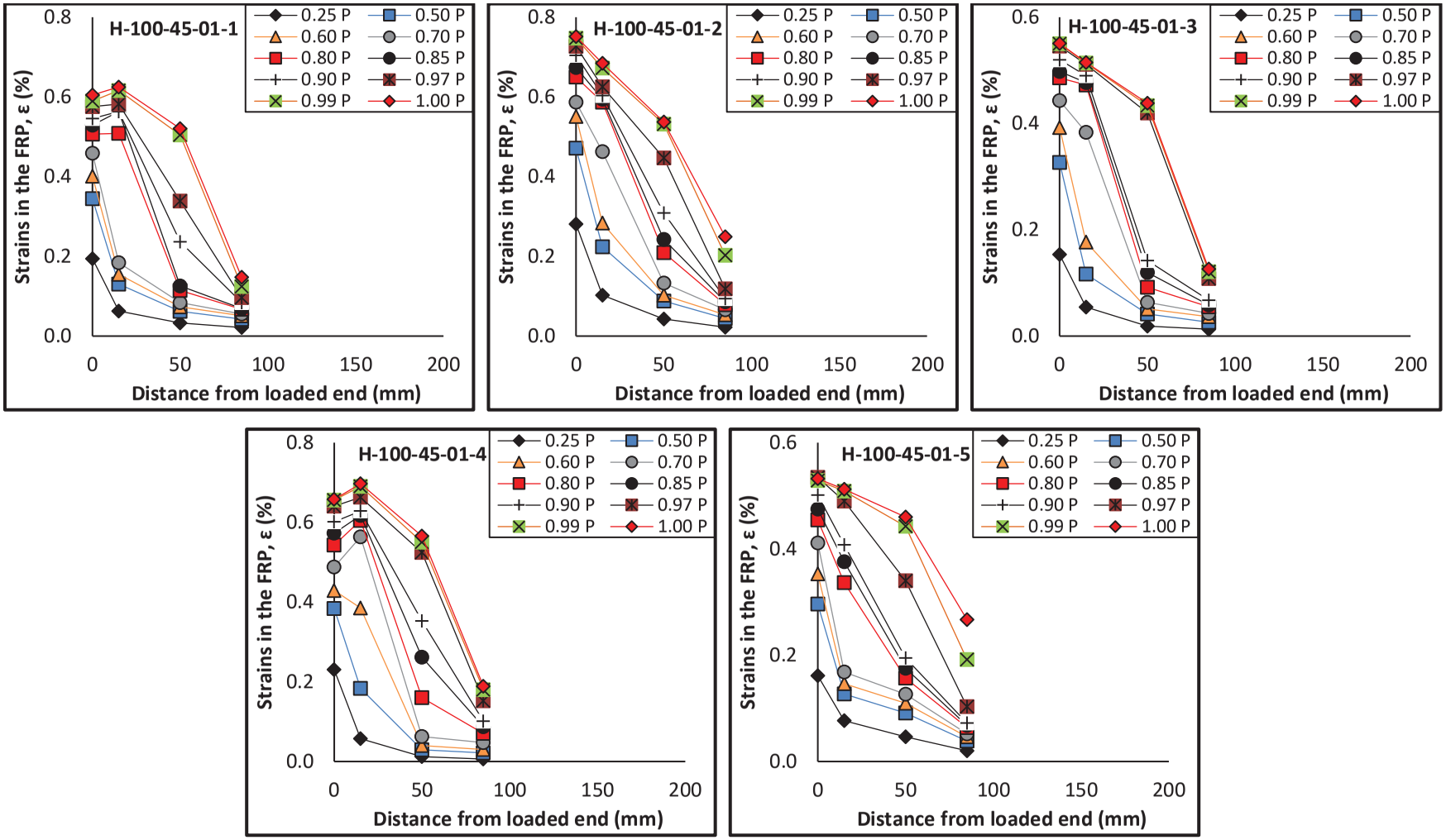
H-100-45-01-1
H-100-45-01-2
H-100-45-01-3
H-100-45-01-4
H-100-45-01-5
0.25 P
0.50 P
0.60 P
0.70 P
0.80 P
0.85 P
0.90 P
0.97 P
0.99 P
1.00 P
Strains in the FRP, ε (%)
Distance from loaded end (mm)

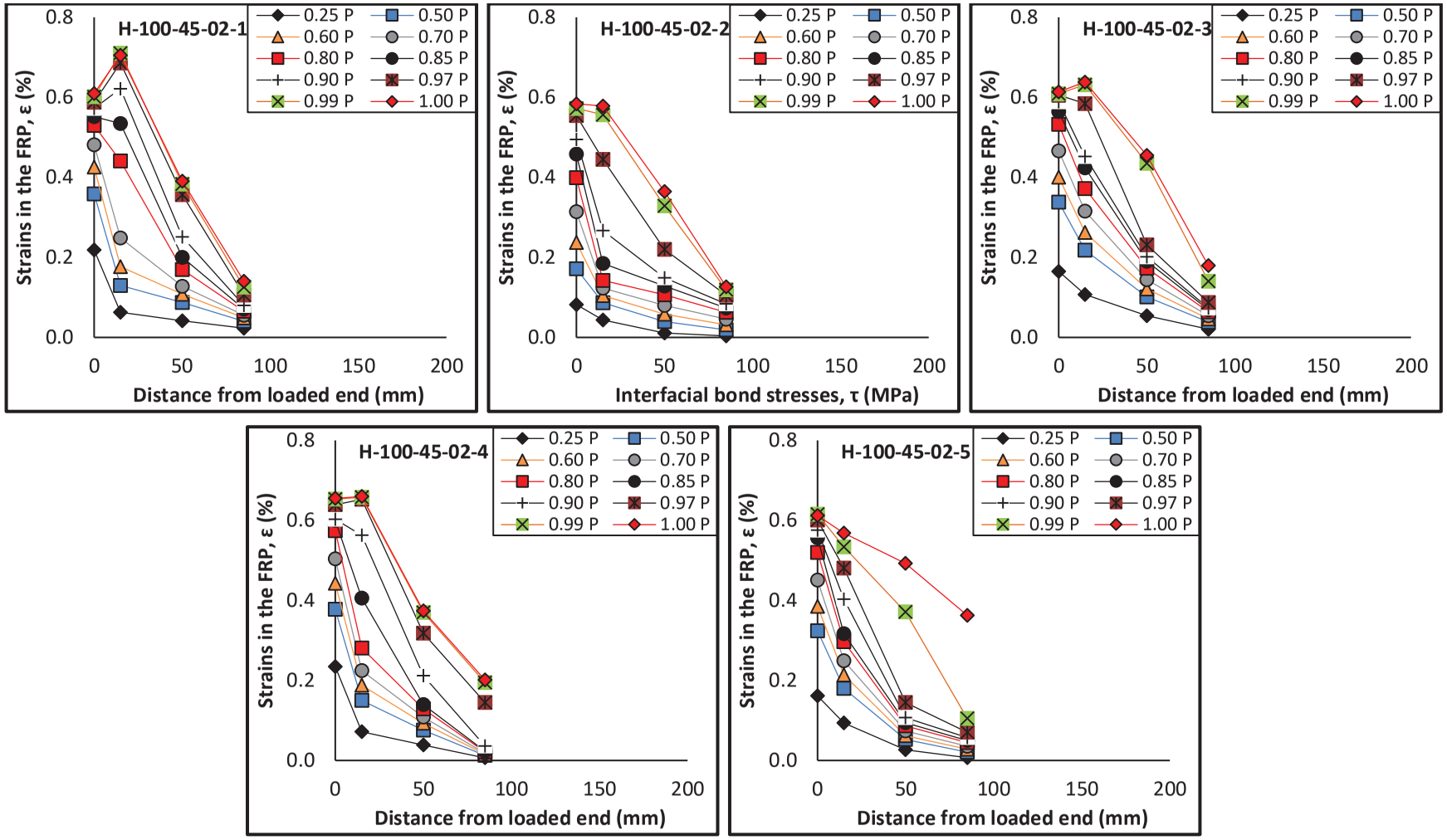
H-100-45-02-1
H-100-45-02-2
H-100-45-02-3
H-100-45-02-4
H-100-45-02-5
0.25 P
0.50 P
0.60 P
0.70 P
0.80 P
0.85 P
0.90 P
0.97 P
0.99 P
1.00 P
Strains in the FRP, ε (%)
Distance from loaded end (mm)
Interfacial bond stresses, τ (MPa)
0.0
0.2
0.4
0.6
0.8
0
50
100
150
200

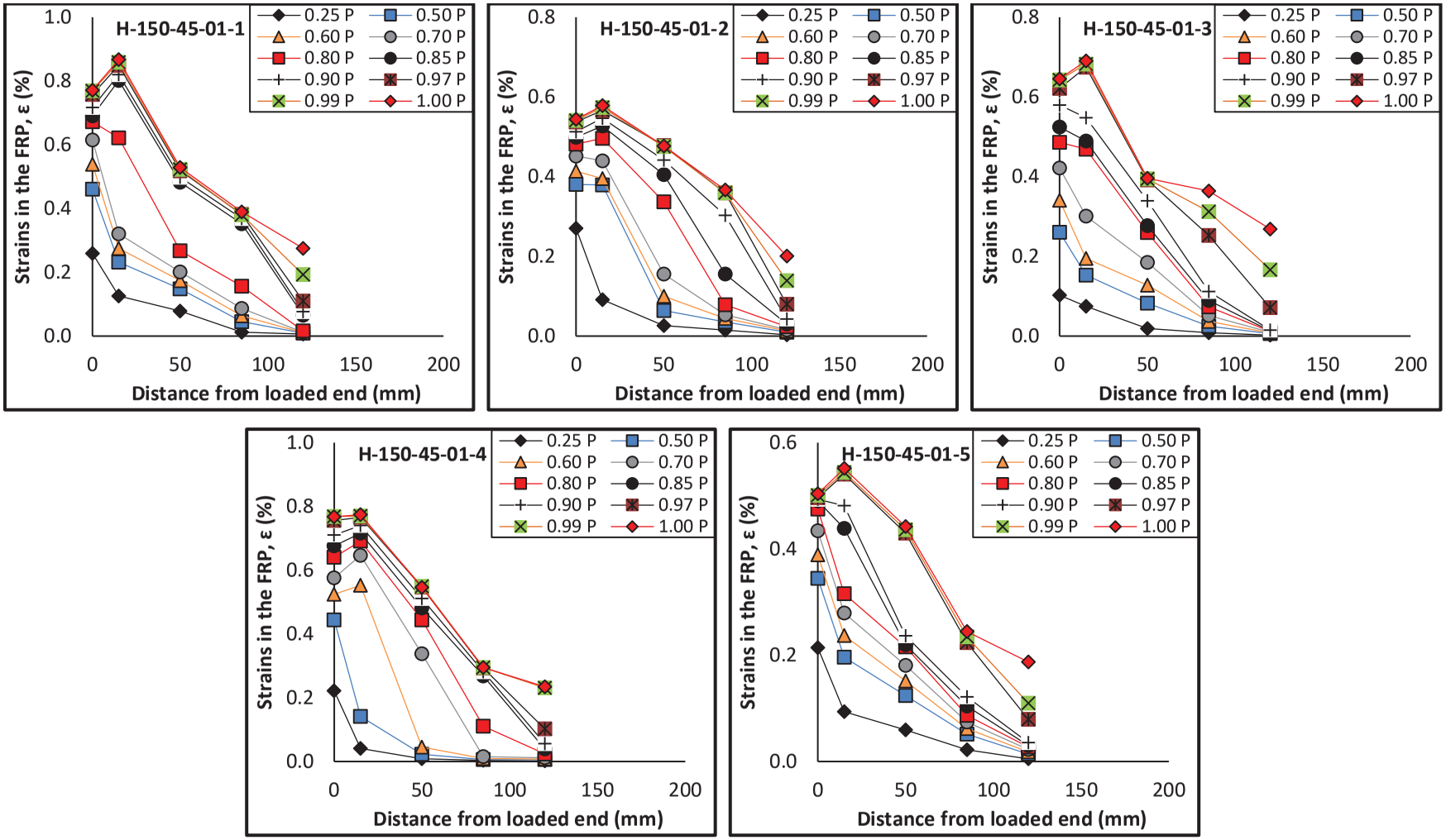
H-150-45-01-1
H-150-45-01-2
H-150-45-01-3
H-150-45-01-4
H-150-45-01-5
0.25 P
0.50 P
0.60 P
0.70 P
0.80 P
0.85 P
0.90 P
0.97 P
0.99 P
1.00 P
Strains in the FRP, ε (%)
Distance from loaded end (mm)

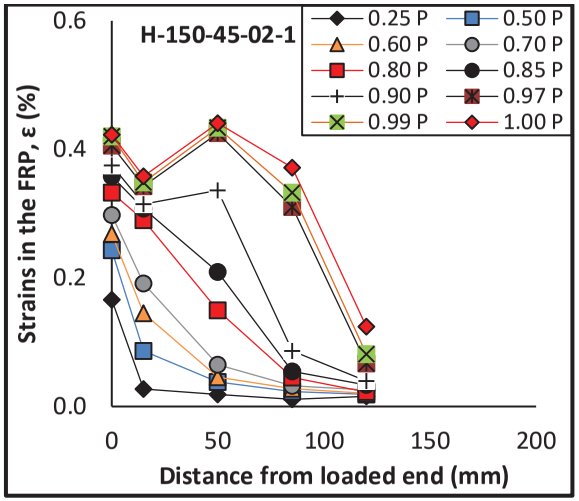
H-150-45-02-1
0.25 P
0.50 P
0.60 P
0.70 P
0.80 P
0.85 P
0.90 P
0.97 P
0.99 P
1.00 P
Strains in the FRP, ε (%)
0.0
0.2
0.4
0.6
0
50
100
150
200
Distance from loaded end (mm)

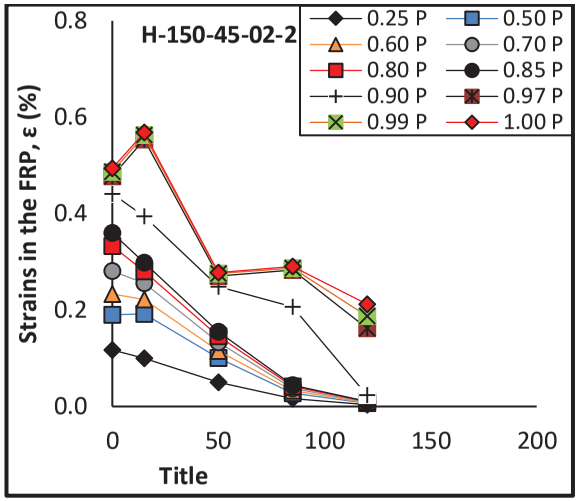
H-150-45-02-2
0.25 P
0.50 P
0.60 P
0.70 P
0.80 P
0.85 P
0.90 P
0.97 P
0.99 P
1.00 P
Strains in the FRP, ε (%)
0.0
0.2
0.4
0.6
0.8
0
50
100
150
200
Title

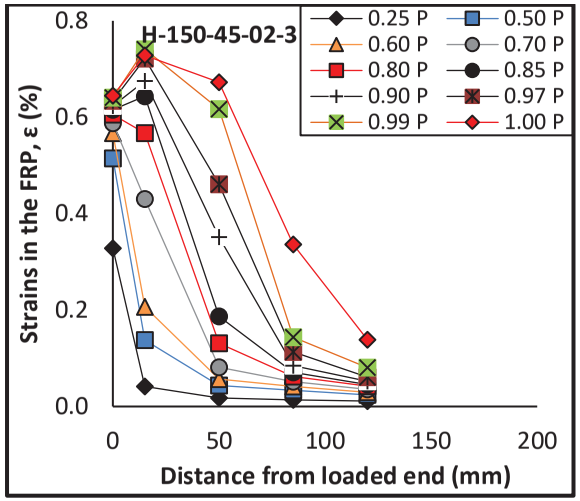
H-150-45-02-3
0.25 P
0.50 P
0.60 P
0.70 P
0.80 P
0.85 P
0.90 P
0.97 P
0.99 P
1.00 P
Strains in the FRP, ε (%)
0.0
0.2
0.4
0.6
0.8
0
50
100
150
200
Distance from loaded end (mm)

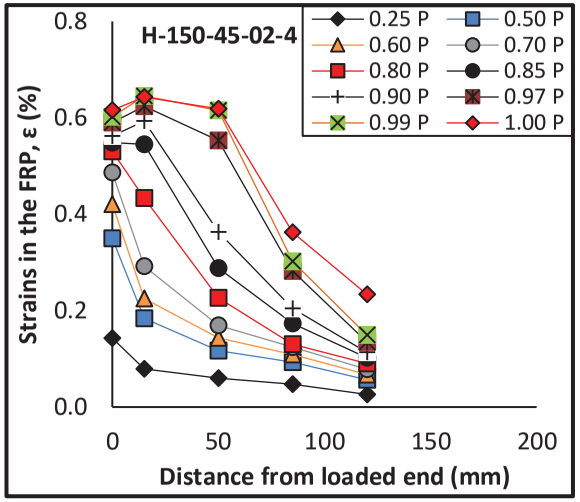
H-150-45-02-4
0.25 P
0.50 P
0.60 P
0.70 P
0.80 P
0.85 P
0.90 P
0.97 P
0.99 P
1.00 P
Strains in the FRP, ε (%)
0.0
0.2
0.4
0.6
0.8
0
50
100
150
200
Distance from loaded end (mm)

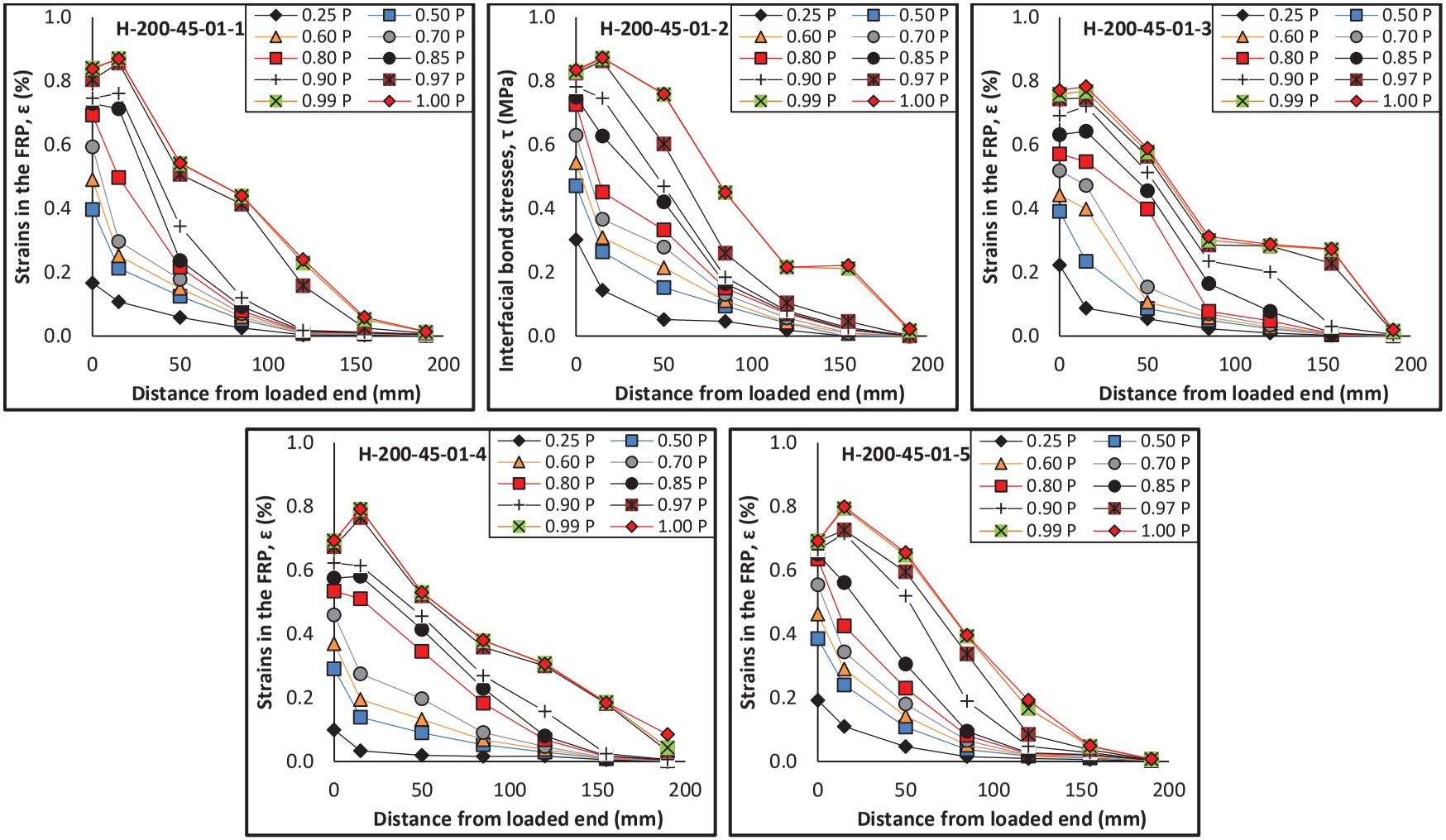
H-200-45-01-1
H-200-45-01-2
H-200-45-01-3
H-200-45-01-4
H-200-45-01-5
0.25 P
0.50 P
0.60 P
0.70 P
0.80 P
0.85 P
0.90 P
0.97 P
0.99 P
1.00 P
Strains in the FRP, ε (%)
Interfacial bond stresses, τ (MPa)
Distance from loaded end (mm)
0.0
0.2
0.4
0.6
0.8
1.0
0
50
100
150
200

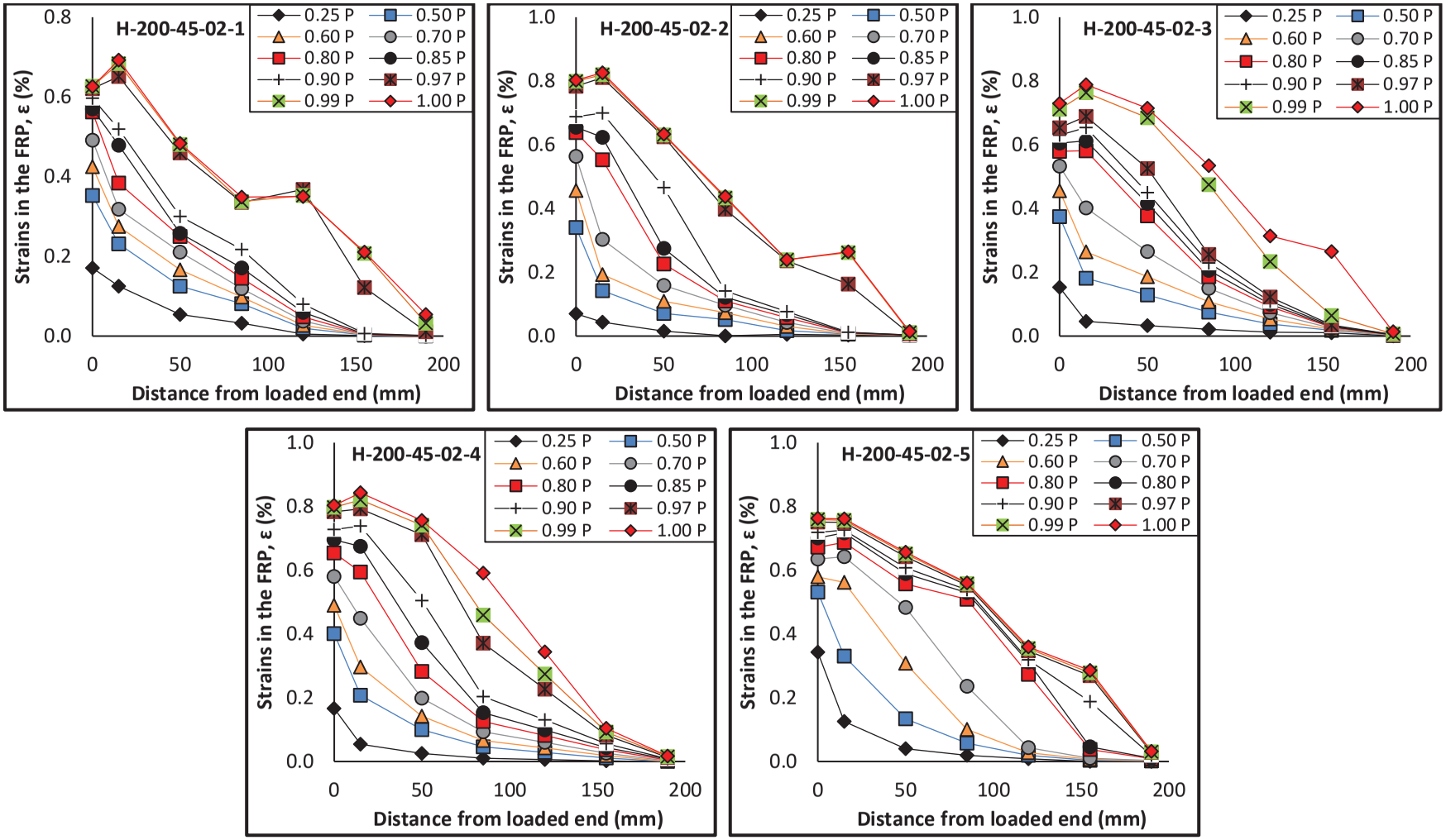
H-200-45-02-1
H-200-45-02-2
H-200-45-02-3
H-200-45-02-4
H-200-45-02-5
0.25 P
0.50 P
0.60 P
0.70 P
0.80 P
0.85 P
0.90 P
0.97 P
0.99 P
1.00 P
Strains in the FRP, ε (%)
Distance from loaded end (mm)

Appendix C.

Strain in the FRP – LVL Series

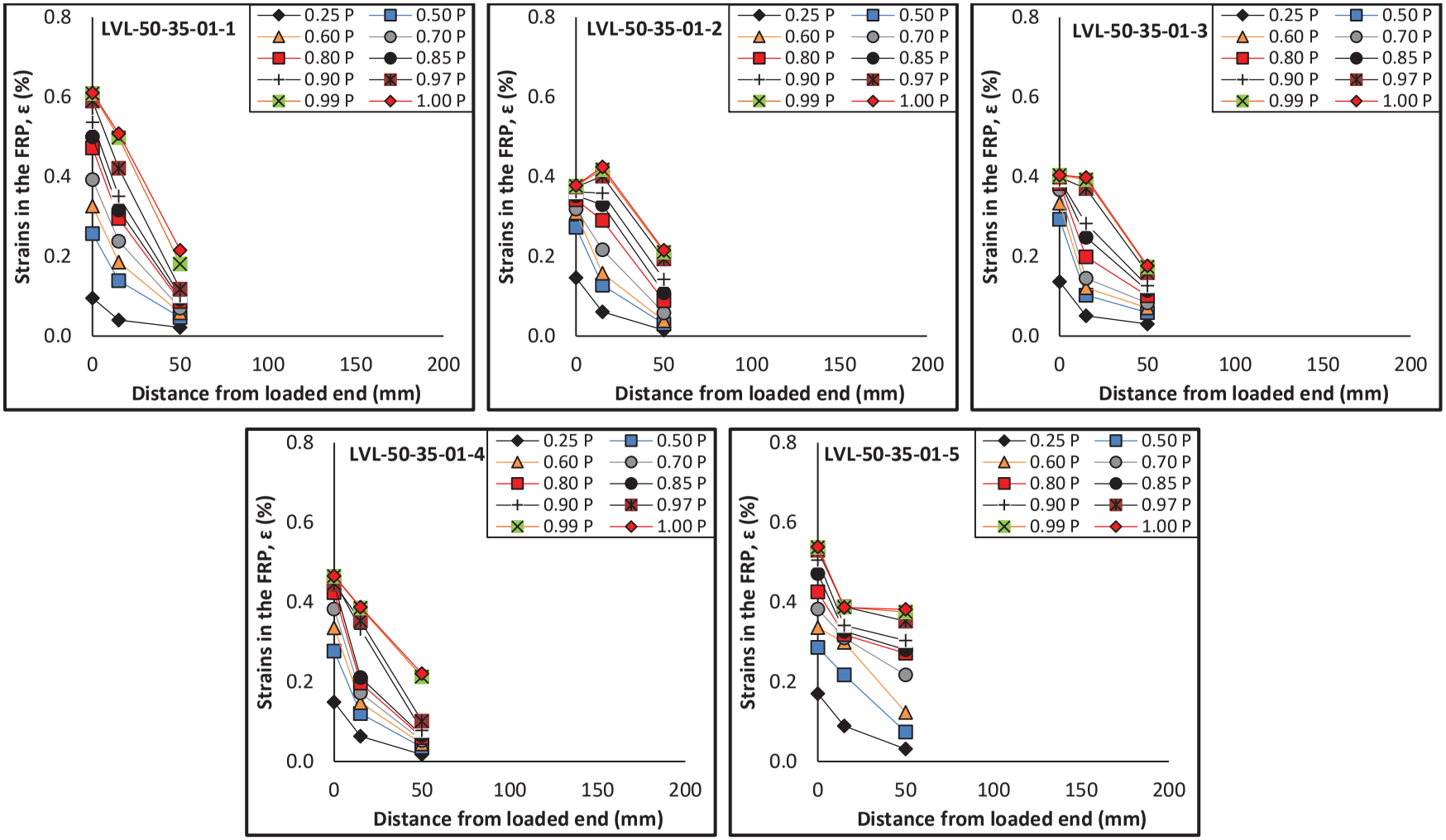
LVL-50-35-01-1
LVL-50-35-01-2
LVL-50-35-01-3
LVL-50-35-01-4
LVL-50-35-01-5
0.25 P
0.50 P
0.60 P
0.70 P
0.80 P
0.85 P
0.90 P
0.97 P
0.99 P
1.00 P
Strains in the FRP, ε (%)
Distance from loaded end (mm)
0.0
0.2
0.4
0.6
0.8
0
50
100
150
200

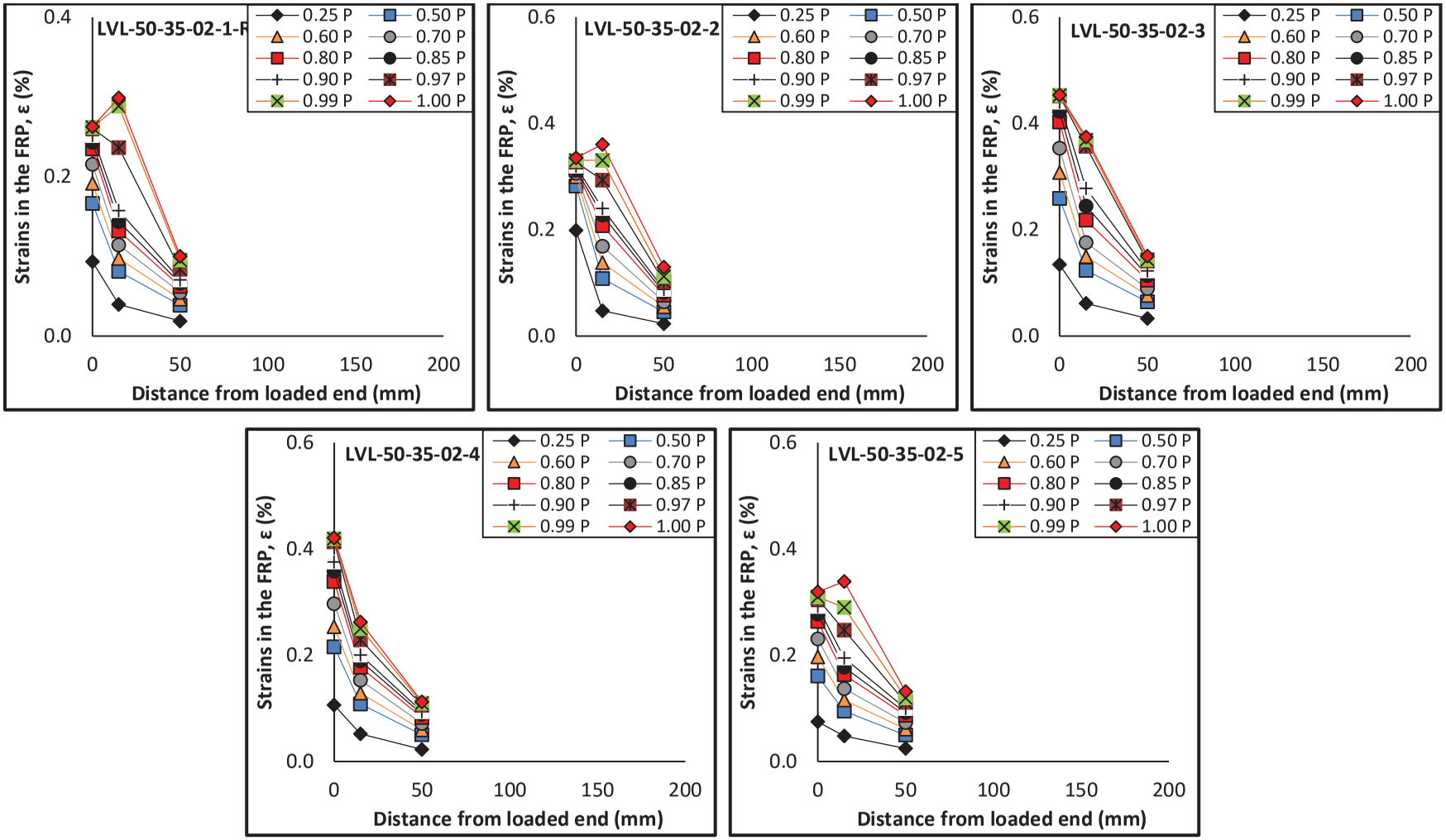
LVL-50-35-02-1-F
LVL-50-35-02-2
LVL-50-35-02-3
LVL-50-35-02-4
LVL-50-35-02-5
0.25 P
0.50 P
0.60 P
0.70 P
0.80 P
0.85 P
0.90 P
0.97 P
0.99 P
1.00 P
Strains in the FRP, ε (%)
Distance from loaded end (mm)

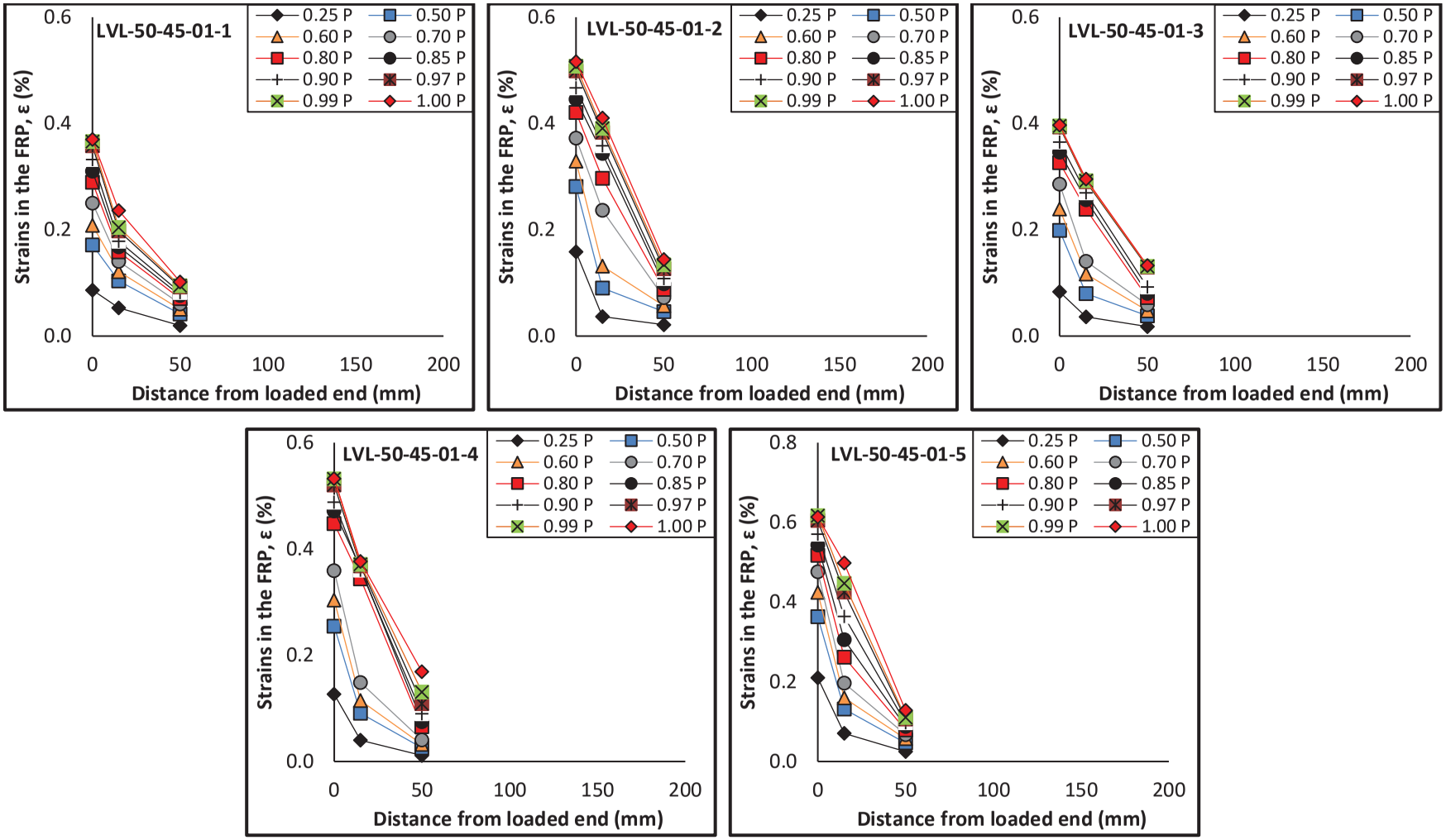
LVL-50-45-01-1
LVL-50-45-01-2
LVL-50-45-01-3
LVL-50-45-01-4
LVL-50-45-01-5
0.25 P
0.50 P
0.60 P
0.70 P
0.80 P
0.85 P
0.90 P
0.97 P
0.99 P
1.00 P
Strains in the FRP, ε (%)
Distance from loaded end (mm)

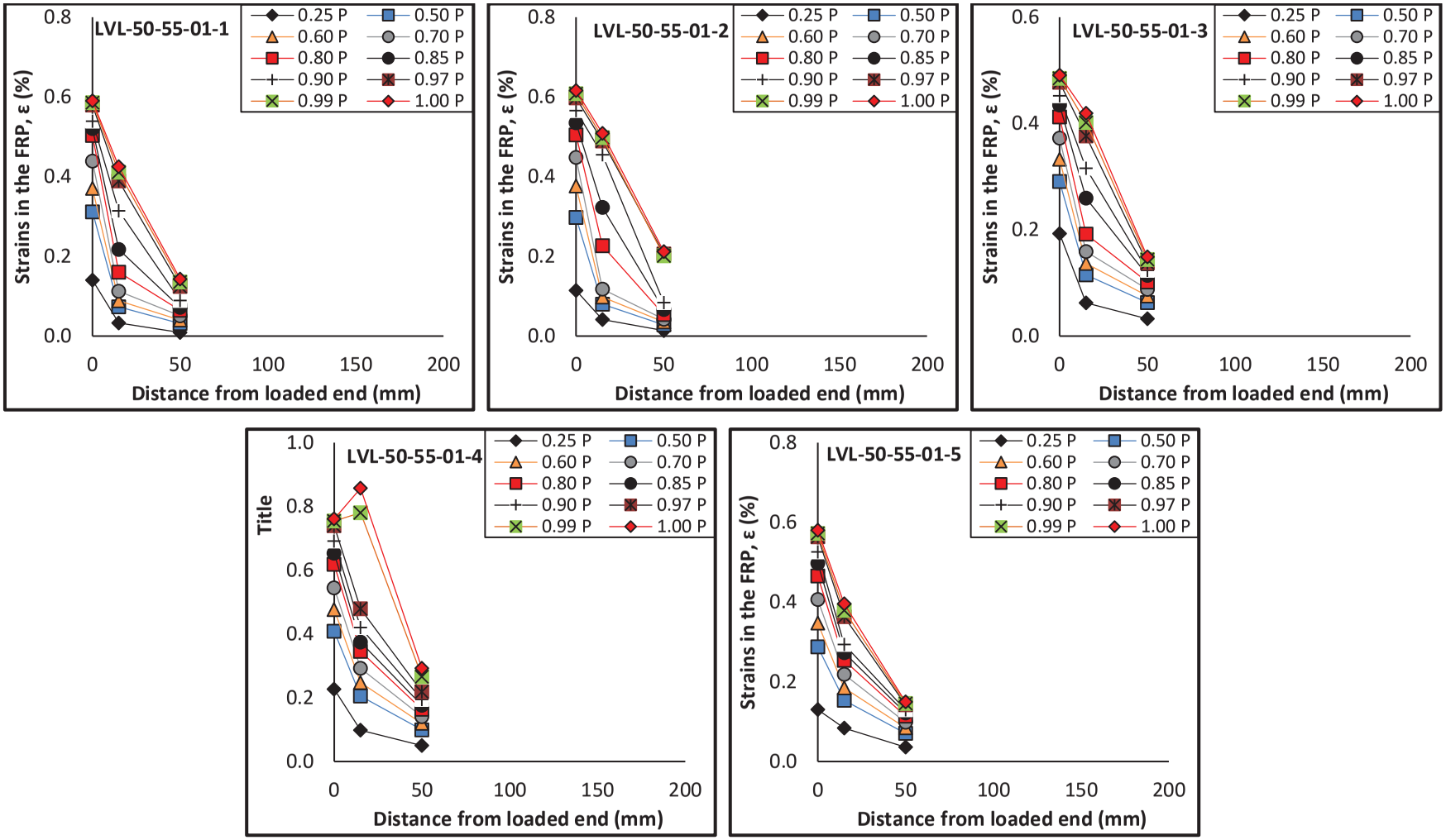
LVL-50-55-01-1
LVL-50-55-01-2
LVL-50-55-01-3
LVL-50-55-01-4
LVL-50-55-01-5
0.25 P
0.50 P
0.60 P
0.70 P
0.80 P
0.85 P
0.90 P
0.97 P
0.99 P
1.00 P
Strains in the FRP, ε (%)
Distance from loaded end (mm)
Title

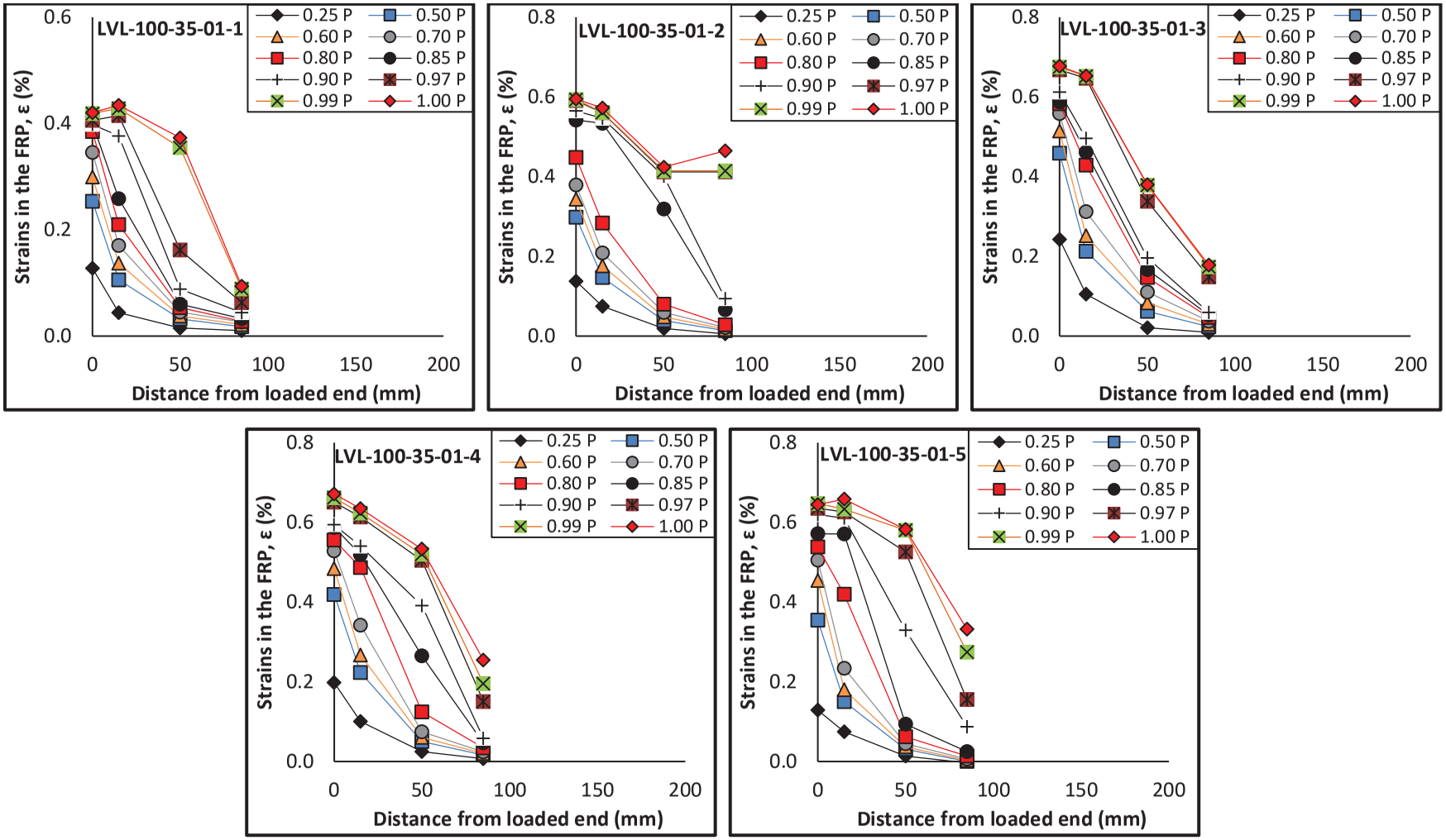
LVL-100-35-01-1
LVL-100-35-01-2
LVL-100-35-01-3
LVL-100-35-01-4
LVL-100-35-01-5
0.25 P
0.50 P
0.60 P
0.70 P
0.80 P
0.85 P
0.90 P
0.97 P
0.99 P
1.00 P
Strains in the FRP, ε (%)
Distance from loaded end (mm)
0.0
0.2
0.4
0.6
0.8
0
50
100
150
200

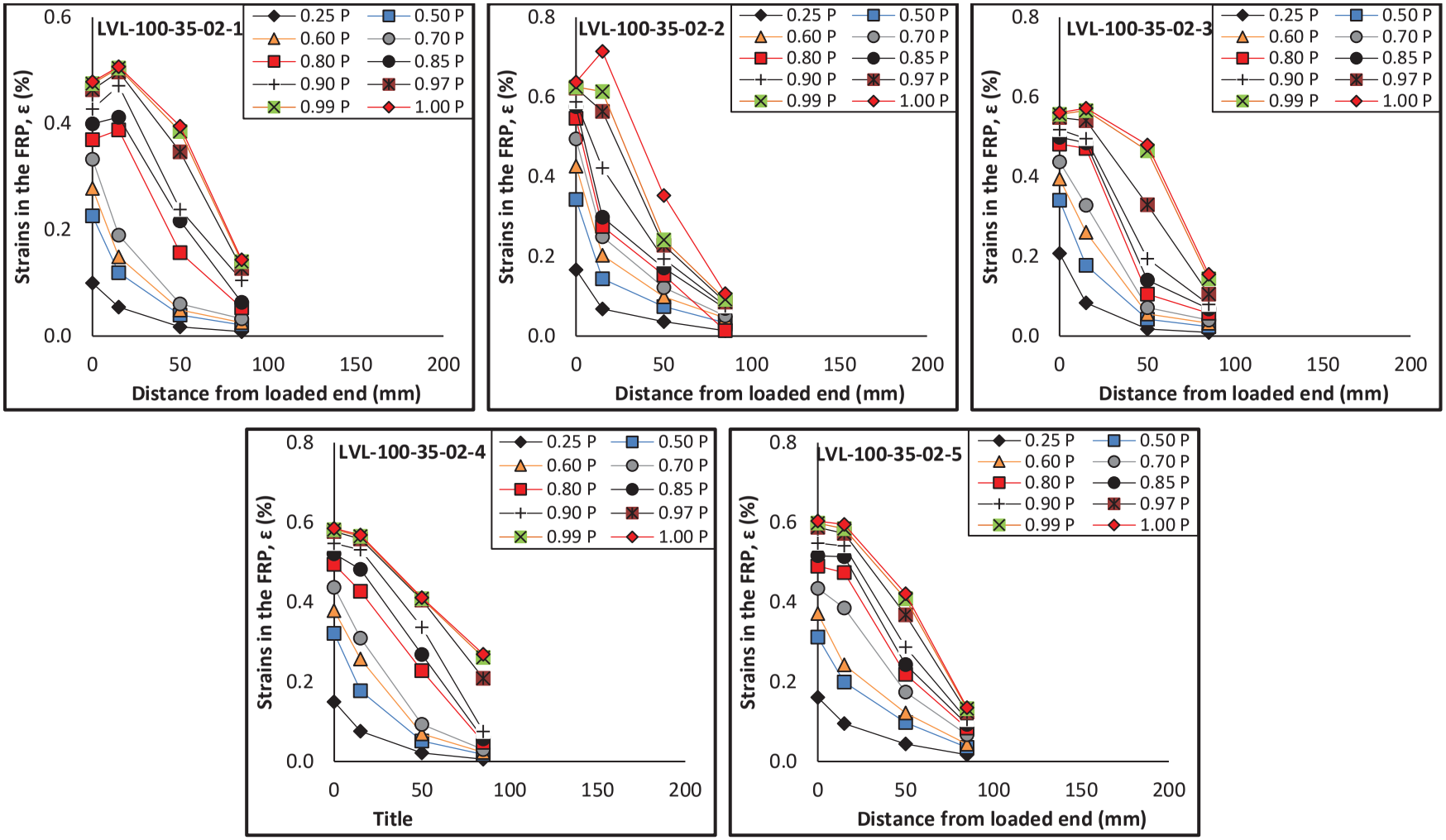
LVL-100-35-02-1
LVL-100-35-02-2
LVL-100-35-02-3
LVL-100-35-02-4
LVL-100-35-02-5
0.25 P
0.50 P
0.60 P
0.70 P
0.80 P
0.85 P
0.90 P
0.97 P
0.99 P
1.00 P
Strains in the FRP, ε (%)
Distance from loaded end (mm)
Title

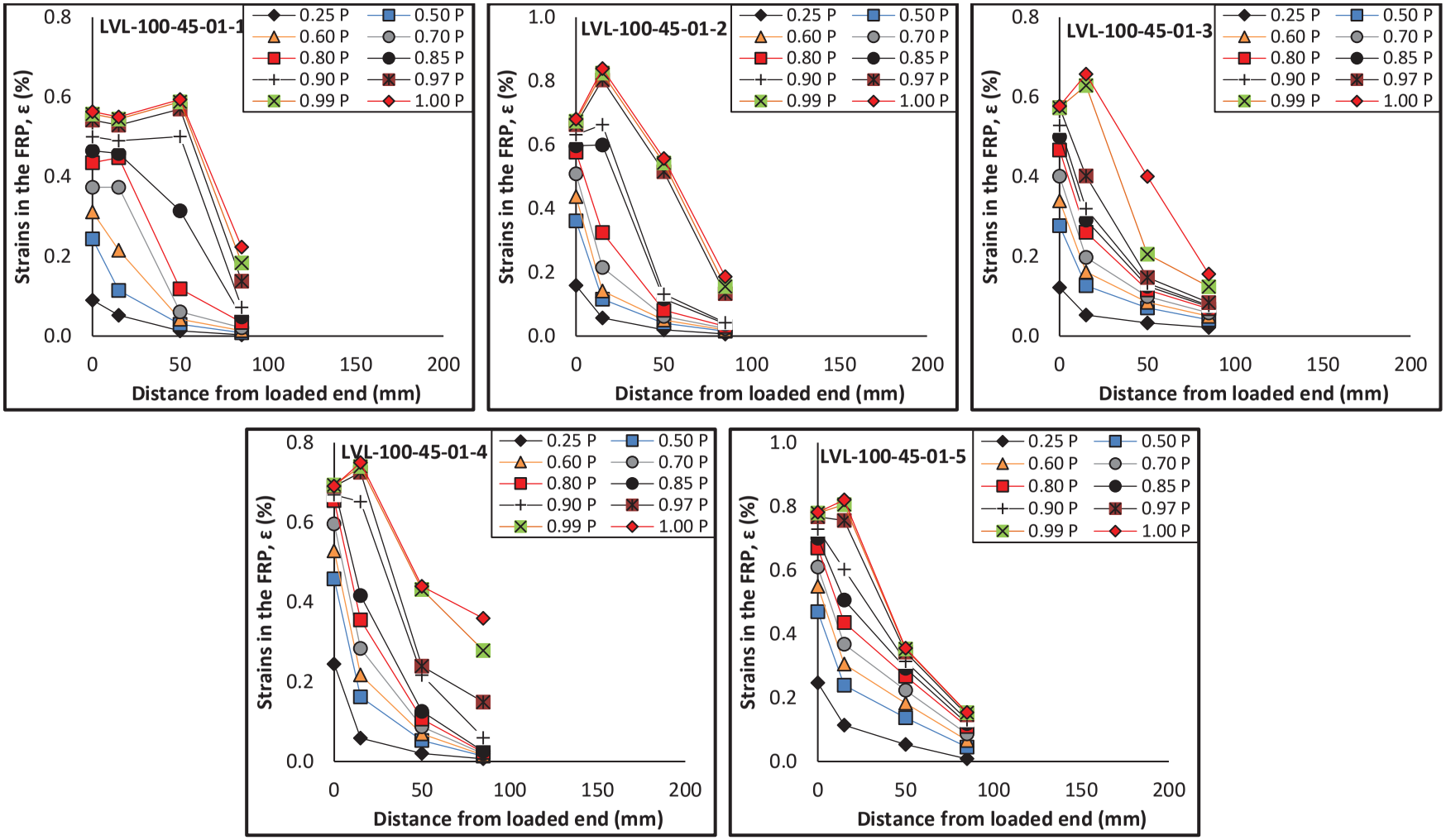
LVL-100-45-01-1
LVL-100-45-01-2
LVL-100-45-01-3
LVL-100-45-01-4
LVL-100-45-01-5
0.25 P
0.50 P
0.60 P
0.70 P
0.80 P
0.85 P
0.90 P
0.97 P
0.99 P
1.00 P
Strains in the FRP, ε (%)
Distance from loaded end (mm)

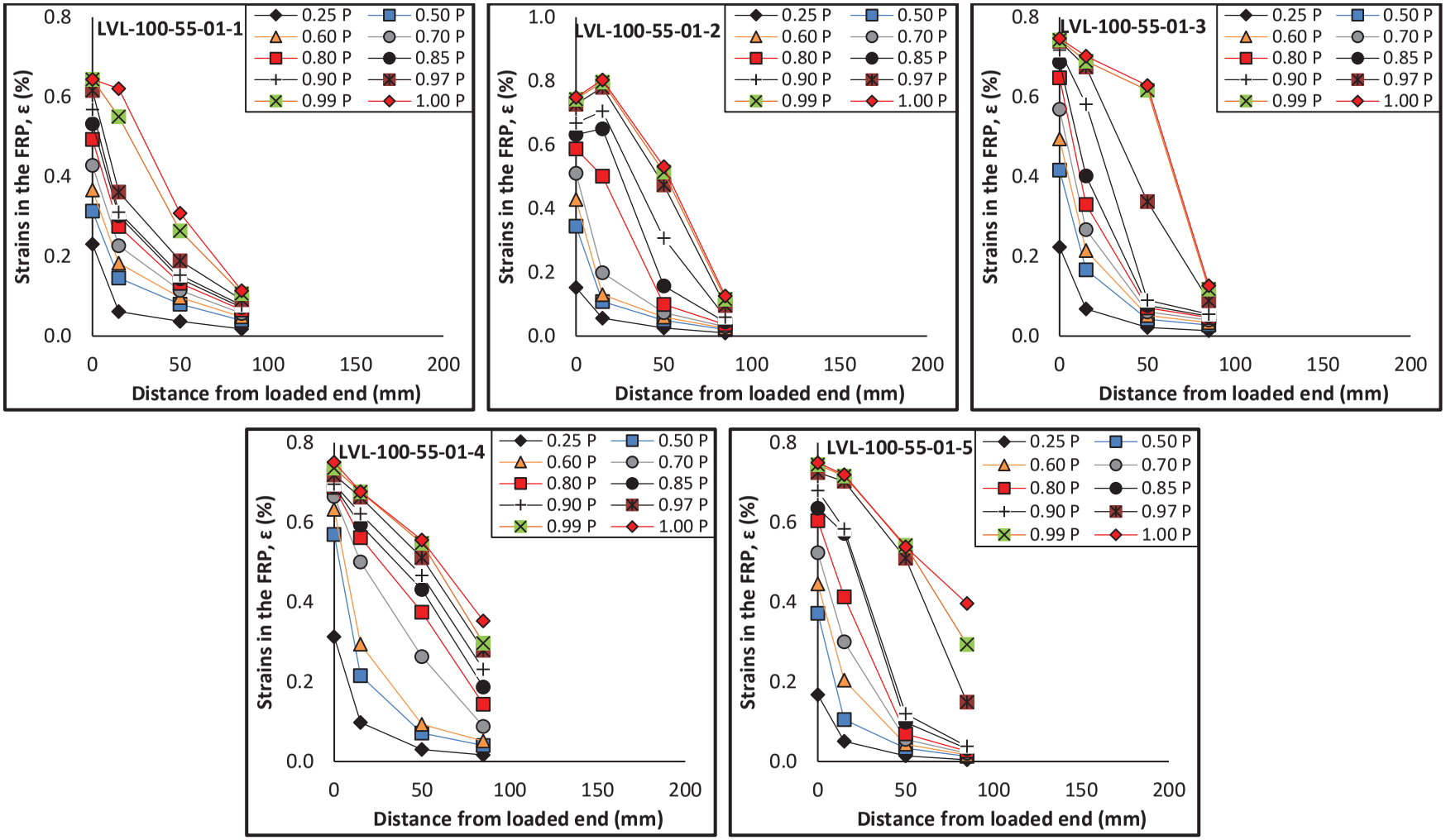
LVL-100-55-01-1
LVL-100-55-01-2
LVL-100-55-01-3
LVL-100-55-01-4
LVL-100-55-01-5
0.25 P
0.50 P
0.60 P
0.70 P
0.80 P
0.85 P
0.90 P
0.97 P
0.99 P
1.00 P
Strains in the FRP, ε (%)
Distance from loaded end (mm)

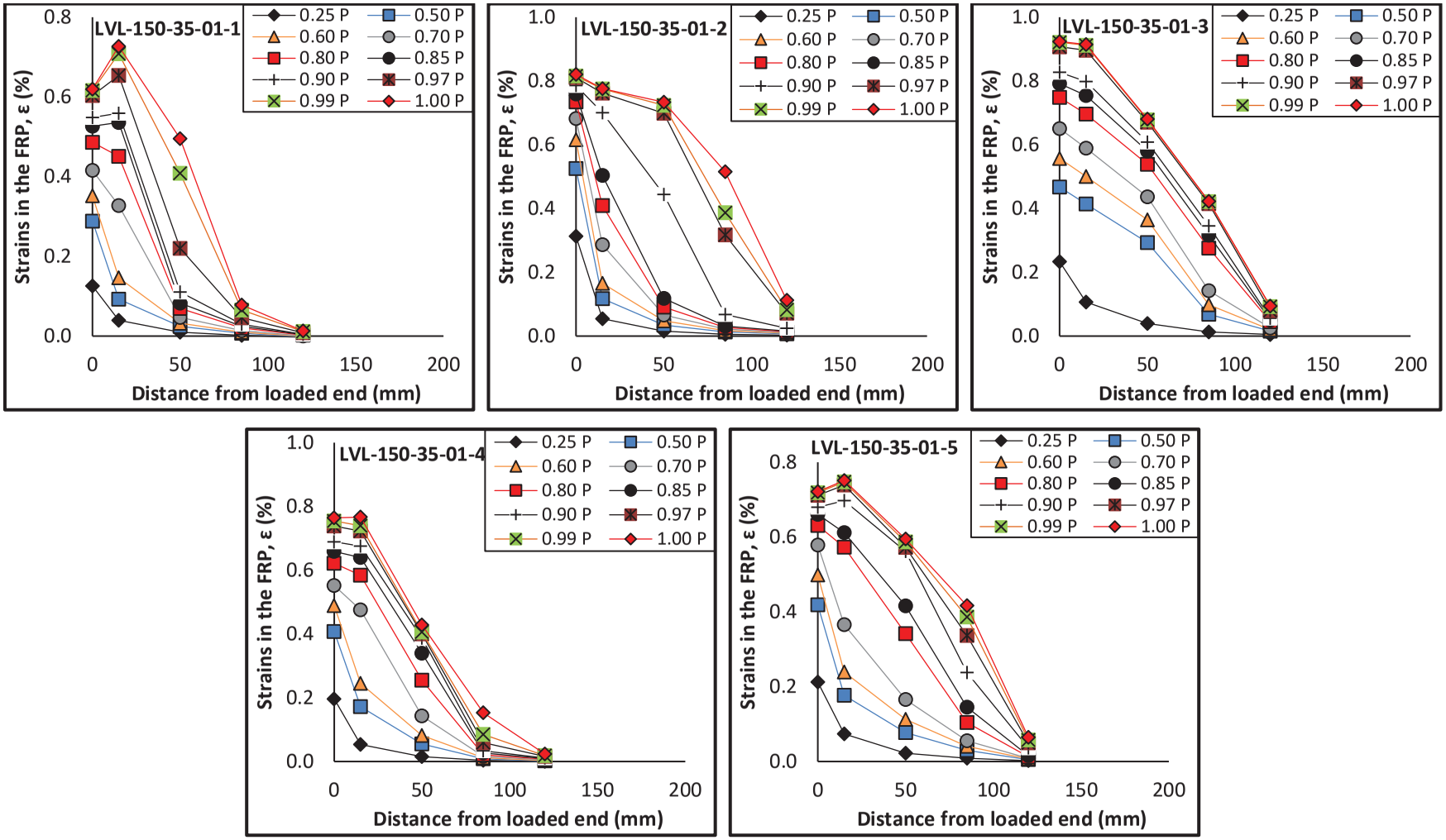
LVL-150-35-01-1
LVL-150-35-01-2
LVL-150-35-01-3
LVL-150-35-01-4
LVL-150-35-01-5
0.25 P
0.50 P
0.60 P
0.70 P
0.80 P
0.85 P
0.90 P
0.97 P
0.99 P
1.00 P
Strains in the FRP, ε (%)
Distance from loaded end (mm)

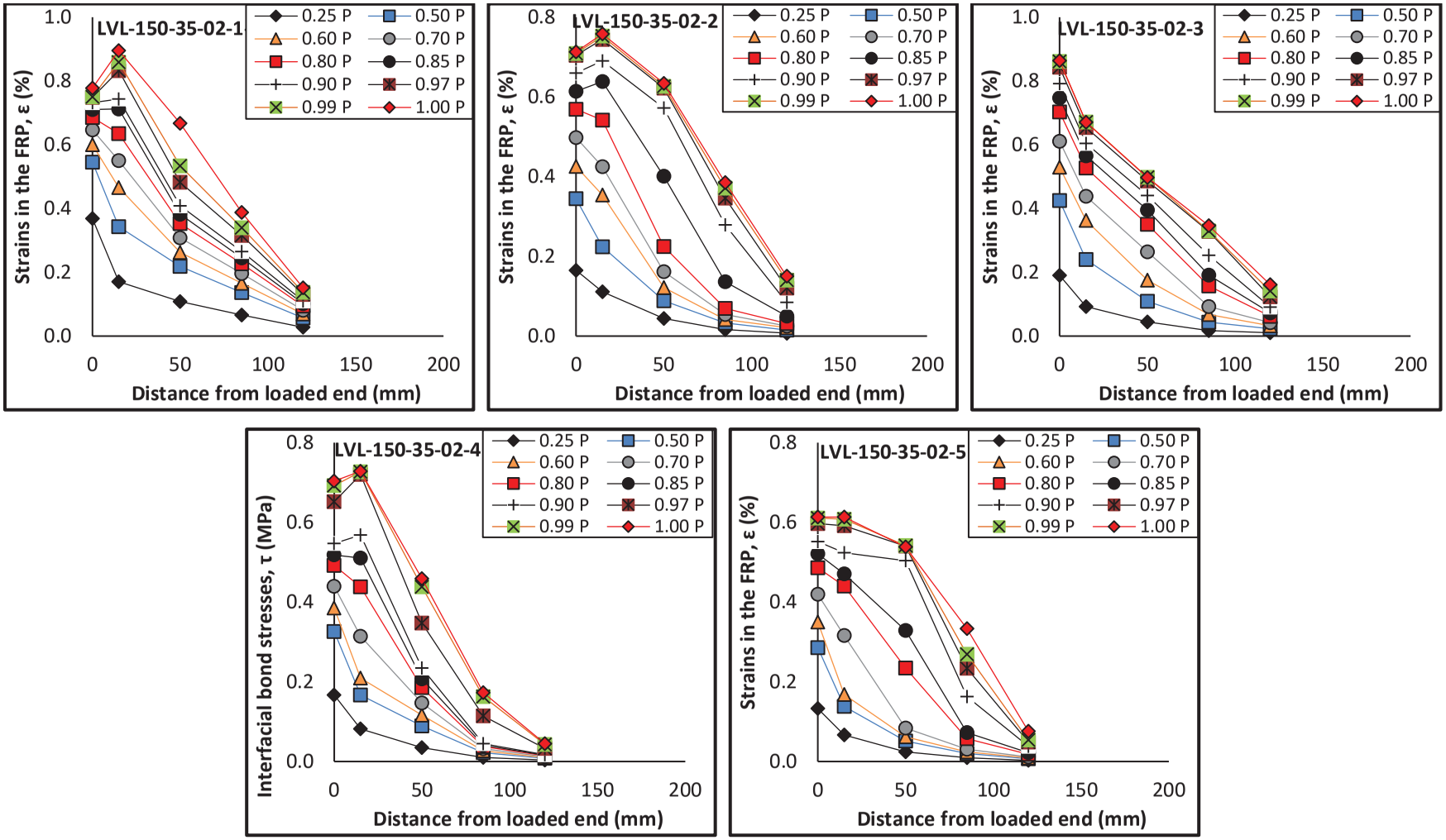
LVL-150-35-02-1
LVL-150-35-02-2
LVL-150-35-02-3
LVL-150-35-02-4
LVL-150-35-02-5
0.25 P
0.50 P
0.60 P
0.70 P
0.80 P
0.85 P
0.90 P
0.97 P
0.99 P
1.00 P
Strains in the FRP, ε (%)
Interfacial bond stresses, τ (MPa)
Distance from loaded end (mm)

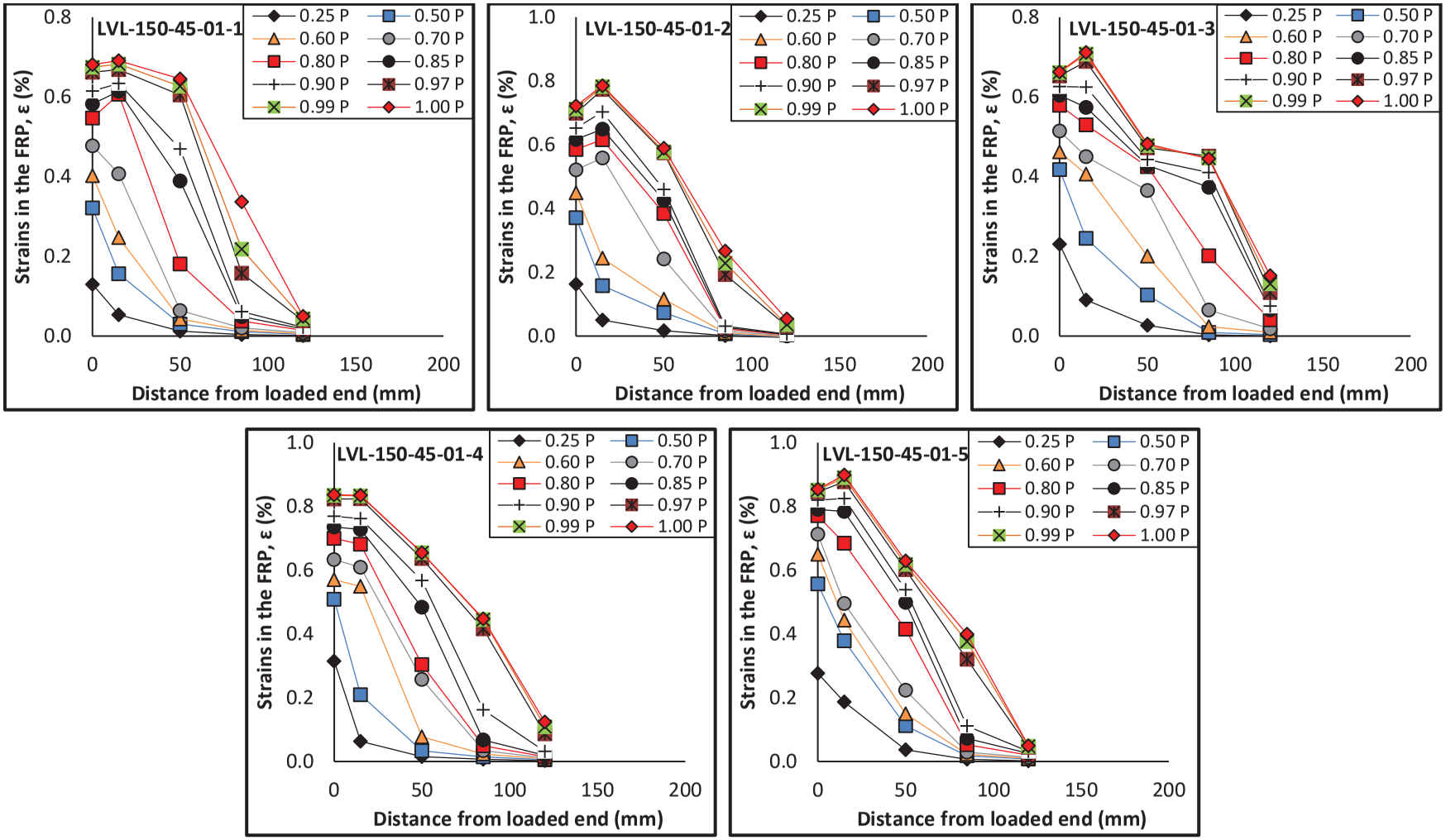
LVL-150-45-01-1
LVL-150-45-01-2
LVL-150-45-01-3
LVL-150-45-01-4
LVL-150-45-01-5
0.25 P
0.50 P
0.60 P
0.70 P
0.80 P
0.85 P
0.90 P
0.97 P
0.99 P
1.00 P
Strains in the FRP, ε (%)
Distance from loaded end (mm)

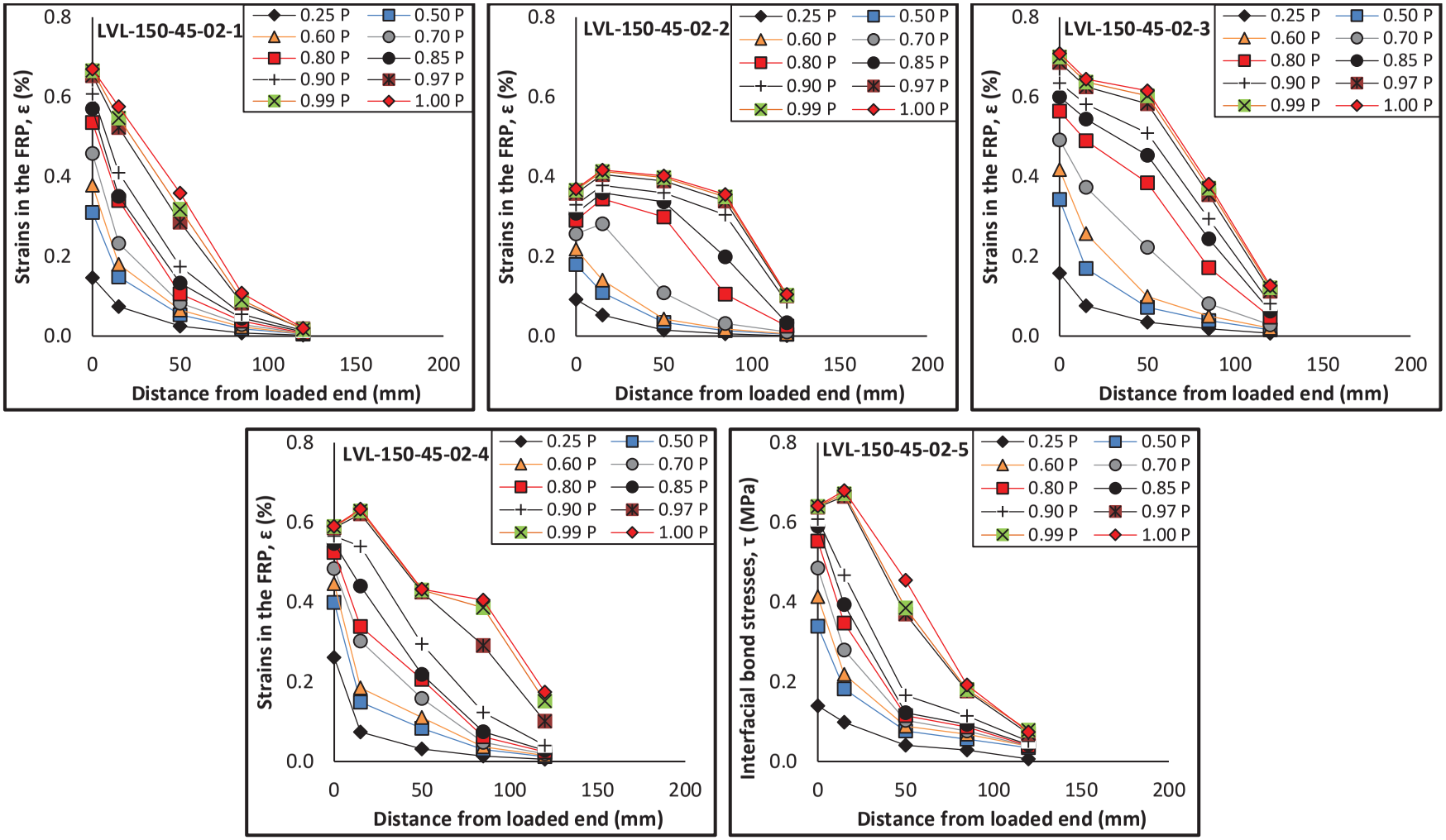
LVL-150-45-02-1
LVL-150-45-02-2
LVL-150-45-02-3
LVL-150-45-02-4
LVL-150-45-02-5
0.25 P
0.50 P
0.60 P
0.70 P
0.80 P
0.85 P
0.90 P
0.97 P
0.99 P
1.00 P
Strains in the FRP, ε (%)
Interfacial bond stresses, τ (MPa)
Distance from loaded end (mm)
0.0
0.2
0.4
0.6
0.8
0
50
100
150
200

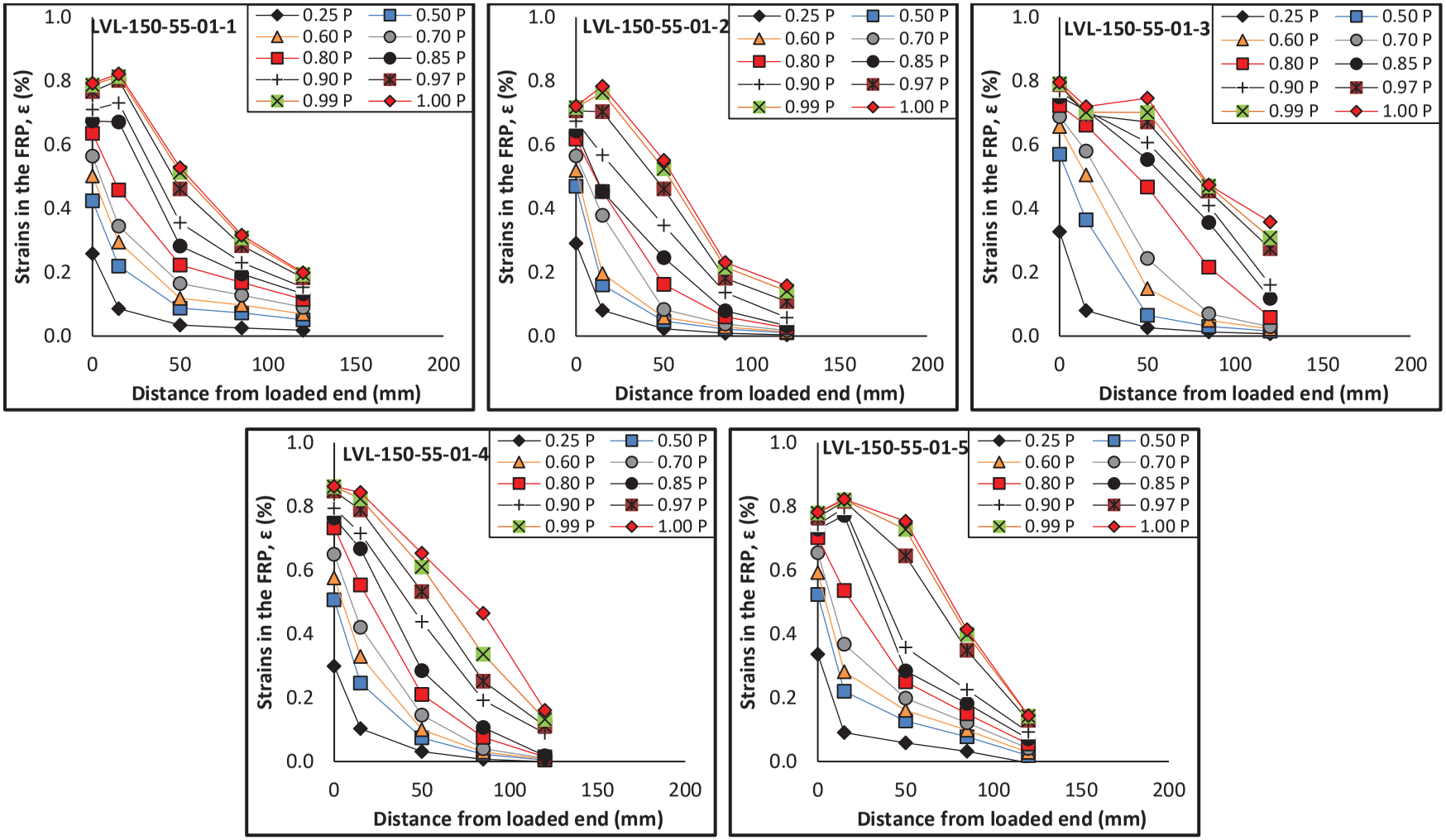
LVL-150-55-01-1
LVL-150-55-01-2
LVL-150-55-01-3
LVL-150-55-01-4
LVL-150-55-01-5
0.25 P
0.50 P
0.60 P
0.70 P
0.80 P
0.85 P
0.90 P
0.97 P
0.99 P
1.00 P
Strains in the FRP, ε (%)
Distance from loaded end (mm)
0.0
0.2
0.4
0.6
0.8
1.0
0
50
100
150
200

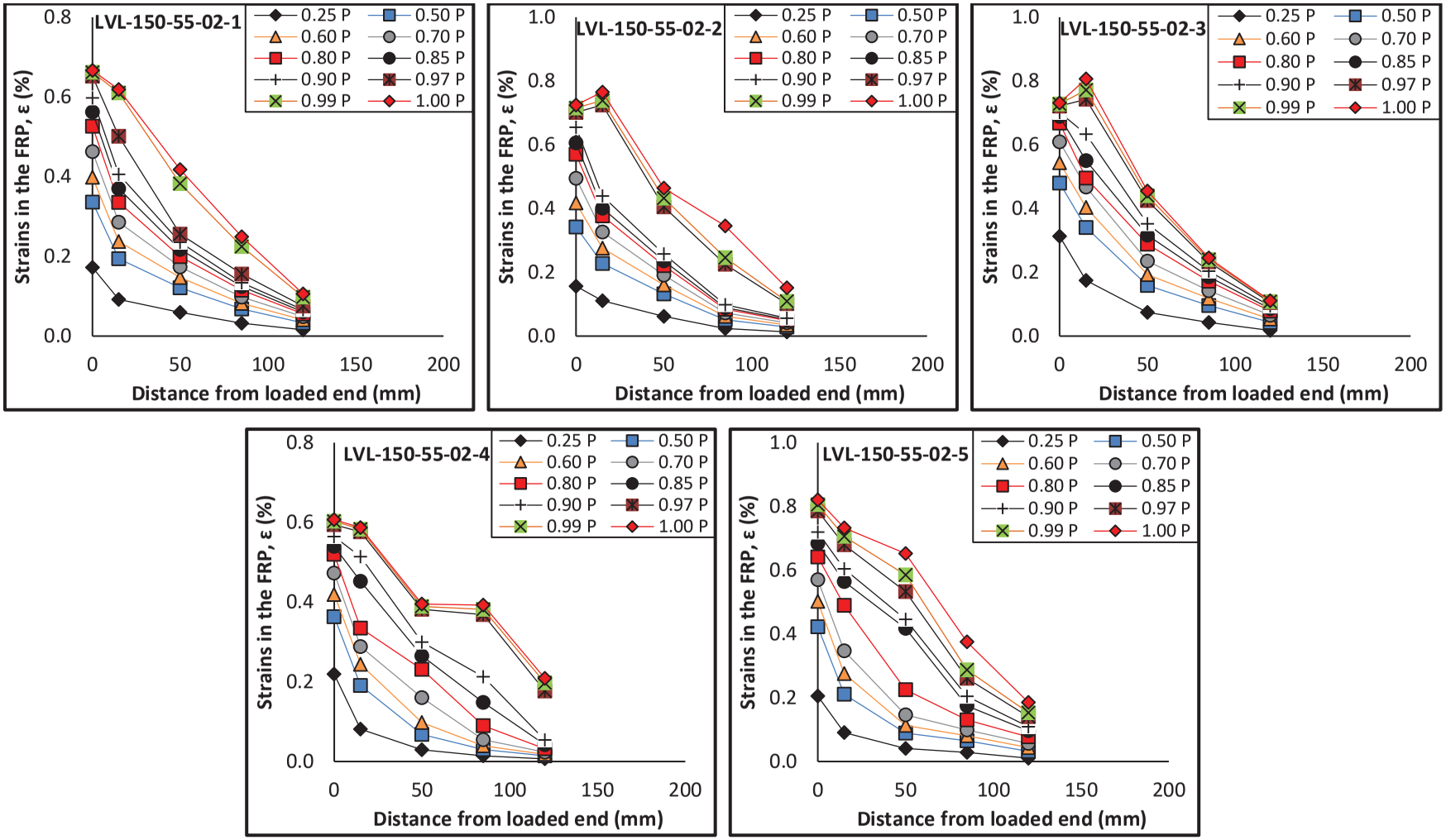
LVL-150-55-02-1
LVL-150-55-02-2
LVL-150-55-02-3
LVL-150-55-02-4
LVL-150-55-02-5
0.25 P
0.50 P
0.60 P
0.70 P
0.80 P
0.85 P
0.90 P
0.97 P
0.99 P
1.00 P
Strains in the FRP, ε (%)
Distance from loaded end (mm)

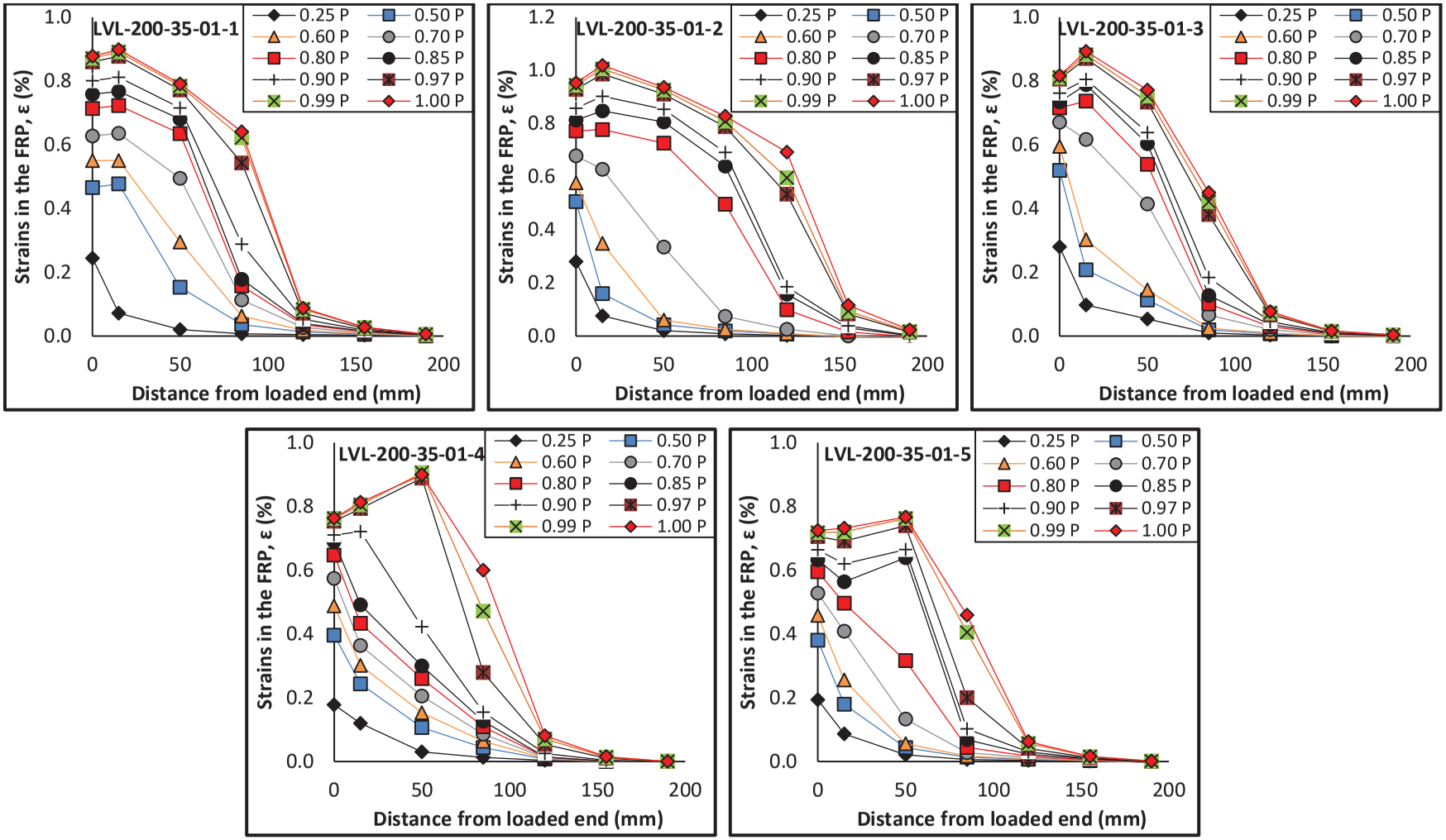
LVL-200-35-01-1
LVL-200-35-01-2
LVL-200-35-01-3
LVL-200-35-01-4
LVL-200-35-01-5
0.25 P
0.50 P
0.60 P
0.70 P
0.80 P
0.85 P
0.90 P
0.97 P
0.99 P
1.00 P
Strains in the FRP, ε (%)
Distance from loaded end (mm)

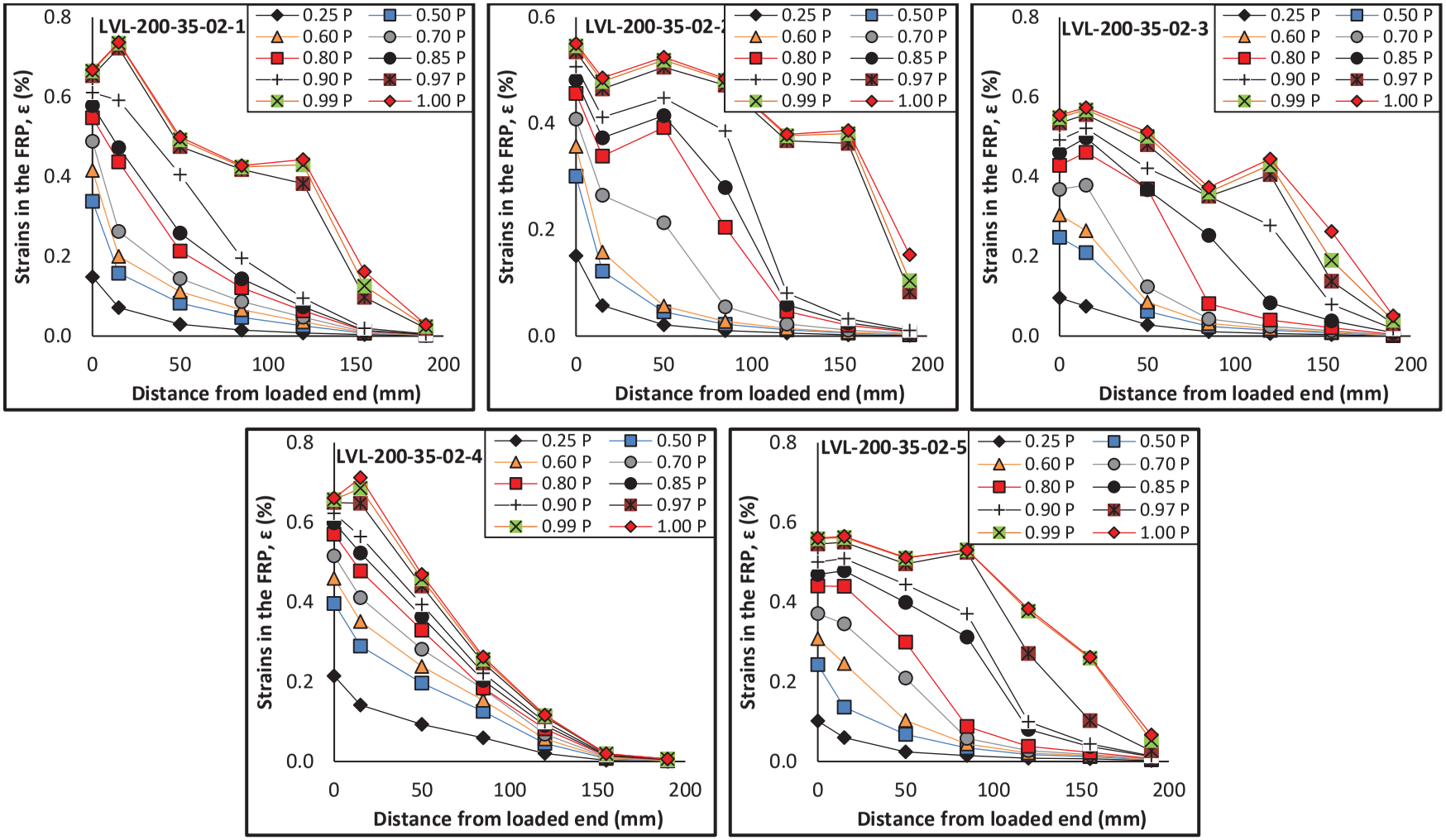
LVL-200-35-02-1
LVL-200-35-02-3
LVL-200-35-02-4
LVL-200-35-02-5
0.25 P
0.50 P
0.60 P
0.70 P
0.80 P
0.85 P
0.90 P
0.97 P
0.99 P
1.00 P
Strains in the FRP, ε (%)
Distance from loaded end (mm)
0.0
0.2
0.4
0.6
0.8
0
50
100
150
200

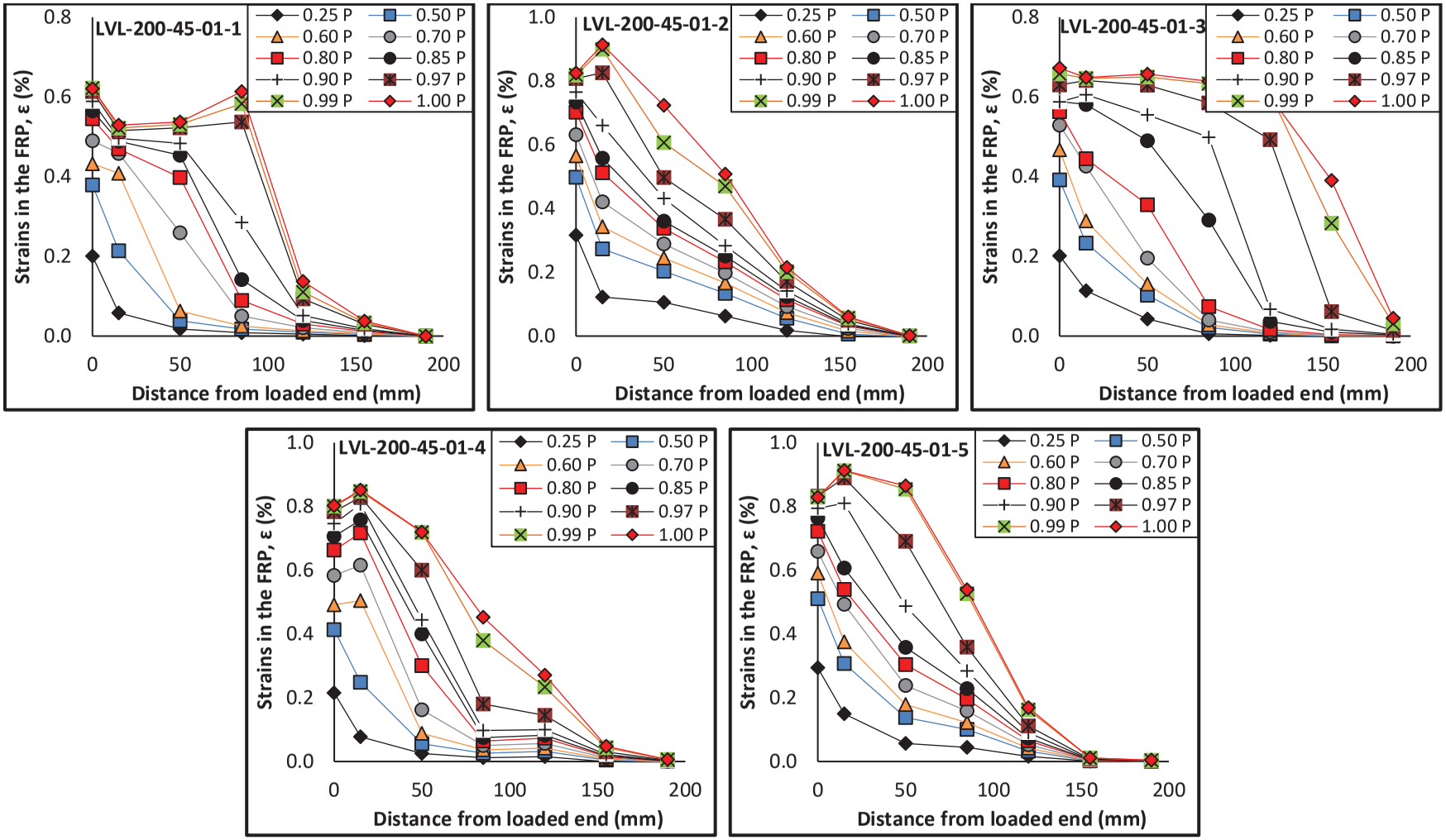
LVL-200-45-01-1
LVL-200-45-01-2
LVL-200-45-01-3
LVL-200-45-01-4
LVL-200-45-01-5
0.25 P
0.50 P
0.60 P
0.70 P
0.80 P
0.85 P
0.90 P
0.97 P
0.99 P
1.00 P
Strains in the FRP, ε (%)
Distance from loaded end (mm)

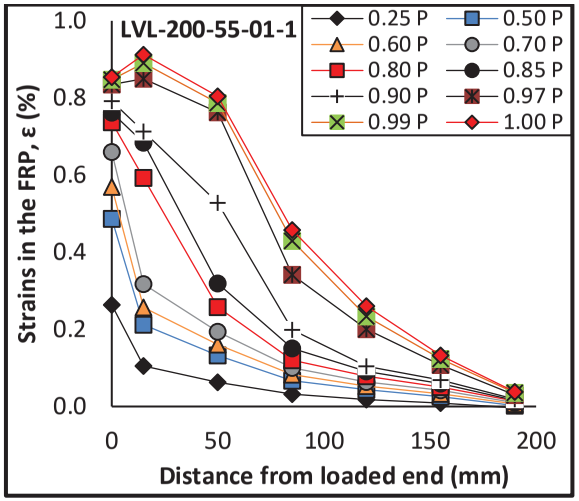
LVL-200-55-01-1
0.25 P
0.50 P
0.60 P
0.70 P
0.80 P
0.85 P
0.90 P
0.97 P
0.99 P
1.00 P
Strains in the FRP, ε (%)
Distance from loaded end (mm)

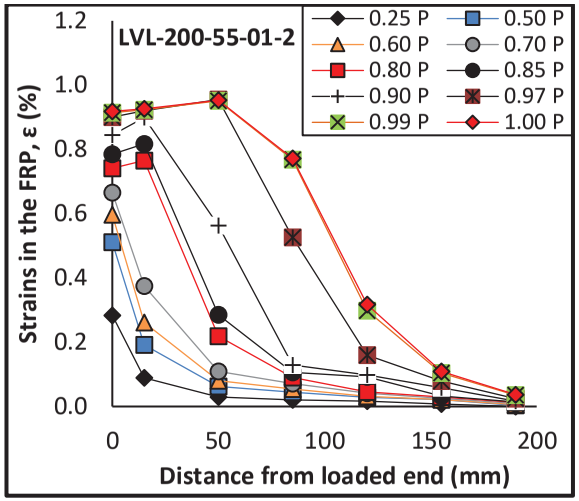
LVL-200-55-01-2
0.25 P
0.50 P
0.60 P
0.70 P
0.80 P
0.85 P
0.90 P
0.97 P
0.99 P
1.00 P
Strains in the FRP, ε (%)
Distance from loaded end (mm)

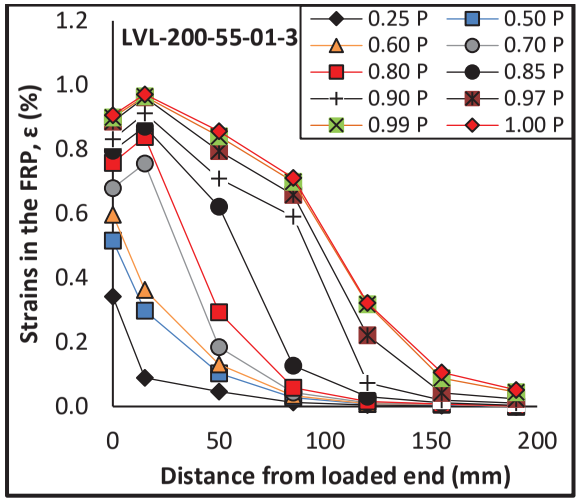
LVL-200-55-01-3
0.25 P
0.50 P
0.60 P
0.70 P
0.80 P
0.85 P
0.90 P
0.97 P
0.99 P
1.00 P
Strains in the FRP, ε (%)
Distance from loaded end (mm)

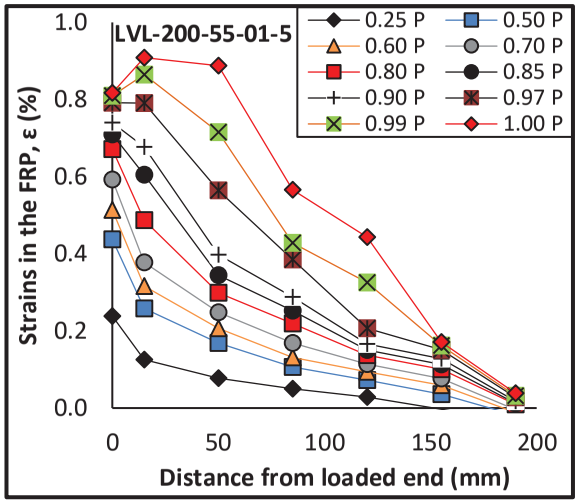
LVL-200-55-01-5
0.25 P
0.50 P
0.60 P
0.70 P
0.80 P
0.85 P
0.90 P
0.97 P
0.99 P
1.00 P
Strains in the FRP, ε (%)
Distance from loaded end (mm)

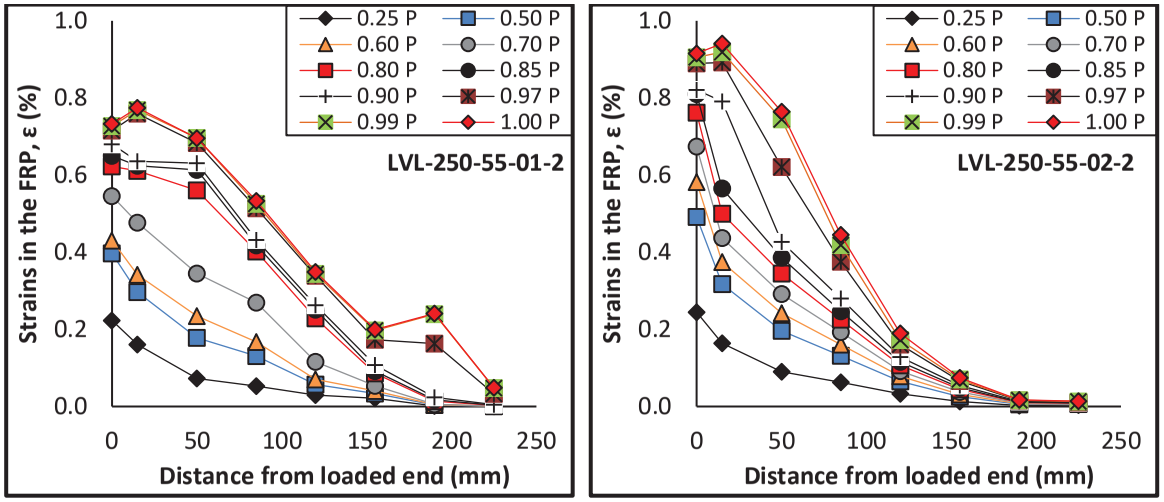
Strains in the FRP, ε (%)
Distance from loaded end (mm)
0.25 P
0.50 P
0.60 P
0.70 P
0.80 P
0.85 P
0.90 P
0.97 P
0.99 P
1.00 P
LVL-250-55-01-2
LVL-250-55-02-2

Appendix D.

Slip of the interface – Hardwood Series

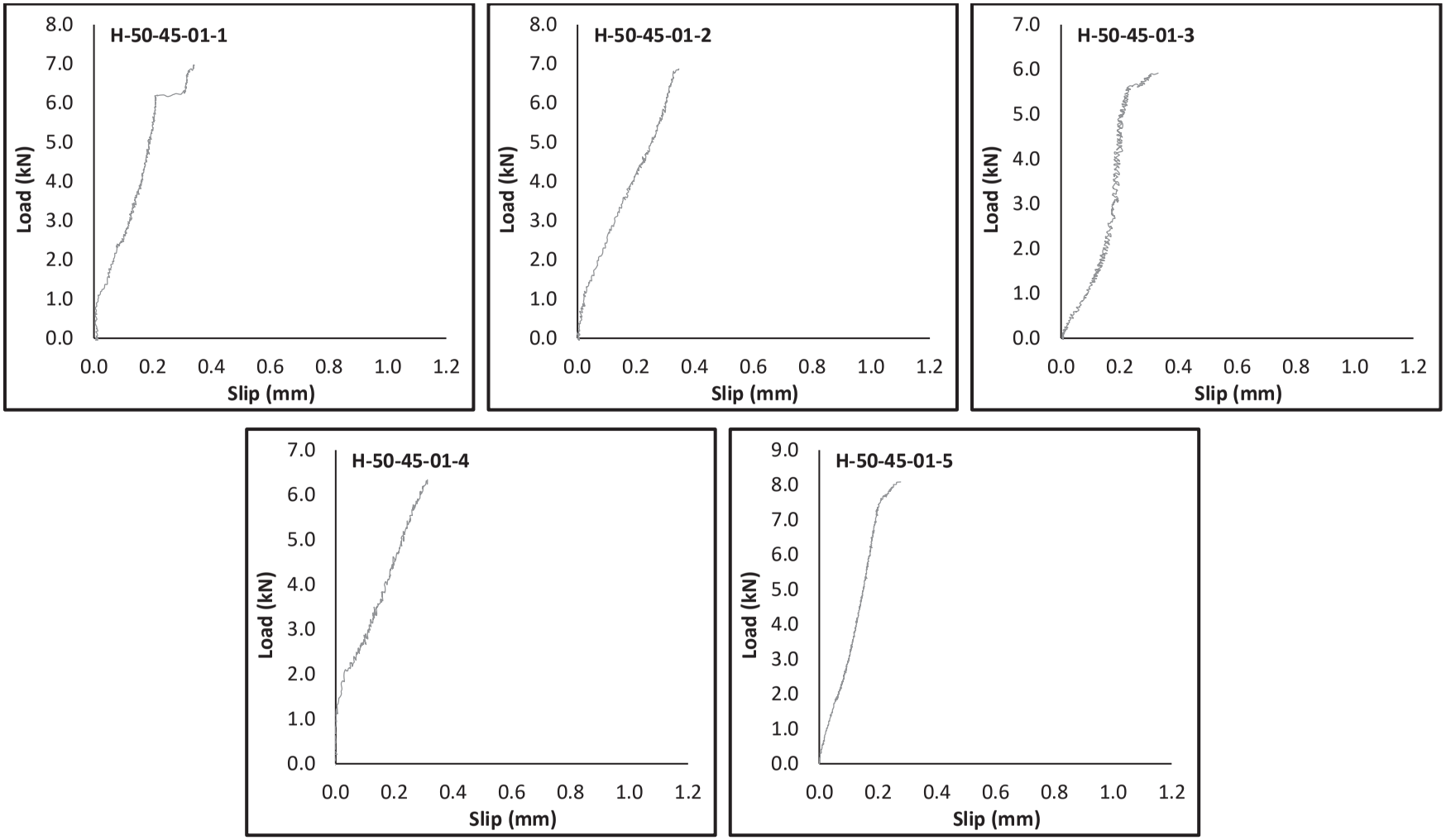
H-50-45-01-1
Load (kN)
Slip (mm)
H-50-45-01-2
Load (kN)
Slip (mm)
H-50-45-01-3
Load (kN)
Slip (mm)
H-50-45-01-4
Load (kN)
Slip (mm)
H-50-45-01-5
Load (kN)
Slip (mm)

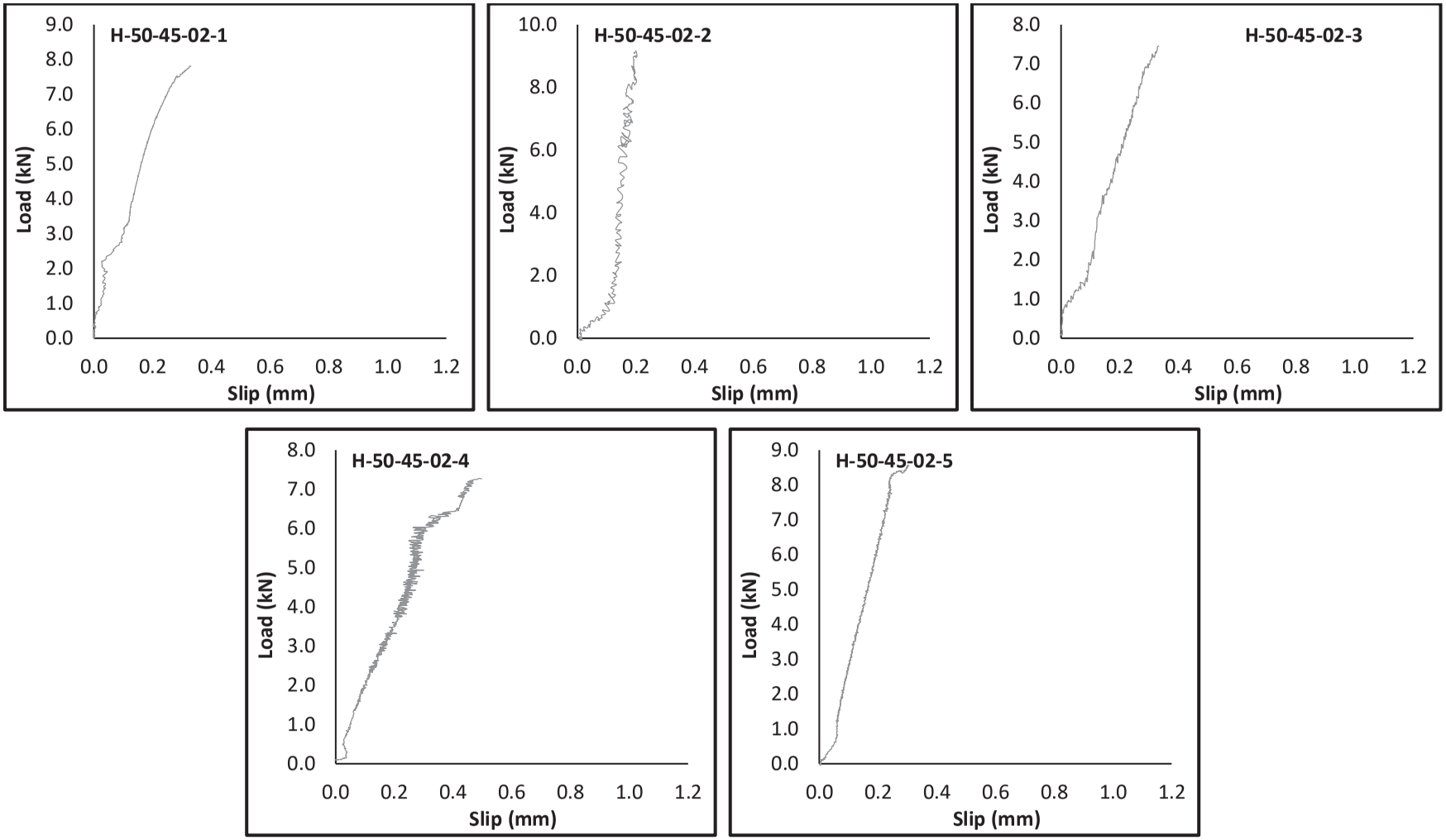
H-50-45-02-1
Load (kN)
Slip (mm)
H-50-45-02-2
Load (kN)
Slip (mm)
H-50-45-02-3
Load (kN)
Slip (mm)
H-50-45-02-4
Load (kN)
Slip (mm)
H-50-45-02-5
Load (kN)
Slip (mm)

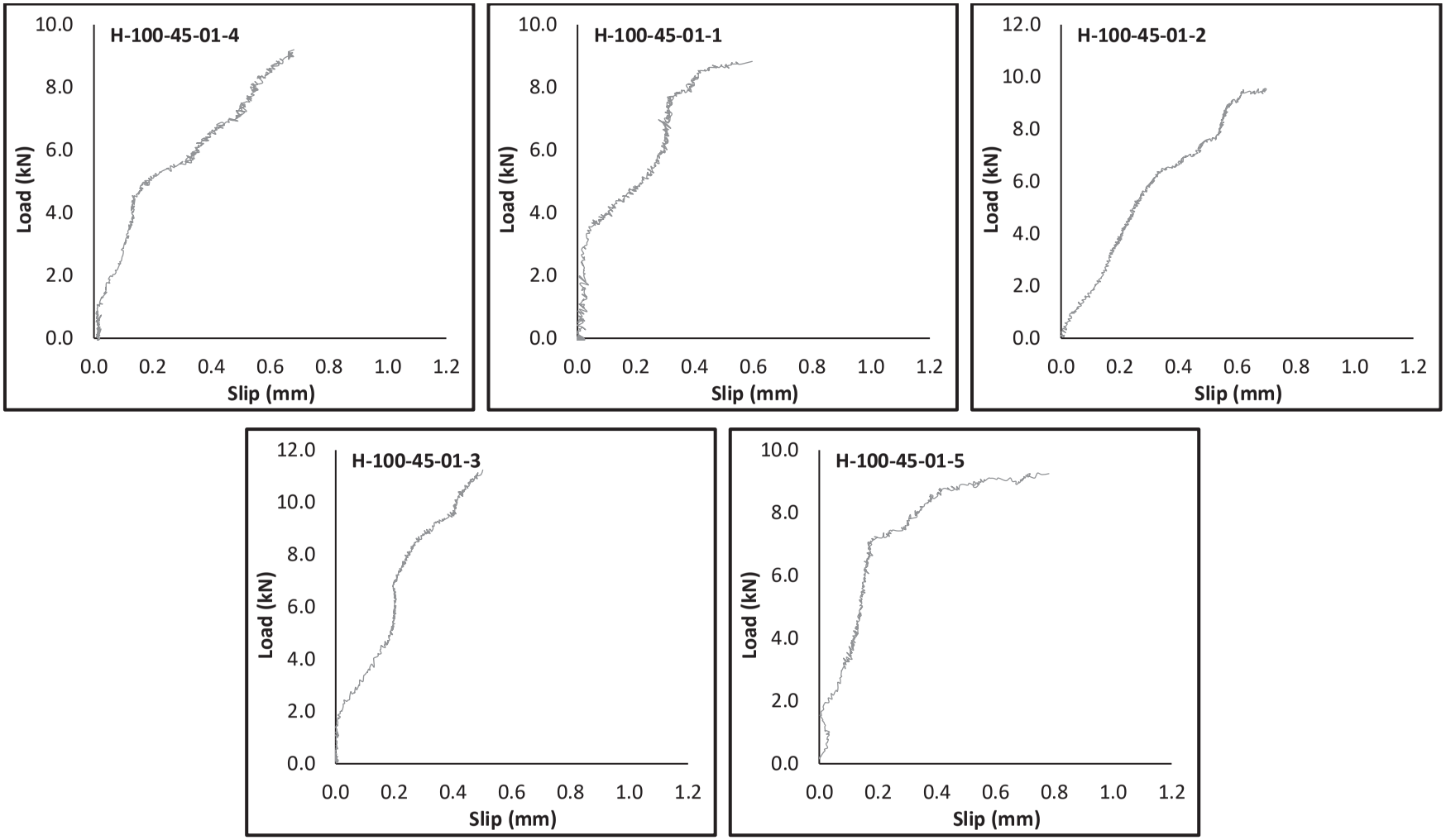
H-100-45-01-4
Load (kN)
Slip (mm)
H-100-45-01-1
Load (kN)
Slip (mm)
H-100-45-01-2
Load (kN)
Slip (mm)
H-100-45-01-3
Load (kN)
Slip (mm)
H-100-45-01-5
Load (kN)
Slip (mm)

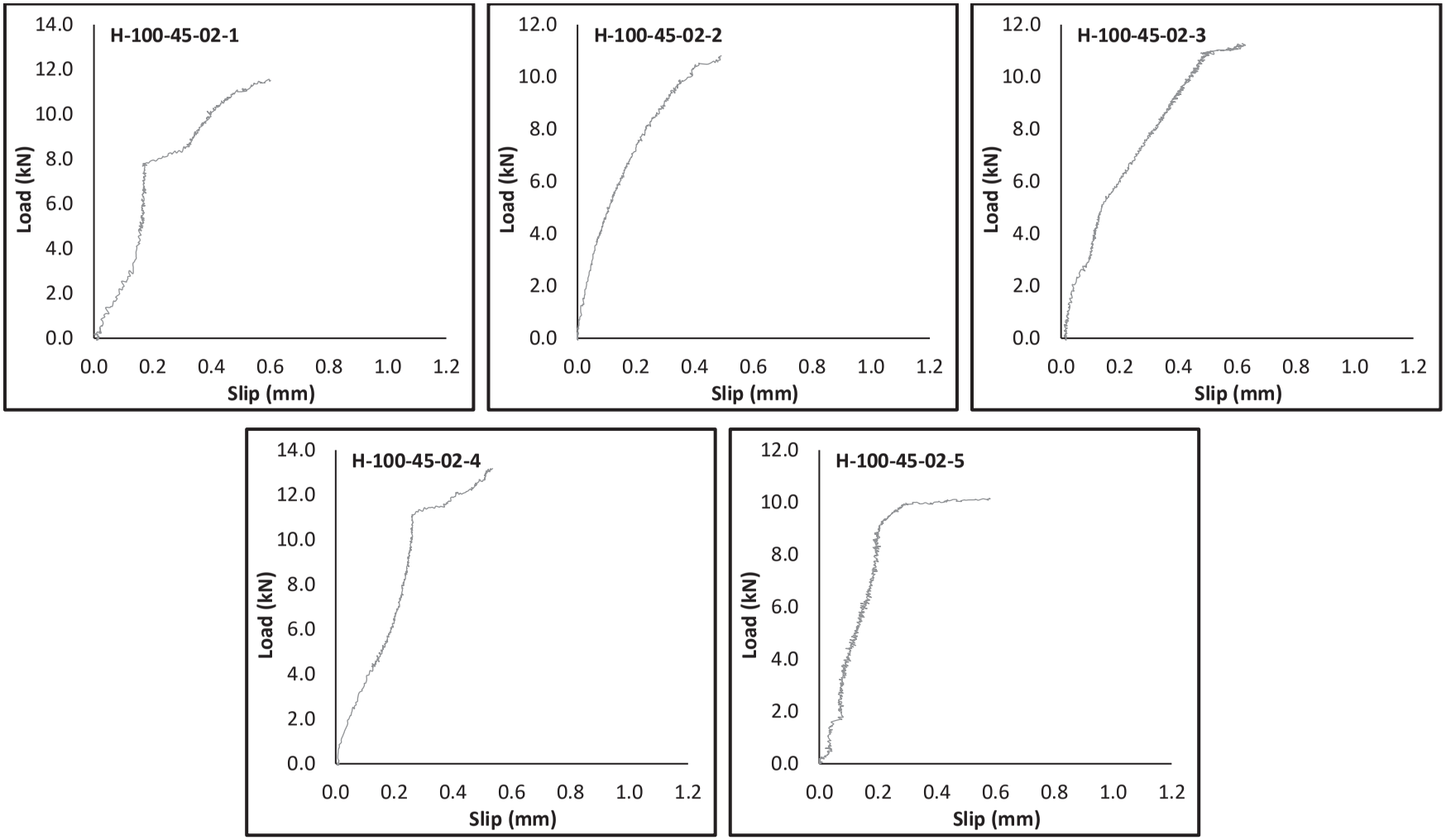
H-100-45-02-1
Load (kN)
Slip (mm)
H-100-45-02-2
Load (kN)
Slip (mm)
H-100-45-02-3
Load (kN)
Slip (mm)
H-100-45-02-4
Load (kN)
Slip (mm)
H-100-45-02-5
Load (kN)
Slip (mm)

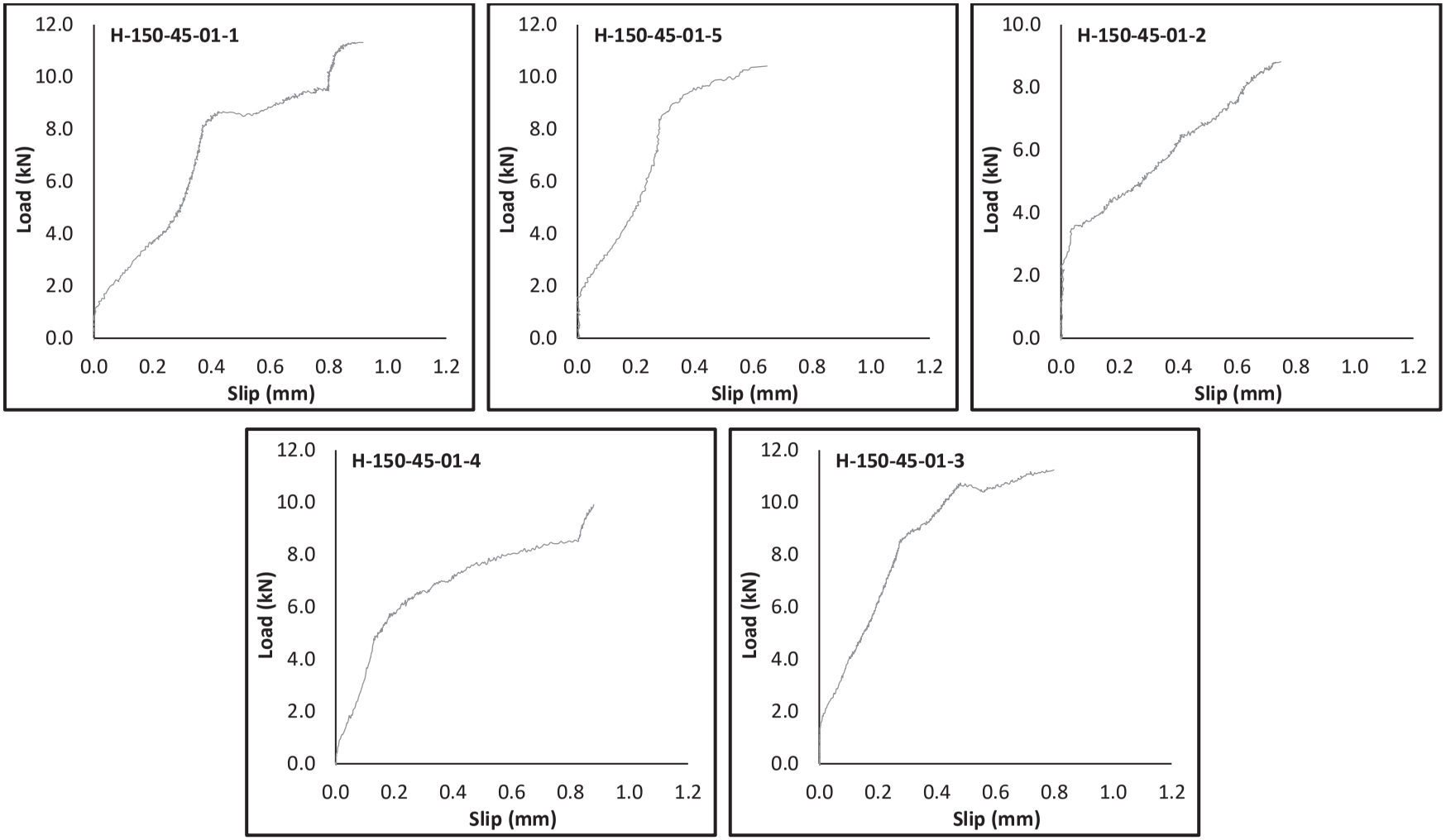
H-150-45-01-1
Load (kN)
Slip (mm)
H-150-45-01-5
Load (kN)
Slip (mm)
H-150-45-01-2
Load (kN)
Slip (mm)
H-150-45-01-4
Load (kN)
Slip (mm)
H-150-45-01-3
Load (kN)
Slip (mm)

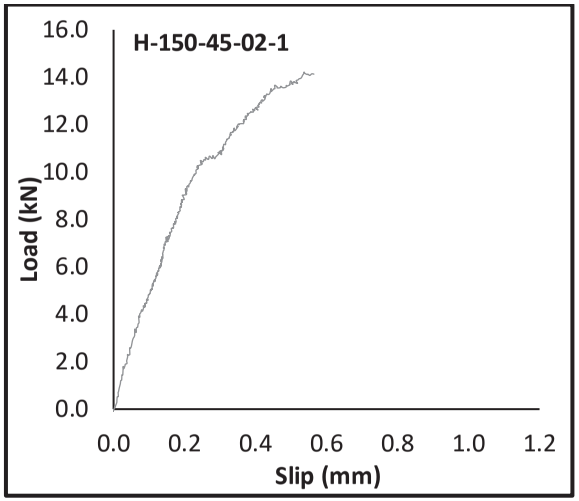
H-150-45-02-1
Load (kN)
Slip (mm)
16.0
14.0
12.0
10.0
8.0
6.0
4.0
2.0
0.0
0.0 0.2 0.4 0.6 0.8 1.0 1.2

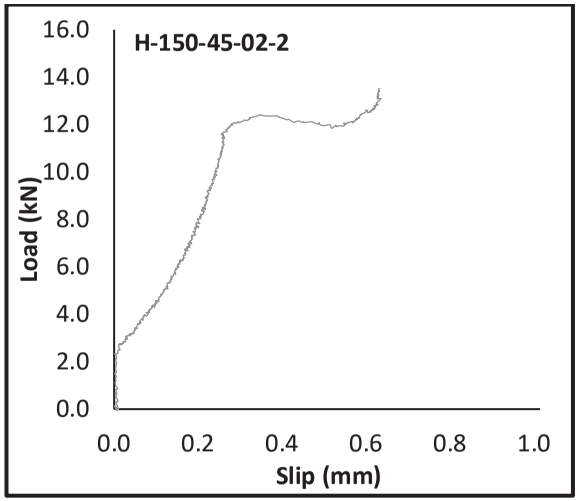
H-150-45-02-2
Load (kN)
Slip (mm)
16.0
14.0
12.0
10.0
8.0
6.0
4.0
2.0
0.0
0.0 0.2 0.4 0.6 0.8 1.0

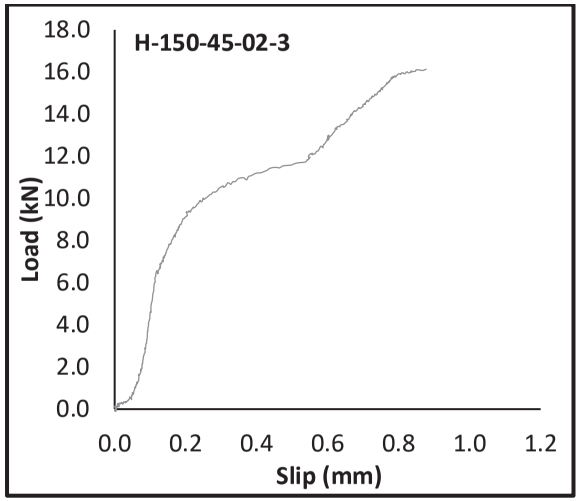
H-150-45-02-3
Load (kN)
Slip (mm)
18.0
16.0
14.0
12.0
10.0
8.0
6.0
4.0
2.0
0.0
0.0 0.2 0.4 0.6 0.8 1.0 1.2

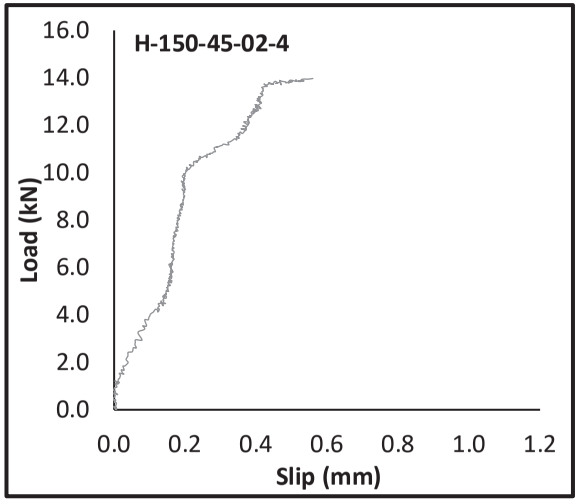
H-150-45-02-4
Load (kN)
Slip (mm)
16.0
14.0
12.0
10.0
8.0
6.0
4.0
2.0
0.0
0.0 0.2 0.4 0.6 0.8 1.0 1.2

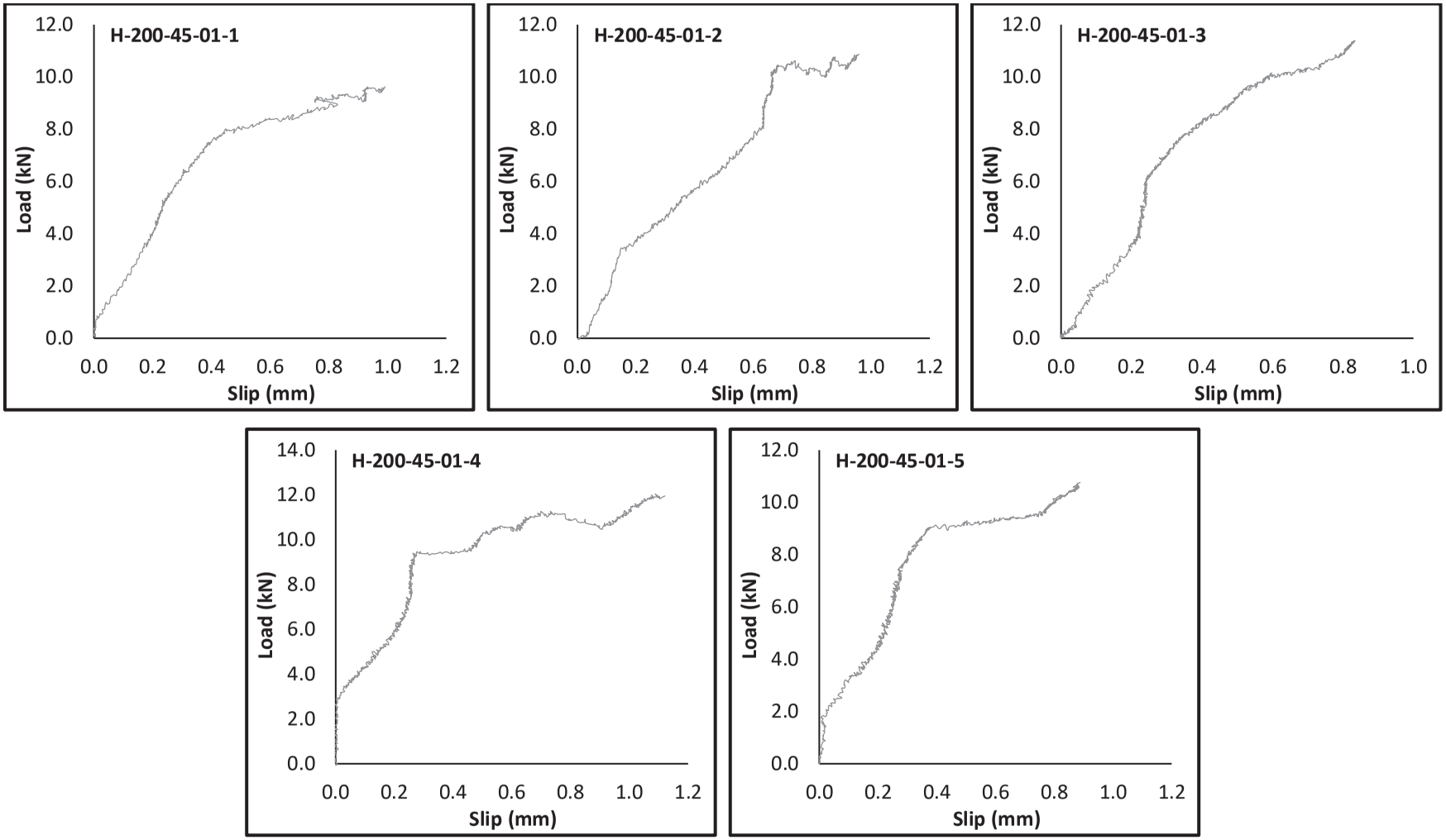
H-200-45-01-1
Load (kN)
Slip (mm)
H-200-45-01-2
Load (kN)
Slip (mm)
H-200-45-01-3
Load (kN)
Slip (mm)
H-200-45-01-4
Load (kN)
Slip (mm)
H-200-45-01-5
Load (kN)
Slip (mm)

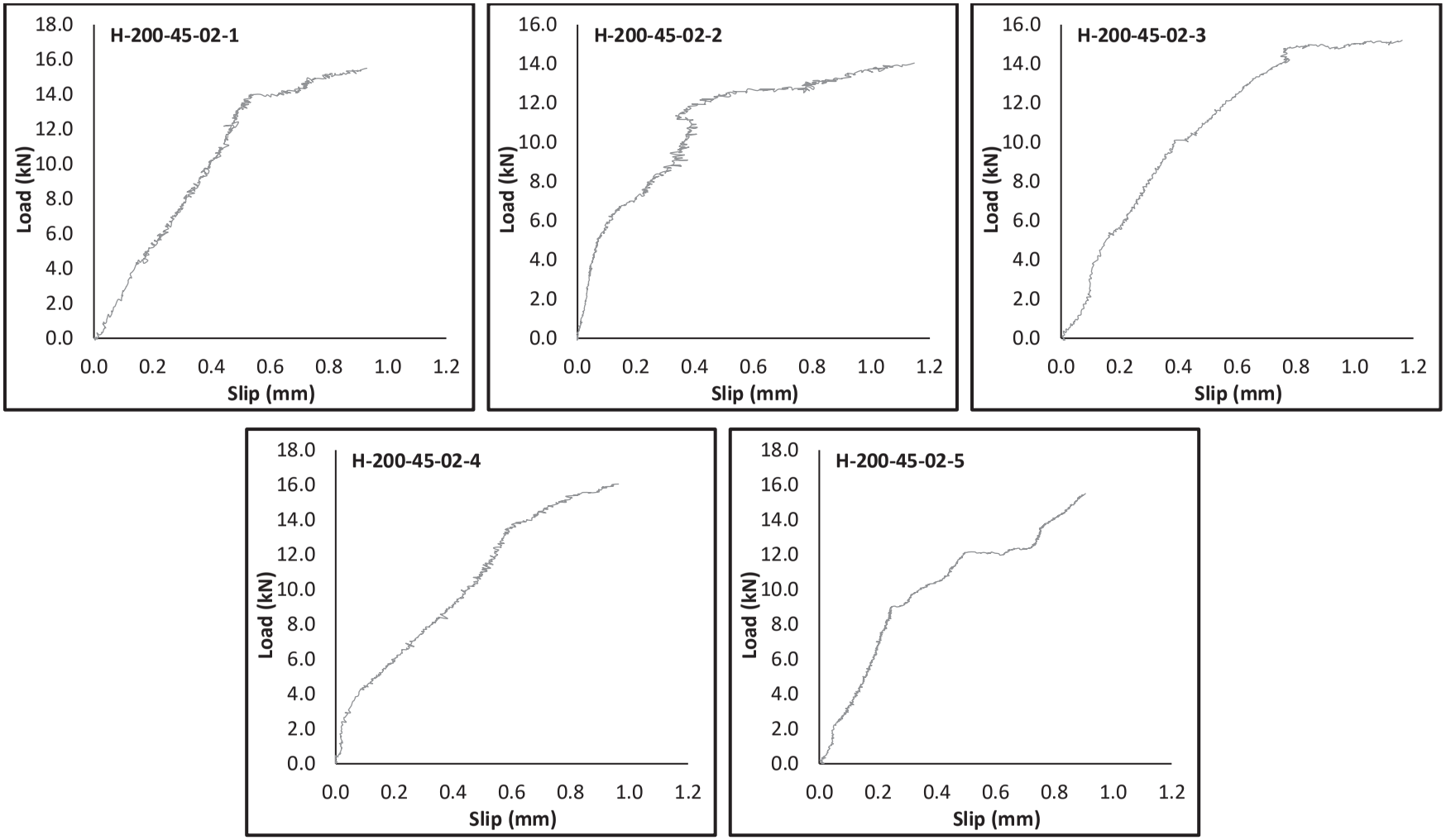
H-200-45-02-1
Load (kN)
Slip (mm)
H-200-45-02-2
Load (kN)
Slip (mm)
H-200-45-02-3
Load (kN)
Slip (mm)
H-200-45-02-4
Load (kN)
Slip (mm)
H-200-45-02-5
Load (kN)
Slip (mm)

Appendix E.

Slip of the interface – LVL Series

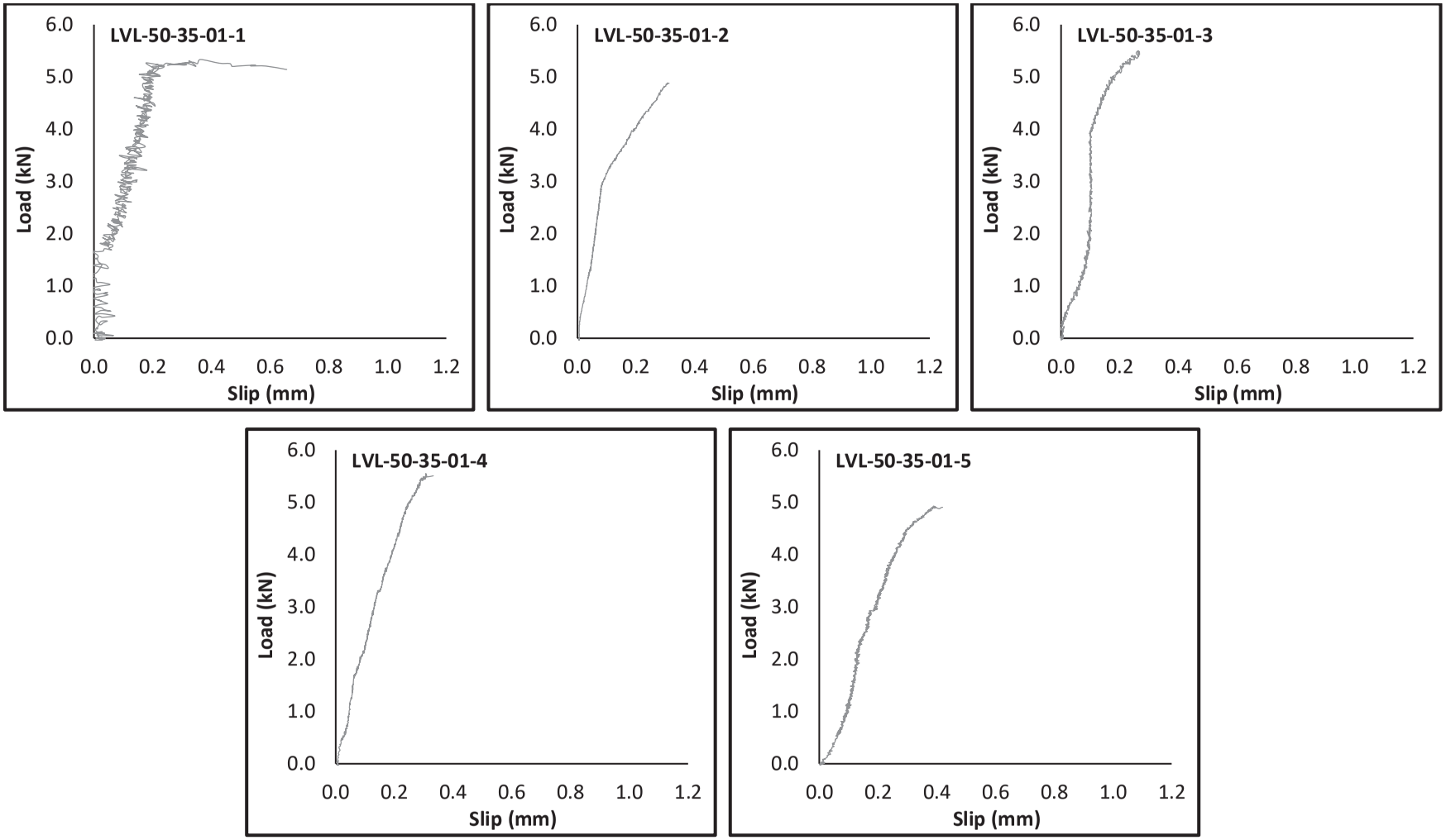
LVL-50-35-01-1
LVL-50-35-01-2
LVL-50-35-01-3
LVL-50-35-01-4
LVL-50-35-01-5
Load (kN)
Slip (mm)
0.0
1.0
2.0
3.0
4.0
5.0
6.0
0.0
0.2
0.4
0.6
0.8
1.0
1.2

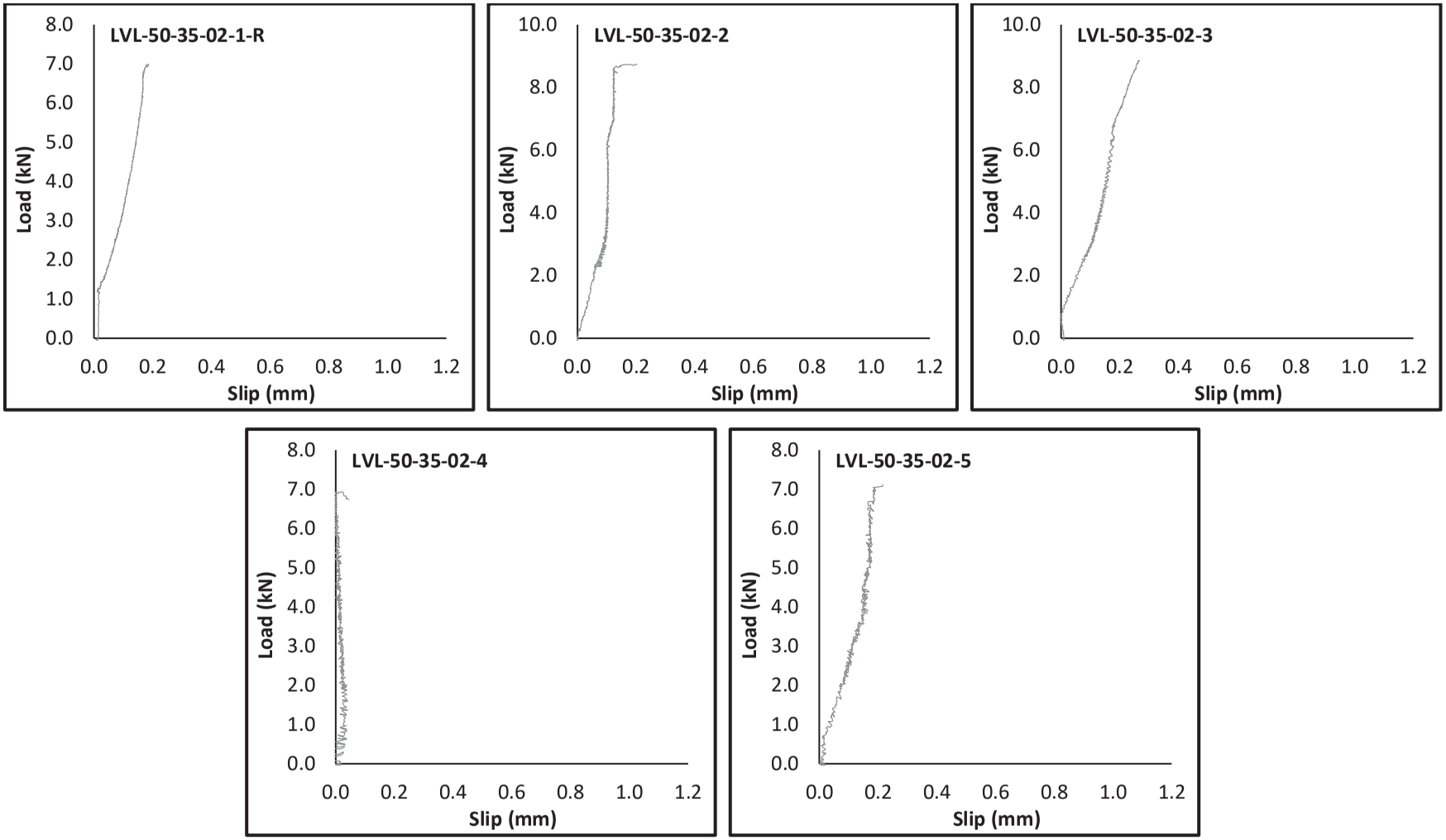
LVL-50-35-02-1-R
Load (kN)
Slip (mm)
LVL-50-35-02-2
Load (kN)
Slip (mm)
LVL-50-35-02-3
Load (kN)
Slip (mm)
LVL-50-35-02-4
Load (kN)
Slip (mm)
LVL-50-35-02-5
Load (kN)
Slip (mm)

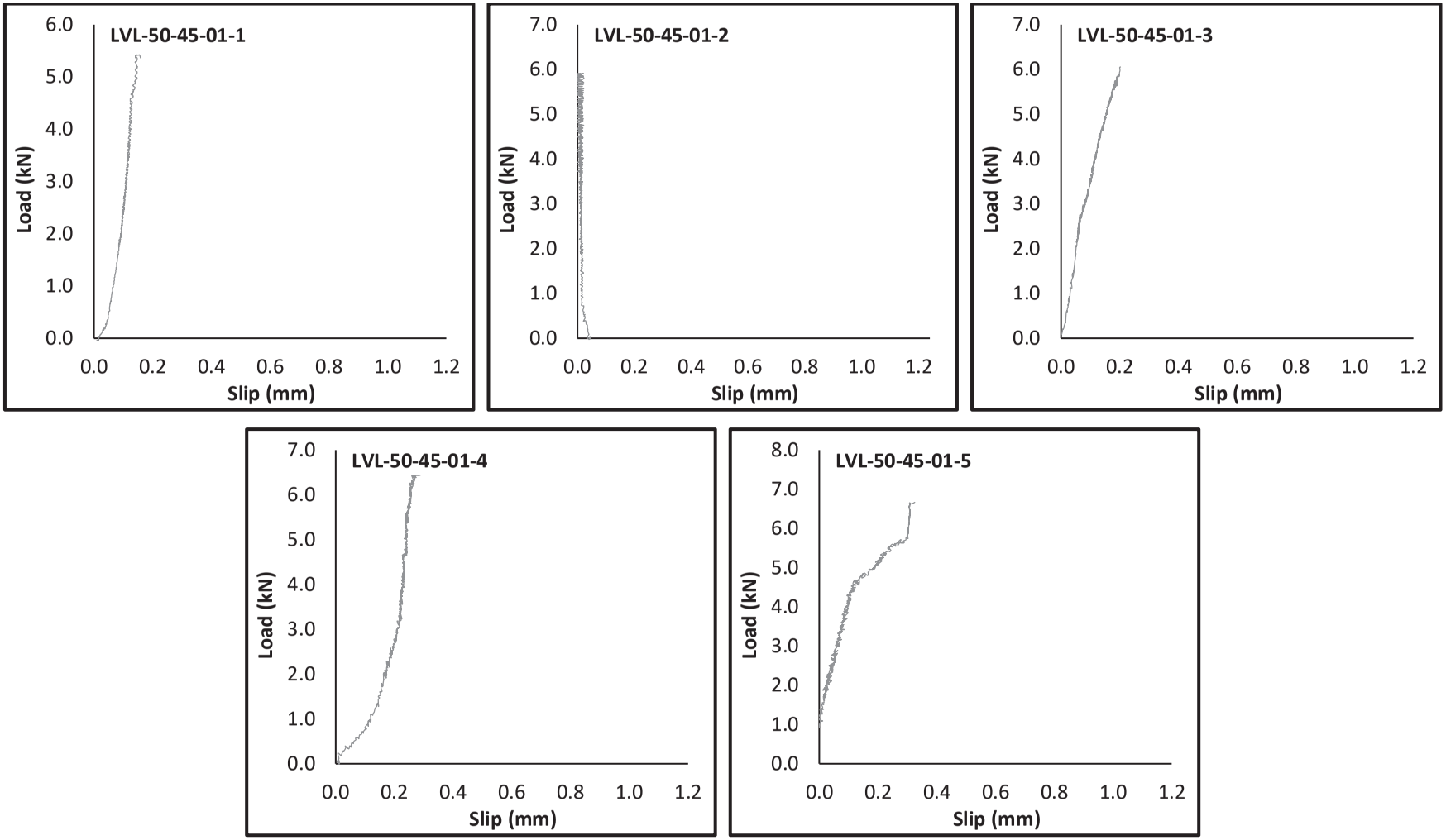
LVL-50-45-01-1
Load (kN)
Slip (mm)
LVL-50-45-01-2
Load (kN)
Slip (mm)
LVL-50-45-01-3
Load (kN)
Slip (mm)
LVL-50-45-01-4
Load (kN)
Slip (mm)
LVL-50-45-01-5
Load (kN)
Slip (mm)

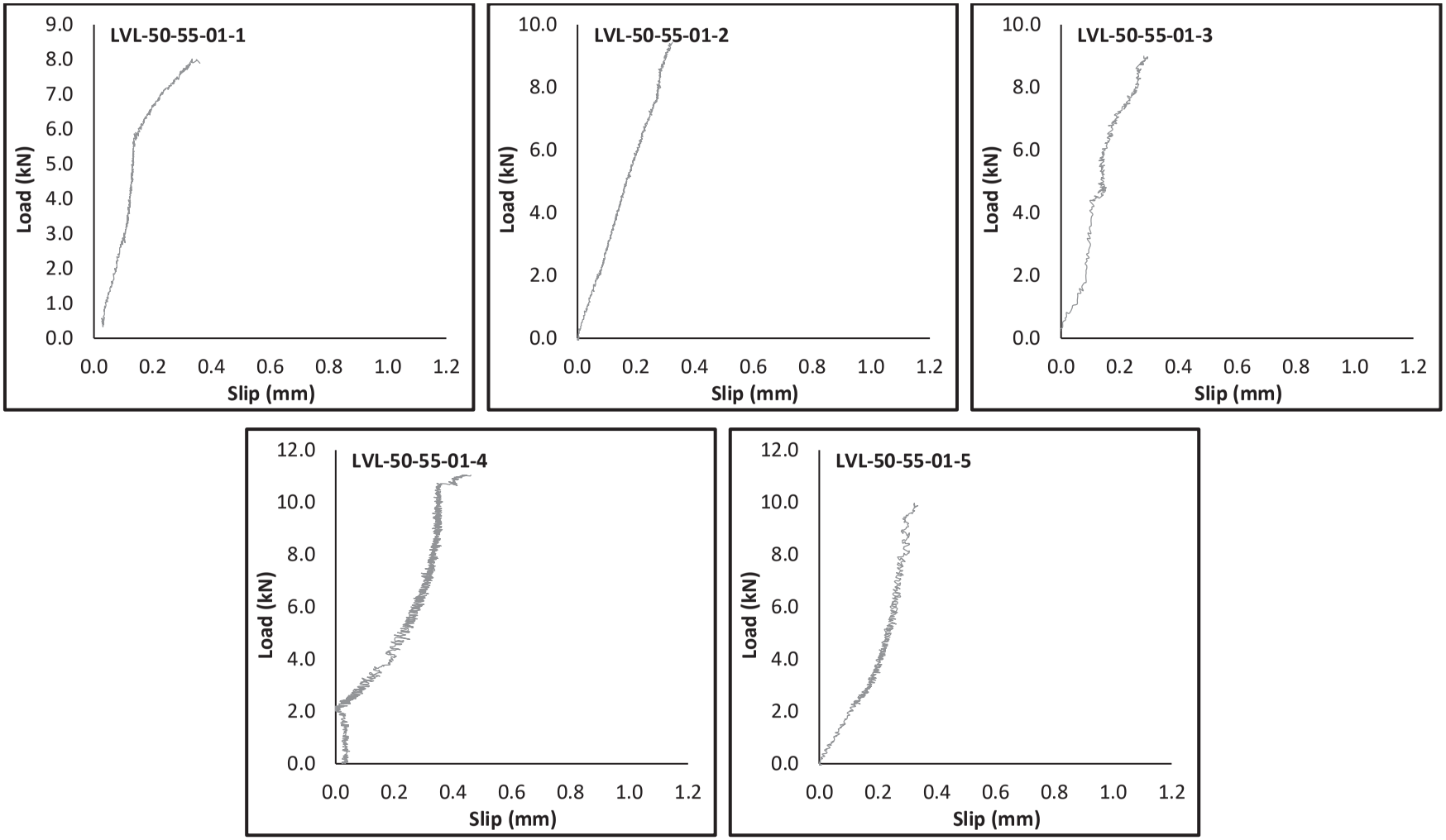
LVL-50-55-01-1
Load (kN)
Slip (mm)
LVL-50-55-01-2
Load (kN)
Slip (mm)
LVL-50-55-01-3
Load (kN)
Slip (mm)
LVL-50-55-01-4
Load (kN)
Slip (mm)
LVL-50-55-01-5
Load (kN)
Slip (mm)

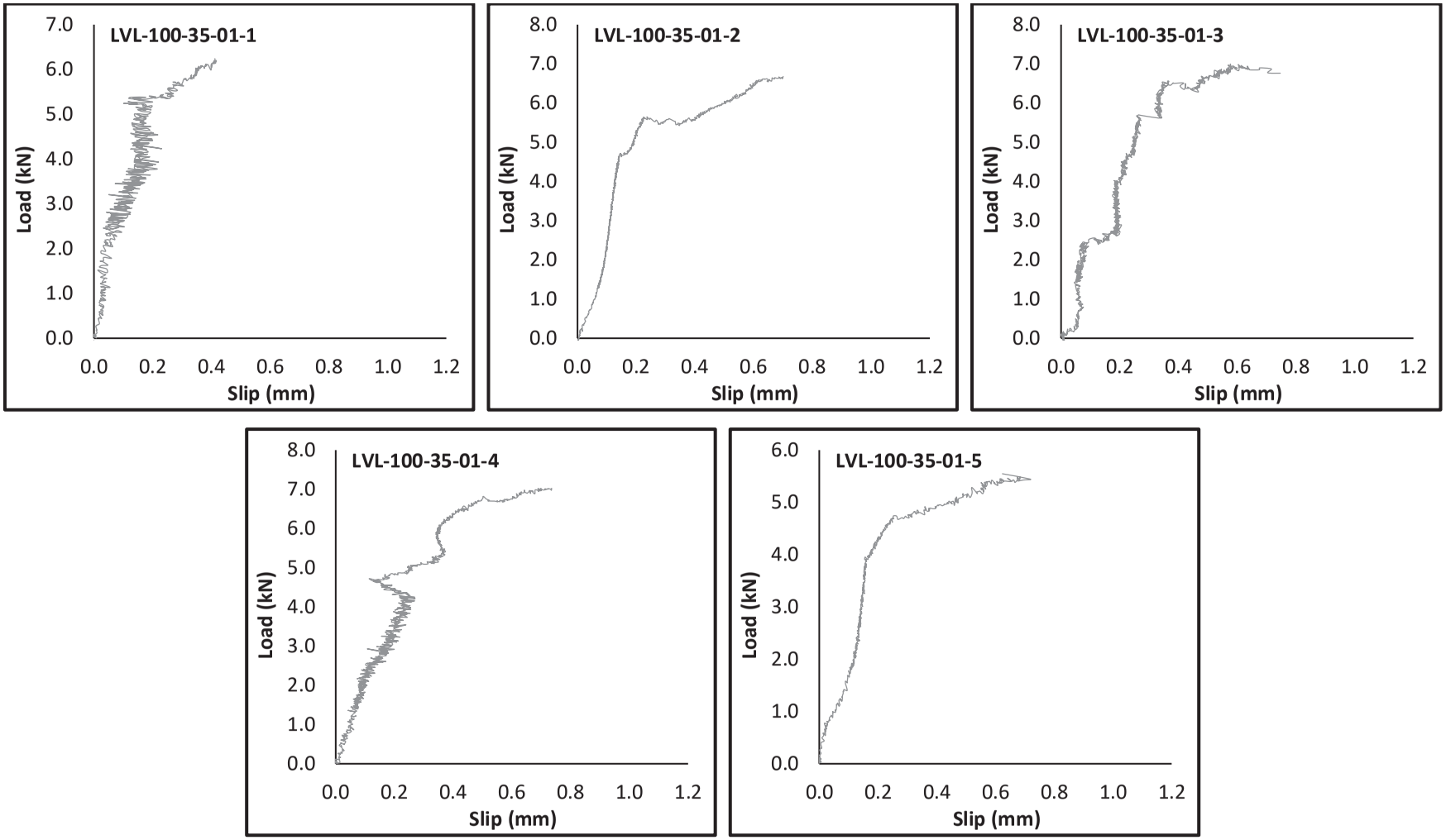
LVL-100-35-01-1
Load (kN)
Slip (mm)
LVL-100-35-01-2
Load (kN)
Slip (mm)
LVL-100-35-01-3
Load (kN)
Slip (mm)
LVL-100-35-01-4
Load (kN)
Slip (mm)
LVL-100-35-01-5
Load (kN)
Slip (mm)

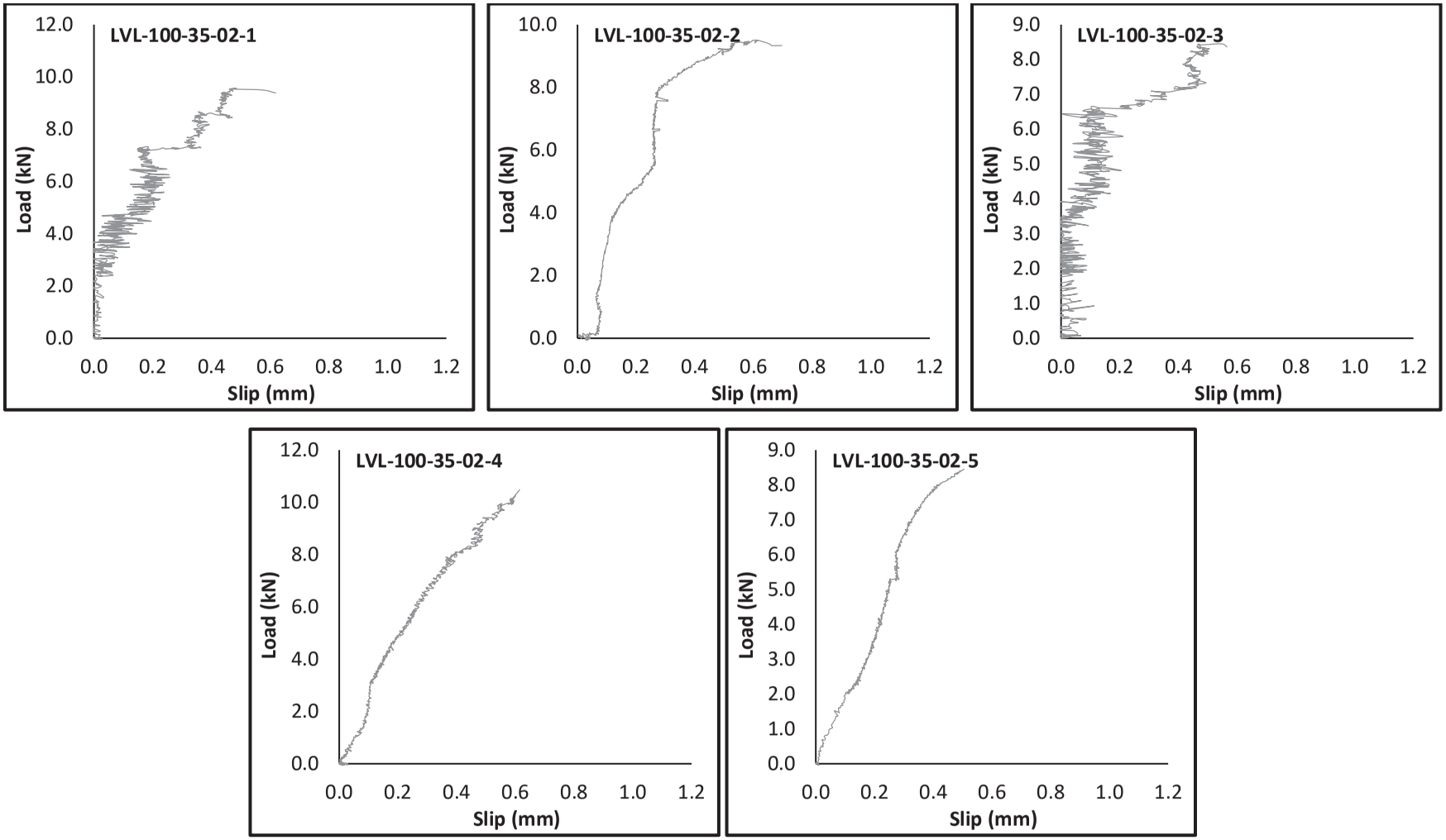
LVL-100-35-02-1
Load (kN)
Slip (mm)
LVL-100-35-02-2
Load (kN)
Slip (mm)
LVL-100-35-02-3
Load (kN)
Slip (mm)
LVL-100-35-02-4
Load (kN)
Slip (mm)
LVL-100-35-02-5
Load (kN)
Slip (mm)

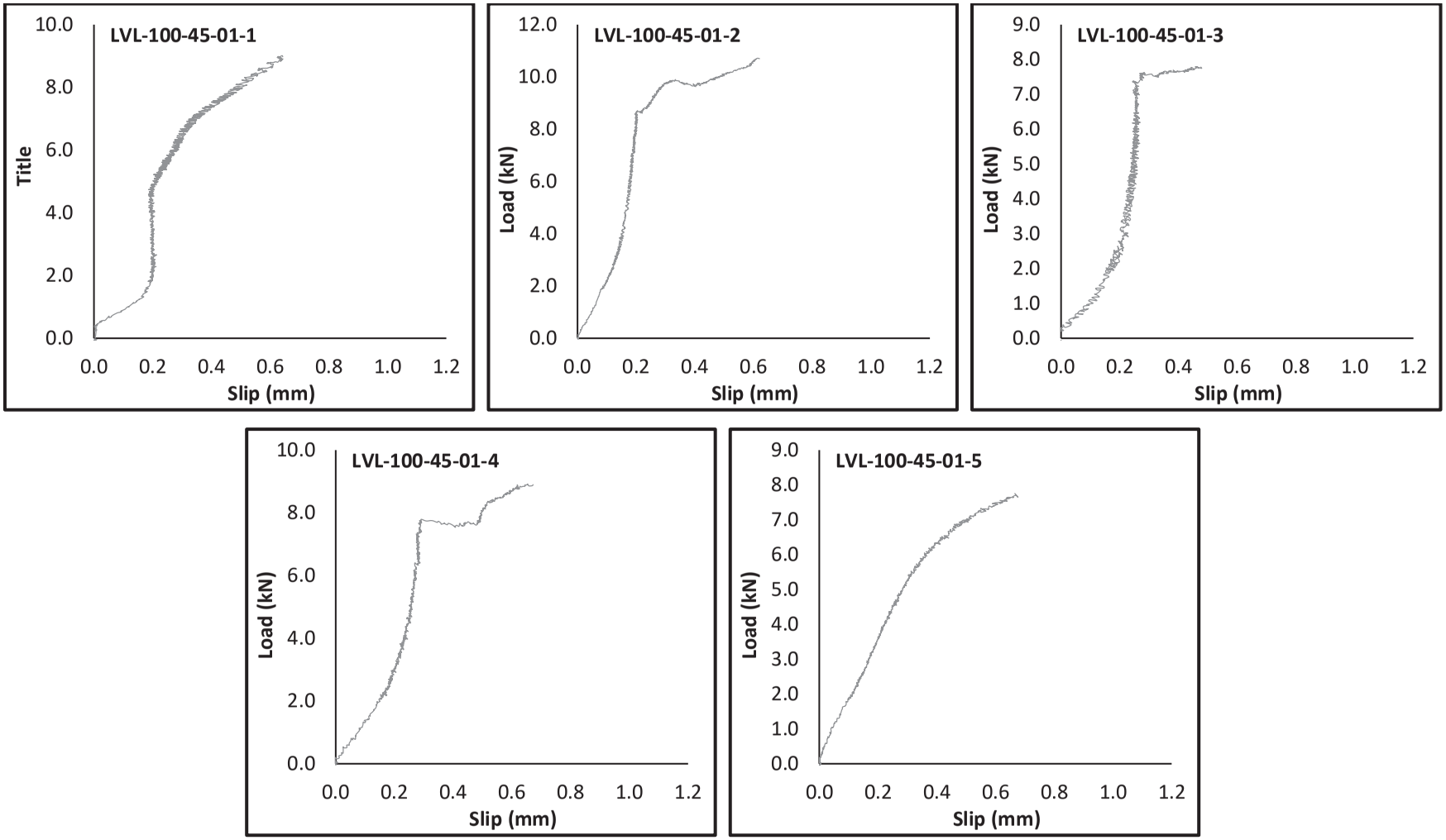
LVL-100-45-01-1
Title
Slip (mm)
LVL-100-45-01-2
Load (kN)
Slip (mm)
LVL-100-45-01-3
Load (kN)
Slip (mm)
LVL-100-45-01-4
Load (kN)
Slip (mm)
LVL-100-45-01-5
Load (kN)
Slip (mm)

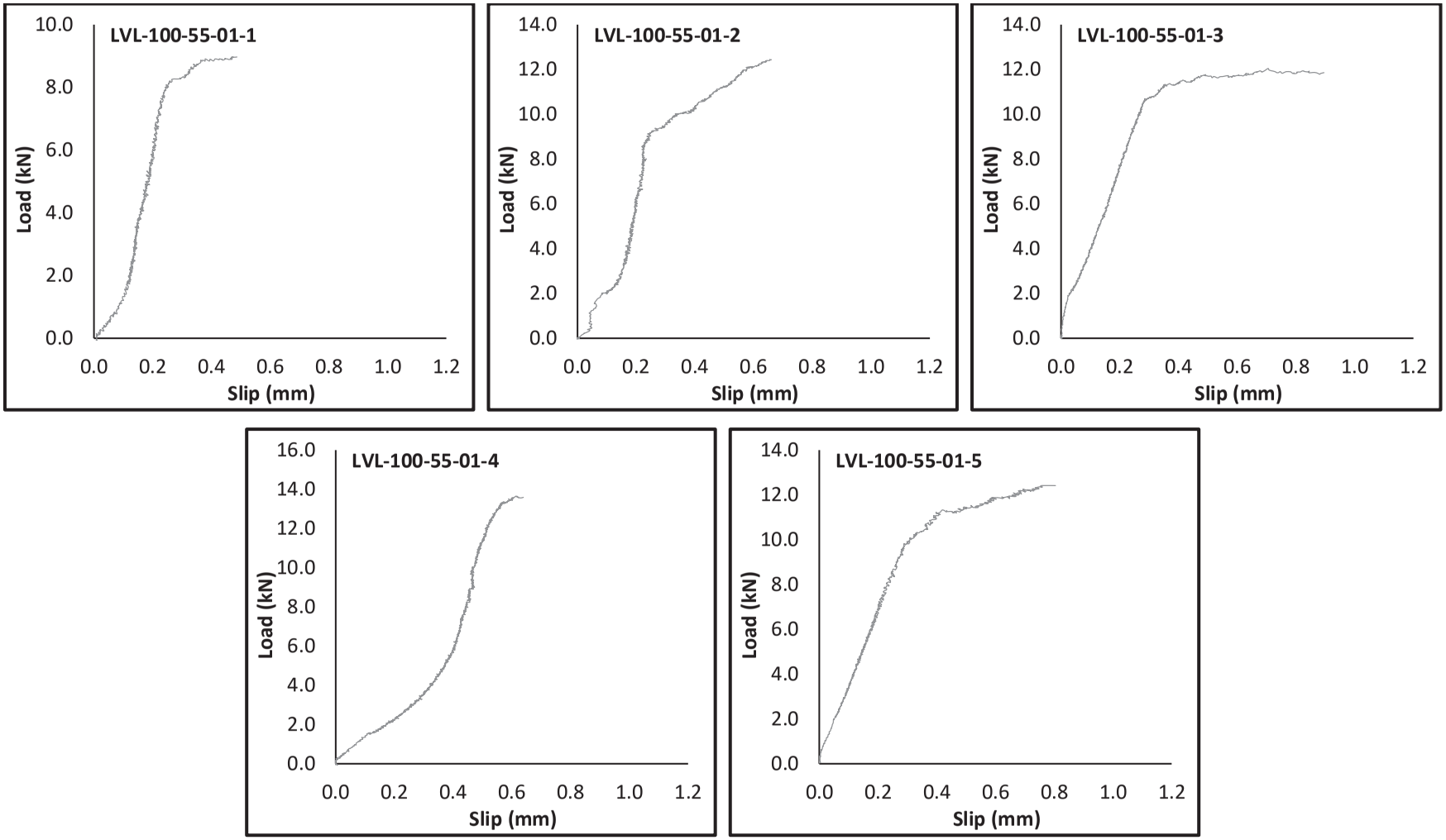
LVL-100-55-01-1
Load (kN)
Slip (mm)
LVL-100-55-01-2
Load (kN)
Slip (mm)
LVL-100-55-01-3
Load (kN)
Slip (mm)
LVL-100-55-01-4
Load (kN)
Slip (mm)
LVL-100-55-01-5
Load (kN)
Slip (mm)

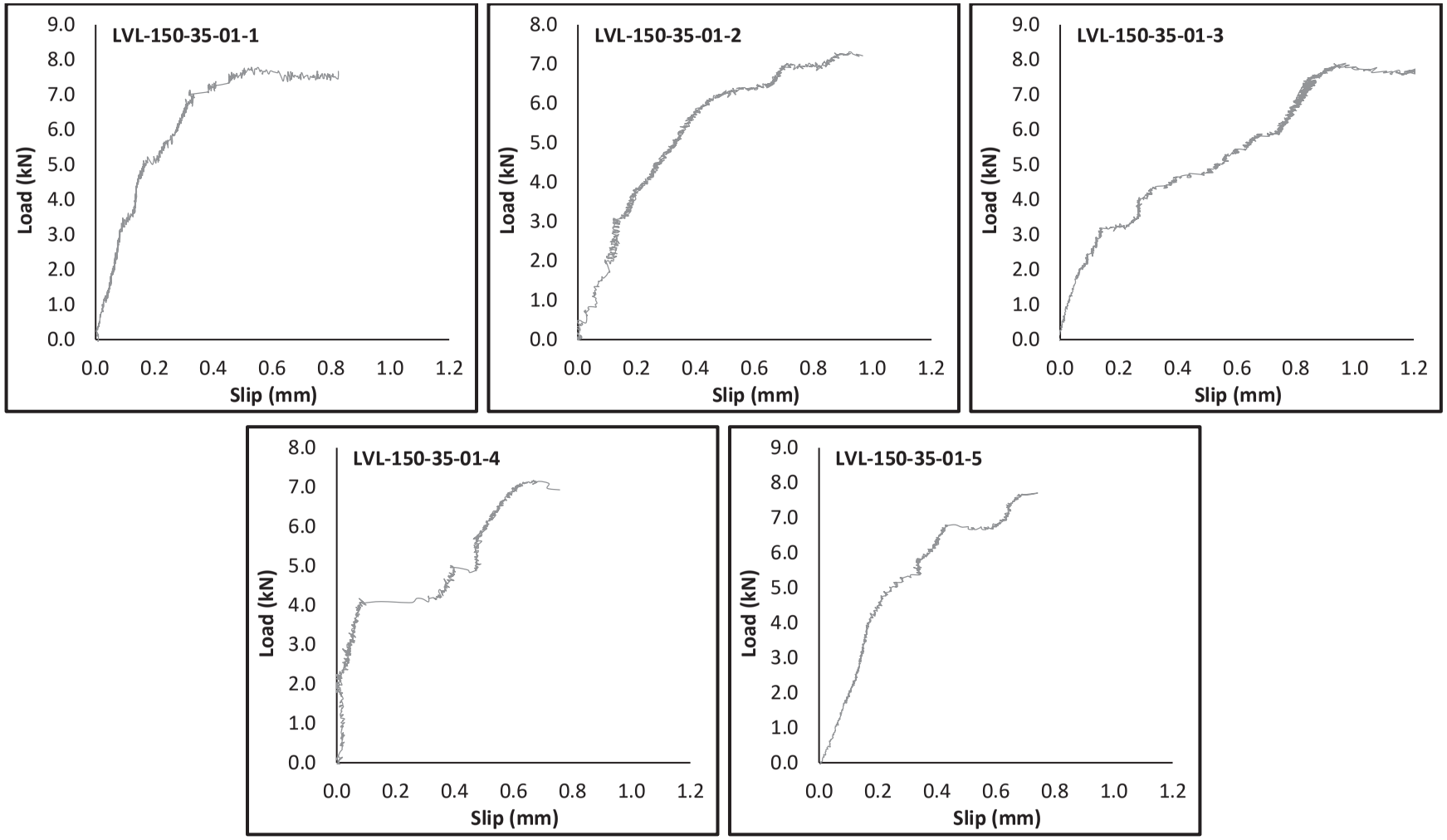
LVL-150-35-01-1
Load (kN)
Slip (mm)
LVL-150-35-01-2
Load (kN)
Slip (mm)
LVL-150-35-01-3
Load (kN)
Slip (mm)
LVL-150-35-01-4
Load (kN)
Slip (mm)
LVL-150-35-01-5
Load (kN)
Slip (mm)

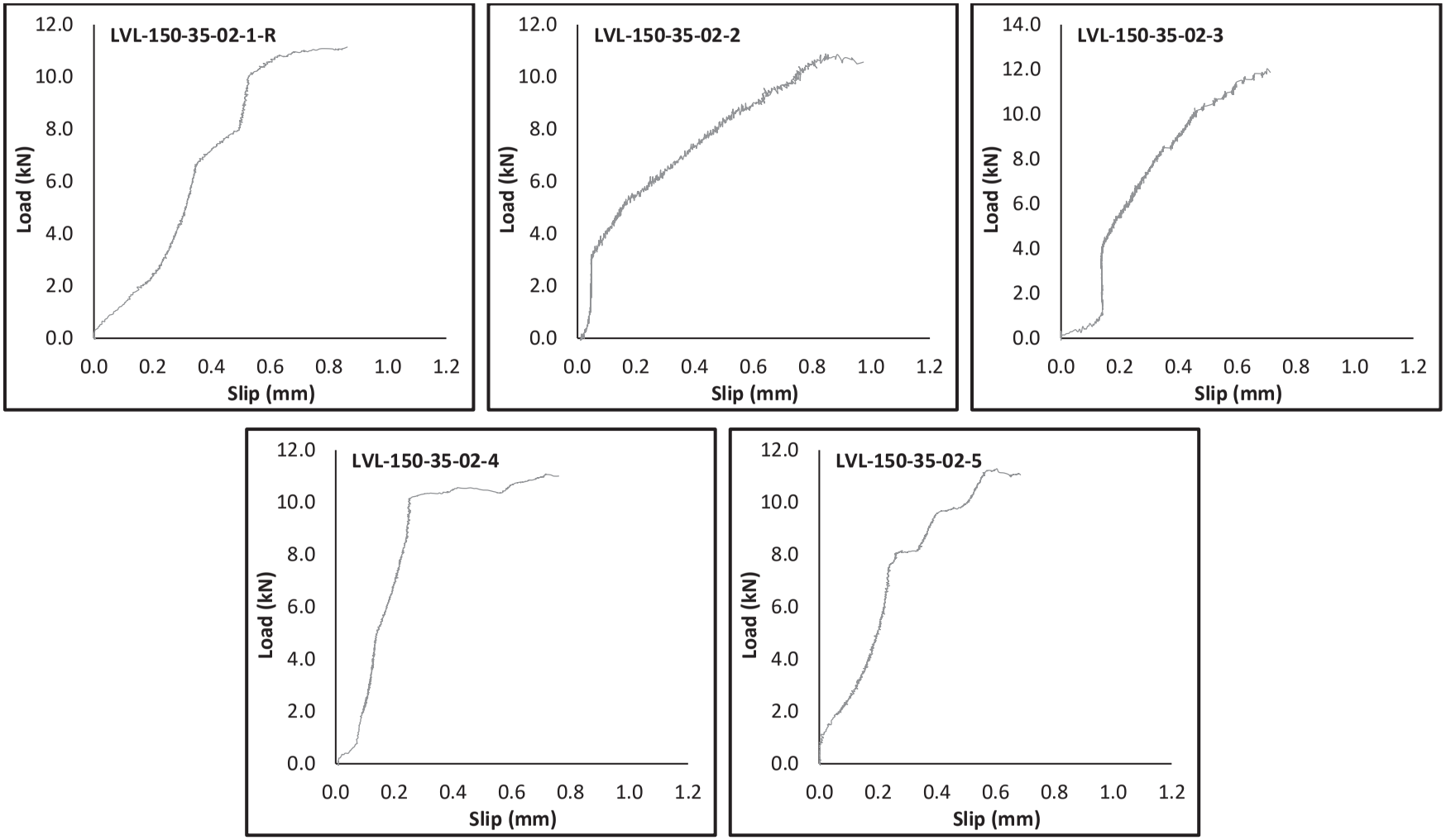
LVL-150-35-02-1-R
LVL-150-35-02-2
LVL-150-35-02-3
LVL-150-35-02-4
LVL-150-35-02-5
Load (kN)
Slip (mm)
0.0
2.0
4.0
6.0
8.0
10.0
12.0
14.0
0.2
0.4
0.6
0.8
1.0
1.2

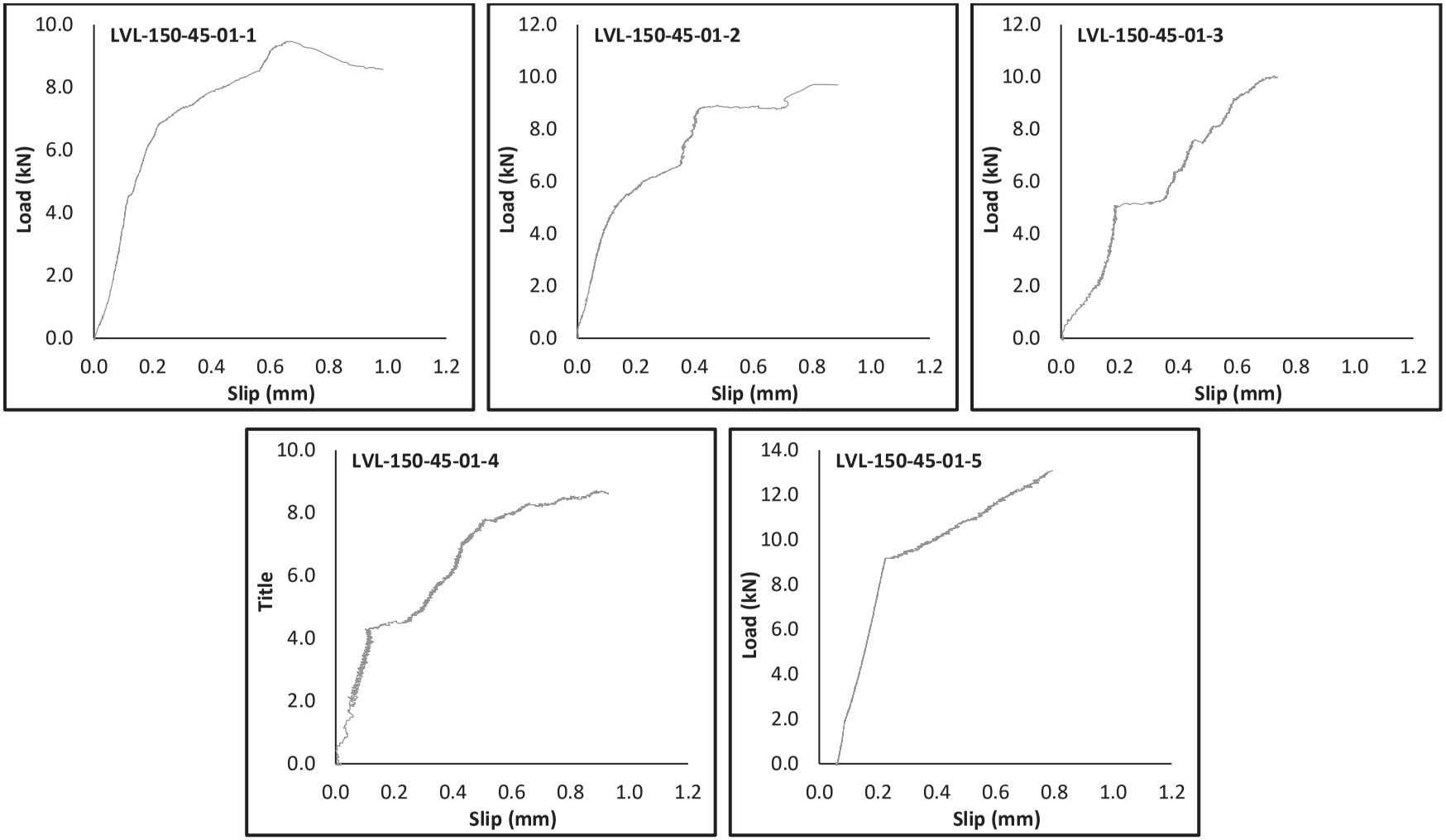
LVL-150-45-01-1
Load (kN)
Slip (mm)
LVL-150-45-01-2
Load (kN)
Slip (mm)
LVL-150-45-01-3
Load (kN)
Slip (mm)
LVL-150-45-01-4
Title
Slip (mm)
LVL-150-45-01-5
Load (kN)
Slip (mm)

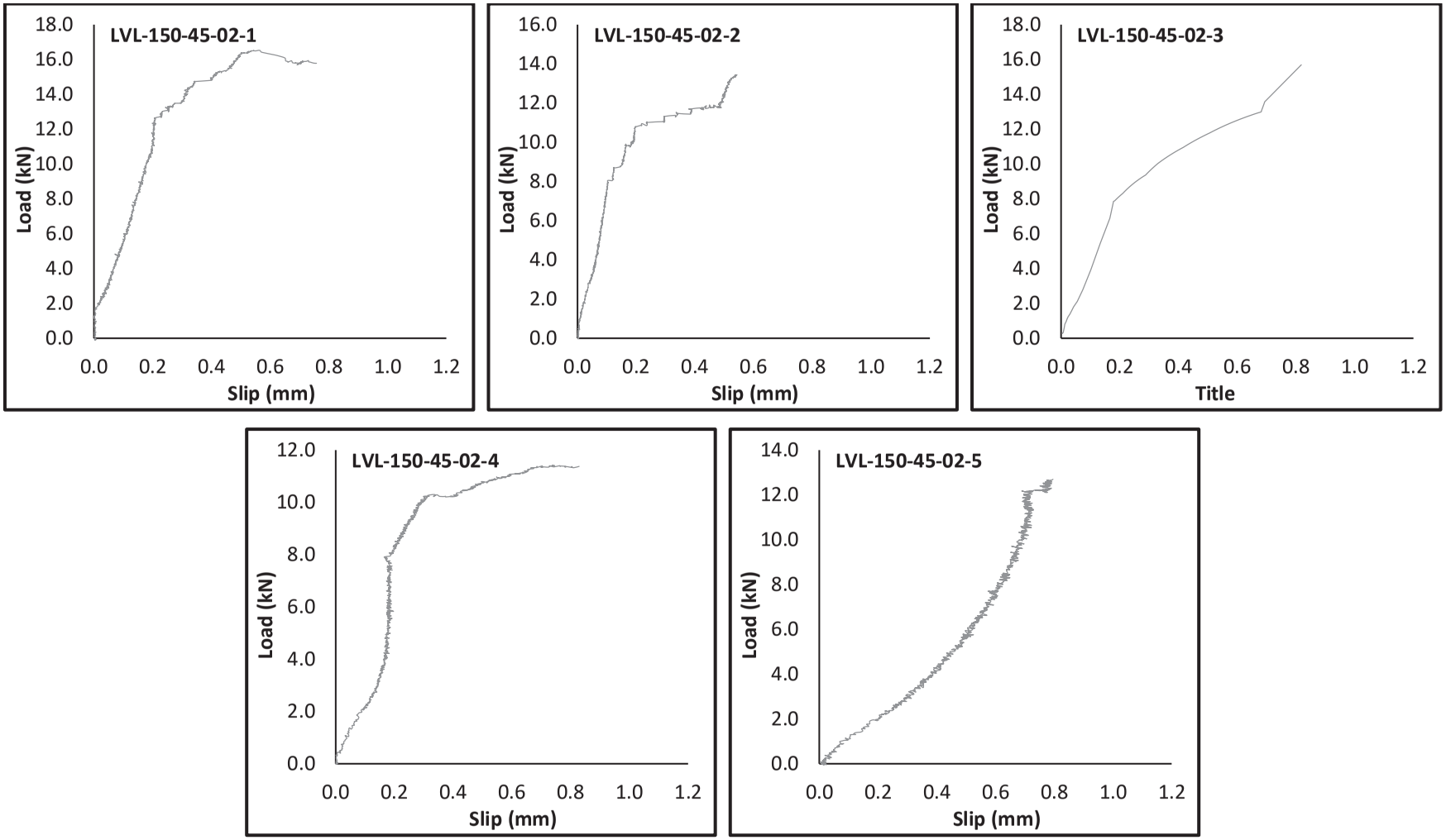
LVL-150-45-02-1
Load (kN)
Slip (mm)
LVL-150-45-02-2
Load (kN)
Slip (mm)
LVL-150-45-02-3
Load (kN)
Title
LVL-150-45-02-4
Load (kN)
Slip (mm)
LVL-150-45-02-5
Load (kN)
Slip (mm)

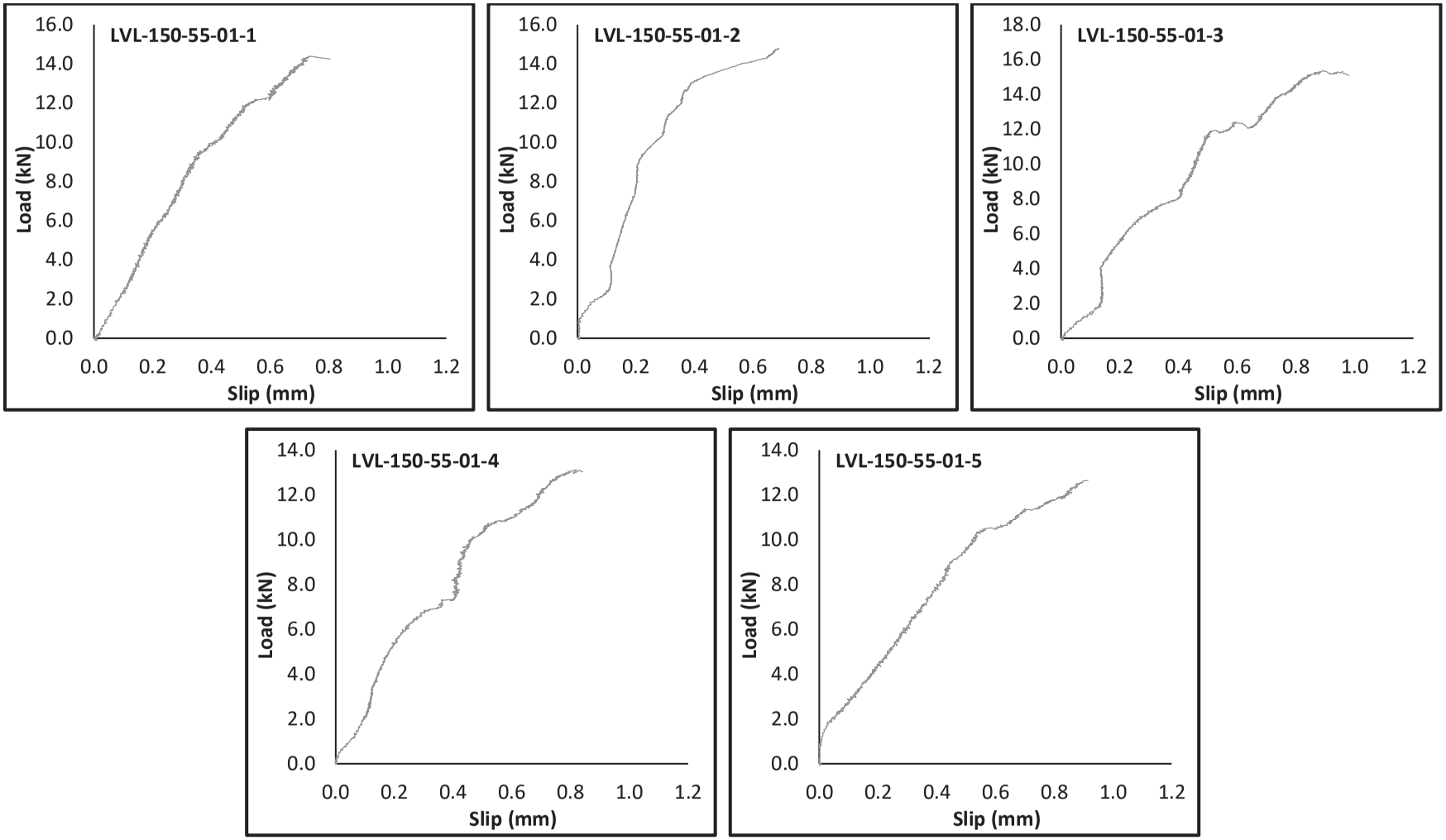
LVL-150-55-01-1
Load (kN)
Slip (mm)
LVL-150-55-01-2
Load (kN)
Slip (mm)
LVL-150-55-01-3
Load (kN)
Slip (mm)
LVL-150-55-01-4
Load (kN)
Slip (mm)
LVL-150-55-01-5
Load (kN)
Slip (mm)

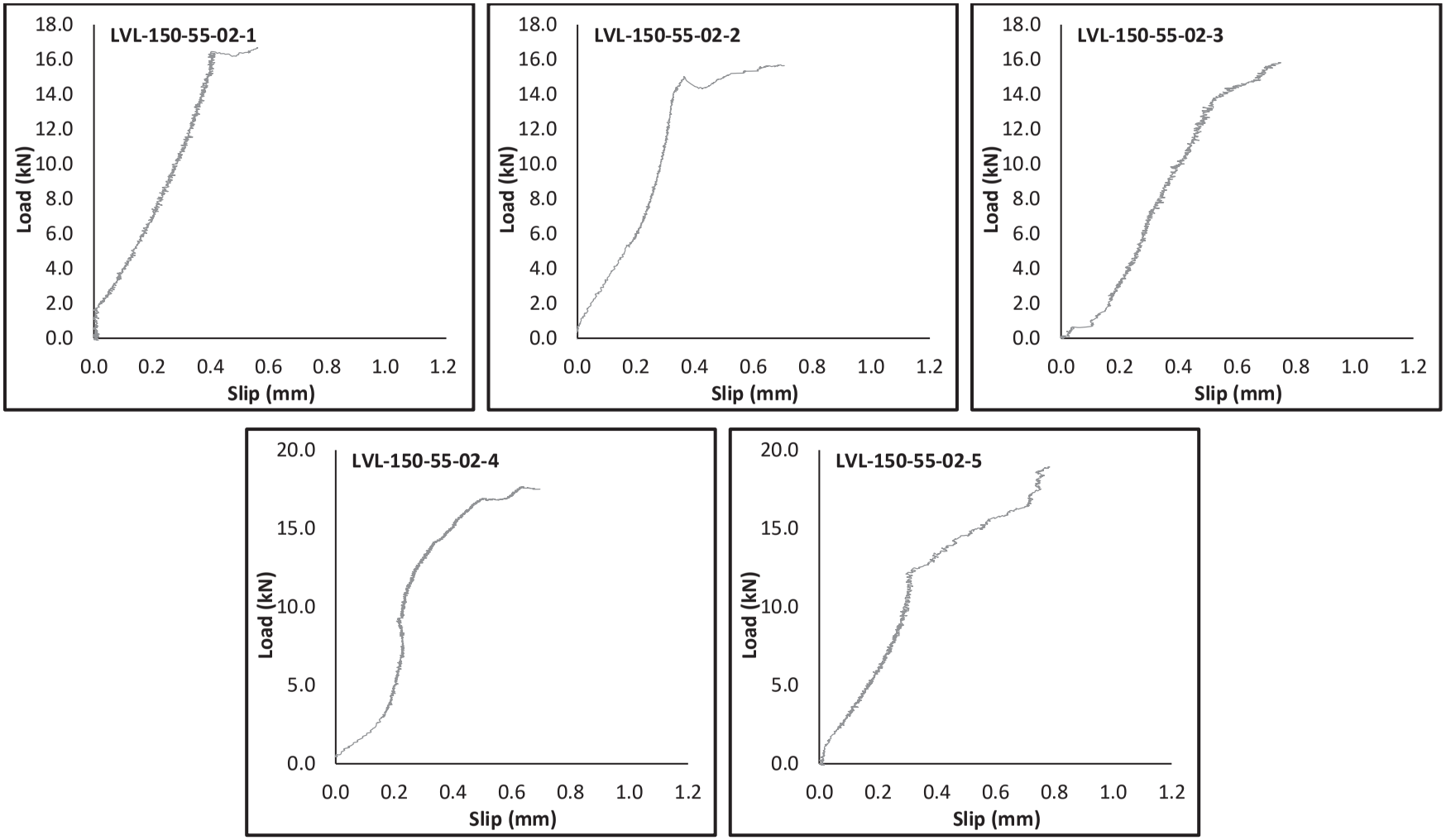
LVL-150-55-02-1
LVL-150-55-02-2
LVL-150-55-02-3
LVL-150-55-02-4
LVL-150-55-02-5
Load (kN)
Slip (mm)
0.0
0.2
0.4
0.6
0.8
1.0
1.2
2.0
4.0
5.0
6.0
8.0
10.0
12.0
14.0
15.0
16.0
18.0
20.0

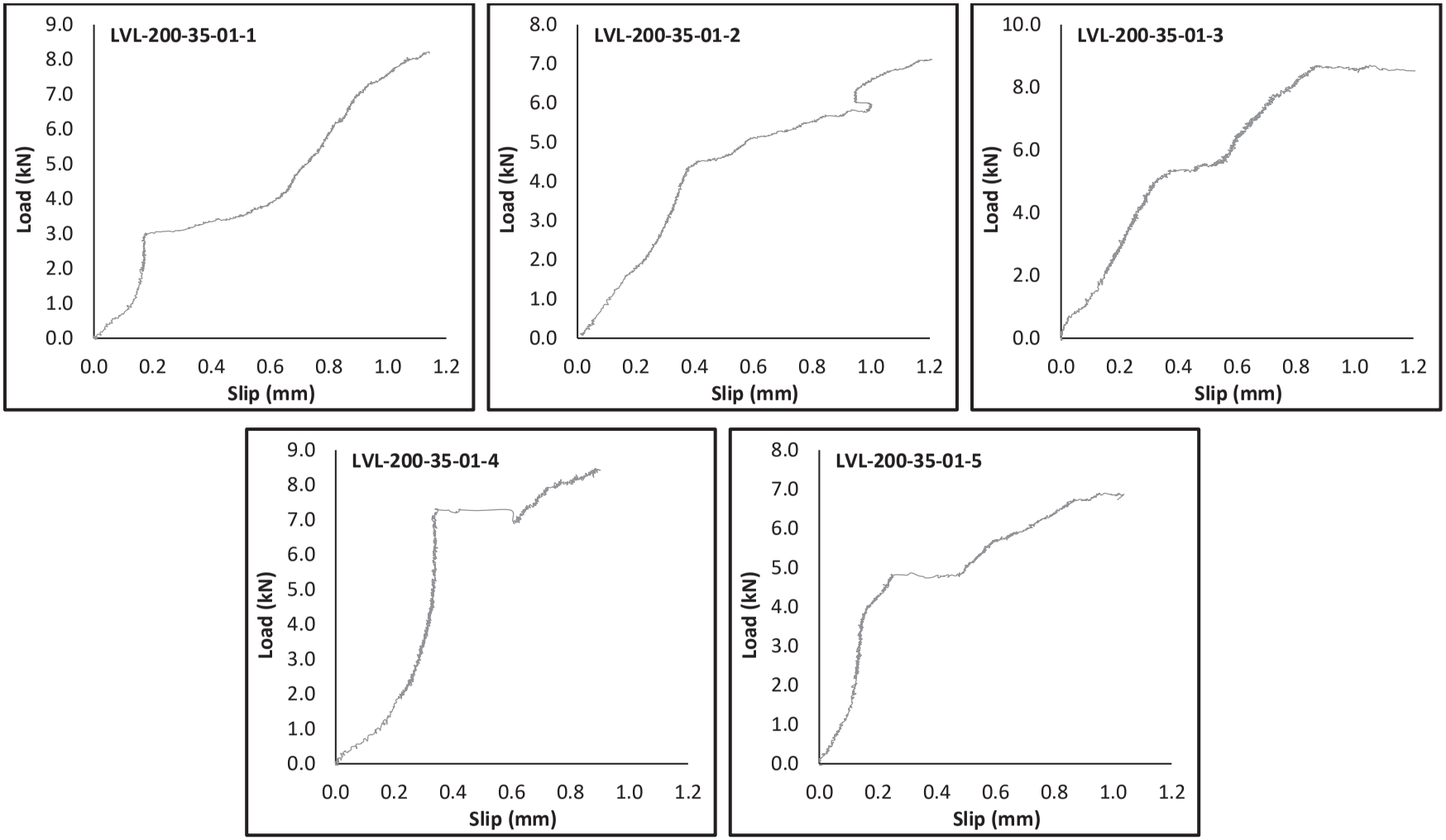
LVL-200-35-01-1
Load (kN)
Slip (mm)
LVL-200-35-01-2
Load (kN)
Slip (mm)
LVL-200-35-01-3
Load (kN)
Slip (mm)
LVL-200-35-01-4
Load (kN)
Slip (mm)
LVL-200-35-01-5
Load (kN)
Slip (mm)

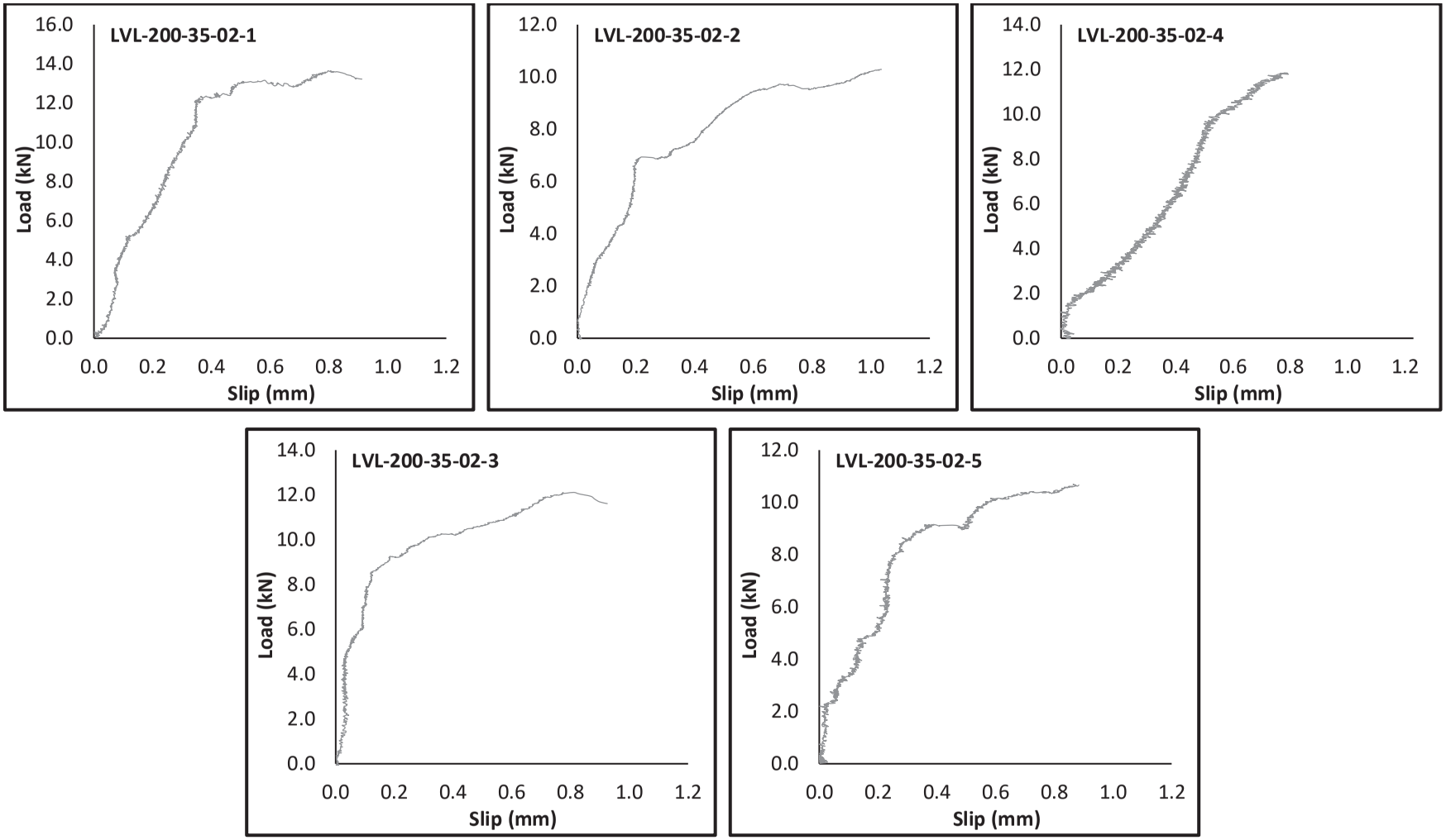
LVL-200-35-02-1
Load (kN)
Slip (mm)
LVL-200-35-02-2
Load (kN)
Slip (mm)
LVL-200-35-02-4
Load (kN)
Slip (mm)
LVL-200-35-02-3
Load (kN)
Slip (mm)
LVL-200-35-02-5
Load (kN)
Slip (mm)

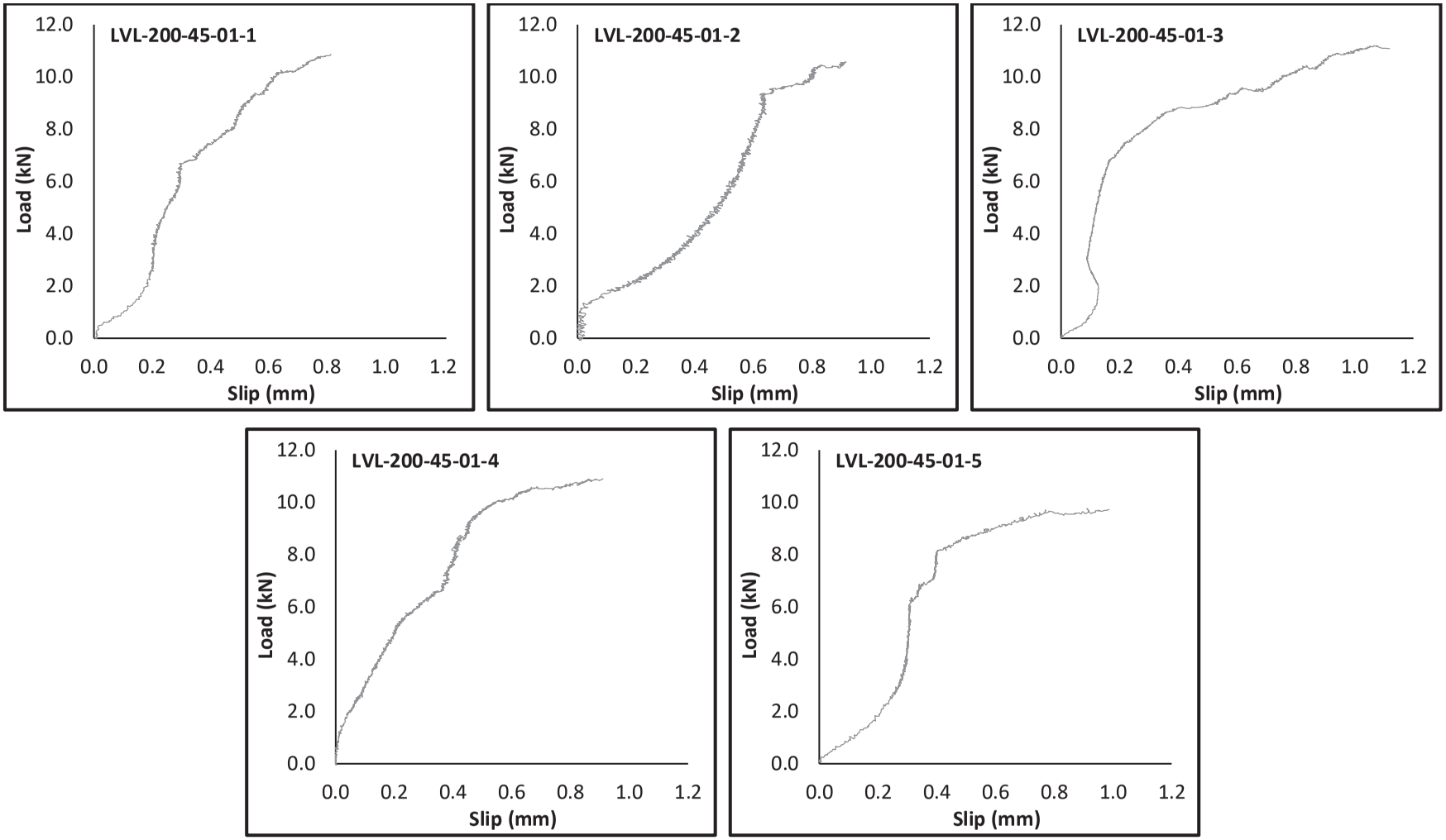
LVL-200-45-01-1
LVL-200-45-01-2
LVL-200-45-01-3
LVL-200-45-01-4
LVL-200-45-01-5
Load (kN)
Slip (mm)
0.0
2.0
4.0
6.0
8.0
10.0
12.0
0.0
0.2
0.4
0.6
0.8
1.0
1.2

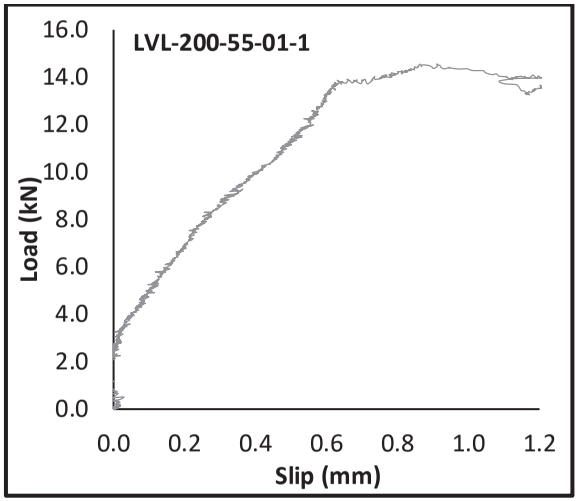
LVL-200-55-01-1
Load (kN)
Slip (mm)
16.0
14.0
12.0
10.0
8.0
6.0
4.0
2.0
0.0
0.0 0.2 0.4 0.6 0.8 1.0 1.2

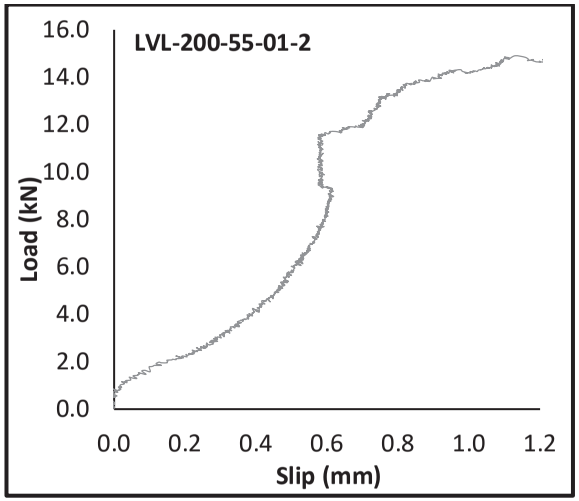
LVL-200-55-01-2
Load (kN)
Slip (mm)
16.0
14.0
12.0
10.0
8.0
6.0
4.0
2.0
0.0
0.0 0.2 0.4 0.6 0.8 1.0 1.2

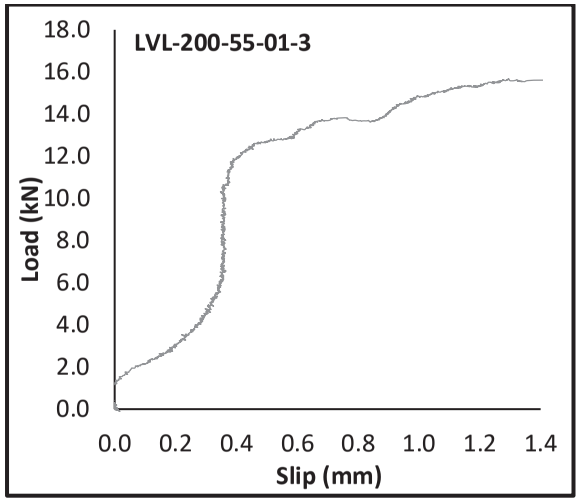
LVL-200-55-01-3
Load (kN)
Slip (mm)
18.0
16.0
14.0
12.0
10.0
8.0
6.0
4.0
2.0
0.0
0.0 0.2 0.4 0.6 0.8 1.0 1.2 1.4

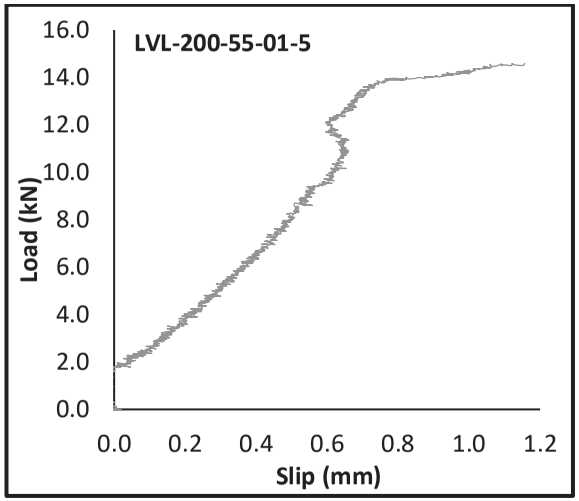
LVL-200-55-01-5
Load (kN)
Slip (mm)
16.0
14.0
12.0
10.0
8.0
6.0
4.0
2.0
0.0
0.0 0.2 0.4 0.6 0.8 1.0 1.2

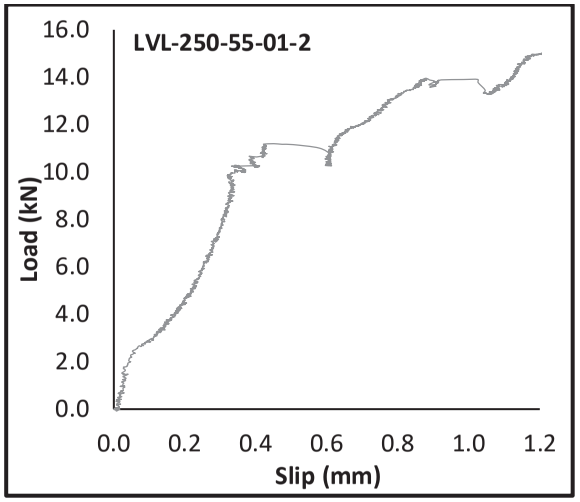
LVL-250-55-01-2
Load (kN)
16.0
14.0
12.0
10.0
8.0
6.0
4.0
2.0
0.0
0.0
0.2
0.4
0.6
0.8
1.0
1.2
Slip (mm)

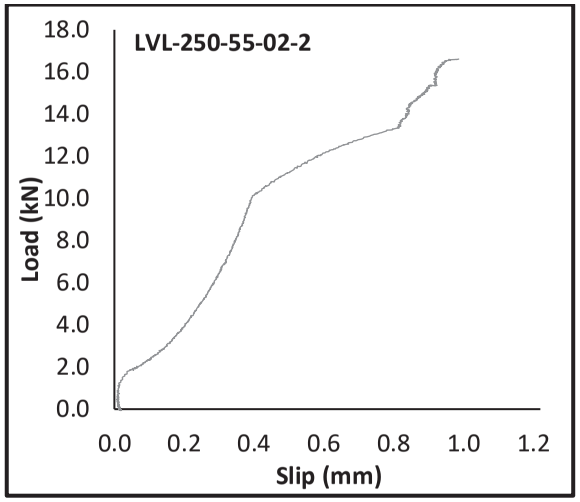
LVL-250-55-02-2
Load (kN)
18.0
16.0
14.0
12.0
10.0
8.0
6.0
4.0
2.0
0.0
0.0
0.2
0.4
0.6
0.8
1.0
1.2
Slip (mm)

Appendix F.

Interfacial bond stress – Hardwood Series

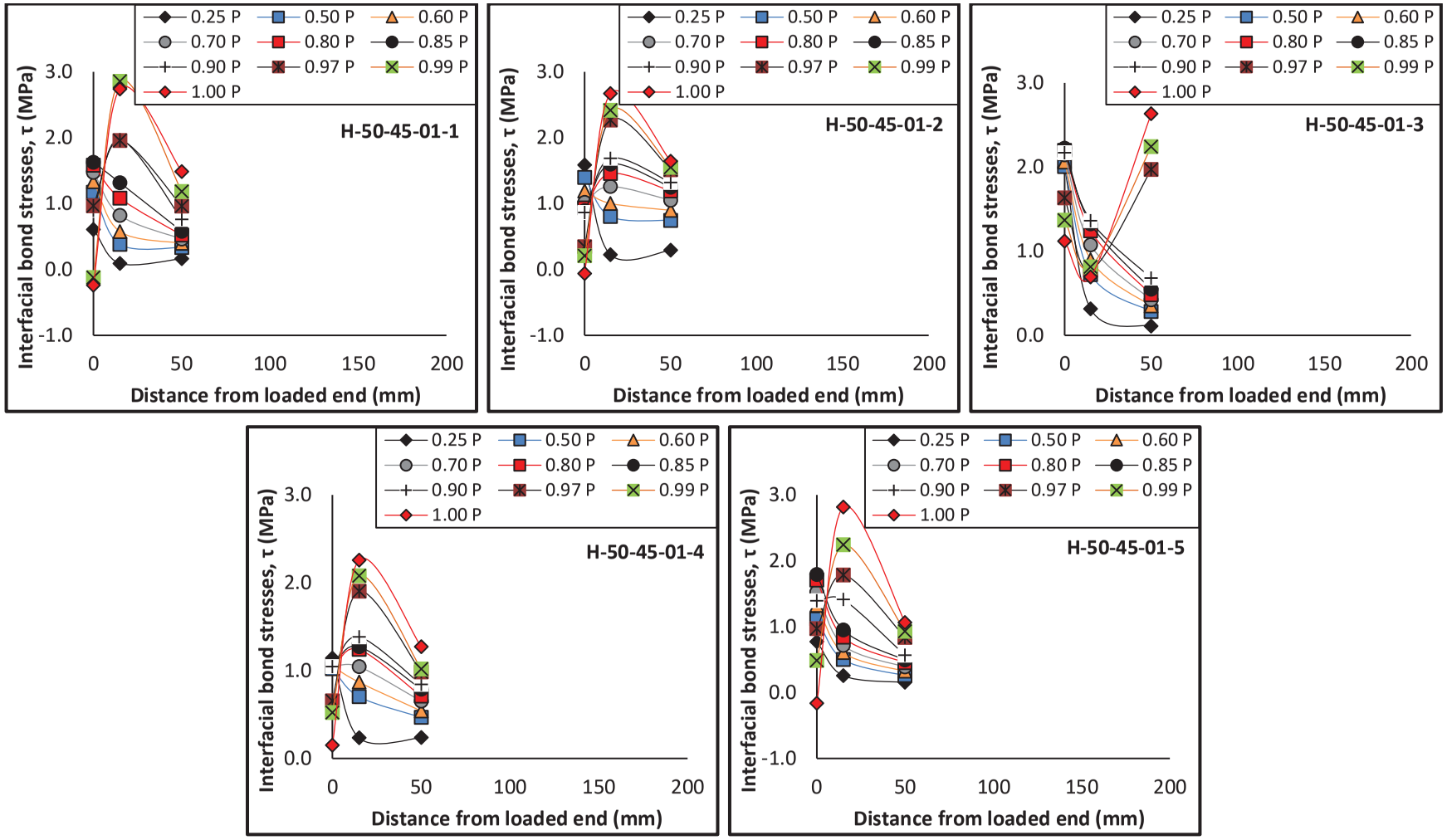
0.25 P
0.50 P
0.60 P
0.70 P
0.80 P
0.85 P
0.90 P
0.97 P
0.99 P
1.00 P
H-50-45-01-1
H-50-45-01-2
H-50-45-01-3
H-50-45-01-4
H-50-45-01-5
Interfacial bond stresses, τ (MPa)
Distance from loaded end (mm)
3.0
2.0
1.0
0.0
-1.0
0
50
100
150
200

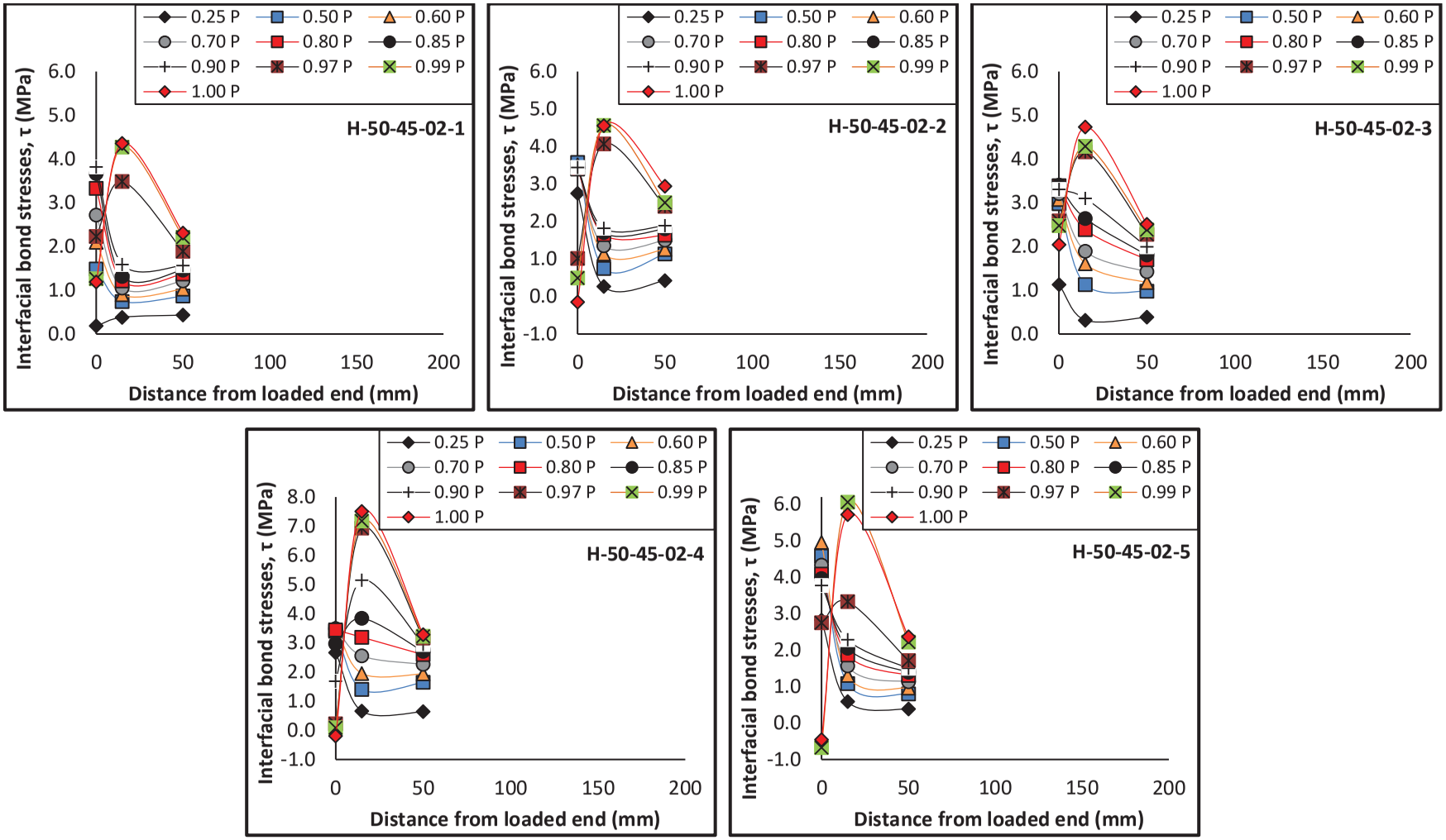
0.25 P
0.50 P
0.60 P
0.70 P
0.80 P
0.85 P
0.90 P
0.97 P
0.99 P
1.00 P
H-50-45-02-1
H-50-45-02-2
H-50-45-02-3
H-50-45-02-4
H-50-45-02-5
Interfacial bond stresses, τ (MPa)
Distance from loaded end (mm)

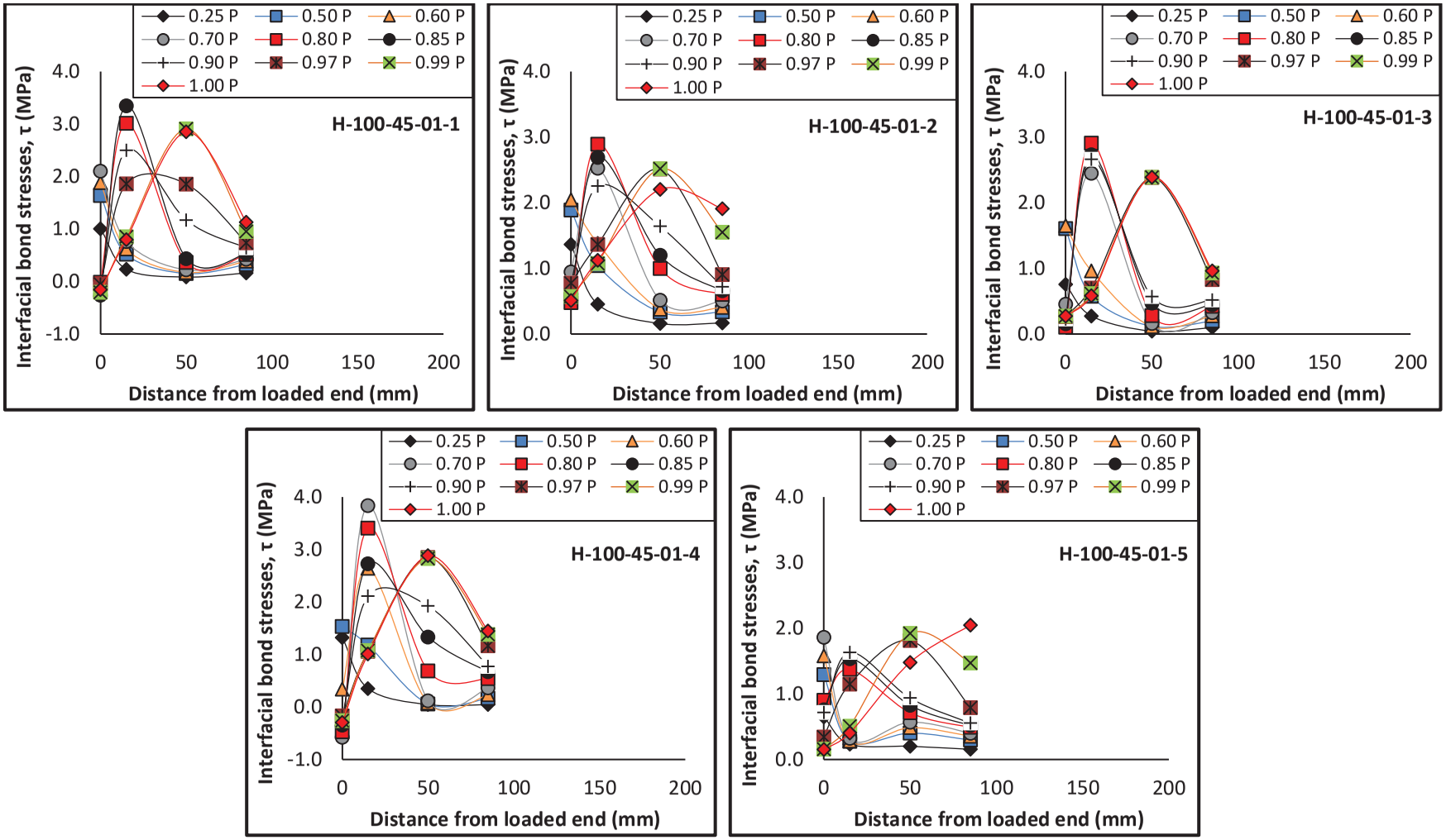
0.25 P
0.50 P
0.60 P
0.70 P
0.80 P
0.85 P
0.90 P
0.97 P
0.99 P
1.00 P
H-100-45-01-1
H-100-45-01-2
H-100-45-01-3
H-100-45-01-4
H-100-45-01-5
Interfacial bond stresses, τ (MPa)
Distance from loaded end (mm)
4.0
3.0
2.0
1.0
0.0
-1.0
0
50
100
150
200

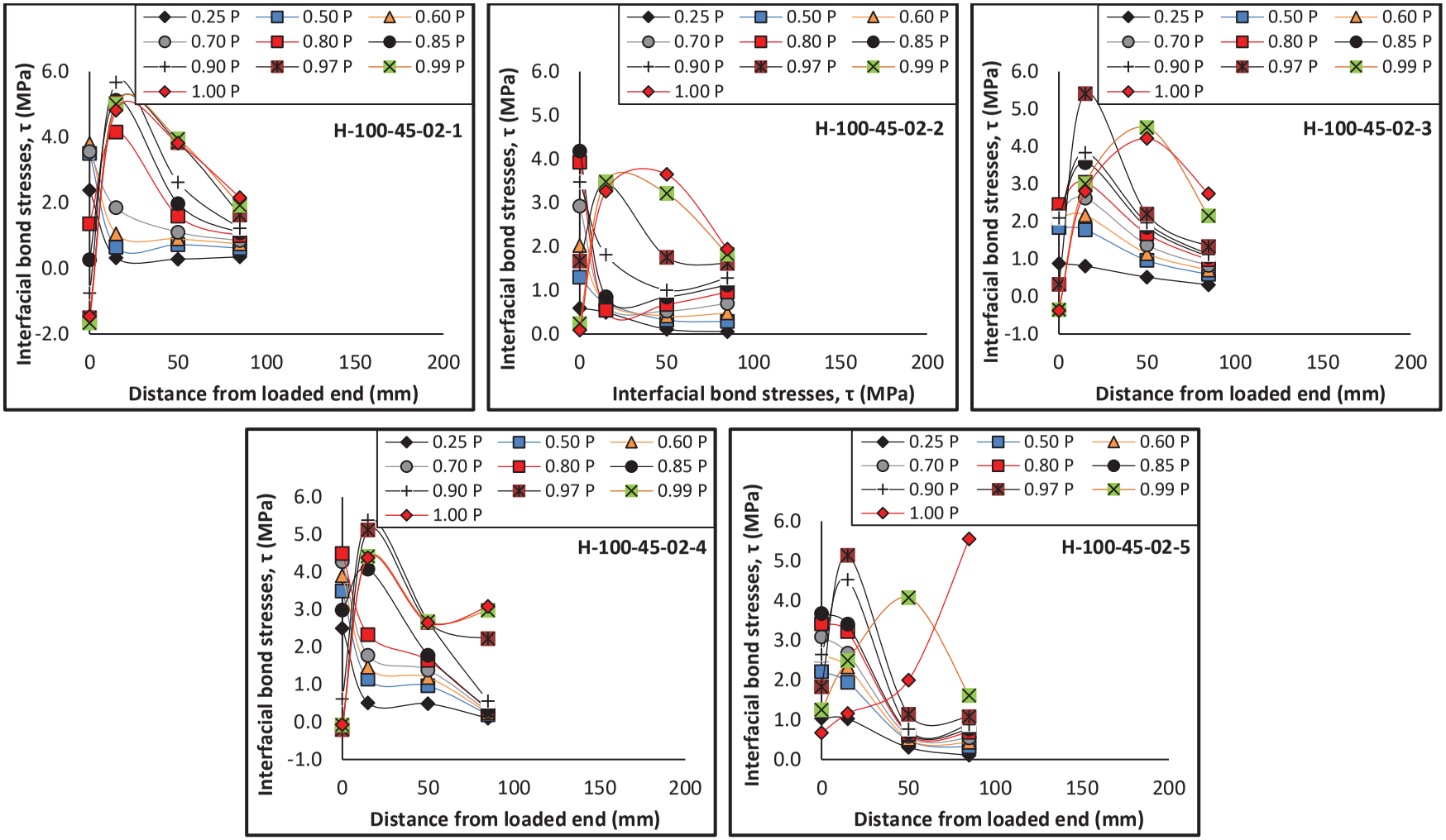
0.25 P
0.50 P
0.60 P
0.70 P
0.80 P
0.85 P
0.90 P
0.97 P
0.99 P
1.00 P
H-100-45-02-1
H-100-45-02-2
H-100-45-02-3
H-100-45-02-4
H-100-45-02-5
Interfacial bond stresses, τ (MPa)
Distance from loaded end (mm)

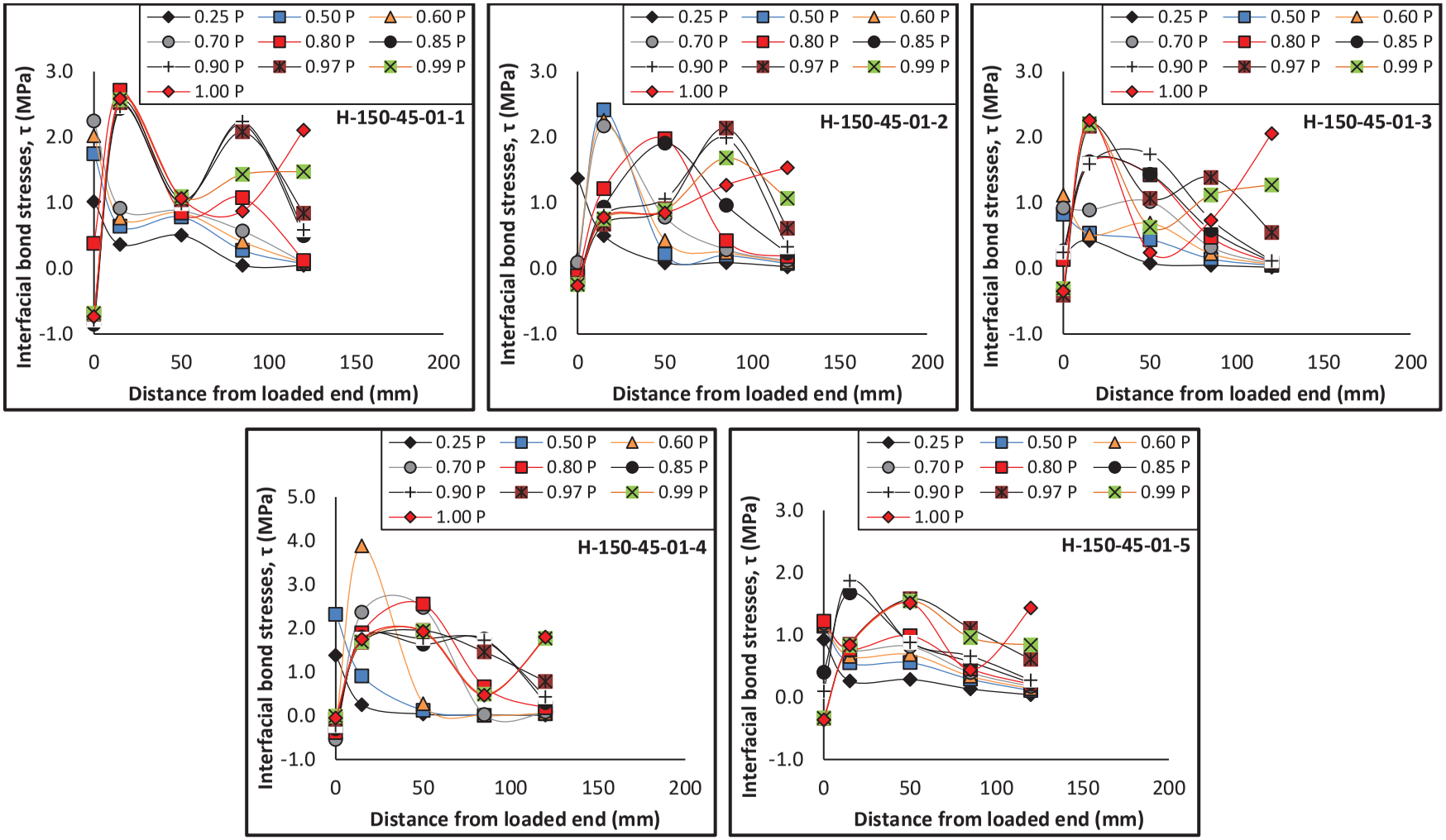
0.25 P
0.50 P
0.60 P
0.70 P
0.80 P
0.85 P
0.90 P
0.97 P
0.99 P
1.00 P
H-150-45-01-1
H-150-45-01-2
H-150-45-01-3
H-150-45-01-4
H-150-45-01-5
Interfacial bond stresses, τ (MPa)
Distance from loaded end (mm)

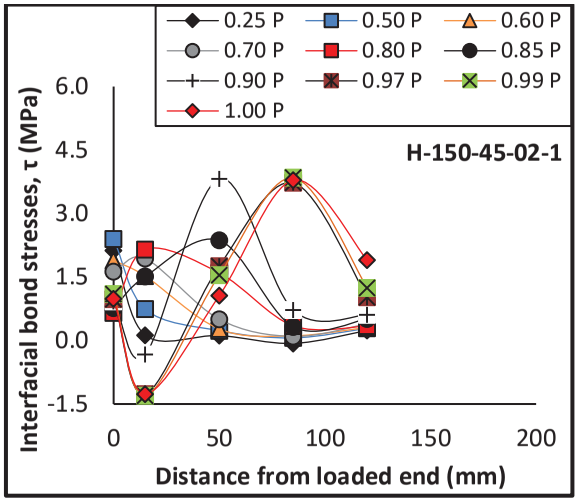
0.25 P
0.50 P
0.60 P
0.70 P
0.80 P
0.85 P
0.90 P
0.97 P
0.99 P
1.00 P
H-150-45-02-1
Interfacial bond stresses, τ (MPa)
6.0
4.5
3.0
1.5
0.0
-1.5
0
50
100
150
200
Distance from loaded end (mm)

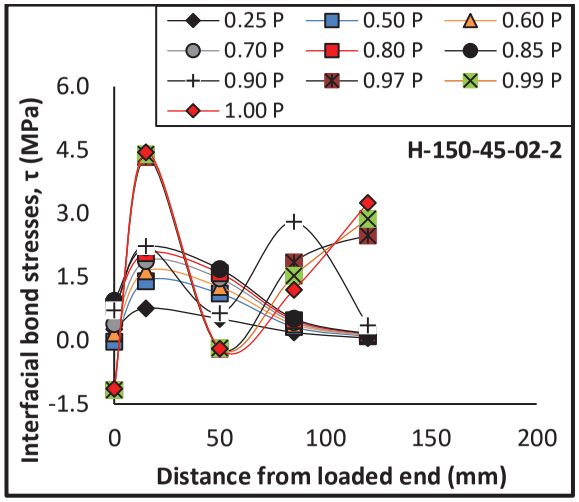
0.25 P
0.50 P
0.60 P
0.70 P
0.80 P
0.85 P
0.90 P
0.97 P
0.99 P
1.00 P
H-150-45-02-2
Interfacial bond stresses, τ (MPa)
6.0
4.5
3.0
1.5
0.0
-1.5
0
50
100
150
200
Distance from loaded end (mm)

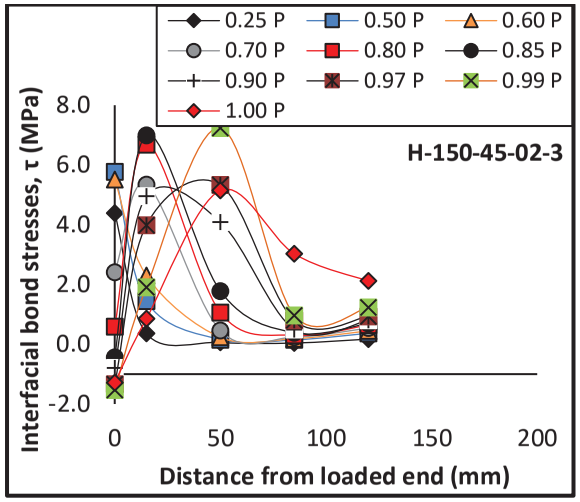
0.25 P
0.50 P
0.60 P
0.70 P
0.80 P
0.85 P
0.90 P
0.97 P
0.99 P
1.00 P
H-150-45-02-3
Interfacial bond stresses, τ (MPa)
8.0
6.0
4.0
2.0
0.0
-2.0
0
50
100
150
200
Distance from loaded end (mm)

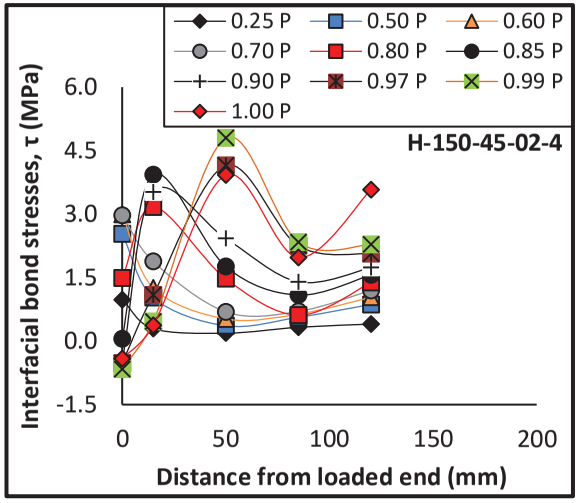
0.25 P
0.50 P
0.60 P
0.70 P
0.80 P
0.85 P
0.90 P
0.97 P
0.99 P
1.00 P
H-150-45-02-4
Interfacial bond stresses, τ (MPa)
6.0
4.5
3.0
1.5
0.0
-1.5
0
50
100
150
200
Distance from loaded end (mm)

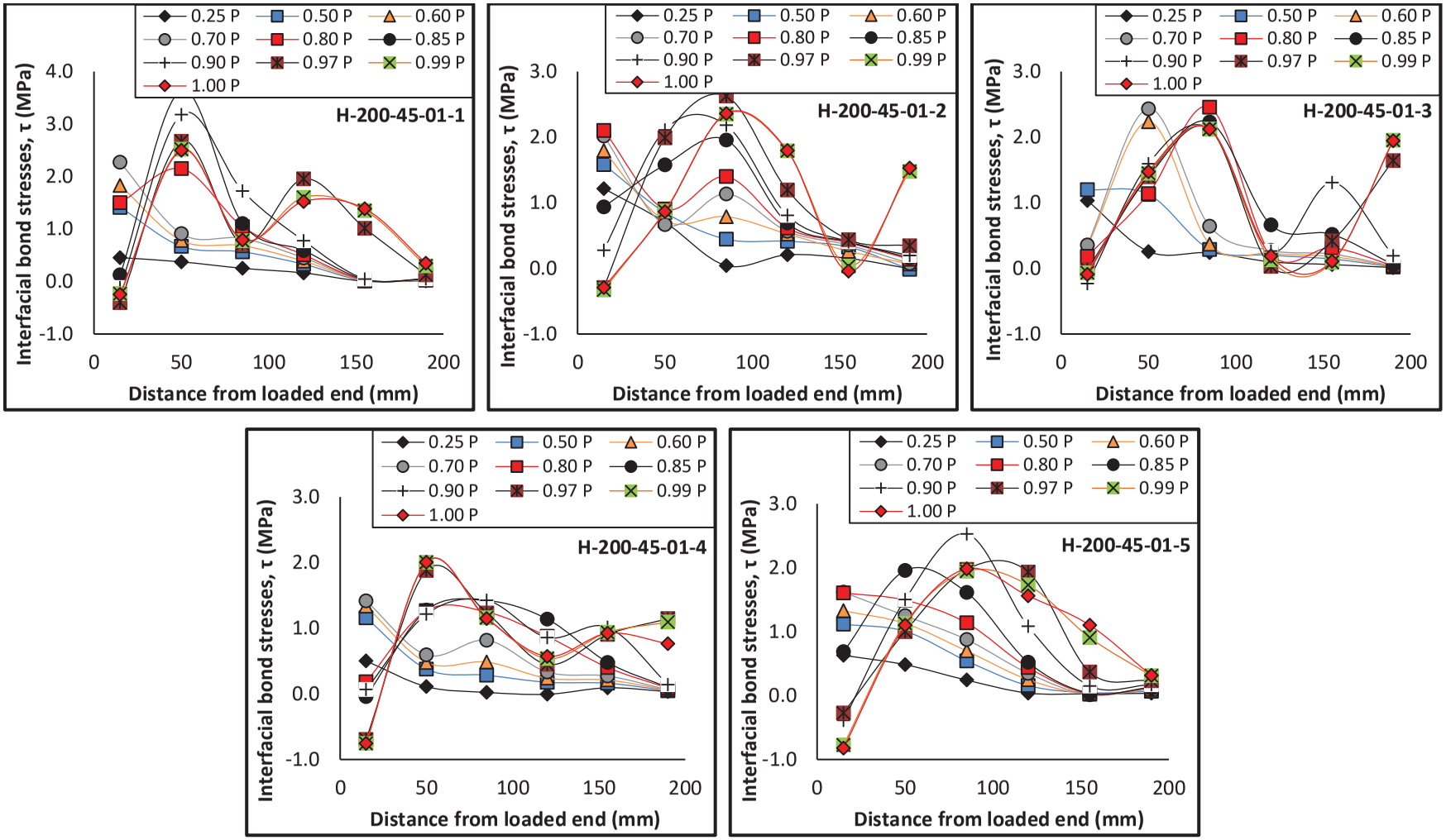
0.25 P
0.50 P
0.60 P
0.70 P
0.80 P
0.85 P
0.90 P
0.97 P
0.99 P
1.00 P
H-200-45-01-1
H-200-45-01-2
H-200-45-01-3
H-200-45-01-4
H-200-45-01-5
Interfacial bond stresses, τ (MPa)
Distance from loaded end (mm)

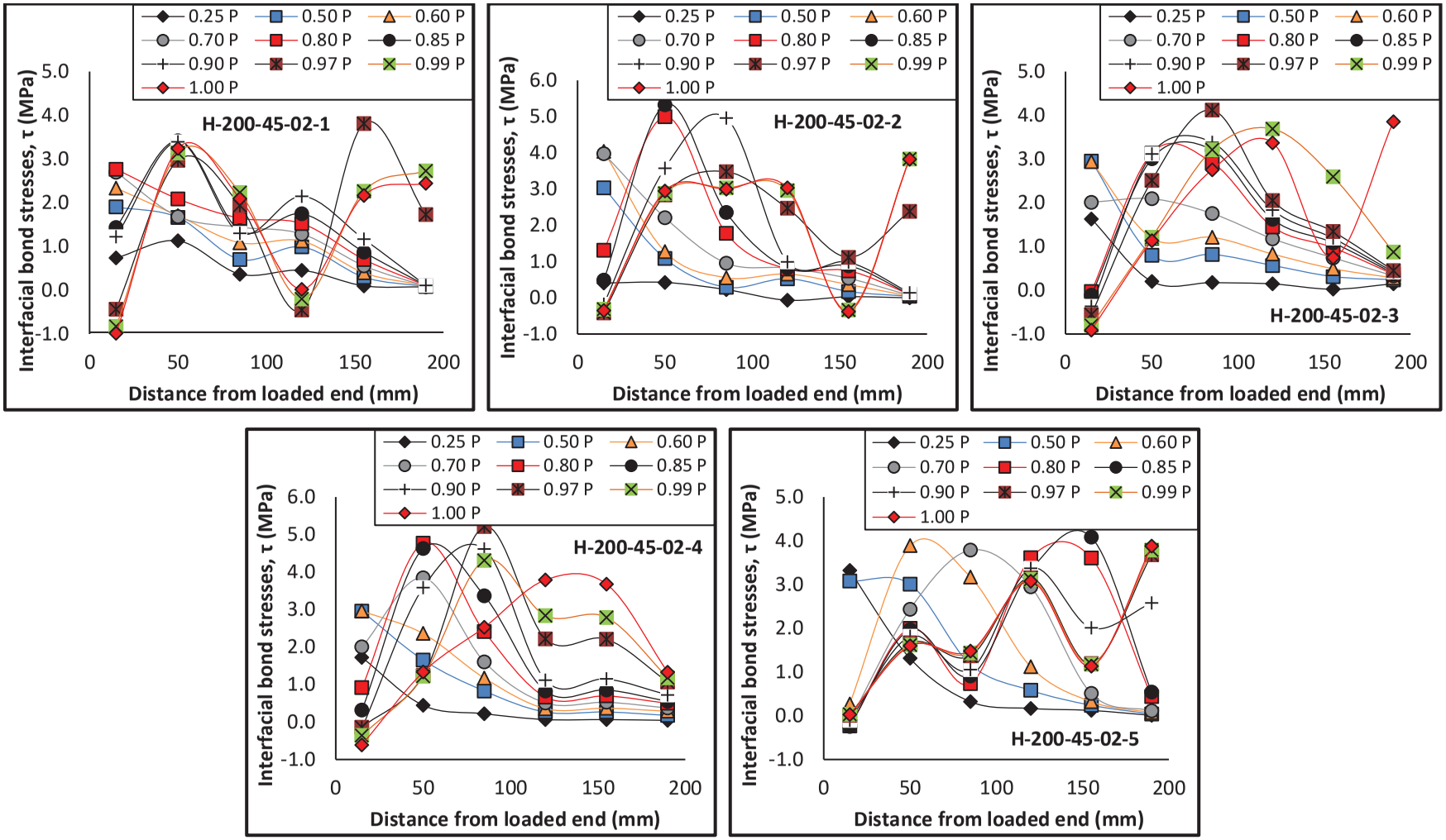
0.25 P
0.50 P
0.60 P
0.70 P
0.80 P
0.85 P
0.90 P
0.97 P
0.99 P
1.00 P
H-200-45-02-1
H-200-45-02-2
H-200-45-02-3
H-200-45-02-4
H-200-45-02-5
Interfacial bond stresses, τ (MPa)
Distance from loaded end (mm)

Appendix G.

Interfacial bond stress – LVL Series

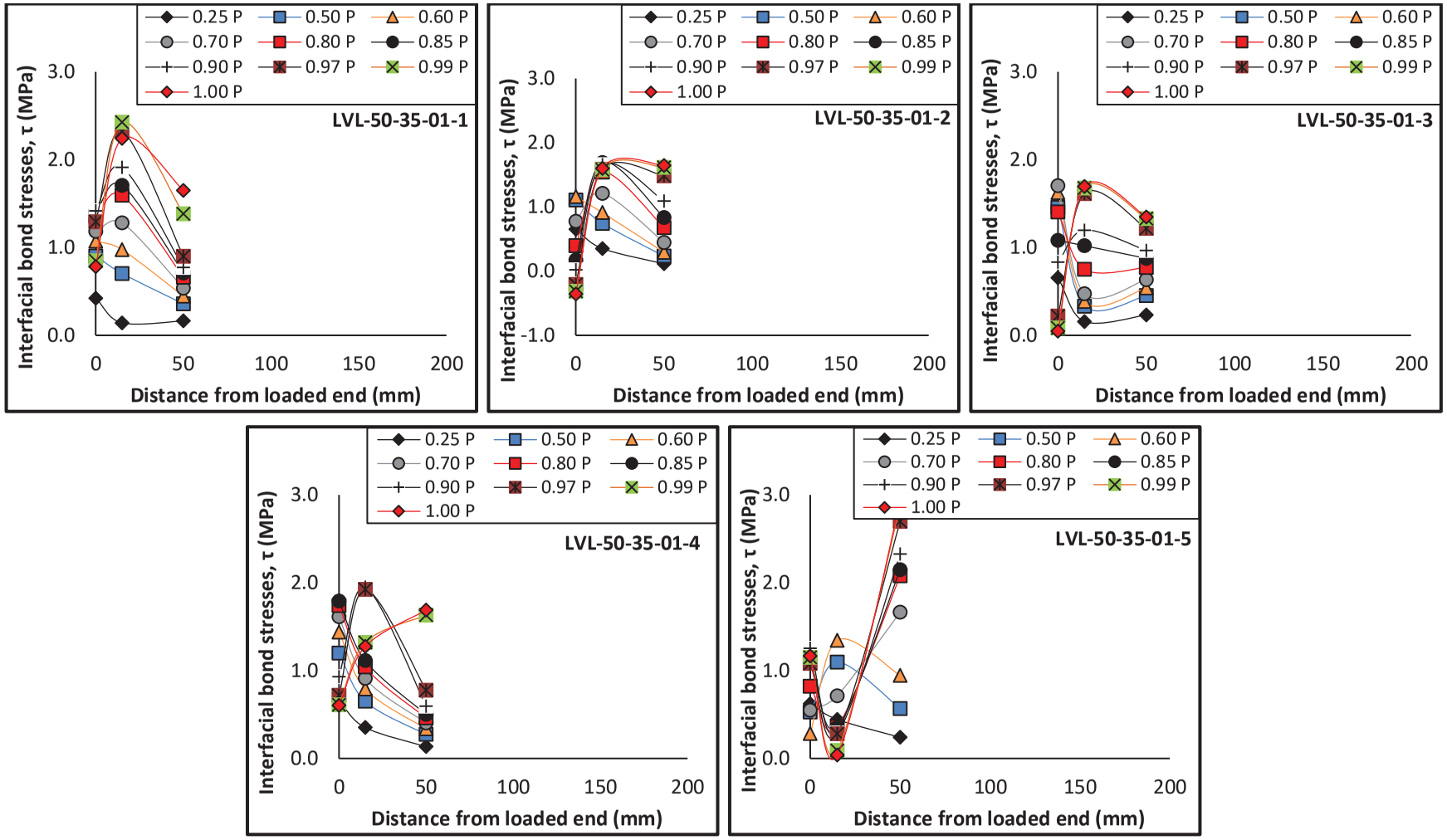
0.25 P
0.50 P
0.60 P
0.70 P
0.80 P
0.85 P
0.90 P
0.97 P
0.99 P
1.00 P
LVL-50-35-01-1
LVL-50-35-01-2
LVL-50-35-01-3
LVL-50-35-01-4
LVL-50-35-01-5
Interfacial bond stresses, τ (MPa)
Distance from loaded end (mm)
3.0
2.0
1.0
0.0
-1.0
0
50
100
150
200

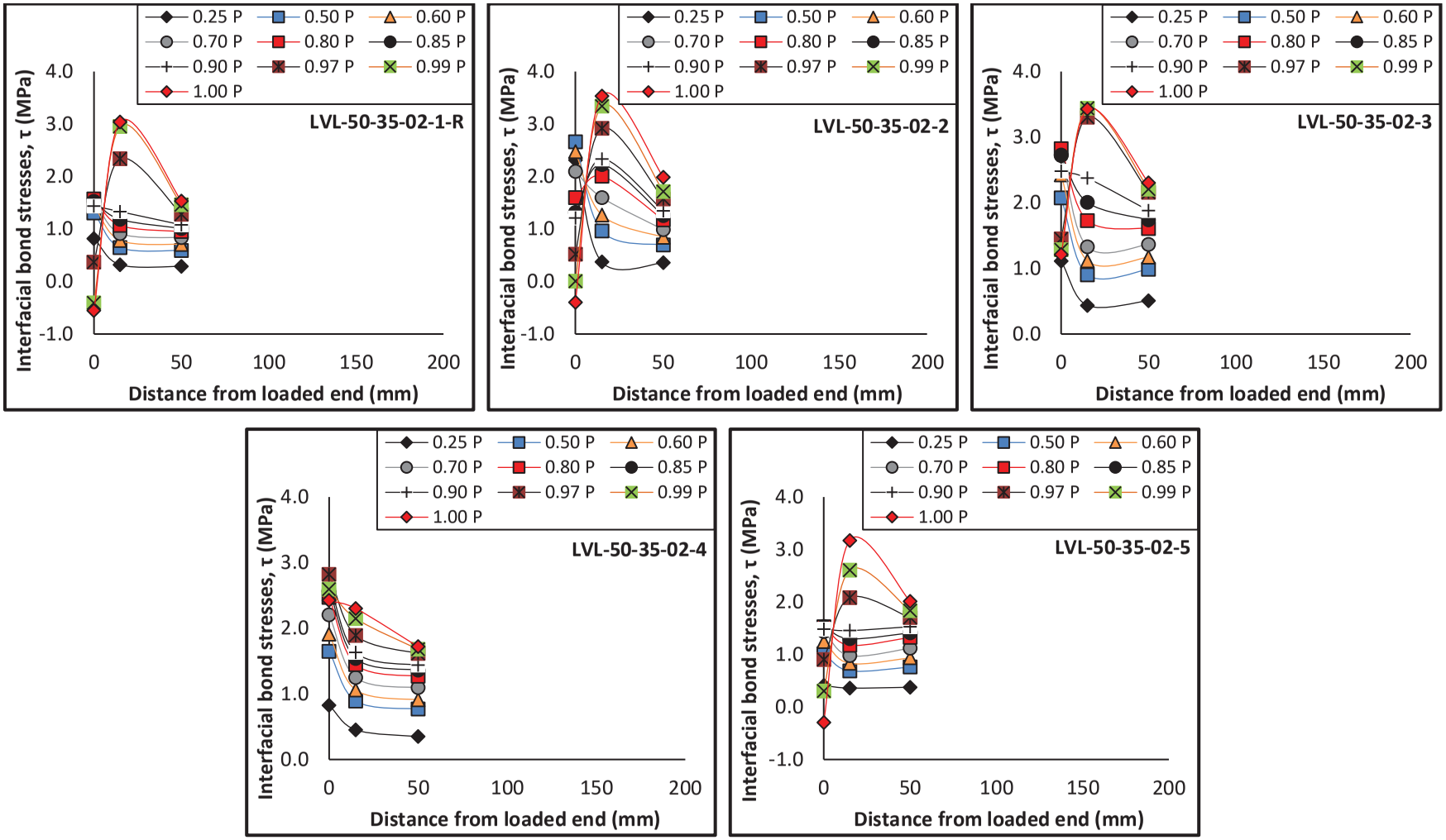
0.25 P
0.50 P
0.60 P
0.70 P
0.80 P
0.85 P
0.90 P
0.97 P
0.99 P
1.00 P
LVL-50-35-02-1-R
LVL-50-35-02-2
LVL-50-35-02-3
LVL-50-35-02-4
LVL-50-35-02-5
Interfacial bond stresses, τ (MPa)
Distance from loaded end (mm)
4.0
3.0
2.0
1.0
0.0
-1.0
0
50
100
150
200

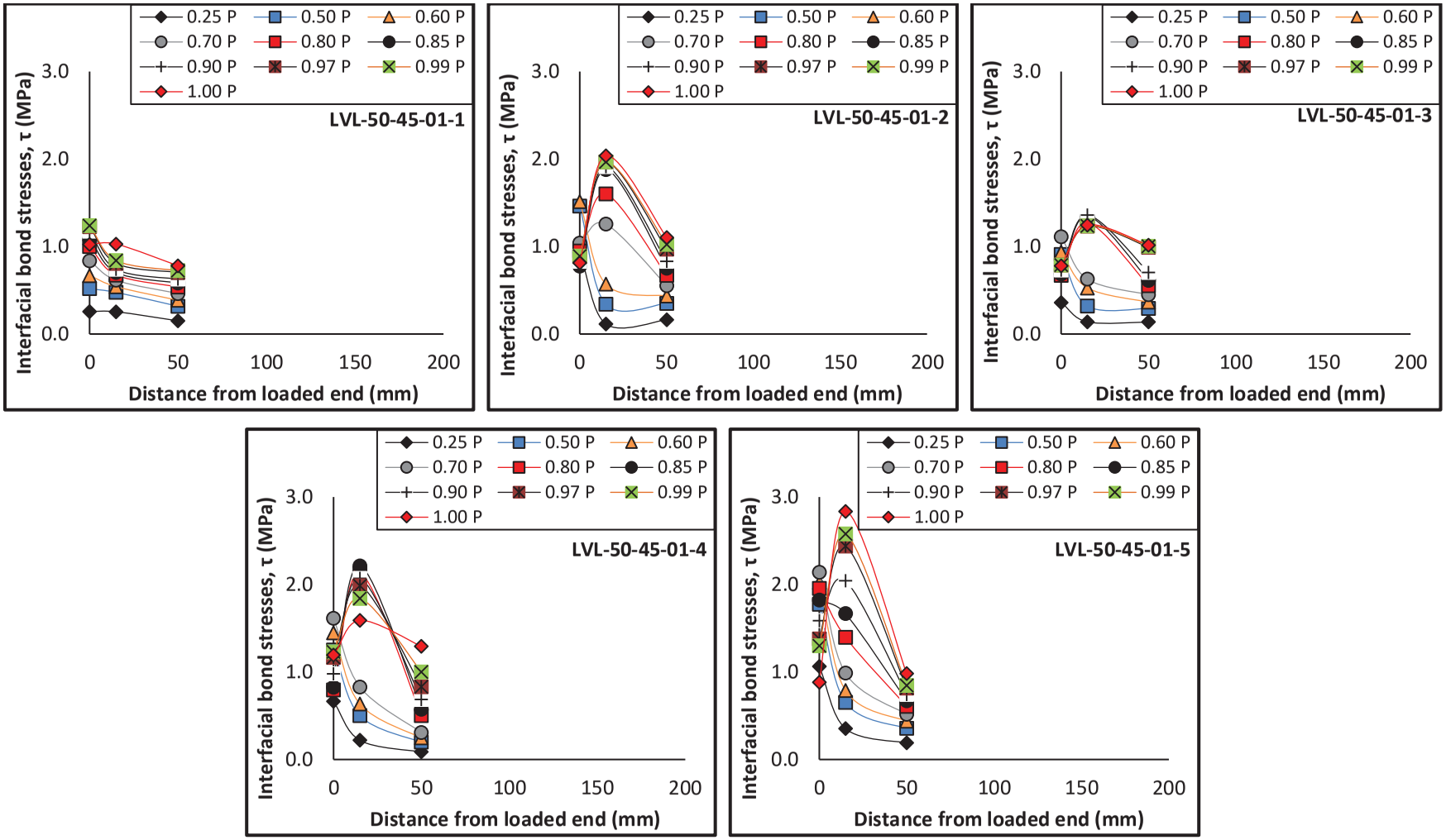
0.25 P
0.50 P
0.60 P
0.70 P
0.80 P
0.85 P
0.90 P
0.97 P
0.99 P
1.00 P
LVL-50-45-01-1
LVL-50-45-01-2
LVL-50-45-01-3
LVL-50-45-01-4
LVL-50-45-01-5
Interfacial bond stresses, τ (MPa)
Distance from loaded end (mm)
0.0
1.0
2.0
3.0
0
50
100
150
200

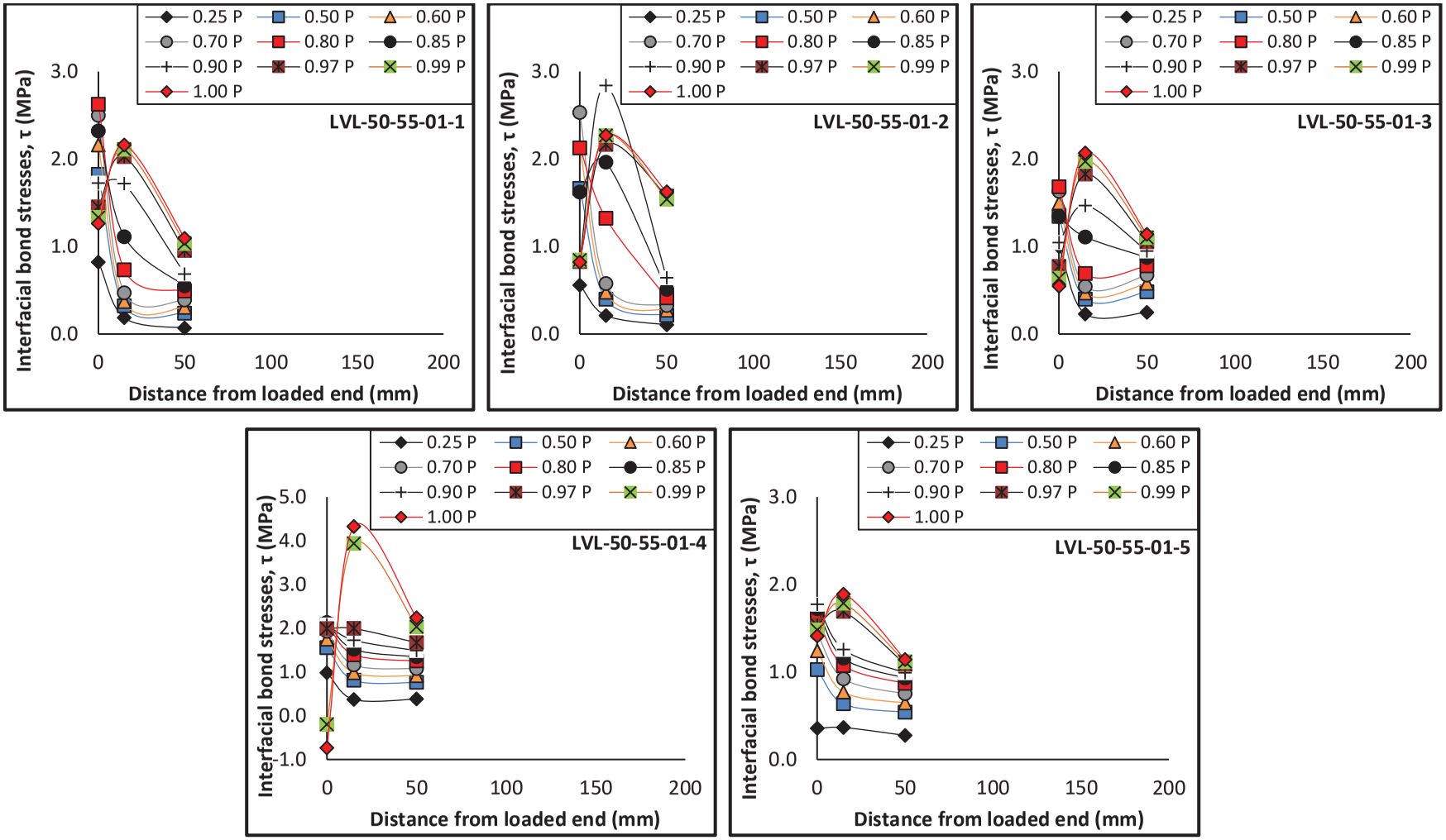
0.25 P
0.50 P
0.60 P
0.70 P
0.80 P
0.85 P
0.90 P
0.97 P
0.99 P
1.00 P
LVL-50-55-01-1
LVL-50-55-01-2
LVL-50-55-01-3
LVL-50-55-01-4
LVL-50-55-01-5
Interfacial bond stresses, τ (MPa)
Distance from loaded end (mm)

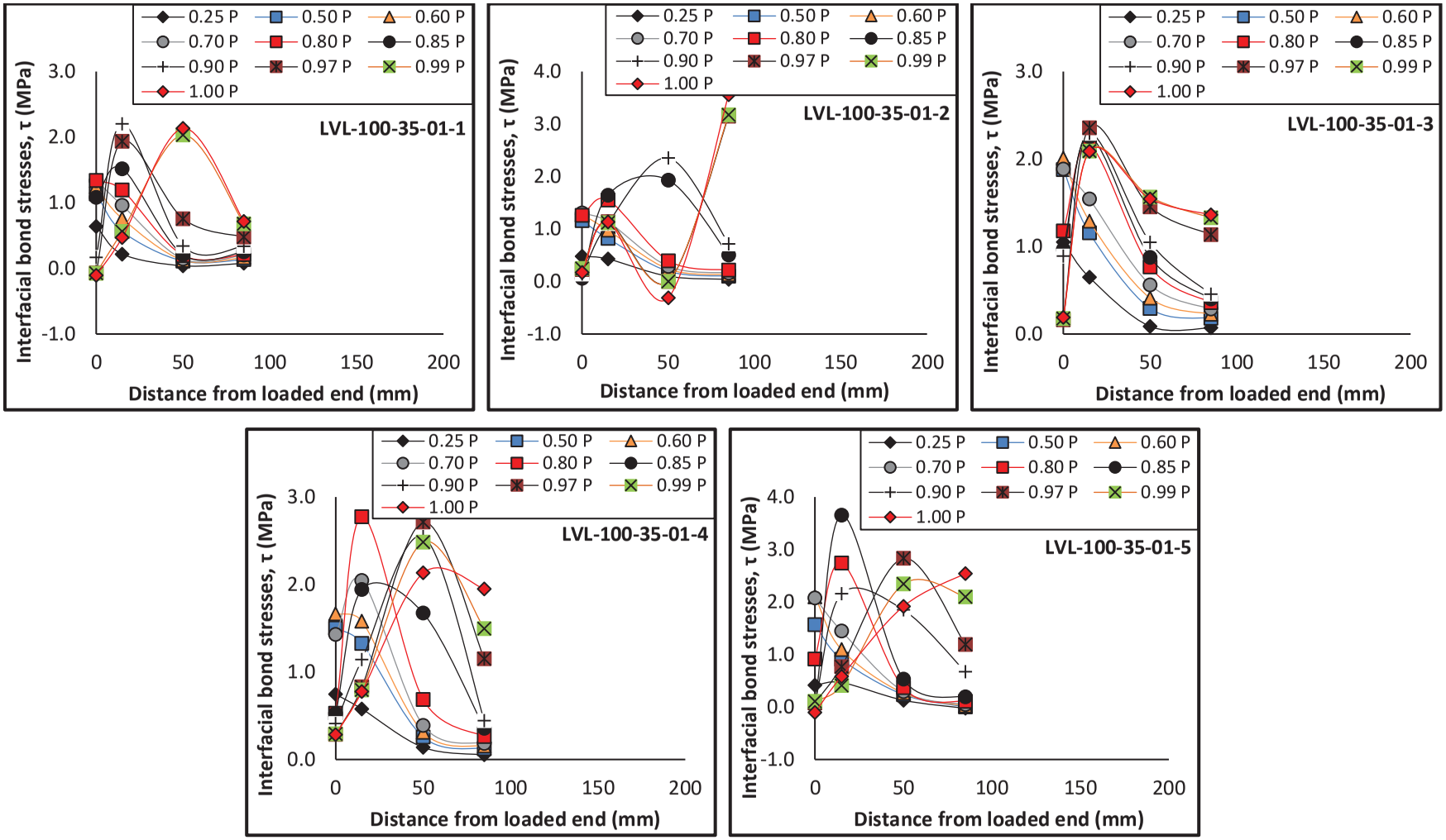
0.25 P
0.50 P
0.60 P
0.70 P
0.80 P
0.85 P
0.90 P
0.97 P
0.99 P
1.00 P
LVL-100-35-01-1
LVL-100-35-01-2
LVL-100-35-01-3
LVL-100-35-01-4
LVL-100-35-01-5
Interfacial bond stresses, τ (MPa)
Distance from loaded end (mm)

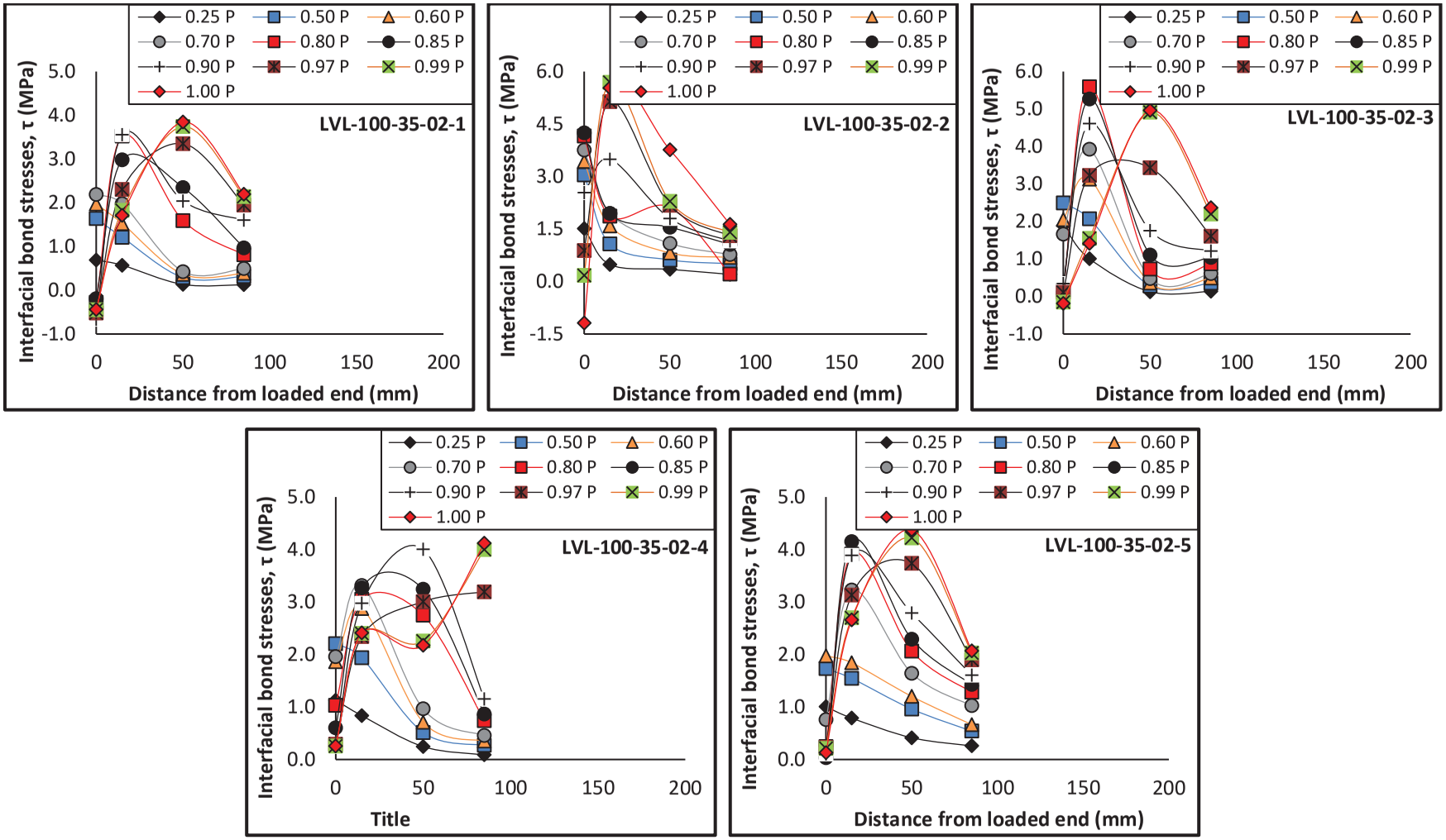
0.25 P
0.50 P
0.60 P
0.70 P
0.80 P
0.85 P
0.90 P
0.97 P
0.99 P
1.00 P
LVL-100-35-02-1
LVL-100-35-02-2
LVL-100-35-02-3
LVL-100-35-02-4
LVL-100-35-02-5
Interfacial bond stresses, τ (MPa)
Distance from loaded end (mm)
Title

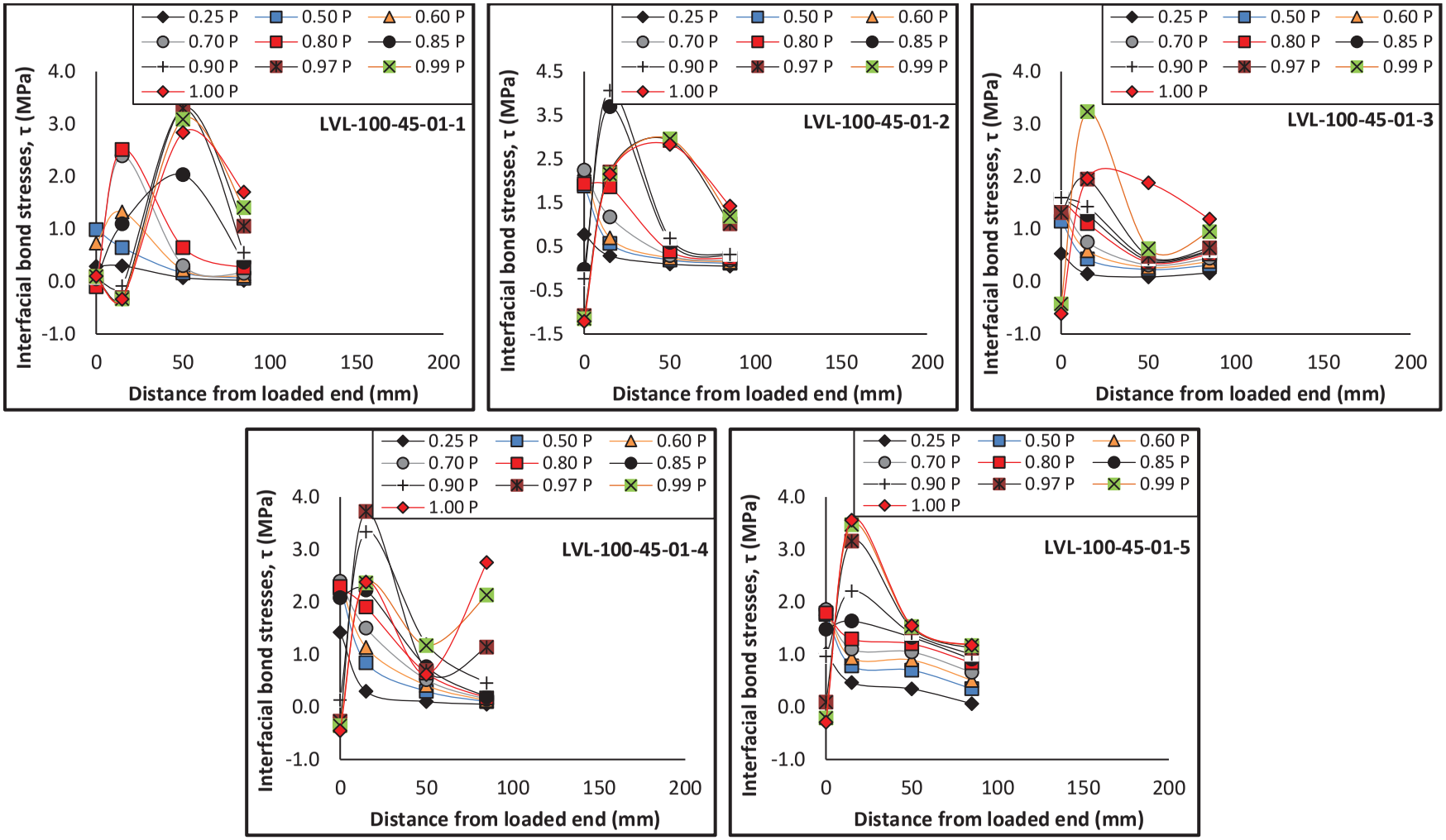
0.25 P
0.50 P
0.60 P
0.70 P
0.80 P
0.85 P
0.90 P
0.97 P
0.99 P
1.00 P
LVL-100-45-01-1
LVL-100-45-01-2
LVL-100-45-01-3
LVL-100-45-01-4
LVL-100-45-01-5
Interfacial bond stresses, τ (MPa)
Distance from loaded end (mm)

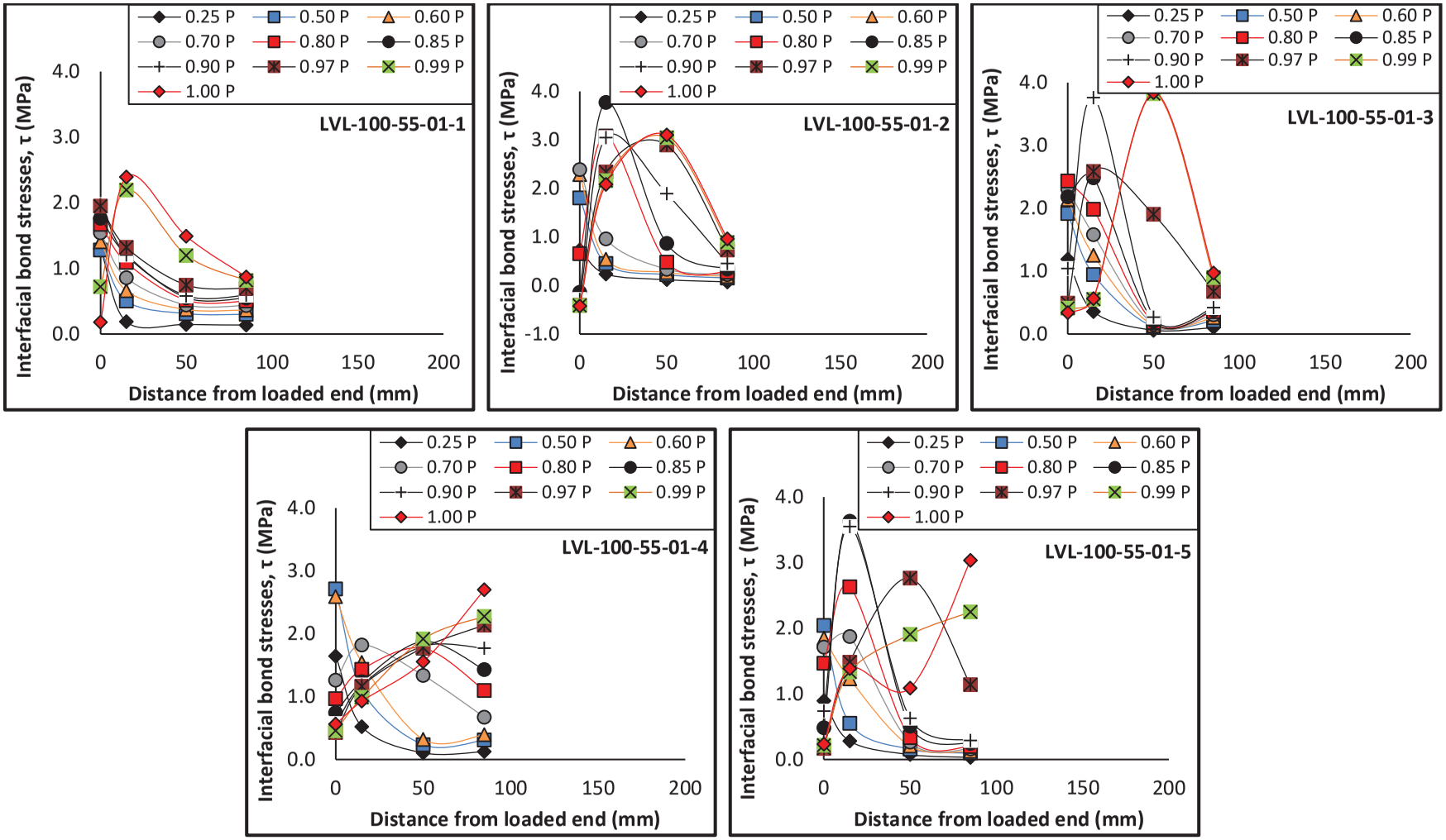
0.25 P
0.50 P
0.60 P
0.70 P
0.80 P
0.85 P
0.90 P
0.97 P
0.99 P
1.00 P
LVL-100-55-01-1
LVL-100-55-01-2
LVL-100-55-01-3
LVL-100-55-01-4
LVL-100-55-01-5
Interfacial bond stresses, τ (MPa)
Distance from loaded end (mm)

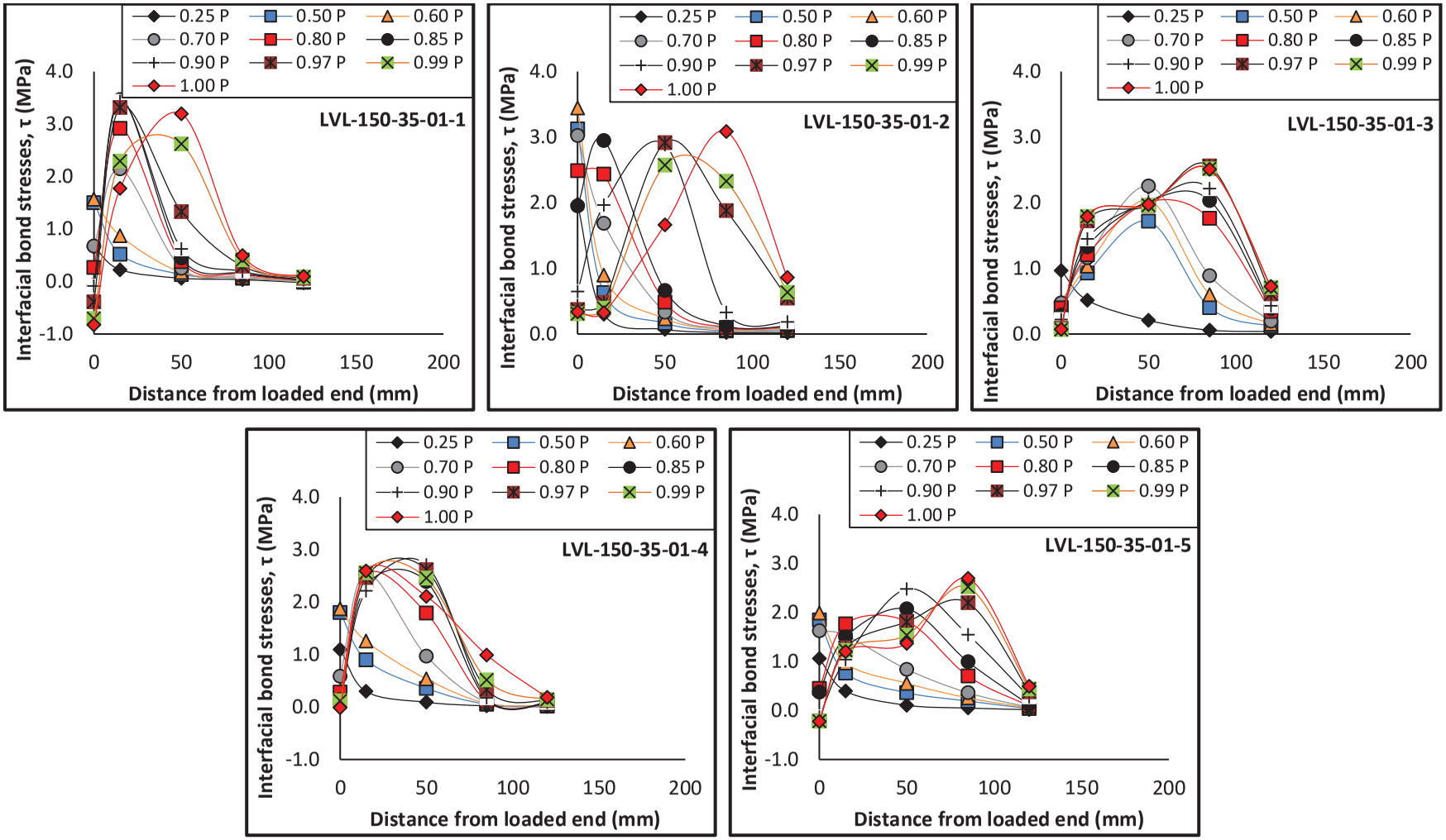
0.25 P
0.50 P
0.60 P
0.70 P
0.80 P
0.85 P
0.90 P
0.97 P
0.99 P
1.00 P
LVL-150-35-01-1
LVL-150-35-01-2
LVL-150-35-01-3
LVL-150-35-01-4
LVL-150-35-01-5
Interfacial bond stresses, τ (MPa)
Distance from loaded end (mm)
4.0
3.0
2.0
1.0
0.0
-1.0
0
50
100
150
200

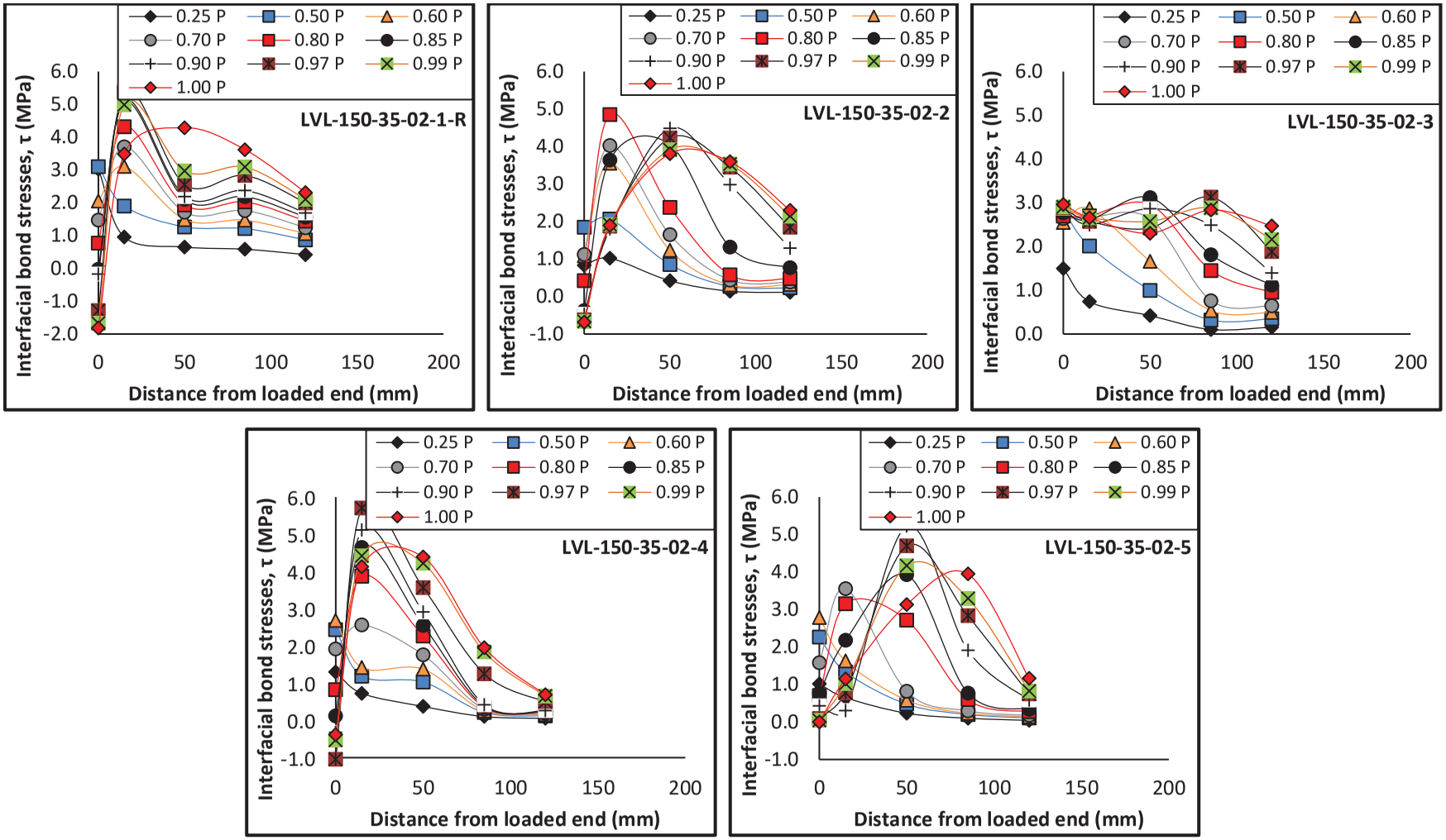
0.25 P
0.50 P
0.60 P
0.70 P
0.80 P
0.85 P
0.90 P
0.97 P
0.99 P
1.00 P
LVL-150-35-02-1-R
LVL-150-35-02-2
LVL-150-35-02-3
LVL-150-35-02-4
LVL-150-35-02-5
Interfacial bond stresses, τ (MPa)
Distance from loaded end (mm)

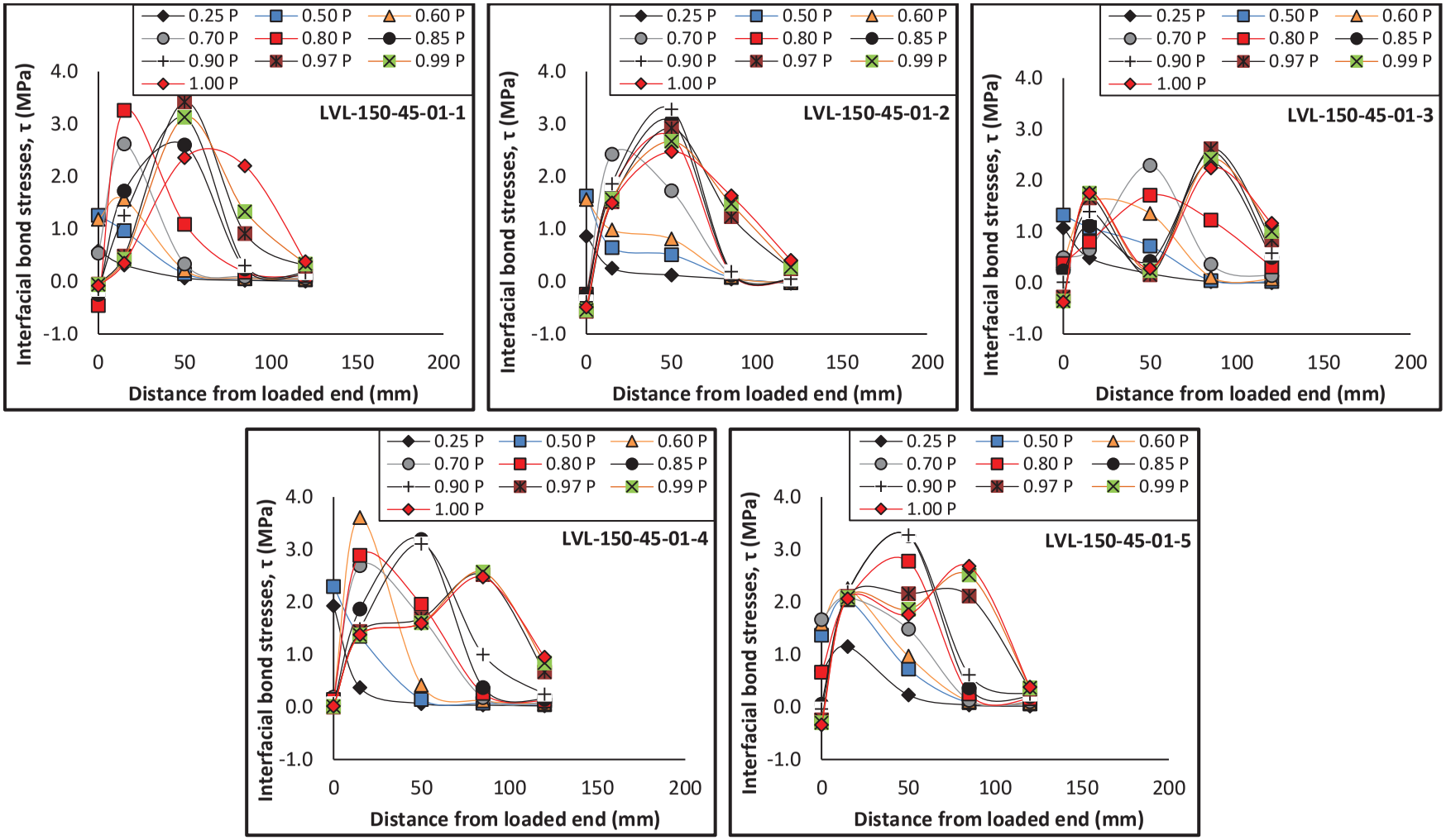
0.25 P
0.50 P
0.60 P
0.70 P
0.80 P
0.85 P
0.90 P
0.97 P
0.99 P
1.00 P
LVL-150-45-01-1
LVL-150-45-01-2
LVL-150-45-01-3
LVL-150-45-01-4
LVL-150-45-01-5
Interfacial bond stresses, τ (MPa)
Distance from loaded end (mm)
4.0
3.0
2.0
1.0
0.0
-1.0
0
50
100
150
200

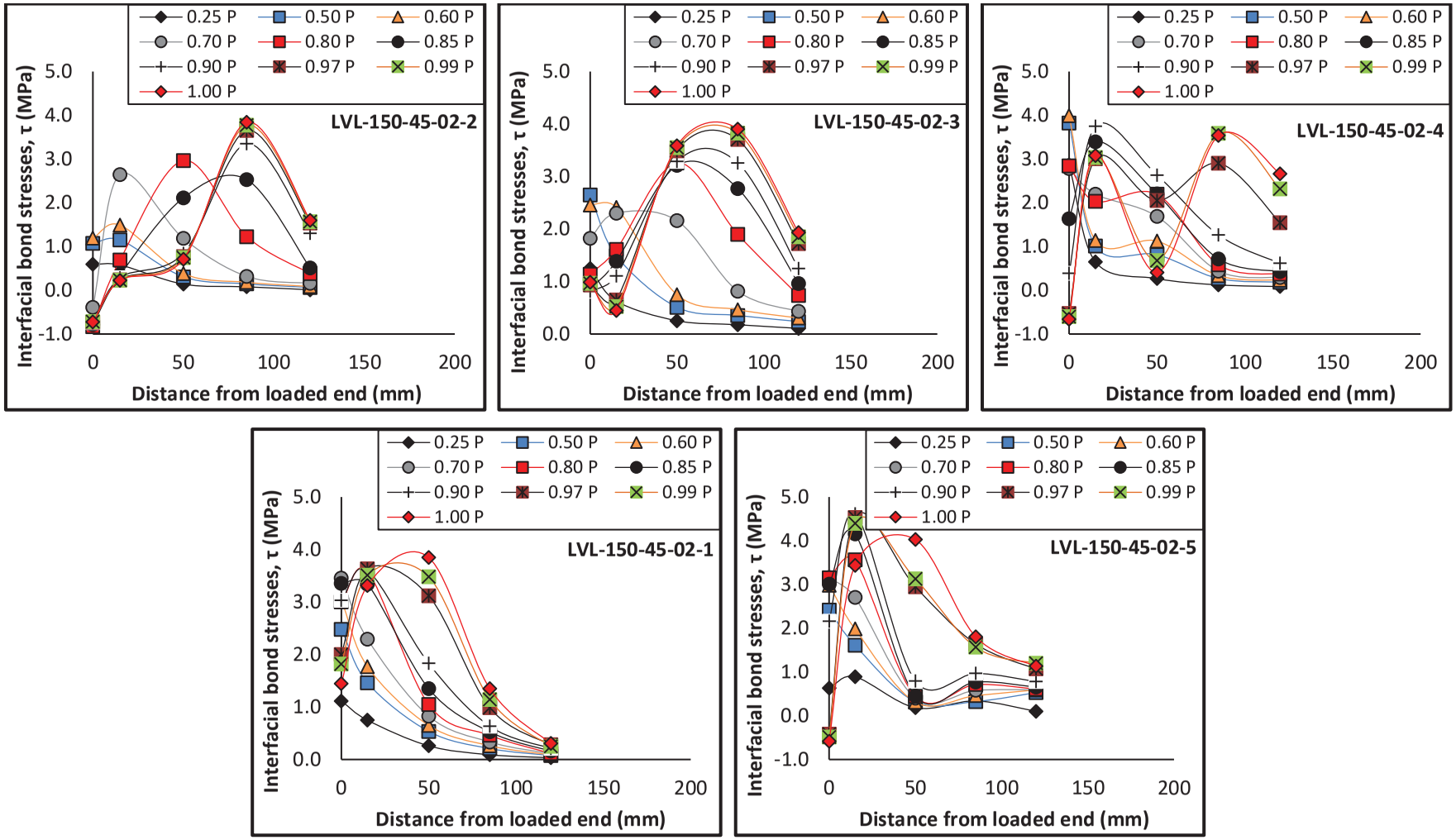
0.25 P
0.50 P
0.60 P
0.70 P
0.80 P
0.85 P
0.90 P
0.97 P
0.99 P
1.00 P
LVL-150-45-02-2
LVL-150-45-02-3
LVL-150-45-02-4
LVL-150-45-02-1
LVL-150-45-02-5
Interfacial bond stresses, τ (MPa)
Distance from loaded end (mm)
5.0
4.0
3.0
2.0
1.0
0.0
-1.0
0
50
100
150
200

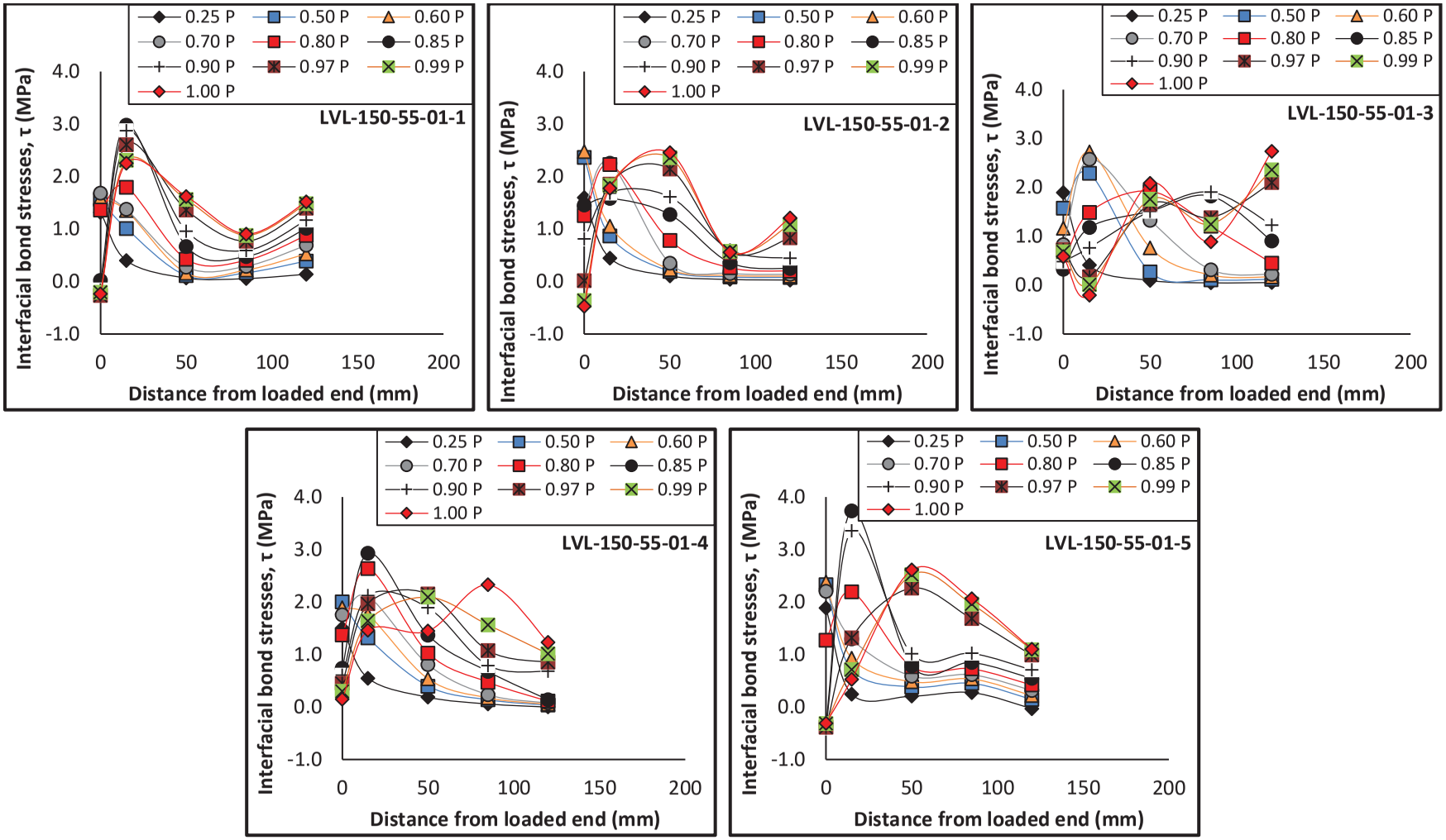
0.25 P
0.50 P
0.60 P
0.70 P
0.80 P
0.85 P
0.90 P
0.97 P
0.99 P
1.00 P
LVL-150-55-01-1
LVL-150-55-01-2
LVL-150-55-01-3
LVL-150-55-01-4
LVL-150-55-01-5
Interfacial bond stresses, τ (MPa)
Distance from loaded end (mm)
4.0
3.0
2.0
1.0
0.0
-1.0
0
50
100
150
200

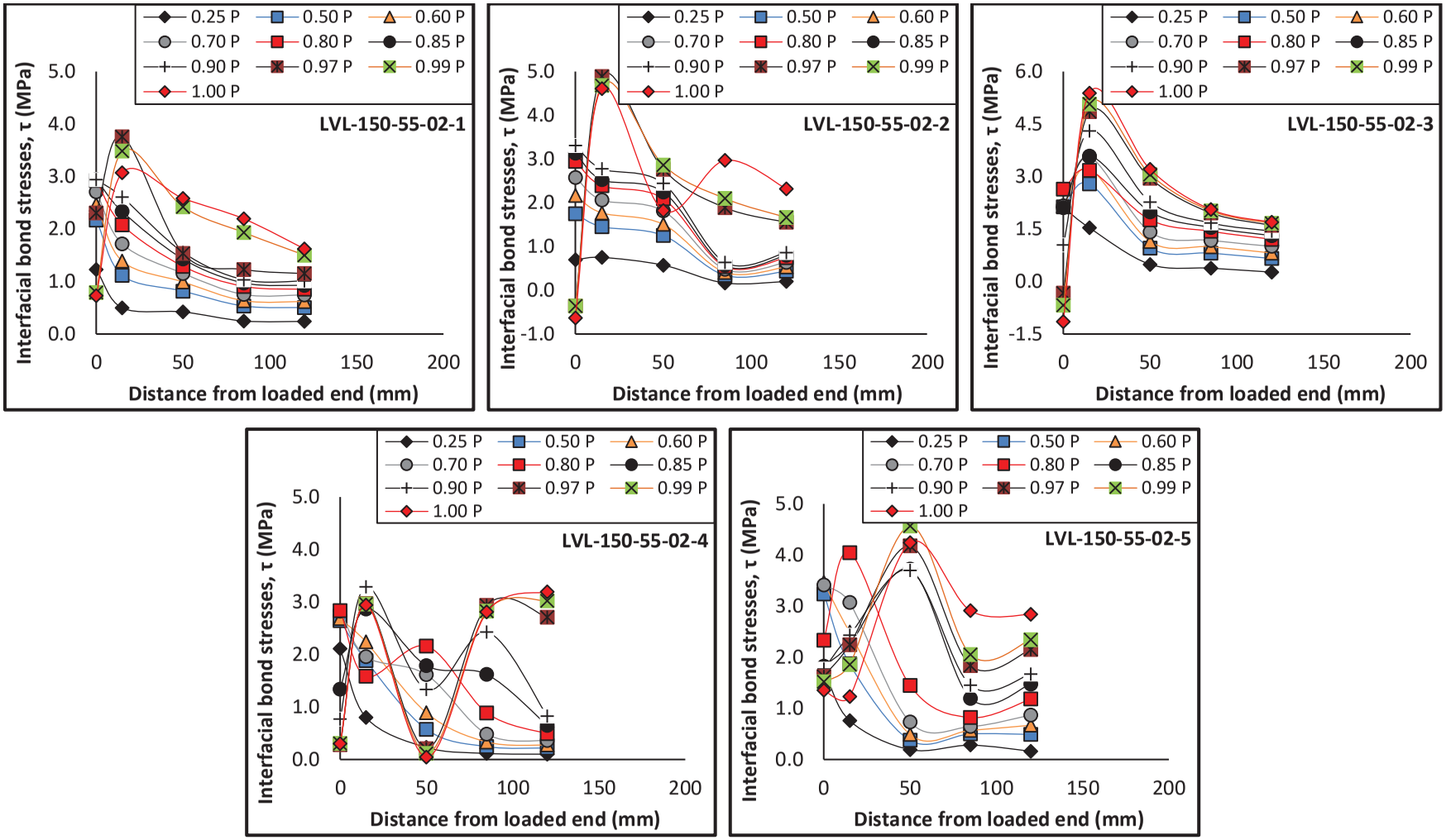
0.25 P
0.50 P
0.60 P
0.70 P
0.80 P
0.85 P
0.90 P
0.97 P
0.99 P
1.00 P
LVL-150-55-02-1
LVL-150-55-02-2
LVL-150-55-02-3
LVL-150-55-02-4
LVL-150-55-02-5
Interfacial bond stresses, τ (MPa)
Distance from loaded end (mm)

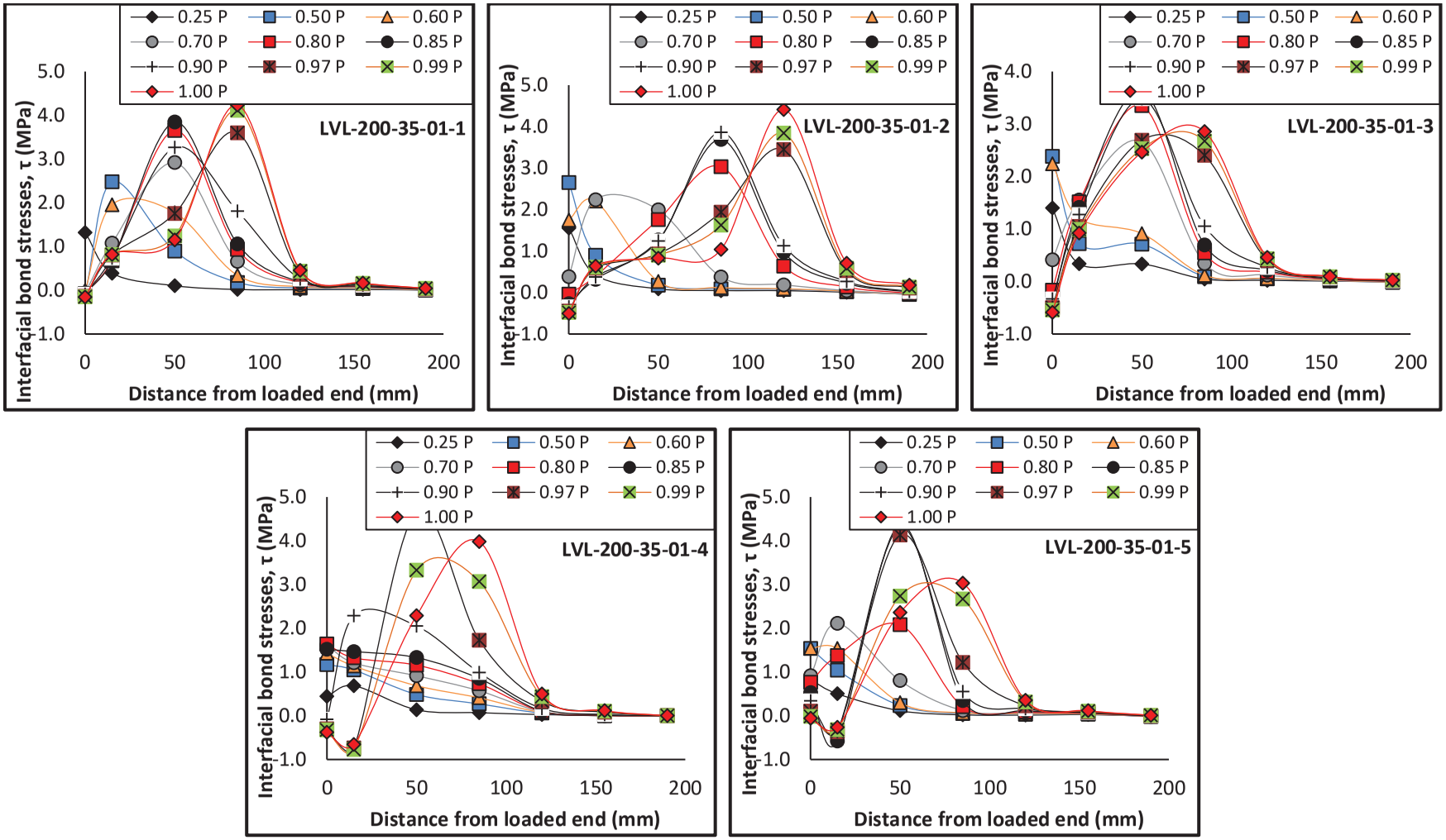
0.25 P
0.50 P
0.60 P
0.70 P
0.80 P
0.85 P
0.90 P
0.97 P
0.99 P
1.00 P
LVL-200-35-01-1
LVL-200-35-01-2
LVL-200-35-01-3
LVL-200-35-01-4
LVL-200-35-01-5
Interfacial bond stresses, τ (MPa)
Distance from loaded end (mm)

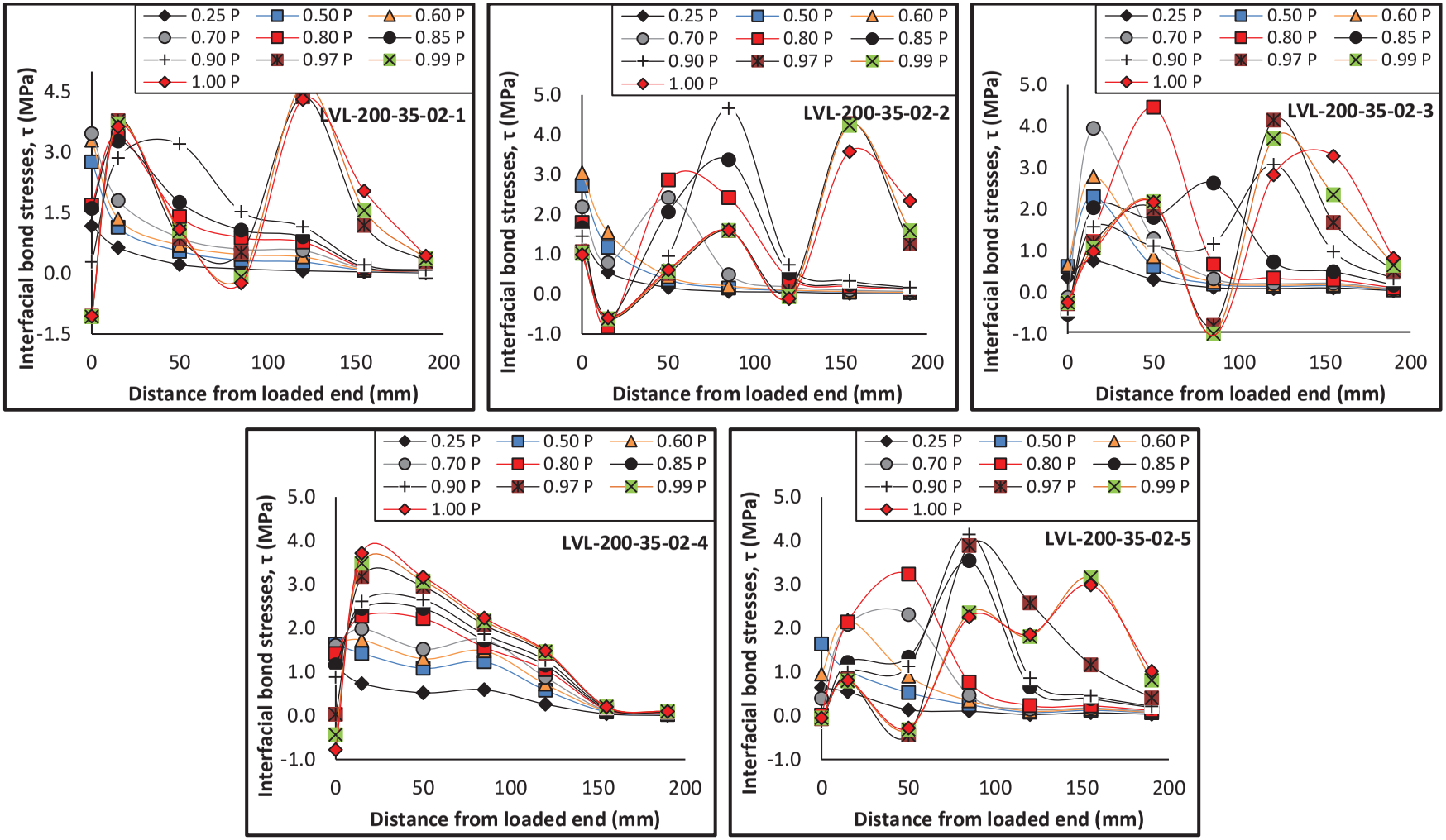
0.25 P
0.50 P
0.60 P
0.70 P
0.80 P
0.85 P
0.90 P
0.97 P
0.99 P
1.00 P
LVL-200-35-02-1
LVL-200-35-02-2
LVL-200-35-02-3
LVL-200-35-02-4
LVL-200-35-02-5
Interfacial bond stresses, τ (MPa)
Distance from loaded end (mm)

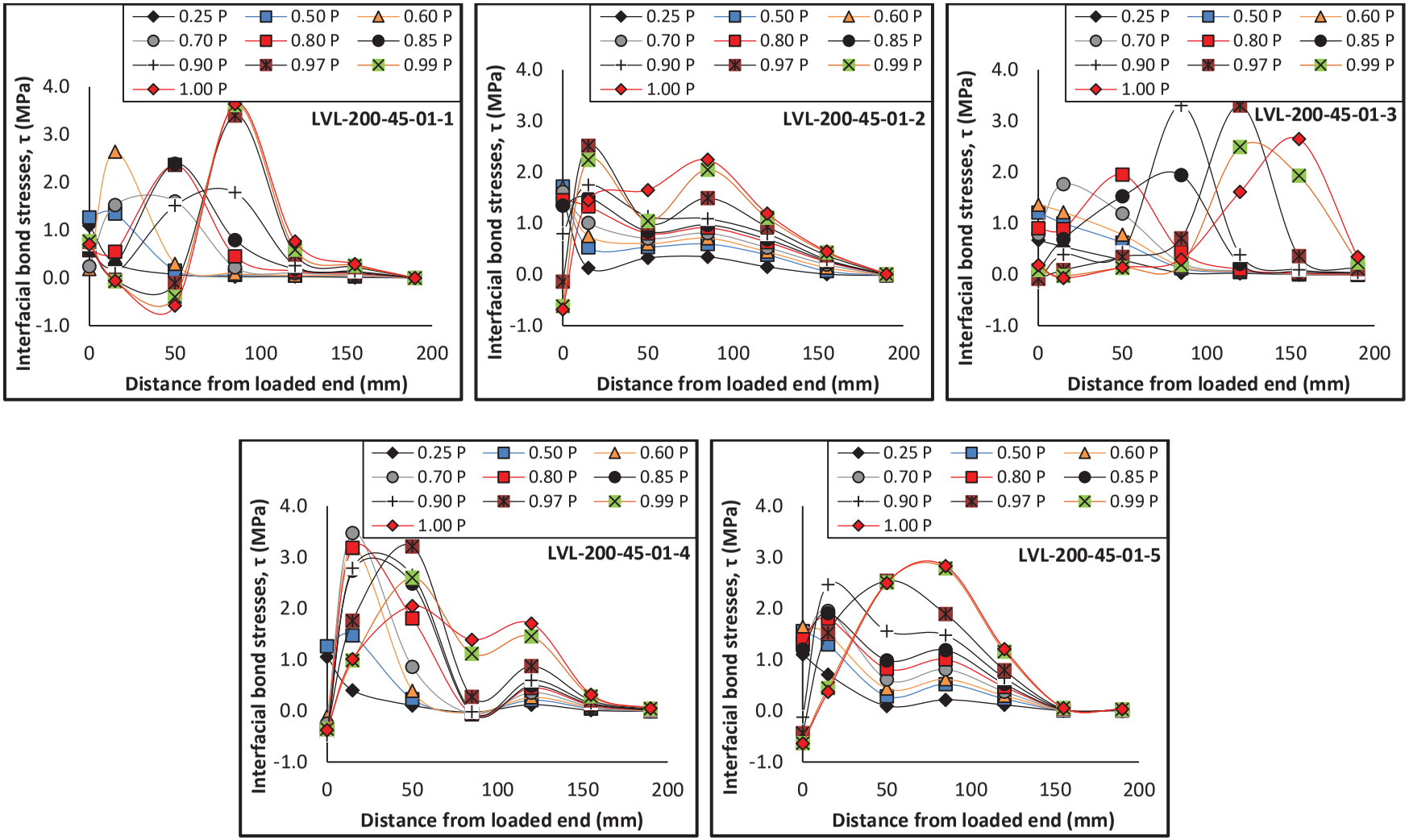
0.25 P
0.50 P
0.60 P
0.70 P
0.80 P
0.85 P
0.90 P
0.97 P
0.99 P
1.00 P
LVL-200-45-01-1
LVL-200-45-01-2
LVL-200-45-01-3
LVL-200-45-01-4
LVL-200-45-01-5
Interfacial bond stresses, τ (MPa)
Distance from loaded end (mm)
4.0
3.0
2.0
1.0
0.0
-1.0
0
50
100
150
200

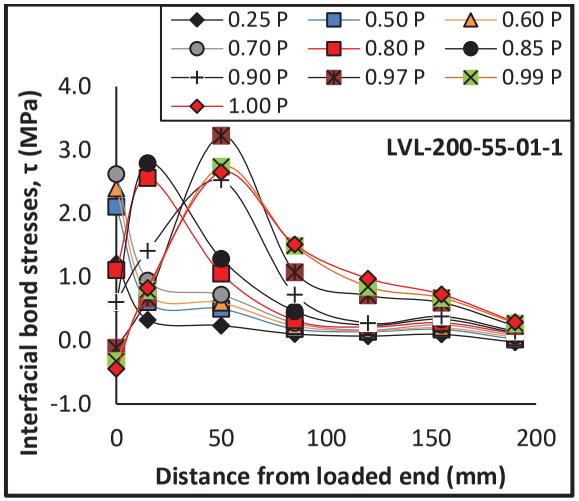
0.25 P
0.50 P
0.60 P
0.70 P
0.80 P
0.85 P
0.90 P
0.97 P
0.99 P
1.00 P
LVL-200-55-01-1
Interfacial bond stresses, τ (MPa)
Distance from loaded end (mm)

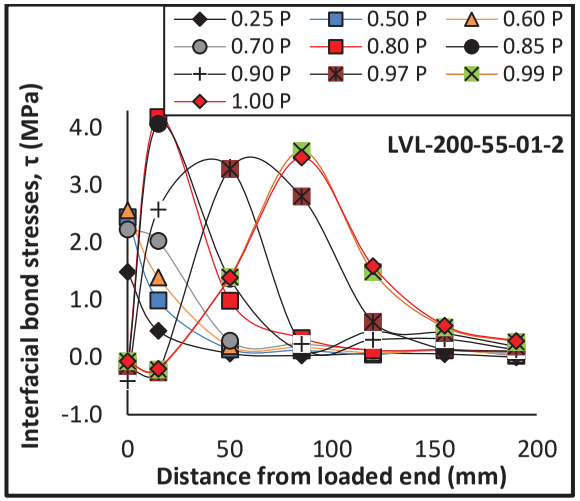
0.25 P
0.50 P
0.60 P
0.70 P
0.80 P
0.85 P
0.90 P
0.97 P
0.99 P
1.00 P
LVL-200-55-01-2
Interfacial bond stresses, τ (MPa)
Distance from loaded end (mm)

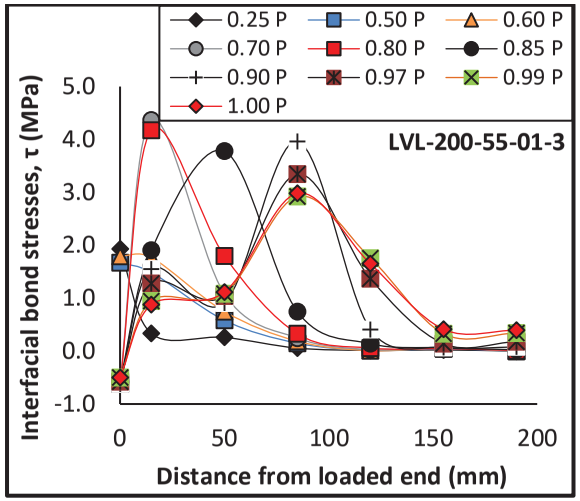
0.25 P
0.50 P
0.60 P
0.70 P
0.80 P
0.85 P
0.90 P
0.97 P
0.99 P
1.00 P
LVL-200-55-01-3
Interfacial bond stresses, τ (MPa)
Distance from loaded end (mm)

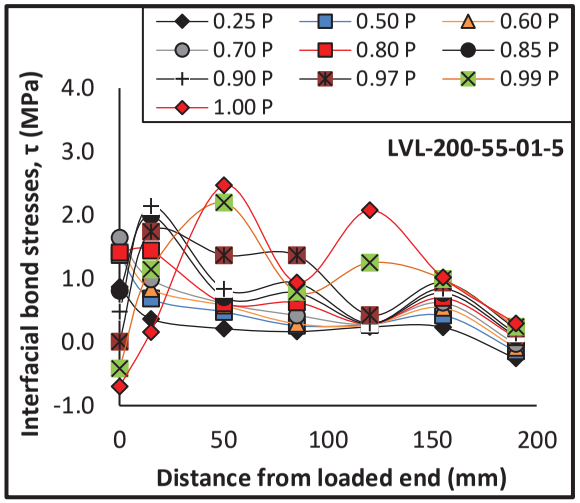
0.25 P
0.50 P
0.60 P
0.70 P
0.80 P
0.85 P
0.90 P
0.97 P
0.99 P
1.00 P
LVL-200-55-01-5
Interfacial bond stresses, τ (MPa)
Distance from loaded end (mm)

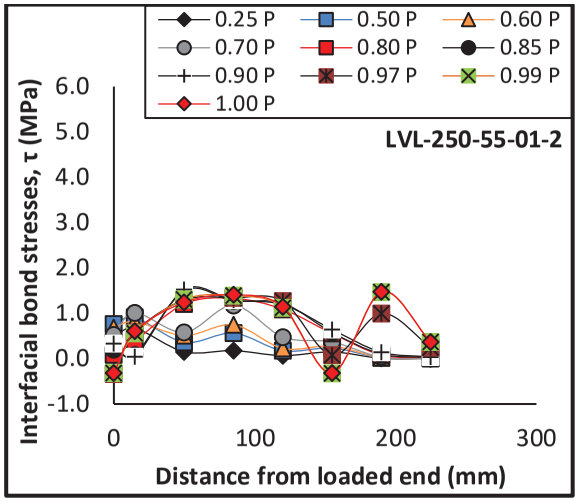
0.25 P
0.50 P
0.60 P
0.70 P
0.80 P
0.85 P
0.90 P
0.97 P
0.99 P
1.00 P
LVL-250-55-01-2
Interfacial bond stresses, τ (MPa)
6.0
5.0
4.0
3.0
2.0
1.0
0.0
-1.0
0
100
200
300
Distance from loaded end (mm)

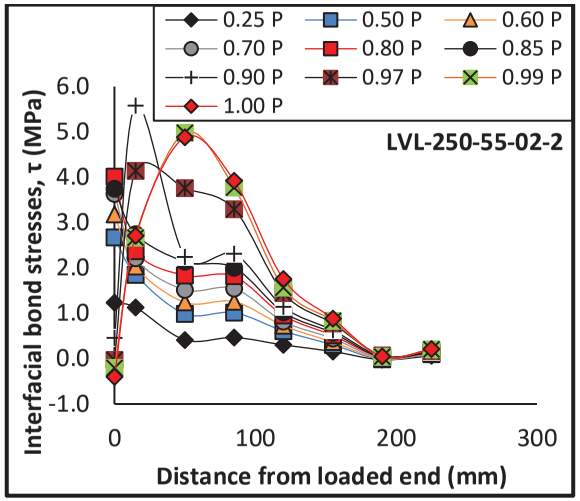
0.25 P
0.50 P
0.60 P
0.70 P
0.80 P
0.85 P
0.90 P
0.97 P
0.99 P
1.00 P
LVL-250-55-02-2
Interfacial bond stresses, τ (MPa)
6.0
5.0
4.0
3.0
2.0
1.0
0.0
-1.0
0
100
200
300
Distance from loaded end (mm)

Appendix H.

Interfacial bond stress as a relative of load along interface – Hardwood Series

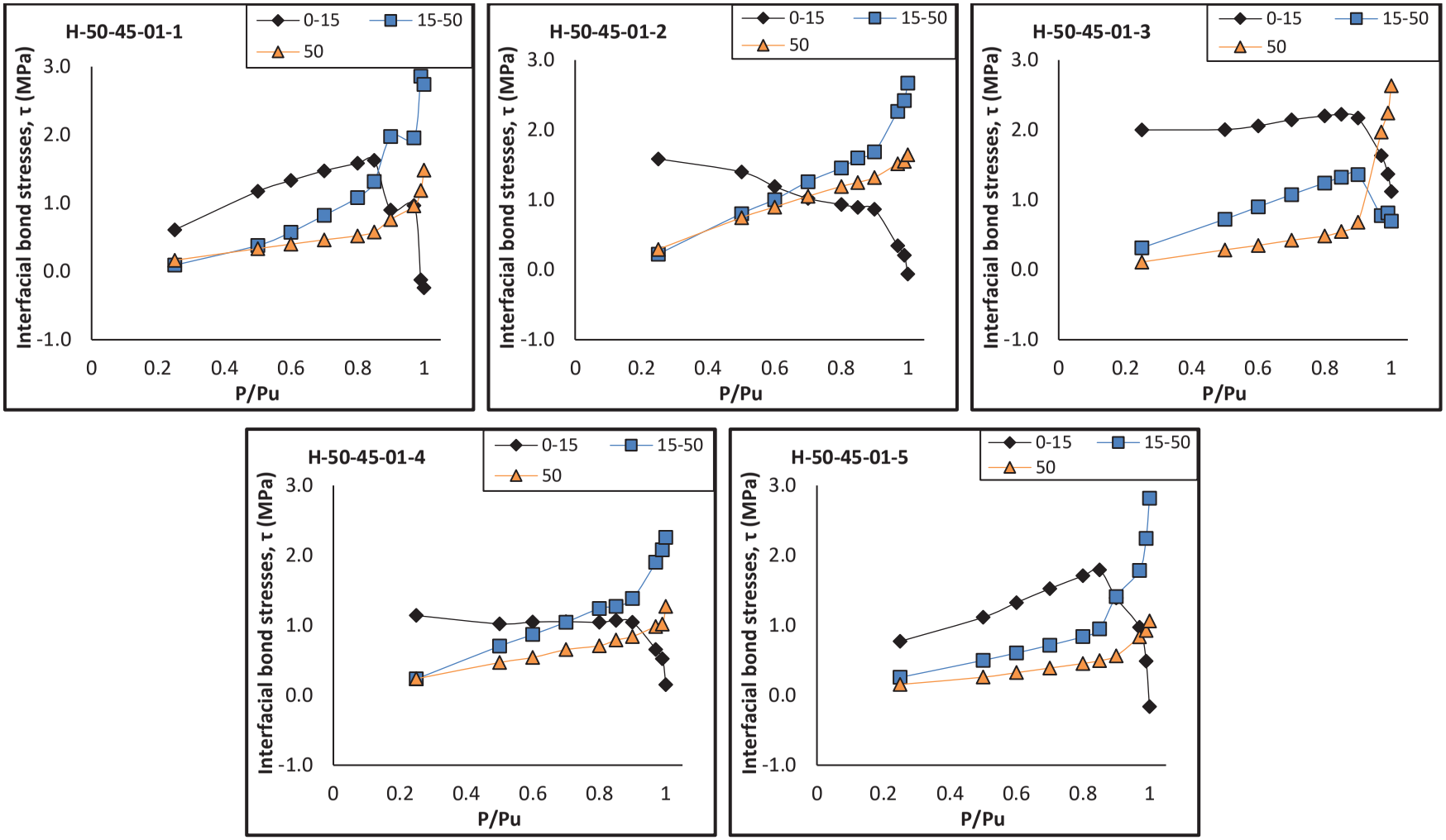
H-50-45-01-1
H-50-45-01-2
H-50-45-01-3
H-50-45-01-4
H-50-45-01-5
0-15
15-50
50
Interfacial bond stresses, τ (MPa)
P/Pu
3.0
2.0
1.0
0.0
-1.0
0
0.2
0.4
0.6
0.8
1

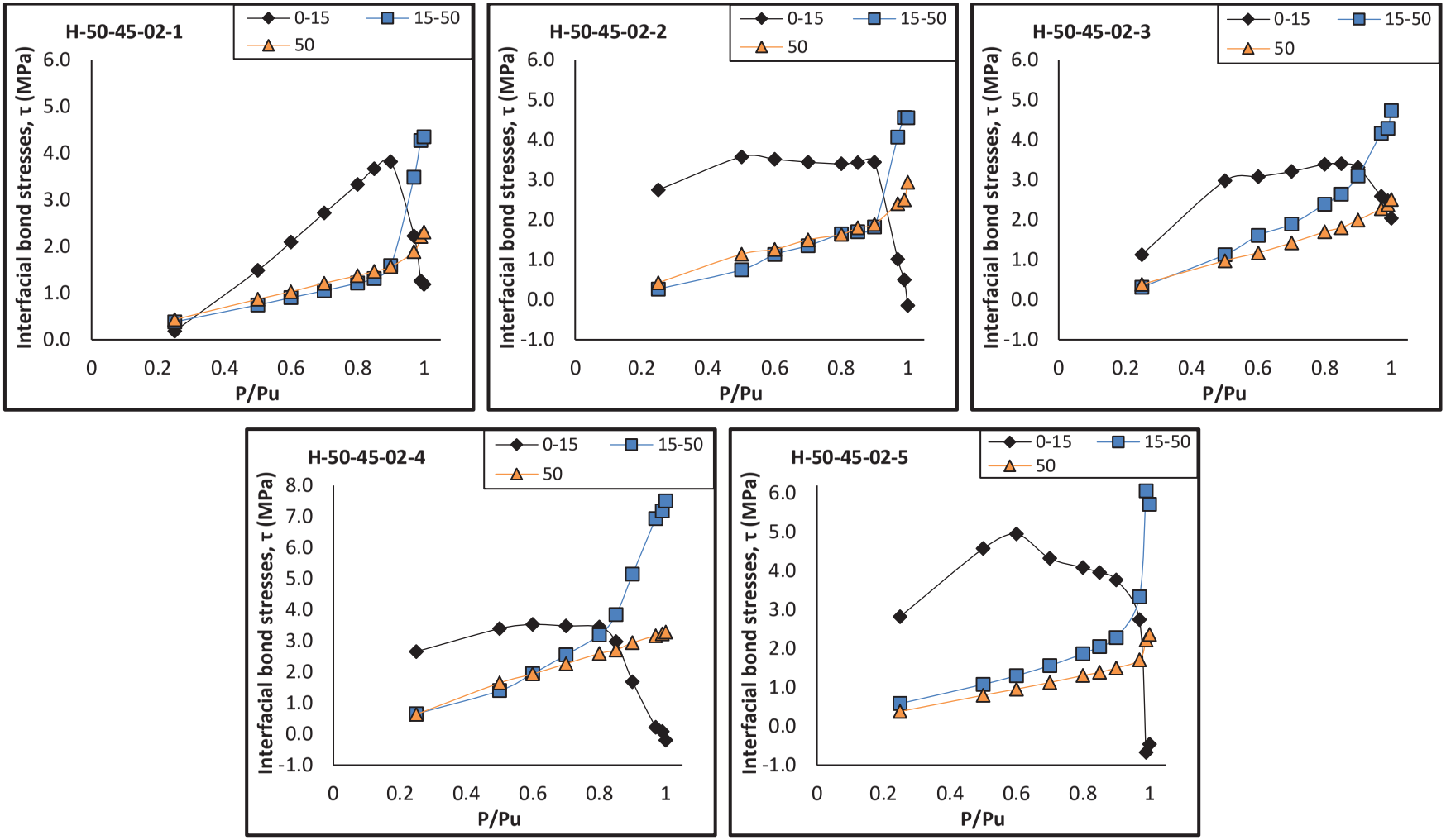
H-50-45-02-1
0-15
15-50
50
Interfacial bond stresses, τ (MPa)
P/Pu
H-50-45-02-2
H-50-45-02-3
H-50-45-02-4
H-50-45-02-5

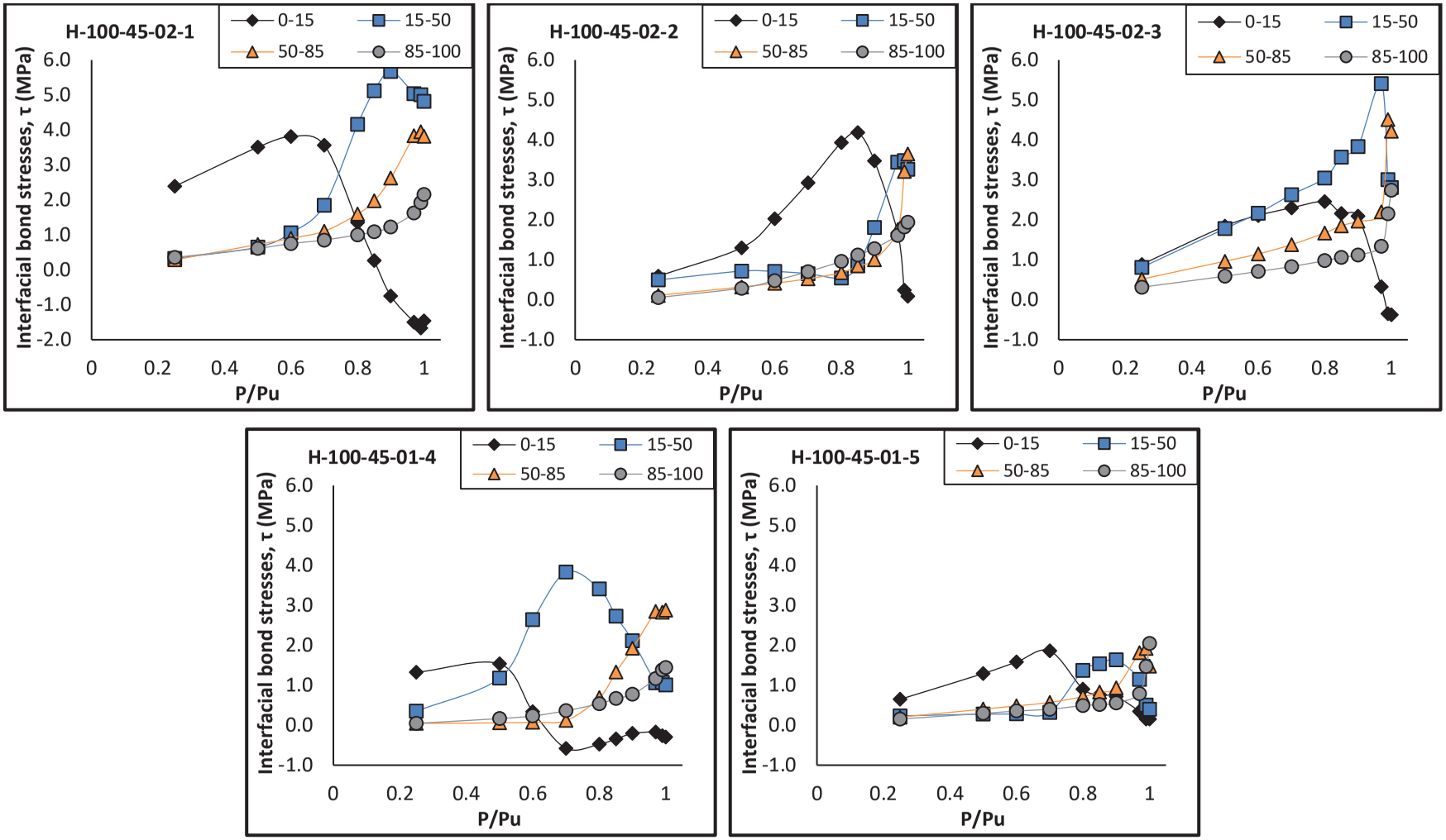
H-100-45-02-1
H-100-45-02-2
H-100-45-02-3
H-100-45-01-4
H-100-45-01-5
0-15
15-50
50-85
85-100
Interfacial bond stresses, τ (MPa)
P/Pu

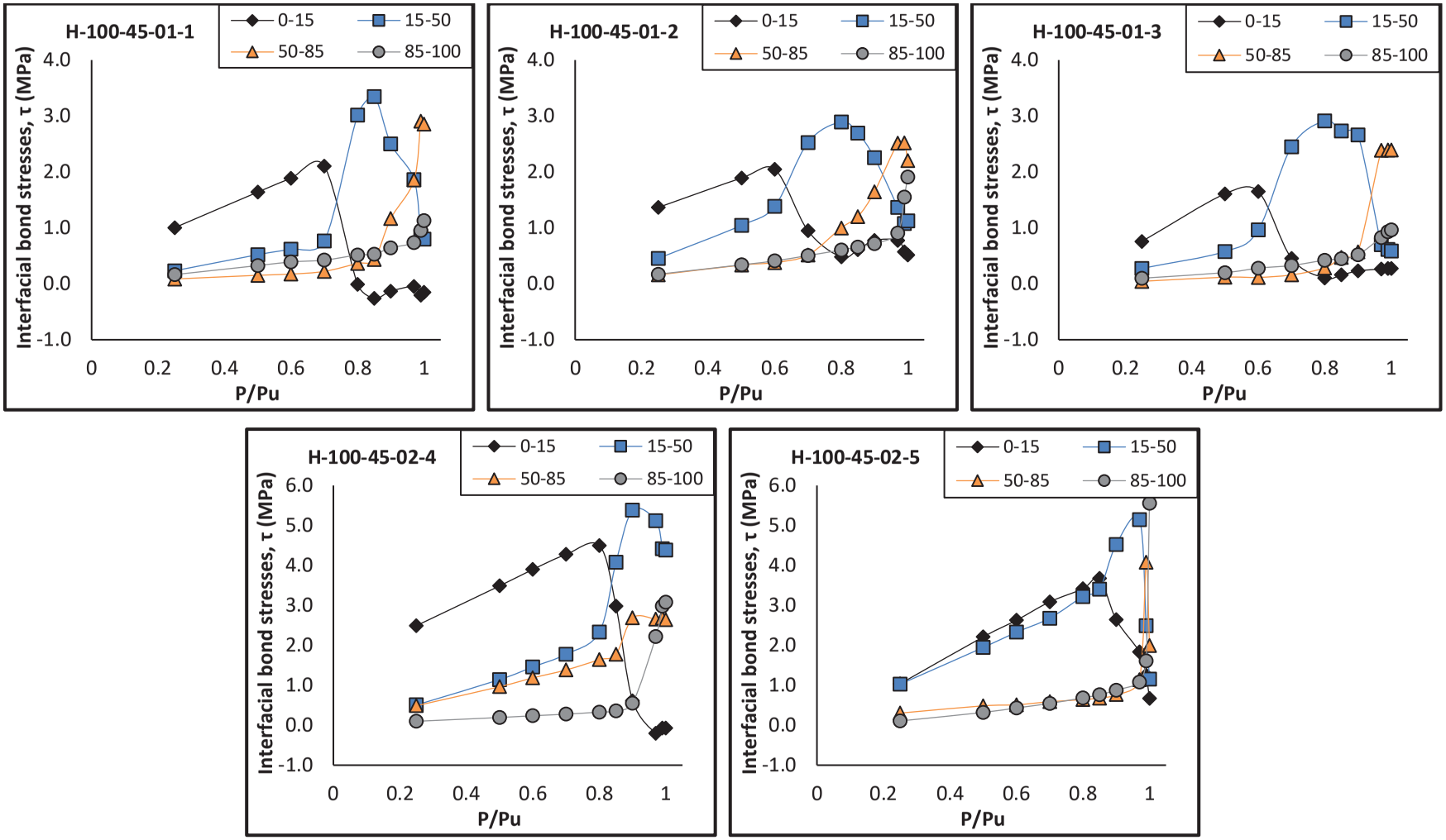
H-100-45-01-1
H-100-45-01-2
H-100-45-01-3
H-100-45-02-4
H-100-45-02-5
0-15
15-50
50-85
85-100
Interfacial bond stresses, τ (MPa)
P/Pu

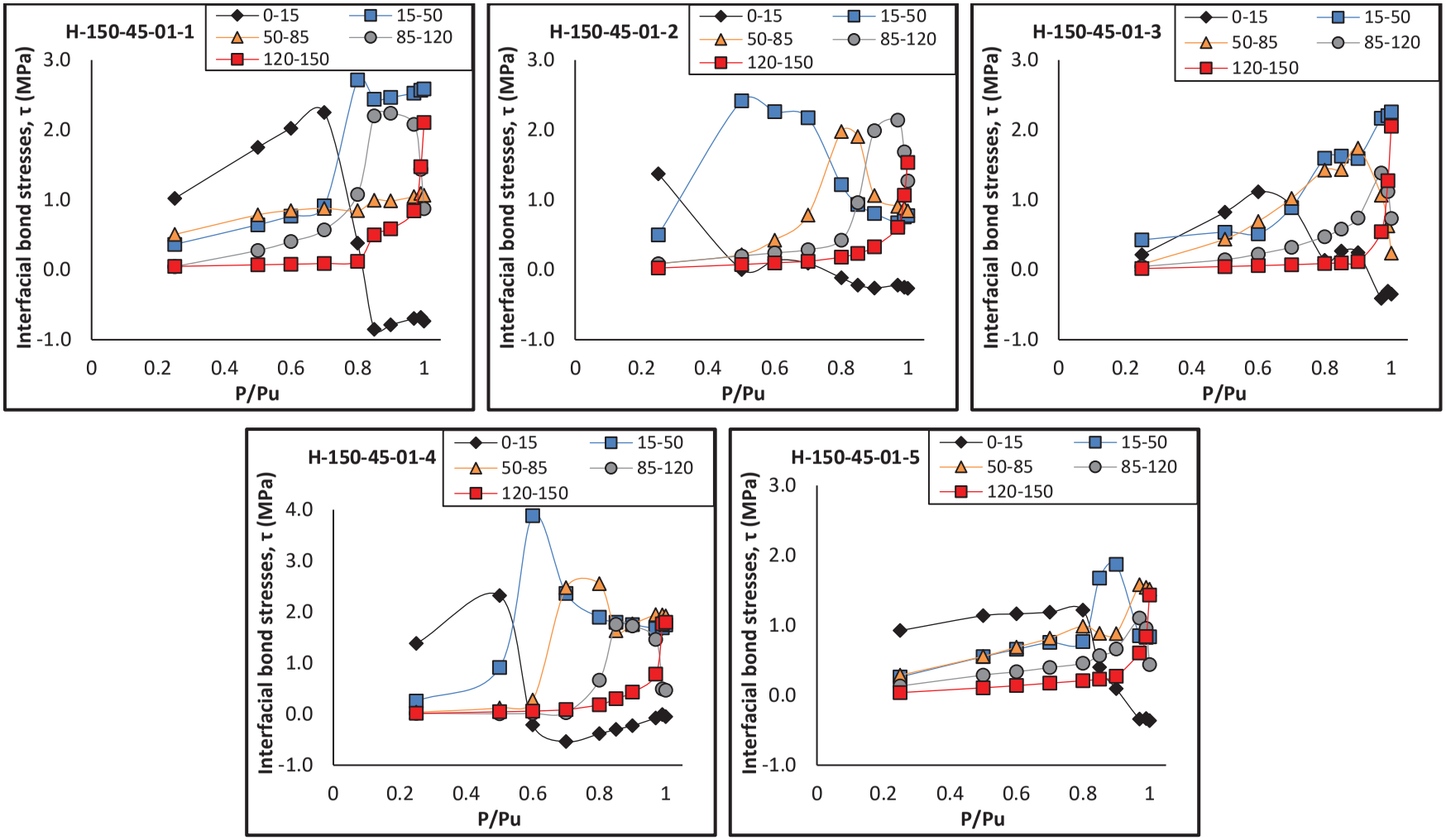
H-150-45-01-1
H-150-45-01-2
H-150-45-01-3
H-150-45-01-4
H-150-45-01-5
0-15
15-50
50-85
85-120
120-150
Interfacial bond stresses, τ (MPa)
P/Pu

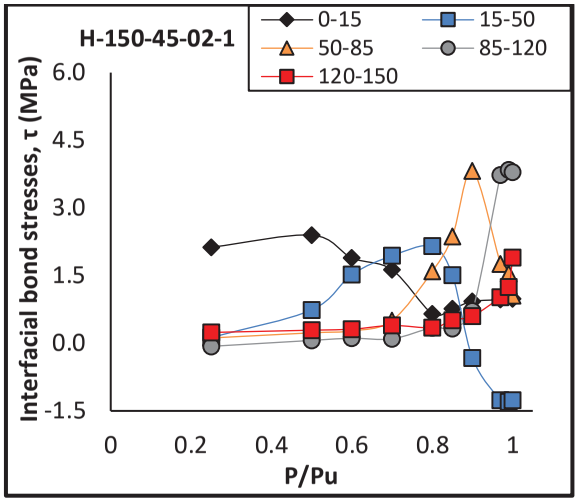
H-150-45-02-1
0-15
15-50
50-85
85-120
120-150
Interfacial bond stresses, τ (MPa)
6.0
4.5
3.0
1.5
0.0
-1.5
0
0.2
0.4
0.6
0.8
1
P/Pu

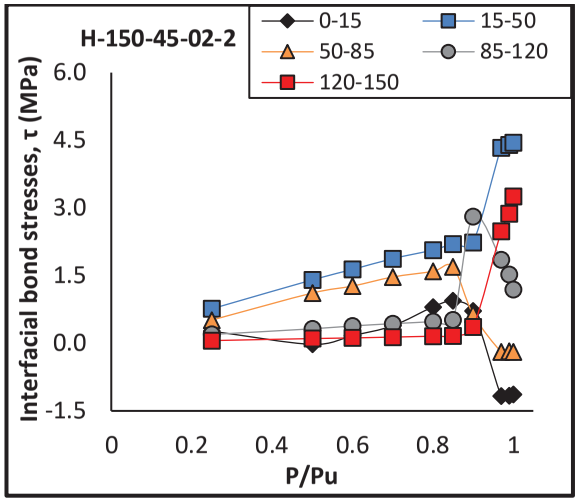
H-150-45-02-2
0-15
15-50
50-85
85-120
120-150
Interfacial bond stresses, τ (MPa)
6.0
4.5
3.0
1.5
0.0
-1.5
0
0.2
0.4
0.6
0.8
1
P/Pu

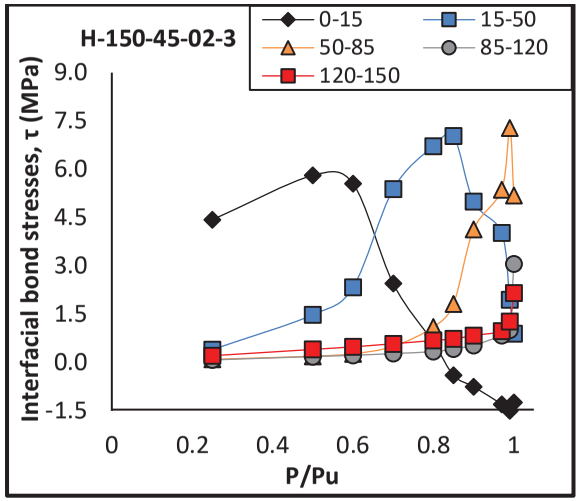
H-150-45-02-3
0-15
15-50
50-85
85-120
120-150
Interfacial bond stresses, τ (MPa)
9.0
7.5
6.0
4.5
3.0
1.5
0.0
-1.5
0
0.2
0.4
0.6
0.8
1
P/Pu

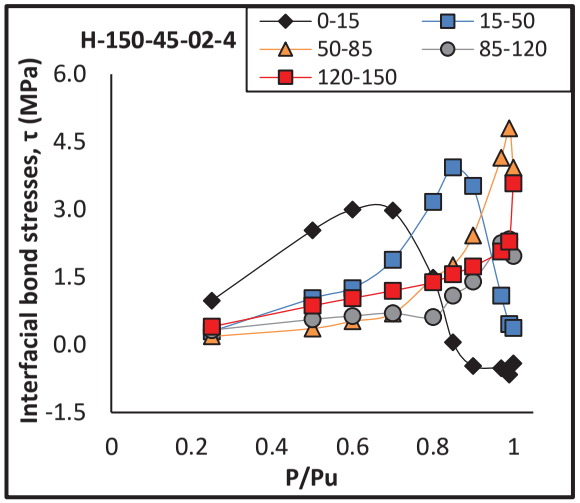
H-150-45-02-4
0-15
15-50
50-85
85-120
120-150
Interfacial bond stresses, τ (MPa)
6.0
4.5
3.0
1.5
0.0
-1.5
0
0.2
0.4
0.6
0.8
1
P/Pu

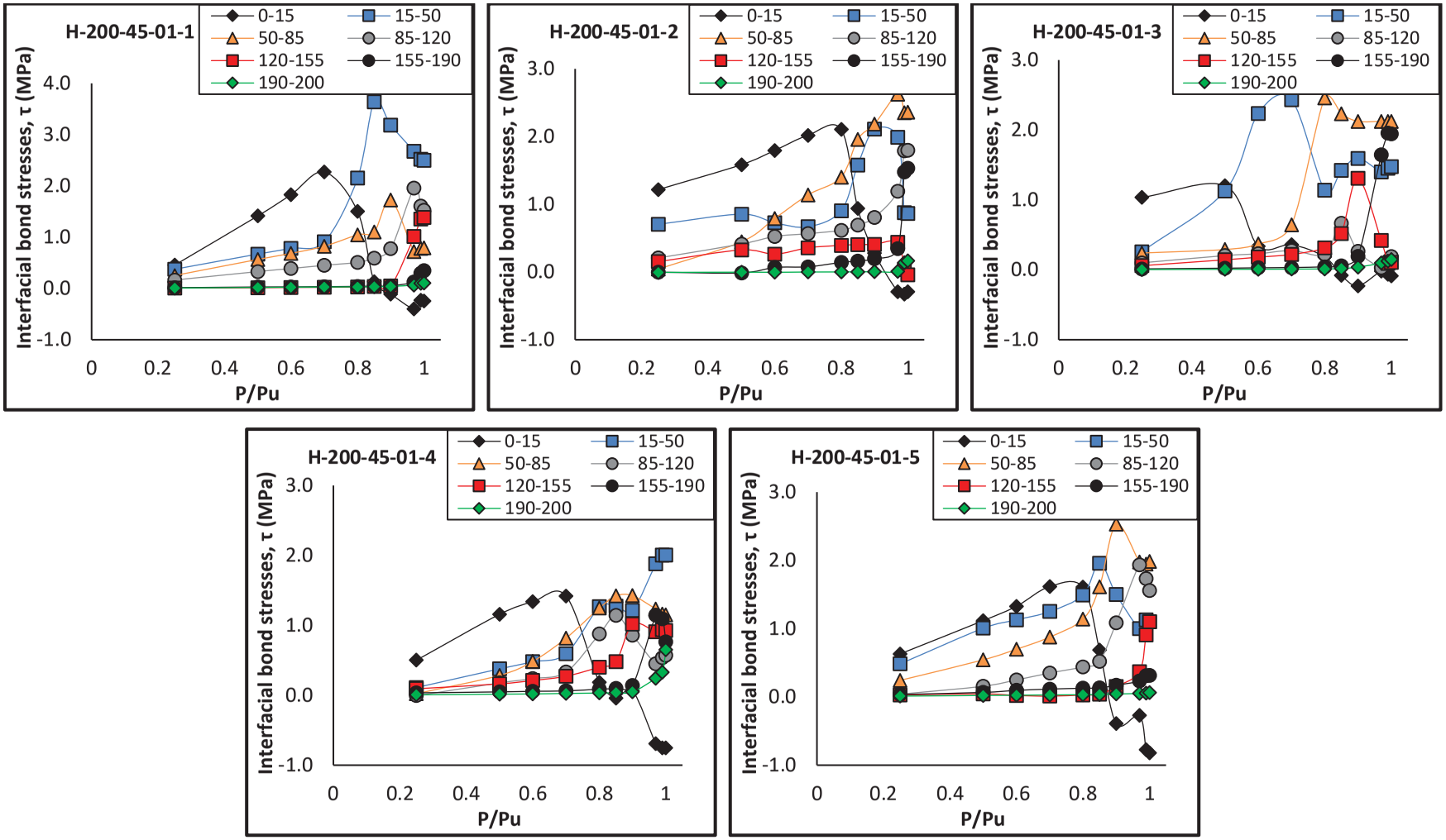
H-200-45-01-1
H-200-45-01-2
H-200-45-01-3
H-200-45-01-4
H-200-45-01-5
0-15
15-50
50-85
85-120
120-155
155-190
190-200
Interfacial bond stresses, τ (MPa)
P/Pu

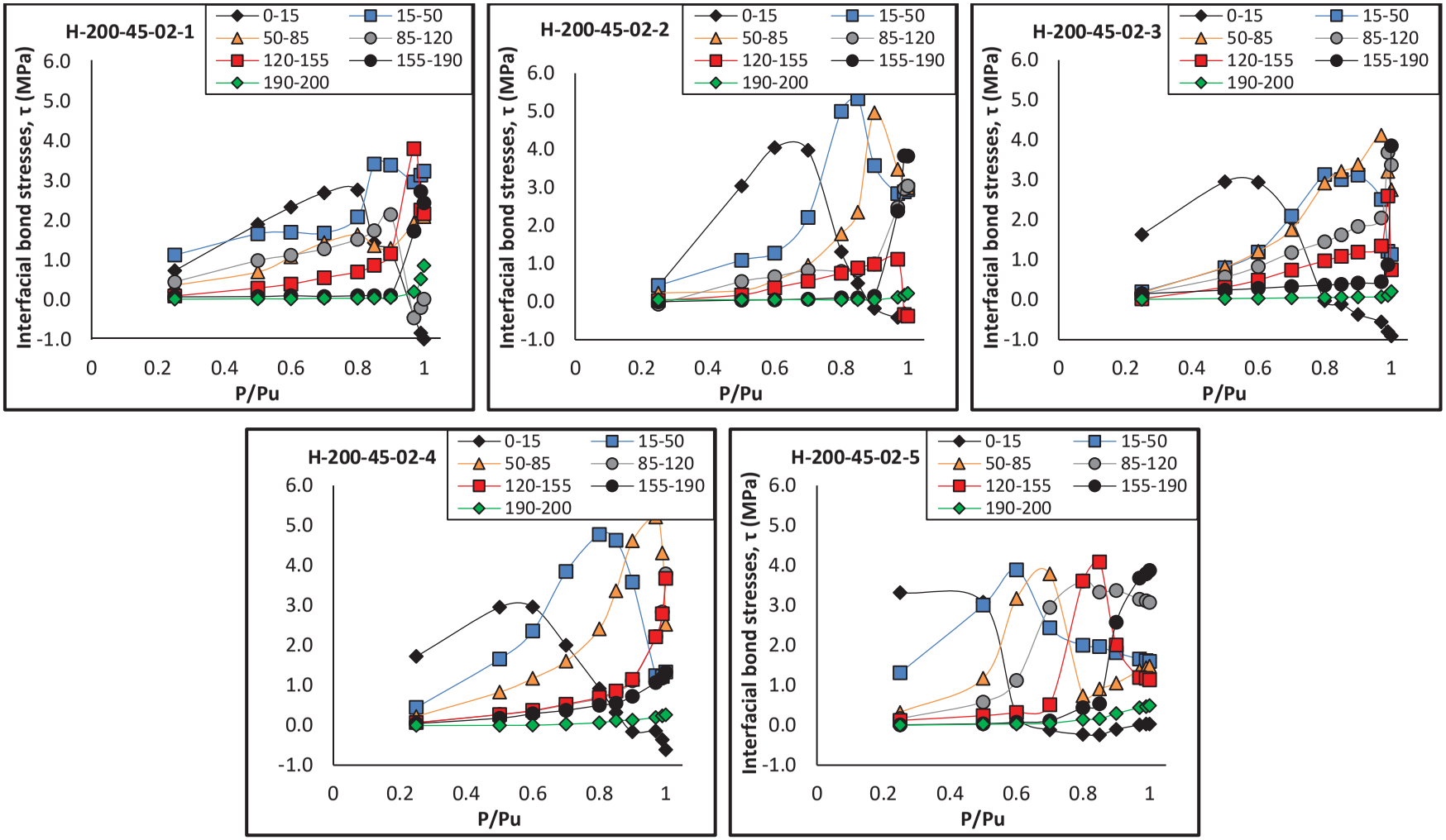
H-200-45-02-1
H-200-45-02-2
H-200-45-02-3
H-200-45-02-4
H-200-45-02-5
0-15
15-50
50-85
85-120
120-155
155-190
190-200
Interfacial bond stresses, τ (MPa)
P/Pu
6.0
5.0
4.0
3.0
2.0
1.0
0.0
-1.0
0
0.2
0.4
0.6
0.8
1

Appendix I.

Interfacial bond stress as a relative of load along interface – LVL Series

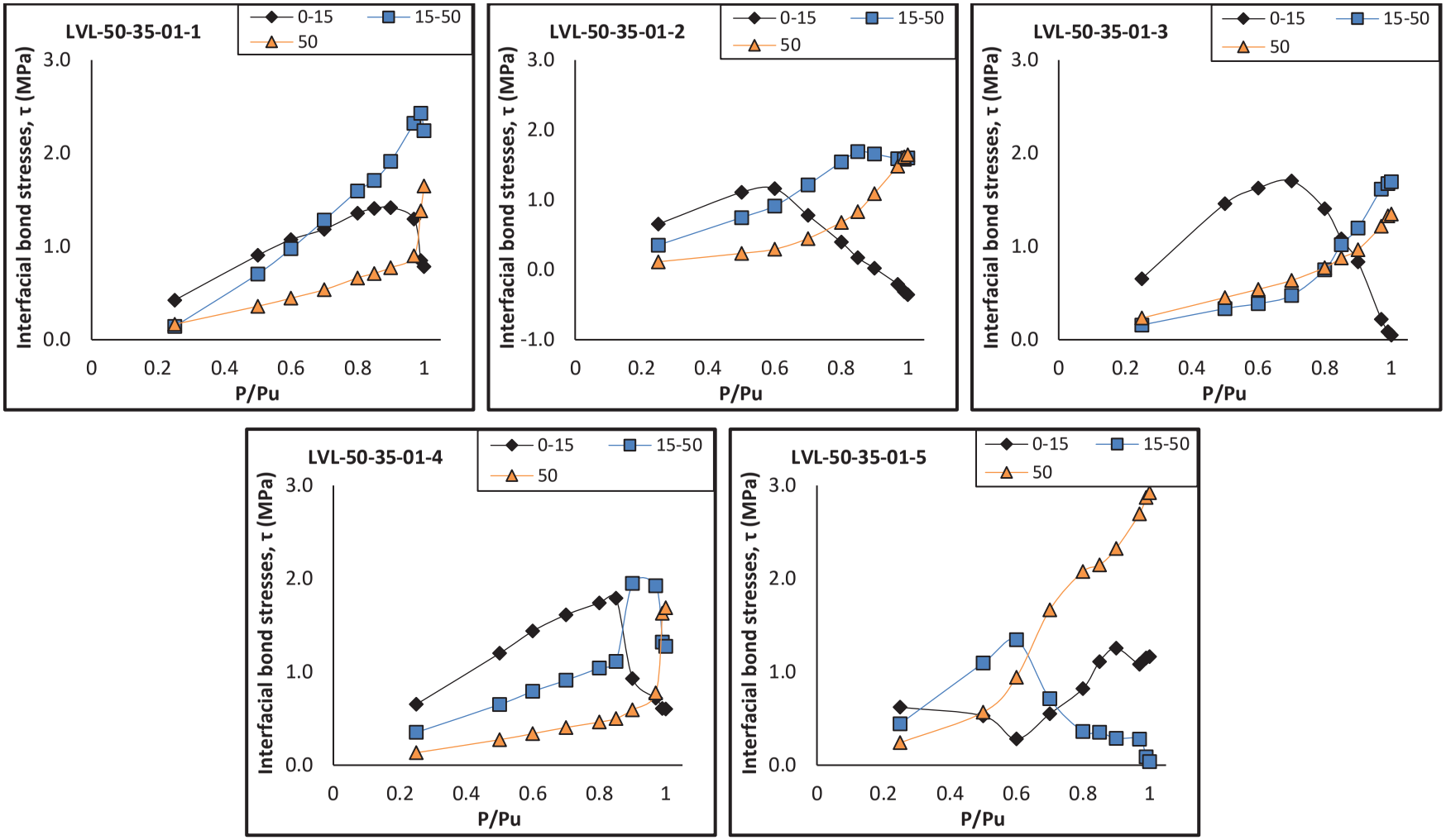
LVL-50-35-01-1
0-15
15-50
50
Interfacial bond stresses, τ (MPa)
P/Pu
LVL-50-35-01-2
LVL-50-35-01-3
LVL-50-35-01-4
LVL-50-35-01-5

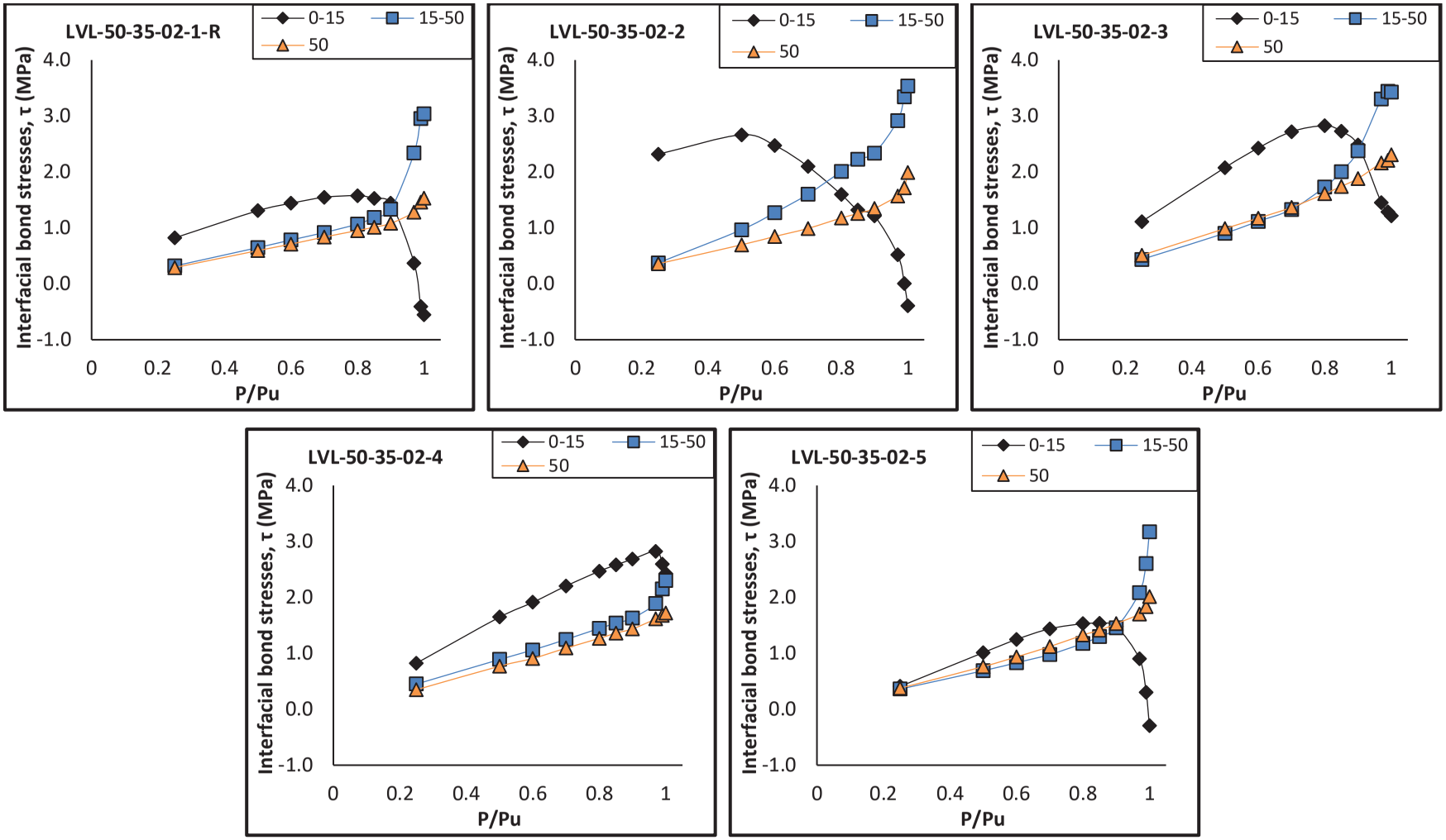
LVL-50-35-02-1-R
LVL-50-35-02-2
LVL-50-35-02-3
LVL-50-35-02-4
LVL-50-35-02-5
0-15
15-50
50
Interfacial bond stresses, τ (MPa)
P/Pu
4.0
3.0
2.0
1.0
0.0
-1.0
0
0.2
0.4
0.6
0.8
1

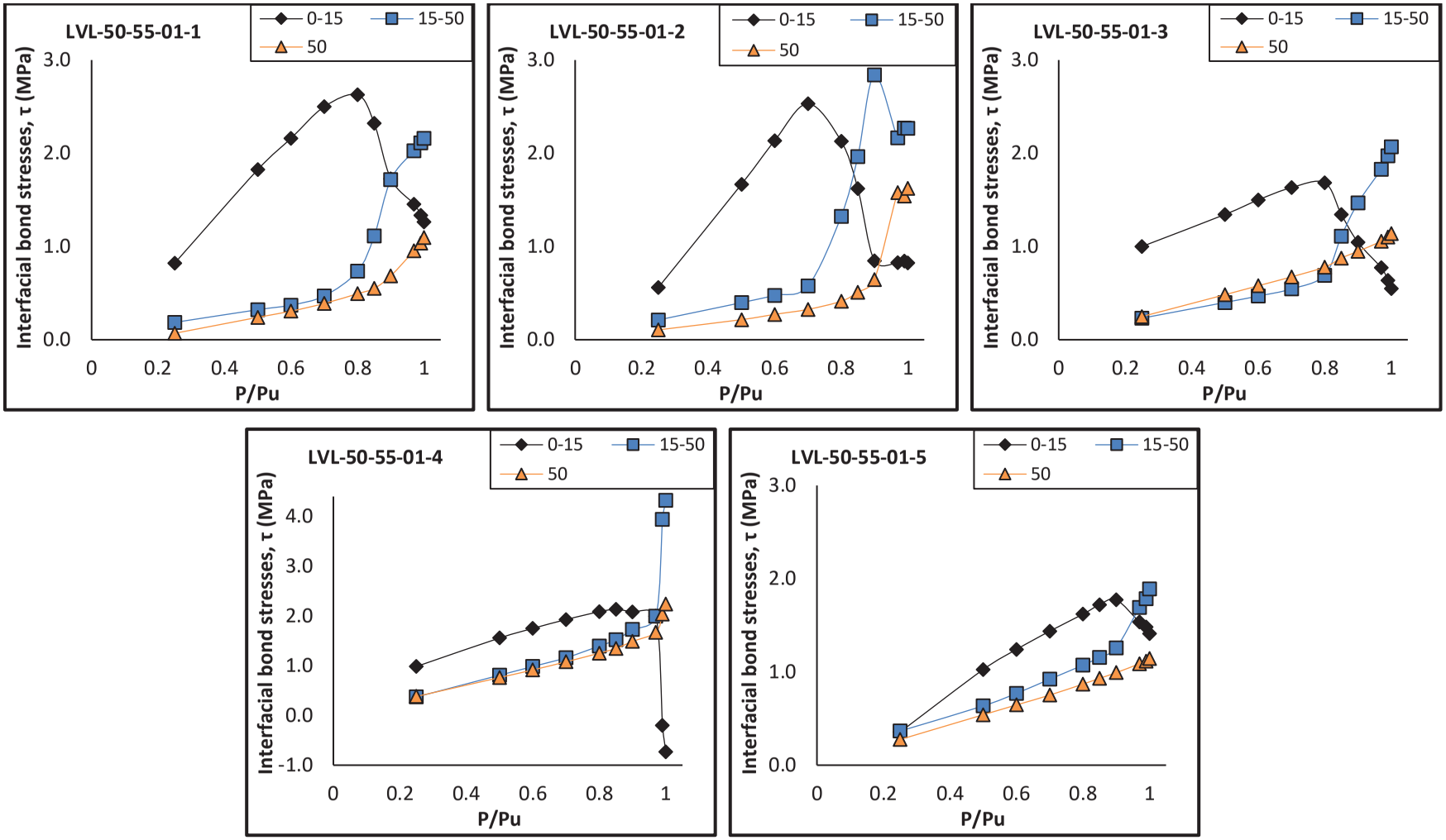
LVL-50-55-01-1
0-15
15-50
50
Interfacial bond stresses, τ (MPa)
P/Pu
LVL-50-55-01-2
LVL-50-55-01-3
LVL-50-55-01-4
LVL-50-55-01-5

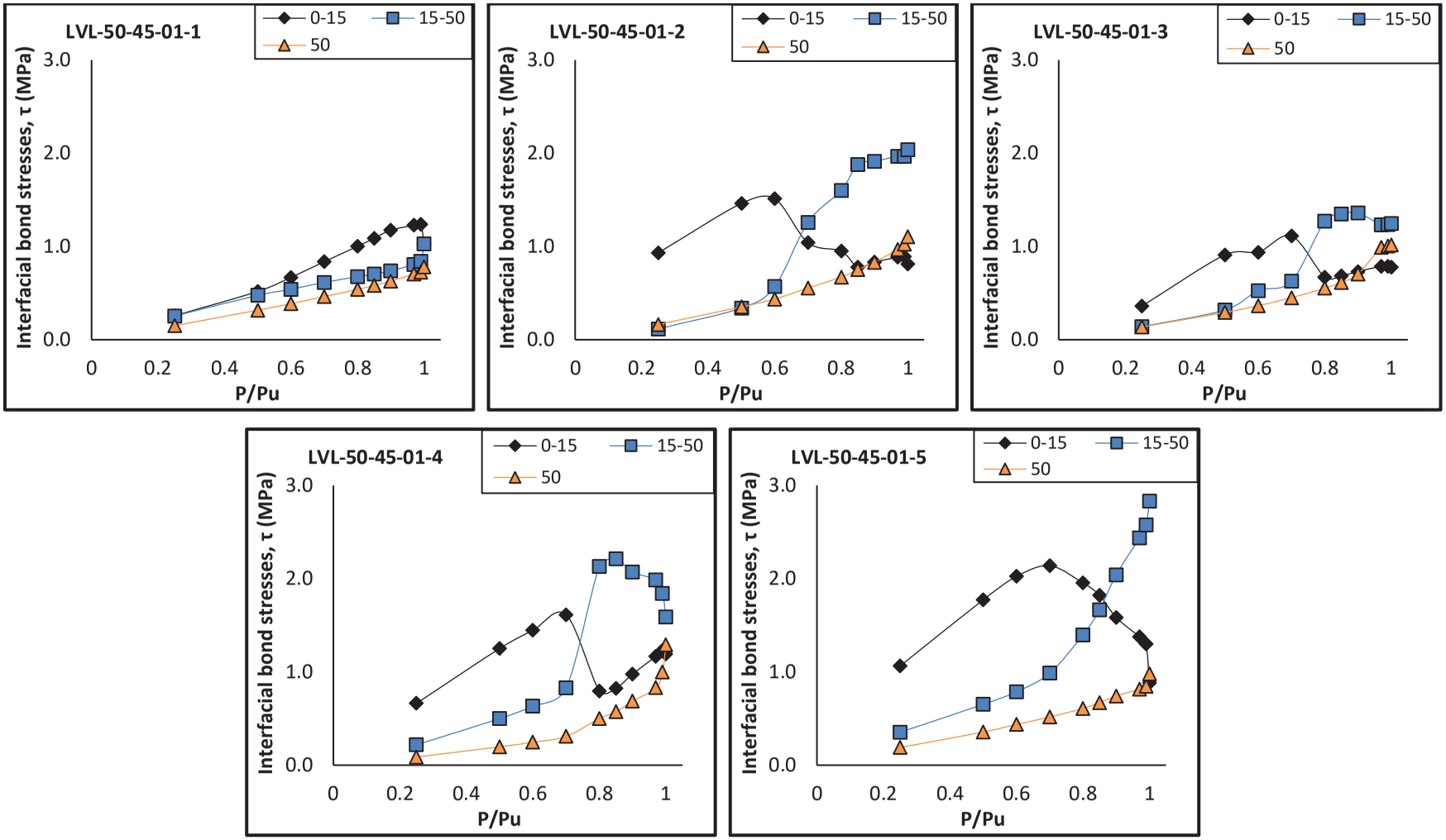
LVL-50-45-01-1
LVL-50-45-01-2
LVL-50-45-01-3
LVL-50-45-01-4
LVL-50-45-01-5
0-15
15-50
50
Interfacial bond stresses, τ (MPa)
P/Pu
0.0
1.0
2.0
3.0
0
0.2
0.4
0.6
0.8
1

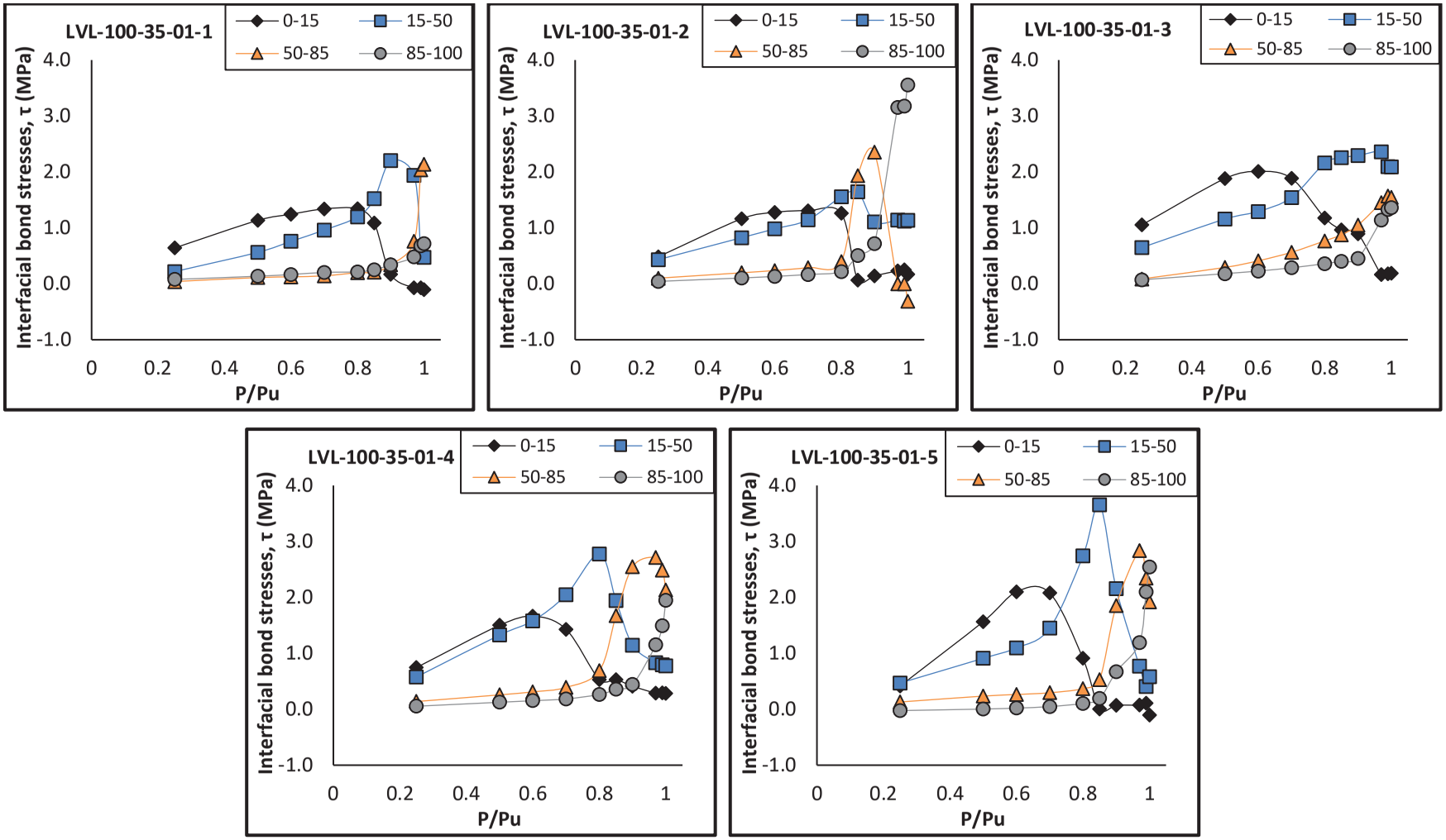
LVL-100-35-01-1
LVL-100-35-01-2
LVL-100-35-01-3
LVL-100-35-01-4
LVL-100-35-01-5
0-15
15-50
50-85
85-100
Interfacial bond stresses, τ (MPa)
P/Pu
4.0
3.0
2.0
1.0
0.0
-1.0
0
0.2
0.4
0.6
0.8
1

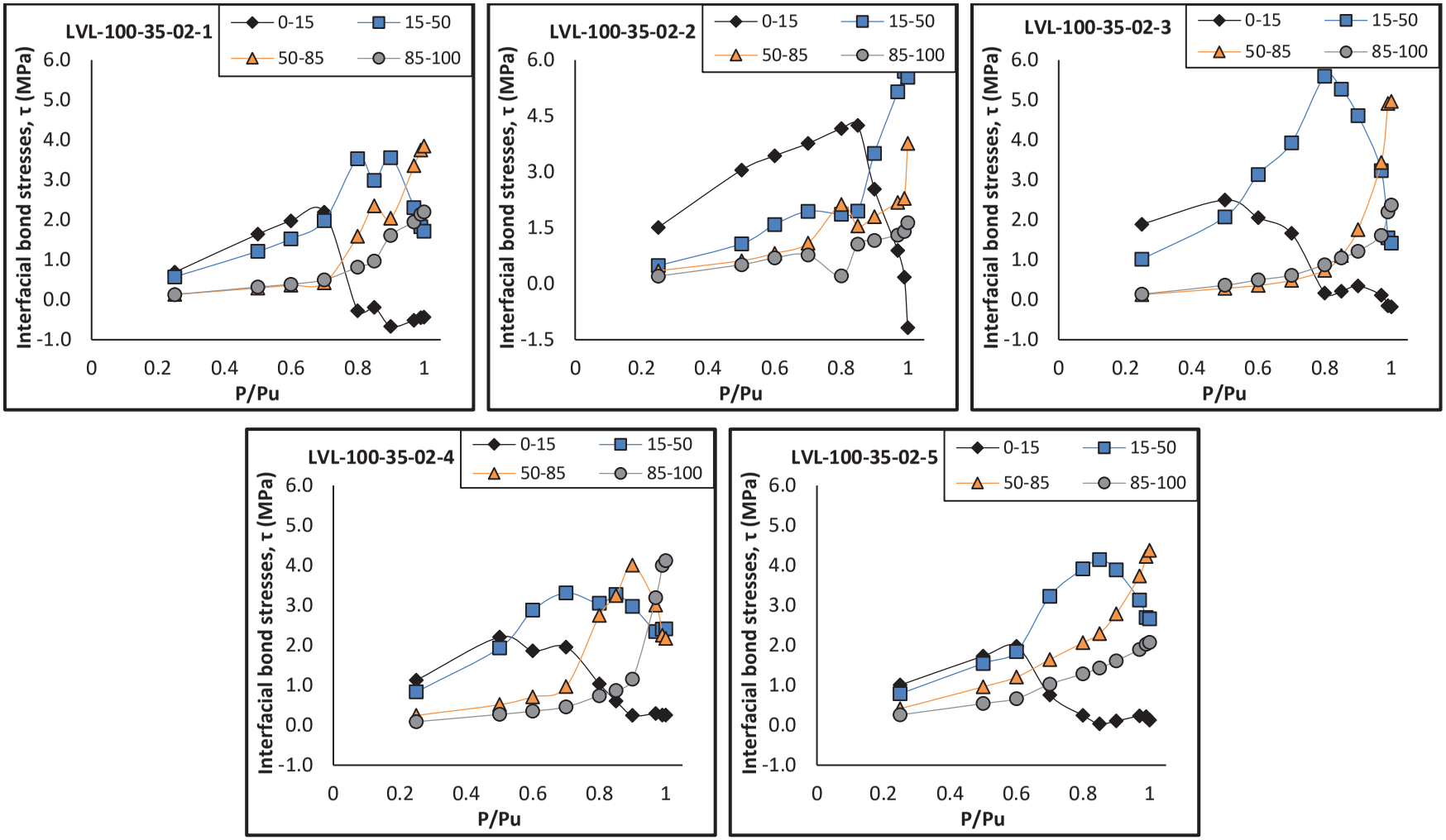
LVL-100-35-02-1
LVL-100-35-02-2
LVL-100-35-02-3
LVL-100-35-02-4
LVL-100-35-02-5
0-15
15-50
50-85
85-100
Interfacial bond stresses, τ (MPa)
P/Pu

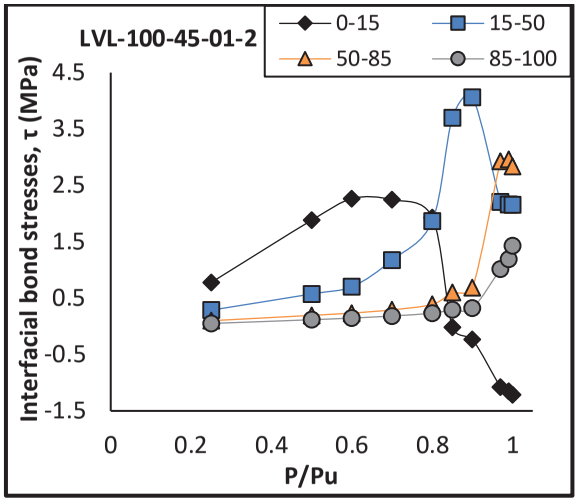
LVL-100-45-01-2
0-15
15-50
50-85
85-100
Interfacial bond stresses, τ (MPa)
4.5
3.5
2.5
1.5
0.5
-0.5
-1.5
0
0.2
0.4
0.6
0.8
1
P/Pu

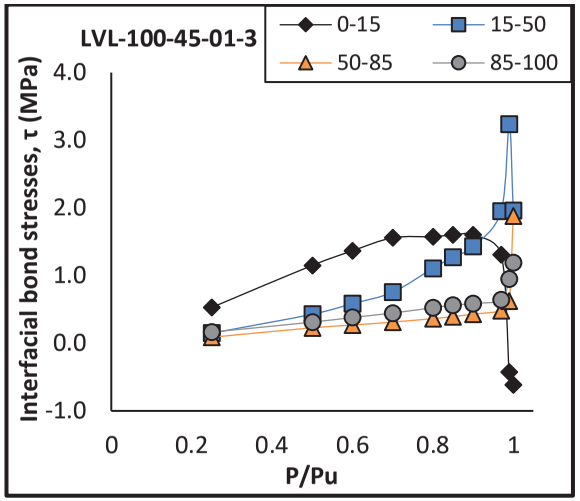
LVL-100-45-01-3
0-15
15-50
50-85
85-100
Interfacial bond stresses, τ (MPa)
4.0
3.0
2.0
1.0
0.0
-1.0
0
0.2
0.4
0.6
0.8
1
P/Pu

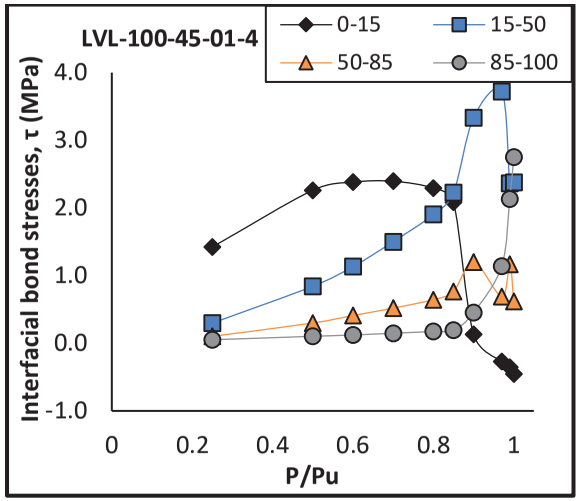
LVL-100-45-01-4
0-15
15-50
50-85
85-100
Interfacial bond stresses, τ (MPa)
4.0
3.0
2.0
1.0
0.0
-1.0
0
0.2
0.4
0.6
0.8
1
P/Pu

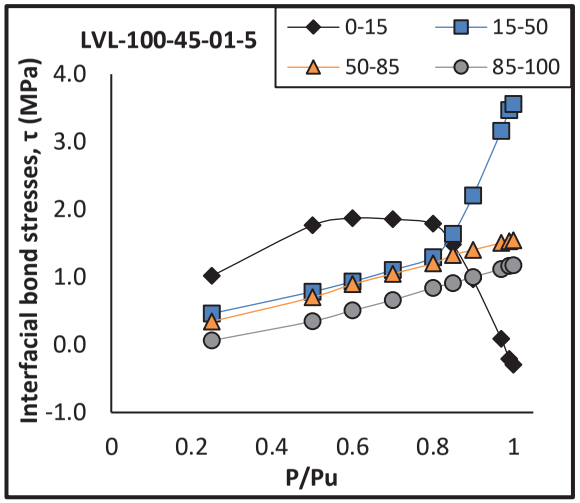
LVL-100-45-01-5
0-15
15-50
50-85
85-100
Interfacial bond stresses, τ (MPa)
4.0
3.0
2.0
1.0
0.0
-1.0
0
0.2
0.4
0.6
0.8
1
P/Pu

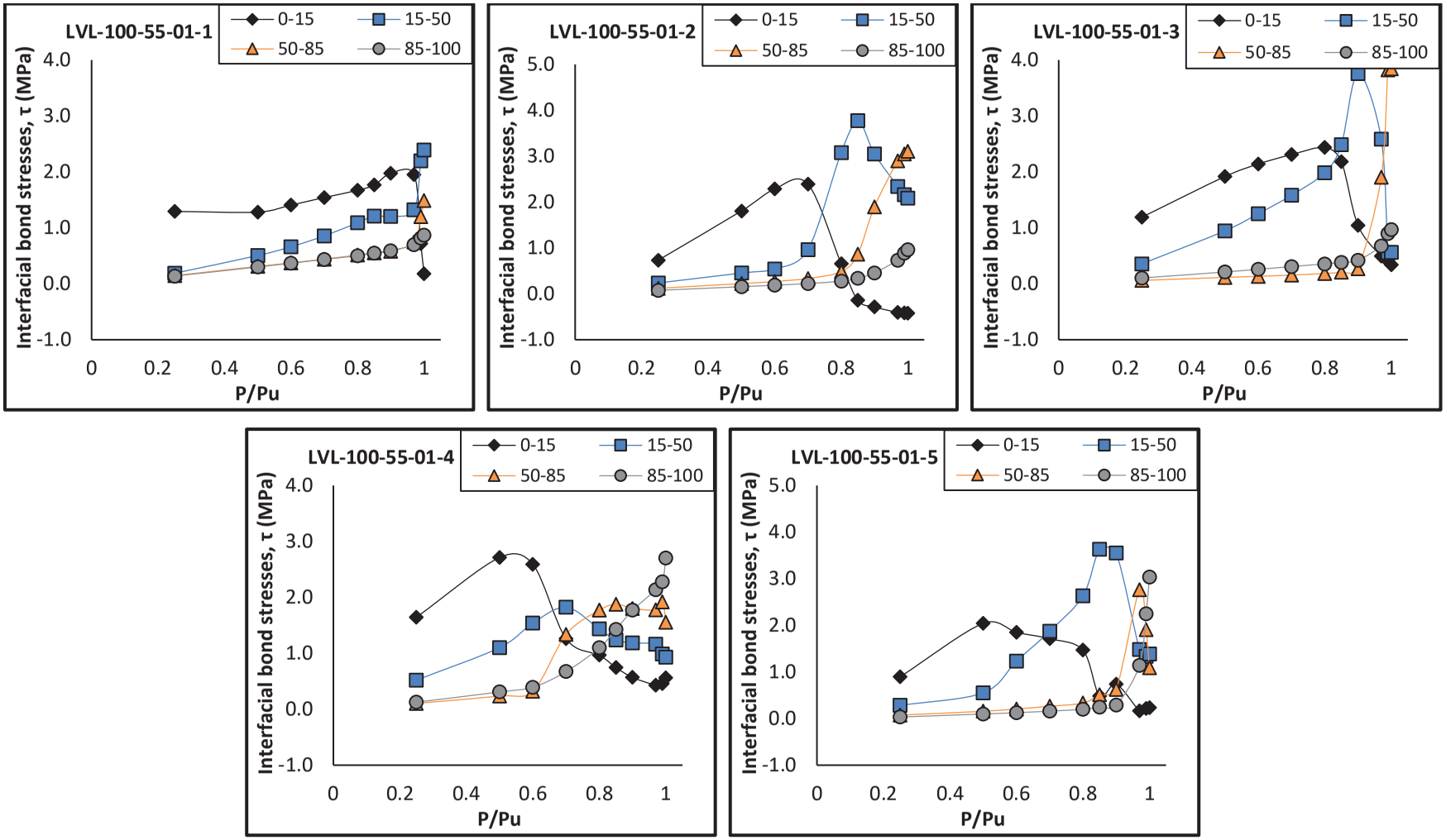
LVL-100-55-01-1
LVL-100-55-01-2
LVL-100-55-01-3
LVL-100-55-01-4
LVL-100-55-01-5
0-15
15-50
50-85
85-100
Interfacial bond stresses, τ (MPa)
P/Pu

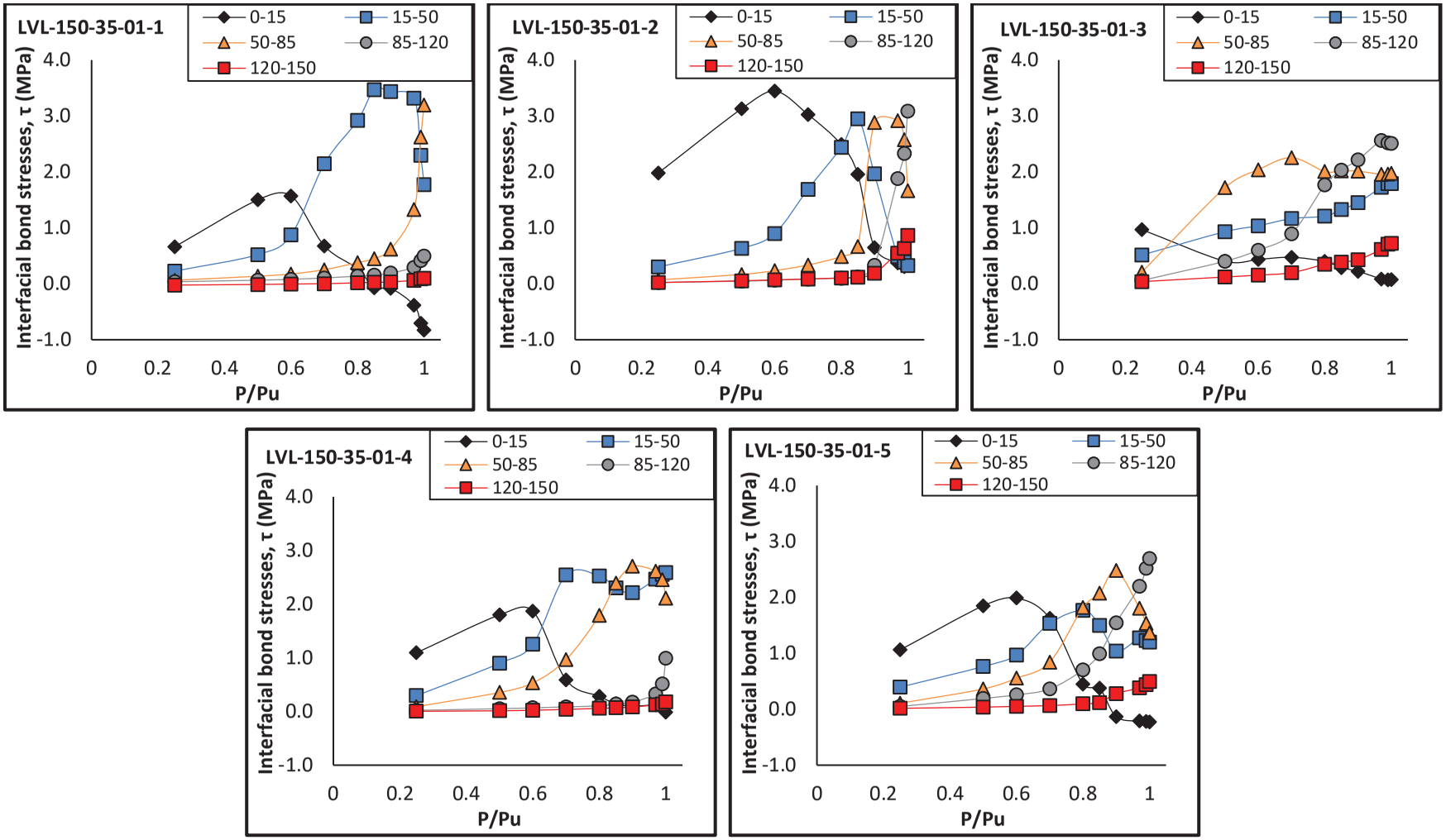
LVL-150-35-01-1
LVL-150-35-01-2
LVL-150-35-01-3
LVL-150-35-01-4
LVL-150-35-01-5
0-15
15-50
50-85
85-120
120-150
Interfacial bond stresses, τ (MPa)
P/Pu
4.0
3.0
2.0
1.0
0.0
-1.0
0
0.2
0.4
0.6
0.8
1

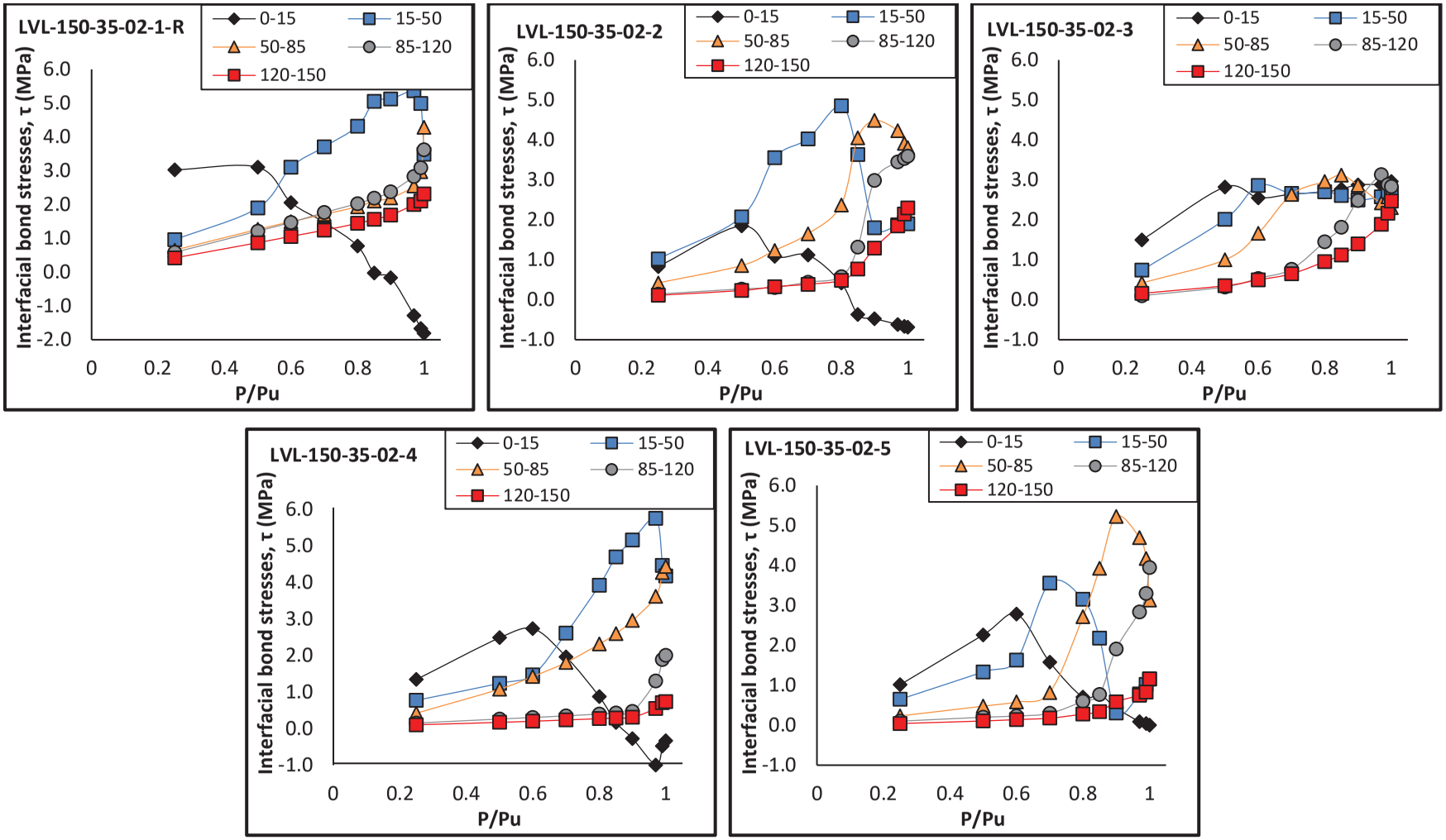
LVL-150-35-02-1-R
LVL-150-35-02-2
LVL-150-35-02-3
LVL-150-35-02-4
LVL-150-35-02-5
0-15
15-50
50-85
85-120
120-150
Interfacial bond stresses, τ (MPa)
P/Pu

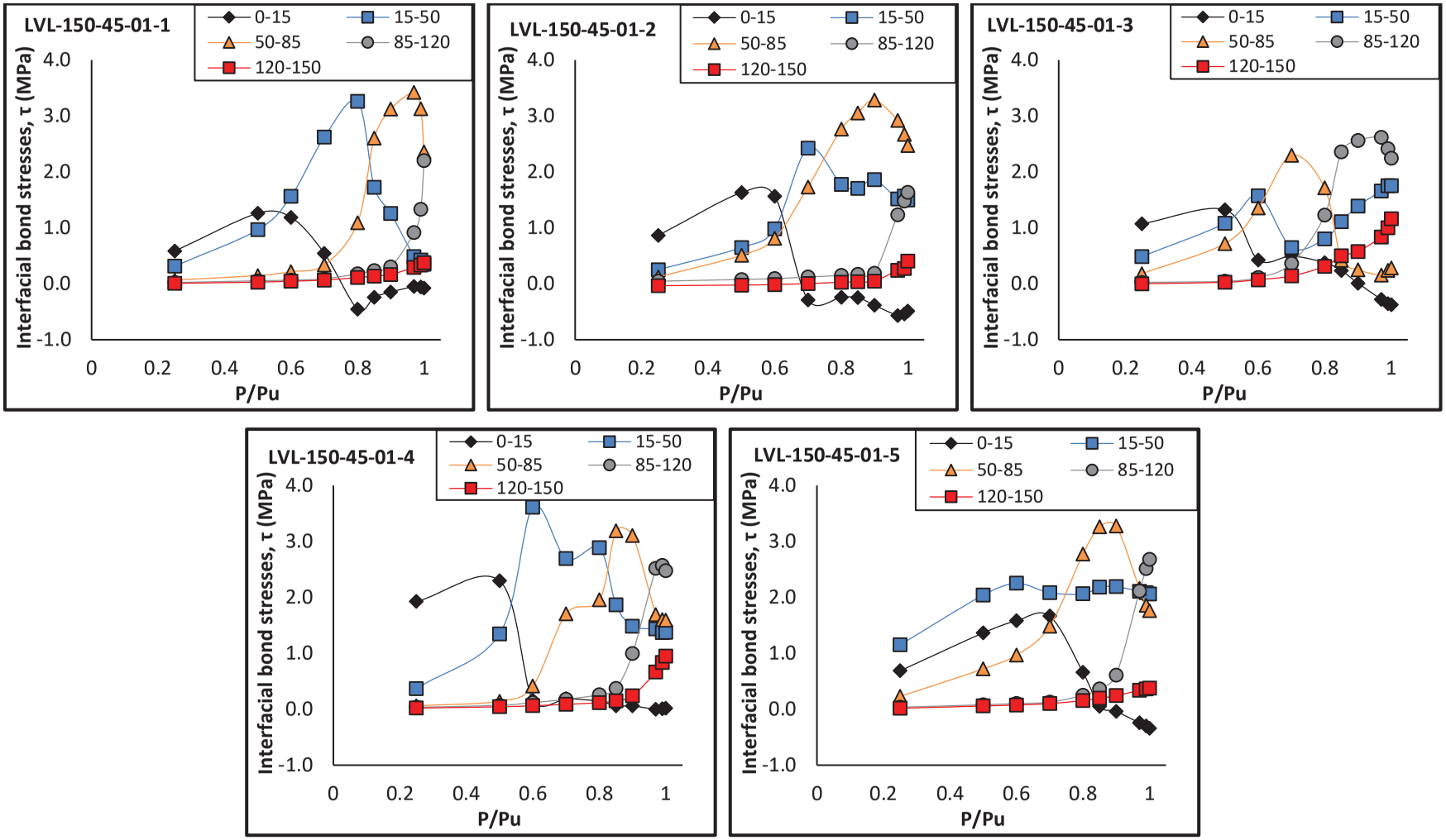
LVL-150-45-01-1
LVL-150-45-01-2
LVL-150-45-01-3
LVL-150-45-01-4
LVL-150-45-01-5
0-15
15-50
50-85
85-120
120-150
Interfacial bond stresses, τ (MPa)
P/Pu
4.0
3.0
2.0
1.0
0.0
-1.0
0
0.2
0.4
0.6
0.8
1

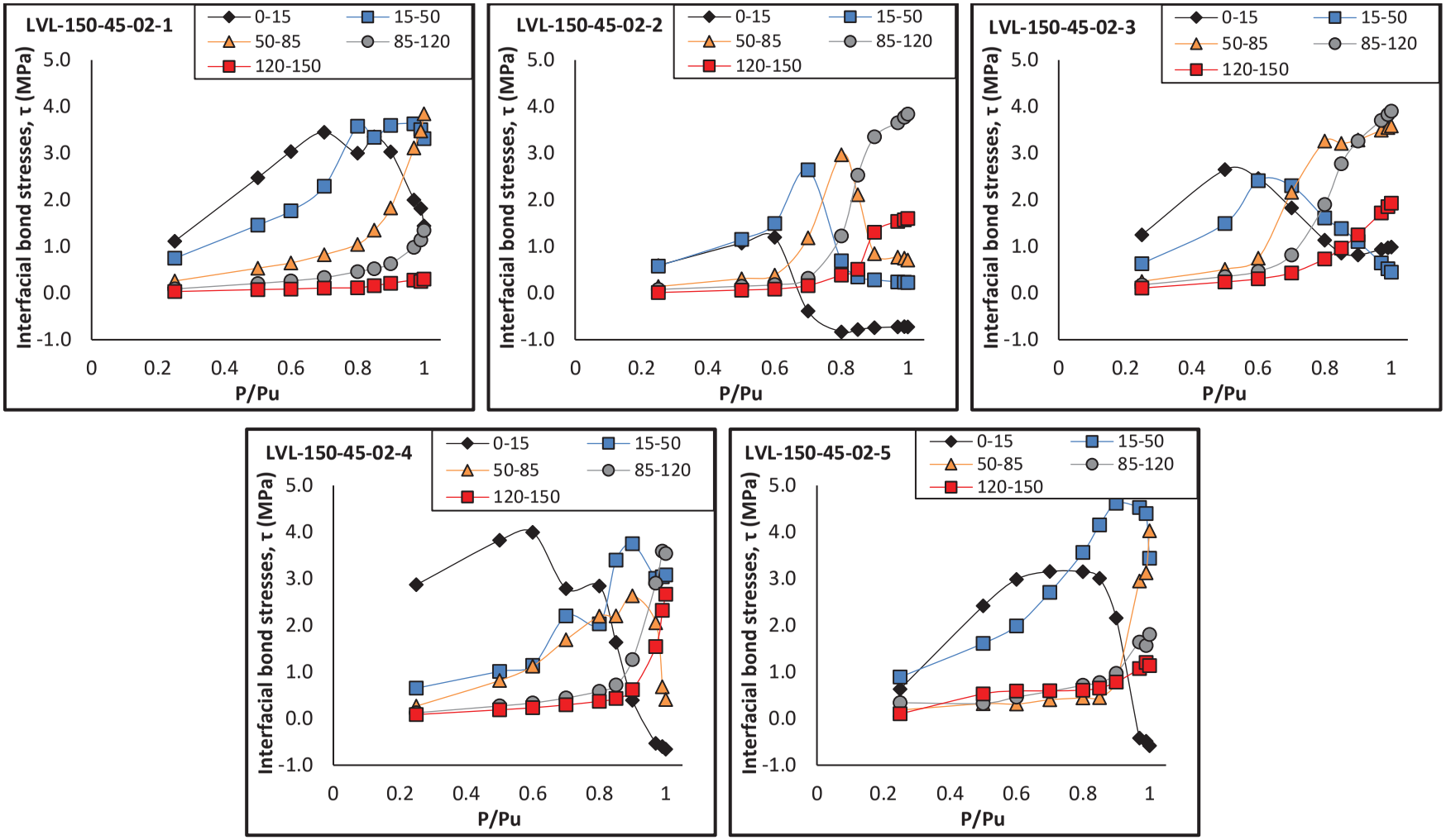
LVL-150-45-02-1
LVL-150-45-02-2
LVL-150-45-02-3
LVL-150-45-02-4
LVL-150-45-02-5
0-15
15-50
50-85
85-120
120-150
Interfacial bond stresses, τ (MPa)
P/Pu
5.0
4.0
3.0
2.0
1.0
0.0
-1.0
0
0.2
0.4
0.6
0.8
1

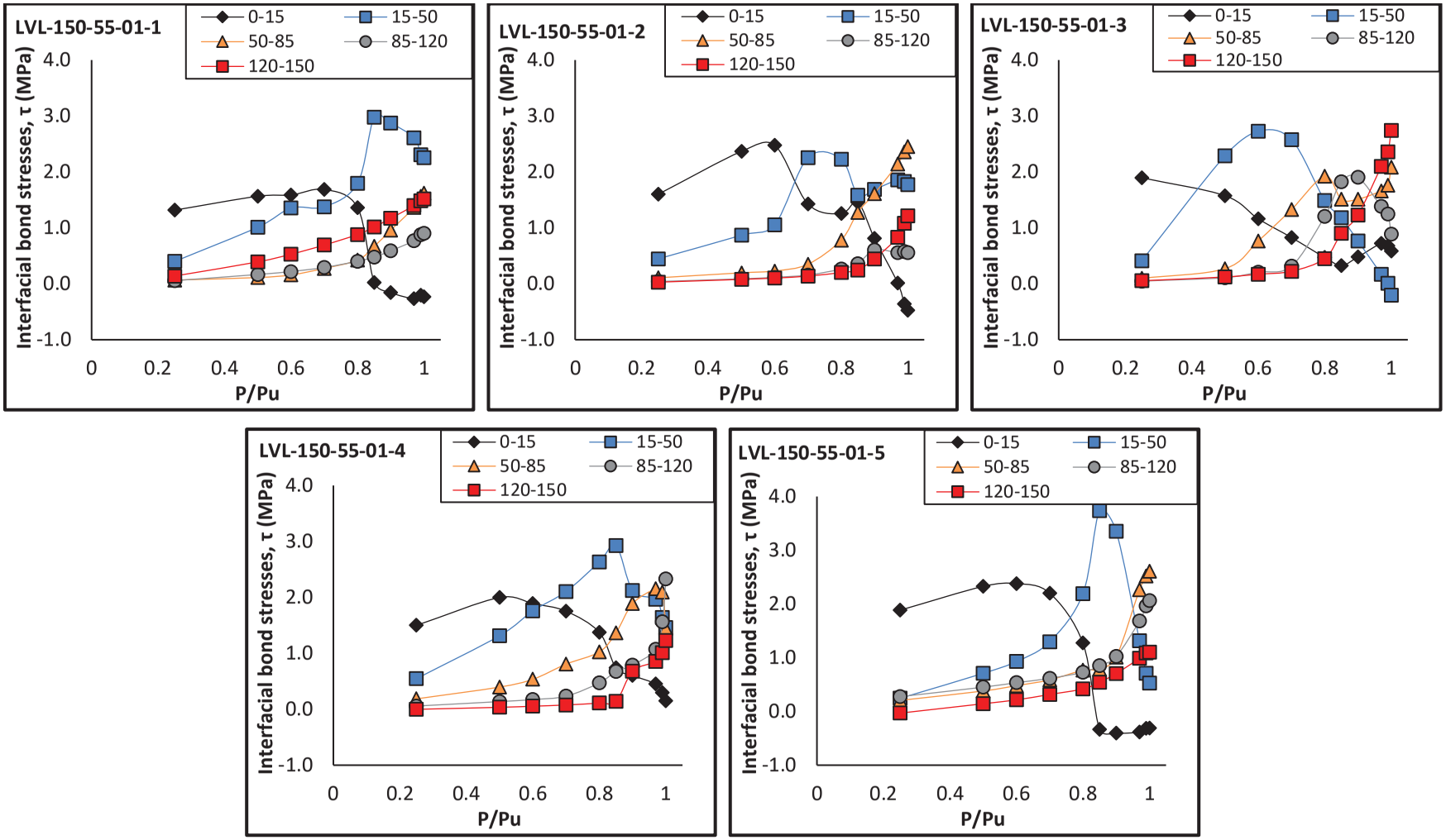
LVL-150-55-01-1
LVL-150-55-01-2
LVL-150-55-01-3
LVL-150-55-01-4
LVL-150-55-01-5
0-15
15-50
50-85
85-120
120-150
Interfacial bond stresses, τ (MPa)
P/Pu
4.0
3.0
2.0
1.0
0.0
-1.0
0
0.2
0.4
0.6
0.8
1

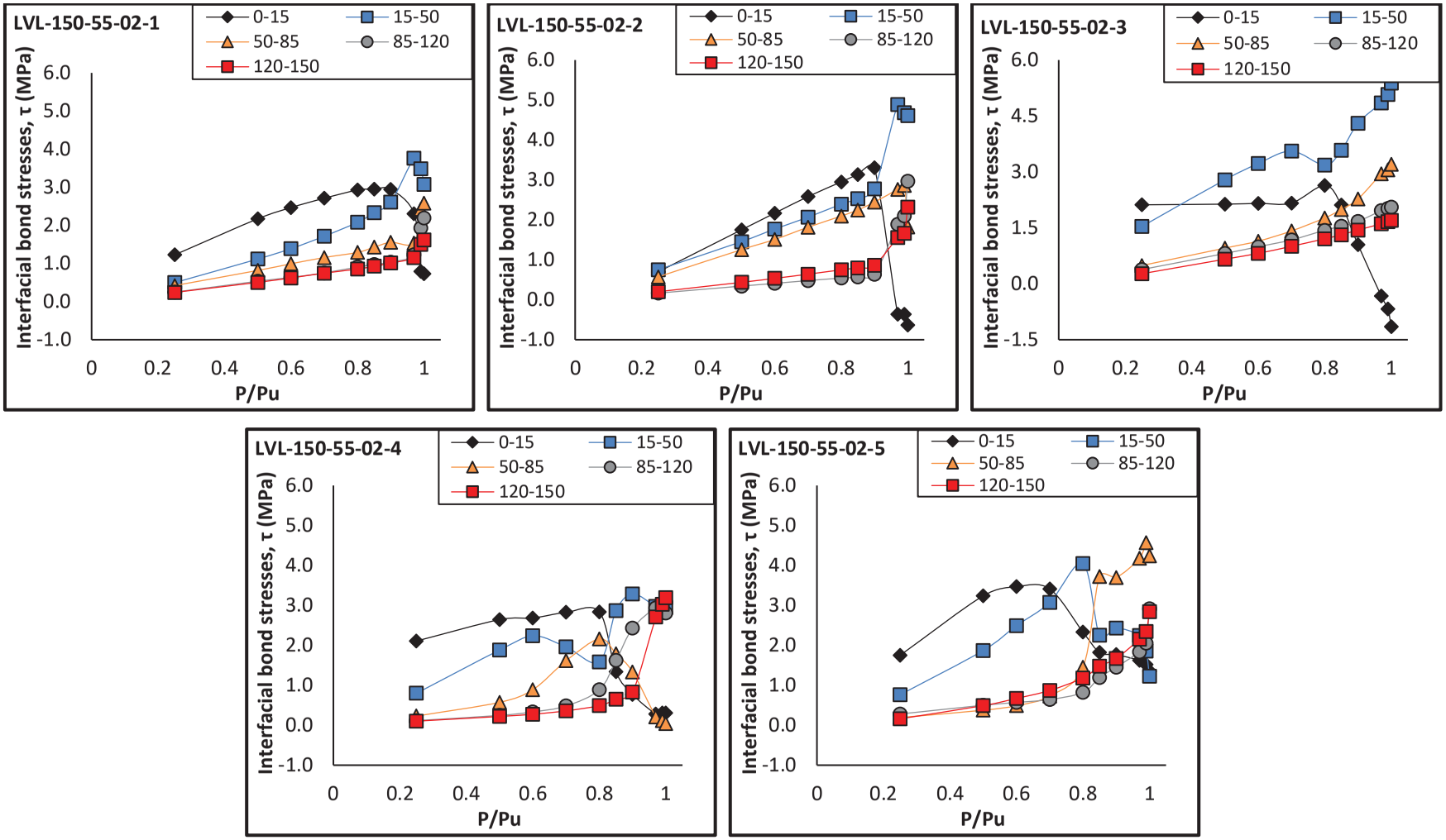
LVL-150-55-02-1
0-15
15-50
50-85
85-120
120-150
Interfacial bond stresses, τ (MPa)
P/Pu
LVL-150-55-02-2
LVL-150-55-02-3
LVL-150-55-02-4
LVL-150-55-02-5

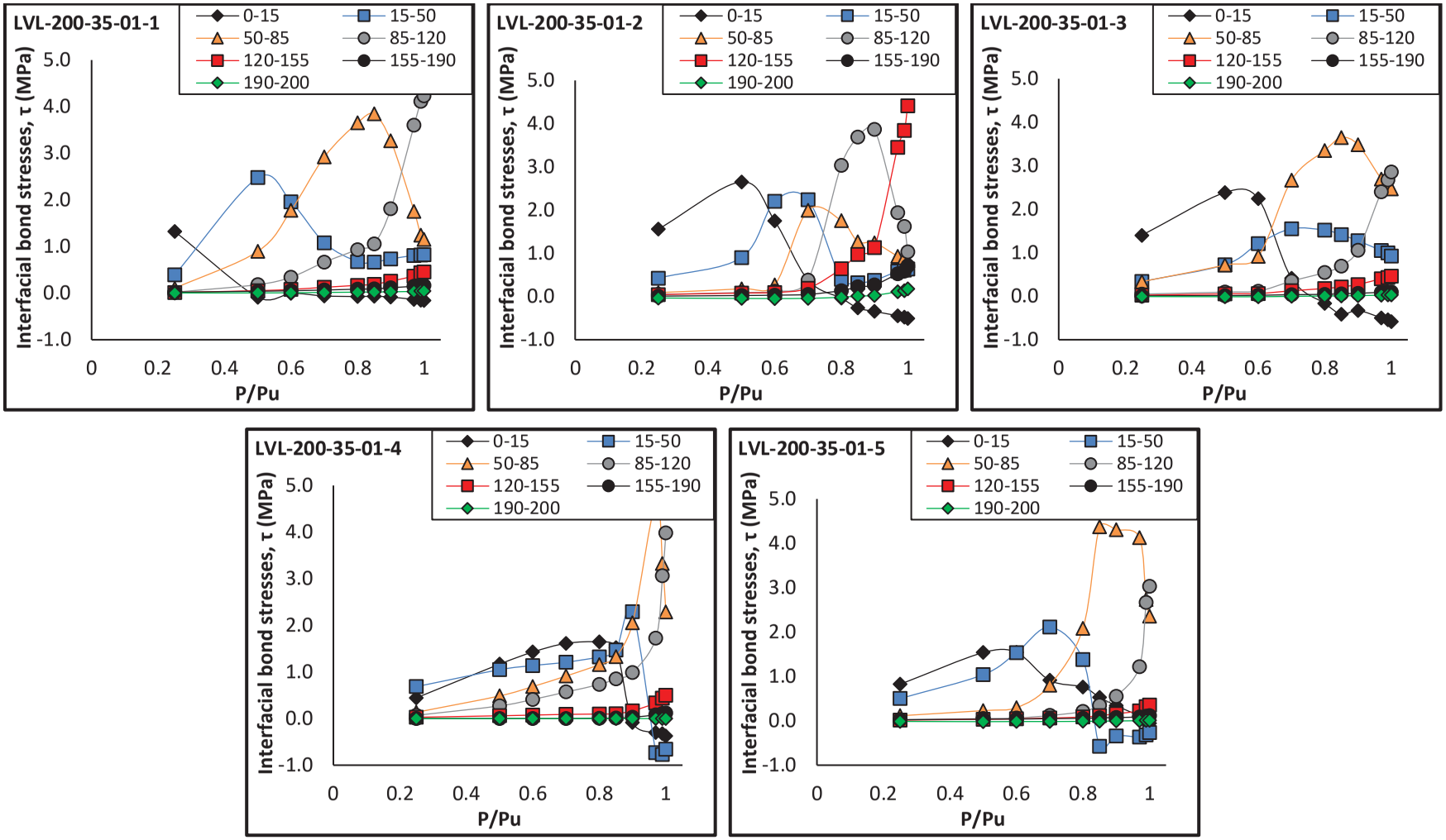
LVL-200-35-01-1
LVL-200-35-01-2
LVL-200-35-01-3
LVL-200-35-01-4
LVL-200-35-01-5
0-15
15-50
50-85
85-120
120-155
155-190
190-200
Interfacial bond stresses, τ (MPa)
P/Pu
5.0
4.0
3.0
2.0
1.0
0.0
-1.0
0
0.2
0.4
0.6
0.8
1

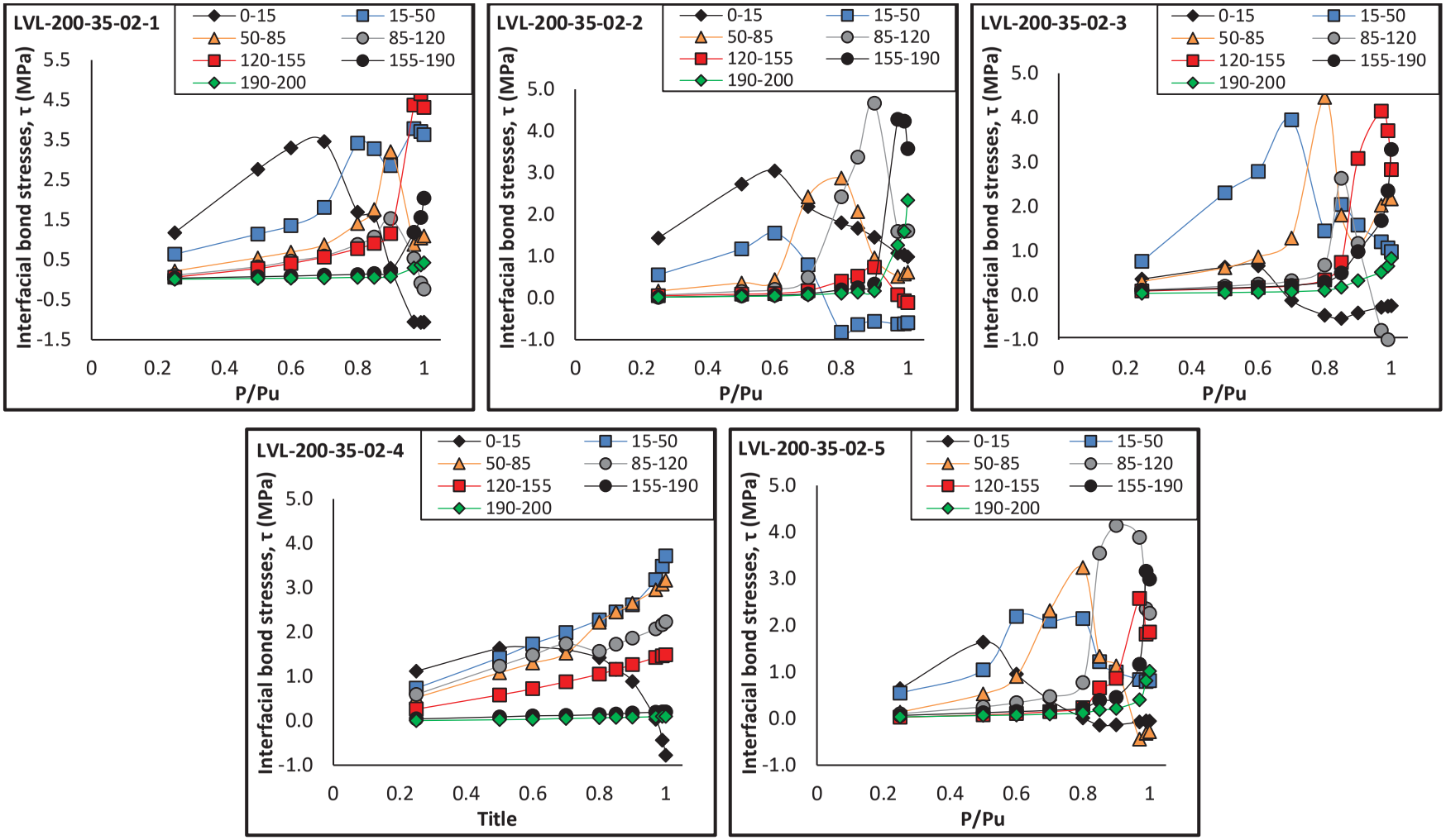
LVL-200-35-02-1
0-15
15-50
50-85
85-120
120-155
155-190
190-200
Interfacial bond stresses, τ (MPa)
P/Pu
LVL-200-35-02-2
LVL-200-35-02-3
LVL-200-35-02-4
LVL-200-35-02-5
Title

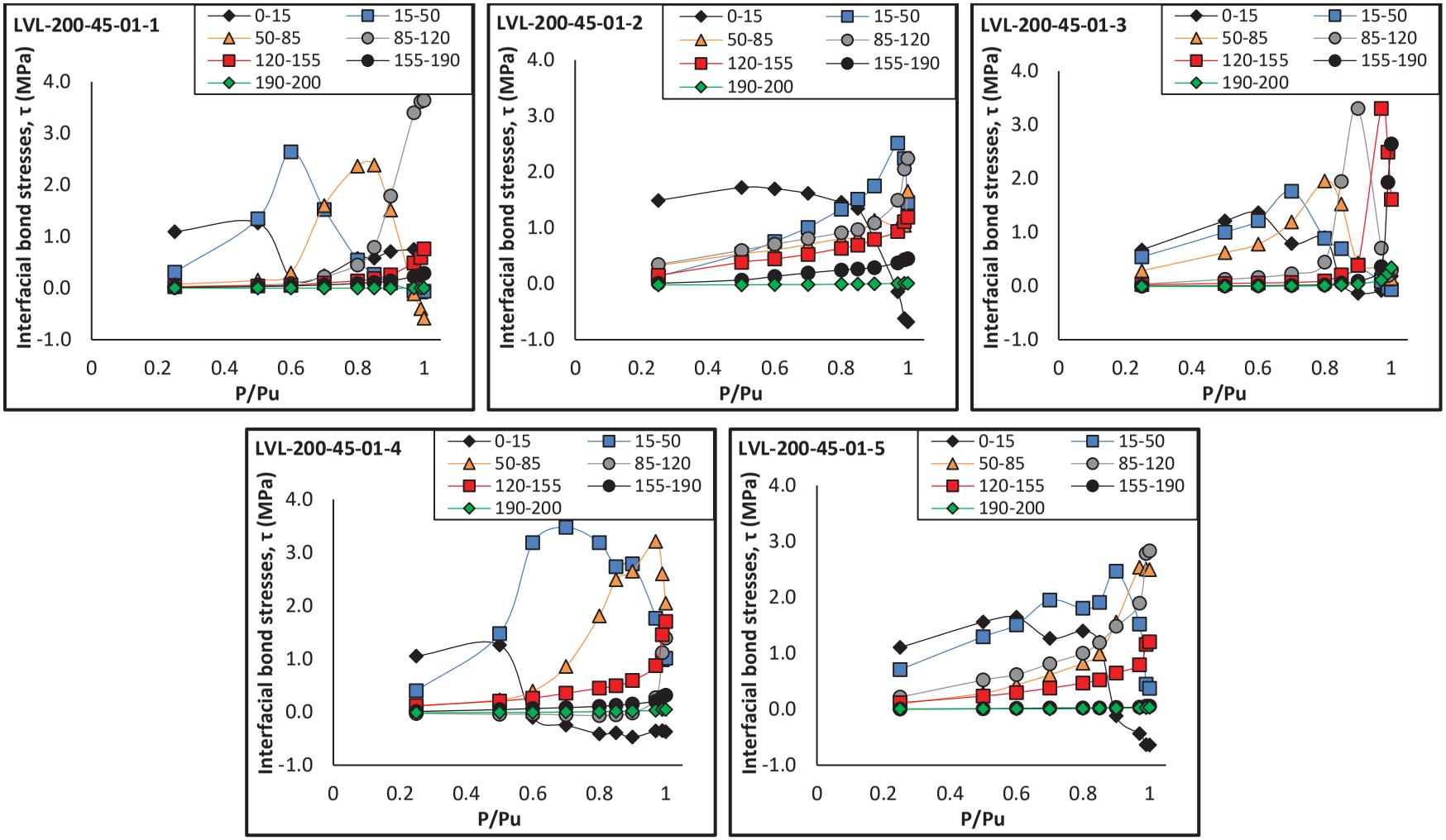
LVL-200-45-01-1
LVL-200-45-01-2
LVL-200-45-01-3
LVL-200-45-01-4
LVL-200-45-01-5
0-15
15-50
50-85
85-120
120-155
155-190
190-200
Interfacial bond stresses, τ (MPa)
P/Pu
4.0
3.0
2.0
1.0
0.0
-1.0
0
0.2
0.4
0.6
0.8
1

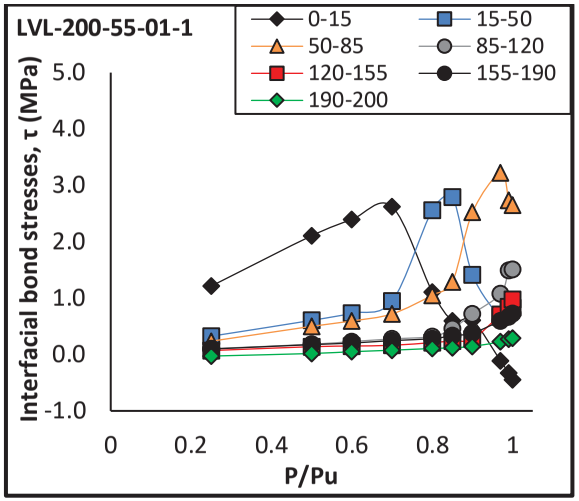
LVL-200-55-01-1
0-15
15-50
50-85
85-120
120-155
155-190
190-200
Interfacial bond stresses, τ (MPa)
5.0
4.0
3.0
2.0
1.0
0.0
-1.0
0
0.2
0.4
0.6
0.8
1
P/Pu

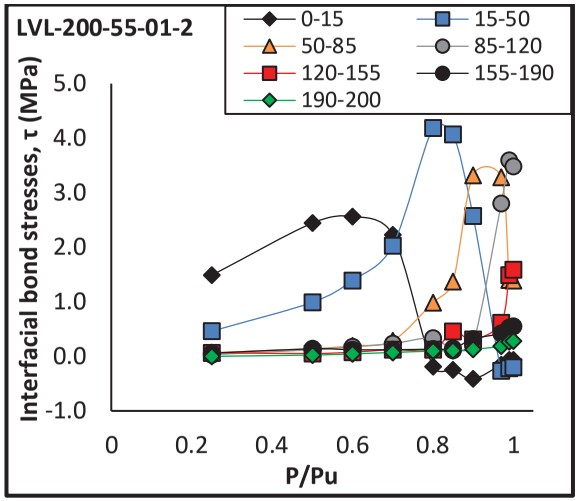
LVL-200-55-01-2
0-15
15-50
50-85
85-120
120-155
155-190
190-200
Interfacial bond stresses, τ (MPa)
5.0
4.0
3.0
2.0
1.0
0.0
-1.0
0
0.2
0.4
0.6
0.8
1
P/Pu

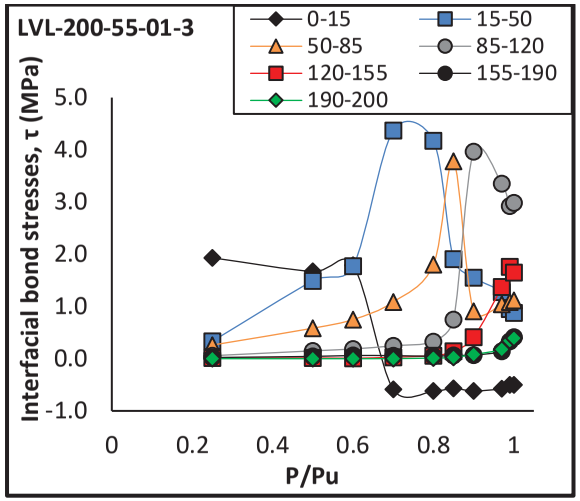
LVL-200-55-01-3
0-15
15-50
50-85
85-120
120-155
155-190
190-200
Interfacial bond stresses, τ (MPa)
5.0
4.0
3.0
2.0
1.0
0.0
-1.0
0
0.2
0.4
0.6
0.8
1
P/Pu

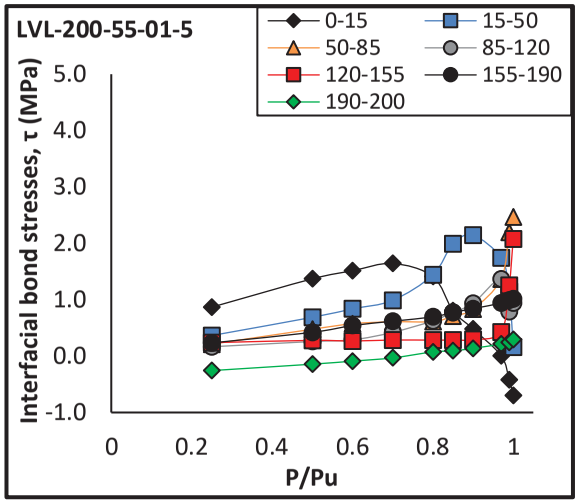
LVL-200-55-01-5
0-15
15-50
50-85
85-120
120-155
155-190
190-200
Interfacial bond stresses, τ (MPa)
5.0
4.0
3.0
2.0
1.0
0.0
-1.0
0
0.2
0.4
0.6
0.8
1
P/Pu

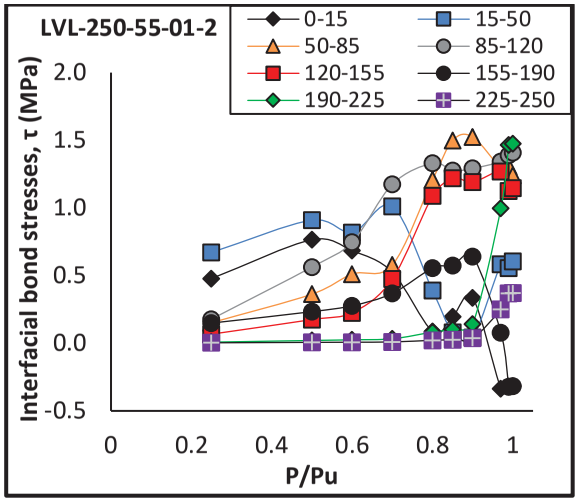
LVL-250-55-01-2
0-15
15-50
50-85
85-120
120-155
155-190
190-225
225-250
Interfacial bond stresses, τ (MPa)
2.0
1.5
1.0
0.5
0.0
-0.5
0
0.2
0.4
0.6
0.8
1
P/Pu

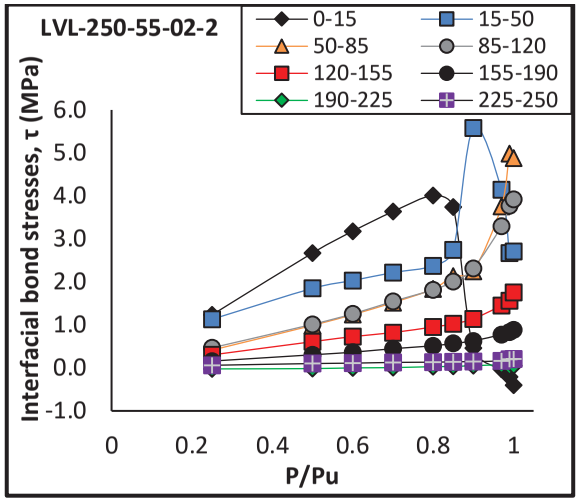
LVL-250-55-02-2
0-15
15-50
50-85
85-120
120-155
155-190
190-225
225-250
Interfacial bond stresses, τ (MPa)
6.0
5.0
4.0
3.0
2.0
1.0
0.0
-1.0
0
0.2
0.4
0.6
0.8
1
P/Pu

Appendix J.

Photos of tested specimens – FRP-to-timber joints – LVL Series


50-35-01-1


50-35-01-2


50-35-01-3


50-35-01-4


50-35-01-5


50-35-02-1


50-35-02-2


50-35-02-3


50-35-02-4


50-35-02-5


50-45-01-1


50-45-01-2


50-45-01-3


50-45-01-4


50-45-01-5


50-55-01-1


50-55-01-2


50-55-01-3


50-55-01-4


50-55-01-5


100-35-01-1


100-35-01-2


100-35-01-3


100-35-01-4


100-35-01-5


100-35-02-1


100-35-02-2


100-35-02-3


100-35-02-4


100-35-02-5


100-45-01-1


100-45-01-2


100-45-01-3


100-45-01-4


100-45-01-5


100-55-01-1


100-55-01-2


100-55-01-3


100-55-01-4


100-55-01-5


150-35-01-1


150-35-01-2


150-35-01-3


150-35-01-4


150-35-01-5


150-35-02-1


150-35-02-2


150-35-02-3


150-35-02-4


150-35-02-4


150-45-01-1


150-45-01-2


150-45-01-3


150-45-01-4


150-45-01-5


150-45-02-1


150-45-02-2


150-45-02-3


150-45-02-4


150-45-02-5


150-55-01-1


150-55-01-3


150-55-01-4


150-55-01-5


150-55-02-1


150-55-02-2


150-55-02-3


150-55-02-4


150-55-02-5


200-35-01-1


200-35-01-2


200-35-01-3


200-35-01-4


200-35-01-5


200-35-02-2


200-35-02-3


200-35-02-4


200-35-02-5


200-45-01-1


200-45-01-2


200-45-01-3


200-45-01-4


200-55-01-1


200-55-01-2


200-55-01-3


200-55-01-4


250-55-01-2


250-55-01-3


250-55-02-1


250-55-02-3

Appendix K.

Photos of tested specimens – FRP-to-timber joints – Hardwood Series


50-45-01-1


50-45-01-2


50-45-01-3


50-45-01-4


50-45-01-5


50-45-02-1


50-45-02-2


50-45-02-3


50-45-02-4


50-45-02-5


100-45-01-1


100-45-01-2


100-45-01-3


100-45-01-4


100-45-01-5


100-45-02-1


100-45-02-2


100-45-02-3


100-45-02-4


100-45-02-5

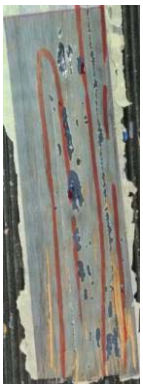
150-45-01-1


150-45-01-2

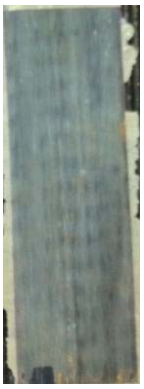
150-45-01-3


150-45-01-4


150-45-01-5


150-45-02-1


150-45-02-2


150-45-02-3


150-45-02-4


150-45-02-5


200-45-01-1


200-45-01-2


200-45-01-3


200-45-01-4


200-45-01-5


200-45-02-1


200-45-02-2


200-45-02-3


200-45-02-4


200-45-02-5

Appendix L.

Material properties – FRP to timber beams

Table F-1 Compression parallel to grain

Samples	P_u (kN)	Compressive Strength (MPa)	MOE (GPa)	Poisson Ratio
C1	162.28	40.07	--	--
C2	166.60	41.14	15.04	--
C3	166.63	41.14	12.08	0.3
Average	165.17	40.78	13.56	0.3
CoV (%)	1.52%	1.52%	15.43%	--

Table F-2 Compression perpendicular to grain

Samples	$f_{c,90,max}$ (kN)	Compressive Strength (MPa)	MOE (GPa)
CP1	8.34	1.65	--
CP2	7.95	1.81	0.46
CP3	9.12	2.01	0.44
Average	8.47	1.89	0.45
CoV (%)	7.02%	9.91%	2.23%

Table F-3 Tension parallel to grain

Samples	P_u (kN)	Tensile Strength (MPa)	MOE (GPa)
T1	106.34	26.26	--
T2	92.65	22.88	18.22
T3	119.59	29.53	14.53
Average	106.19	26.22	16.38
CoV (%)	12.69%	12.69%	15.91%

Table F-4 FRP tensile test results

Samples	Tensile Strength (MPa)	MOE (GPa)	Ultimate Strain
1	2664	224	0.013
2	2628	261	0.011
3	2718	235	0.013
4	2819	238	0.008
5	2416	267	0.012
Average	2649	245	0.011
CoV (%)	5.62%	7.38%	18.09%

CoV: co-efficient of variation.

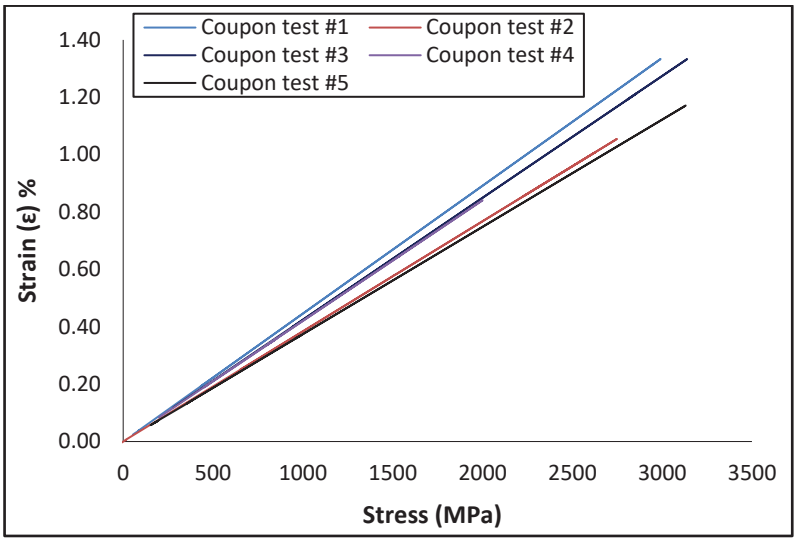

Figure F-8-1 FRP coupon test specimens and results

Appendix M.

Beam test results- Strains in the FRP sheets

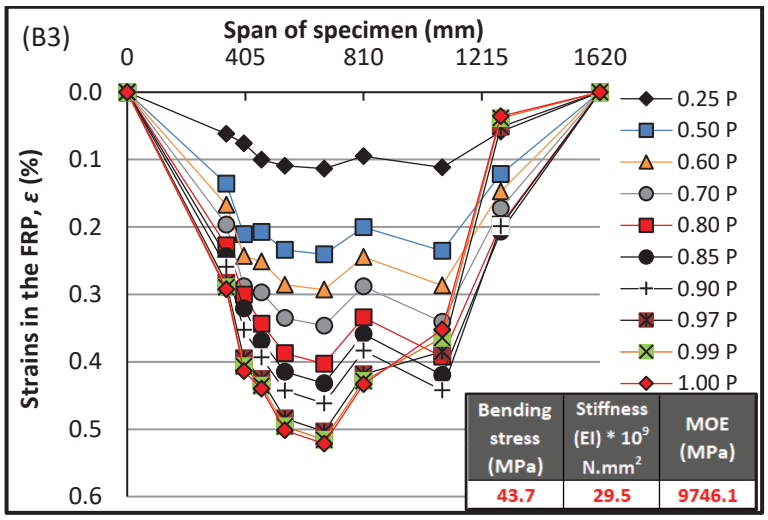

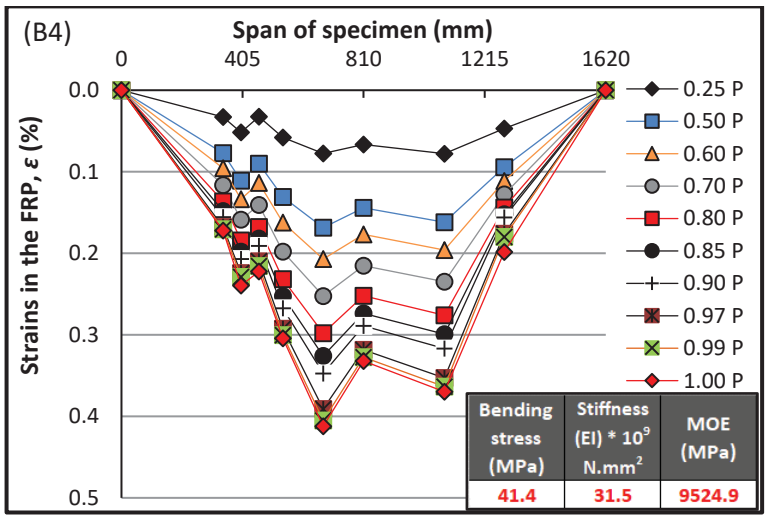

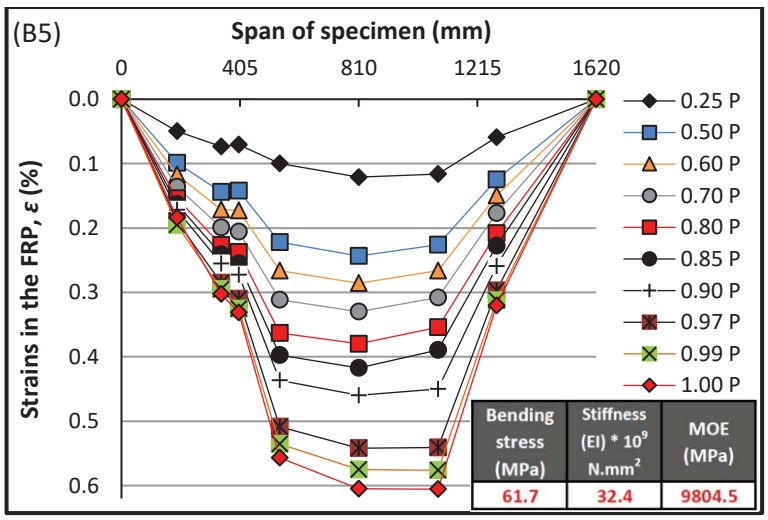

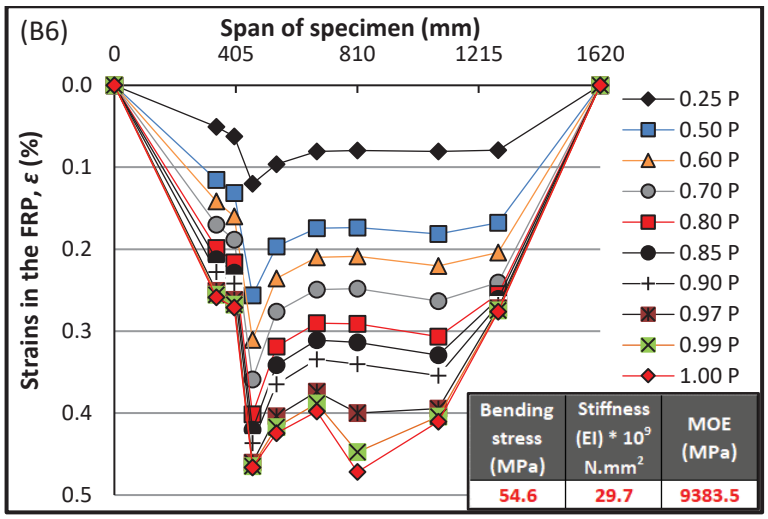
(B6)
Span of specimen (mm)
0
405
810
1215
1620
0.0
0.1
0.2
0.3
0.4
0.5
Strains in the FRP, ε (%)
0.25 P
0.50 P
0.60 P
0.70 P
0.80 P
0.85 P
0.90 P
0.97 P
0.99 P
1.00 P
Bending stress (MPa)
Stiffness (EI) * 10^9 N.mm^2
MOE (MPa)
54.6
29.7
9383.5

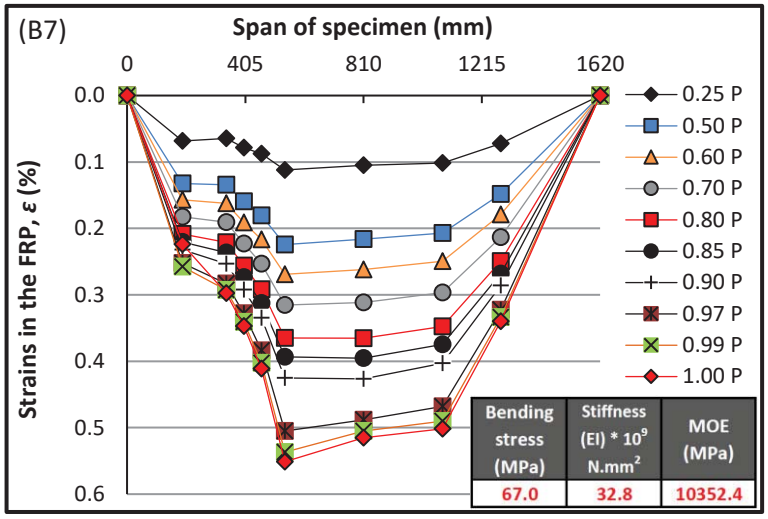
(B7)
Span of specimen (mm)
0
405
810
1215
1620
0.0
0.1
0.2
0.3
0.4
0.5
0.6
Strains in the FRP, ε (%)
0.25 P
0.50 P
0.60 P
0.70 P
0.80 P
0.85 P
0.90 P
0.97 P
0.99 P
1.00 P
Bending stress (MPa)
Stiffness (EI) * 10^9 N.mm^2
MOE (MPa)
67.0
32.8
10352.4

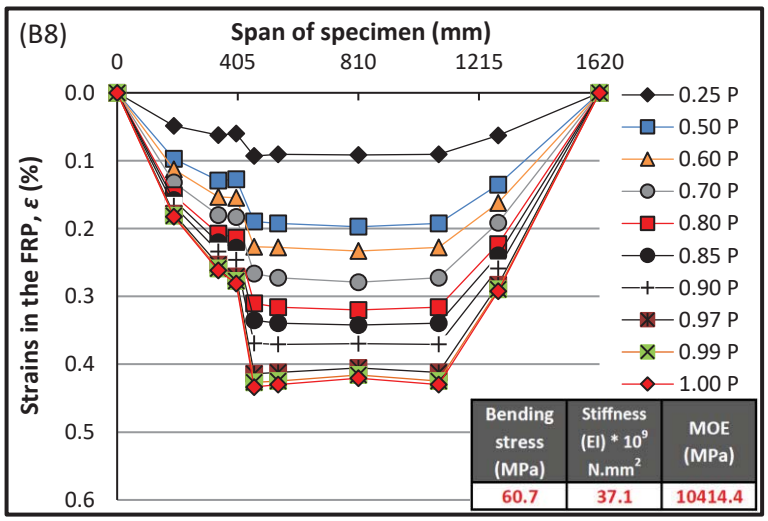
(B8)
Span of specimen (mm)
0
405
810
1215
1620
0.0
0.1
0.2
0.3
0.4
0.5
0.6
Strains in the FRP, ε (%)
0.25 P
0.50 P
0.60 P
0.70 P
0.80 P
0.85 P
0.90 P
0.97 P
0.99 P
1.00 P
Bending stress (MPa)
Stiffness (EI) * 10^9 N.mm^2
MOE (MPa)
60.7
37.1
10414.4

Appendix N.

Beam test results- Shear stress in the interface

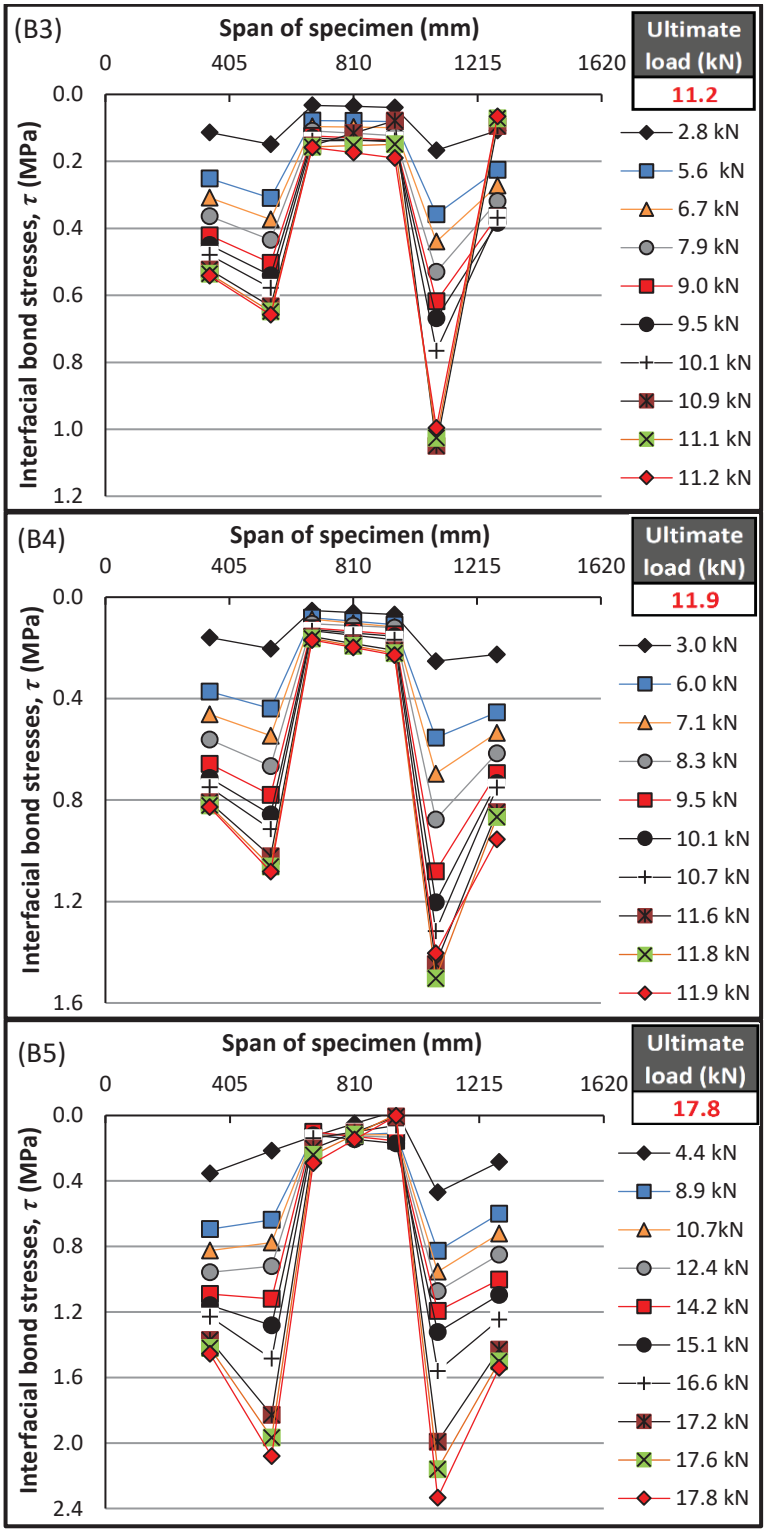

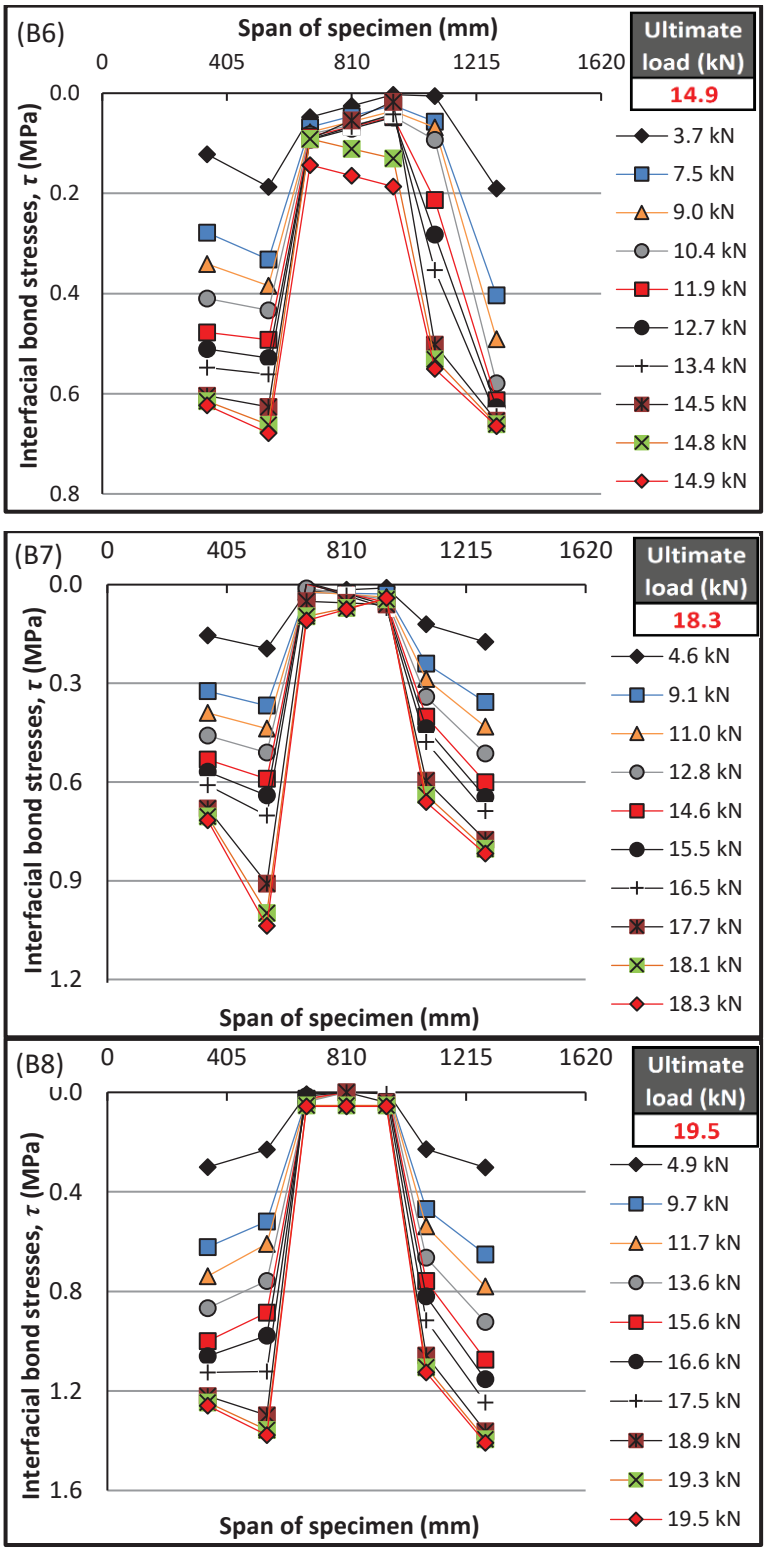
(B6)
Span of specimen (mm)
0
405
810
1215
1620
Ultimate load (kN)
14.9
Interfacial bond stresses, τ (MPa)
0.0
0.2
0.4
0.6
0.8
3.7 kN
7.5 kN
9.0 kN
10.4 kN
11.9 kN
12.7 kN
13.4 kN
14.5 kN
14.8 kN
14.9 kN
(B7)
0
405
810
1215
1620
Ultimate load (kN)
18.3
Interfacial bond stresses, τ (MPa)
0.0
0.3
0.6
0.9
1.2
4.6 kN
9.1 kN
11.0 kN
12.8 kN
14.6 kN
15.5 kN
16.5 kN
17.7 kN
18.1 kN
18.3 kN
Span of specimen (mm)
(B8)
0
405
810
1215
1620
Ultimate load (kN)
19.5
Interfacial bond stresses, τ (MPa)
0.0
0.4
0.8
1.2
1.6
4.9 kN
9.7 kN
11.7 kN
13.6 kN
15.6 kN
16.6 kN
17.5 kN
18.9 kN
19.3 kN
19.5 kN
Span of specimen (mm)

Numerical results FRP-to-LVL series - shear stress

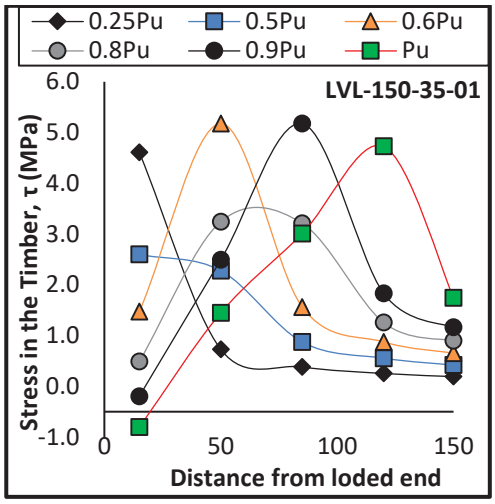

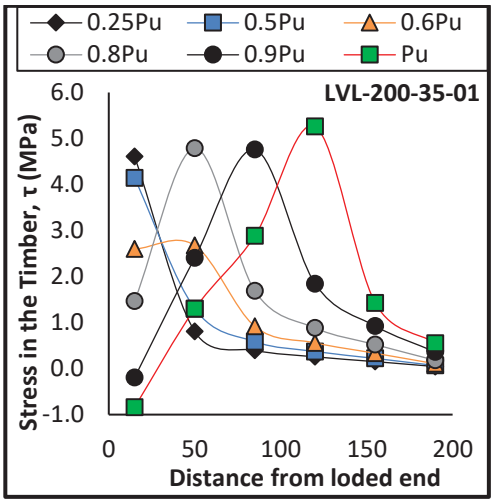

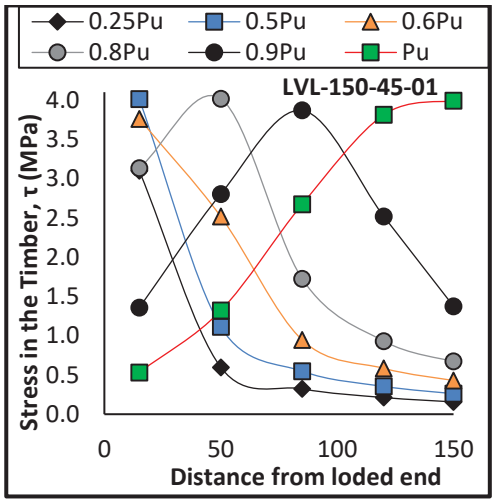

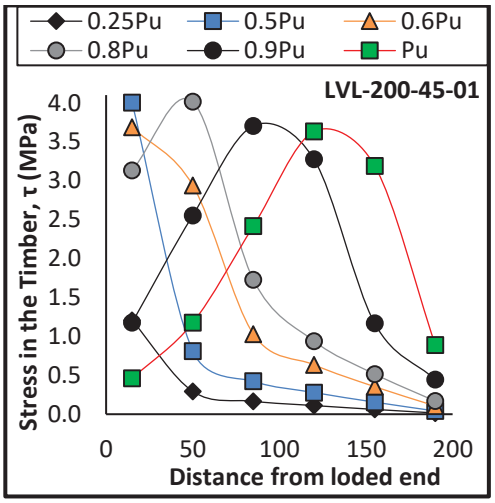

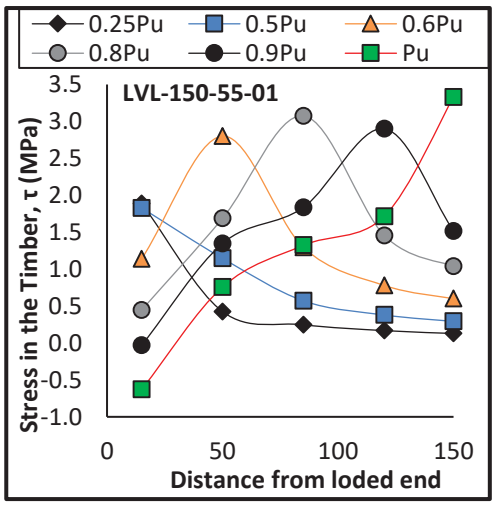

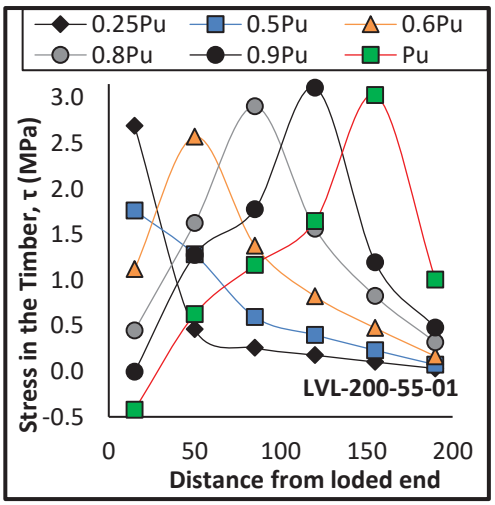

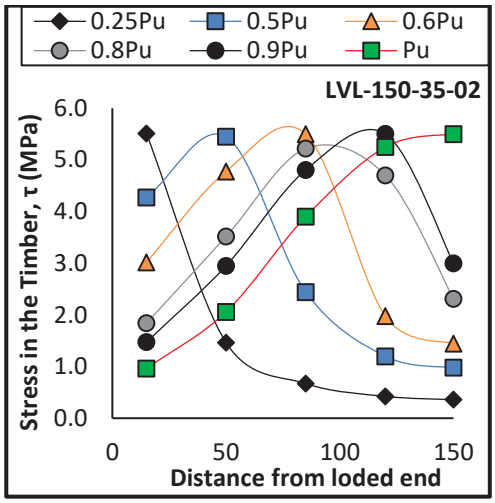
0.25Pu
0.5Pu
0.6Pu
0.8Pu
0.9Pu
Pu
LVL-150-35-02
Stress in the Timber, τ (MPa)
6.0
5.0
4.0
3.0
2.0
1.0
0.0
0
50
100
150
Distance from loded end

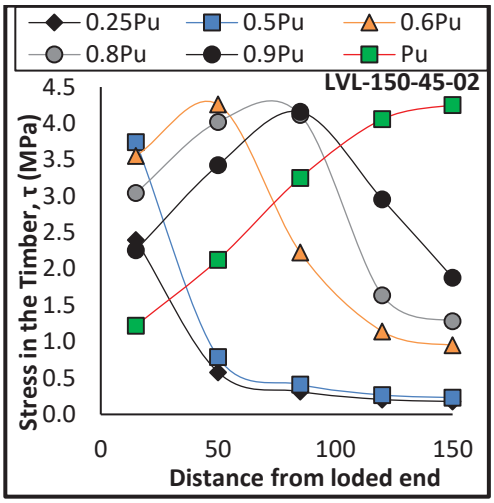
0.25Pu
0.5Pu
0.6Pu
0.8Pu
0.9Pu
Pu
LVL-150-45-02
Stress in the Timber, τ (MPa)
4.5
4.0
3.5
3.0
2.5
2.0
1.5
1.0
0.5
0.0
0
50
100
150
Distance from loded end

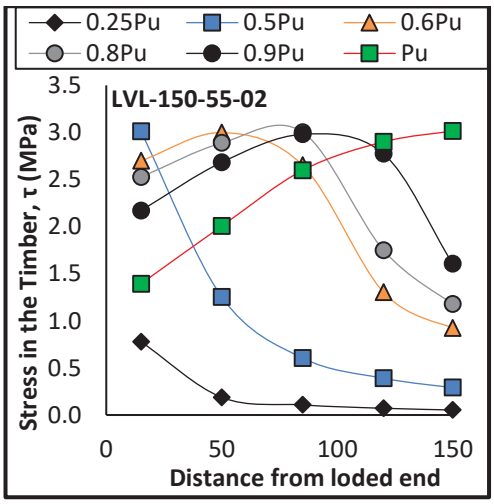
0.25Pu
0.5Pu
0.6Pu
0.8Pu
0.9Pu
Pu
LVL-150-55-02
Stress in the Timber, τ (MPa)
3.5
3.0
2.5
2.0
1.5
1.0
0.5
0.0
0
50
100
150
Distance from loded end

Appendix P.

Numerical results FRP-to-LVL series - strain distribution

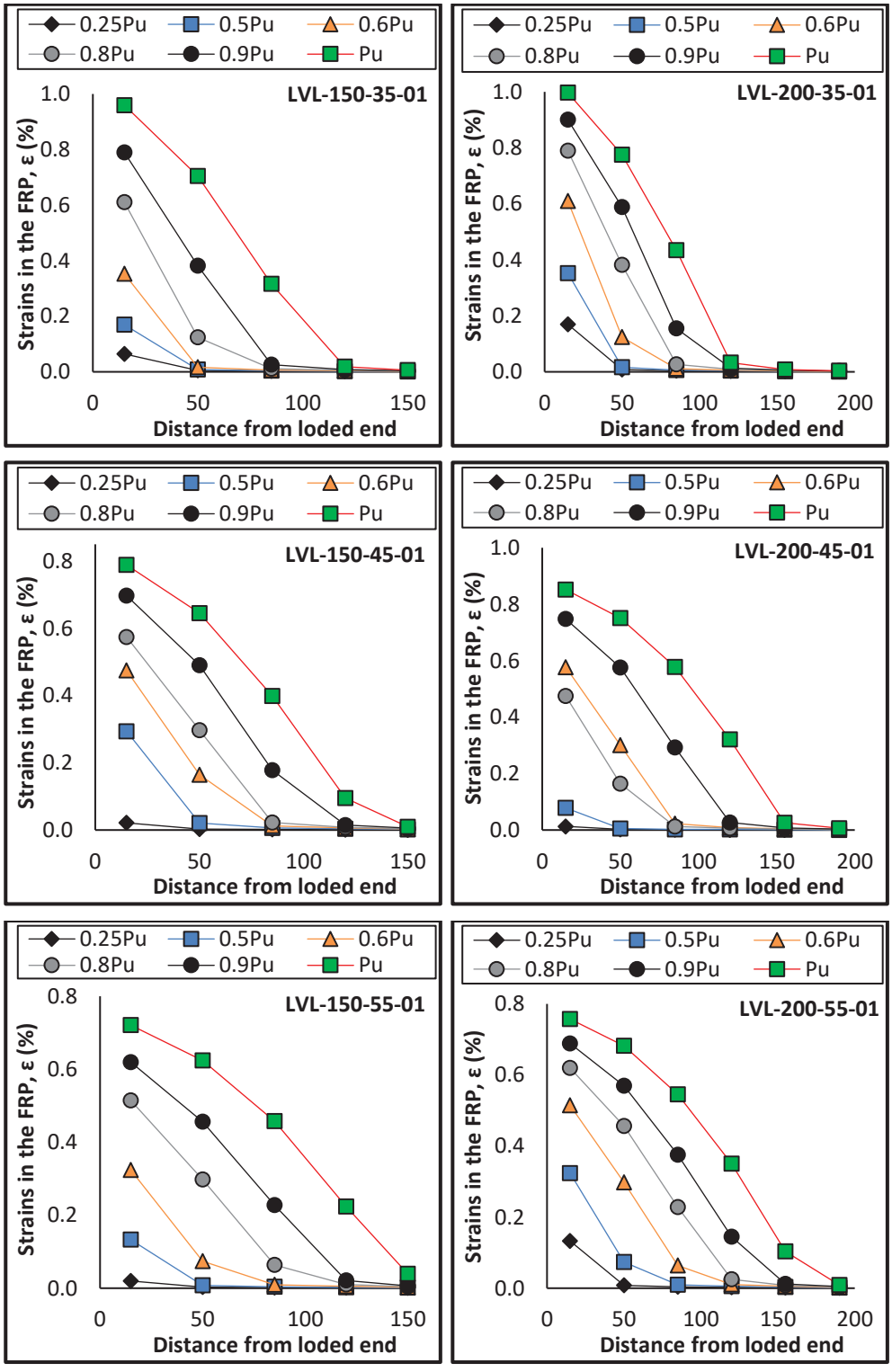

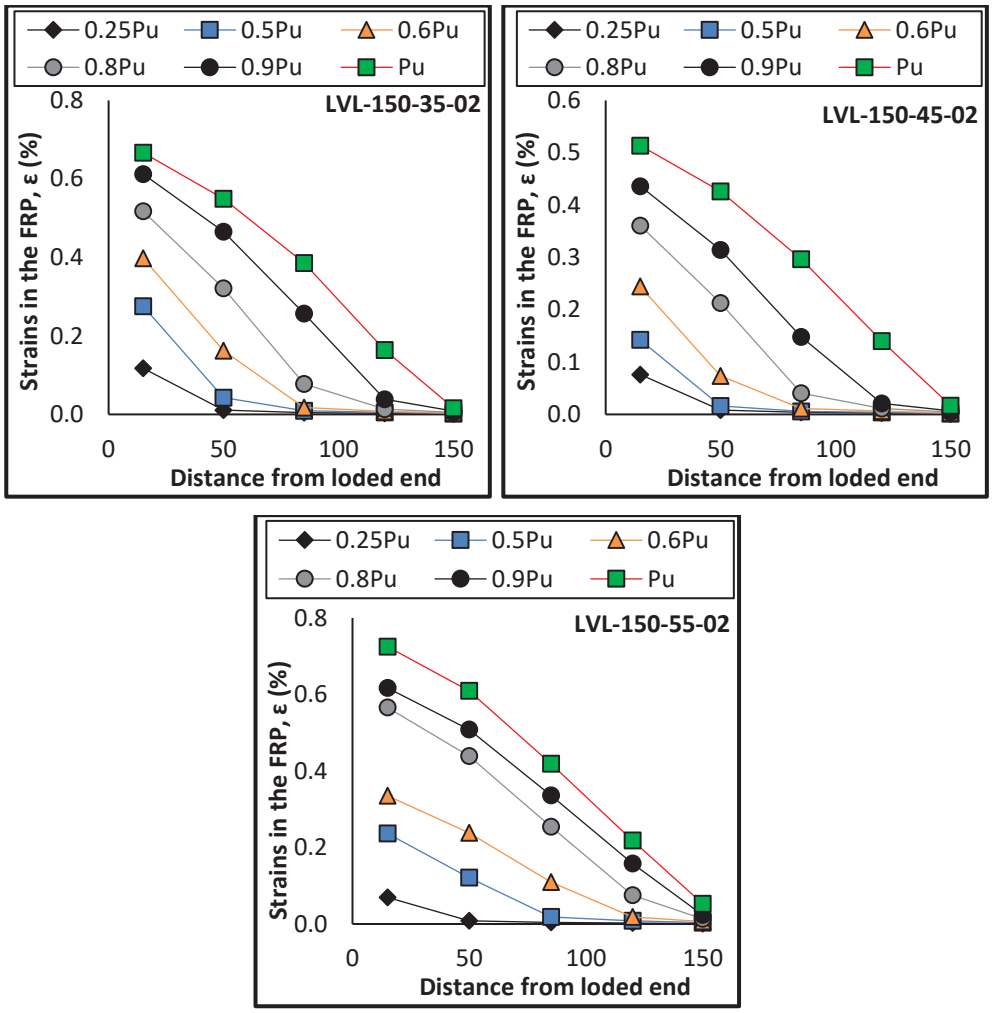
0.25Pu
0.5Pu
0.6Pu
0.8Pu
0.9Pu
Pu
LVL-150-35-02
Strains in the FRP, ε (%)
Distance from loded end
LVL-150-45-02
LVL-150-55-02

Appendix Q.

Numerical results FRP-to-Hardwood series - shear stress

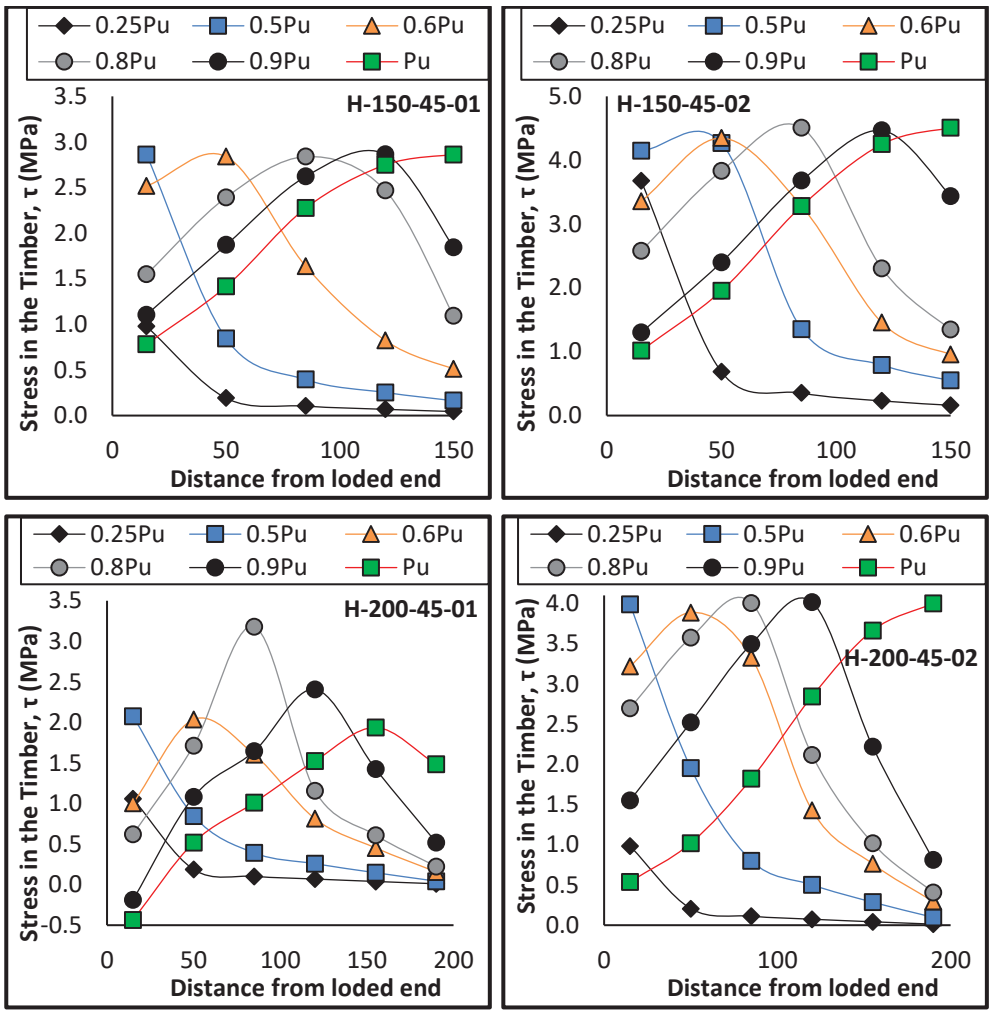

Appendix R.

Numerical results FRP-to- Hardwood series - strain distribution

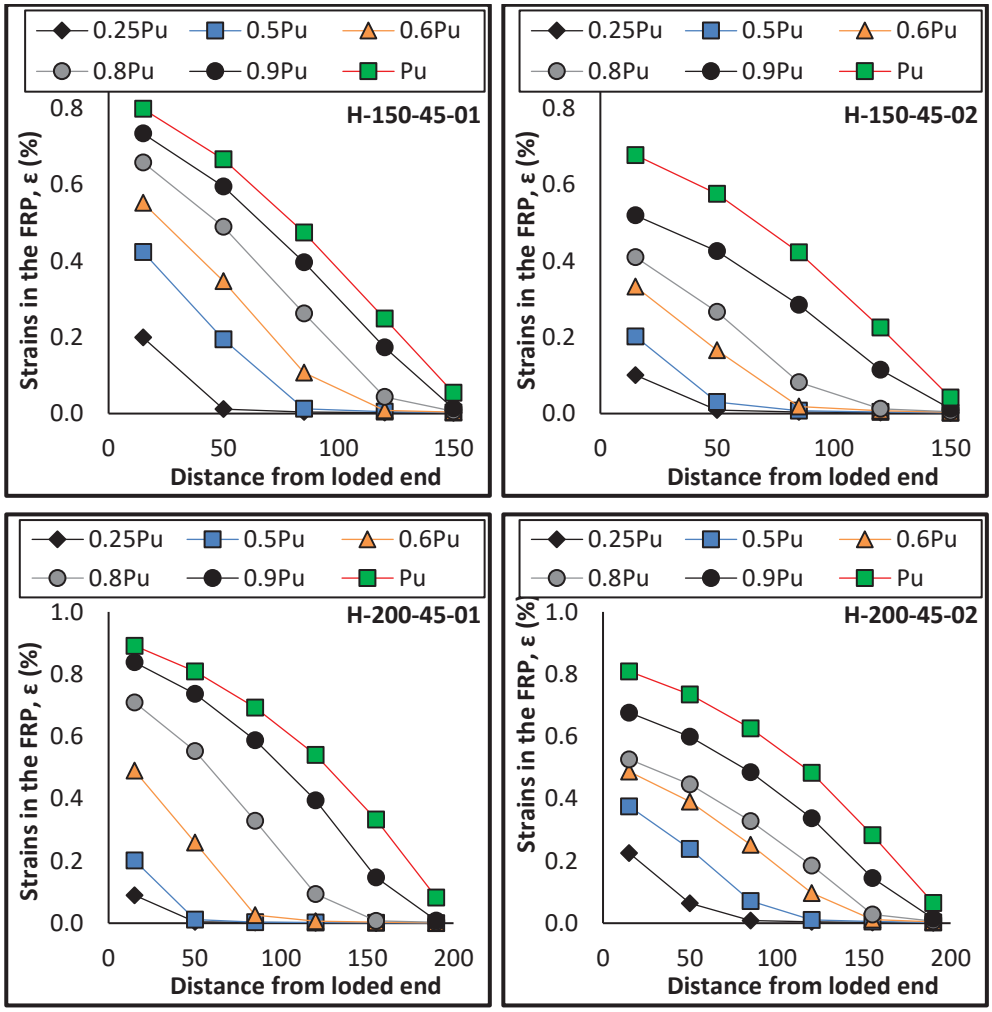

Appendix S.

Numerical simulation, FRP-to-LVL Series; Stress distributions

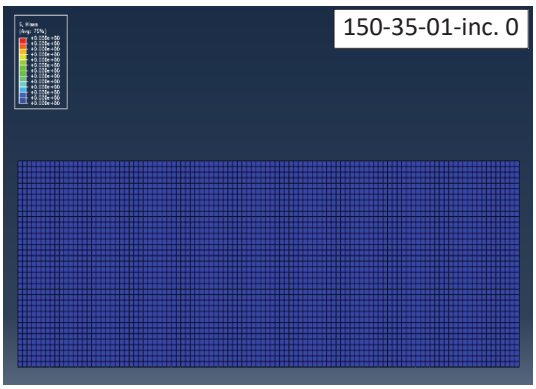

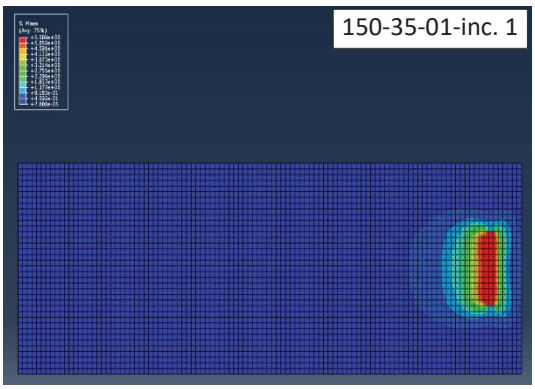

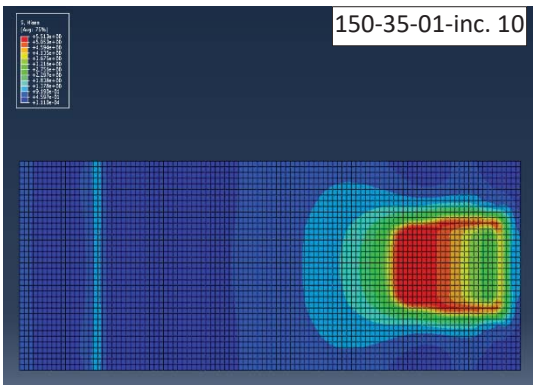

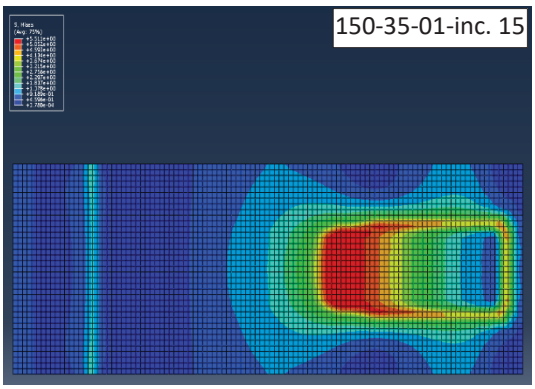

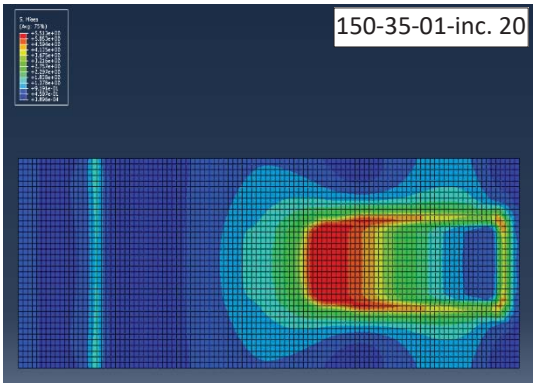

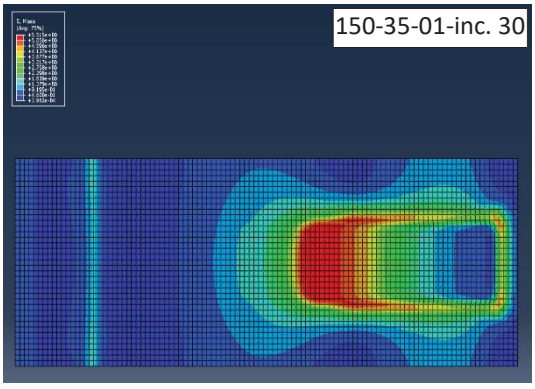

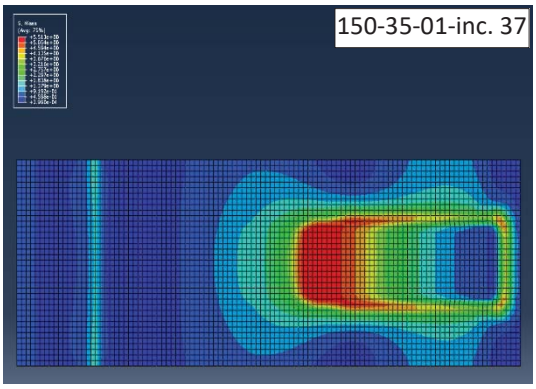

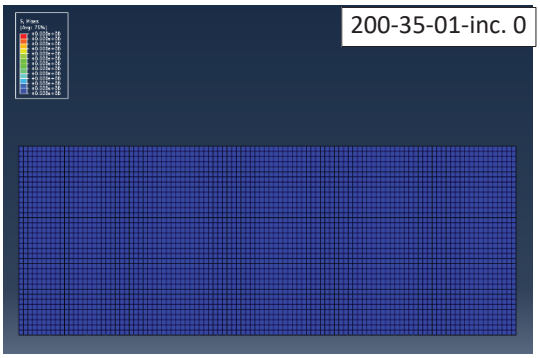
200-35-01-inc. 0

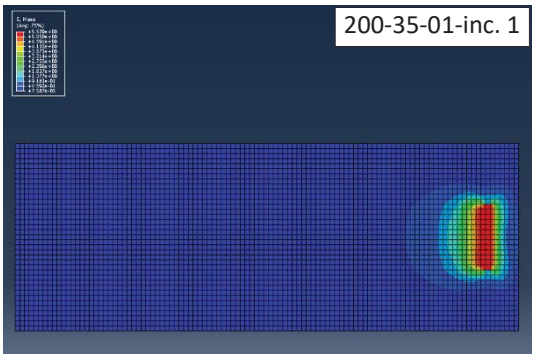
200-35-01-inc. 1

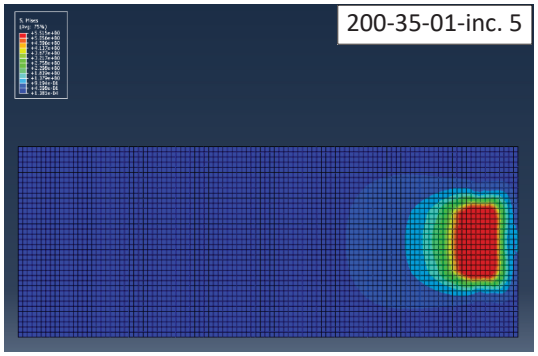
200-35-01-inc. 5

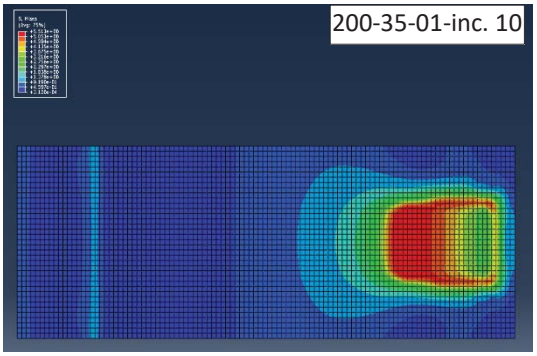
200-35-01-inc. 10

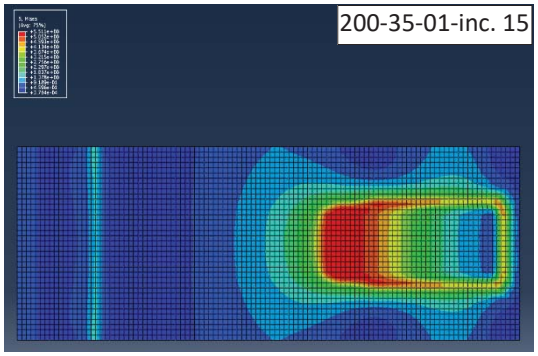
200-35-01-inc. 15

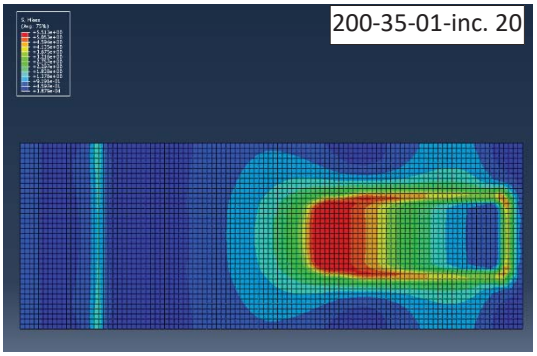
200-35-01-inc. 20

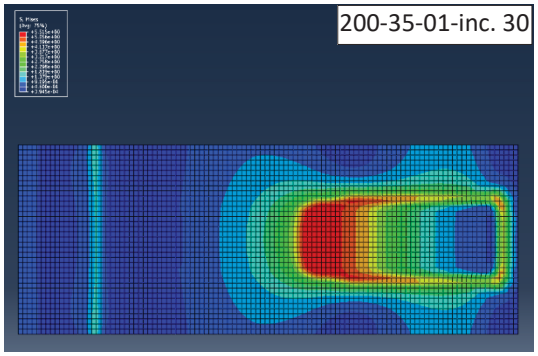
200-35-01-inc. 30

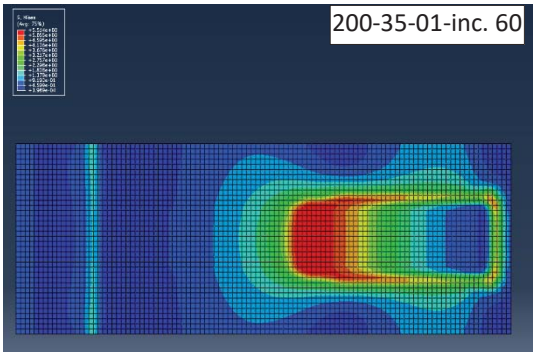
200-35-01-inc. 60

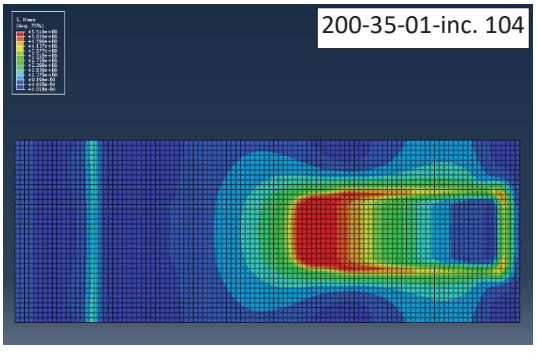
200-35-01-inc. 104

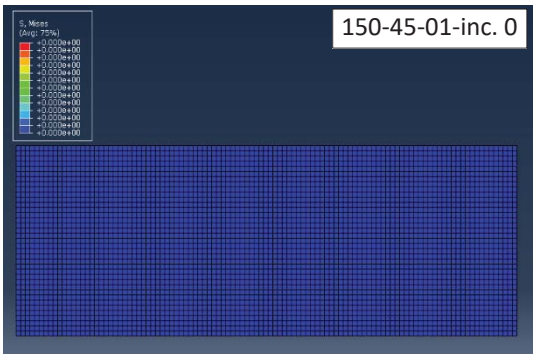
150-45-01-inc. 0

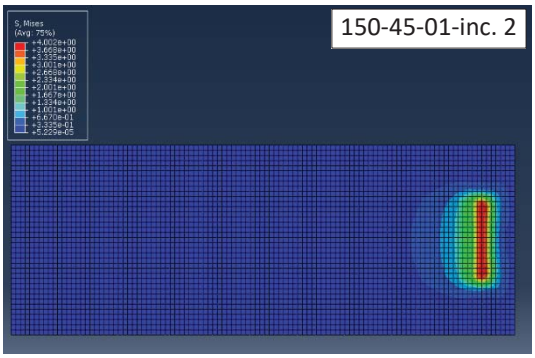
150-45-01-inc. 2

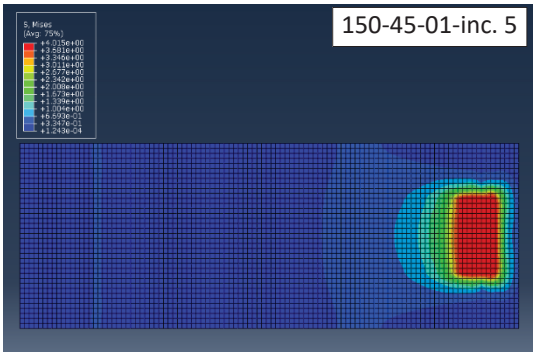
150-45-01-inc. 5

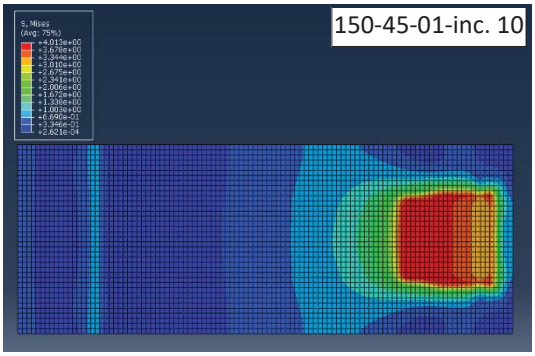
150-45-01-inc. 10

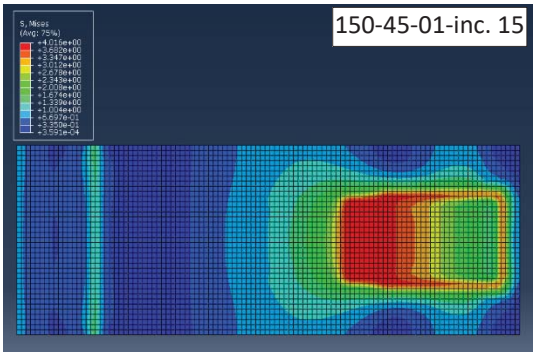
150-45-01-inc. 15

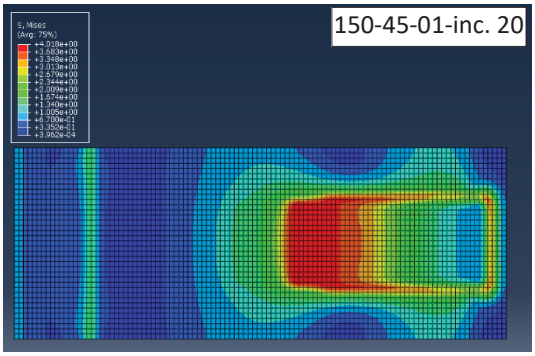
150-45-01-inc. 20

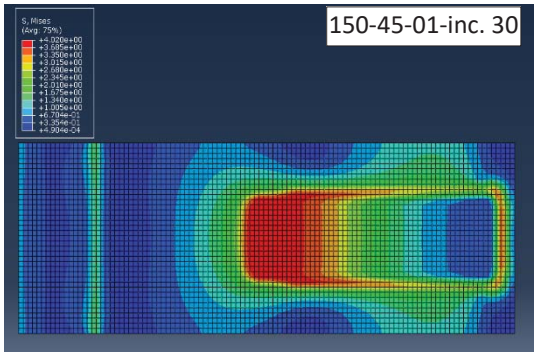
150-45-01-inc. 30

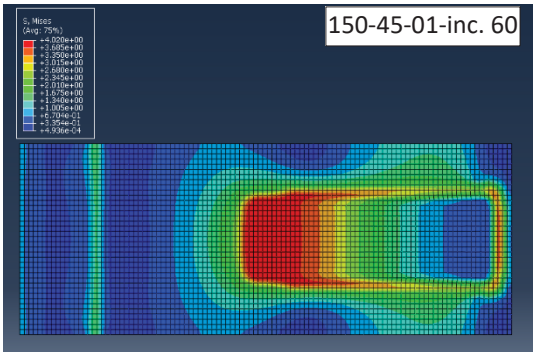
150-45-01-inc. 60

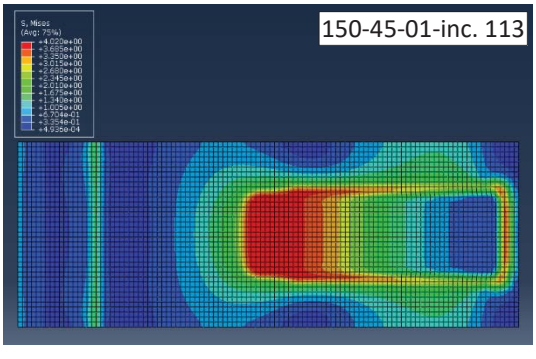
150-45-01-inc. 113

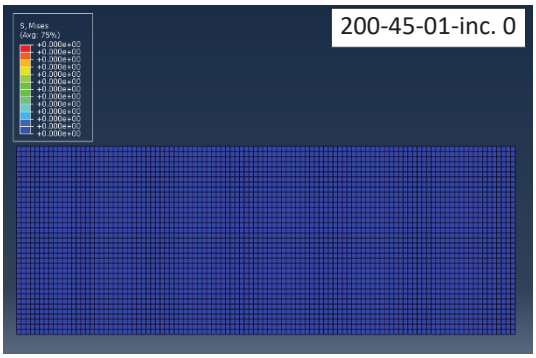
200-45-01-inc. 0

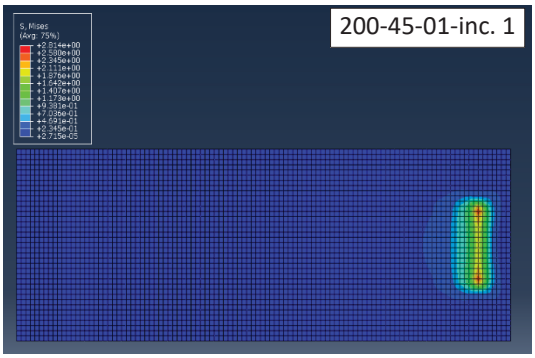
200-45-01-inc. 1

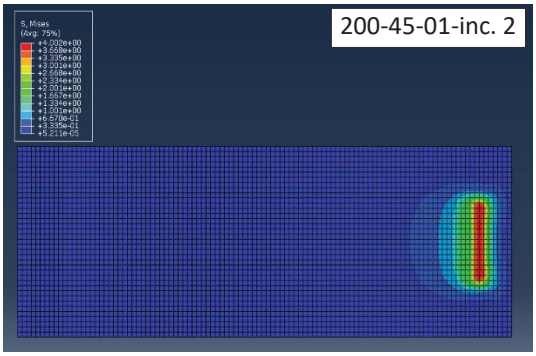
200-45-01-inc. 2

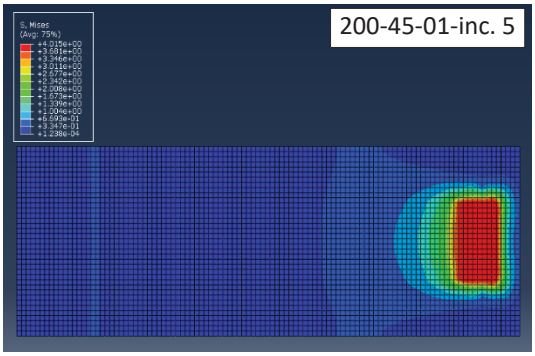
200-45-01-inc. 5

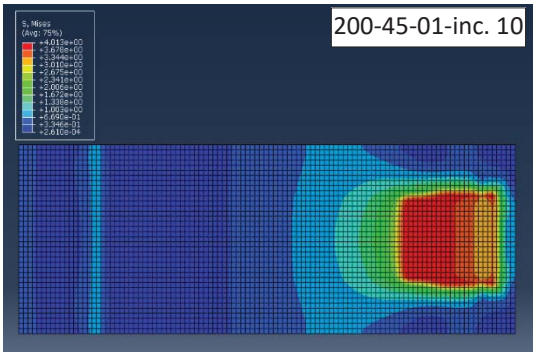
200-45-01-inc. 10

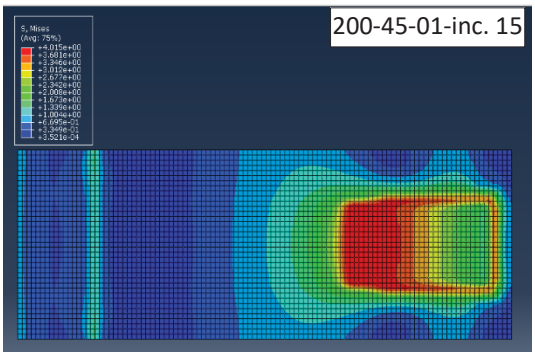
200-45-01-inc. 15

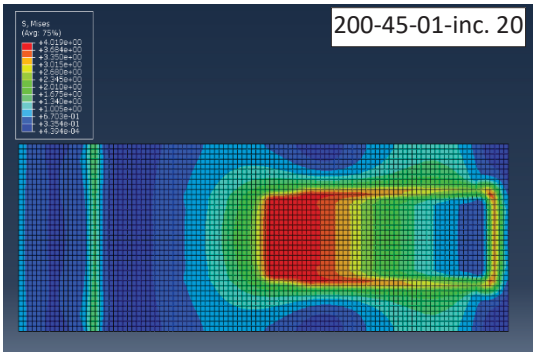
200-45-01-inc. 20

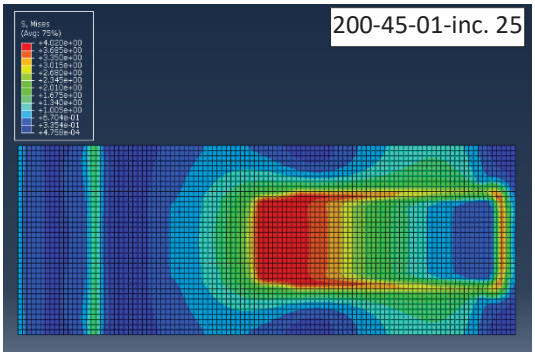
200-45-01-inc. 25

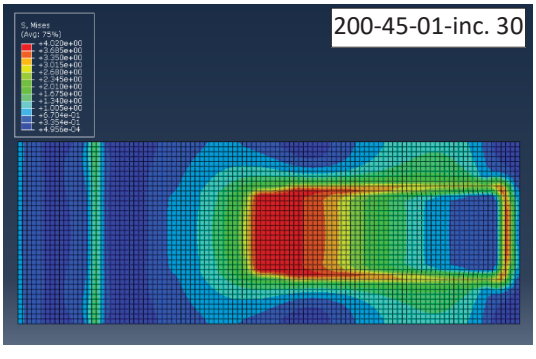
200-45-01-inc. 30

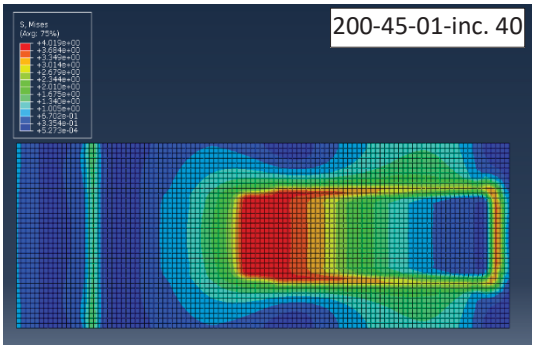
200-45-01-inc. 40

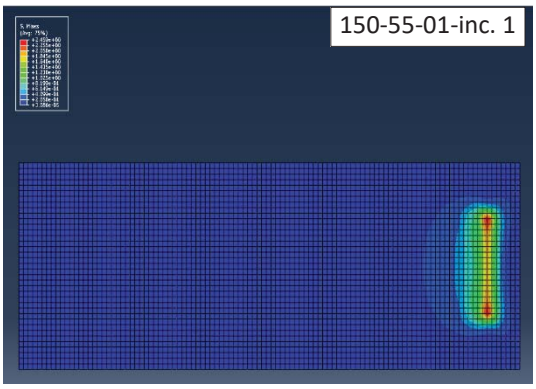
150-55-01-inc. 1

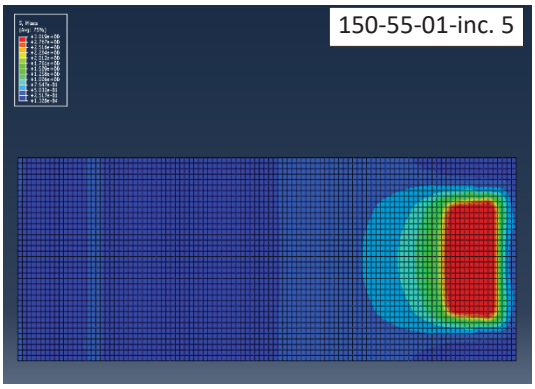
150-55-01-inc. 5

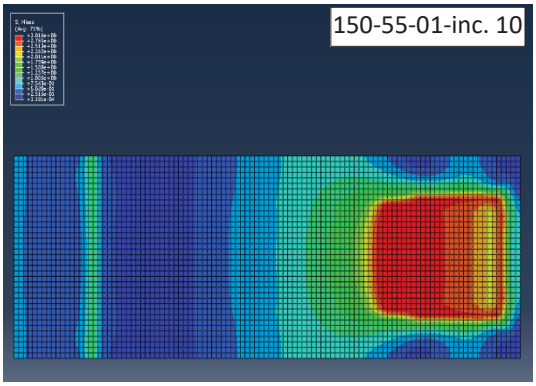
150-55-01-inc. 10

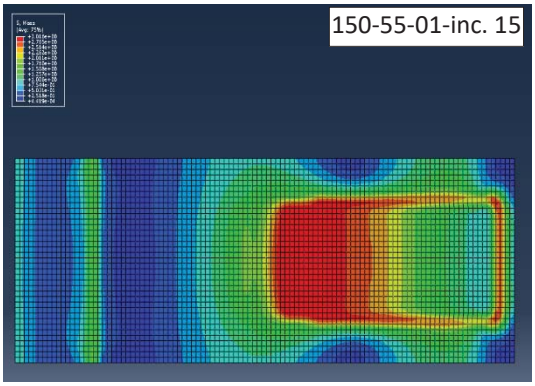
150-55-01-inc. 15

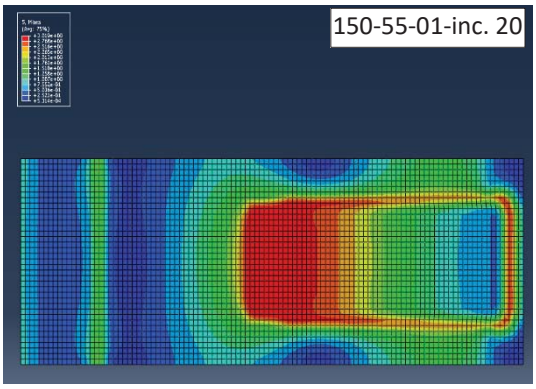
150-55-01-inc. 20

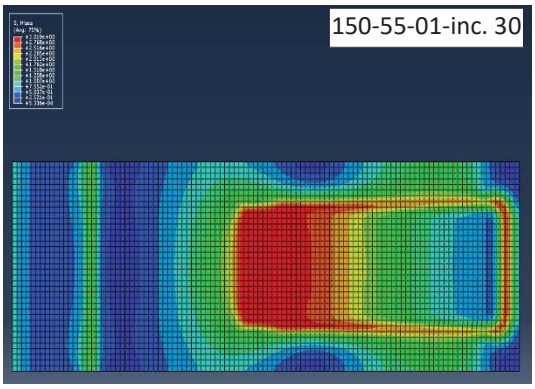
150-55-01-inc. 30

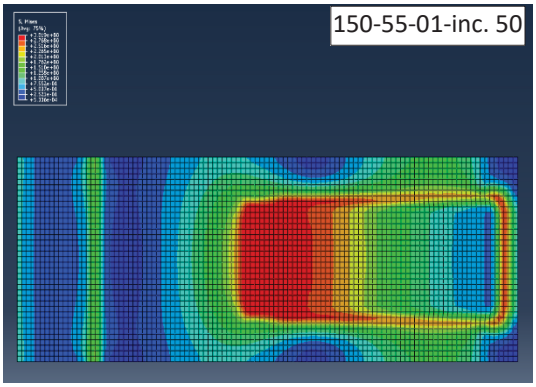
150-55-01-inc. 50

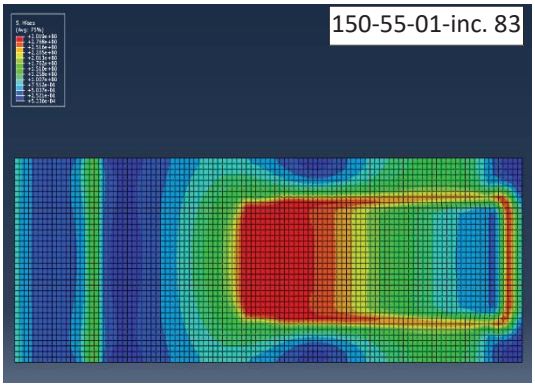
150-55-01-inc. 83

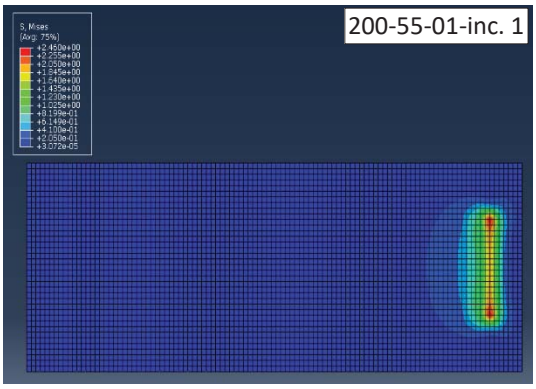
200-55-01-inc. 1

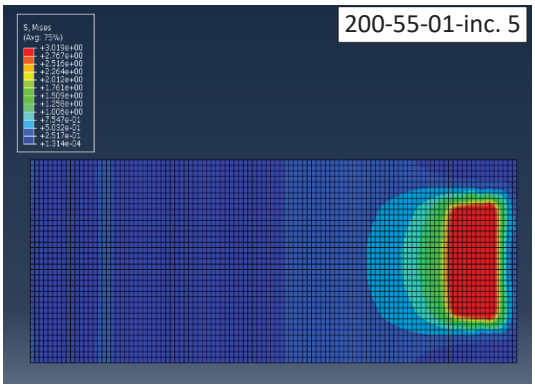
200-55-01-inc. 5

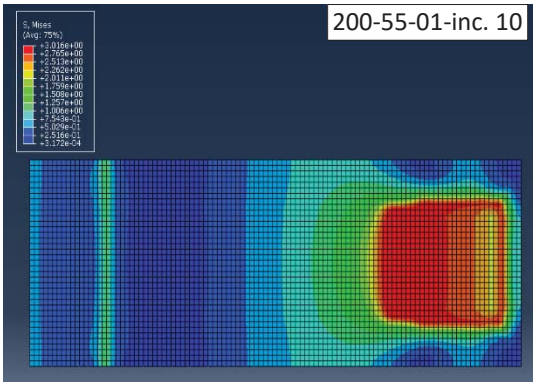
200-55-01-inc. 10

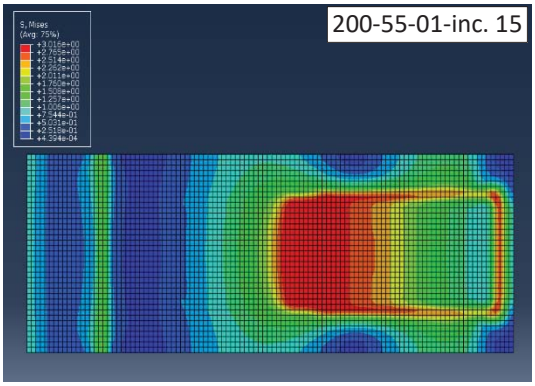
200-55-01-inc. 15

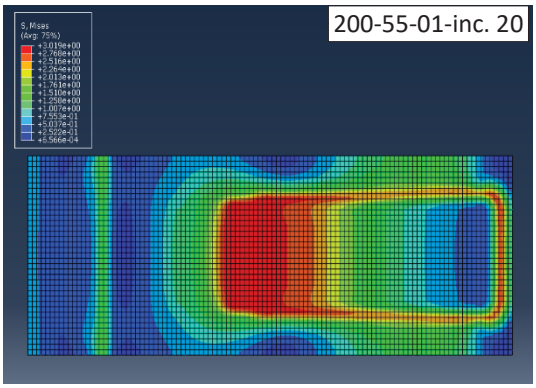
200-55-01-inc. 20

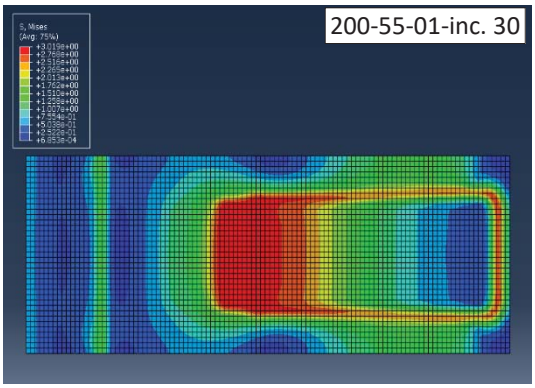
200-55-01-inc. 30

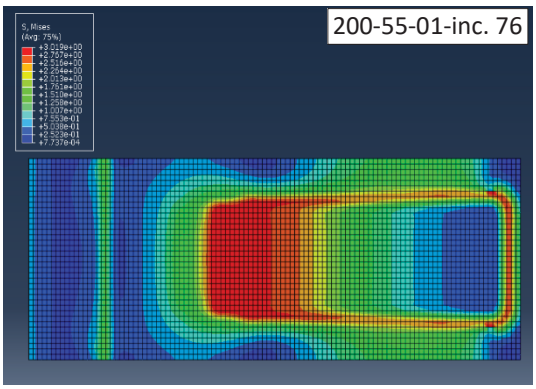
200-55-01-inc. 76

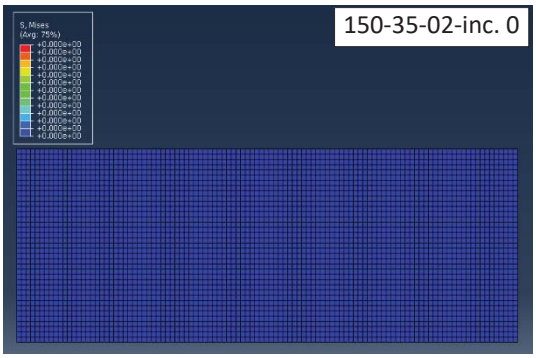
150-35-02-inc. 0

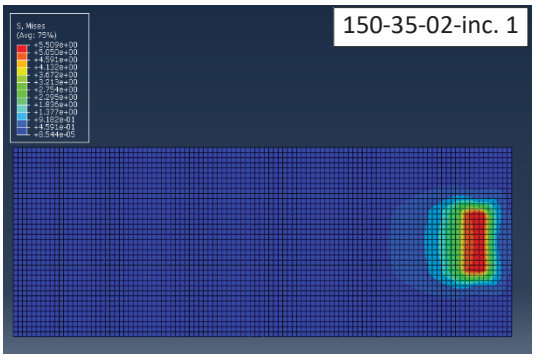
150-35-02-inc. 1

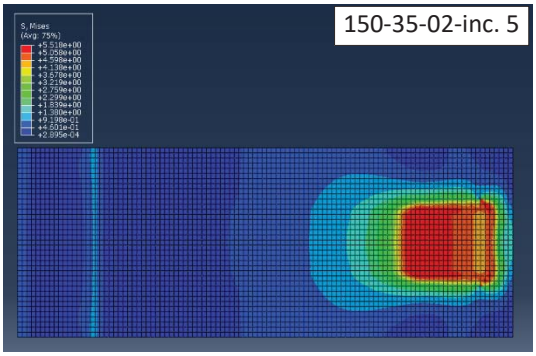
150-35-02-inc. 5

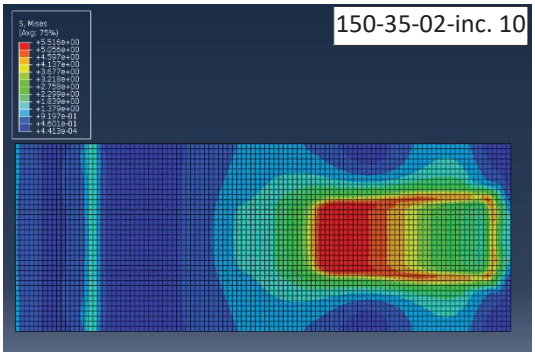
150-35-02-inc. 10

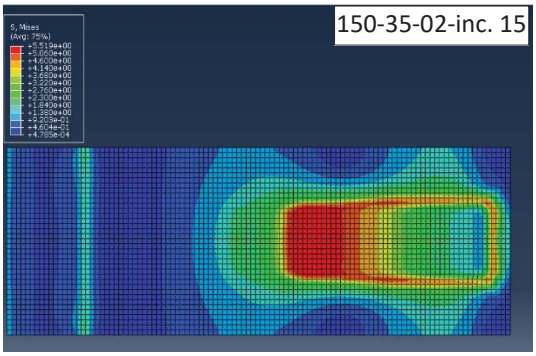
150-35-02-inc. 15

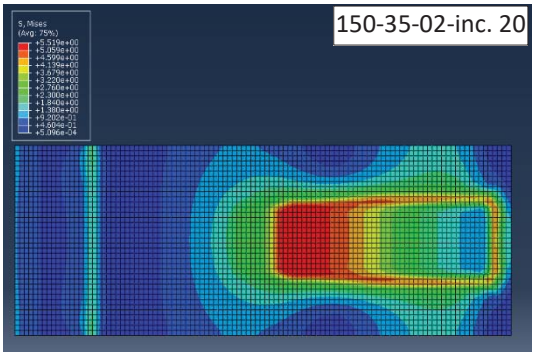
150-35-02-inc. 20

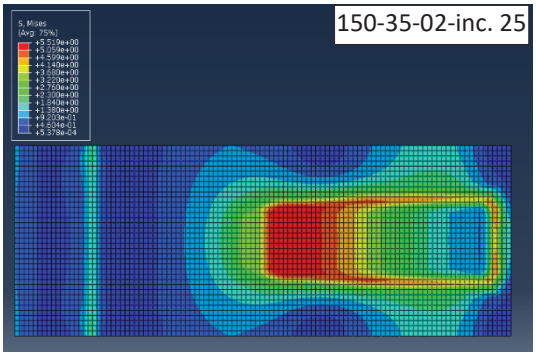
150-35-02-inc. 25

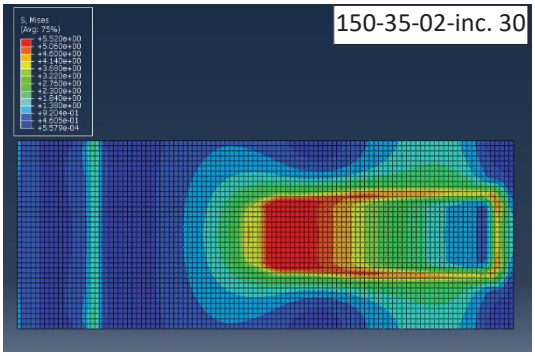
150-35-02-inc. 30

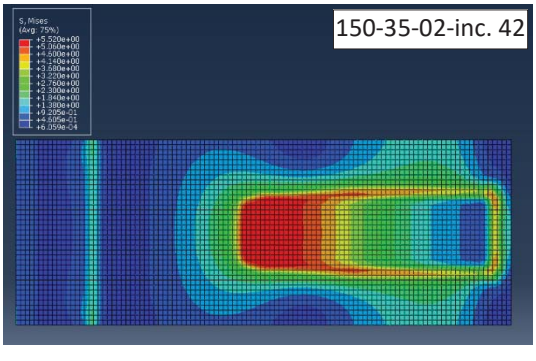
150-35-02-inc. 42

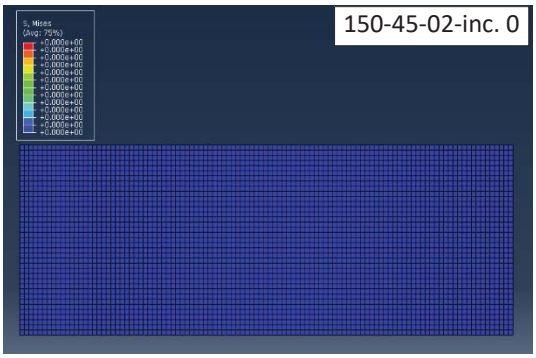
150-45-02-inc. 0

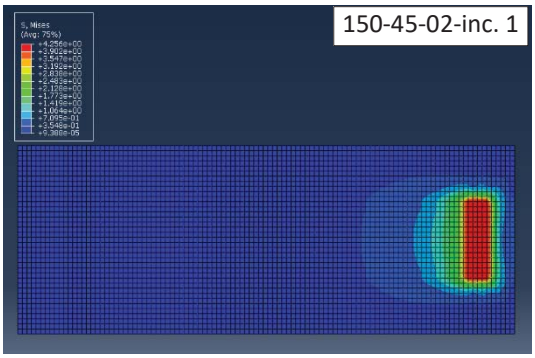
150-45-02-inc. 1

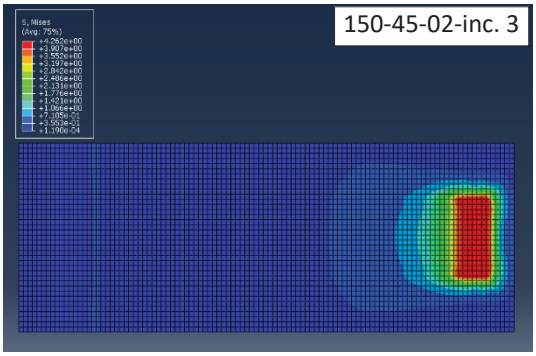
150-45-02-inc. 3

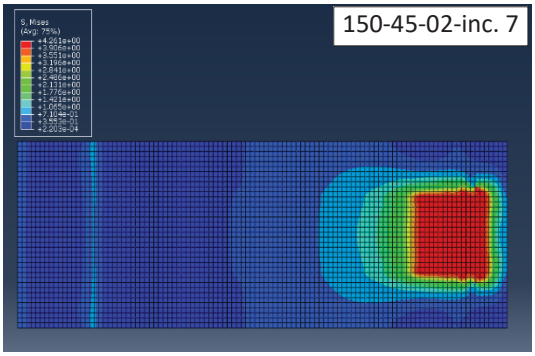
150-45-02-inc. 7

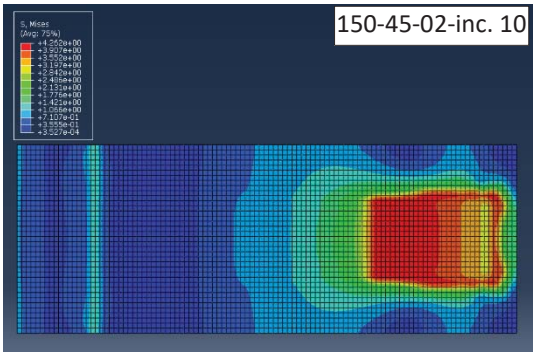
150-45-02-inc. 10

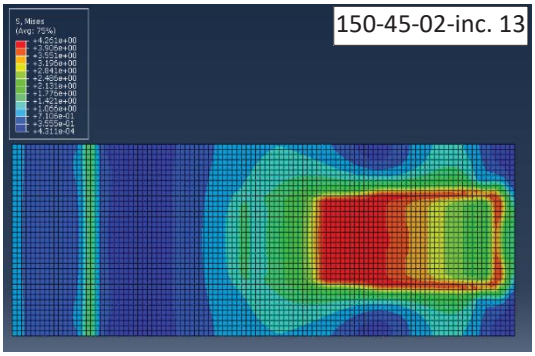
150-45-02-inc. 13

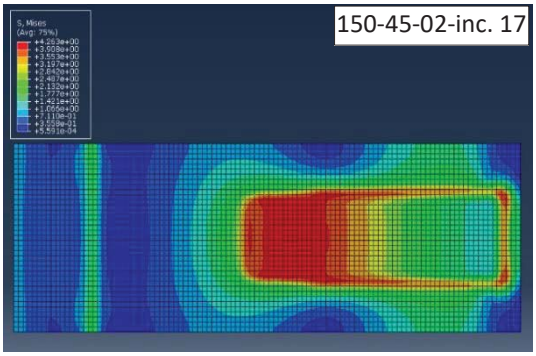
150-45-02-inc. 17

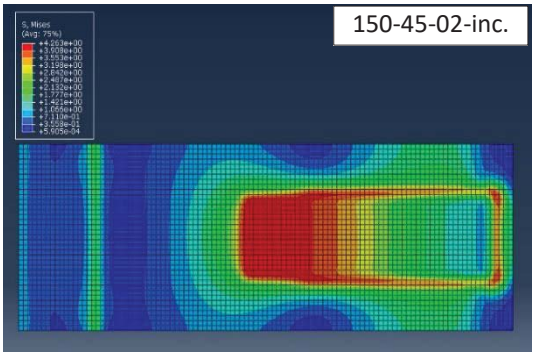
150-45-02-inc.

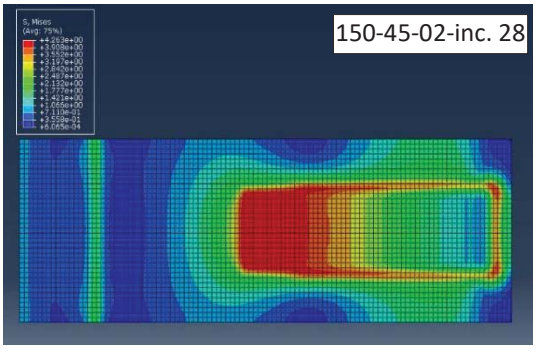
150-45-02-inc. 28

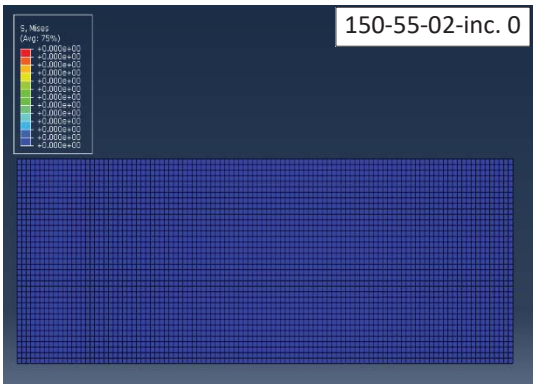
150-55-02-inc. 0

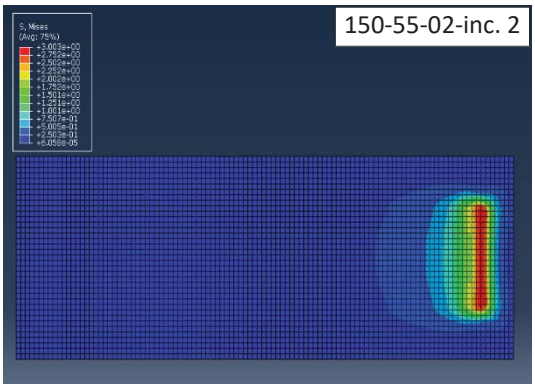
150-55-02-inc. 2

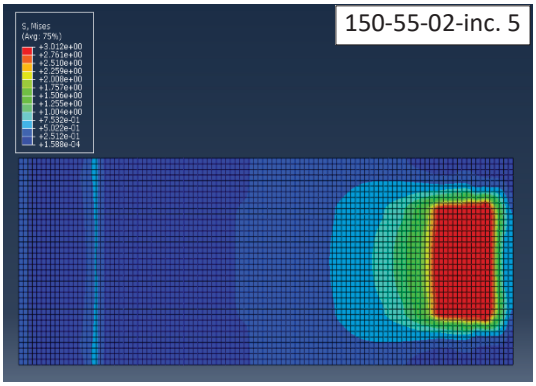
150-55-02-inc. 5

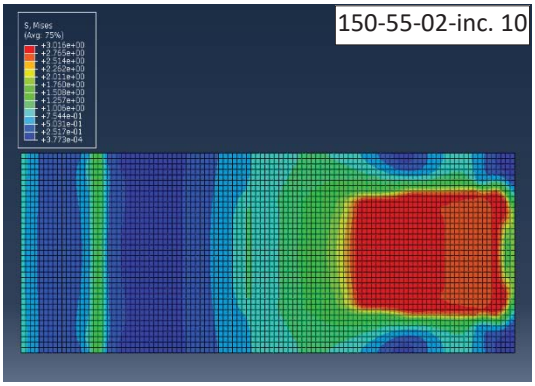
150-55-02-inc. 10

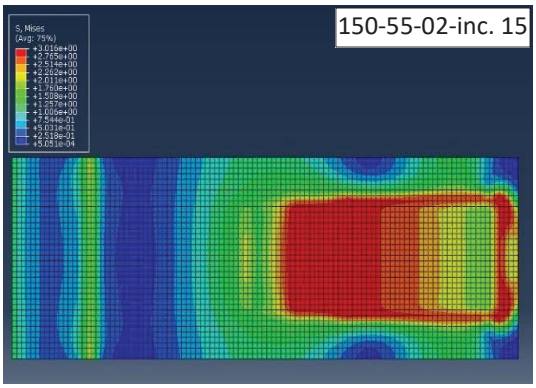
150-55-02-inc. 15

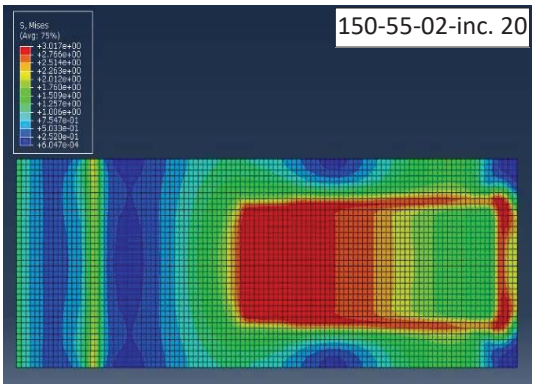
150-55-02-inc. 20

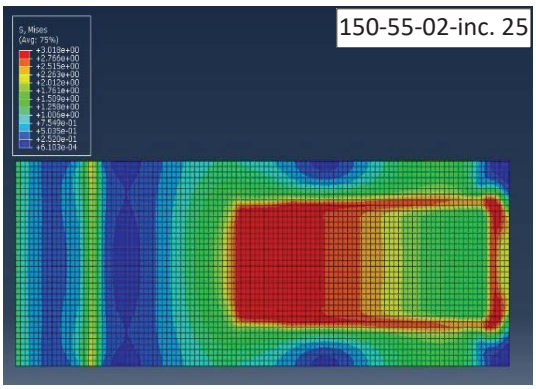
150-55-02-inc. 25

Numerical simulation, FRP-to-LVL Series; Damage distributions

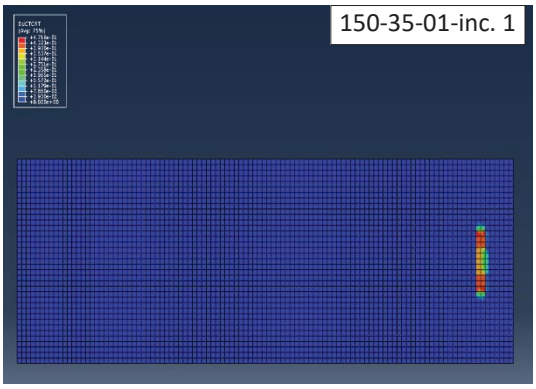

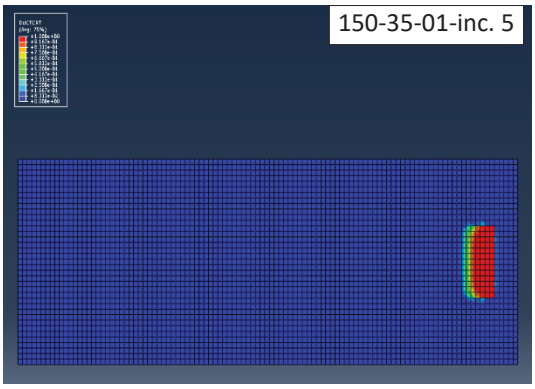

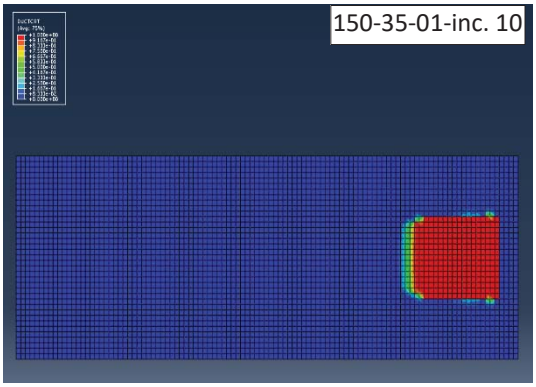

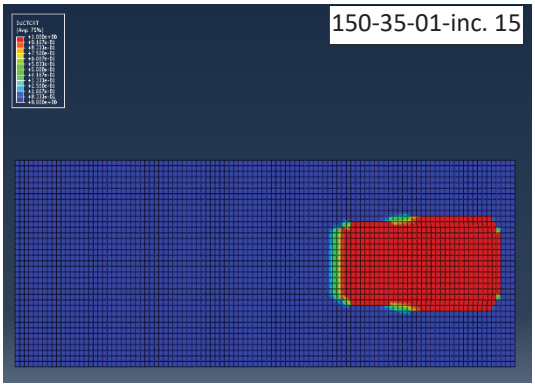

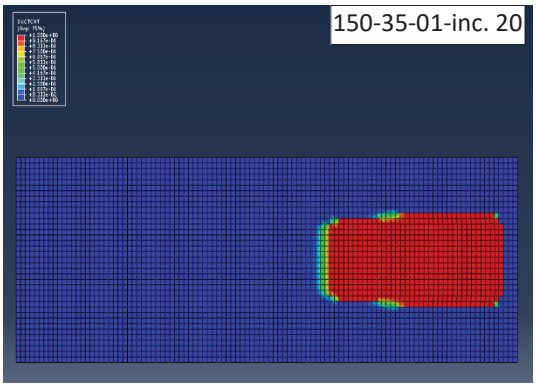

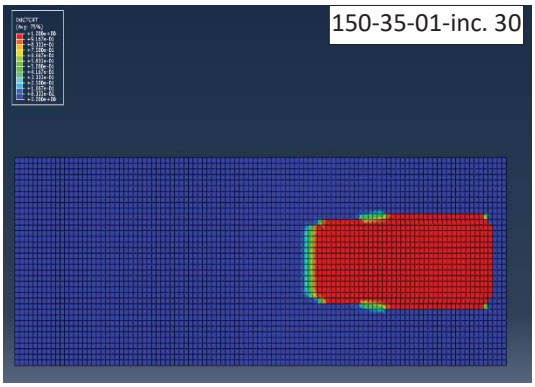

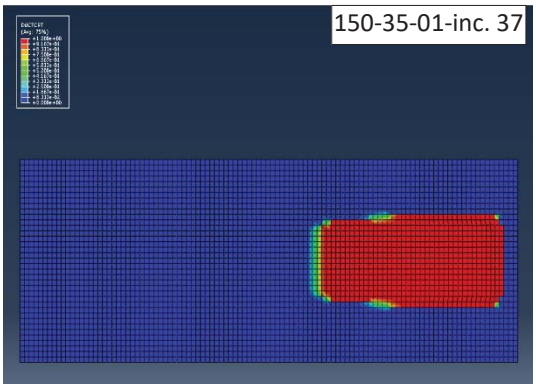

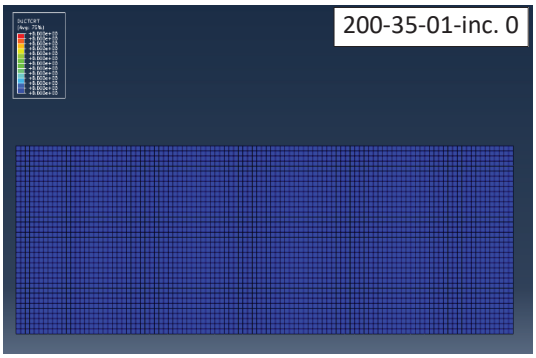
200-35-01-inc. 0

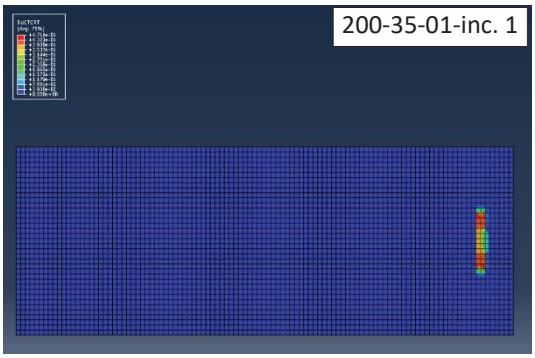
200-35-01-inc. 1

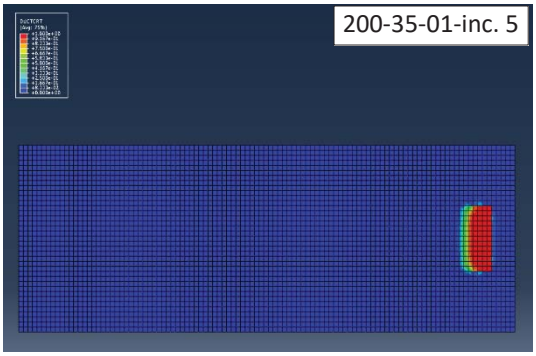
200-35-01-inc. 5

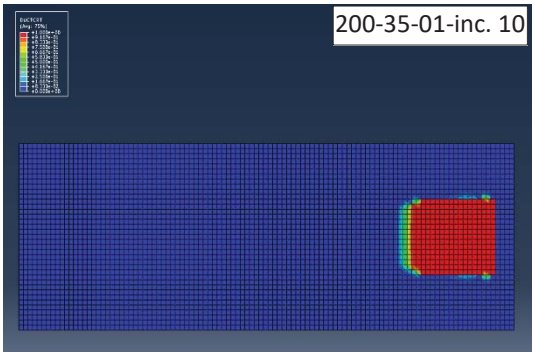
200-35-01-inc. 10

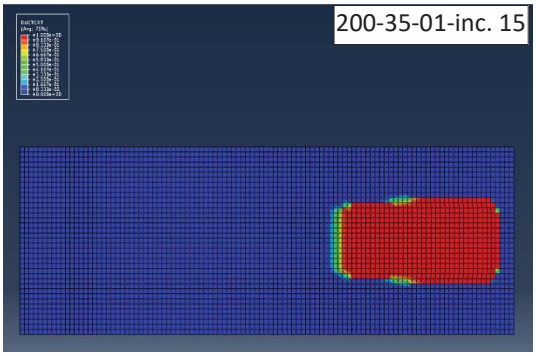
200-35-01-inc. 15

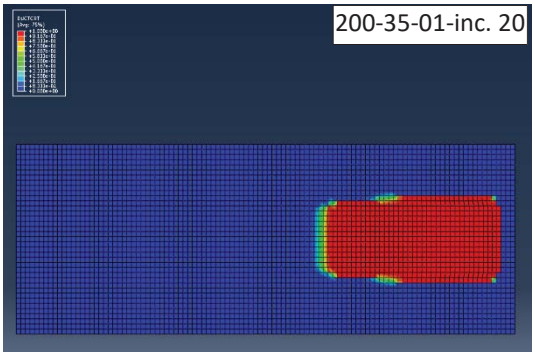
200-35-01-inc. 20

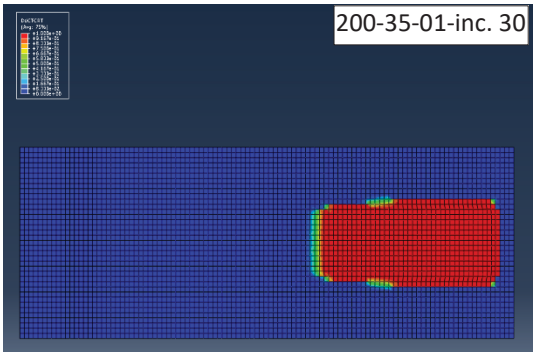
200-35-01-inc. 30

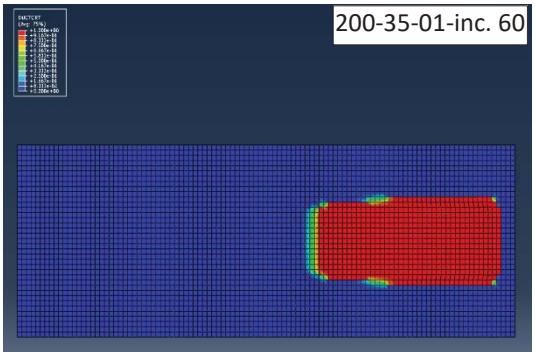
200-35-01-inc. 60

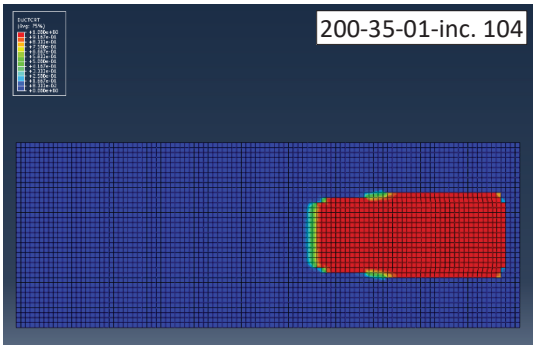
200-35-01-inc. 104

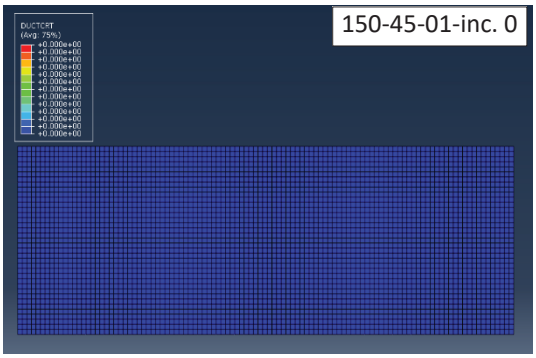
150-45-01-inc. 0

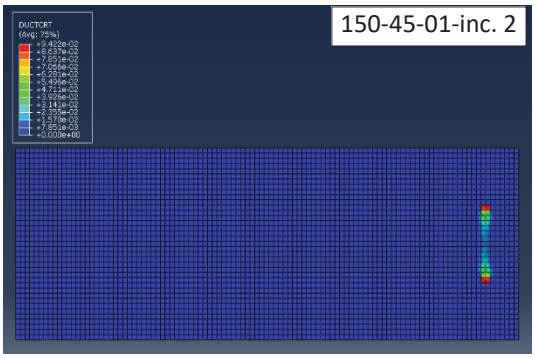
150-45-01-inc. 2

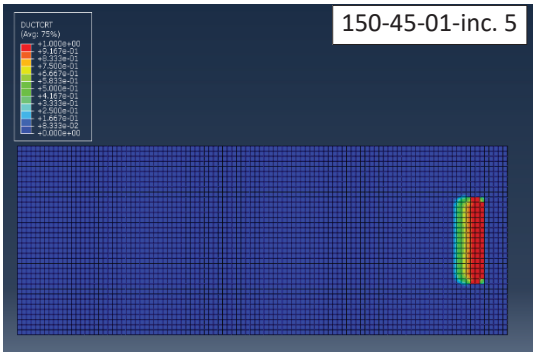
150-45-01-inc. 5

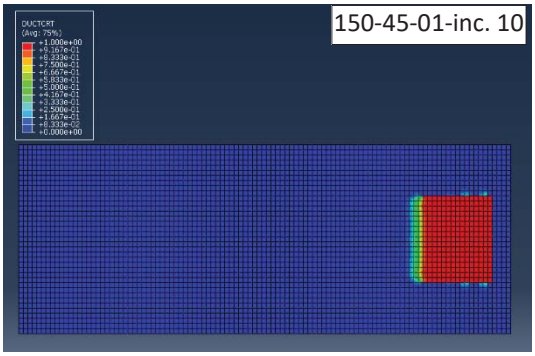
150-45-01-inc. 10

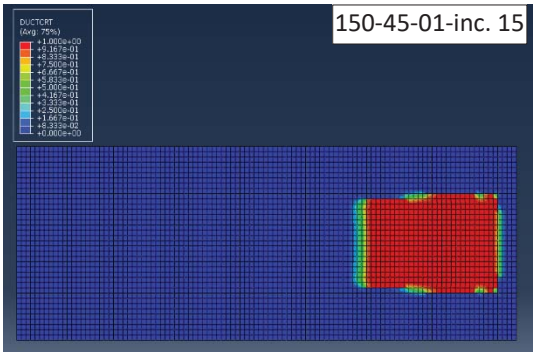
150-45-01-inc. 15

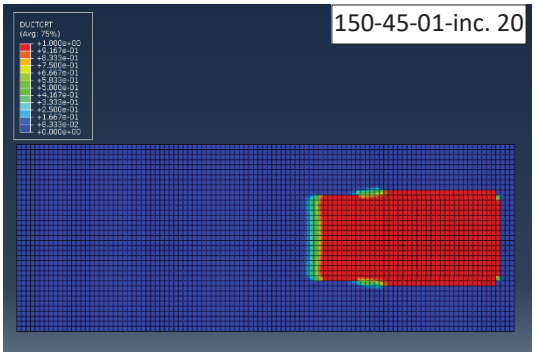
150-45-01-inc. 20

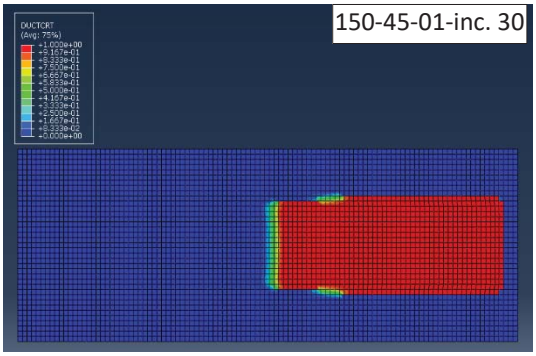
150-45-01-inc. 30

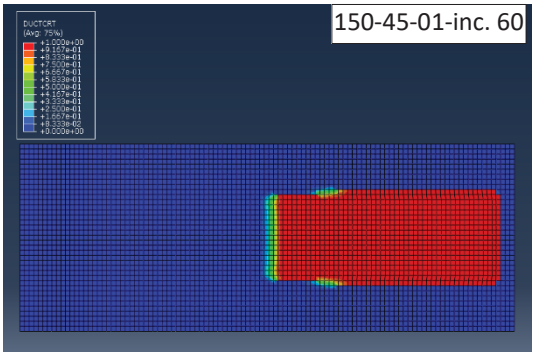
150-45-01-inc. 60

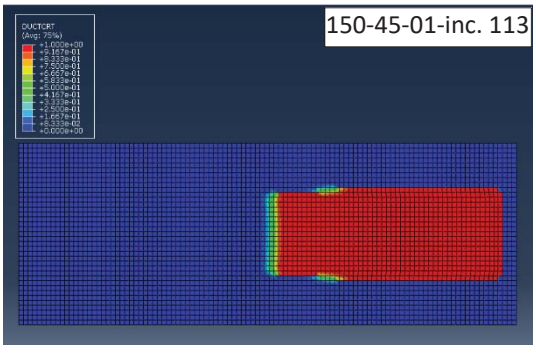
150-45-01-inc. 113

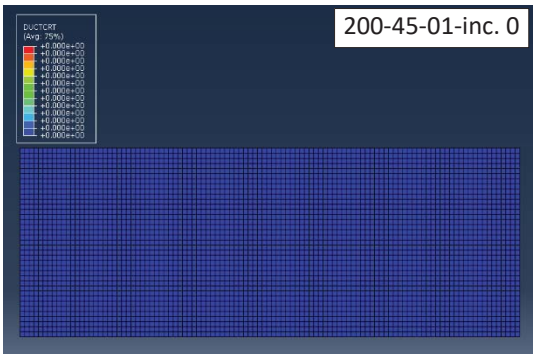
200-45-01-inc. 0

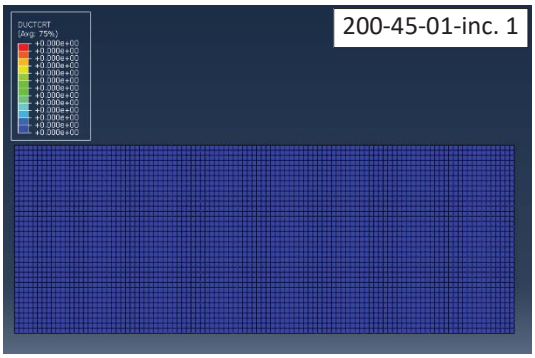
200-45-01-inc. 1

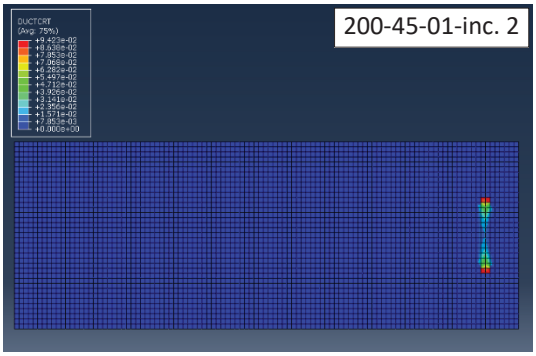
200-45-01-inc. 2

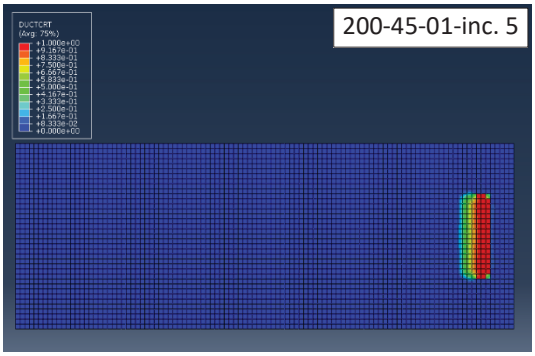
200-45-01-inc. 5

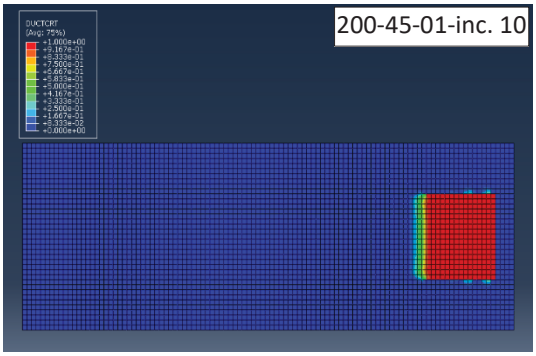
200-45-01-inc. 10

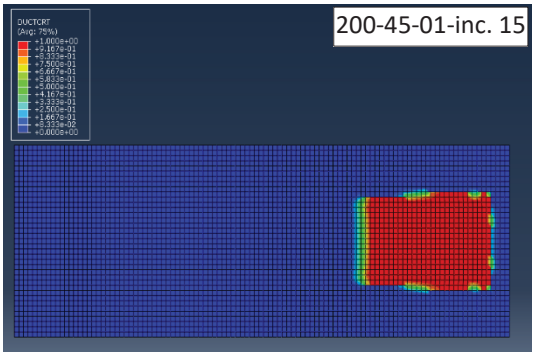
200-45-01-inc. 15

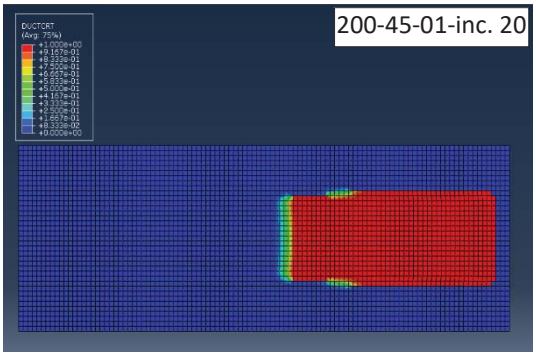
200-45-01-inc. 20

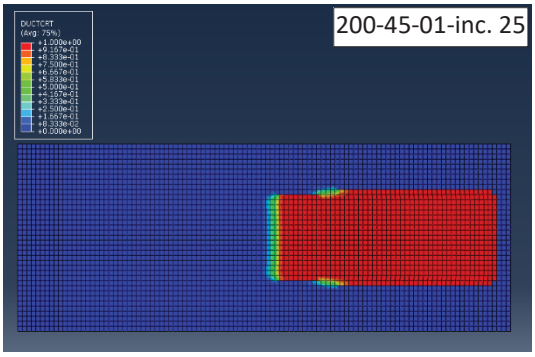
200-45-01-inc. 25

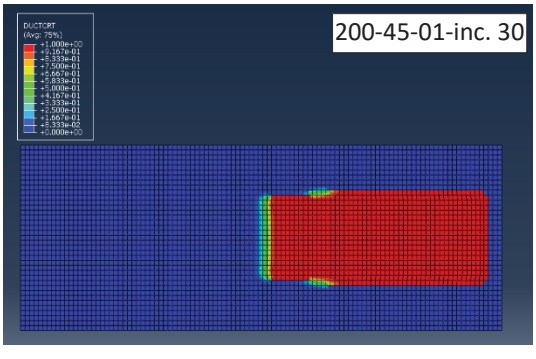
200-45-01-inc. 30

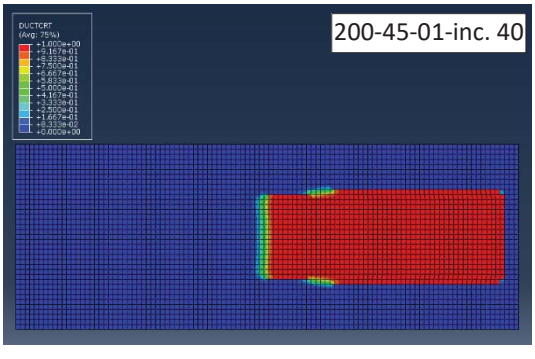
200-45-01-inc. 40

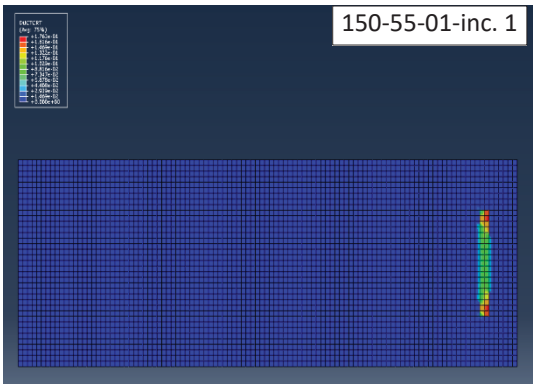
150-55-01-inc. 1

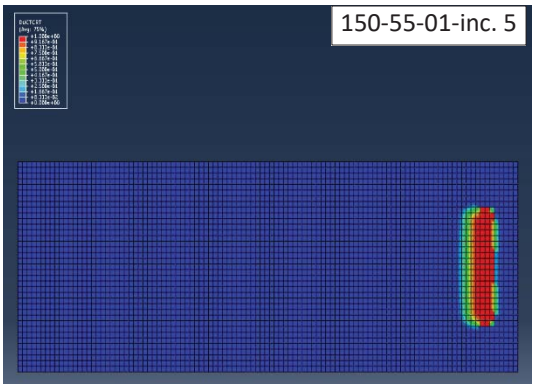
150-55-01-inc. 5

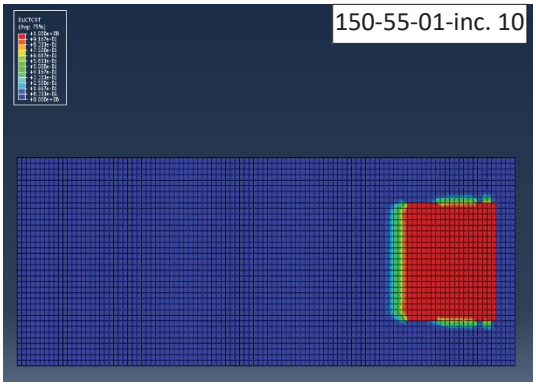
150-55-01-inc. 10

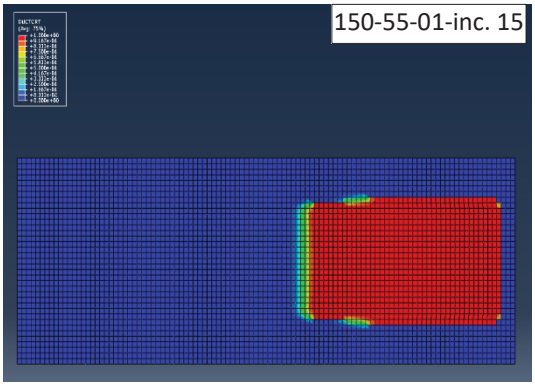
150-55-01-inc. 15

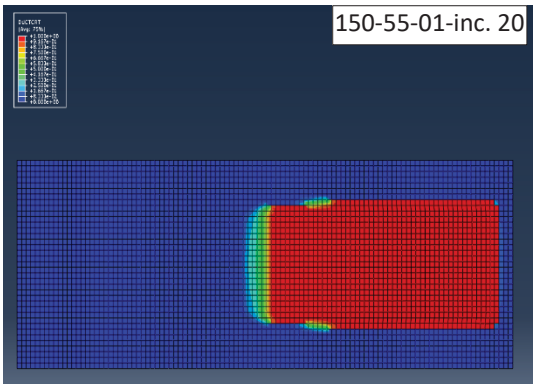
150-55-01-inc. 20

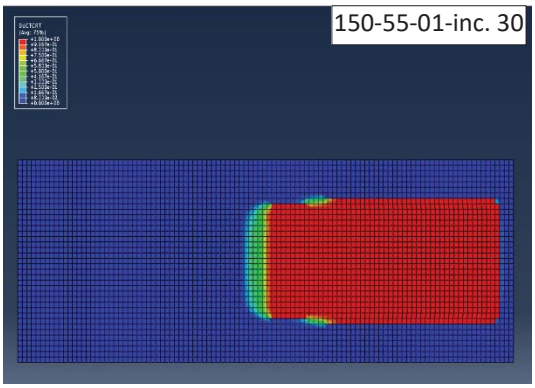
150-55-01-inc. 30

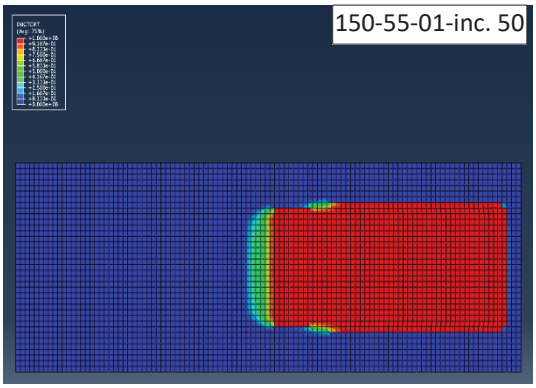
150-55-01-inc. 50

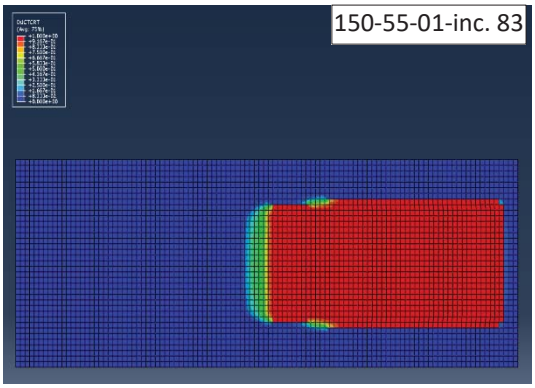
150-55-01-inc. 83

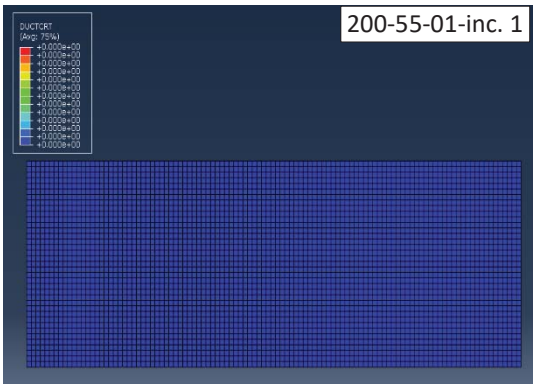
200-55-01-inc. 1

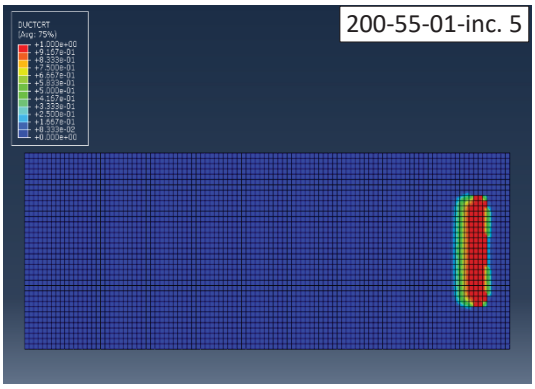
200-55-01-inc. 5

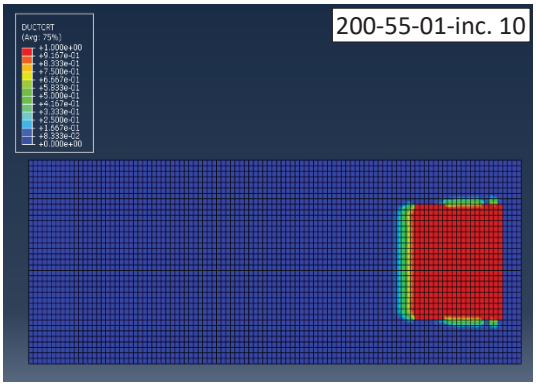
200-55-01-inc. 10

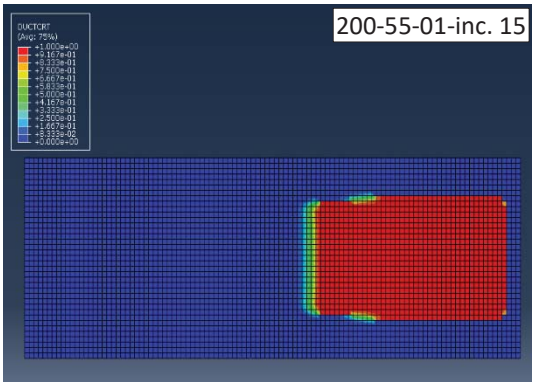
200-55-01-inc. 15

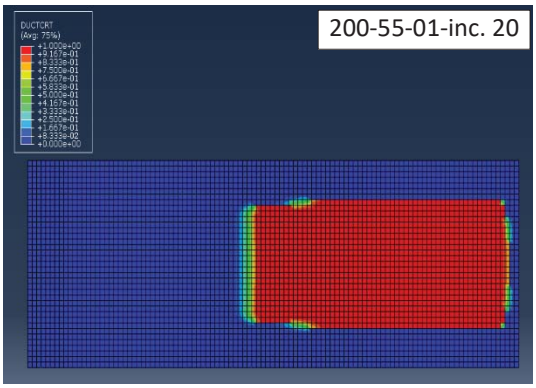
200-55-01-inc. 20

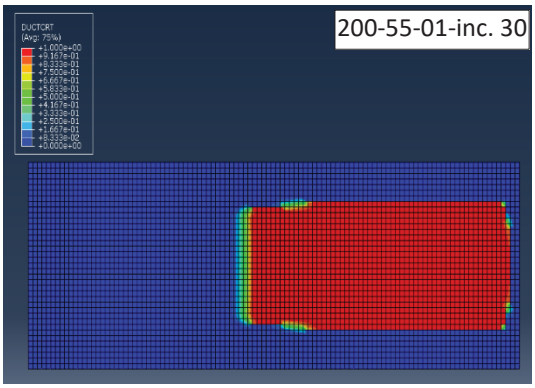
200-55-01-inc. 30

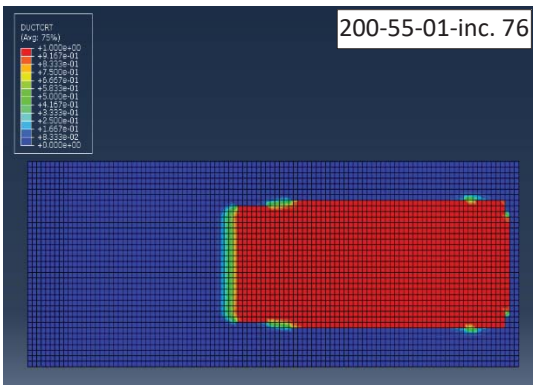
200-55-01-inc. 76

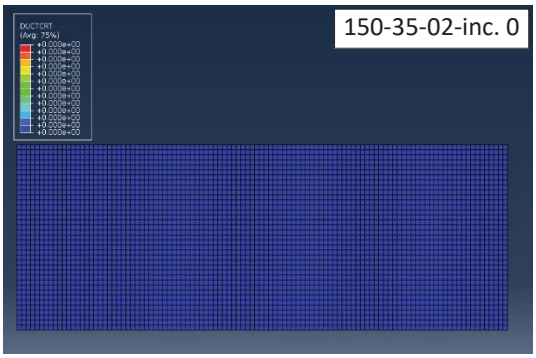
150-35-02-inc. 0

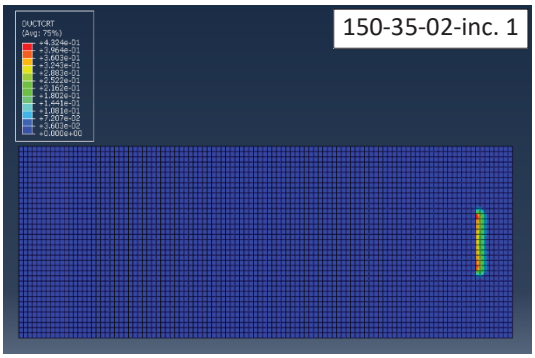
150-35-02-inc. 1

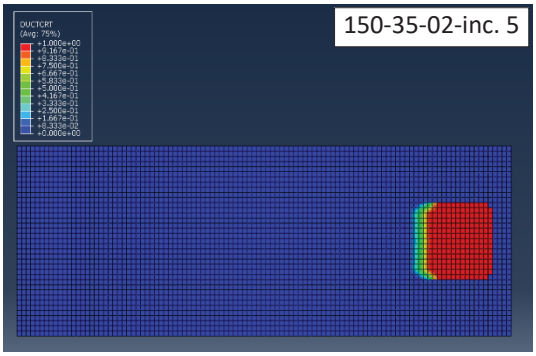
150-35-02-inc. 5

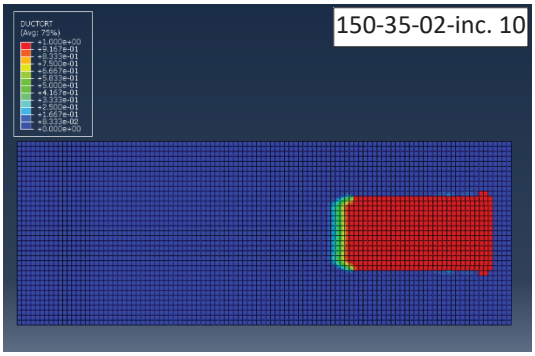
150-35-02-inc. 10

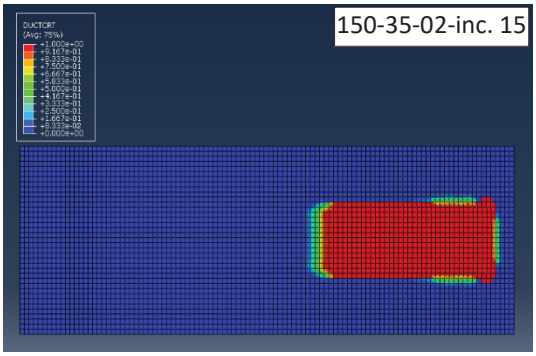
150-35-02-inc. 15

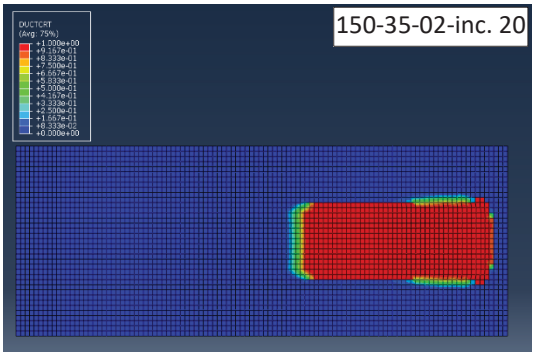
150-35-02-inc. 20

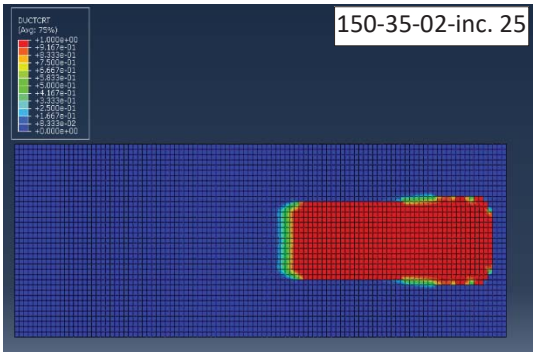
150-35-02-inc. 25

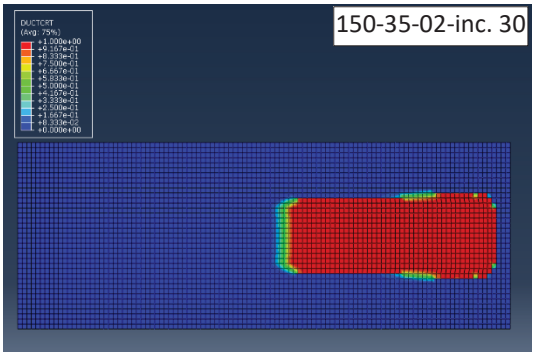
150-35-02-inc. 30

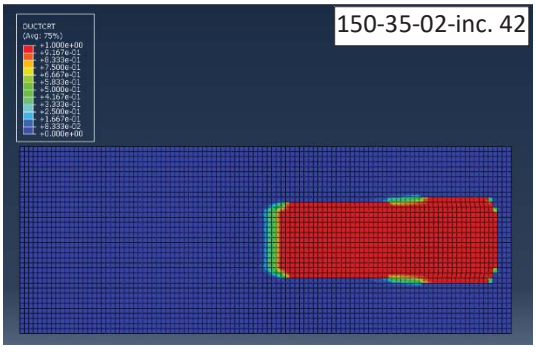
150-35-02-inc. 42

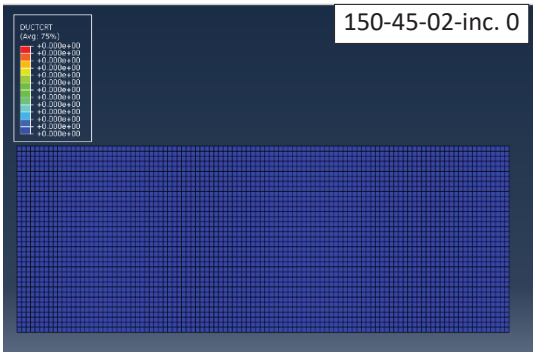
150-45-02-inc. 0

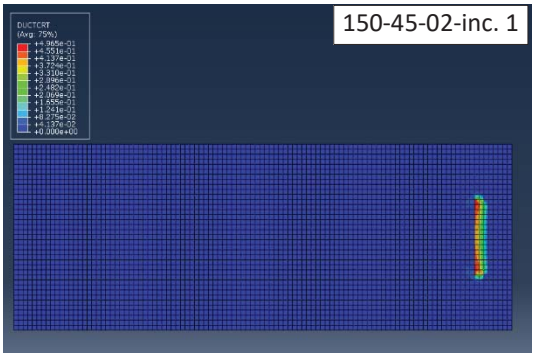
150-45-02-inc. 1

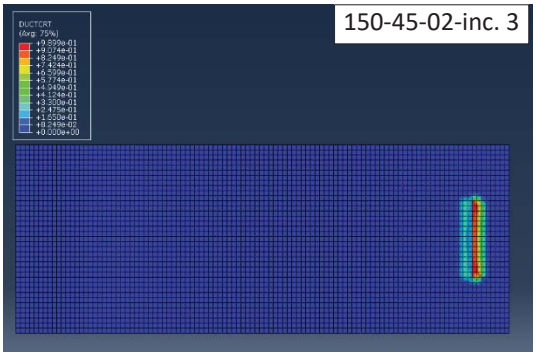
150-45-02-inc. 3

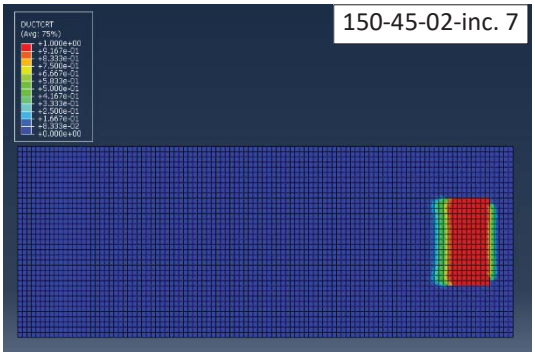
150-45-02-inc. 7

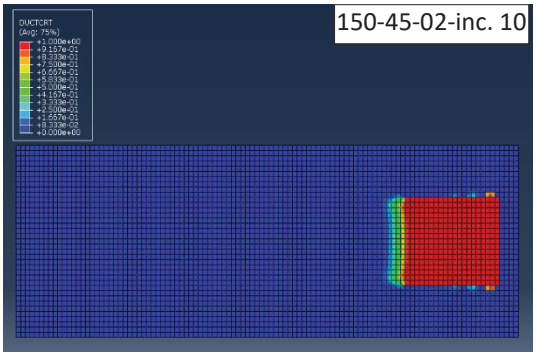
150-45-02-inc. 10

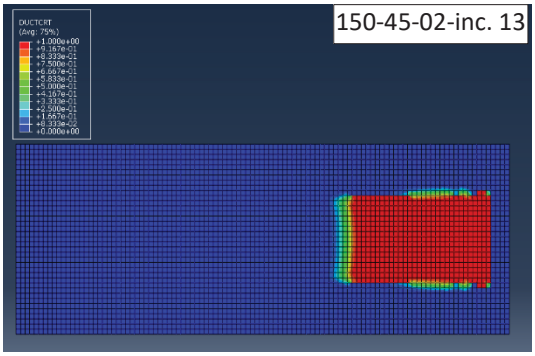
150-45-02-inc. 13

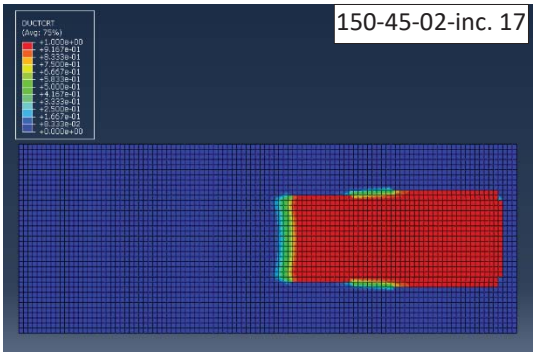
150-45-02-inc. 17

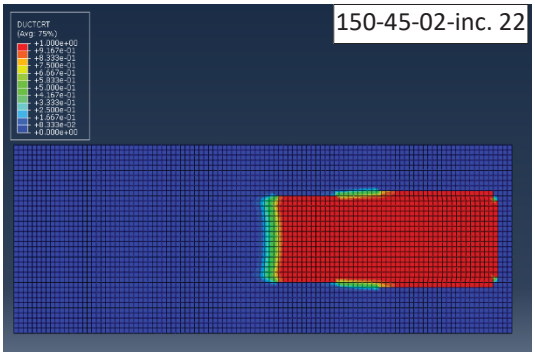
150-45-02-inc. 22

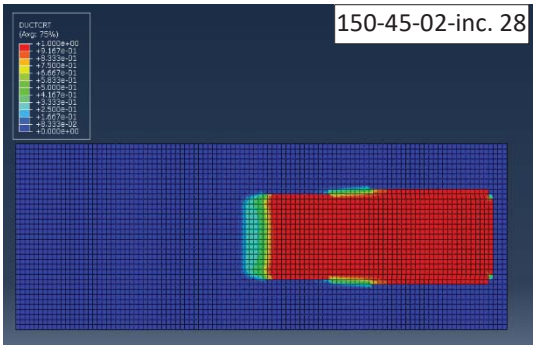
150-45-02-inc. 28

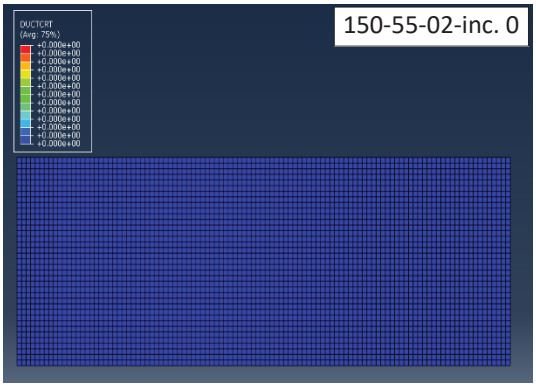
150-55-02-inc. 0

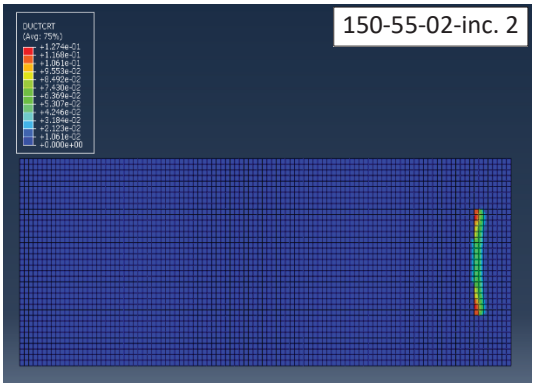
150-55-02-inc. 2

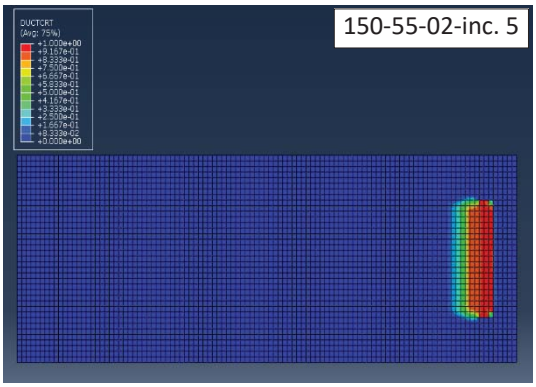
150-55-02-inc. 5

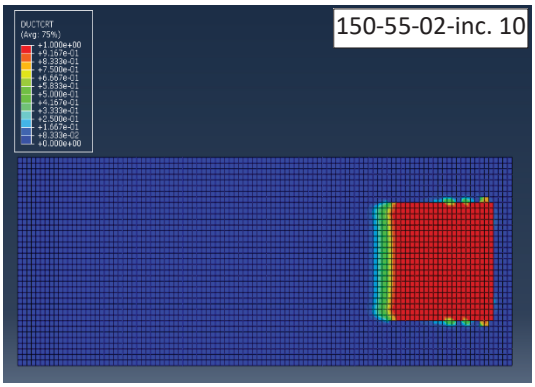
150-55-02-inc. 10

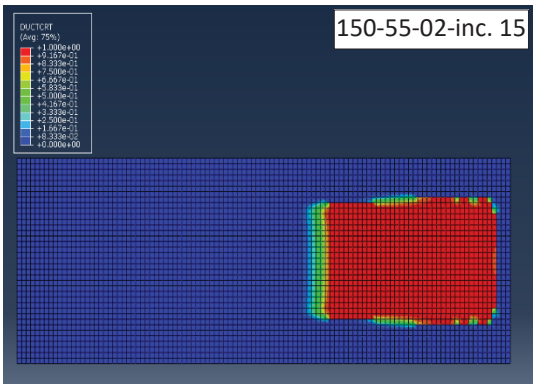
150-55-02-inc. 15

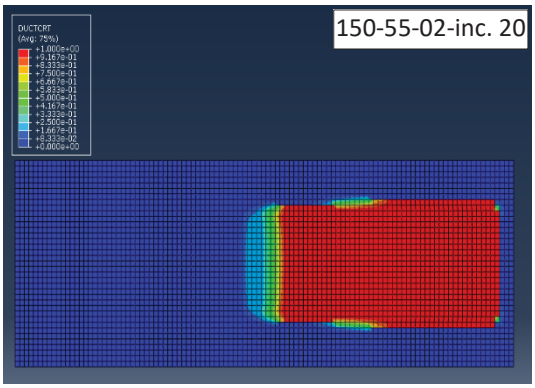
150-55-02-inc. 20

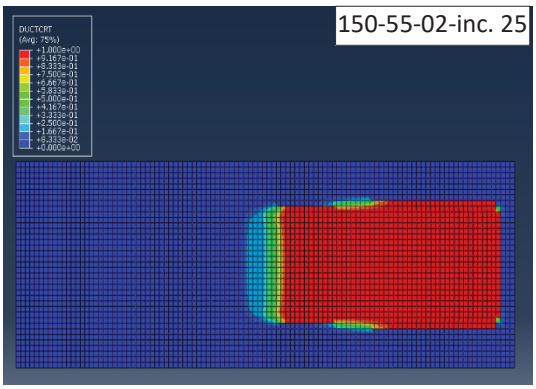
150-55-02-inc. 25

Numerical simulation, FRP-to-Hardwood Series; Stress distributions

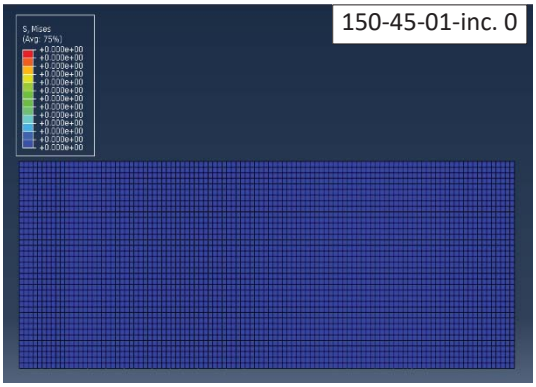

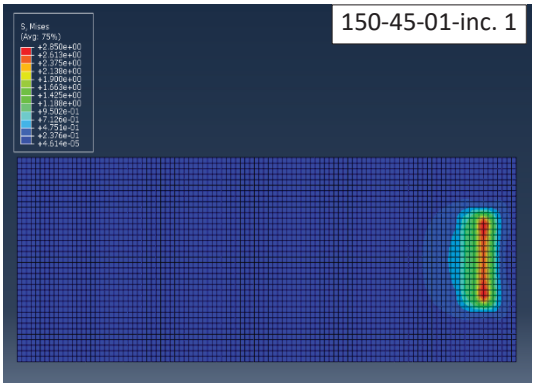

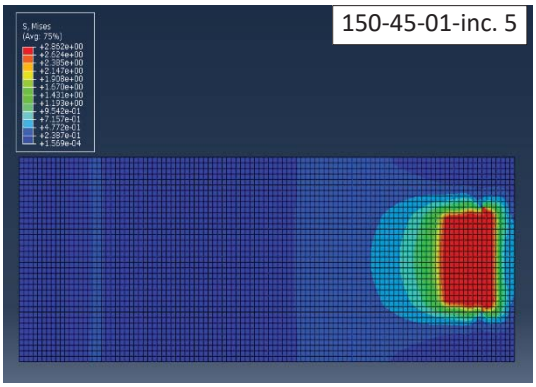

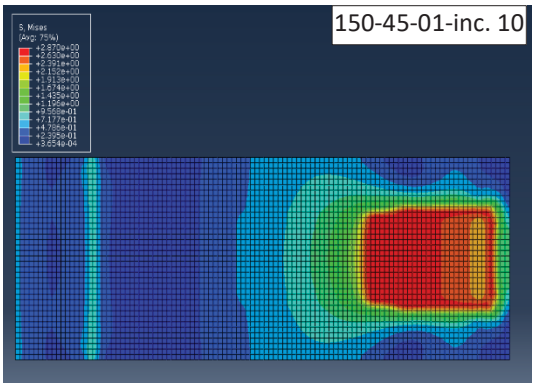

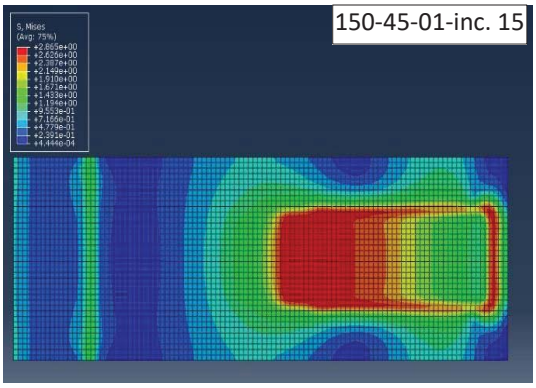

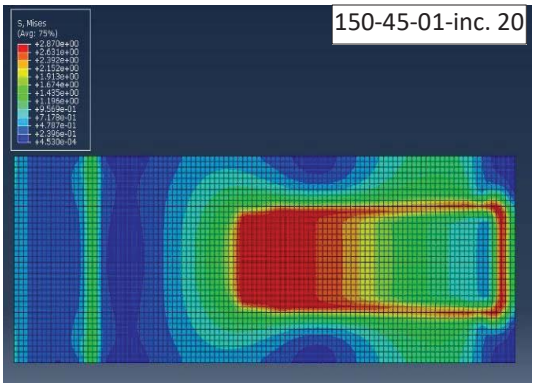

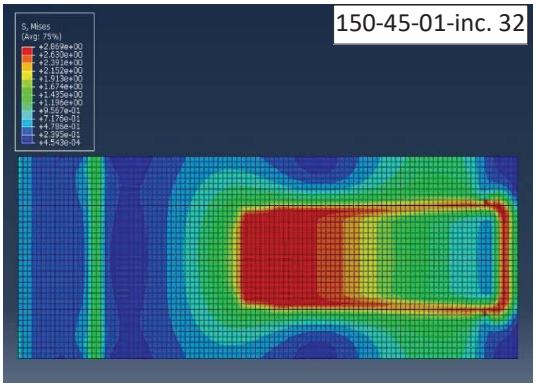

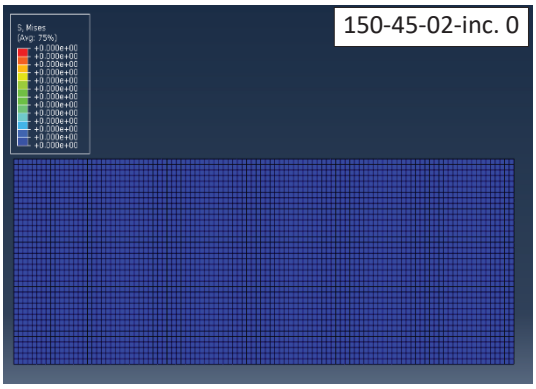
150-45-02-inc. 0

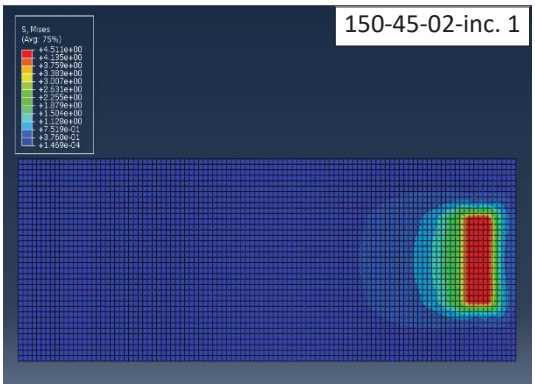
150-45-02-inc. 1

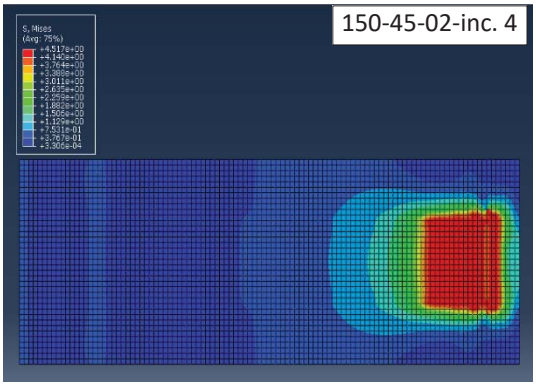
150-45-02-inc. 4

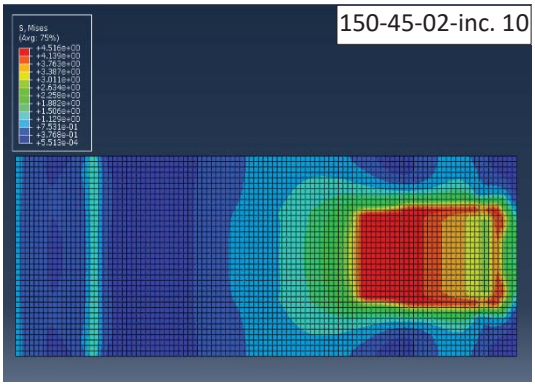
150-45-02-inc. 10

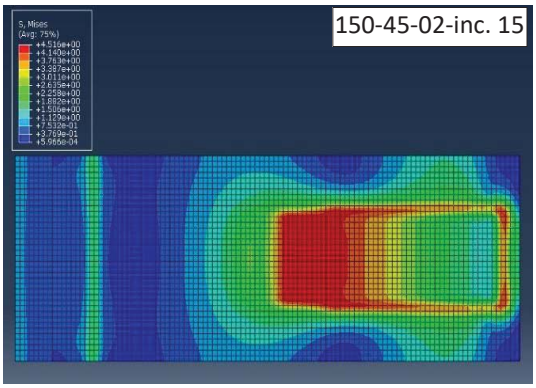
150-45-02-inc. 15

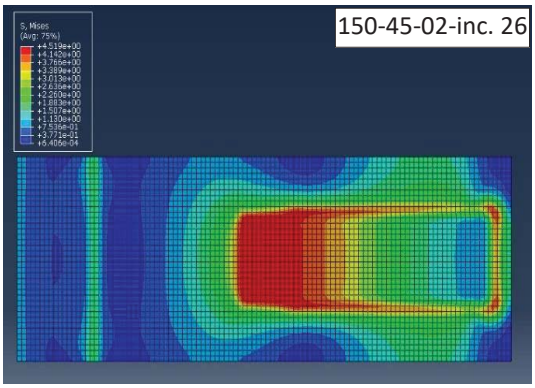
150-45-02-inc. 26

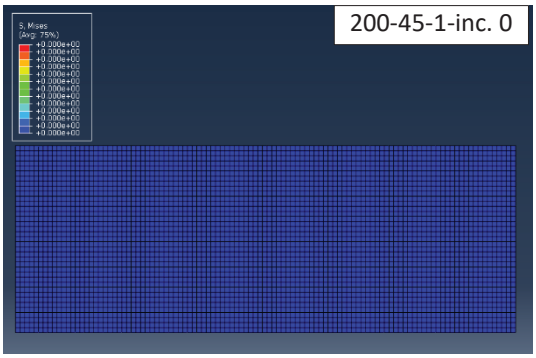
200-45-1-inc. 0

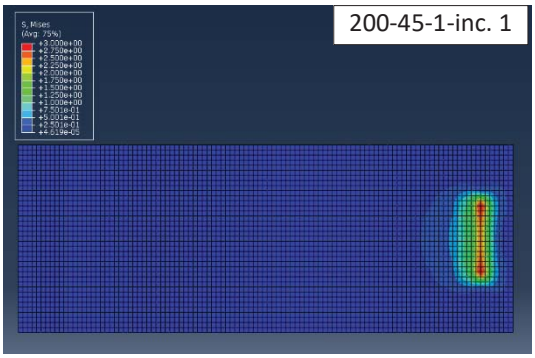
200-45-1-inc. 1

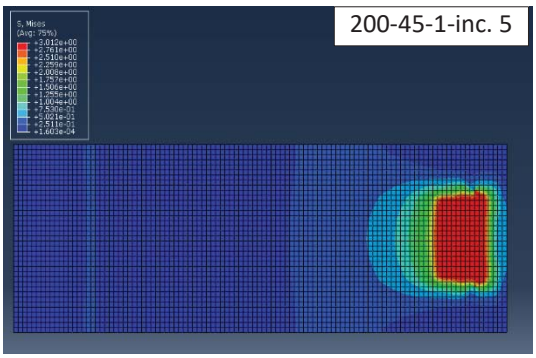
200-45-1-inc. 5

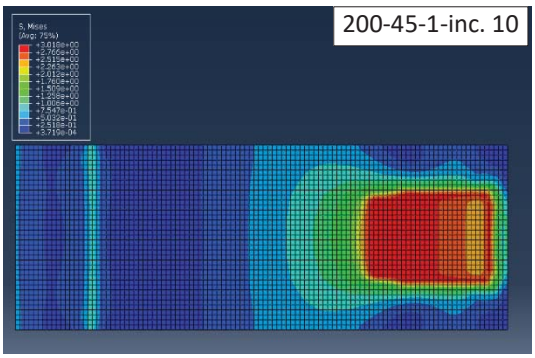
200-45-1-inc. 10

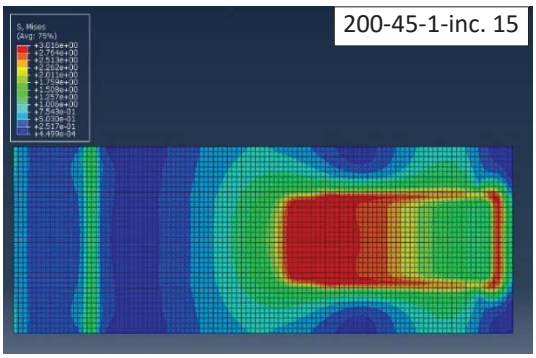
200-45-1-inc. 15

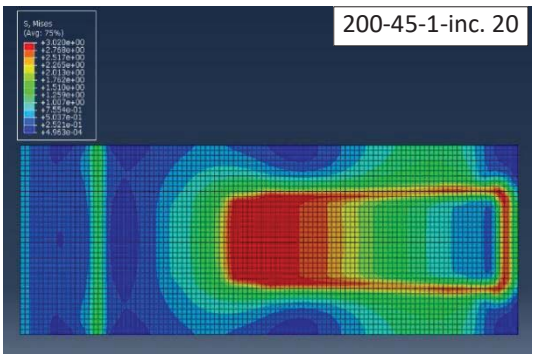
200-45-1-inc. 20

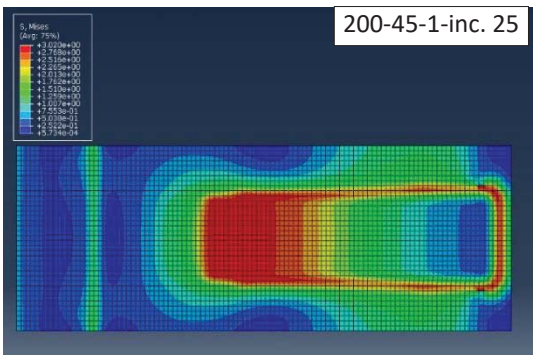
200-45-1-inc. 25

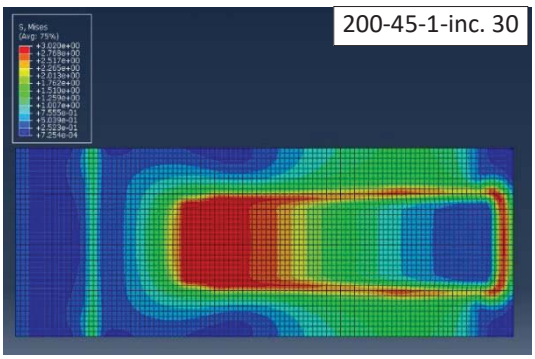
200-45-1-inc. 30

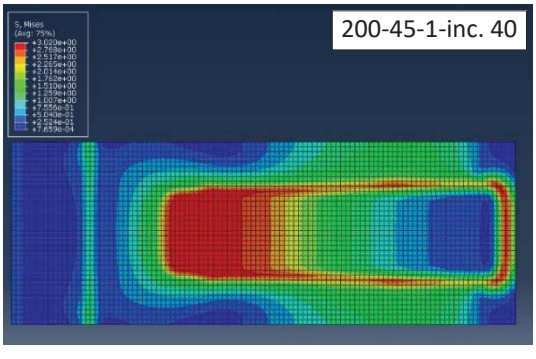
200-45-1-inc. 40

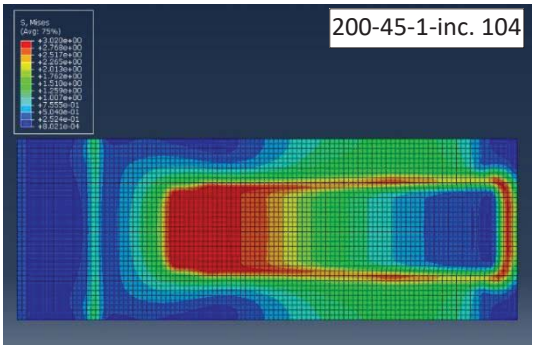
200-45-1-inc. 104

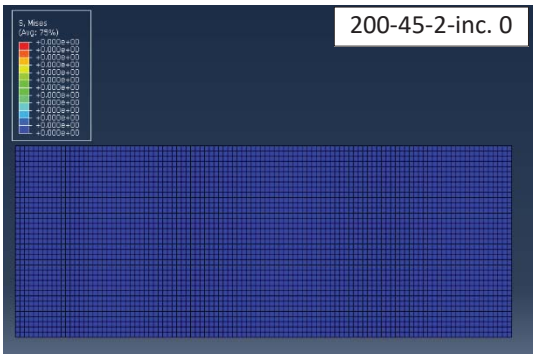
200-45-2-inc. 0

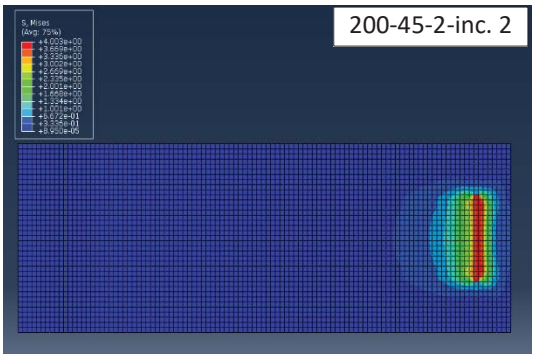
200-45-2-inc. 2

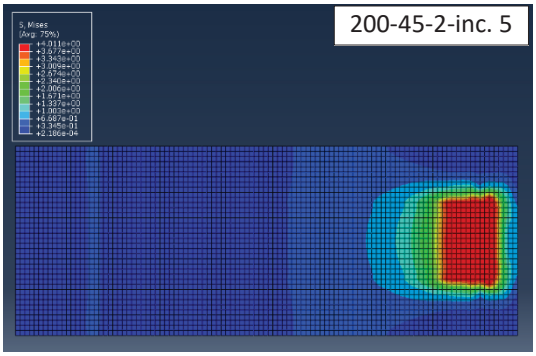
200-45-2-inc. 5

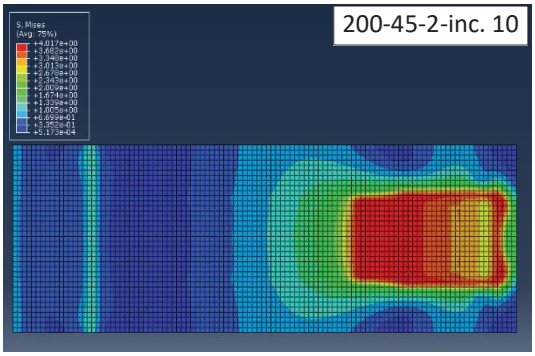
200-45-2-inc. 10

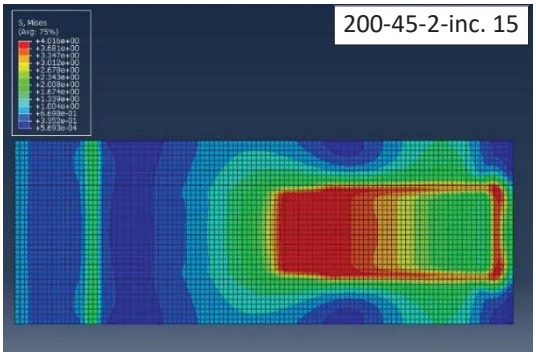
200-45-2-inc. 15

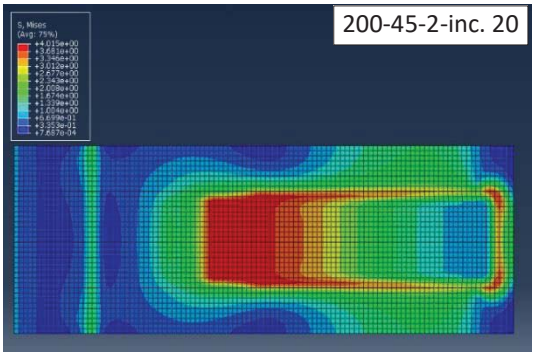
200-45-2-inc. 20

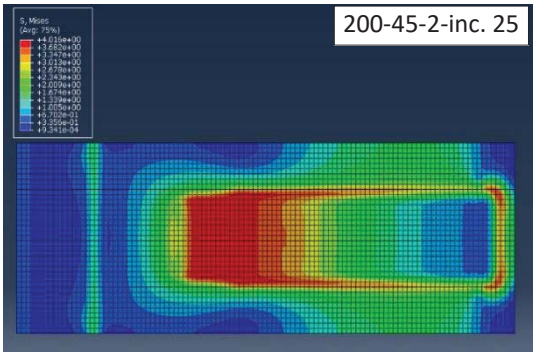
200-45-2-inc. 25

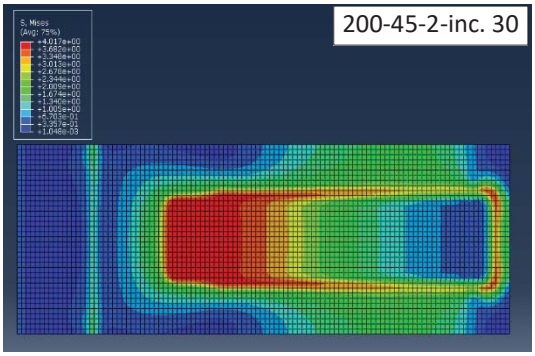
200-45-2-inc. 30

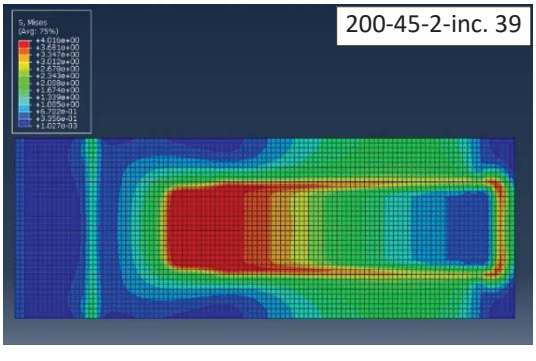
200-45-2-inc. 39

Numerical simulation, FRP-to-Hardwood Series; Damage distributions

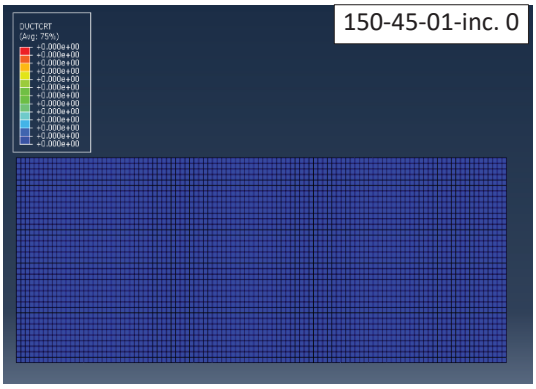

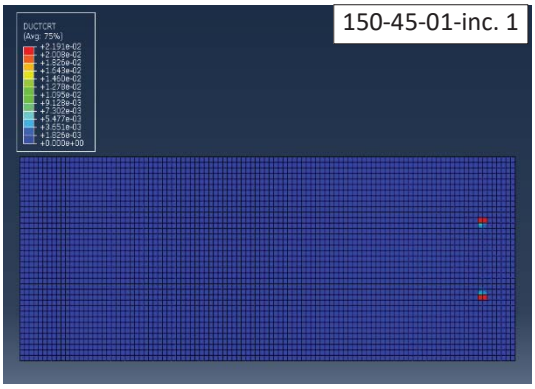

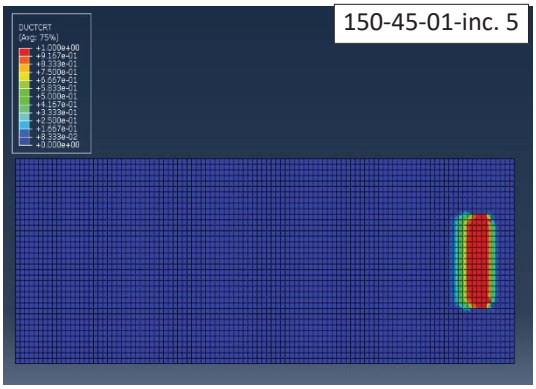

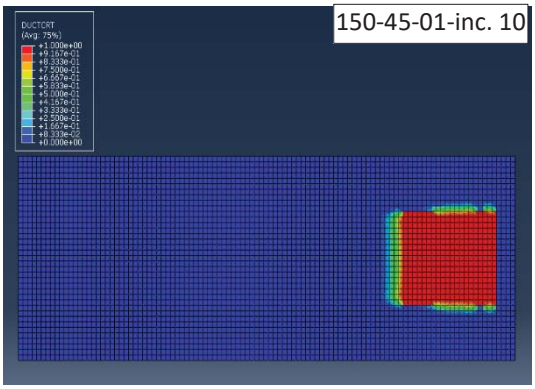

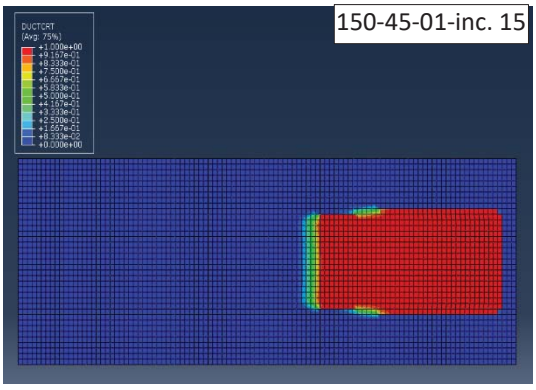

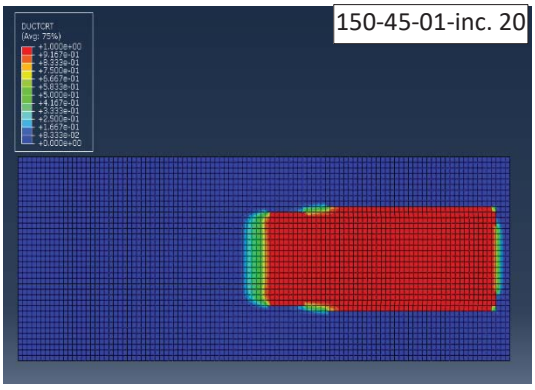

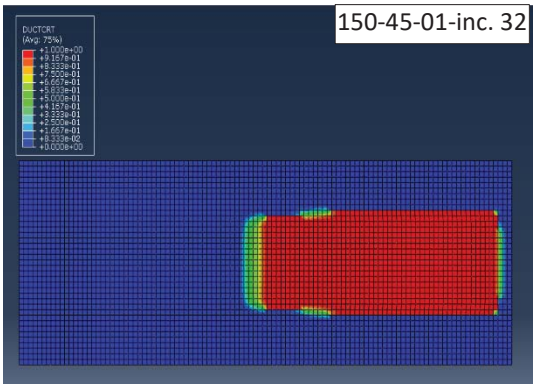

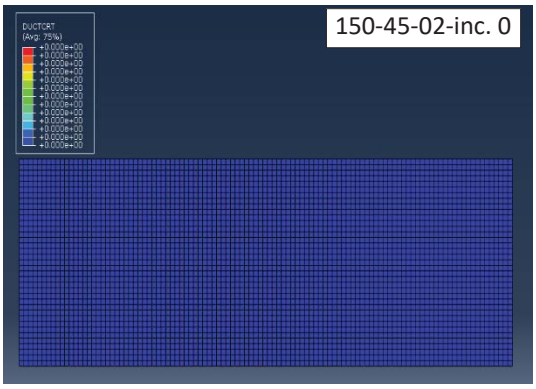
150-45-02-inc. 0

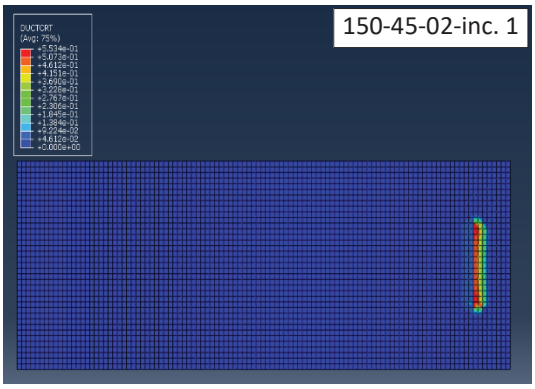
150-45-02-inc. 1

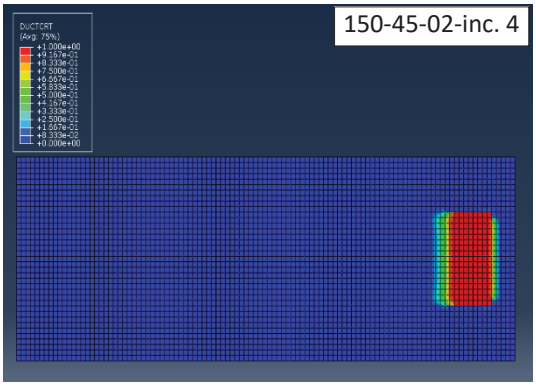
150-45-02-inc. 4

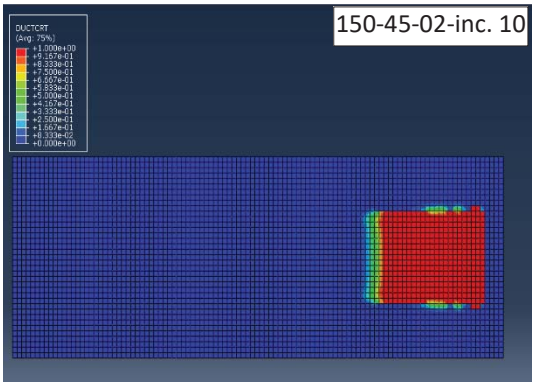
150-45-02-inc. 10

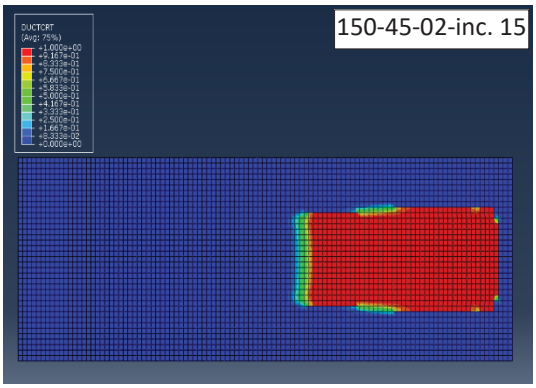
150-45-02-inc. 15

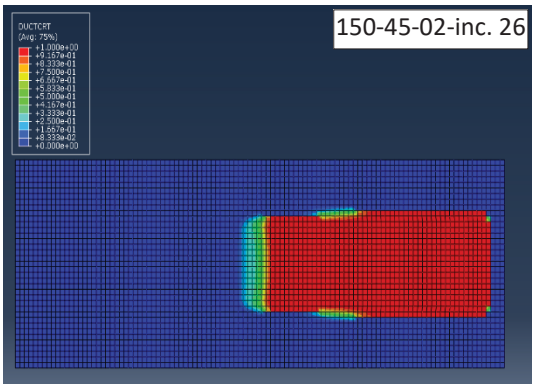
150-45-02-inc. 26

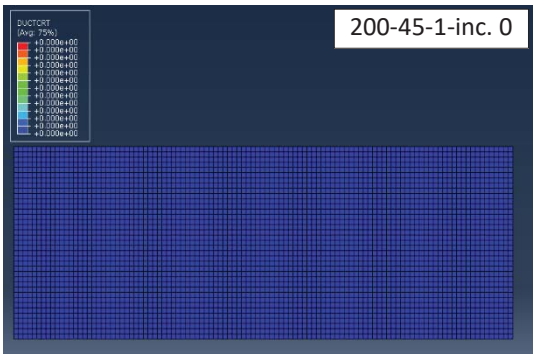
200-45-1-inc. 0

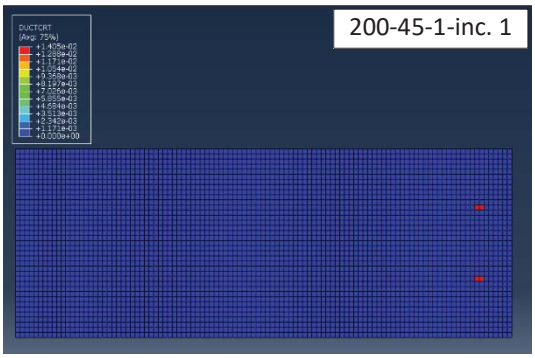
200-45-1-inc. 1

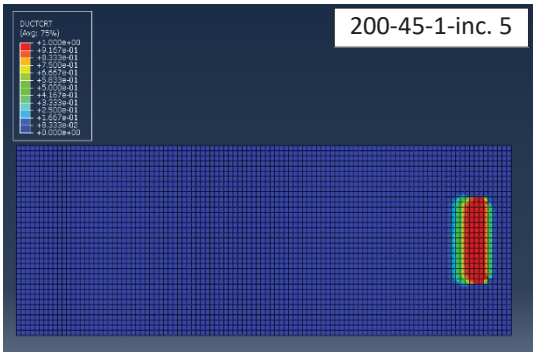
200-45-1-inc. 5

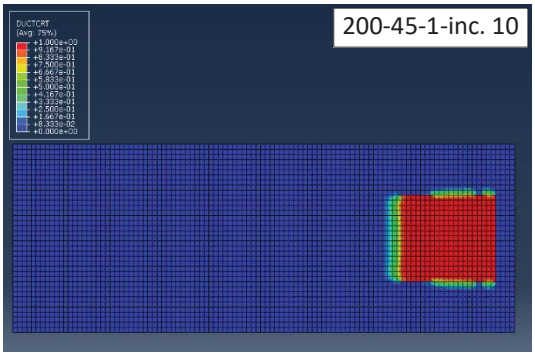
200-45-1-inc. 10

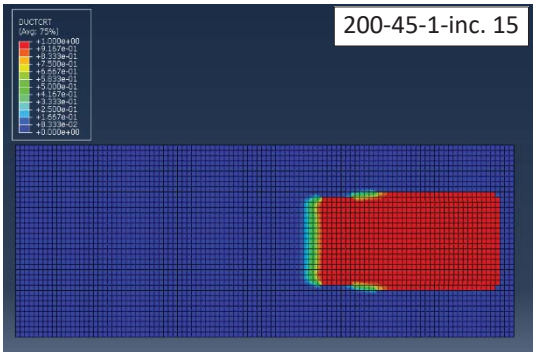
200-45-1-inc. 15

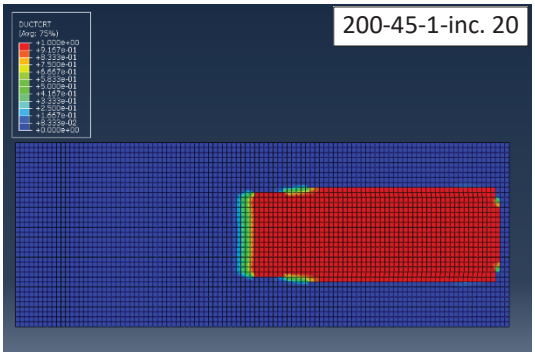
200-45-1-inc. 20

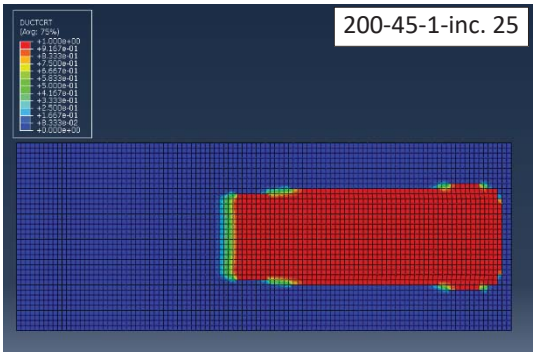
200-45-1-inc. 25

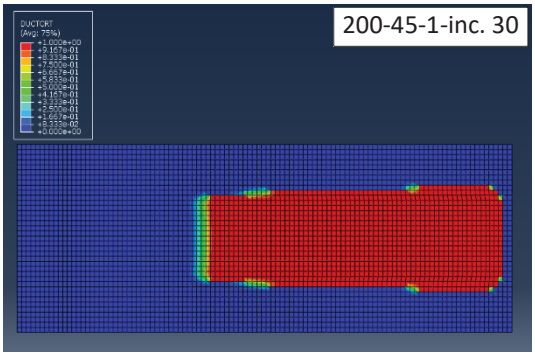
200-45-1-inc. 30

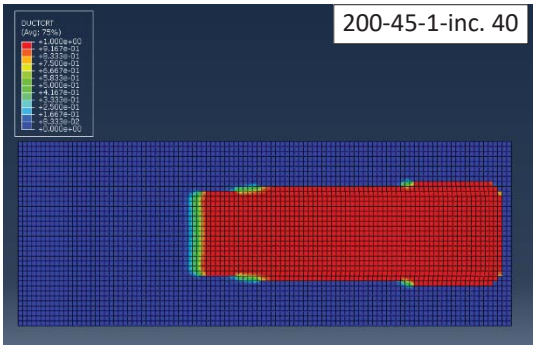
200-45-1-inc. 40

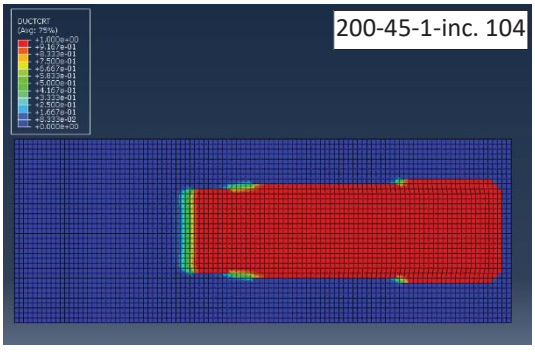
200-45-1-inc. 104

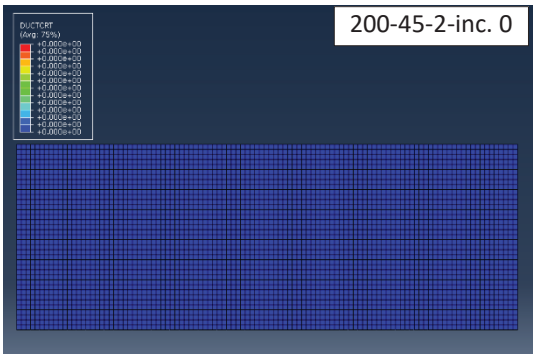
200-45-2-inc. 0

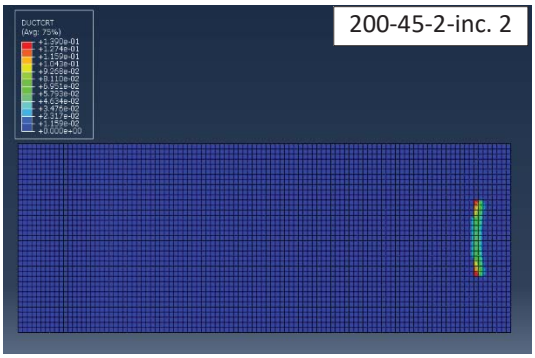
200-45-2-inc. 2

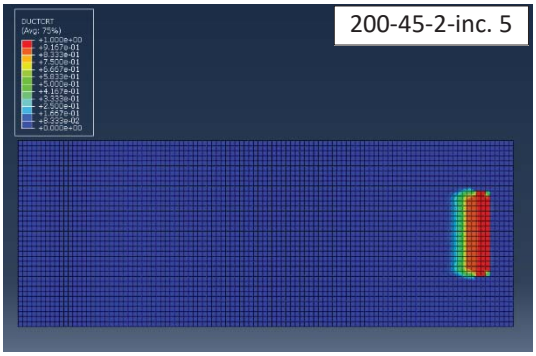
200-45-2-inc. 5

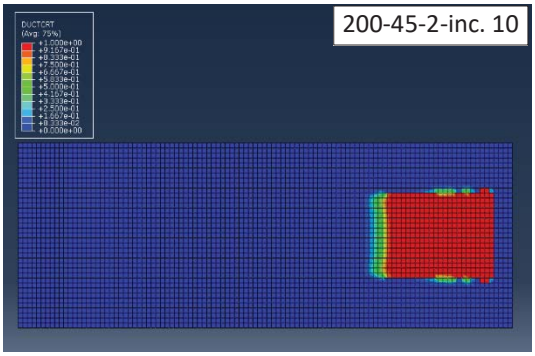
200-45-2-inc. 10

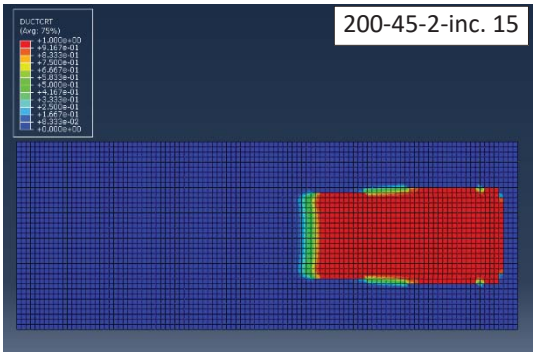
200-45-2-inc. 15

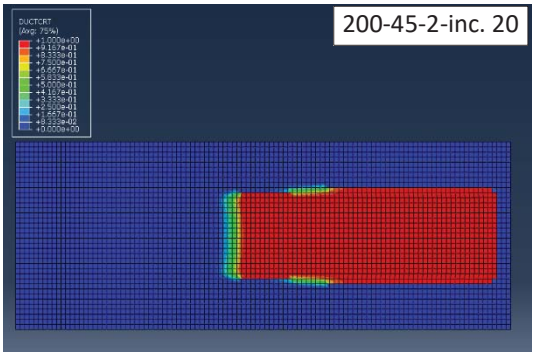
200-45-2-inc. 20

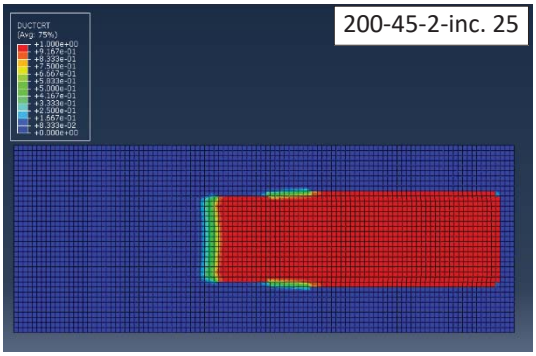
200-45-2-inc. 25

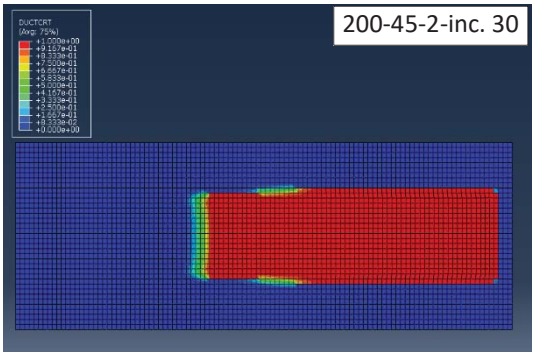
200-45-2-inc. 30

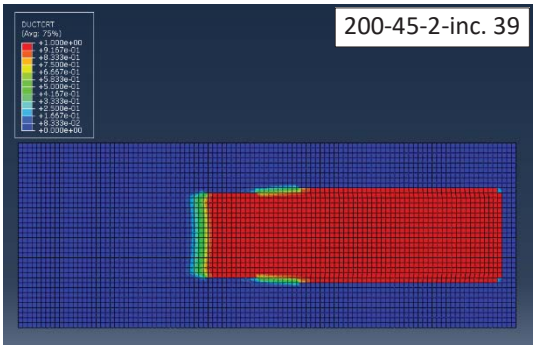
200-45-2-inc. 39